ORNL-4145
UC-10 – Chemical Separations Processes
for Plutonium and Uranium

CHEMICAL TECHNOLOGY DIVISION
ANNUAL PROGRESS REPORT
FOR PERIOD ENDING MAY 31, 1967

OAK RIDGE NATIONAL LABORATORY
operated by
UNION CARBIDE CORPORATION
for the
U.S. ATOMIC ENERGY COMMISSION

Printed in the United States of America. Available from Clearinghouse for Federal
Scientific and Technical Information, National Bureau of Standards,
U.S. Department of Commerce, Springfield, Virginia 22151
Price: Printed Copy $3.00; Microfiche $0.65

ORNL-4145

Contract No. W-7405-eng-26

CHEMICAL TECHNOLOGY DIVISION

ANNUAL PROGRESS REPORT

for Period Ending May 31, 1967

D. E. Ferguson – Division Director
K. B. Brown – Assistant Division Director
R. G. Wymer – Chemical Development Section A Chief
R. E. Blanco – Chemical Development Section B Chief
M. E. Whatley – Unit Operations Section Chief
H. E. Goeller – Process Design Section Chief
R. E. Brooksbank – Pilot Plant Section Chief

OCTOBER 1967

OAK RIDGE NATIONAL LABORATORY
Oak Ridge, Tennessee
operated by
UNION CARBIDE CORPORATION
for the
U. S. ATOMIC ENERGY COMMISSION

Reports previously issued in this series are as follows:

ORNL-2392	Period Ending August 31, 1957
ORNL-2576	Period Ending August 31, 1958
ORNL-2788	Period Ending August 31, 1959
ORNL-2993	Period Ending August 31, 1960
ORNL-3153	Period Ending May 31, 1961
ORNL-3314	Period Ending May 31, 1962
ORNL-3452	Period Ending May 31, 1963
ORNL-3627	Period Ending May 31, 1964
ORNL-3830	Period Ending May 31, 1965
ORNL-3945	Period Ending May 31, 1966

Contents

Summary

1. POWER REACTOR FUEL PROCESSING

1.1 Development of Mechanical Processes

Several reactor and reactor fuel manufacturers were visited to obtain the most recent detailed designs for third-generation PWR and BWR fuel (and proposed FBR fuel) assemblies. Evaluation of these data indicated that fuel element disassembly and shear-leach methods and equipment were suitable for handling the newer designs. Leaching of sheared Zircaloy-clad ThO_2-UO_2 in Thorex dissolvent [13 *M* HNO_3–0.05 *M* HF–0.05 *M* $Al(NO_3)_3$] resulted in the dissolution of about 99.8% of the uranium and thorium and 1.5% of the Zircaloy. Most of the zirconium precipitated during feed adjustment; however, subsequent solvent extraction processing of the unclarified solution was satisfactory. Operability of the full-sized delayed-neutron leached-hull monitor was evaluated; even in the presence of an 830-r/hr gamma field as little as 0.01 g of ^{235}U was still detectable. Further refinement of this monitoring technique, which we believe is the most sensitive and accurate for stainless steel cladding, is now in progress. Mechanical processing studies of graphite-base HTGR fuels were begun. Tests were made of the rough-breaking of large graphite fuel blocks with the ORNL 250-ton shear and of a "pile-driver" technique to provide feed for a jaw crusher; neither method was satisfactory. Use of a high-pressure (1000-psi) multinozzle water jet for removing coated fuel particles embedded in a sintered binder from holes in prototype graphite fuel sticks (Public Service of Colorado Reactor) was successful; the removal rate was 0.2 to 0.3 in./sec. A large fraction of the particle coatings were broken; however, this did not interfere with the almost quantitative separation of simulated fuel (–40 mesh) from fertile (+30 mesh) particles. Further development of this technique is in progress.

1.2 Development of Burn-Leach Process for Graphite-Base Fuels

The burn-leach process for graphite-base HTGR fuels was successfully demonstrated in hot-cell tests using General Atomic GAIL-3A and GAIL-3B compacts; these were composed of pyrolytic-carbon-coated $(Th,U)C_2$ particles in a graphite matrix and had been irradiated to (U + Th) burnups of 8800 and 41,500 Mwd/ton respectively. The broken compacts were burned in a fluidized bed of alumina at temperatures up to 750°C. Decontamination factors up to about 10^7 (based on the fission product activity in the bed and that in the discharged off-gas) were obtained after passing the off-gas through a 20-μ-porosity sintered metal filter held at $\leq$300°C. Further filtration of the off-gas through ordinary fiber-glass mats removed all the radioactive particulate matter. Nearly quantitative recovery of the thorium and uranium (>99%) was obtained when the $(Th,U)O_2$ ash was leached with boiling 13 *M* HNO_3–0.05 *M* HF–0.1 *M* $Al(NO_3)_3$; however, small quantities of insoluble fission products contaminated the leached alumina slightly. A system was developed for separating the bulk of the ThO_2-U_3O_8 from the alumina by screening, thus allowing part of the alumina bed to be recycled to the burner without leaching.

1.3 Development of Grind-Leach Process for Graphite-Base Fuels

Although laboratory experiments with unirradiated HTGR fuel samples [carbon-coated $(Th,U)C_2$ particles] indicated that the grind-leach process is feasible, hot-cell tests were disappointing because of the high (>1%) thorium and uranium losses and fission product retention (10 to 20%) by the leached graphite. The new ORNL roll crusher, which uses two 4-in. by 12-in.-diam rolls,

was tested; crushing of all fuels having fuel particle diameters of $\geq 150\ \mu$ to -140 mesh was completely successful. Single-step leaching with 13 *M* HNO_3–0.05 *M* HF–0.05 *M* $Al(NO_3)_3$ of unirradiated ground Peach Bottom and UHTREX fuel, even for extended times, was unsuccessful; results indicated uranium and thorium losses of ≥ 0.25 and 0.75% respectively. Two-step leachings were satisfactory, however, and resulted in uranium and thorium losses of $\leq 0.1\%$. Leaching tests with crushed carbon-coated sol-gel ThO_2 were very satisfactory, resulting in thorium losses of only 0.01%. All leach solutions contained about 1% of the carbon from the fuel as soluble organic compounds. Washing the graphite residue first with nitric acid and then with water was shown to give the highest fuel recovery for a minimum of wash volume. Hot-cell studies with irradiated Peach Bottom [GAIL-3A, irradiated to a (U + Th) burnup of 8850 Mwd/ton, and GAIL-3B, irradiated to a (U + Th) burnup of 41,500 Mwd/ton] fuel compacts and AVR fuel spheres [irradiated to a (U + Th) burnup of 23,000 Mwd/ton] were disappointing. Uranium and thorium losses varied from 1 to 5% and 2.5 to 7% respectively; in all experiments 10 to 20% of the fission products, principally ^{106}Ru, ^{137}Cs, and ^{144}Ce were retained in the leached and washed graphite residues.

1.4 Solvent Extraction Studies

The fuel solutions prepared in the grind-leach head-end experiments were used to evaluate a high-acid TBP extraction flowsheet that is capable of handling feeds containing 1% soluble organic compounds. The thorium-uranium strip product from the process has only low concentrations of organic material and fission products, and tests have demonstrated that it is a suitable feed for the standard Acid Thorex process. Preliminary results indicate that uranium and thorium can be leached directly from acidified HTGR fuel with TBP in *n*-dodecane. In other solvent extraction studies, we measured the solubility of (1) uranyl nitrate in di-sec-butyl phenylphosphonate–diethylbenzene and (2) thorium nitrate in TBP (diluted with benzene, diethylbenzene, or various straight- and branched-chain aliphatic compounds).

1.5 Development of Processes for Heavy-Water-Moderated Organic-Cooled Reactor Fuels

Development of head-end methods for heavy-water-moderated organic-cooled (HWOCR) fuels was continued. Studies were made of UC, (Th,U)C, and $(Th,U)O_2$ fuels clad in Zircaloy and in SAP (a dispersion of 5 to 15% Al_2O_3 in aluminum). Since the shear-leach process appears to be adequate for Zircaloy-clad fuels, the major development effort was devoted to SAP-clad fuels (particularly SAP-clad UC), for which the shear-leach process seems inadequate because of the high solubility of the aluminum (in the SAP) in HNO_3. The most promising processing method for this fuel appears to be dissolution of the cladding in 2 *M* NaOH–2 *M* $NaNO_3$, dissolution of the residual UC in nitric acid, and decontamination and recovery of the uranium and plutonium by solvent extraction or ion exchange. Alternatively, the aluminum in the SAP can be volatilized as $AlCl_3$ at 300 to 350°C with anhydrous HCl, and the residue can be processed further.

1.6 Development of Processes for Fast-Breeder-Reactor Fuels

Mechanical fuel disassembly and shear-leach studies were made on the basis of data recently obtained from a number of reactor and reactor fuel manufacturers relative to their proposed fast-reactor fuel assembly designs. The evaluations indicate that, mechanically, processing problems, while similar to those for LWR fuels, are more severe in degree. For instance, based on computer calculations, fission product heat dissipation for short-cooled (30 days), highly irradiated (burnup, 100,000 Mwd/ton) fuels will be quite difficult. Laboratory studies were made to find safe methods for disposal of the residual sodium coolant and bond that are associated with fast-breeder-reactor (FBR) fuels. External coolant can be reacted to form oxide and oxygen and/or water-vapor–inert-gas mixtures at room temperatures. Destruction of the sodium bonding material after fuel rod shearing is more difficult. The best method appears to be exposure to 3% H_2O–97% He at 300°C. Exposure at 300°C in air gave erratic reaction rates. The reaction with CO_2 to form Na_2CO_3 was too slow at temperatures below 600°C to be useful. Because the quantities of plutonium are quite large (10 to

20% plutonium in uranium), it is undesirable to use ferrous sulfamate or U(IV) as a reagent for reducing the Pu(IV) to Pu(III) for the solvent extraction partitioning of plutonium and uranium; therefore, an alternative method using hydrogen and a platinized-alumina catalyst was studied. When 4% H_2 in argon was used, quantitative reduction was obtained; in solutions containing only uranium, 1% reduction of U(VI) to U(IV) was observed.

In initial studies of amine extractants as potential alternatives to TBP, coefficients for the extraction of Pu(IV) from 1 *M* $UO_2(NO_3)_2$–3 *M* HNO_3 were obtained for a number of amines of different types and alkyl structures. A branched secondary amine, di(tridecyl)amine, which showed the desired degree of plutonium extraction power to allow complete recovery and still permit stripping of the plutonium with dilute acid, was selected for more intensive study.

In order to obtain a unit processing cost for FBR oxide fuel containing 10% plutonium, a conceptual plant study was made to determine what additions to the Nuclear Fuel Services (NFS) plant would be required to permit the processing of this type of fuel. A processing rate of 0.52 ton of U + Pu (50 kg of Pu) per day was found to be compatible with present NFS operating license restrictions; however, 1.4 tons/day is technically feasible. The latter capacity is commensurate with the discharge rate from sixteen 1000-Mw (electrical) reactors and would result in a processing charge of 0.09 mill/kwhr for a core-plus-blanket burnup of 38,500 Mwd/ton. In any case, a new, shielded plutonium ion exchange system, costing up to $5 million, would have to be added to the existing NFS plant. Computations made in this study indicated that the processing of FBR fuel decayed as short a time as 30 days would not be limited by the radiation degradation of the solvent.

2. FLUORIDE-VOLATILITY PROCESSING

The present investigation of fluoride-volatility processing at ORNL is part of an intersite effort to develop an alternative to the aqueous method for recovering valuable components that are present in spent UO_2 fuel from power reactors. Our main contribution will be the installation and operation of a "hot" pilot plant in Building 3019. The installation of head-end process equipment and the design of the distillation system for purifying UF_5 have begun.

We continued laboratory-scale and small-scale engineering studies in support of the fluidized-bed volatility process. Laboratory efforts were centered on (1) gaining a better understanding of the recently adopted BrF_5 flowsheet and (2) attempting to develop a sorption method for separating and purifying plutonium. Hot-cell studies of the process were initiated. The small-scale engineering studies are simulating head-end steps that are planned for the pilot plant; special emphasis is being placed on in-line instrumentation and sampling of solids from a fluidized-bed reactor.

2.1 Status of Fluidized-Bed Volatility Pilot Plant

The Fluidized-Bed Volatility Pilot Plant (FBVPP) is being designed for installation in Building 3019 to study the processing of Zircaloy-clad UO_2 power reactor fuels at high irradiation levels. Later, the processing of stainless-steel-clad UO_2 may also be studied.

Use of BrF_5 as the fluorinating agent for uranium was agreed upon during the year. Plans to install leaching equipment in the FBVPP were abandoned.

Nearly all the equipment required in the decladding, oxidation, and fluorination of "cold" uranium fuel has been fabricated. Structural steel and much of the shielding have been installed in cell 3 for head-end equipment, and installation of process equipment has begun. Purchasing and fabrication are progressing on mechanical handling equipment and instrumentation (including a computer-based data acquisition system). Electrical gear and ventilation components are being installed.

Design of the distillation system for separating and purifying UF_6 was begun, and cell 2 was prepared for installation of that equipment. A satisfactory method for purifying PuF_6 is not yet available.

LABORATORY-SCALE STUDIES

2.2 New Decladding and Oxidation Method for Zircaloy-Clad UO_2 Fuels Using Hydrogen, Oxygen, and HF-O_2 in Sequence

In laboratory studies an alternative decladding and oxidation scheme was developed for UO_2 fuels clad in Zircaloy. It consists in: (1) reacting the

zirconium with hydrogen ("hydriding") to fracture the cladding, (2) converting the UO_2 to U_3O_8 by reaction with oxygen, (3) pulverizing the cladding by exposing it to $HF-O_2$, and (4) fluorinating to volatilize the uranium and plutonium. Use of this method should eliminate difficulties now being experienced with filtering $ZrCl_4$ that is obtained from the HCl-Zr reaction. Also, compared with the $HF-O_2$ process, the ratio of fuel charged to bed volume is about four times greater. The hydriding reaction proceeds very rapidly, making this method advantageous for thick Zircaloy pieces. However, before the process could be seriously considered for large-scale application, process tests to study plutonium retention would be required.

2.3 Particle Size and Filtration of U_3O_8 During Oxidation

Members of an MIT practice school team studied the size distribution of U_3O_8 particles formed by the oxidation of UO_2 pellets. Of the two distinct classes of U_3O_8 particles formed, the larger particles were irregular in shape and had a number-average diameter of 4.2 μ; the other class consisted of spherical particles with a number-average diameter of about 0.6 μ. Filters made of sintered nickel fibers (10-μ rating) satisfactorily removed U_3O_8 from the exit gases from fluidized beds during the tests.

2.4 Effects of Five Process Variables on Retention of Uranium by Alumina After Treatment with Fluorine

The fluorination step was studied, in the absence of plutonium, in both a 0.94-in.-ID fluidized-bed reactor and in a $\frac{5}{8}$-in.-ID rotating-bed reactor. A statistically designed experiment was conducted to determine the effects of the following variables on the final uranium concentration in the alumina bed: temperature, fluorinating gas concentration, reaction time, and the initial concentration of uranium in the bed. The results of this experiment indicated that, over the ranges studied, these five variables had no effect on the amount of uranium retained by the alumina bed.

2.5 Relative Effectiveness of Fluorine, BrF_5, and BrF_3 in Minimizing Retention of Uranium by Alumina

In other experiments using the $\frac{5}{8}$-in.-ID rotating-bed reactor, some evidence was found that fluorine leaves less residual uranium than does BrF_5, particularly at temperatures above 300°C. Treatment of the alumina with BrF_3 between the BrF_5 and the fluorine steps may be required to reduce the carry-over of uranium during the fluorination of plutonium with fluorine. In several experiments with a 0.94-in.-ID fluidized-bed reactor, BrF_3 was used successfully as a cleanup agent for the disengaging section, filter, and lines. After fluorination at 600°C, with either fluorine or BrF_3, the final fluoride content of the alumina bed was twice that after fluorination at 500°C.

2.6 Fluorine Calorimetric Reactor for Determining Bromine and BrF_3 Contents of Primary Reactor Off-Gas

An experimental fluorine calorimetric reactor was built and tested. The concentration of bromine or BrF_3 in a gas stream can be determined by mixing fluorine with the stream in the reactor and measuring the rise in temperature. Such a device should be able to measure as little as 5% utilization of BrF_5 in the off-gas from the fluidized-bed reactor and thus provide an indirect measurement of the UF_6 concentration in the off-gas product stream. Consideration is being given to using this device as a means of maintaining the required excess fluorine in the $UF_6-BrF_5-N_2-F_2$ gas stream from the BrF_5 regenerator and to the 400°C NaF bed. In this instance, the gas of unknown fluorine content would be reacted with bromine to hold the fluorine concentration constant.

2.7 LiF and Fluorine as a Sorption-Desorption System for PuF_6

The investigation of LiF for use in a sorption-desorption method of purifying PuF_6 was extended during this report period.

Last year, 31 metal fluorides were tested for possible use as sorbents; LiF was the only one from which PuF_6 could be desorbed at reasonable rates. The chemical equilibrium between PuF_6, fluorine,

and the PuF_4-LiF complex was found, by the transpiration method, to be defined by the relationship: $\log K = 2047/T\ (°K) + 0.827$, where K is the $F_2 : PuF_6$ equilibrium constant in terms of mole ratio.

The sorption rate for PuF_6 by LiF was shown to be dependent on the sorption temperature and the surface area of the LiF. When LiF having a specific surface area of 1 to 3 m^2/g was used, the sorption reaction with PuF_6 was about 99% complete in 0.04 min at 275°C. High-surface-area LiF (20 to 37 m^2/g) was similarly effective at 175°C. Satisfactory separation of PuF_6 was demonstrated by the selective sorption of PuF_6 by low-surface-area LiF (1 to 3 m^2/g) at 275°C; however, separation was incomplete with the high-surface-area LiF (20 to 37 m^2/g) at 175°C owing to the partial cosorption of UF_6.

Desorption of PuF_6 from low-surface-area LiF was about 98% complete in 5 hr in the presence of fluorine at 500°C. Desorption from the high-surface-area LiF was only 93% complete after 35 hr at 475°C. The high-surface-area LiF degenerated, during desorption, to a specific surface area of about 1 m^2/g.

The limitations of an LiF sorption process were confirmed in process application tests in which an LiF bed was used to recover PuF_6 that had been volatilized from a 0.94-in.-ID fluidized-bed reactor. A reasonable degree of PuF_6 sorption (96.1%) was obtained only by using a high-surface-area LiF bed that was relatively large in proportion to the amount of plutonium involved. Fluorine flow rate and F_2: PuF_6 mole ratio, as well as sorption bed temperature and specific surface area, were shown to be important variables. Under process conditions the undesirable thermal decomposition of PuF_6 to PuF_4 within the sorption bed was found to occur during the sorption reaction.

Further work on the LiF system for PuF_6 sorption has been terminated in favor of the use of NaF as a sorbent for PuF_6.

2.8 Sorption-Desorption Systems for NpF_6

The separation and recovery of NpF_6 from both PuF_6 and UF_6 product streams may be required in volatility processing. The separation from PuF_6 may be satisfied by the current BrF_5 flowsheet, but the problem of separation from UF_6 remains. The sorption of NpF_6 by MgF_2 has been used previously to collect NpF_6 at low concentrations from UF_6 process streams; however, this sorbent requires a retention time of more than 0.8 min, and the NpF_6 is not recoverable from the sorbent by refluorination. The compounds LiF, CaF_2, and BaF_2 appear unsuitable as sorbents for NpF_6. However, NaF has been found to sorb NpF_6 effectively at temperatures from 200 to 450°C, producing a violet-colored complex. The NpF_6 may be desorbed either with nitrogen or fluorine. The dissociation pressure of the NpF_6 complex with NaF appears to be about one one-hundredth of that found for the comparable UF_6-NaF complex.

2.9 Corrosion in Volatility Processes

Because of the highly reactive reagents and the elevated temperatures required in volatility processing, corrosion of equipment and piping must be given careful consideration. In addition to corrosion studies at each of the participating sites, we have had a subcontract with Battelle Memorial Institute – Columbus Laboratories (BMI) to study corrosion problems, particularly those relating to the FBVPP. This subcontract was continued, and their results are presented.

A major portion of the BMI work during this period was a continuation of the study of intergranular corrosion of nickel 200 and 201, and of high-nickel alloys. The additional data from this study tended to support the earlier conclusion that the contaminant sulfur is a factor in such corrosion. During the last part of this period, several failures by corrosion of nickel pipe at the engineering-scale test reactor led to a renewed and intensive study of the problem; this study is nearing completion, and, again, results are indicating that sulfur is the principal contributor to corrosion.

The second major area of BMI work concerned the determination of corrosion characteristics of nickel and nickel alloys upon exposure to bromine and to bromine and oxygen at 300°C, the normal maximum temperature expected in the processing steps where bromine is present. Corrosion of nickel and most nickel alloys was not of significant proportions at 300°C; in other tests at 500°C, corrosion rates were about tenfold higher. Monel was more rapidly attacked, apparently because of the copper content, and copper itself dissolved quickly. Monel, when exposed in the same system with nickel, accelerated the nickel corrosion by a factor of more than 5 – apparently from deposition

of $CuBr_2$ (formed by reactions with the copper in the Monel). A laboratory-scale system is being installed at BMI to study corrosion under fluidized-bed conditions.

2.10 Leaching of Uranium and Plutonium from Primary Reactor Waste Solids, and Related Corrosion Studies

Leaching of waste solids from the primary reactor, and possibly other sources, is being considered mainly as a means of supplementing accountability and analytical data. Laboratory studies have demonstrated that uranium and plutonium recoveries are 85% or greater when the initial uranium or plutonium concentration in the waste solids is 0.03% or higher; recoveries decrease rapidly for concentrations below the 0.03% level. Reproducibility of data in the lower ranges is poor. However, the proposed leaching of entire beds of reactor waste solids would be useful for detecting "pockets" or agglomerates of plutonium or uranium that might escape detection by other analytical means. The most effective leachant is 13 *M* HNO_3 up to 0.1 *M* in HF; $Al(NO_3)_3$ at about the same concentration as the HF is effective in reducing fluoride corrosion and may be added if required. Small-scale engineering work has demonstrated operating feasibility. Corrosion studies have been concluded; they indicated HAPO-20 alloy (50% Ni–25% Cr–16% Fe–6% Mo–1% Cu) to be the best choice for equipment construction. In view of a decision not to install the leaching system in the FBVPP, engineering design progressed only through preliminary versions of a flowsheet, of vessel designs, and of equipment layout.

SMALL-SCALE ENGINEERING STUDIES

2.11 Process Flowsheet Tests

Tests of process flowsheets have been continued in the small-scale engineering test facility to obtain experience with remotely operated fluidized-bed equipment. These tests, using unirradiated UO_2 fuel clad in stainless steel or Zircaloy-2, were performed in a 2-in.-ID fluidized-bed reactor. Instruments and controls duplicated as closely as possible those proposed for installation in the FBVPP. No process steps involving plutonium were tested.

Evaluation of the HF-oxygen flowsheet for decladding UO_2 fuel was completed. Stainless steel cladding was completely destroyed and the UO_2 was oxidized to U_3O_8 by using 40% HF–60% oxygen to initiate the reaction and 20% HF–80% oxygen to complete it. Although massive pieces of stainless steel, such as end plugs, were only partially reacted, operation of the fluidized bed appeared to be unaffected, and subsequent treatment of the bed with fluorine resulted in uranium losses consistently less than 0.2%. Zircaloy-2 cladding can also be destroyed and the UO_2 oxidized by use of similarly programmed HF-oxygen reagent flows. The massive shards of ZrO_2 produced are not detrimental to bed fluidization; however, their conversion to ZrF_4 in the subsequent fluorination step would be slow.

During preliminary experiments in decladding Zircaloy-2-clad UO_2 fuel elements with HCl, unsteady flow conditions existed in the pyrohydrolyzer as a consequence of a high gas velocity, which resulted from the increased volume of gas produced during the pyrohydrolysis of $ZrCl_4$ to ZrO_2. Operating difficulties with the pyrohydrolyzer can be minimized by keeping the superficial velocity of the HCl reagent in the primary reactor at or below 1 fps. Decladding times of 2 hr or less were obtained when using 60% HCl–40% oxygen, a 450°C reactor temperature, and a $UO_2 : Al_2O_3$ ratio of 1 : 1.6. Uranium losses to the pyrohydrolyzer were about 0.2%, and 1 to 2% of the zirconium remained in the primary reactor bed. The UO_2 pellets from the HCl decladding test were oxidized to U_3O_8 by air without sintering. The chloride content in the bed after oxidation was about 0.1%.

2.12 Sampling of Solids from a Fluidized-Bed Reactor

A system is being developed for sampling bed material in fluidized-bed reactors. It uses a gas-powered jet to transfer particles from the fluidized bed through an external loop and back into the reactor. After numerous tests a jet was designed; these jets will be integral parts of the sample takeoff nozzles installed on the primary reactor in the FBVPP. A prototype unit was built and will be tested to determine the correlation between the amount of uranium in the sample and the total amount in the bed.

2.13 Continuous In-Line Monitoring of Process Gas Streams

Proper control of the various steps in the fluoride volatility process depends on developing in-line monitoring devices that measure, preferably continuously, some component in the off-gas stream whose concentration varies directly with the reaction rate. The HCl–Zircaloy-2 reaction can be followed by measuring the hydrogen concentration in the pyrohydrolyzer off-gas stream with a thermal conductivity cell. In the oxidation step, the oxygen concentration can be measured by taking advantage of its high magnetic susceptibility. At present, a gas chromatograph that measures either the bromine-BrF_3 or the UF_6 concentration appears to be a promising method for monitoring the BrF_5 fluorination step; however, further development effort is needed. Fluorine concentrations in the off-gas from the plutonium fluorination step can be monitored with an ultraviolet spectrophotometer.

2.14 Estimation of Critical Constants for NbF_5

As an extension of earlier experiments to determine vapor-liquid equilibria of the UF_6-NbF_5 system, the pressure-density-temperature relationships of the liquid and vapor phases of NbF_5 were determined.

3. MOLTEN-SALT REACTOR PROCESSING

3.1 Continuous Fluorination of Molten Fluoride Mixtures in 1-in.-diam Columns

Processing of the fuel stream of a molten-salt breeder reactor (MSBR) requires complete removal of uranium from the salt by continuous fluorination. A high uranium recovery can be obtained by using a tower in which molten salt and fluorine are contacted countercurrently, with the molten salt as the continuous phase. Experimental data indicate that the fluorination rate is satisfactory and that the required axial concentration gradient will not be destroyed by the inherent axial mixing resulting from rising bubbles of fluorine. The effects of salt throughput, operating temperature, and initial UF_4 concentration on uranium removal during steady-state operation were studied in fluorinators having a salt depth of 48 in. Removal of the uranium fed to the fluorinator ranged from 97.4 to 99.9%, with removal in most of the runs being greater than 99%.

3.2 Corrosion Control by Use of a Frozen Wall

Corrosion of a continuous fluorinator can be controlled by maintaining a layer of frozen salt on the fluorinator wall. We are making preparations for the demonstration of frozen-wall protection. In these forthcoming experiments, the molten salt will contact an inert gas countercurrently in equipment of a design suitable for continuous fluorination.

3.3 Relative Volatilities of Rare-Earth Fluorides in MSBR Salts

The method currently proposed for processing the fuel stream of an MSBR includes a distillation step in which the major components of the stream, LiF and BeF_2, are vaporized and separated from less-volatile fission products, primarily rare-earth fluorides (REF). Relative volatilities of a number of REF's with respect to LiF have been measured in a recirculating equilibrium still, using the binary system LiF-REF and the ternary system LiF-BeF_2-REF. The still was operated at 1000°C in all instances; the operating pressures were 0.5 and 1.5 mm Hg with the binary and the ternary systems respectively. Relative volatilities of the trifluorides of La, Pr, Nd, Ce, and Sm ranged from 2×10^{-4} to 2×10^{-3}, with Ce and Pr showing the highest values. These values indicate that the required REF removal efficiencies can be obtained in stills of simple design without rectification.

3.4 Vaporization Rates in Fluoride Salt Distillation

Data on the variation of vaporization rate with total pressure are necessary to predict vaporization rates in equipment that is suitable for MSBR fuel processing and to assess errors in relative volatilities that are measured in recirculating equilibrium stills. The rate of vaporization of a mixture of LiF and PrF_3 was measured at several condenser pressures in the range 0.1 to 1.0 mm Hg in an inverted-U-shaped distillation unit constructed from 1-in. nickel tubing. The vapor pressure of the

salt mixture was 0.50 mm Hg at the vaporization temperature of 1000°C.

Salt vaporization rates at condenser pressures of 1.0 and 0.1 mm Hg were 7.8×10^{-6} and 2.4×10^{-4} g sec^{-1} cm^{-2} respectively. The vaporization rate for a condenser pressure of 1.0 mm Hg is comparable with the calculated rate of diffusion of salt vapor through stationary argon, which was present between the vaporization and condensation surfaces. Viscous drag in the passage between the vaporization and condensation surfaces limits the vaporization rate when condenser pressures are lower than the vapor pressure of the salt at the vaporization surface.

3.5 Prevention of the Buildup of Low-Volatility Materials at a Vaporization Surface

During the vaporization of a multicomponent mixture, materials that are less volatile than the bulk of the mixture tend to remain in the liquid phase and are removed from the surface of the liquid by convection and molecular diffusion. Low-pressure vaporization does not generate deeply submerged bubbles and therefore provides little convective mixing in the liquid. The concentration of materials of low volatility at the vaporization surface may be appreciably higher than the average liquid concentration if these materials are removed by diffusion alone. The increased surface concentration will result in the vaporization of a greater quantity of low-volatility material than would occur in a comparable system having a uniform liquid-phase concentration and will decrease the separation efficiency of the still.

The effect of the surface buildup of materials having low volatilities has been considered for both transient and steady-state operation of several still types. Liquid-phase mixing by liquid circulation is a necessary characteristic of molten-salt stills.

3.6 Demonstration of Fuel-Salt Distillation at the MSRE

Equipment has been designed and fabricated for a large-scale demonstration of the distillation of molten-salt reactor fuel. The system consists of a 48-liter feed tank, a 12-liter still pot, a condenser, a 48-liter condensate receiver, and associated auxiliaries required for removing condensate samples during operation and for maintaining desired operating conditions.

The system will be operated for 500 to 700 hr using nonradioactive salt having the MSRE fuel carrier composition (65-30-5 mole % LiF-BeF_2-ZrF_4) and containing small quantities of rare-earth fluorides. The system will be used in early 1968 to distill approximately 48 liters of radioactive MSRE fuel salt from which the uranium has been removed by fluorination.

3.7 Alternative Processing Methods

The stability of lanthanum beryllide ($LaBe_{13}$) in contact with liquid bismuth was studied in connection with possible reductive precipitation and reductive extraction methods for processing MSBR fuel. Over the temperature range investigated, 318 to 832°C, the beryllide was decomposed by the bismuth, the extent of decomposition being governed mainly by the solubility of lanthanum in bismuth. Formation of insoluble beryllides can, therefore, probably be avoided in the reductive extraction method if enough bismuth is present to satisfy the solubilities of the rare-earth metals.

3.8 Preparation of ^{233}U Fuel for the MSRE

Approximately 71 kg of $^{233}UF_4 \cdot {}^{7}LiF$ eutectic salt will be prepared for refueling the MSRE in early 1968. The starting material will consist of $^{233}UO_3$ containing 240 ppm of ^{232}U, which is presently available at the Laboratory. The chemical flowsheet involves simultaneous reduction and hydrofluorination in the presence of lithium fluoride. Equipment has been designed and is being installed in the TUFCDF.

4. WASTE TREATMENT AND DISPOSAL

4.1 High-Level Radioactive Waste

Development work on the disposal of aqueous high-level waste by the Pot Calcination process is now complete except for the pilot-plant demonstration of this process at the Pacific Northwest Laboratories. Currently, the major objectives in high-level waste development are to develop and to demonstrate, on a pilot-plant scale, processes for putting the waste powders from the Fluidized-

Bed Volatility Process (FBVP) into a form suitable for permanent disposal. Processes are being developed concurrently at Oak Ridge National Laboratory (ORNL) and Brookhaven National Laboratory (BNL); ORNL's primary responsibility is to determine the problems associated with the storage of the waste as a powder and BNL's to develop an economical process for dispersing the waste in a glass matrix.

Studies at ORNL on the thermal stability of untreated wastes have shown that fluorides such as those of aluminum and cesium have substantial vapor pressures at temperatures of about 500°C. Further, these studies have shown that the presence of trace quantities of water on the untreated wastes causes release of corrosive hydrogen fluoride during the heating cycle. Thermochemical calculations indicate that alkaline-earth oxides should stabilize these systems by reacting with the volatile fluorides to yield a more-stable fluoride and a stable oxide. Laboratory experiments with calcium oxide as a "fluoride getter" confirm these calculations. The 1 to 3% weight loss observed when the untreated powder is held at 550°C for 74 hr can be reduced to essentially zero if calcium oxide is added to the waste powder in a 1:9 weight ratio prior to heating. Thermal conductivity measurements made on the alumina powders used as fluidizing media in the FBVP gave values ranging from 0.26 Btu hr^{-1} ft^{-1} $°F^{-1}$ at 327°F to 0.42 Btu hr^{-1} ft^{-1} $°F^{-1}$ at 1680°F. Leaching tests with water showed that in one week essentially all the ^{137}Cs tracer, about 30% of the fluoride, and 3% of the aluminum are removed from these powders. Lead borosilicate and lead silicate glasses have been tested at ORNL in an attempt to find a commercial glass frit for use as a glass matrix in the dispersion process. Dense, void-free products have been obtained using Pemco 716 (nominally 67.6% PbO, 26.8% SiO_2, and 5.6% CaO) in a glass:powder waste weight ratio of about 1.7:1. The measured thermal conductivity of this dispersion is about 1.22 Btu hr^{-1} ft^{-1} $°F^{-1}$ at 140°F, which is about five times that of the waste powder alone. Leaching studies on waste dispersed in glass have shown that 0.002% of the cesium and 0.07% of the fluoride and aluminum are leached from the dispersion in 21 days.

The pilot-plant demonstration of the ORNL and BNL waste disposal processes, which will be carried out simultaneously with the fluidized-bed volatility process demonstration, will be located in cell I of Building 3019. The necessary equipment is being designed to be compatible with both processes. Process operations will be performed remotely with a crane and manipulators.

4.2 Intermediate-Level Radioactive Waste

A process for incorporating all types of intermediate-level wastes in asphalt is being developed. The waste types studied include alkaline evaporator residues, an aluminum cladding solution, and a second-cycle solvent extraction raffinate with added caustic. In this process, the wastes are mixed with emulsified asphalt (~35% H_2O), the water is volatilized, and the product is heated to 160°C. The leach rates of cesium from the asphalt products were reduced by factors of 2 to 10 by adding 2 wt % Grundite clay and 2 wt % water glass to the original wastes. These additives also increased the ignition temperatures of the products by at least 65°C. The effect of radiation on the products is being studied using samples that contain 60 wt % salts and 2 to 52 curies of mixed radionuclides per gallon of asphalt product. After seven months and an absorbed dose of 4×10^7 rads, no swelling, gas evolution, or increase in leach rates of salts have been observed. A nonradioactive pilot plant was constructed to determine the feasibility of using a wiped-film evaporator for the incorporation of intermediate-level wastes in asphalt. The equipment operated for 62 hr at rates up to 11 gal of waste solution per hour yielding product containing up to 64 wt % waste salts. No serious operating difficulties were encountered, and wiper-blade wear was negligible. The water distillate was decontaminated from sodium by a factor greater than 4000 as compared with the original waste solution. The estimated capital cost of an asphalt plant for annually treating 400,000 gal of ILW containing 5 curies/gal was $330,500; the estimated unit operating cost, including amortization and burial at ORNL, was 37¢ per gallon.

4.3 Low-Level Radioactive Waste

A process is being developed to decontaminate low-level radioactive waste to the degree required to permit recycle and reuse of the wastes. This would be an improvement on the current practice of partial decontamination and the dependence on discharge to streams and dilution to meet the

maximum permissible concentration limits for radionuclides. Micro-pilot-plant experiments included flocculation and clarification by alum, demineralization by ion exchange, and final cleanup by activated carbon. Overall decontamination factors of 1000 to 10,000 were obtained for all major radioactive species for up to 2400 volumes of low-salt-content recycle waste water treated per bed volume of cation resin. Wastes with the same concentration of dissolved solids but containing different amounts of suspended solids require the same amount of the coagulant alum. Wastes containing tripolyphosphate and alkylbenzenesulfonate (synthetic detergents) may require treatment with an organic polyelectrolyte in addition to alum. With polyphosphate in solution, a calcium : phosphate ratio of 1 or higher is needed for floc formation to minimize the amount of alum required.

4.4 Engineering, Economic, and Safety Evaluation

The management of wastes produced at nuclear power plants will become increasingly significant in an economy that is expected to grow to 50 times its present size within the next 13 years. As a preliminary step in assessing future implications, the operating experience in waste management at Dresden-I, Big Rock Point, Humboldt Bay, Elk River, Yankee, and Indian Point-I has been reviewed. In this study, to be published as ORNL-4070, the sources and characteristics of the wastes are reviewed, the waste management systems and techniques in use at the power stations are described, and the operating experience is analyzed from the standpoint of the radioactivity released to the environment.

4.5 Separation of Noble Gases from Air Using Permselective Membranes

A thin (~1 mil) dimethyl silicone rubber membrane was used to separate noble gases from air. The permeability factors of krypton, oxygen, and nitrogen at 150 psig were 45, 16, and 10 respectively. Preliminary estimates indicate that the cost for removing noble gases from a reactor containment shell following a reactor accident by using a cascade of permselective membranes compares favorably with other processes that have been proposed.

4.6 Computer Code for Calculating Nuclear Properties of Accumulated Wastes

Three computer programs have been written to calculate the buildup and decay of gross fission product activity and heat in waste tanks and systems. Steady or variable waste addition rates may be considered.

5. TRANSURANIUM-ELEMENT PROCESSING

The Transuranium Processing Plant (TRU) and the High Flux Isotope Reactor (HFIR) were built at ORNL to produce large quantities of the heavy actinide elements as part of the USAEC Heavy Element Production Program. These materials will be used in basic research in laboratories throughout the country. During the past year TRU began "hot" operations, $^{242}PuO_2$ target irradiation was started in the HFIR, and isotopic enrichment of ^{244}Pu was carried out in the Isotopes Division. More than 40 shipments of transuranium elements were made to fulfill requests from national laboratories, universities, and industry in this country and in three foreign countries. The phases of the program that are under the direction of the Chemical Technology Division are reported here; these include operation of TRU, final isolation and purification of the transuranium elements, and development of chemical separation processes and equipment.

Design and development work on the target elements, which are to be remotely fabricated in TRU, is under the direction of the Metals and Ceramics Division and is reported elsewhere. However, the premature failure of targets during irradiation in the HFIR and the possible effect on the Transuranium Element Production Program are discussed.

5.1 TRU Operations

The purpose of the Transuranium Processing Plant is to recover transuranium elements from irradiated targets for distribution to research workers and to refabricate targets from some of the intermediate isotopes, especially americium and curium, to produce heavier elements. Complete processing is expected to include:

1. dissolution of irradiated targets;
2. recovery of unburned plutonium;

3. separation of the transplutonium elements from fission products (Tramex);
4. separation of transcurium elements from americium and curium;
5. separation of berkelium from californium, einsteinium, and fermium;
6. isolation of californium, einsteinium, and fermium;
7. preparation of oxides of some of the actinides;
8. remote fabrication of targets for reirradiation of some of the actinides in the HFIR.

The first three processing steps were performed successfully this year in TRU, at full levels of solution power density and alpha and beta-gamma radioactivity. Operation in TRU of equipment for the main-line process steps that are to follow Tramex has been held up by flowsheet problems in the next step, separation of transcurium elements from the americium and curium. In the meantime, subsequent actinide separations have been done using laboratory-type equipment and alternative flowsheets.

Eighteen targets, which had been irradiated at the Savannah River Plant for a year, were inspected and repaired in TRU and then transferred to HFIR for continued irradiation. Four HFIR prototype targets and six SRP reactor slugs were processed. When laboratory-scale isolation and purification of the resulting solutions (now in the final stages) are completed, we will have produced 50 g of ^{242}Pu, 10 mg of ^{244}Pu, 25 g of ^{243}Am, 80 g of ^{244}Cm, 200 μg of ^{249}Bk, and 2 mg of ^{252}Cf.

Target dissolution is done by first dissolving the aluminum (jacket and matrix) in 6 *M* NaOH – 3 *M* $NaNO_3$ and decanting the aluminum-bearing solution through a filter and centrifuge, leaving the undissolved particles of actinide oxides. Less than 0.2% of the actinides has been lost during aluminum removal, and no difficulty has been encountered in filtering the solutions. The actinides are then dissolved in either 6 *M* HCl or 15.8 *M* HNO_3 (with or without fluoride catalyst). If fluoride is used, a fluoride-removal step is required to prevent excessive corrosion of Zircaloy-2 and tantalum equipment.

Plutonium is removed initially. The well-known nitrate-based anion exchange process and a new batch solvent extraction process were used successfully. A chloride-based anion exchange process, which worked well in glass equipment, was unsatisfactory for use with metal equipment in TRU. The plutonium was apparently reduced to Pu(III), which will not load on the resin; oxidants that are strong enough to keep the plutonium oxidized caused excessive corrosion of equipment.

After only cursory tests, we obtained satisfactory results with a batch solvent extraction process that uses di-*tert*-butylhydroquinone to reduce the extracted plutonium in the organic phase and to cause it to be stripped into concentrated HCl. The plutonium product was decontaminated from gross gamma activity by a factor of 150, which is approximately equal to that achieved with nitrate-based anion exchange. Separation between plutonium and transplutonium actinides was very sharp, and losses were low. Zirconium, which is introduced into process solutions by corrosion and which causes equipment operating problems during subsequent processing steps, was completely removed from the actinides and discarded with the waste solvent. This feature (zirconium removal) is a key advantage of the extraction flowsheet.

The Tramex solvent extraction process, for continuous separation of fission products from the transplutonium actinides, is operational in TRU. Equipment operability still needs to be improved, and the flowsheet parameters need to be optimized. Nevertheless, process operation is routine, and product recovery is good. The transplutonium elements are decontaminated from gross gamma activity by a factor of 75, which is adequate since remote fabrication techniques will be used to make recycle targets.

TRU was shut down for an extensive program of equipment repair and modification in February 1967, after about seven months of operation. No single problem was serious enough to have forced a shutdown, but the combined effects had made plant operation inefficient. Eventually, remote maintenance techniques will be required in the tank pits, but thus far direct maintenance has been possible. A total of 28 entries by personnel were made into the tank pits; the radiation dose received per entry (about 20 min average duration) ranged up to 150 millirems; no weekly doses exceeded 300 millirems. Although surface contamination in the pits was in excess of 10^5 alpha disintegrations per second per 100 cm^2 and a number of internally contaminated lines were disconnected in the pits, the level of airborne contamination in the "limited access" area, into which the pits were opened, never exceeded normal tolerance.

Two computer programs, which are operational, were written to allow the prediction of compositions of targets irradiated in the HFIR. Such predictions are required in order to determine target compositions that can be safely irradiated in the reactor, to plan irradiation and processing schedules, and to forecast the availability of various isotopes of the transuranium elements. One of the computer programs, which is used to calculate production rates of various isotopes during neutron irradiation, is an extension of earlier programs that are based on the CRUNCH code. This expanded version computes explicit contributions from epithermal neutrons and makes an approximation of resonance self-shielding effects. The second program is used to interpolate and weigh the results from the first program, by the method of least squares, to determine the set of cross sections that most nearly results in the observed target compositions. The prediction of HFIR effective cross sections for ^{242}Pu and ^{243}Am, which was based on the analysis of SRP irradiations, was found to be within 10% of the values determined by the analysis of irradiations in the HFIR. This indicates that no gross deficiencies exist in the mathematical models. As larger quantities of transuranium elements are produced, these programs will be used repeatedly to reevaluate cross-section data and to more accurately predict the availability of various isotopes.

5.2 Transplutonium Element Isolation from Tramex Products

Generally accepted processes for isolating actinides from small-scale targets of highly irradiated plutonium, americium, and curium were satisfactorily scaled up for processing Tramex product from TRU operations. The successful processing of Tramex product has demonstrated the feasibility of using these laboratory-type isolation methods to separate significantly larger amounts of transplutonium elements than was previously considered possible.

Four major processing steps were required for isolation of the actinides. Following adjustment of the feed an LiCl–anion exchange process was used to provide additional decontamination from fission products and ionic contaminants and to separate the actinides into three fractions that could be subsequently processed for final actinide isolation. Most of the americium and curium was eluted using 9 *M* LiCl; continued elution with 8 *M* LiCl provided a second fraction, which contained the remainder of the curium and about 60% of the berkelium; final elution with 8 *M* HCl gave a third fraction, which contained the remainder of the berkelium, all of the californium, and about 0.5% of the original americium-curium. Highly pure californium was recovered by chromatographic elution from cation exchange resin with ammonium α-hydroxyisobutyrate. The americium-curium-berkelium fractions from both columns were combined, and berkelium was recovered by extraction of Bk(IV) with di(2-ethylhexyl)phosphoric acid from 8 *M* HNO_3. When the separation of americium and curium was required, americium was precipitated from potassium carbonate solution as a double potassium americium(V) carbonate.

5.3 Development of Chemical Processes

Laboratory support was provided to investigate chemical problems that arose during initial high-activity-level processing in TRU. Process development was continued in the areas of plutonium recovery by an HCl–anion exchange process, actinide partitioning by solvent extraction, Cf-Es-Fm separations, and americium-curium oxide preparation.

We studied methods for removing fluorides from dissolver solutions when HNO_3-HF was used to ensure complete dissolution of oxide target materials of low burnup. (Fluoride is not compatible with main-line TRU process equipment.) Hydroxide precipitation was determined to be the simplest method readily available, and process parameters for this procedure were evaluated. It was found that unless the hydroxide precipitate is washed very thoroughly, two or more precipitation-filtration cycles are required for complete fluoride removal; when appreciable amounts of aluminum are present, complete fluoride removal in a single cycle is impossible.

Since highly burned plutonium targets can be dissolved in HCl media and since it is convenient to have the transplutonium elements in HCl solution following plutonium removal, development of a process to recover plutonium by an HCl–anion exchange system was continued. Laboratory studies were made to determine the effects of several variables on plutonium loading for three different resins. Distribution coefficients for Pu(IV) were determined as a function of HCl and LiCl concentration; also, the effect of the addition of ethanol on plutonium sorption was investigated.

In recent studies of the Pharex process, in which the heavy actinides are separated from americium and curium by preferential extraction into 2-ethylhexyl phenylphosphonic acid (HEH[ϕP]) from dilute hydrochloric acid, we found that the presence of small amounts of zirconium significantly reduces available curium-berkelium separation factors; for example, 100 ppm of zirconium in the feed causes a fourfold reduction. This reduction is explained by the fact that berkelium and californium distribution coefficients are not affected by zirconium, while the americium-curium distribution coefficients increase with increasing zirconium concentration. Since feed solutions for this separation step will probably contain enough zirconium to preclude Pharex, other separation methods were sought. It was found that, by using di(2-ethylhexyl)phosphoric acid (HDEHP) as the extractant, the deleterious effect of zirconium can be avoided and a berkelium-curium separation factor of 12 to 14 can be obtained. Laboratory studies of this process (named Hepex) are presently under way; details are reported in Sect. 8.9.

Chromatographic elution from cation exchange resin with α-hydroxyisobutyrate solutions will be used for the separation of Cf-Es-Fm and the purification of some final products. Column scale-up studies to high activity levels, using ^{242}Cm as a stand-in, confirmed that this method can probably be used to process 100-mg quantities of ^{252}Cf in conventional equipment; however, very careful control of conditions, and rapid processing, are required to limit radiolytic gas formation and radiation damage to the resin.

We are developing a new ion exchange technique that improves control and decreases processing time. Feed is pumped rapidly at high pressure through a long bed of very fine particles of ion exchange resin. The use of fine-mesh resin increases the kinetics of ion exchange, and the high pressure permits greater freedom in the selection of operating parameters. Tests with neodymium and praseodymium indicated that this technique is promising for the separation of actinides. Systems have been installed in glove boxes, and testing with actinide tracers is in progress.

Particles of dense americium-curium oxide in the range of 20 to 100 μ diameter are required for incorporation into HFIR targets. The sol-gel method has several advantages over alternative processes for preparing such particles. Two techniques that are potentially applicable to in-cell preparation of 10-g batches of sol were investigated: (1) filtration and washing in a jacketed filter funnel that can be heated to convert the hydroxide paste to a sol, and (2) filtration and washing in a sintered-metal bowl centrifuge, which can also be heated. After conversion, the sol can be separated from unconverted hydroxide paste by applying pressure across the porous material, either by centrifuging or by applying vacuum; the fluid sol passes through to a collection vessel, and the unconverted paste remains. Both techniques appeared promising during initial evaluations in which europium hydroxide sols were prepared. The filter was used to prepare 5-g batches of americium-241 hydroxide sol; the behavior of americium closely paralleled that of europium.

5.4 Development of Process Equipment

We continued the development of equipment for use with solvent extraction processes for the separation of americium and curium from other transplutonium elements. Last year it was found that severe plate wetting by the solvent precluded operation of the Pharex process in TRU solvent extraction equipment with the aqueous phase continuous, as designed. Two alternative solutions were investigated: operation with the organic phase continuous, or the use of ceramic sieve plates, which are preferentially wetted by the aqueous phase. Both solutions are workable. However, Pharex was found to be unsatisfactory for use in TRU because the presence of zirconium in the feed, which is introduced by corrosion of TRU equipment, reduced separation factors to intolerably low values. We are developing a new process, Hepex, which employs a chemical system that is insensitive to zirconium; however, Hepex exhibits hydraulic behavior that is similar to Pharex. It must be operated with the organic phase continuous, or ceramic sieve plates must be used. At present our development work indicates that operation with the organic phase continuous is the preferred method. Only limited data on stage heights have been obtained as yet.

5.5 HFIR Target Rod Failures

In February 1967, it was observed that several TRU target rods had ruptured during irradiation in the HFIR. This was six to eight months before the processing of these targets had been scheduled. When the failures were detected, the target island

in the HFIR flux trap contained 14 targets that had been irradiated only in the HFIR and 17 targets that had been previously irradiated about one year at the Savannah River Plant. Both groups of targets had received the same amount of irradiation in the HFIR. Examination of the SRP-irradiated targets showed cracked cladding on five. The 14 targets that had been irradiated only in the HFIR apparently remained intact. It was concluded that the failures occurred because the ductility of the cladding was reduced by the effects of irradiation, to the extent that the cladding was unable to deform to accommodate the normal swelling of the target pellets and the fission-gas pressures generated within the pellets. The Metals and Ceramics Division has begun an extensive program to determine the mechanisms that caused the failures and to develop an improved design for the targets; this work will be reported elsewhere.

The transuranium-element production program should not be seriously affected as a result of these premature target failures. On the other hand, the failures will have a rather important effect on production in the coming year, since processing the failed targets and recycling the americium and curium to the HFIR will require six months. Since contamination problems in HFIR have not been severe, the remaining SRP targets will be irradiated either until they fail or until they have been irradiated as originally planned; the actual reduction in product availability will depend on how long these targets are irradiated.

6. DEVELOPMENT OF THE THORIUM FUEL CYCLE

During the past year notable advances were made in the Thorium Utilization Program. A solvent extraction process for preparing mixed ThO_2-UO_3 sols was developed in the laboratory and was demonstrated in engineering equipment on the scale that will be required in the Thorium-Uranium Recycle Facility (TURF). Conditions were determined for producing thorium dicarbide microspheres at greater than 90% of theoretical density, with acceptably low oxygen and free carbon. A sphere-forming pilot plant was built and operated on the scale that will be required in the TURF. The TURF building, procurement of major equipment, and the design of processing equipment are nearly complete.

6.1 Sol Preparation by Solvent Extraction

A simple solvent extraction process has been developed for preparing mixed ThO_2-UO_3 sols directly from an aqueous solution of thorium and uranyl nitrates. The solution is denitrated by use of a multistage solvent extraction process; the nitrate extractant is a long-chain amine, dissolved in an *n*-paraffin diluent. Digestion of the partially denitrated aqueous phase, after the first stage of extraction, forms the sol and releases more nitrate, which is extracted in the additional stages to produce the desired nitrate content. The sol may be evaporated to a concentrate that is suitable for use in forming microspheres, or it may be dried to form gel fragments. Laboratory studies have defined the important chemical variables for the preparation of sols containing up to 68 mole % uranium. Engineering studies have demonstrated the feasibility of the continuous production of sols at the rate of 1 kg of oxide per hour. Representative batches of sol have been concentrated to 1.5 *M* by continuous evaporation. Good-quality ThO_2-UO_2 microspheres have been formed by firing gel microspheres that were prepared from these sols.

6.2 Sol-Gel Process: Further Development and New Applications

Continued studies of the preparation of thorium dicarbide particles showed that the major problem is gross porosity. The method of firing ThO_2-C gel to ThC_2 involves a critical balance between grain growth, sintering, and chemical conversion. An argon atmosphere and the presence of CO aid in controlling the conversion at a temperature where grain growth is optimized and high-density (>90% of theoretical) microspheres are obtained. Typical microspheres had the composition $ThC_{1.8-1.9}$, and contained 0.1 to 0.2% free carbon and 0.03 to 0.1% oxygen. They were characterized by an open porosity of 1% and a closed porosity of 6 to 8%. They resisted crushing loads of 700 to 900 g. Electron micrographs and electrophoretic and viscosity measurements of the ThO_2-C sols showed strong association between the particles. Thoria (and urania) dispersed and stabilized carbon blacks, the quantity of carbon depending on the specific surface of the thoria.

We have been studying methods for preparing UO_2-ThO_2 sols accurately at any desired ratio of thorium to uranium, with emphasis on a ratio of ≈ 3. Uranium dioxide–thorium dioxide can be prepared by coprecipitating and peptizing the hydroxides or by mixing the separately prepared sols. Control of the thorium:uranium ratio proved to be precise, and

the products were of excellent chemical and physical quality. A coprecipitation-peptization method was developed for preparing UO_3-ThO_2 sols and was demonstrated through calcination to dense UO_2-ThO_2 microspheres having a thorium: uranium ratio of 3.

We studied the chemistry of gel microsphere formation in the 2-ethyl-1-hexanol column, emphasizing control of surfactant concentrations and possible effects of long-term operation. Conductivity measurements proved useful for monitoring the concentration of Ethomeen S/15. Little, if any, surfactant was sorbed on ThO_2 sol or gel. Some oxidation of 2-ethyl-1-hexanol by air and/or nitrate during distillation was indicated.

6.3 Development of Methods for Producing Microspheres

A pilot plant for preparing microspheres was built and operated as a part of the ORNL Coated Particle Development Laboratory. This pilot plant operates at the rate of 25 cc of thoria sol feed per minute, or about 1 kg of product per hour. This system has demonstrated long-term, stable operation with respect to the water extractant (2-ethyl-1-hexanol, 2EH) and surfactants. Several problems of remote operation were solved; however, we still need simple remote techniques for monitoring the operation of the gel-forming column and the quality of the gel spheres.

We have continued the study of sol-dispersing equipment in an effort to attain higher throughputs and a closer control of drop sizes. Results are reported for single and multiple two-fluid nozzles, mechanically vibrated nozzles, and free-fall orifices (for large sol droplets only). The two-fluid nozzles have been the most useful; at optimum operating conditions, the mechanically vibrated nozzles produced the most uniform droplets. The choice of equipment that is most suitable for gelation by extraction of water with 2EH depends on the desired droplet size; a fluidized bed in a tapered column is best for larger sizes (e.g., to produce thoria microspheres 150 μ, or larger, in diameter); direct agitation produces (nonuniform) spheres 80 μ, or less, in diameter; a long "fall-through" column is promising for intermediate- and small-sized spheres.

The key step – extraction of water by 2EH – is being studied by observing the resultant shrinkage of single suspended sol droplets. The mass transfer characteristics during gelation appear to be different from any that have been reported in the literature.

Empirical observations of the drying and firing of thoria gel microspheres indicate that, in general, the conditions that will prevent cracking are those that minimize concentration gradients within the spheres. The desirable conditions (most stringent in the case of the largest microspheres) include relatively slow drying in argon and superheated steam at temperatures reaching 200°C, before firing in air. A new gel dryer for removing water and alcohol from the gel spheres was installed and successfully operated in the Coated Particle Development Laboratory.

6.4 Thorium-Uranium Recycle Facility

The Thorium-Uranium Recycle Facility (TURF) is being built to provide adequate shielded space for the development of processes and equipment for remotely processing and fabricating Th-^{233}U fuels of various types. The building and the procurement of special materials (exclusive of process equipment) are virtually complete. Contracted work yet to be completed consists mainly in installation of the in-cell crane and manipulator system, cell access plugs, and viewing windows.

During the past year, various items of process equipment to be used by the development groups were designed. These include equipment for continuous uranium reduction by hydrogen at atmospheric pressure, a bench-scale solvent extraction unit for sol production by nitric acid extraction, equipment for continuous sol production by precipitation, an evaporator to concentrate dilute sol, a settler to remove gel fines from the gel-forming 2EH stream, and a furnace for batch gel drying and firing. Most of these have been fabricated; some have been tested. The original sphere-forming equipment flowsheet has been simplified; the number of equipment items, as well as the space required, has been reduced. Equipment design is scheduled for completion by June 30, 1967.

6.5 ^{233}U Storage and Distribution Facility

Oak Ridge National Laboratory serves as a storage, purification, and dispensing center for ^{233}U. During the past year, the ^{233}U handling facility received 180 kg of ^{233}U (31 shipments) and

transferred out 190 kg of ^{233}U (54 shipments). Most of this material contained less than 5 ppm of ^{232}U. Five solvent extraction runs were made to purify 46 kg of ^{233}U.

The new 5-kg/day dissolver-leacher performs satisfactorily; it has proved very efficient in dissolving high-fired sol-gel ThO_2-UO_2. A study of the stability of uranyl nitrate solutions containing rare-earth neutron poisons for criticality control, in anticipation of semipermanent storage of a large amount of mixed $^{233-235}UO_2(NO_3)_2$, indicated that the use of these poisons is feasible.

7. SOL-GEL PROCESSES FOR THE URANIUM FUEL CYCLE

The uranium fuel cycle, especially as it relates to fast reactors, occupies an important place in the reactor development program of the United States. Fuel preparation is an essential part of the uranium fuel cycle, and the investigations reported in this section constitute part of our effort to apply sol-gel techniques to the uranium cycle. Emphasis was on the preparation of urania and plutonia sols, which can be readily converted into UO_2-PuO_2 mixtures. Zirconia (and UO_2-ZrO_2) sol preparation is also being investigated since ZrO_2 is used as an inert diluent in oxide fuels.

7.1 Urania

A flowsheet for the engineering-scale preparation of urania sol was developed. The hydrous oxide is first precipitated at pH 9 from a U(IV) nitrate-formate solution (NO_3^-/U mole ratio = 2.0; $HCOO^-$/U mole ratio = 0.5 to 1.0). The precipitate is then washed free of electrolyte by decantation. To form the sol, the washed precipitate is resuspended, HNO_3 and HCOOH are added, and the suspension is stirred at 60 to 63°C until peptized. Initial studies of the engineering flowsheet and the use of HNO_3 as the sole peptizing agent indicated that peptization was not always achieved and sol yields were not good. The use of hydrazine in the precipitation and washing stages and of formic acid in the peptizing steps made the process more reproducible and increased sol yields to more than 90%.

Kilogram quantities of urania microspheres, containing both natural and highly enriched uranium, for use in various applications were made from batch-prepared urania sol; however, the desirability of continuous preparation methods for the engineering scale was recognized. Therefore, a continuous urania sol preparation system for remote, large-scale, critically safe operation with enriched uranium was designed and fabricated. Sol products prepared in the initial tests were dilute and had to be concentrated before they were suitable for use in the preparation of microspheres. Operational experience indicated the need for additional equipment development to make the system suitable for remote operations. Countercurrent washing of the uranous hydroxide precipitate in a simple column was demonstrated as a possible means of removing electrolyte on an engineering scale.

A process for the preparation of urania sol by solvent extraction was developed. In this process, NO_3^- is extracted from a dilute U(IV) nitrate-formate solution (aqueous phase) into an immiscible organic phase containing Amberlite LA-2, a long-chain secondary amine. This removal of the nitrate ion causes the U(IV) to hydrolyze and form a sol. The process consists of a reduction step, for preparation of the U(IV) solution; nitrate extraction in two stages, with an intervening digestion step to produce a dilute sol; and concentration of the dilute sol by evaporation at reduced pressure.

Drying and firing studies of sol-gel urania microspheres are being made in order to establish firing conditions that will provide products of low carbon content (<50 ppm) and near-theoretical density. Although the use of a CO_2 atmosphere has, in many tests, yielded adequate products, the most effective atmosphere for attaining low carbon content and high density has been Ar–4% H_2 saturated with water vapor at 90°C. The shrinkage rate, crystallite growth, and decrease in surface area during firing were studied. Analyses of the evolved gases by chemical, thermogravimetric, and differential-thermal methods were used to study phenomena that occur during the firing, in various atmospheres, of UO_2 gels.

A necessary first step in the production of urania sol by precipitation-peptization or solvent extraction is the preparation of a U(IV) solution. Work on the preparation of such solutions included the development of a redox-potential measurement to determine the completeness of reduction, an investigation of slurry catalysts, and studies of the nature of the hydrogen reduction process. A commercially available platinized-alumina powder containing 5 wt % Pt appeared to be the most suitable catalyst for the reduction reaction.

A urania sol preparation method involving the direct reduction of U(VI) suspensions was developed on a laboratory scale; however, in considering engineering scaleup, it was set aside in favor of the two sol preparation methods described above.

Urania sols were analyzed by means of chemical methods, pH and conductivity measurements, viscometry, electron microscopy, and x-ray diffraction techniques.

Concentrated zirconia sols ($\lesssim$3.4 *M*) were prepared by autoclaving zirconyl nitrate solutions at 200°C to promote hydrolysis and grow zirconia crystallites. The resulting slurries were peptized by successive decantation-washing procedures to give nitrate-rich zirconia sols. The nitrate contents were decreased to acceptable levels by solvent extraction with a long-chain amine dissolved in a hydrocarbon solvent. Gel microspheres were prepared in the usual manner and fired in air at 1100°C to yield dense porcelain-white zirconia spheres.

Urania-zirconia sols with a Zr/U mole ratio of 0.3 were prepared by an adaptation of the laboratory method for preparing urania sol. Zirconyl nitrate or zirconia sol was added to U(IV) solution, the mixed hydrous oxides were precipitated at pH 7, and the filtered, washed precipitate was heated at 60 to 63°C to form the sol. Strong, dense microspheres of urania-zirconia were prepared from the sols.

7.2 Plutonia

Laboratory studies and engineering scaleup of the plutonia sol-gel process were continued during this report period. The objective of this work was to develop processes for preparing plutonia sols that (1) could be used to prepare dense PuO_2, (2) would be compatible with other oxide sols so that mixed oxides could be prepared, and (3) would have the same versatility with regard to forming techniques as the sols already developed at ORNL. The sols produced by this procedure are 1 to 3 *M* in plutonium and have NO_3^-/Pu mole ratios of 0.1 to 0.15. They are stable for several months and are compatible with thoria or urania sols that are produced by the ORNL sol-gel process. The ability to produce dense plutonia microspheres, as well as homogeneous plutonia-urania or plutonia-thoria microspheres at desired heavy-metal mole ratios, has now been demonstrated on an engineering scale.

The plutonia sol is prepared by precipitating the hydrous oxide from a nitrate solution with ammonium hydroxide. After it is washed, the oxide is peptized by the addition of nitric acid to give a nitrate-rich plutonia sol having an NO_3^-/Pu ratio greater than, or equal to, 1. The nitrate concentration is reduced by drying and baking the sol. The residue is then resuspended in water to give a dilute sol, which is concentrated by evaporation to the desired plutonium concentration.

The operability and the reproducibility of the basic flowsheet were demonstrated by the production of 20 batches of sol (50 to 150 g of plutonium per batch) containing over 1500 g of plutonium. During sol preparation, engineering efforts were concentrated on the development of essential equipment components having increased reliability and ease of operation. Oxide microspheres from plutonia sols and mixed sols were successfully prepared.

Laboratory efforts were continued in an effort to optimize variables in the plutonia sol process, to investigate the basic nature of colloidal plutonia particles, to examine alternative procedures for preparing plutonia sol, and to define characteristics of oxide microsphere products. A substantial improvement in sol characteristics was obtained by the simple flowsheet modification of boiling the washed precipitate of plutonium hydroxide prior to peptization with dilute HNO_3. Several laboratory preparations employing this technique were characterized by high yields, improved stability, and good handling and sphere-forming characteristics.

Plutonia and PuO_2-UO_2 microspheres calcined at 1150°C are characterized by high density, low surface area, and high resistance to crushing. Density determinations by mercury porosimetry indicate densities of 95 to 99% of the theoretical crystal density for typical products. Surface areas of 0.02 m^2/g are obtained for 300- to 600-μ-diam microspheres. The crush resistances of 250- and 500-μ-diam microspheres calcined at 1150°C average about 550 g and more than 1 kg respectively. Calcined PuO_2 spheres were water-washed, dried in air, and smeared. Extensive contact with 50 to 100 spheres produced smears that demonstrated a very low level of transferable alpha activity (20 dis/min per smear). The homogeneity of urania-plutonia microspheres was investigated by electron microprobe techniques. Examination of micro-

spheres containing 20 wt % PuO_2 indicated a homogeneous mixture with a uniform distribution of urania.

An investigation of the thermal stability of various actinide compounds of interest to transplutonium element production by use of thermonuclear devices is in progress. Equipment for thermogravimetric and differential thermal analyses was installed in a glove-box facility, cold-tested with europia gels, and used to analyze plutonia sol-gel materials. Weight changes in europia gels are (tentatively) attributed to water loss below 300°C (1 mole of H_2O per mole of Eu, 250 to 300°C) and to nitrate decomposition between 350 and 500°C. Plutonia gels lose weight in two merging steps; the first involves the loss of water and nitrogen oxides, while the second corresponds to the measured loss in nitrate. Analyses of gel microspheres are complicated by the presence of organic residues that are introduced during the microsphere forming process.

7.3 Oxides of Controlled Porosity

Methods of producing sol-gel oxide (ThO_2 and UO_2) microspheres having controlled porosity were investigated by incorporating, in the oxide sols, materials that volatilize during the firing of gel spheres. In the preparation of porous ThO_2, carbon black was dispersed in the ThO_2 sols, gels were then prepared from the sols, and, finally, the carbon was removed by firing the gels in air. Porous UO_2 was prepared by volatilizing either chloride or molybdic oxide (MoO_3) from the urania gel.

8. SEPARATIONS CHEMISTRY RESEARCH

New separations methods and reagents are being developed, principally for uses in radiochemical processing but also for other purposes extending from extractive metallurgy to biochemical separations. Solvent extraction technology retains the principal emphasis, although increasing attention is being given to other separation methods. Reagents developed in the former ORNL raw-materials program and in subsequent studies continue to show extended utility. The program in separations chemistry can be divided into three interdependent types of research activity: (1) descriptive chemical studies (Sects. 8.1–8.4, 8.9) of the reactions of substances to be separated and of separations reagents, of the controlling variables in particular separations, and of new compounds that may be potential reagents; (2) development (Sects. 8.5–8.8) of selected separations into specific complete processes, both where no workable process has yet been devised and where existing processes can be improved, carried where warranted to the point that large-scale performance can be predicted; (3) fundamental chemical studies (Sects. 8.10–8.15) of the species, equilibria, and reaction mechanisms involved in separation systems, both to increase knowledge and to help define potential applications.

8.1 Extraction of Metal Sulfates and Nitrates by Amines

As part of the program surveying the extraction characteristics of many metals from various systems, data were obtained for extractions from acidified lithium nitrate (0.5–10 N NO_3^-) and lithium sulfate (0.3–0.5 N SO_4^{2-}) solutions with representative primary, secondary, tertiary, and quaternary amines. Data are presented for extraction of 16 metals in the nitrate system and 12 metals in the sulfate system. Relatively high extraction coefficients were found for Tc(VII) from both sulfate and nitrate solutions with all classes of amines, and for Sc, Fe(III), and Y from sulfate solutions with primary amine.

8.2 New Separations Agents

We are continuing to investigate, for potential utility in solvent extraction or other separations methods, compounds that are: (1) newly available commercially, (2) submitted by manufacturers for testing, or (3) specially procured for testing of class or structure.

A supply of 3,7-di-*n*-dodecylnaphthalenesulfonic acid (HDDNS) was prepared and used to extract strontium and europium from concentrated acid solutions. Two new carboxylic acids of relatively high molecular weight were obtained for testing: a mixed "neo" acid $R\text{-}C(CH_3)_2\text{-}CO_2H$ (15 to 19 carbon atoms) and 3,7,11,15-tetramethylhexadecanoic acid.

Three aminopolycarboxylic acids, needed for the investigation of the effects of structure on complexing of the trivalent actinides, were synthesized by reaction of sodium chloroacetate with polyamines. After the acids were purified by multiple recrystal-

lization from aqueous alcohol, the successive pK_a's were determined by titration to be 2.46, 2.52, 4.00, 5.98, 9.35, and 10.33 for triethylenetetraaminehexaacetic acid; 1.99, 2.19, 2.55, 3.19, 5.80, 9.46, and 11.11 for tetraethylenepentaaminеheptaacetic acid; and ~1.60, 2.65, 6.98, and 9.50 for 2-hydroxy-1,3-diaminopropanetetraacetic acid.

Reported complexing of lithium by low-molecular-weight sterically hindered β-diketones suggested that higher-weight analogs might be effective lithium extractants. By use of a new method, 2,2,6,6-tetramethylpentadecanedione-3,5 was synthesized; this compound has been shown to extract lithium from concentrated potassium hydroxide solutions.

The previous observation that several symmetrical dialkyl sulfoxides extracted only metals likely to coordinate with sulfur rather than with oxygen was confirmed with seven different symmetrical sulfoxides. In contrast, the unsymmetrical methyl 2-ethylhexyl sulfoxide extracted metals that are more likely to coordinate with the sulfinyl oxygen than with the sulfur, for example, uranium as UO_2Cl_2 and $UO_2(NO_3)_2$ and iron as chloride, but not iron, silver, and cobalt as nitrates or cobalt, copper, zinc, and rare earths as chlorides.

A supply of 1-(3-ethylpentyl)-4-ethyloctylamine (3,9-diethyltridecyl-6-amine, "heptadecylamine," "HDA," "Amine 21F81"), which was obtained on special order, assays 93.8% primary amine, 4.8% secondary and tertiary amines, and 1.4% inert material. Previously, this amine had not been available from any commercial source.

8.3 Selectivity of Polyacrylamide Gels for Certain Cations and Anions

Polyacrylamide gels, used primarily for separating macromolecules, also show selectivity for certain small cations and anions; this indicates a separation mechanism other than that based on matching the size of the solute species to the size of the gel pores. In chromatographic elution with water from Bio-Gel P-2 (macromolecule exclusion above a molecular weight of 1600), the order of elution was: (chlorides) K, Na, Li, Mg, Ca; (nitrates) Cs-Na, Mn-Tl, Ag; (sodium salts) F, SO_4, Cl, NO_3.

8.4 Performance of Degraded Reagents and Diluents

We have begun a study of the role of iodine in solvent extraction processing. The objectives are to determine the types of organic iodine compounds formed and the effects of their presence on the extraction process, and to establish methods for separating them from the solvent phase, if necessary. Initial tests showed that oxidation of iodide ion by nitric acid is rapid when the aqueous phase is stirred with TBP in a hydrocarbon diluent. Irradiation of the system to an absorbed dose of 100 whr/liter apparently iodinated about 2% of the diluent molecules.

8.5 Recovery of Beryllium from Ores

In further studies of the primary amine extraction process for recovering beryllium from low-grade ore sulfate liquors, optimum conditions were established for stripping the beryllium from the solvent with sulfuric acid and for recovering a beryllium oxide product from the strip solution. Development work on this process is now complete. A brief study of beryllium extraction with di(2-ethylhexyl)phosphoric acid showed that extractions of beryllium with this reagent, which are usually very slow, can be accomplished rapidly under certain conditions.

8.6 Beryllium Purification by Solvent Extraction

In the study of new and potentially less-expensive methods for preparing high-purity beryllium compounds, effective extraction of beryllium from sodium and ammonium carbonate solutions was obtained with quaternary ammonium extractants. The beryllium extraction coefficients increase with increasing pH and have a strong inverse dependence on total carbonate concentration in the range of about 0.5 to 1.5 *M*. The beryllium is stripped readily from 0.1 *M* Adogen 464 in diethylbenzene with 2 *M* NH_4HCO_3.

8.7 Separation of Zirconium and Hafnium with Amines

Preliminary results obtained in the separation of zirconium from hafnium by extraction with amines

in the sulfate system were promising. The Zr/Hf separation factors are strongly dependent on the amine type and alkyl structure. The highest separation factors (6 to 10) were obtained with an extensively branched secondary amine and with certain tertiary amines.

8.8 Separation of Rare Earths

The potential usefulness of di(2-ethylhexyl)-phosphoric acid (D2EHPA) extractant for large-scale separation of rare earths is being studied. Efficient separations of small quantities of rare earths can be obtained by extraction chromatography (sequential elution of the rare earths from a column containing D2EHPA on diatomaceous earth support material), but whether this method can be scaled up successfully is questionable. The comparison of results from runs in 0.9-, 2.5-, and 5.0-cm-diam columns indicated a partial loss of resolution in the largest column compared with the smaller columns. Preliminary tests in a mixer-settler system with a static organic phase, 0.5 *M* D2EHPA in Amsco 125-82, were encouraging.

8.9 Comparative Chemistry of Lanthanides and Trivalent Actinides

In the extraction of lanthanides from mineral acid solutions by di(2-ethylhexyl)phosphoric acid (HDEHP) and 2-ethylhexyl phenylphosphonic acid (HEH[ϕP]), the increase of the extraction coefficients with increasing atomic number is not uniform for successive pairs of these elements. In extractions from carboxylic acid solutions the irregularities increase until neodymium, instead of lanthanum, is the least extractable. The addition of aqueous aminopolyacetic acid complexers decreases and further alters the extractions so that, with diethylenetriaminepentaacetic acid (DTPA), lanthanum is the most extractable of the light lanthanides. Extraction coefficients for americium and californium are inversely proportional to DTPA concentrations above 10^{-4} *M*; a comparable relationship exists above 10^{-3} to 10^{-2} *M* for the lanthanides.

Extraction dependences on extractant concentration and on (inverse) acid concentration are not simply third-power, and they vary between elements. The practicable separation factors are about the same with either HEH[ϕP] or HDEHP. For the separation of greatest interest, berkelium from curium, the factor is around 12 in extraction from HCl solution.

Lanthanide and actinide extractions by HEH[ϕP], from HCl and especially from HNO_3 solutions, are enhanced by the presence of small concentrations of some cations of the type MO^{2+}. The enhancement decreases with increasing atomic number in both series, thus impairing or eliminating intergroup separations with HEH[ϕP]. This synergism has not been found with HDEHP.

Trace amounts of berkelium are quantitatively carried with cerium in iodate precipitation after bromate oxidation.

8.10 Transplutonium Element Compound Preparation and X-Ray Characterization

A coherent particle of berkelium oxide was prepared by saturating a single bead of ion exchange resin with purified berkelium and then calcining it. Activation analysis of the resultant oxide detected only Ce ($\leq$1.3%), Nd (<0.5%), La (0.008%), and Eu (<0.005%). X-ray diffraction measurements showed that the air-stable oxide is BkO_2 (face-centered cubic, lattice parameter $a = 5.334 \pm 0.005$ A) and that the hydrogen-reduced form is Bk_2O_3 (body-centered cubic, lattice parameter $a = 10.880 \pm 0.005$ A).

8.11 Aminopolycarboxylic Acid Complexes of Trivalent Actinides

To aid in the theoretical understanding of stability trends and to permit enhanced separations, we are determining the stability constants of a variety of transplutonium actinide chelate compounds. Complexing with a series of aminopolycarboxylic acids was studied by both spectrophotometric and cation exchange techniques. The stability constants found for four different ligands with americium were: Imidodiacetic acid: 1:1, $pK_s = 6.1$ (two additional complexes detected). Hydroxyethylimidodiacetic acid: 1:1, $pK_s = 10.44$; 1:2, $pK_s = 7.4$. Ethylenediaminetetraacetic acid (EDTA): 1:1, $pK_s = 18.15$ (one additional complex detected). Diethylenetriaminepentaacetic acid: 1:1, $pK_s = 24.6$. Stability constants (pK_s) for 1:1 complexes with 2-hydroxy-1,3-diaminopropanetetraacetic acid were: Am, 12.14 $\pm$ 0.05; Cm, 12.30 $\pm$ 0.05; Cf, 13.18 $\pm$ 0.05; and Eu, 12.21 $\pm$ 0.05. The

CHOH group caused a larger decrease in the pK_s (as compared with EDTA) than was expected. Also, the difference between americium and californium was greater than with other ligands tested.

8.12 Lanthanide and Actinide Sulfate Complexes

A primary amine, 1-*n*-nonyl-*n*-decylamine (as sulfate), was found to have sufficiently high solubility in benzene, low distribution to aqueous phases, and high extraction coefficients for europium sulfate that it could be used in a solvent extraction study of the aqueous sulfate complexes of europium. The extraction series that were completed at constant sulfuric acid activity levels of $3.58 \times 10^{-10}\ M^3$ (pH ≈ 3) and $6.45 \times 10^{-5}\ M^3$ (pH ≈ 1) (ionic strength varying) indicate qualitatively that positive species (Eu^{3+} and $EuSO_4^{+}$) preponderate over negative species [$Eu(SO_4)_2^{-}$, etc.] at a total sulfate concentration of about 1 *M*. The quantitative results (formation constants) are being calculated.

8.13 Equilibria and Mechanisms of Extractions

The study of the synergistic extraction of strontium by HDEHP-TBP was completed with a continuous-variations examination of the effect of the TBP:DEHP ratio, and a brief direct test of possible TBP-H_2O aggregation (in *n*-octane) that is suggested by the extraction results. We concluded that changing diluents (or additives) has two separate effects: (1) shift of the E_{Sr} vs pH curve along the pH axis, reflecting changes in the apparent acidity of HDEHP, and (2) synergistic enhancement or antagonistic depression of E_{Sr}, due, respectively, to direct association of the additive with the extracted strontium species or to competitive association of the additive with DEHP. TBP replaces HDEHP = HA in coordination with SrA_2, probably to give $SrA_2 \cdot 2HA \cdot TBP$ when little sodium salt (NaA) is present and $SrA_2 \cdot 4TBP$ when $NaA/\Sigma A > 0.2$.

Extractions of strontium and europium by didodecylnaphthalenesulfonic acid (HDDNS) confirmed the expectation that this strong acid should act as a liquid cation exchanger for metals in concentrated acid solutions. They also indicated that no coordination of additional acid with the extracted metals occurred, in contrast to the extensive additional coordination in the case of organophosphorus acids. Thus, extensive synergism by added organic-phase complexers may be expected.

Extraction coefficients of strontium and barium with several carboxylic acid–sodium carboxylate mixtures were an order of magnitude higher than those with HDEHP at the same $NaA/\Sigma A$ ratios. Positions of maxima in the *E* vs pH curves indicated coordination of the strontium and barium carboxylates with differing amounts of additional carboxylic acid.

In a test of the possible critical effects of water activity in the equilibria of uranyl extraction by amine sulfate, extractions were measured from saturated $(NH_4)_2SO_4$ ($a_w = 0.80$) and saturated Na_2SO_4 ($a_w = 0.93$) and compared with those from 1 *M* Na_2SO_4 ($a_w = 0.96$). The log *E* vs log [amine] plots were parallel at a given pH, with a slope near 1; this eliminated any possibility that the deviations from the mass action law in this system involve some abrupt change at high water activities.

8.14 Kinetics of Metal-Ion Extraction by Di(2-ethylhexyl)phosphoric Acid (HDEHP)

In the continued study of the kinetics of the slow extraction of iron(III) from acid perchlorate solutions by HDEHP (=HA), an explanation was found for the increase in extraction rate with decreasing acidity. It is analogous to a published mechanism for the formation of aqueous iron complexes and assumes that two steps occur at the interface:

$$Fe(H_2O)_6^{3+} + \underset{\cdot\cdot}{\underset{\cdot\cdot}{A^-}} \xrightarrow{\text{slow}} FeOH(H_2O)_5^{2+} + \underset{\cdot\cdot}{\underset{\cdot\cdot}{HA}} \xrightarrow{\text{fast}}$$

$$\underset{\cdot\cdot\cdot\cdot\cdot\cdot\cdot\cdot\cdot\cdot\cdot}{FeA(H_2O)_5^{2+}} + H_2O\ ,$$

followed by further fast reactions to yield $FeA_3 \cdot 3HA$. This leads to the prediction that the addition of aqueous proton-accepting complexers should speed up the extraction. Results obtained by adding several complexers at 0.1 *M* to a solution that was 0.002 *M* in Fe^{3+} and 2 *M* in ClO_4^{-}, pH 1, showed that the rate of extraction by 0.1 *M* HDEHP was increased by factors of up to 18.

In contrast to the iron extraction, the rate of beryllium extraction from acid perchlorate solution by HDEHP does not fit well to an equation of any order, integral or fractional. This could result from rate control by two slow extraction re-

actions in parallel, or more likely from a slow first-order extraction of a particular beryllium species accompanied by slow reequilibration to replenish that species from other aqueous beryllium species.

8.15 Aggregation and Activity Coefficients in Solvent Phases

Isopiestic measurement of average aggregations in TBP–HDEHP–NaDEHP–*n*-hexane confirmed the previous qualitative evidence from dielectric measurements that TBP is associated with DEHP and suggested that the principal adduct may be NaA·2HA·TBP.

Tests of the usefulness of a commercial matched-thermistor osmometer for measurements of aggregation numbers and activity coefficients showed that it is usable to lower concentrations (0.005 *m*) than is our isopiestic system but that its reproducibility above 0.01 *m* (with the solutions tested) was not as good as is desired for calculation of activity coefficients. Brief tests of a new principle for osmometry gave promising results: we equilibrated a solution with pure diluent through the vapor phase in a sealed container, as in isopiestic balancing, but with a pressure gradient established by holding the solution at a measured elevation above the solvent. This method would give absolute measurements, in contrast to the comparison measurements of isopiestic balancing and matched-thermistor osmometry, at much lower pressure differences than can be measured by our direct differential manometer system.

We measured the solubility of water in eight common organic diluents by liquid-liquid equilibration, with tritiated water as analytical tracer. The precision of the results is better than we have been able to obtain by Karl Fischer titration or to find in the literature. Five of these diluents, tested over a range of water activities, conformed to Henry's law throughout, with constants varying from 3.00×10^{-4} for cyclohexane to 3.05×10^{-3} for benzene (mole fraction scale). Previous isopiestic measurements of water distribution and TBP activities in the TBP-H_2O system were confirmed and extended to the TBP-D_2O system by liquid-liquid equilibration, with tritium as analytical tracer. The Henry's law constants found were 2.09 ± 0.04 at $a_{H_2O} < 0.7$ and 2.03 ± 0.06 at $a_{D_2O} < 0.06$ (mole fraction scale).

The previously reported aggregation numbers for dry tri-*n*-octylamine bisulfate in benzene were fitted up to 0.4 *m* by a model involving monomers, tetramers, and some dimers:

$$2R_3NH\cdot HSO_4 \leftrightharpoons (R_3NH\cdot HSO_4)_2, \quad Q_{12} = 11.7 ;$$
$$2(R_3NH\cdot HSO_4)_2 \rightleftharpoons (R_3NH\cdot HSO_4)_4, \quad Q_{24} = 2.99 \times 10^5 .$$

With the aid of this model, improved extrapolation of osmotic coefficients to infinite dilution gave a more complete evaluation of the stoichiometric activity coefficients than was previously reported.

Infrared absorption spectra in the system water–tri-*n*-octylamine–H_2SO_4–diluent indicated that the water is associated with the sulfate and not with the alkylammonium ion.

9. CHEMICAL APPLICATIONS OF NUCLEAR EXPLOSIONS

9.1 Copper Ores

Recent studies continued to show that ^{106}Ru would probably be the only significant radiocontaminant of cement copper produced by nuclear fracturing of a copper ore body, in-situ leaching, and recovery of copper from solution by cementation on scrap iron. In laboratory tests effective separation of copper from ruthenium was obtained in upgrading the cement copper to electrolytic copper. The final copper product, therefore, should not be hazardous to the user.

9.2 Stimulation of Natural Gas Wells

Laboratory measurements of tritium-hydrogen exchange in water-methane systems indicate that the rate of exchange will probably be low during methane production from a natural gas well that has been stimulated under the conditions of the proposed Gasbuggy experiment. The rate at room temperature and atmospheric pressure in a 1-liter glass vessel is

$$R \sim 2.3 \times 10^{-8} \ [HTO]^2 \text{ mc liter}^{-1} \text{ day}^{-1}$$

when the tritium concentration is in the range of 10 to 50 mc/liter.

9.3 Recovery of Oil from Shale

The use of a nuclear device to crush oil shale in place has been proposed. The recovery of oil from the crushed shale in the nuclear chimney would then involve in-situ retorting. The proposed demonstration experiment is called Project Bronco. ORNL is assisting in this project by studying the potential contamination of the product shale oil by radionuclides and potential problems involved in producing and handling the oil. In a small laboratory retort, shale moistened with tritiated water produced oil that was slightly contaminated with tritium. When shale oil was heated with radioactive debris from an underground test shot, small amounts of radionuclides (predominantly ^{106}Ru) were detected in the oil.

9.4 Development of Hypervelocity Jet Samplers

In final tests to demonstrate a jet-sampler method for recovering a target irradiated about a meter from a detonating nuclear device, five highly symmetrical copper cones containing gold targets were jetted. The gold will be recovered from the wood used to catch the jetted targets to determine the efficiency with which the jets were focused within the flight chamber.

10. RECOVERY OF FISSION PRODUCTS BY SOLVENT EXTRACTION

A new process flowsheet for isolating fission product rare earths, strontium, and cesium from Purex waste was demonstrated on a bench scale at tracer level. The rare earths and bulk metal contaminants are extracted from unadjusted waste solution with the sodium salt of di(2-ethylhexyl)-phosphoric acid, and the rare earths are selectively stripped from the extract. The raffinate from this operation is adjusted to a pH of about 6 to precipitate residual metal contaminants, and the resulting solution is contacted first with di(2-ethylhexyl)phosphoric acid to recover strontium and then with a substituted phenol to recover cesium. The process yields less-pure concentrates than processes developed previously, but it is simpler and does not require the use of large amounts of aqueous-phase complexing agents.

11. BIOCHEMICAL SEPARATIONS

11.1 Development of Processes for Macromolecular Separations

We have developed a new reversed-phase chromatographic system that gives superior resolution of *E. coli* transfer ribonucleic acids (tRNA's). The system employs a quaternary ammonium extractant in a Freon diluent, which is immobilized as a film on a hydrophobic diatomaceous earth support. The chromatograms are developed by elution with a sodium chloride solution of increasing concentration.

A revised procedure for the preparation of larger quantities of phenylalanyl-RNA synthetase has been devised. In the first test of the complete flowsheet, 22.4 mg of highly purified phenylalanyl-RNA synthetase was obtained from 4.3 kg of *E. coli* cells.

11.2 Scaleup of Processes for Macromolecular Separations

Engineering-scale research and development have provided information on scaled-up procedures for the preparation of purified tRNA's. During the latter half of this report period an intensified development campaign was undertaken to prepare a gram-sized sample of phenylalanine tRNA.

E. coli B cells were grown by batch fermentation techniques; 390 kg of cells were obtained after four weeks of intermittent three-shift operation. These cells yielded approximately 500 g of crude tRNA, which was fractionated by reversed-phase chromatography on large coupled columns. The eluted phenylalanine tRNA product was pooled, desalted on Sephadex G-25 columns, concentrated in a wiped-film evaporator, and separated from high-molecular-weight components by gel filtration on Sephadex G-100 columns.

The product, which represented about a 23% overall recovery, was accumulated in two purity grades: approximately 1 g that assayed 64% active phenylalanine tRNA, and 0.5 g that assayed 51% phenylalanine tRNA.

11.3 Molecular Weights of Transfer Ribonucleic Acids

Molecular weight values obtained by membrane osmometry ranged from 41,300 to 46,200 for crude,

mixed tRNA. After purification of the tRNA by gel permeation chromatography, the molecular weight values ranged from 30,100 to 32,800 (pH 7) and from 35,200 to 38,400 (pH 4) at 10 to 50°C.

11.4 Behavior of Transfer Ribonucleic Acids on Polyacrylamide Gel Columns

Transfer ribonucleic acids can be partially separated into groups on a Bio-Gel P-100 column by means of polyacrylamide gel chromatography. The tRNA's are eluted with a buffered solution containing NaCl and $MgCl_2$. The position of the tRNA's on the chromatogram is affected by temperature, pH, and NaCl and Mg^{2+} concentrations.

11.5 Body-Fluid Analysis

We are developing automatic high-resolution analyzers that are capable of quantifying the molecular constituents of human body fluids. Currently, emphasis is centered on the development of a chromatographic analyzer for the low-molecular-weight (less than 1000) uv-absorbing constituents of human urine. Several pathological and normal samples have been analyzed by a prototype system, and differences between normal urine chromatograms and those from lymphocytic leukemics and schizophrenics have been observed.

A search of the literature, for a two-year period (1964–65), dealing with molecular constituents of urine has resulted in the accumulation of more than 800 references to more than 300 low-molecular-weight constituents.

Urine collection and processing procedures include: collection of a refrigerated 24-hr composite sample; filtration through a membrane filter; pH adjustment to 4.4; and, in some cases, pressure filtration through dialysis tubing. A 1- to 2-ml sample is injected into the analytical system for analysis.

Several different separations media have been tested for chromatographically separating the absorbing constituents. Biorad AG-1-X8 (purified Dowex 1-X8) provided the highest resolution.

A uv photometer with solid-state detectors is being developed for use in the continuous monitoring of the chromatographic column effluent.

Fifteen urinary components have been tentatively identified by cochromatography; the identities of five of these have been further verified by comparison of uv spectral data. Other techniques being developed for a more complete identification include thin-layer chromatography, spot tests, other physical comparisons, and computer resolution of complex uv spectra.

A data acquisition system for digitizing the output of the spectrophotometer column monitor has been designed.

12. CHEMISTRY OF PROTACTINIUM

In the continued study of the chemistry of protactinium in aqueous sulfate systems, a solid protactinium sulfate was prepared by precipitation from fuming sulfuric acid. It was hoped that more reproducible solutions could be prepared from this compound than have been obtained by dissolving protactinium oxide or hydroxide in sulfuric acid. However, its apparent solubility in sulfuric acid varied with the amount of solid present, suggesting heterogeneity. Absorption spectra of the resulting solutions were, in general, similar to those previously obtained from protactinium hydroxide dissolved in sulfuric acid. They did not show the band near 2000 A that is shown by the protactinium remaining in the fuming sulfuric acid from which the protactinium sulfate was precipitated. Resolution of these spectra awaits computer analysis.

A novel protactinium purification procedure was demonstrated, in which fired Pa_2O_5, together with anion exchange resin, was contacted in a closed circuit with 10 *M* HCl solution. The slowly dissolving protactinium was sorbed by the resin. After two months, elution with HCl-HF solution gave 15 mg of highly pure protactinium (from an initial 100 mg of Pa_2O_5).

13. IRRADIATION EFFECTS ON HETEROGENEOUS SYSTEMS

The study of the radiolysis of adsorbed water was continued in an effort to determine the mechanism by which the adsorbent influences the yield of molecular hydrogen. Several molecular sieves with different surface cations were tested, and the results were compared with those previously found for silica gels of varying specific surface area. These studies indicate a highly efficient transfer of energy from the adsorbent to the adsorbate, probably in the form of inelastically scattered electrons. These electrons become hydrated

at the surface and then react with water or hydronium ions to give H atoms and hence molecular hydrogen. The efficiency of this latter process depends on the nature of the surface, the total amount of water present, and the total irradiation dose received by the system. Competing reactions with radiation-induced radicals in the excess water and with accumulated positively charged species reduce the hydrogen yields.

14. SPECTROPHOTOMETRIC STUDIES OF SOLUTIONS OF ALPHA-ACTIVE MATERIALS

14.1 Spectral Studies of Uranium Solutions

The ultraviolet (1795 to 3565 A) and visible spectra of the uranyl ion in perchlorate solution were resolved into 24 absorption bands, which were subsequently grouped into 7 major bands with an average spacing of 6137 cm^{-1} and progressively increasing oscillator strengths or transition probabilities. The relative energy levels for the complete ultraviolet and visible absorption spectra and fluorescence emission spectra, as determined from the resolved bands, are presented in an energy-level diagram.

The spectrum (2000 to 13,000 A) of U(IV) in perchloric acid solution contains 23 overlapping bands, which have not yet been assigned to particular transitions. The resolved spectra at various stages of U(IV) hydrolysis can be associated with the changes in the nature of the U(IV) species. Further progress is contingent on our ability to prepare and maintain a pure $U(ClO_4)_4$ solution, completely free of higher oxidation states of uranium.

14.2 Installation and Testing of the Spectrophotometer System for High Alpha Levels

The spectrophotometer system is mounted in a "cold" laboratory for testing. The spectrophotometer is operating satisfactorily and is showing a resolution essentially twice that of a standard Cary model 14 spectrophotometer. Initial checkout of the associated equipment is nearly complete. The system is being operated with dummy cells at high temperature prior to actual operation with uranium and lanthanide solutions.

15. CHEMICAL ENGINEERING RESEARCH

15.1 Performance of a Prototype Stacked-Clone Contactor with Integral Pumps

The 14-stage prototype stacked-clone contactor has been tested, by using the Purex and other flowsheets, and found to be equal in performance to its experimental predecessor. It is currently being evaluated for use in "hot" ^{233}U recovery operations in the Chemical Technology Division Pilot Plant. Operability with the light (organic) phase continuous and with an internal interface has been demonstrated; this will greatly increase the range of usefulness of the device.

15.2 Scaleup of the Stacked-Clone Contactor

A study of the scaleup of the stacked-clone contactor has been completed. Experimental units 0.5 and 1.4 times the size of the standard contactor were tested. The smaller unit provides several advantages, including flow capacities 60% higher than expected, mass transfer efficiencies 20% higher than those obtained with the standard contactor, and solution residence times of only 1 sec per stage; thus the most effective scaleup can be provided by the manifolding of several small clones in each stage.

15.3 Mass Transfer of Water from Sol Droplets During Microsphere Gelation

The mass transfer of water from single thoria sol droplets into 2-ethyl-1-hexanol is being investigated by optically measuring the diameters of single fluidized drops, at magnifications of 20 to 40×. A small tapered Plexiglas column that will stabilize the droplets for this purpose has been developed. The experimental data are correlated with a model that assumes that the controlling resistance to mass transfer is the organic-phase film surrounding the drops.

15.4 Hyperfiltration of Spent Sulfite Liquor with a Self-Rejecting Membrane

Hyperfiltration using a dynamically cast membrane is a new technique that is potentially useful for various radiochemical applications such as

concentration of low- and intermediate-level wastes. We have been participating in its development by assisting in programs with similar applications, for example, the concentration of dissolved solids in paper-mill wastes. Work has demonstrated the recovery and recycle of 90% of the water from spent sulfite liquor and the collection of solids in concentrations that are sufficiently high to make evaporation and burning feasible. We have obtained 95% rejection of dissolved salts with high production rates (35 gal day^{-1} ft^{-2}) at moderate pressures (400 psig) by hyperfiltration with a self-rejecting membrane. Our technique consists in pumping the spent liquor through a porous ceramic or carbon tube under pressure and allowing the spent liquor to form its own membrane.

16. REACTOR EVALUATION STUDIES

This program, sponsored jointly by the Reactor Division and the Chemical Technology Division, consists of studies of various proposed advanced reactor and fuel-cycle systems to evaluate their technical and economic feasibility. Currently, the bulk of this work is being done in support of the USAEC Fuel Recycle Task Force and the Systems Analysis Task Force. Evaluations completed during the past year included estimations of the costs of fuel-material preparation (conversion), processing spent fuel, and shipping fresh and spent fuel for advanced converter reactors (HWOCR, HWBLWR, and HTGR), fast breeder reactors, and various proposed desalination reactors. In addition, computer codes were developed for the analysis of the overall cost of nuclear power and for calculation of the decay properties of mixed fission products resulting from the fission of ^{235}U. The optimization of the size of fuel processing plants in a growing economy was also studied.

17. PREPARATION AND PROPERTIES OF ACTINIDE-ELEMENT OXIDES

Studies of the electrophoretic behavior of thoria sols have essentially been completed. The multiple boundaries observed in the Tiselius type of apparatus were shown to be caused by the presence of small amounts ($\sim 10^{-4}$ *M*) of Th^{4+} in the intermicellar fluid. The method of preparation of the sol is not an important variable, and the electrophoretic mobility, in general, is not very sensitive to environmental effects such as changes in pH or ionic strength.

Studies of the shrinkage and of the sintering of thoria gels with and without additives have also been completed; reports summarizing this work are being prepared.

Attention is now being focused on urania sols, and a few measurements of their viscosities and electrophoretic mobilities have been made. The most remarkable effect observed to date is the sharp decrease in the viscosity of concentrated (6.2 to 6.4 *M*) chloride-stabilized UO_2 sols upon the addition of a small amount of UO_3. A decrease from 10^4 to 100 centipoises was observed as the calculated oxygen:uranium atom ratio was increased from 2.00 to 2.07.

18. ASSISTANCE PROGRAMS

18.1 Eurochemic Assistance Program

The Laboratory continued to coordinate the exchange of technical information between Eurochemic and the AEC production sites and national laboratories for the AEC Division of International Affairs. E. M. Shank completed his fifth year at Mol, Belgium, as U.S. Technical Advisor to Eurochemic during the construction and startup of the Eurochemic fuel-processing plant. Construction of the plant and its auxiliary facilities and startup operations are complete. Discharged fuels from several European reactors have now been processed.

18.2 Evaluation of the Radiation Resistance of Selected Protective Coatings and Other Materials

In a continuing program the radiation resistance of a number of protective coatings, lubricants, gasket materials, sealants, electrical insulation materials, and glasses were tested in a ^{60}Co gamma field having a radiation intensity of 8×10^5 r/hr. Epoxy and polyurethane coatings were satisfactory for total doses, in air, of up to 10^{10} rads; failure of epoxy and modified phenolic coatings exposed in deionized water occurred at doses between 1×10^8 and 3×10^9 rads. The other materials tested failed at total doses between 5×10^8 and 5×10^9 rads.

19. WATER RESEARCH PROGRAM

Oak Ridge National Laboratory is carrying out a program of basic research on the properties of water and its solutions under the auspices of the Office of Saline Water, Department of the Interior. This program has as its long-range goal the development of methods for the economical purification of water in such amounts and of such purity that it may be used for irrigation and for drinking. Work in this interdivisional program is under the direction of K. A. Kraus. It is reported in part in a series of reports issued annually by the Department of the Interior. The most recent report in the series is *Saline Water Conversion Report, 1966*. Because the work is reported formally in the above series, only this abstract of the work carried out by Chemical Technology Division personnel is presented in this report.

Studies carried out in the Chemical Technology Division have followed several lines. In one, we have measured thermodynamic properties of water-organic liquid mixtures, in order that such mixtures can serve as models for salt-excluding organic membranes. This part of the program has now been terminated; results will be published that show the correlation of activity coefficients and miscibility gaps with class and structure of the organic liquids, dielectric constants, and thermodynamic activity of water.

In another line of study, methods are being sought to alter the hydrodynamic conditions near a solid surface to promote higher rates of transfer of a solute between the surface and the circulating fluid. (This study is under the direct supervision of D. G. Thomas, Reactor Division, ORNL.) This research is specifically intended to reduce the concentration polarization problems encountered in reverse osmosis and electrodialysis of brackish waters; the effort is focused upon studying the effects of cylindrical obstructions supported slightly above the transfer surface. Earlier, we reported that mass transfer rates at a given point can be increased eightfold through the use of such promoters and that a threefold increase can be achieved over a large transfer surface. These increased mass transfer rates are accompanied by higher pressure losses or pumping power requirements. However, the pumping power required to achieve given mass transfer rates with detached promoters has now been shown to be less than that required to obtain the same rates in clear, or "unpromoted," channels. The investigation has included studies of the effects of promoters on local velocity and mass transfer rate fluctuations at the wall; this has provided insight into the manner in which velocity disturbances near the wall affect instantaneous and time-averaged mass transfer rates. An analytical model describing many features of these effects has been developed.

In a third line of study, hyperfiltration (reverse osmosis) is being tested as a means of treating waste water. One of the principal wood-pulping processes is the calcium-base sulfite process, which produces a spent liquor containing mostly calcium lignosulfonate. The recovery and recycle of 90% of the water would concentrate the liquor so that evaporation and burning would be feasible, and thus would eliminate a water pollution problem. We have obtained 95% rejection of dissolved solids with high product rates (35 gal day^{-1} ft^{-2}) at moderate pressures (400 psig) by hyperfiltration with a self-forming membrane. Our technique involves pumping the spent liquor through a porous ceramic or carbon tube under pressure and allowing the spent liquor that forms a concentrated layer at the porous surface to act as its own membrane. Tubes with a uniform pore size distribution of 1 μ in diameter gave highest rejection and product fluxes.

20. CHEMISTRY OF CARBIDES AND NITRIDES

Fundamental studies of the reactions of metal carbides with aqueous solutions were continued. The reactions of high-purity uranium and thorium carbides with 3 to 9 *M* HCl and 6 *M* H_2SO_4 were found to be hydrolysis reactions, yielding hydrocarbons, with no oxidation of the U(IV) or formation of C–S, C–O–S, or C–Cl bonds. In 2 to 18 *M* NaOH some of the tetravalent uranium in uranium monocarbide was oxidized to a higher valence state, with the accompanying evolution of hydrogen; the carbide carbon was hydrolyzed to methane. Other studies showed that the rate-determining step in the hydrolysis of the uranium and thorium carbides probably does not involve cleavage of the H–O bond in the water, since the reaction with D_2O at 80°C was identical to the corresponding reaction with H_2O except that deuterium was substituted for hydrogen in the products.

Pronounced differences in chemical behavior between the alkaline-earth dicarbides and the

actinide dicarbides were found. The reactions of calcium dicarbide with 0 to 16 *M* HNO_3 and of barium dicarbide with 0 to 8 *M* HNO_3 yielded acetylene as the only carbon-containing product. In contrast, the uranium and thorium dicarbides yielded complex aliphatic hydrocarbon mixtures when hydrolyzed, and complex aromatic compounds when oxidized by nitric acid.

21. INDUSTRIAL APPLICATIONS OF NUCLEAR ENERGY

21.1 Survey of Process Applications in a Desalination Complex

A survey of the chemical and metallurgical industries was made to ascertain which processes should be given priority for further detailed study as possible components of a nuclear industrial-desalination complex. Investigated factors included market potential, demand for large quantities of power or steam, shipping costs, production costs, and economics expressed as turnover ratios.

A comparison of 20 industrial processes showed that nitrogenous and phosphatic fertilizer production should be given first priority, after which chlorine and caustic production should be considered. The production of metals such as iron, steel, aluminum, ferroalloys, and magnesium falls next in priority. The production of acetylene via calcium carbide and the electric arc furnace also appeared promising.

21.2. Production of Hydrogen by the Electrolysis of Water

A recent survey indicated that the production of ammonia for fertilizer using electrolytic hydrogen is economically feasible if newly developed electrolytic cells prove successful in industrial applications. One of the new cells is being studied on a laboratory scale.

Galvanic corrosion was found to be a problem in a bimetallic electrolytic system exposed to aqueous KOH at temperatures in excess of 80°C. Mechanical coupling of types 316 and 304 stainless steels increased the corrosion of the former by 75% when exposed to 34% KOH at 116°C; nickel, however, did not corrode under these conditions. Evaluations of several different types of membranes showed that type 10 Quinterra asbestos produced significantly lower internal resistance losses without sacrificing any gas separation qualities. An 82-hr laboratory test was performed at 90°C and at a current density of 1860 amp/ft^2. The results showed no measurable degradation of cell performance during this period. Ultrahigh current densities, up to about 4600 amp/ft^2, had no apparent effect on electrodes and membranes at temperatures up to 90°C.

22. SAFETY STUDIES OF FUEL TRANSPORT

A new program has been organized to develop an acceptance *Criteria* for casks that are designed for transporting irradiated fuel. The intent of the *Criteria* is to provide a uniform engineering basis for cask design and fabrication that will ensure compliance with the performance specifications imposed by AEC regulations as stated in chapter 0529 of the *AEC Manual*.

The *Criteria* will consider engineering standards for the design, fabrication, testing, and analysis of shipping casks for irradiated fuel. It will provide a uniform basis for assessing design adequacy without inhibiting the ingenuity or technical aggressiveness of the designer.

Data and information are presented on cask structural design, materials and fabrication, shielding, criticality, and heat transfer.

1. Power Reactor Fuel Processing

Laboratory- and engineering-scale development of processes for recovering fissionable and fertile material from spent power-reactor fuels is continuing. This work has included basic chemical studies on unirradiated samples of new types of fuel and cladding materials, chemical and engineering development of mechanical and aqueous chemical processes for present-day and advanced fuels, and hot-cell testing of new processes to determine the effects of radiation and fission products on the chemical reactions. The major processes studied this year included a burn-leach process and a grind-leach process for uranium-thorium-graphite HTGR (high-temperature gas-cooled reactor) fuel, mechanical methods applicable to HTGR and metal-clad oxide fuels, and caustic decladding and high-temperature HCl decladding methods for SAP-clad UC fuel for a heavy-water-moderated, organic-cooled reactor (HWOCR). Work on fuel recovery processes for liquid-metal fast breeder reactor (LMFBR) fuel was begun. A limited number of solvent extraction studies were also made.

Various reactor and fuel manufacturers were visited to obtain the most up-to-date information on existing and proposed third-generation PWR's and BWR's and on proposed fast breeder reactor (FBR) fuel element designs; such information was needed to determine whether existing fuel disassembly and shear-leach methods and equipment can be satisfactorily used to process these fuels. Evaluation of the accumulated data indicates that the new fuel designs can be adequately handled; however, computer calculations show that fission product heat removal from short-cooled (30 days), highly irradiated (burnup, 100,000 Mwd/ton) FBR fuels will be a very difficult problem. The safe disposal of residual sodium coolant and bonding (on and in FBR fuel rods) was evaluated in laboratory tests. Residual sodium on the fuel rod exteriors can be destroyed easily by controlled reaction with oxygen and/or water-vapor–inert-gas atmospheres. Destruction of the sodium bond at 300°C with 3% H_2O–97% He is satisfactory; subsequent pyrohydrolysis at 750°C adequately converts PuC-UC to the more desirable PuO_2-UO_2. Treatment with air and with CO_2 was less satisfactory for destroying sodium. Leaching of sheared Zircaloy-clad ThO_2-UO_2 with 13 *M* HNO_3–0.05 *M* HF resulted in the dissolution of 1.5% of the cladding, part of which precipitated during feed adjustment; however, solvent extraction processing (employing TBP or amines) of the resulting feed solution was satisfactory. The development and evaluation of a full-sized delayed-neutron leached-hull monitor was continued. The detection of 0.01 g of ^{235}U in an 830-r/hr gamma field was demonstrated.

The development of the burn-leach and grind-leach processes for carbon- and SiC-coated $(Th,U)C_2$ and $(Th,U)O_2$ fuel particles in graphite was continued. Mechanical processing tests indicated that both shearing and breaking the large compacts by a "pile-driver" technique were unsatisfactory. The removal of coated-particle compacts from the holes in unirradiated Public Service of Colorado Reactor prototype graphite fuel sticks with a high-pressure water jet was successful; screening of the removed material provided adequate separation of fissile and fertile particles of different sizes. A series of hot-cell demonstrations of the burn-leach process showed this process to be satisfactory for HTGR fuels that had been irradiated to exposures as high as 50,000 Mwd/ton. Burning rates were adequate, and decontamination of off-gases by a factor of 10^6 with a sintered-metal filter at $\leq$300°C was consistently achieved. The dissolution of the ThO_2-U_3O_8 burner ash was $\geq$99.7% complete in 5 to 7 hr in boiling 13 *M* HNO_3–0.05 *M* HF–0.01 *M* Al^{3+}.

Although laboratory experiments with unirradiated HTGR fuel samples [carbon-coated $(Th,U)C_2$ particles] indicated that the grind-leach process is feasible, hot-cell tests were disappointing be-

cause of the high (>1%) thorium and uranium losses and fission product retention (10 to 20%) by the leached graphite. The development of the method is continuing, however, since it may be essential for the processing of fuels composed of SiC-coated particles. The demonstration of the new ORNL-designed roll crusher showed that this device is adequate for all fuels containing particles with diameters $\geq 150\ \mu$. Leaching tests with unirradiated Peach Bottom and UHTREX fuel samples showed that a two-step leaching procedure and a thorough washing of the leached graphite are required to achieve >99.5% fuel dissolution. The leaching of ground carbon-coated sol-gel ThO_2 resulted in a thorium loss of only 0.01%. All leachates contained about 1% of the carbon from the fuels as soluble organic compounds. An improved equation for calculating the filtration and washing characteristics of the graphite residue was formulated; also, an acid recycle flowsheet, which uses the first acid wash as the dissolvent for the next batch, was developed.

The Acid-Thorex flowsheet was modified to permit the processing of grind-leach solutions containing small amounts of soluble organic compounds. The recovery of thorium and uranium was adequate, and a fission product decontamination factor of 400 was obtained in a system containing five extraction and three scrub steps. The leaching of ground fuel (after treatment with HNO_3 and drying) with acidified 30% TBP in *n*-dodecane gave satisfactory thorium and uranium recoveries; a two-step stripping flowsheet, in which relatively good uranium-thorium separation was achieved, was also demonstrated.

Other solvent extraction studies included determinations of the solubility of $UO_2(NO_3)_2$ in di-sec-butyl phenylphosphonate–diethylbenzene mixtures and of the solubility of $Th(NO_3)_4$ in 30% TBP with various diluents, including several normal and branched saturated hydrocarbons, benzene, and diethylbenzene. Measurements were also made of the adsorbability of 0.1 *M* HF on Dowex 50W ion exchange resin saturated with $Th(NO_3)_4$. Further demonstrations of the reduction of Pu(IV) to Pu(III) with hydrogen and a platinized-alumina catalyst were made; this method will be used for the partitioning of plutonium and uranium from FBR fuels.

The development of head-end processes for the most promising HWOCR fuel candidate, UC clad in SAP (a dispersion of Al_2O_3 in aluminum), was continued. Decladding in $NaOH$-$NaNO_3$ solutions, followed by dissolution in nitric acid and solvent extraction or anion exchange, appears to be the most satisfactory process. Another method investigated involves volatilization of the aluminum (as $AlCl_3$) in the cladding by reaction with HCl at 300°C, pyrohydrolysis to remove the residual HCl and to convert UCl_3 to U_3O_8, and, finally, dissolution of the U_3O_8 in HNO_3; alternatively, the U_3O_8 may be processed subsequently by fluidized-bed volatility methods. Processing of this fuel by the shear-leach process appears to be an unlikely choice because a significant amount of the aluminum from the SAP cladding dissolves in HNO_3.

1.1 DEVELOPMENT OF MECHANICAL PROCESSES

The engineering-scale development of the basic technology of the shear-leach process (with full-size unirradiated first- and second-generation stainless-steel-clad and Zircaloy-clad UO_2 and ThO_2-UO_2 power reactor fuel elements) has been completed. The process is now being used by Nuclear Fuel Services, Inc., in their reactor fuel processing plant near Buffalo, New York.

Work this year included studies and mechanical tests of the applicability of the shear-leach process to third-generation LWR fuels, leaching studies of Zircaloy-clad urania-thoria fuels, and continued development of the delayed-neutron leached-hull monitor. In addition, we began mechanical processing studies of HTGR fuels [coated $(Th,U)C_2$ or $(Th,U)O_2$ fuel particles incorporated in a graphite matrix or cemented in holes in a graphite block] and LMFBR fuels (UO_2-PuO_2 and UC-PuC).

Fuel Disassembly and Shearing Studies

The large number of thermal power reactors (LWR's) that are expected to begin operation during the period 1969–72 prompted a detailed study of the designs of third-generation fuel assemblies to determine if the latter could be satisfactorily processed by conventional fuel disassembly and shear-leach methods.

The study was preceded by on-site visits to most of the principal producers of power reactors and power reactor fuels. Based on detailed data obtained during these visits, a typical third-genera-

tion assembly will be comprised of 49 to 173 Zircaloy-2 or -4 tubes containing UO_2 (^{235}U enrichment ~3%) and having stainless steel ends. It will be about $7\frac{3}{8}$ or $8\frac{1}{4}$ in. square in cross section and will have 12 ft of active length. Grids will be made from either brazed Zircaloy with Inconel or stainless steel inserts or from sheet metal with wire inserts. All fuel tubes will contain springs to hold the fuel pellets in place during handling and transport. These springs will vary in length from 3 to 16 in. and will usually be made of Inconel or carbon steel; however, other materials, including Zircaloy, are being tested for this application. In general, Zircaloy-4 appears to be the most popular alloy for use in fabricating the assemblies.

The results of the subsequent study indicated that all third-generation fuels now in existence or currently proposed can be processed by a shear-leach head-end method. The inert end hardware holding the multitubular assembly together can easily be removed by a simple transverse sawing operation or the removal of nuts from threaded tie rods. Then, all assemblies can be completely taken apart by withdrawing the individual fuel tubes or rows of tubes in a tube puller. The remaining part of the assembly, which becomes a solid waste, consists of grids held together by several empty tubes (formerly containing control rods) or by several solid-metal, small-diameter tie rods. Casings and sheaths no longer present a problem in disassembly operations since they either are not used or are removed by the reactor operator prior to the shipping of fuel to the processor. A cropped assembly can be sheared intact or, if disassembled, as individual fuel tubes, rows of tubes, or a reassembled bundle of loose tubes. However, when assemblies are sheared intact, grids used to align and support fuel tubes and to tie an assembly together can be troublesome in the shearing operation. For example, if a shear cut is made immediately before and after a grid, or directly on one, chunks are produced which may clog the shear discharge chute or the fuel baskets. If continuous leachers, such as vibratory conveyors, are used, portions of such chunks may protrude above the surface of the leach acid, causing incomplete leaching of core material. There is no obvious practical answer to this problem at present.

In order to evaluate the shearing of third-generation fuel assemblies, the ORNL 250-ton prototype shear was modified so that prototypes as large as 10 in. square could be accommodated. The shear stroke was increased from 9 to $10\frac{3}{16}$ in., and the gag stroke was increased from $2\frac{5}{8}$ to $4\frac{5}{8}$ in. New gag guides, fixed and moving blades to shear 10- by 10-in. shapes across flats, and a new feed envelope and collapsible pusher head were installed. The shear ram was also equipped with new D-2 gibs and Stellite 6-B liners.

For the tests, two prototype assemblies (one of which is shown in Fig. 1.1) were fabricated from two Consolidated Edison core B fuel assemblies. One of the reconstituted prototypes was a $9\frac{1}{2}$-in.-square, 24- by 24-tube array consisting of 576 lead-filled tubes 0.300 in. in diameter by 21 in. long on $\frac{3}{8}$-in. centers; the other was a 10-in.-square, 22- by 22-tube array consisting of 484 porcelain-filled tubes 0.340 in. in diameter by 21 in. long on 0.425-in. centers. Each assembly contained two leaf-spring grids fabricated by welding together sections of prototype Consolidated Edison core B grids.

Leaching of Zircaloy-Clad ThO_2-UO_2

Leaching tests of sheared Zircaloy-clad urania-thoria were made to determine the extent to which the cladding and cladding fines are dissolved by fluoride-catalyzed Thorex dissolvent (13 *M* HNO_3–0.05 *M* F^-–0.05 *M* Al^{3+}) and to determine whether the dissolved zirconium interferes in the subsequent Acid-Thorex solvent-extraction step. About 99.8% of the thorium and the uranium were leached from unirradiated sol-gel ThO_2-UO_2 in 24 hr by the dissolvent; during this time about 1.5% of the Zircaloy cladding was also dissolved. The product solution contained 264 g of thorium per liter, 8.3 g of uranium per liter, and 1.5 g of zirconium per liter. Several experiments showed that only ~0.05 and ~0.01% of the Zircaloy were present in the potentially hazardous size range (–40 mesh) after 7 and 24 hr, respectively, of leaching. Preliminary solvent extraction tests indicated that about 70% of the zirconium in solution is precipitated when the leachate is made acid deficient. It was concluded that the shear-leach process can be used satisfactorily with this type of fuel despite the disadvantage of having some dissolved Zircaloy in the waste stream.

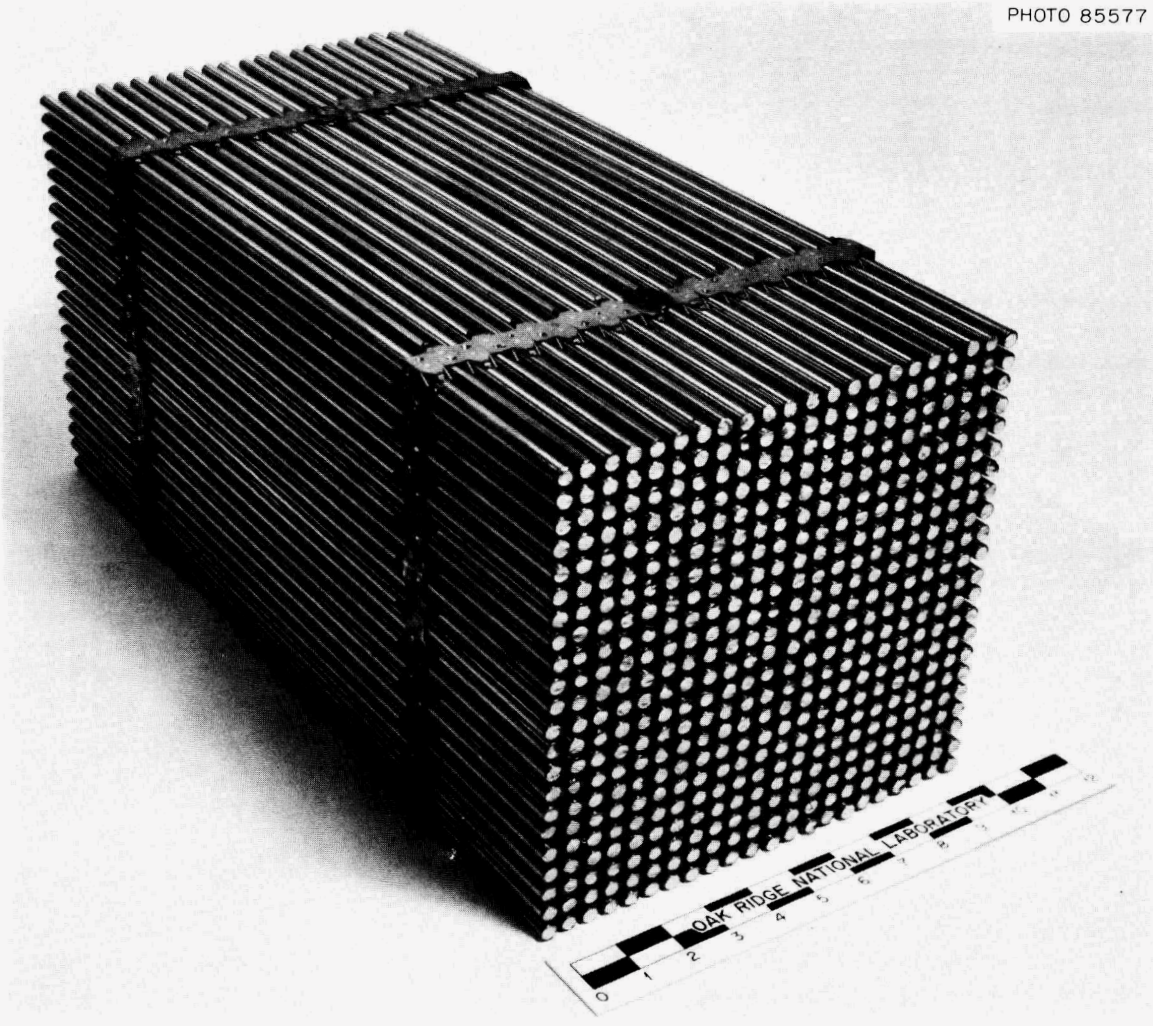

Fig. 1.1. Prototype Fuel Assembly Consisting of 484 (22 by 22 Array) Porcelain-Filled 0.340-in.-diam by 21-in.-long Stainless Steel Tubes. Leaf-spring grids were fabricated by welding together sections of Consolidated Edison core B grids.

Leached-Hull Monitor Development[1]

Two devices for monitoring sheared and leached cladding hulls are under development in the United States: a delayed-neutron monitor (ORNL), and a gamma spectrometer monitor (General Electric) for the proposed Midwest Fuel Reprocessing Plant. The latter instrument appears to be satisfactory for all Zircaloy-clad fuels but is, we believe, of marginal use for stainless-steel-clad fuels. Since the fuel for thermal power reactors is almost exclusively clad in Zircaloy, the General Electric monitor is probably satisfactory for use in the processing of LWR fuels; however, for a fast-breeder fuel, which will be clad in stainless steel, the delayed-neutron monitor appears to be the better choice.

In order to provide basic data for the evaluation of the leached-hull monitor, calculations[2] have been made to determine the induced activities in nuclear reactor cladding materials. Results have been obtained for stainless steel, Zircaloy, and

[1] J. E. Strain and W. J. Ross of the Analytical Chemistry Division have assisted in this work.

[2] E. D. Arnold, *Calculated Induced Activities in Nuclear Reactor Fuel Cladding Materials*, ORNL-4065 (in press).

graphite. They are presented in terms of specific activities (at the time of reactor discharge) per gram of parent element, as a function of flux and irradiation time. Decay-factor tables and graphs are also provided to enable the user to calculate the specific activity after any decay period. Gamma emission rates are given for use in shielding calculations, and beta and gamma watts are shown for heat calculations. The report[2] also includes a few sample problems to illustrate the use of the data.

Evaluation of the delayed-neutron monitor for leached cladding is being continued; a full-sized prototype unit (Fig. 1.2) was operated under hot-cell conditions to detect undissolved fissionable material in the presence of an 830-r/hr ^{60}Co gamma source to simulate the induced radioactivity in the leached cladding. The detection instruments were able to detect and locate as little as 0.010 g of ^{235}U. The minimum amount of uranium could be detected within a maximum factor of 2.3, depending on its location in an 8-in.-diam by 8-in.-high section of leacher basket. Figure 1.3 shows the delayed-neutron count as a function of the distance from the center line of the neutron beam passing through the basket.

The operating sequence of the monitor provided for a leacher basket (8 in. diam by 5 ft long), containing leached fuel cladding, to be lowered in 8-in. increments through an axial hole in a 25-in.-diam by 24-in.-high polyethylene moderator. A 2-in.-thick inner lead liner in the moderator hole and 0.5-in.-thick lead shields around the detector tubes were used to help prevent degradation of the tubes by gamma radiation. The ^{60}Co gamma source was pneumatically inserted from a lead carrier to the center position of the leacher basket. A 150-kv Cockcroft-Walton accelerator was used to generate neutrons (3 to 5 $\times$ 10^{10} neutrons/sec) to activate any residual fuel in the hulls in the leacher basket. A sequence timer controlled the analysis cycle automatically. Delayed neutrons

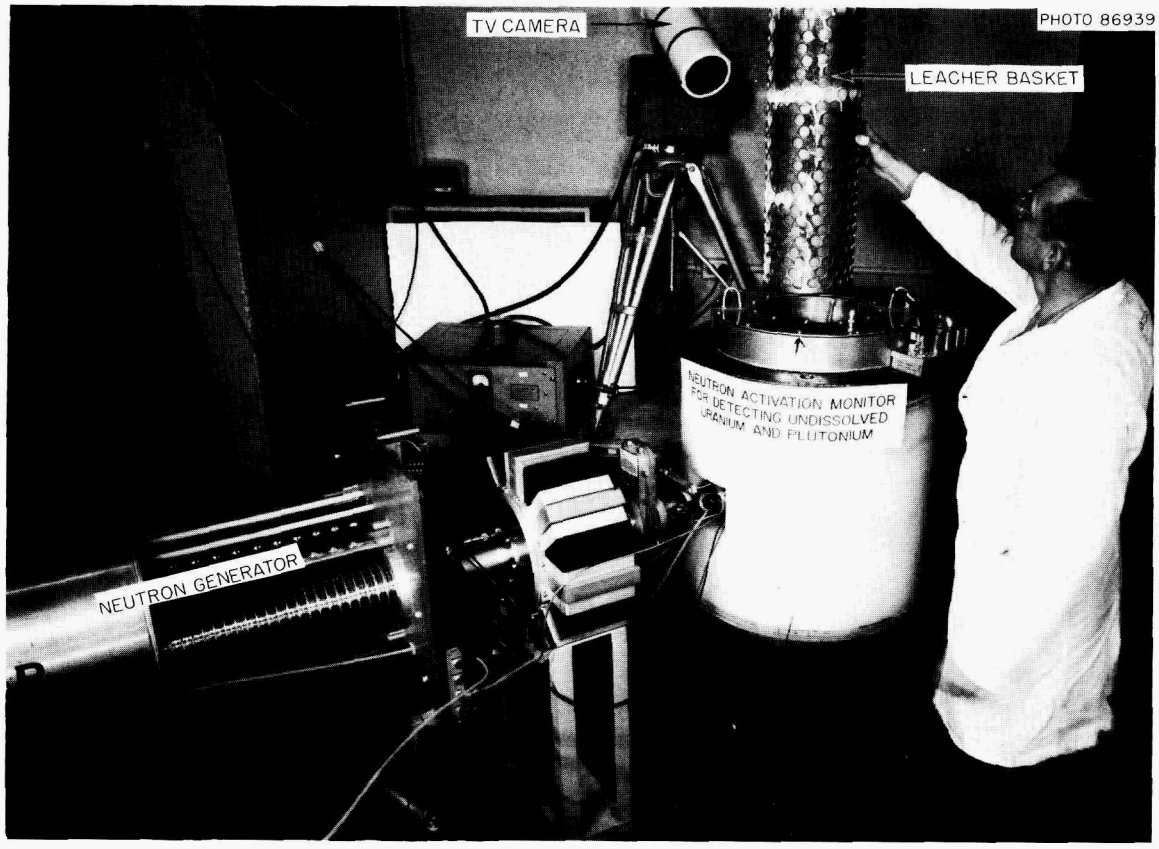

Fig. 1.2. Neutron Activation Apparatus and Prototype Leached-Hull Monitor.

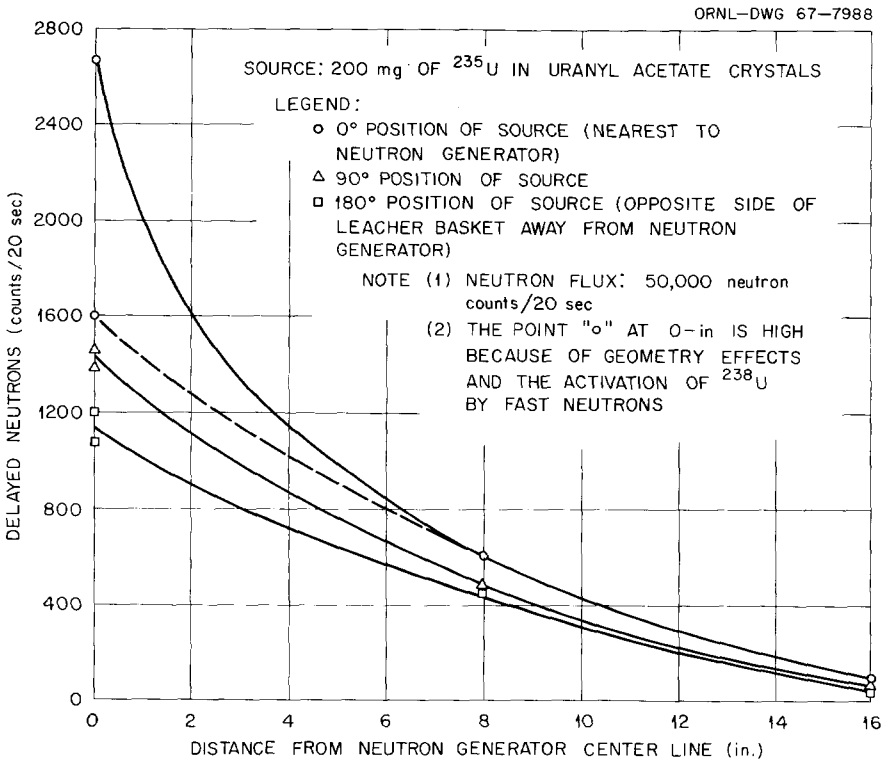

Fig. 1.3. Delayed Neutrons Detected vs Source Distance from Center Line of Generator Beam.

from any ^{235}U and ^{239}Pu present were detected by the BF_3 tubes and counted by using two decade scalers.

The six standard 1-in.-diam BF_3 detector tubes, equally spaced on a 7.625-in. radius, operated efficiently during initial tests; however, degradation from gamma radiation reduced the efficiency by 10 and 25% after exposures for 5 and 60 min respectively. This rapid degradation can be retarded, however, by the use of a getter such as charcoal, which was used in 2-in.-diam BF_3 tubes in previous experiments.

A modified version of the leached-hull monitor, designed to operate in radiation fields with intensities as high as 1×10^5 r/hr, will be evaluated in future tests. If this detector and its associated nanosecond electronics system operate as expected, the monitor can be used in the processing of either short- or long-cooled reactor fuel, regardless of the type of cladding, with a sensitivity that is lower than the allowable ^{235}U loss level by a factor of 50.

Mechanical Processing of HTGR Fuels

The presently proposed graphite-base HTGR fuel designs employ either a dispersion of coated fuel particles in a graphite matrix (Peach Bottom) or the use of holes in graphite blocks that are filled with loose or cemented coated fuel and fertile particles (TARGET, PSC). Mechanical processing experiments were begun this year to evaluate various means of size-reducing both types and of selectively removing fuel particles from the latter.

We investigated the feasibility of shearing as a method of reducing graphite-base HTGR fuel to a size that is suitable for fluidized-bed burning or subsequent grinding to -140 mesh prior to leaching. The graphite fuel pieces that were sheared were prototype Public Service of Colorado (PSC) blocks, $6\frac{1}{4}$ in. square by 6 in. long, with 0.580-in.-diam coolant holes and 0.420-in.-diam unfilled fuel holes. The fuel blocks were sheared across the diagonal with a conventional stepped blade

to $\frac{1}{2}$- and 1-in. lengths and across the flats, using a straight blade, to $\frac{1}{2}$-in. lengths. In both cases, the fuel did not shear evenly but fractured into random-shaped and -sized chunks varying from fine dust to wedge-shaped pieces 2 to 3 in. on a side and of a thickness equal to the length of cut. The fuel sheared in an acceptable fashion for approximately 50% of the cross-sectional area, but large irregular pieces were dislodged from the remainder of the cross section. The force required to shear the prototypes was insignificant. It was concluded from these tests that the non-uniformity of product and the uncertainty of holding and feeding blocks of graphite that break randomly makes size reduction by shearing an unattractive operation.

In other tests, the unirradiated prototype PSC fuel blocks were mechanically broken to determine whether such an approach would produce suitable feed for a hammer mill or roll crusher. The test specimens were 6-in.-thick sections of prototype PSC graphite fuel blocks (hexagons measuring 14 in. across the flats, with coolant and unfilled fuel holes). In these tests a fuel block was placed on edge in an open-top metal box, and a 500-lb cylindrical weight was dropped axially from heights of 5, 7, and 10 ft. In each case, approximately 30% of the graphite section was broken into various-sized pieces ranging from splinters 6 in. long to fine powder; the remainder of the section was broken into four or five large wedge-shaped pieces. The results of these tests indicate that breaking PSC graphite fuel blocks by the "pile-driving" technique is not practical and does not warrant further investigation.

Several methods of removing the coated fuel particles from holes in PSC type fuel blocks have been suggested: (1) pressing the cylindrical compact of cemented fuel particles (beads) from the channel, (2) burning out the low-density binder holding the beads together, and (3) using a high-velocity water flow to erode the binder and thus dislodge the beads from the channel. The beads might then be screened into two size fractions in order to separate the fissile beads from the fertile beads for further processing in separate chemical systems.

The initial testing of hydraulic or jet erosion methods for removing the fuel beads was encouraging. A three-hole nozzle, which delivered water at 1000 psi, eroded the cemented fuel beads from a 0.45-in.-diam graphite hole at a penetration of about 0.2 to 0.3 in./sec. Unfortunately, many of the pyrolytic carbon coatings were fractured. The irregular coatings of carbonized phenolic binder did not interfere with sieving of the beads into two fractions in the proper proportions. The original charge of coated beads was 60% +30 mesh and 40% −40 mesh.

Addition of 15% carbon-black filler to the phenolic binder, followed by carbonization, resulted in a fuel compact that was very resistant to jet erosion. The rate of bead dislodgment was only about 5% of that found in the previous tests. Modifications to the test equipment are being made to increase the operating pressure to about 6000 psi.

1.2 DEVELOPMENT OF BURN-LEACH PROCESS FOR GRAPHITE-BASE FUELS

The prime contender in the United States for a high-temperature gas-cooled reactor fuel consists of coated $(Th,U)C_2$ or $(Th,U)O_2$ fuel particles incorporated in a graphite matrix (Peach Bottom) or cemented into holes in a graphite block (TARGET, PSC). Several processes are being developed for this fuel. The burn-leach process is described below, and the grind-leach process is discussed in the following section. Work on a pressurized aqueous combustion (PAC) process was abandoned because it appeared to be inferior to the first two methods. Mechanical preprocessing is also being investigated (see Sect. 1.1).

The burn-leach process is the preferred process for fuels containing carbon-coated fuel particles; however, for SiC-coated fuel particles, grind-leach, or a modified grind-burn-leach process, must be employed.

The burn-leach process involves rough crushing of the graphite fuel to −4 mesh, burning in air or oxygen at 600 to 750°C in a fluidized bed of alumina, and leaching of the thorium and uranium oxide ash with fluoride-catalyzed nitric acid for subsequent solvent extraction. Development of the process, using unirradiated carbon-coated-particle fuel samples, was completed previously;[3] work during this period has consisted of the hot-cell demonstration of the process. The two major unsolved problems in the "cold" tests were: the

[3] *Chem. Technol. Div. Ann. Progr. Rept. May 31, 1965*, ORNL-3830, pp. 34–36.

ORNL DWG 67-1519R1

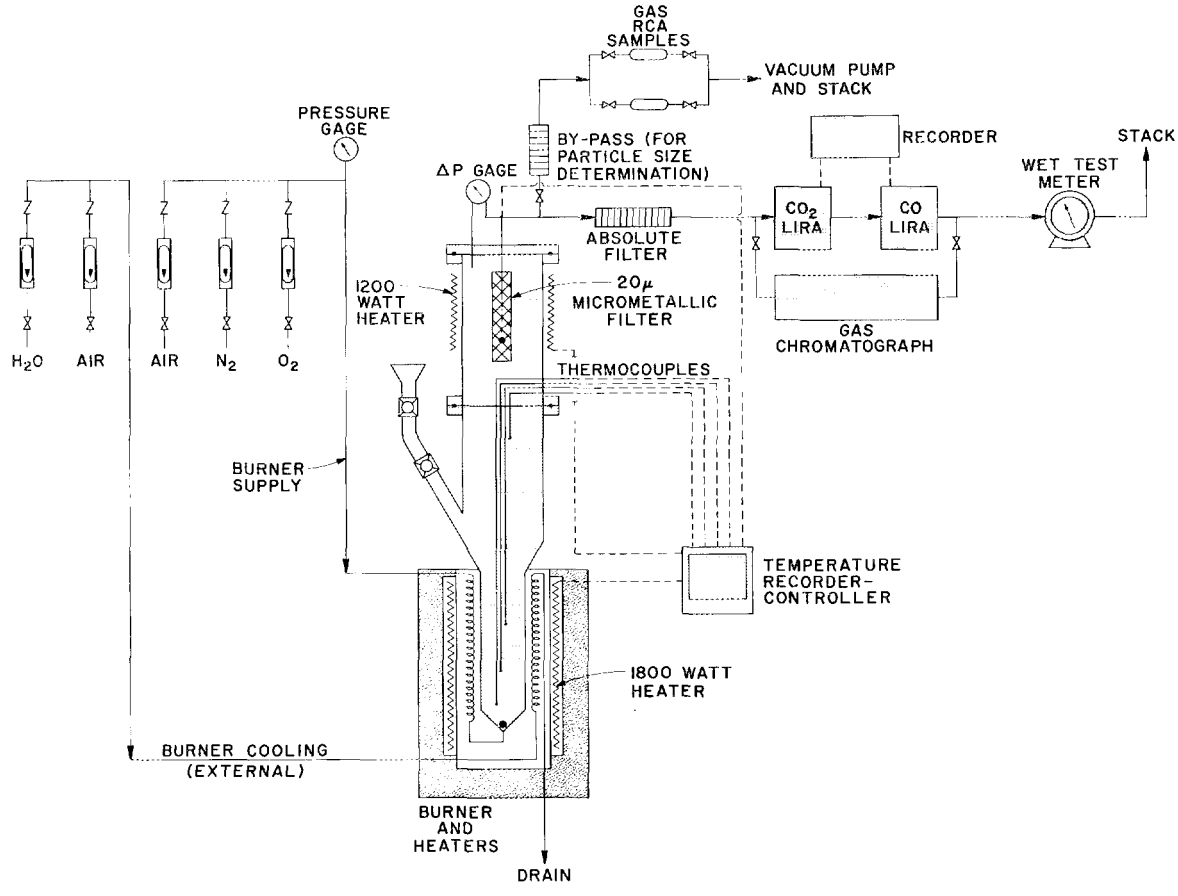

Fig. 1.4. Schematic Flowsheet of Hot-Cell Fluidized-Bed Burning Equipment.

determination of the amount of fission products that would be present in the burner off-gas, and the best method for removing these contaminants.

In the hot-cell tests the volatility and the fate of the fission products during burning and leaching, the decontamination of the off-gas stream, and the combustion of the fuel itself were intensively investigated.[4] Irradiated fuel samples were burned in a batch-operated nickel burner (Fig. 1.4) that contained a fluidized bed of 200 g of equal weights of nominal 60-, 90-, and 120-mesh Norton RR alumina as the heat-transfer medium. Nominal 100-g batches of −4 mesh General Atomic GAIL-3A fuel compacts (irradiated to a burnup of 8800 Mwd/ton) and GAIL-3B fuel compacts (irradiated to a burnup of 41,500 Mwd/ton) containing 7% uranium and 16% thorium as carbon-coated $(Th,U)C_2$ particles were burned at 750 ± 25°C in a stream of nitrogen and oxygen (flow rate 4 liters/min). Overall oxygen utilization was greater than 90%. The bed temperatures, the oxygen utilization, and the CO and CO_2 content of the off-gas during a run are shown in Fig. 1.5. The burner off-gas was first passed through a primary filter (20-μ sintered stainless steel having a $\frac{1}{4}$-in. coating of carbon dust) located in the top of the burner. It was then passed through absolute filters (for final removal of fission products), continuous CO_2 and CO analyzers (for process control), and a wet test meter. Gas samplers and a bypass filter (for the determination of particulate size) were also provided.

After each burning, the ash (or a representative fraction) was leached with boiling fluoride-catalyzed nitric acid, and the solutions and the leached Al_2O_3 were analyzed for heavy metals

[4] J. R. Flanary *et al.*, *Hot-Cell Evaluation of the Burn-Leach Process Using Irradiated Graphite-Base HTGR Fuels*, ORNL-4120 (in preparation).

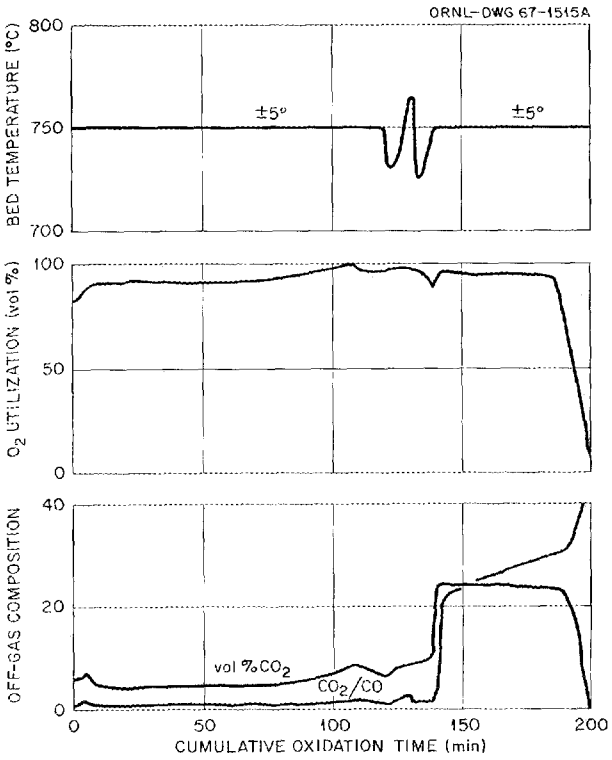

Fig. 1.5. Off-Gas Data, Oxygen Utilization, and Bed Temperatures During Fluidized-Bed Combustion.

and fission products. The dust adhering to the primary micrometallic filter was also collected and analyzed.

Fluidized-Bed Combustion

Data collected during the burning tests showed the influence of important parameters on the combustion of the HTGR fuel. By assuming that the rate of combustion is dependent upon the chemical reaction of carbon with oxygen at the reaction surface and upon the mass transport of oxygen to the reaction surface, an equation was derived[5] that qualitatively relates the combustion rate to the oxygen pressure and the nitrogen pressure in the feed gas, the bed temperature, and the particle size:

$$\frac{r_c}{W} = \frac{K_2\,\phi(T)\,P_{O_2}}{\frac{P_i}{P}K_3\,\frac{1}{K_4 T^{0.17} d^{-0.78} + 2T^{0.5} d^{-1}} + T^{0.5}\cdot\frac{1}{K_1}\,e^{E/RT}},$$

where

r_c = rate of carbon combustion, g/min,

W = fuel inventory, g,

K_{1-4} = constants,

$\phi(T)$ = temperature function of primary CO production,

P_{O_2} = oxygen pressure in feed gas, atm,

P_i = inert gas pressure in feed gas, atm,

P = total pressure, atm,

T = bed temperature, °K,

d = mean particle diameter, cm,

E = activation energy of carbon-oxygen reaction, cal/mole,

R = gas constant, cal mole^{-1} (°K)$^{-1}$.

Our data showed that the reaction of the graphite fuel with oxygen in the fluidized bed was first order with respect to oxygen pressure. Below 600°C the rate-controlling factor appeared to be the kinetics of the chemical reaction (Fig. 1.6); the apparent activation energy was about 18.9 kcal/mole. Above 600°C, the preferred operating condition, the reaction rate appears to be controlled by the diffusion of oxygen through a stagnant film surrounding the fuel particles, and the apparent activation energy was about 2.8 kcal/mole at the higher temperatures.

An increase in the partial pressure of the combustion products in the stagnant film produces a slight decrease in the exponent of the oxygen pressure because of increased diffusional resistance. In the diffusion-controlled region, a decrease in the pressure of the inert gas causes a more rapid increase in the reaction rate than can be attributed to the oxygen pressure alone; this is due to decreasing diffusional resistance. Our experience showed that the oxygen should be

[5] H. O. Witte, "Fluidized-Bed Combustion of Graphite-Base Nuclear Fuels," paper submitted for publication to *Industrial and Engineering Chemistry, Process Design and Development.*

diluted with about 20% nitrogen to facilitate control of the burner temperature.

Off-Gas Decontamination

During fluidized-bed combustion of irradiated HTGR fuel, the burner off-gas was contaminated by gaseous fission products, volatile fission product oxides, and radioactive solids that were entrained in the fly ash. The average size of the combustion ash particles was about 40 μ; entrained particles, along with unburned fuel and carbon, were efficiently trapped by the 20-μ-porosity sintered-metal filter. The total amount of dust on the filter was about 1% of the original bed weight and contained from 43 to 78% carbon fines. The remainder consisted of heavy-metal and fission product oxides. The dust layer acted as a highly efficient filter aid. Decontamination factors (ratio of total activity in the bed to that passing through the dust-covered filter) were on the order of 10^6. No significant effect of oxygen pressure on the volatility of individual fission products was noted during portions of the burning runs having high (>90%) or low (<50%) oxygen utilization.

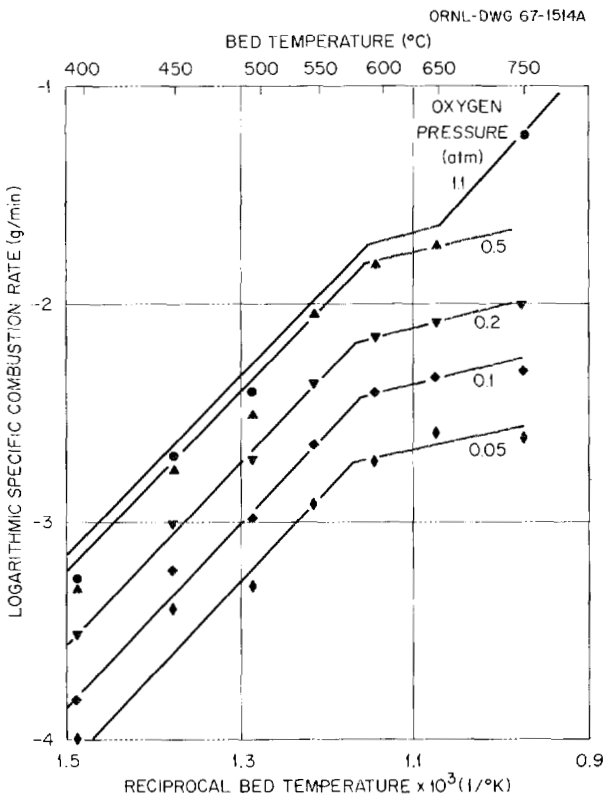

Fig. 1.6. Arrhenius Plot of Combustion Rate in Fluidized-Bed Burning of HTGR Fuel.

The amount of fission products released through the sintered-metal filter was found to be dependent on the filter temperature. Table 1.1 shows that decontamination factors of 10^6 to 10^7 were obtained when the filter temperature was held below 300°C; however, at 500°C it was only 10^2, probably because of the passage or release of volatile fission products.

The activity of the off-gas leaving the sintered-metal filter was predominantly due to ^{137}Cs. The specific activities were 1.3×10^{-11}, 8.1×10^{-11}, and 8.1×10^{-8} μc/cc at filter temperatures of 100, 285, and 500°C. These activities may be compared with the maximum permissible concentration of ^{137}Cs in air (2×10^{-9} μc/cc) for continuous exposure of the general population in the vicinity of an atomic energy plant. It must be remembered, however, that the fuel used in these

Table 1.1. Effect of the Temperature of the Sintered-Metal Filter on the Removal of Fission Products by Primary Burner Filter

Filter Temperature (°C)	Decontamination Factors for Filtered Off-Gas				
	Gross Gamma	^{106}Ru	^{125}Sb	^{137}Cs	^{144}Ce
100	2.71×10^7	5.87×10^7	3.60×10^6	2.08×10^7	5.68×10^7
160	8.10×10^6	1.36×10^6		8.74×10^6	9.35×10^5
285	7.23×10^6	1.85×10^7	1.15×10^7	9.55×10^6	6.11×10^6
500	8.10×10^2	$\geq 1.5 \times 10^4$	$>7.2 \times 10^3$	8.47×10^3	$\geq 9.73 \times 10^4$

experiments was cooled for about four years and that the shorter-lived isotopes have not been studied.

In the filter cartridges that were attached to the burner for final cleanup of the off-gas stream leaving the sintered-metal filter, five layers of air-conditioning filter (American Air Filter No. 50 FG Filterdown, each about $\frac{1}{2}$ in. thick before compression) reduced the particulate activity of the off-gas to background level. This filter medium is made of 1.5-μ-diam glass fibers that are coated with a phenol-formaldehyde binder; its density is 20 mg/cm^2. Krypton-85 was the only radioactive component that could be detected in the gas that was released to the atmosphere.

Leaching of Fluidized-Bed Products

Thorium, uranium, and fission products were leached from the fluidized bed with boiling Thorex reagent, 13 *M* HNO_3–0.05 *M* HF–0.01 *M* $Al(NO_3)_3$. Table 1.2 summarizes the data obtained in the leaching experiments. Nearly quantitative recovery of the heavy metals was achieved with one 5-hr plus one 2-hr reflux with fresh dissolvent, followed by washing with water. These results suggest that a small, variable fraction of each fission product may have become adsorbed on the alumina as a refractory film during the high-temperature combustion of individual fuel particles. Additional leaching and washing dissolved only 0.3% of the deposited gamma emitters from the alumina.

Table 1.2. Averaged Results from Leaching Alumina–Fuel-Ash Beds Derived by Burning Irradiated General Atomic GAIL-3A and GAIL-3B Fuels

Runs FB-17 to FB-24

	Recovered by Leaching[a] (%)	Retained by Alumina[a] (%)
Thorium	99.3 ± 0.4	0.7 ± 0.4
Uranium	99.8 ± 0.2	0.07 ± 0.07
Gross gamma	94.4 ± 4.8	5.0 ± 2.7
^{106}Ru	83 ± 15	17.0 ± 16.1
^{125}Sb	90 ± 16	10 ± 16
^{136}Cs	97 ± 2.8	5.9 ± 2.0
^{144}Ce	96 ± 3.4	3.1 ± 2.8

[a]Within 95% confidence level.

Bed Recycle Studies

The major product of the fluidized bed is alumina, which must be recycled to minimize solid waste volumes. The alumina : ash weight ratio should always be greater than 3 to provide sufficient inert material in the fluidized bed[4] for the adequate dissipation of fission product heat. Since the average diameter of the alumina particles is about 200 μ and the average diameter of the ash particles was found to be about 40 μ in once-through tests, screening the bed through a 120-mesh sieve should separate the bulk of the fuel ash from the alumina. By leaching only the −120 mesh fraction, one should be able to drastically reduce the amount of bed that must be circulated through the leacher.

This procedure was tested for five cycles using two types of fuel: unirradiated Peach Bottom fuel and irradiated GAIL-3B fuel. Fresh alumina and fuel were added after each sieving to maintain a constant initial weight for the bed. We found that the thorium (and uranium) in the +120 mesh fraction increased about 4% per cycle, rendering this simple approach impractical. However, it was calculated that, if part of the +120 mesh fraction is also leached, the heavy metals removed by leaching could be made to balance the input to the burner and permit steady-state operation. To maintain a weight ratio of 2 for feed material to recycle material, calculations predict that about 35% of the total +120 mesh alumina must be leached with the −120 mesh fraction. Other recycle ratios, sizes of fluidized-bed particles, and types of operation may reduce this fraction significantly. The smaller the amount of material that must be leached, the smaller will be the required size of the leacher and the associated handling equipment.

1.3 DEVELOPMENT OF GRIND-LEACH PROCESS FOR GRAPHITE-BASE FUELS

In the grind-leach process, graphite-base fuels containing carbon- or SiC-coated $(Th,U)C_2$ or $(Th,U)O_2$ fuel particles are crushed to −4 to −6 mesh and then ground in a roll crusher to −100 to −140 mesh to fracture all the particle coatings. The ground fuel is leached with nitric acid or Thorex dissolvent [13 *M* HNO_3–0.05 *M* HF–0.01 *M* $Al(NO_3)_3$]. The unreacted graphite is washed free of soluble heavy metals, and the leach and

wash solutions are combined for feed adjustment prior to solvent extraction.

The new experimental roll crusher that was designed and built last year[6] was evaluated with broken (−6 mesh) HTGR fuel; additional laboratory leaching tests were made with ground unirradiated HTGR and UHTREX fuel samples and with pyrolytic-carbon-coated ThO_2 sol-gel fuel beads; further engineering-scale graphite residue filtration tests were performed, and a hot-cell evaluation of the grind-leach process was made with irradiated HTGR (General Atomic GAIL compacts and AVR) fuel samples.

Roll Crusher Evaluation Tests

Quantitative recovery of uranium and thorium from coated-particle fuels requires that the coating of every fuel particle be broken prior to leaching. Previously reported work[6] with a small commercial double-roll crusher demonstrated its applicability to the Peach Bottom type of HTGR fuel [carbon-coated $(Th,U)C_2$ fuel particles in a graphite matrix] and led to the fabrication of a much improved ORNL-designed roll crusher. This machine has several notable features that have not been incorporated in commercially available units:

1. a preloading mechanism between shafts, which minimizes undesirable deflections that would otherwise result in a significant increase in the spacing between rolls during operation;
2. hardening of the two 4-in. by 12-in.-diam rolls to Rockwell 60 (C scale) for maximum resistance to abrasion and indentation;
3. a clearance of only 0.003 in. between the ends of the rolls and the heavy ($1\frac{1}{2}$-in.-thick) side plates to ensure that the material fed to the crusher will not bypass the two roll faces;
4. a pivoting yoke that supports one roll to permit rapid and precise adjustment of the roll-to-roll spacing;
5. horizontal gage rods (riding on the shaft of the adjustable roll) to provide a means of continuously monitoring the shaft position to detect translational movement that would indicate a change in the preset roll-to-roll spacing under load.

The performance of the new roll crusher was not accurately predicted from earlier measurements of nip angle that were made with the small commercial machine; in general, the new rolls can accommodate larger particles than expected. Three of these roll crushers in series would provide a capacity of about 0.25 metric ton (U + Th) of HTGR fuel per day.

A typical size distribution of Peach Bottom compacts crushed to about −6 mesh in a 15- by 8-in. hammer mill is shown in the lower curve of Fig. 1.7 (a Rosin-Rammler distribution diagram); the upper curve describes the size distribution of the final product from the roll crusher, using the optimum sequence of three roll spacings: 0.030, 0.004, and 0.002 in.

The effectiveness of hammer milling and roll crushing in fracturing the coatings of the fuel particles was evaluated by leaching tests. These tests showed that about 30% of the coatings of Peach Bottom fuel particles [150- to 200-μ-diam $(Th,U)C_2$ coated with a 50- to 60-μ-thick layer of pyrolytic carbon] were broken during rough crushing to −6 mesh in the hammer mill. Three passes of the hammer mill product through the roll crusher were required to increase the proportion of fractured coatings to $\geq$99.8%. When graphite fuel consisting of 75-μ-diam UC_2 particles was crushed and leached under similar conditions, the uranium recovery was only 99.0%. This suggests that coated-particle fuel containing $\sim$150-μ $(Th,U)C_2$ kernels may define the lower limit for fully effective grinding in the 12- by 4-in. double-roll crusher.

The rate of roll wear was not well established because the limited quantity of fuel (35 kg) that was crushed produced a barely measurable change ($\sim$0.0005 in.) in roll radius; the surface finish was unchanged at 12 to 15 μin.

Leaching Experiments with Unirradiated Fuel

Laboratory-scale studies[7] of the leaching of unirradiated HTGR fuels (Peach Bottom and carbon-coated sol-gel ThO_2) and UHTREX fuels have been made using samples that were rough-crushed to −6 mesh and then roll-crushed to −140 mesh[6] to ensure rupture of the coated particles.

---

[6] *Chem. Technol. Div. Ann. Progr. Rept. May 31, 1966*, ORNL-3945, pp. 28–32.

[7] L. M. Ferris, *Grind-Leach Process for Graphite-Base Reactor Fuels That Contain Coated Particles: Laboratory Development*, ORNL-4110 (June 1967).

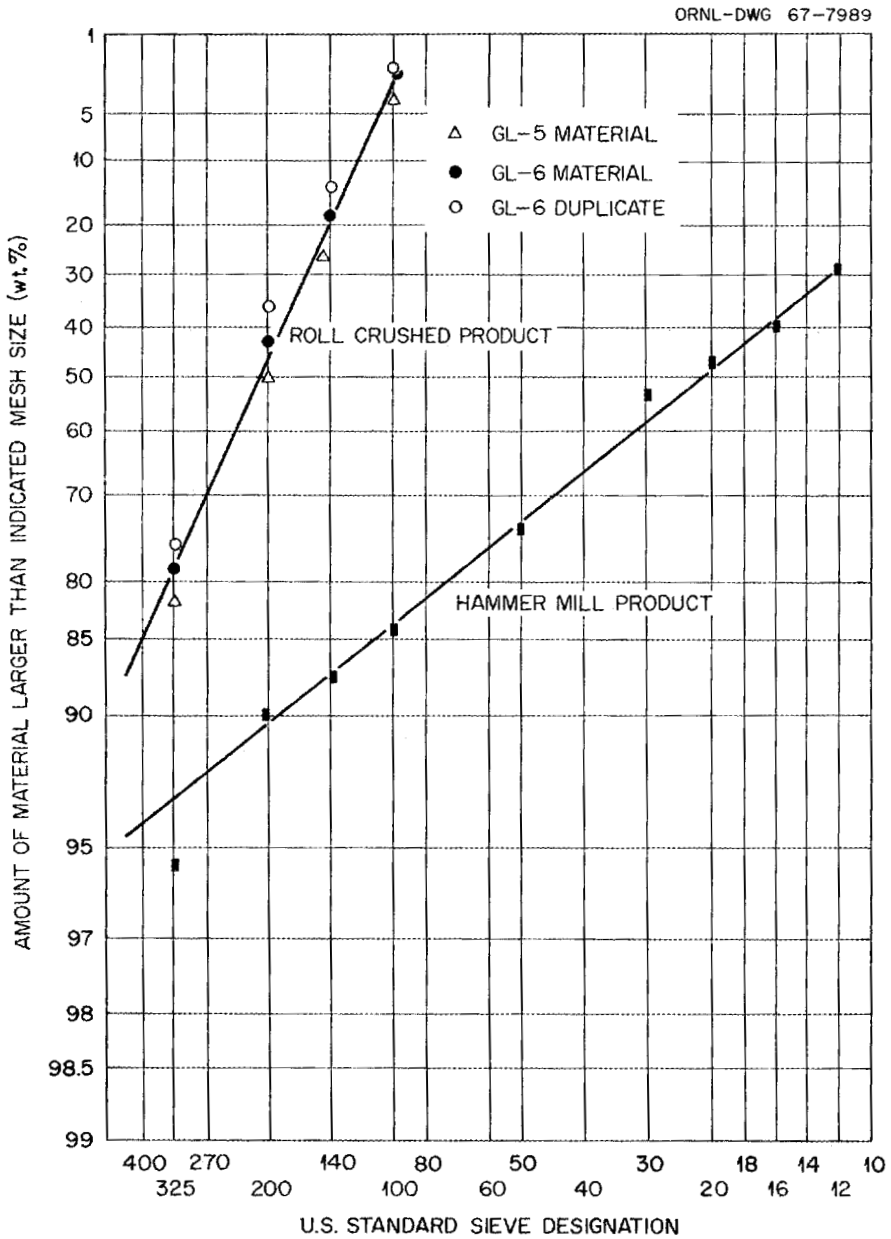

Fig. 1.7. Particle Size Distribution of Peach Bottom Fuel Compacts After Hammer Milling and After Roll Crushing at Optimum Roll Spacing.

Most of the leaching studies were conducted with prototype Peach Bottom fuel. This fuel (3% uranium and 13% thorium) was composed of $(Th,U)C_2$ particles, coated with a single layer of pyrocarbon, that were dispersed in a graphite matrix. The prototype UHTREX fuel[8] (about 8% uranium) consisted of triplex-coated UC_2 particles dispersed in a graphite matrix. The three coatings were: (1) an inner buffer layer of porous carbon, (2) an intermediate layer of isotropic pyrocarbon, and (3) an outer layer of granular pyrocarbon.

In one series of experiments, samples of roll-crushed Peach Bottom fuel were leached for 5 hr with the volumes of boiling nitric acid solution required to produce solutions 0.2 *M* in Th + U (if

[8] J. M. Taub and R. J. Bard, *Coated Particle Fuel Elements for UHTREX*, LA-3378 (Mar. 1, 1966).

all the contained uranium and thorium were leached). After leaching, the residue was washed thoroughly with water to ensure maximum recoveries. In a 5-hr leach the amount of uranium left in the graphite residue was usually between 0.25 and 0.5% regardless of the acid concentration, which was varied from 2 to 21.5 *M* (Table 1.3). Corresponding thorium losses to the residue were between 0.8 and 1.8%. Increasing the leaching time to 24 hr did not appear to increase the recovery of uranium or thorium. Also, the presence in the nitric acid of $Al(NO_3)_3$ and/or HF, at concentrations of 0.05 *M* each, produced no beneficial effect on the recoveries.

Multiple leaching of Peach Bottom fuel, especially with concentrated nitric acid, usually resulted in the adequate recovery of both uranium and thorium (Table 1.3). For example, after two 5-hr leaches with boiling 13 *M* HNO_3 followed by a water wash of the residue, uranium and thorium losses to the residue generally were 0.2% or less.

In leaching experiments with crushed UHTREX fuel, high uranium recoveries were difficult to achieve even when boiling 13 *M* HNO_3 was used as the leachant. After a single 5-hr leach, nearly 1% of the uranium remained in the residue; after three 5-hr leaches, the uranium loss to the residue was still about 0.24% (Table 1.3).

A few leaching tests were also made with unirradiated carbon-coated ThO_2 microspheres. One batch (OR-520) was composed of ThO_2 kernels coated with a single layer of dense pyrocarbon. Another batch (OR-521) consisted of ThO_2 kernels with a duplex coating (an inner layer of porous carbon surrounded by an outer layer of pyrocarbon). Samples of each batch were crushed to −100 mesh to rupture the particles. The crushed samples were then leached with the amounts of boiling 13 *M* HNO_3–0.05 *M* HF required to produce solutions 0.5 *M* in thorium (if all the ThO_2 dissolved). In all instances, leaching of the ThO_2 was nearly quantitative; thorium losses to the carbon residues were less than 0.01%.

The product solutions from all the above experiments contained soluble organic compounds. These compounds (mellitic acid, for example) are formed

Table 1.3. Uranium and Thorium Losses to Residue After Leaching Roll-Crushed HTGR and UHTREX Fuels with Boiling Nitric Acid

Duration of each leach: 5 hr

Experiment	Nitric Acid Concentration (*M*)	Fuel	Number of Leaches	Losses to Residue (%)		Percent of Graphite Matrix Oxidized[a]	Carbon in Leach Solution (% of total carbon in fuel)
				Uranium	Thorium		
1	2	PB[b]	1	0.39	1.80	0	0.56
2	5	PB	1	0.44	1.08		
3	13	PB	1	0.25	0.81	0	0.30
4	13	PB	1	0.25	0.89	0	0.35
5	13	UH[c]	1	0.93		2.6	0.39
6	15.8	PB	1	0.24	1.20	2.8	0.06
7	21.5	PB	1	0.38	1.70	9.4	1.6
8	3	PB	2	0.21	0.28	5.3	0.10
9	5	PB	2	0.12	0.17	5.1	0.04
10	13	PB	2	0.12	0.025	3.9	0.66
11	13	PB	2	0.057	0.12	4.6	1.2
12	13	UH	2	0.40		6.0	0.31
13	13	UH	3	0.24		6.0	0.58

[a]Based on initial composition of fuel and the assumption that the residue after leaching was pure graphite.

[b]Peach Bottom fuel.

[c]UHTREX fuel.

by reaction of nitric acid with carbon[9] (graphite and/or particle coatings) and/or uranium and thorium carbides.[10-12] In single 5-hr leaches of crushed HTGR fuels with boiling 2 to 5 *M* HNO_3, no measurable oxidation of the graphite matrix occurred; however, about 3 to 9% was oxidized as the HNO_3 concentration was increased from 13 to 21.5 *M* (Table 1.3). In two 5-hr leaches with boiling 3 to 13 *M* HNO_3, 4 to 6% was oxidized. Less than 1% of the total carbon from the fuel was generally found in the leach solution as soluble organic compounds, even when the amount of graphite matrix oxidized was significant (Table 1.3). This amount of carbon corresponded to 30 to 50% of the carbide carbon from the ThC_2-UC_2 or UC_2 particles. These results indicate that oxidation of the graphite matrix and/or the carbide particles gives CO_2 and CO as the main products and that the soluble organic compounds stem principally from the carbide carbon. Some oxidation of the carbon was also noted in the leaching experiments with the carbon-coated ThO_2 microspheres; consequently, soluble organic compounds can be expected in the solutions resulting from the leaching of practically all types of graphite-base reactor fuels.

Graphite Residue Filtration Tests

Previous filtration experiments have confirmed that the maximum recovery of uranium and thorium requires extensive washing of the graphite residue.[6] In order to measure the effects of acid concentration and acid temperature, a series of small engineering-scale washing experiments were made using ~2-ft-deep beds, each of which was contained in a 1½-in.-diam glass column; the latter was maintained at a constant temperature by heated mineral oil circulating through a glass jacket. A perforated stainless steel plate covered with graded Al_2O_3 (−6 +30 mesh) was used to support a bed of previously leached −140 mesh HTGR fuel. Preheated wash solution was metered into the filter at a rate sufficient to maintain a shallow pool over the flooded bed. Air overpressure in the vapor space at the top of the column provided the driving force to push the wash downward through the bed.

The results of seven such experiments are summarized in Table 1.4. The data indicate that acid washing, followed by a short water wash, results in lower thorium and uranium losses than extended water washing (compare all other runs with GL-5A). Losses were also reduced by increasing the temperature of the wash. A moderate reduction in acid concentration (13 to 10 *M*) and temperature (90 to 75°C) resulted in a small increase in uranium loss and no change in thorium loss.

Figure 1.8 shows the amount of soluble thorium remaining in the bed as a function of the volume of filtrate collected. When the normal ratio of filtrate volume to fuel weight (about 2 liters/kg) is used, approximately 75% of the soluble thorium is removed in the filtered leachate before the addition of wash liquid to the column is begun. About 5 liters of wash solution per kilogram of residue is required for essentially complete removal of the soluble thorium (lower curve). Washing is less efficient at the higher flow rate (upper curve) in terms of wash volume required.

To provide a solvent extraction feed that requires only dilution with water to achieve final adjustment, a recycle acid flowsheet was developed (Fig. 1.9) in which the bulk of the wash acid is returned to the head end of the process for leaching a subsequent batch of ground fuel. The leachate and the water wash are combined and diluted to obtain a final HNO_3 concentration of about 4 *M*; this treatment produces a solution that is suitable for an acid-feed thorium extraction flowsheet,[13] despite the presence of a small amount of dissolved organic compounds formed during leaching.

Previous experiments showed that a deep bed of graphite residue permits more efficient utilization of acid and water washes than a shallow bed but that it has the disadvantage of a greater pressure drop. In order to develop an improved permeability correlation, permeabilities for typical residues were measured as functions of pressure drop (ΔP), bed depth (L), and liquid viscosity (μ). Filtration rate (V) plotted vs the product of pressure gradient and reciprocal viscosity showed

[9] L. M. Ferris, *J. Chem. Eng. Data* 9, 387 (1964).

[10] L. M. Ferris and M. J. Bradley, *J. Am. Chem. Soc.* 87, 1710 (1965).

[11] P. L. Pausen, J. McLean, and W. J. Clelland, *Nature* 197, 1200 (1963).

[12] H. Imai and S. Uruno, *Nature* 206, 691 (1965).

[13] R. H. Rainey, Oak Ridge National Laboratory, personal communication (May 1967).

Table 1.4. Summary of Grind-Leach Washing Results

Run[a]	Wash Conditions[b]			Thorium in Residue		Uranium in Residue	
	Wash Liquid	Temperature (°C)	Pressure Gradient (psi/ft)	Concentration (μg/g)	Loss (%)	Concentration (μg/g)	Loss (%)
GL-5A	H_2O	90	15	1300	0.75	200	0.40
GL-5B	13 *M* HNO_3	90	15	260	0.15	69	0.14
GL-5C	10 *M* HNO_3	75	15	290	0.17	124	0.21
GL-5D	13 *M* HNO_3	90	10	260	0.15	70	0.14
GL-6A	13 *M* HNO_3	90	15	110	0.063	32	0.065
GL-6B	13 *M* HNO_3	90	3.7	110	0.063	37	0.075
GL-6C	13 *M* HNO_3	25	15	370	0.21	64	0.13

[a]A common batch of leached Peach Bottom fuel was used for GL-5 runs; another common batch was used for GL-6 runs.

[b]The graphite residue was contacted with the flowing wash liquid for 5 to 6 hr and then washed with flowing water until the uranium concentration in the effluent was reduced to approximately 1 mg/liter.

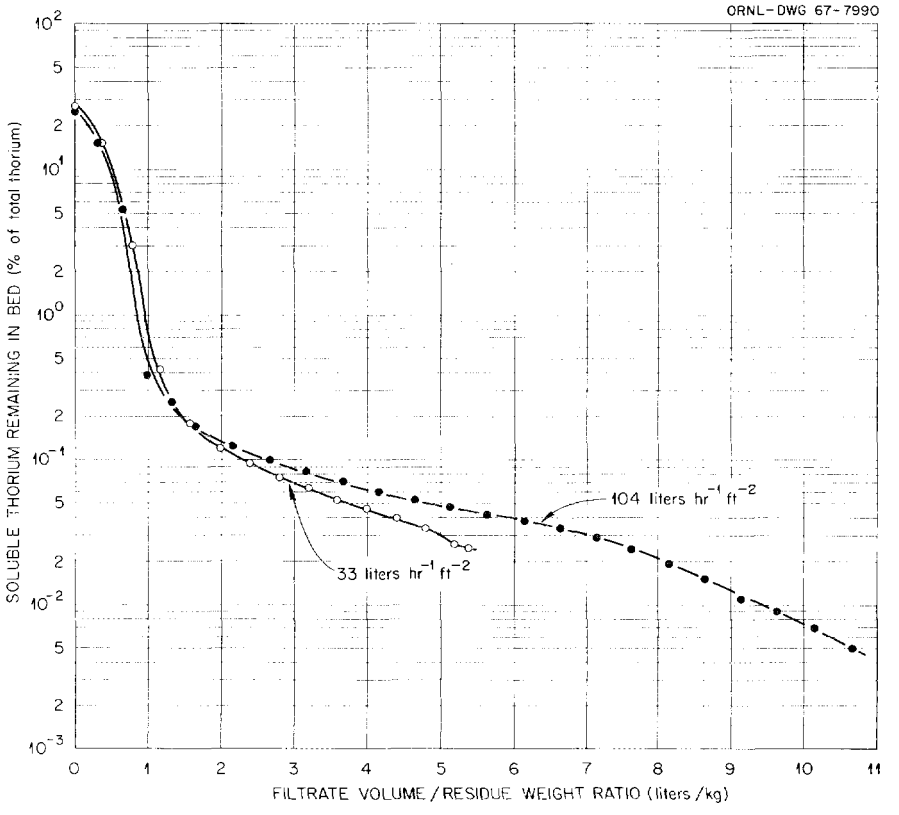

Fig. 1.8. Soluble Thorium Remaining in the Bed vs Filtrate Volume. Bed $L/D \cong 15$; temperature = 90°C; contact time = 6 hr.

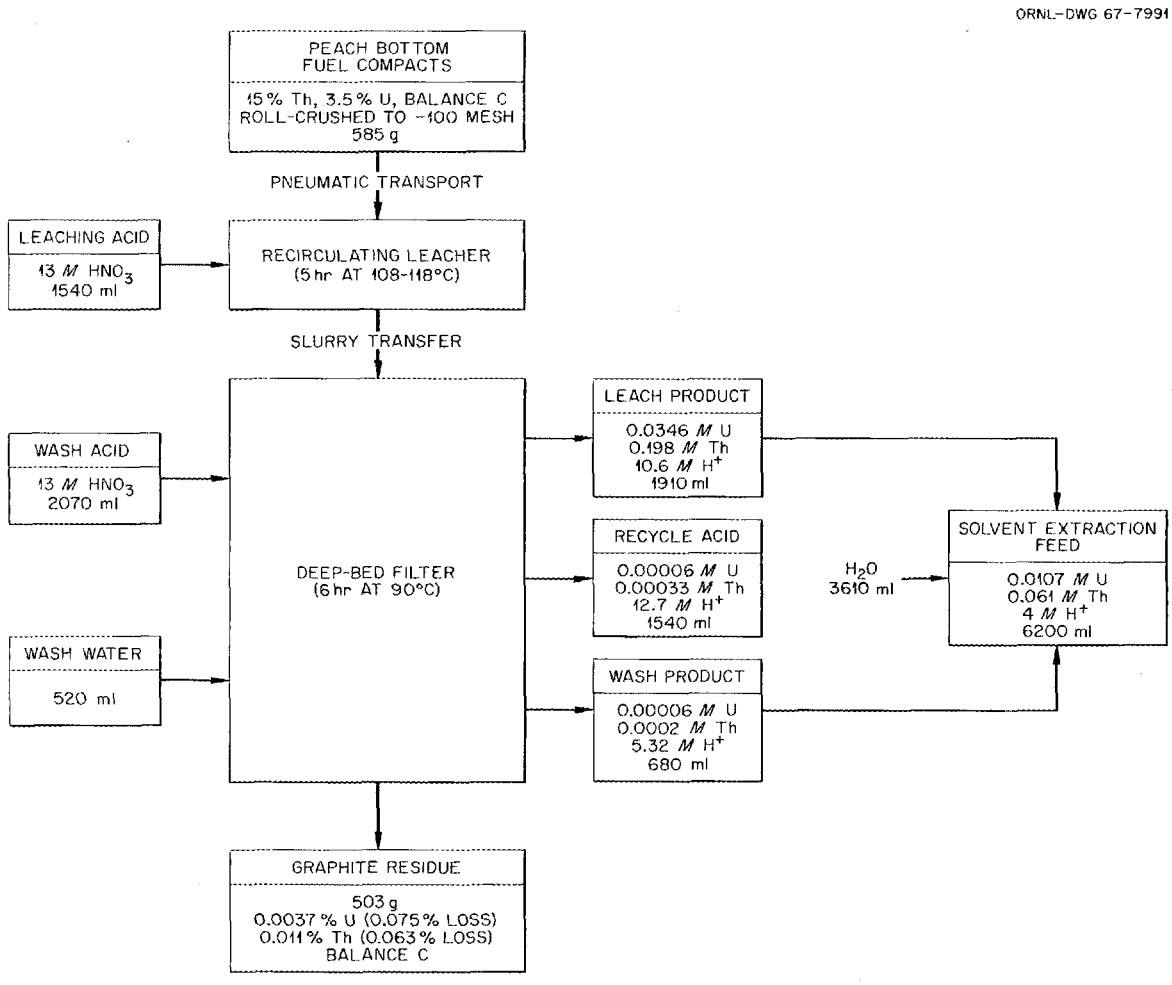

Fig. 1.9. Recycle Acid Flowsheet for Leaching Roll-Crushed HTGR Fuel (Run GL-6B).

that the previously reported[6] expression $V = 0.9\ (\Delta P/L)\ (1/\mu)$, where V is in gal hr^{-1} ft^{-2}, generally provides a conservative estimate of filtration rate. Three different residues were examined over the ranges $L = 0.5$ to 2.3 ft, $\Delta P/L = 3.7$ to 29 psi/ft, and $\mu = 0.32$ to 1.78 centipoises. Some of the scatter in the data is due to small variations in the manner in which the concentrated slurry compacted during initial pressurization and to small amounts of air trapped in the bed. The material in all these experiments was contained in a thermostated $1\frac{1}{2}$-in.-diam glass column.

Hot-Cell Evaluations

Hot-cell studies were made in order to evaluate the grind-leach process for two types of HTGR fuels:[14] prototype Peach Bottom fuel (GAIL-3A and GAIL-3B compacts) and ORNL-produced experimental AVR fuel spheres. The GAIL-3A compacts, GAIL-3B compacts, and AVR spheres had average burnups of 8850, 41,500, and 23,000 Mwd/ton respectively. Postirradiation examination showed that almost all the pyrolytic carbon coatings on the GAIL $(Th,U)C_2$ fuel particles had ruptured, whereas those on the AVR $(Th,U)C_2$ fuel particles were intact. Unirradiated GAIL and AVR fuel specimens from corresponding batches were used as controls in the hot-cell tests.

The fuel was ground in a Waring Blendor and sieved to -100 mesh (149 μ); then 10- to 20-g

[14] J. R. Flanary and J. H. Goode, *Hot-Cell Evaluation of the Grind-Leach Process. I. Irradiated HTGR Candidate Fuels: Pyrocarbon-Coated $(Th,U)C_2$ Particles Dispersed in Graphite*, ORNL-4117 (in press).

Table 1.5. Summary of Processing Conditions and Data Obtained in Grind-Leach Hot-Cell Experiments

Run No.	Type of Fuel	Irradiation (Mwd/ton)	Leaches			Washes		Amount Retained in Graphite Residue (%)			
			Number	Contact Time (hr)	Reagent	Number	Reagent	Uranium	Thorium	Gross Gamma	Gross Beta
PB-2	GAIL-3A	0	2	7	13 *M* HNO_3–0.05 *M* HF	3	H_2O	0.15	0.01		
PB-3	GAIL-3A	0	2	7	13 *M* HNO_3–0.05 *M* HF	5	13 *M* HNO_3–0.05 *M* HF	0.02	0.002		
PB-4	GAIL-3A	0	2	7	13 *M* HNO_3	5	13 *M* HNO_3	0.02	0.001		
PB-5	GAIL-3A	0	4	9	13 *M* HNO_3	3	H_2O	0.16	0.26		
PB-6	GAIL-3A	0	4	9	13 *M* HNO_3	3	H_2O	0.14	0.27		
PB-7	GAIL-3A	0	4	9	13 *M* HNO_3	3	H_2O	0.16	0.25		
PB-8	GAIL-3A	0	4	9	13 *M* HNO_3	3	H_2O	0.19	0.33		
AVR-1	AVR	0	2	8	13 *M* HNO_3–0.05 *M* HF	3	H_2O	0.90	1.04		
AVR-2	AVR	0	2	7	13 *M* HNO_3–0.05 *M* HF	3	H_2O	0.33	0.27		
AVR-3	AVR	0	4	9	13 *M* HNO_3–0.05 *M* HF	3	H_2O	0.38	0.24		
3A-1	GAIL-3A	8,800	3	9	13 *M* HNO_3–0.05 *M* HF	5	H_2O	0.90	1.11	19.22	15.66
3A-2	GAIL-3A	10,400	3	9	13 *M* HNO_3–0.05 *M* HF	5	H_2O	0.96	4.0	9.54	10.43
3B-1	GAIL-3B	33,500	2	7	13 *M* HNO_3	5	13 *M* HNO_3	0.84	1.31	2.48	8.25
3B-2	GAIL-3B	41,200	2	7	13 *M* HNO_3	5	13 *M* HNO_3	2.15	3.29	8.99	18.82
3B-3	GAIL-3B	34,100	2	7	13 *M* HNO_3–0.05 *M* HF	5	13 *M* HNO_3–0.05 *M* HF	0.44	3.82	7.38	22.52
3B-4	GAIL-3B	33,400	2	7	13 *M* HNO_3–0.05 *M* HF	5	13 *M* HNO_3–0.05 *M* HF	1.40	0.92	8.21	26.27
3B-5	GAIL-3B	41,000	2	9	13 *M* HNO_3–0.05 *M* HF	5	13 *M* HNO_3–0.05 *M* HF	1.29	2.83	10.22	26.97
3B-6	GAIL-3B	38,500	2	9	13 *M* HNO_3–0.05 *M* HF	5	13 *M* HNO_3–0.05 *M* HF	1.37	2.51	14.43	
3B-7	GAIL-3B	36,200	3	9	13 *M* HNO_3–0.05 *M* HF	5	H_2O	0.54	0.40	8.17	
3B-8	GAIL-3B	33,300	3	9	13 *M* HNO_3	5	H_2O	1.38	1.07	10.53	
3B-9	GAIL-3B	36,800	4	9	13 *M* HNO_3	3	H_2O	2.54	4.45	18.22	
3B-10	GAIL-3B	30,600	4	9	13 *M* HNO_3	3	H_2O	4.46	6.89	8.80	
3B-11	GAIL-3B	25,100	4	9	13 *M* HNO_3	3	H_2O	1.88	6.27	0.93	
AVR-4	AVR	23,200	3	9	13 *M* HNO_3–0.05 *M* HF	5	H_2O	0.70	4.07	19.01	22.74
AVR-5	AVR	26,400	3	9	13 *M* HNO_3–0.05 *M* HF	5	H_2O	2.50	1.19	34.86	25.10

samples of the pulverized fuel were leached and washed several times with boiling 13 *M* HNO_3 or 13 *M* HNO_3–0.05 *M* HF and fresh dissolvent or water respectively. Finally, the graphite residues were dried and submitted for chemical and radiochemical analysis. Table 1.5 summarizes the data obtained in these grind-leach experiments.

Tests with the unirradiated control samples gave consistent recoveries of $\geq$99.7% of the thorium and uranium; the nonleachable fraction is probably associated with the pyrocarbon coatings and presumably results from diffusion during the fuel fabrication process. The irradiated GAIL-3A samples yielded residues containing an average of about 1% of the total uranium, 2.5% of the thorium, 15% of the gross gamma activity, and 13% of the gross beta activity in each sample. The residues from the more highly irradiated GAIL-3B samples, leached under optimum conditions, contained up to 4.5% of the uranium, 6.9% of the thorium, and 18.2% of the gross gamma activity in the samples. Unsatisfactory results were also obtained with the irradiated AVR material (Table 1.5).

As many as four leaches for total contact times up to 9 hr resulted in no significant additional recovery after the first leach. From these results it was concluded that, at most, two leaches (total contact time 7 hr) will recover all the readily acid-soluble $(Th,U)C_2$. The recovery of the heavy metals from the dicarbide was not enhanced by the presence of 0.05 *M* HF in the leachant [fluoride is necessary, however, for leaching $(Th,U)O_2$ fuel particles]. Water was found to be as effective as fresh acid for washing the leached graphite; furthermore, a boiling water wash could be filtered about three times as fast as an acid wash. The use of fluoride in the wash solution did not improve the recovery of the heavy metals or fission products.

The presence of significant amounts of uranium and thorium, along with major quantities of fission products (particularly ^{106}Ru, ^{137}Cs, and ^{144}Ce), in the leached and washed residues from the grind-leach head-end process makes this method appear unattractive for the reprocessing of HTGR fuels that contain pyrolytic-carbon-coated $(Th,U)C_2$ particles dispersed in a graphite matrix.

Additional tests will be made with irradiated samples of ORNL carbon-coated sol-gel ThO_2 and $(Th,U)O_2$ fuel microspheres and General Atomic SiC-coated $(Th,U)C_2$ to determine the applicability of the grind-leach process to these fuels. The latter work is quite important since the burn-leach process cannot be used directly for SiC-coated-particle fuels.

1.4 SOLVENT EXTRACTION STUDIES

Aqueous solutions obtained from the head-end processes that are being developed for various reactor fuel types will be treated by solvent extraction (or anion exchange) to effect the required recovery and decontamination of uranium, thorium, and plutonium from radioactive fission products. To demonstrate that such separations processes are adequate, experiments are performed, first with solutions of unirradiated fuel to establish flowsheet conditions and later with solutions of fully irradiated fuel, in hot-cell tests, to determine decontamination factors and to verify that the separations systems are valid for use with irradiated material. During this report period, the major effort involved the development of a solvent extraction process for treating grind-leach fuel solutions. The new process was then demonstrated in hot-cell tests. In addition, some survey studies of alternative solvents and diluents were made.

Solvent Extraction Studies with HTGR Grind-Leach Solutions

Solutions from the grind-leach head-end process for graphite-base HTGR fuels contain small amounts of soluble organic materials (mellitic and oxalic acids); during the subsequent extraction process, these materials cause troublesome emulsions when the standard Acid-Thorex flowsheet[15] is used for fuel recovery. We have found, however, that the thorium and uranium can be extracted from the solution by TBP without formation of an emulsion if the acid concentration of the aqueous phase is high. The thorium-uranium strip product solution from this head-end extraction cycle contains only small amounts of organic material and fission products; it is a suitable feed solution (after heating and evaporating to effect concentration and conversion to an acid-deficient condition) for the

[15] R. H. Rainey and J. G. Moore, *Nucl. Sci. Eng.* 10, 367 (1961).

standard Acid-Thorex process. Flowsheet conditions for the new process are as follows:

Feed	41 g of Th per liter, 7.7 g of U per liter, 4.6 *N* HNO_3; 1 volume
Solvent	30% TBP in *n*-dodecane (NDD); 1.5 volumes
Scrub solution	Water; 0.3 volume
Strip solution	0.002 *N* HNO_3; 1.5 volumes
Stages	Five extraction, three scrub, five strip

In a batch countercurrent demonstration run at tracer level, no difficulties were encountered with emulsions or crud formations. The gross gamma decontamination factor (DF) from fission products was 400; the fission product that limited the decontamination was ruthenium. The uranium loss to the aqueous raffinate was <0.01%, but the thorium loss was about 5%; however, the latter loss could have been decreased by the use of additional extraction stages or a small increase in the volume of the solvent. This head-end solvent extraction treatment has advantages over other proposed head-end treatments (e.g., treatment of the aqueous feed solution with permanganate to destroy the organic material) in that it (1) effectively separates uranium and thorium from the fission products and (2) does not add chemical reagents to the feed that would complicate subsequent waste treatment.

Using the organic extract from the above tests, we then obtained separate thorium and uranium products by use of a compound strip column. Nearly all the thorium and nitric acid and 6% of the uranium were first stripped from the extract (composition: 0.14 *M* in thorium, 0.03 *M* in uranium, and 0.12 *N* in HNO_3) with 0.4 volume of water, using a five-stage countercurrent contactor. The remaining uranium was then stripped, in a second five-stage contactor, with 0.5 volume of 0.01 *M* NH_4NO_3. The column separation factors of thorium from uranium and of uranium from thorium were 16 and 45 respectively. A similar experiment employing an organic feed that did not contain any free acid produced similar results; however, the separation factors were about 12 and 300 respectively. Besides providing separate uranium and thorium products, the compound strip system has the advantage of yielding products at concentrations about twice those that are obtainable from a co-stripping system.

Subsequently, hot-cell experiments were performed with feeds derived from the burn-leach and the grind-leach head-end hot-cell tests (Sects. 1.2 and 1.3) with irradiated GAIL-3B fuel compacts and pyrolytic-carbon-coated thorium oxide particles. Based on extraction isotherms, five ideal extraction stages should provide greater than 99.9% recovery of uranium and thorium from these feeds. In a series of batch tests the aqueous feeds (of varying fission product contents ranging from 9.4 to 37 beta-plus-gamma curies/liter) were equilibrated with the organic solvent for periods ranging from 3 min to 24 hr to evaluate the effects of radiation or chemical damage to the organic solvent. The extracts were then scrubbed, in three successive steps, with water or nitric acid; each was finally stripped, in five successive steps, with very dilute acid. Table 1.6 summarizes the data obtained in these tests. In equilibrations with feeds containing long-decayed (4 years and 19 months respectively) fuel that was derived from mixed burn-leach and grind-leach tests, thorium and uranium losses were low and decontamination factors (gross gamma DF = 750) were essentially constant. The radiation dose absorbed by the organic solvent ranged up to 0.35 whr/liter. Ruthenium was the principal contaminant in the product. Tests with solutions containing shorter-decayed (10 months) fuel, derived from the grind-leach process, showed that losses of uranium during stripping increased from less than 0.01 to 0.17% as the absorbed dose increased from 0.006 to 1.49 whr/liter. The ^{95}Nb decontamination factor decreased as the absorbed dose was increased; the gross gamma DF decreased from 180 to less than 100. The effect of the acid concentration of the scrub solution was also evident; low acid concentrations gave greater decontamination from zirconium-niobium, whereas higher concentrations removed more ruthenium. More recent solvent extraction tests show that the retention of fission products by the solvent is principally associated with the presence of dissolved organic materials contained in solutions from the grind-leach processing. In these tests the loss of decontamination efficiency and the increase in uranium retention by the solvent with increased solvent radiation exposure are due to the combined effects of the organic materials in the feed and of the radiation damage to the process solvent (and should not be attributed entirely to the latter).

A 12-stage modified Eurochemic mixer-settler with five extraction, three scrub, and four strip

Table 1.6. Effect of Absorbed Radiation Dose on the Recovery of Thorium and Uranium from Solutions Obtained During Burn-Leach and Grind-Leach Processing: Results of Batch Extraction Tests Employing 30% TBP in *n*-Dodecane

Feed Solutions				Scrub Solution HNO_3 (*M*)	Contact Time (hr)	Calculated Absorbed Dose (whr/liter)	Loss to Stripped Solvent (%)		Decontamination Factors[b]					
Source	Period of Decay	Activity[a] (curies/liter)	HNO_3 (*M*)				U	Th	Gross Gamma	^{95}Zr	^{95}Nb	^{106}Ru	^{137}Cs	^{144}Ce
Burn-leach	4 years	9.4	3.4	0	0.05	0.001	<0.01	0.05	750			36	1500	1200
(GAIL-3B) plus grind-leach (GCR-ORR-Loop 1-14)	19 months	9.4	3.4	0	19	0.35	<0.01	0.08	760			54	1160	1160
Grind-leach	10 months	37	3.9	0	0.1	0.006	<0.01	<0.02	180	55	540	51	570	590
(GCR-ORR	10 months	37	3.9	0	24	1.49	0.18	0.07	100	380	36	18	104	630
Loop 1-15)				3	24	1.49	0.17	0.07	71	35		205	2300	1380

[a]Beta and gamma.

[b]Based on uranium concentration (feed vs product).

stages was used to test the new flowsheet. A single 1-liter batch of solvent was continuously recirculated without cleanup during runs with aqueous feeds having two different acid concentrations. The aqueous feeds consisted of 3400 ml of mixed burn-leach and grind-leach fuel solutions and 480 ml of grind-leach solutions containing short-decayed fuel; the latter feed analyzed 9.4 beta-plus-gamma curies/liter. The nitric acid concentration of the feed used in the first mixer-settler run was 2.5 *M*; this was increased to 5.4 *M* in the second run. Physical operation of the mixer-settler system was satisfactory; no problems were experienced with phase separation or crud formation. Extraction losses (about 40%) of the thorium and uranium and stripping losses (up to 4%) of the uranium, however, were high because of the poor stage efficiency of the contactor; for example, the five mechanical extraction stages were found to be equivalent to slightly less than two ideal stages.

Direct Leaching of Acidified HTGR Fuel with TBP

Scouting tests were performed to determine the feasibility of leaching crushed graphite fuel with TBP. The ground, unirradiated Peach Bottom graphite fuel was wetted with 13 *M* HNO_3 and heated; the amount of acid used was only slightly in excess of the stoichiometric amount required for reaction with the thorium and uranium. The resultant material was then dried, loaded in a column, and finally leached by passing acidified 30% TBP–NDD through the column. Major fractions of the thorium and uranium were readily dissolved in the solvent phase; however, the run was too short to accurately define the recoveries that may be obtainable by this procedure. It is expected that most of the fission products would be retained by the graphite, but this expectation needs to be verified in tests with irradiated fuels.

General Solvent Extraction Studies

It has been shown that a solvent composed of di-sec-butyl phenylphosphonate in diethylbenzene (DSBPP in DEB) has some advantages over TBP-NDD for use in the extraction of uranium (especially ^{233}U) because of its greater stability at high irradiation levels and because of the higher ratio of the uranium distribution coefficient to the thorium distribution coefficient.[16] Studies with DSBPP in DEB showed that the complexed uranium species is $UO_2(NO_3)_2 \cdot 2DSBPP$. The limit of solubility of this complex in DEB at about 25°C is 0.37 *M*; therefore, 20 vol % DSBPP ($\sim$0.75 *M*) in DEB is the maximum concentration that can be used at this temperature in the presence of high concentrations of uranium without precipitation of the complex.

In other experiments the solubility of thorium nitrate in 30% TBP (1.06 *M*) in various diluents was found to be strongly influenced by the diluent; however, the solubility of uranyl nitrate in all the tested diluents was about 0.50 *M*. The solubilities of the thorium nitrate–TBP complexes were determined by equilibrating $Th(NO_3)_4 \cdot 4H_2O$ crystals with various solvents containing TBP (dissolved in the normal aliphatic hydrocarbons from hexane to tetradecane, in several branched isomers of these compounds, and in benzene and diethylbenzene). The solubility of the thorium nitrate–TBP complex in the aliphatic hydrocarbons was limited by the formation of a second organic phase. The solubility varied linearly from 0.33 *M* in hexane to 0.15 *M* in tetradecane and can be approximately represented by: thorium concentration (*M*) = 0.48 – 0.025*C*, where *C* is the number of carbon atoms in the diluent molecule. Throughout this series, the hydrocarbon : thorium mole ratio at saturation had a nearly constant value of about 20. The TBP : thorium mole ratio observed at the beginning of the formation of a second organic phase did not change as the concentration of TBP in the diluent was varied. If addition of thorium nitrate to the solution was continued until solid crystals remained undissolved, the TBP : thorium mole ratio was found to be approximately 2.6 in the heavy organic phase and 2.9 in the light phase. The solubility of the TBP-thorium complex in branched aliphatic diluents was as much as 10% greater than in the corresponding normal aliphatic compound. In benzene and diethylbenzene, indicated maximum thorium solubilities were 0.39 and 0.38 *M* respectively; no second organic phase formed.

---

[16] C. A. Blake, Jr., A. T. Gresky, J. M. Schmitt, and R. G. Mansfield, *Comparison of Dialkyl Phenyl Phosphonates with Tri-n-butyl Phosphate in Nitrate Systems: Extraction Properties, Stability, and Effect of Diluent on the Recovery of Uranium and Thorium from Spent Fuels*, ORNL-3374 (Jan. 8, 1963).

1.5 DEVELOPMENT OF PROCESSES FOR HEAVY-WATER-MODERATED ORGANIC-COOLED REACTOR FUELS

Several conceptual reactor designs are being considered by the Atomic Energy Commission in connection with its heavy-water-reactor program. Uranium monocarbide (UC) clad in SAP (a dispersion of 5 to 15% Al_2O_3 in an aluminum matrix) has emerged as the leading candidate for a heavy-water-moderated organic-cooled reactor (HWOCR) fuel.[17] Other types of fuel considered were: (1) SAP-clad UO_2, (2) Zircaloy-clad UC, (3) Zircaloy-clad UO_2, (4) SAP-clad (Th,U)C (thorium : uranium atom ratio of about 40), (5) SAP-clad $(Th,U)O_2$, and (6) Zircaloy-clad thorium-uranium alloy (alloy and cladding coextruded). Possible methods for processing these fuels were studied on a laboratory scale.[18,19] Shearing followed by leaching with nitric acid solution appeared to be the most promising head-end method for fuels clad in zirconium. For the SAP-clad fuels, decladding either with caustic solution or with gaseous HCl appeared attractive. Since SAP seems to be the leading candidate for the cladding material for HWOCR fuels, only the development work on the processing of SAP-clad fuels is reviewed here.

Caustic Decladding Process Development

Previous work[18,20] has shown that the aluminum matrix of SAP dissolves readily in boiling NaOH and NaOH-$NaNO_3$ solutions, leaving the Al_2O_3 as a residue. It is also well known that both UO_2 and ThO_2-UO_2 are almost totally insoluble in caustic and sodium aluminate solutions. Consequently, the chemistry of aqueous decladding processes for SAP-clad oxide fuels is straightforward, and processes for these fuels can probably be devised utilizing existing technology. On the other hand, caustic decladding processes for SAP-clad carbide fuels will probably have to be developed by using irradiated fuel samples. Formulation of such processes utilizing existing data is difficult because of the unpredictable behavior of the heavy-metal carbides in aqueous systems. Examples of the erratic behavior of uranium and thorium carbides in aqueous systems are numerous. Unirradiated UC is inert in boiling 2 *M* NaOH–2 *M* $NaNO_3$ (a desirable decladding reagent), but ThC reacts rapidly. Unirradiated UC and ThC are both hydrolyzed by boiling water and nitrate-free sodium hydroxide solutions; however, UC irradiated to burnups of 0.6 at. % or higher is inert to both water and 6 *M* NaOH.[21] The behavior of irradiated ThC in aqueous systems has not yet been studied.

Conceptual caustic decladding flowsheets for SAP-clad carbide fuels have been devised[18] in which irradiated UC is assumed to be inert to the decladding solution. Consequently, the first step in the conceptual process for SAP-clad UC (Fig. 1.10) would consist in dissolution of the SAP in boiling NaOH-$NaNO_3$ solution (to minimize hydrogen formation); UC and the Al_2O_3 from the SAP would comprise the residue. The UC and most of the Al_2O_3 would then be dissolved in concentrated nitric acid. The product solution would contain 20 to 50% of the carbide carbon as soluble organic compounds,[10,11] and would therefore not be suitable as a feed for a conventional Purex solvent extraction purification process. Several alternative procedures appear feasible for recovering the uranium, and especially the plutonium, from the product solution. In one method[22] the organic compounds would be oxidized to CO_2 and CO after adding $KMnO_4$ (or another suitable oxidant) to the system. After removal of the solid MnO_2 that would be formed, the resulting solution could be used as a feed for the Purex extraction process. An oxidation step to remove the organic compounds does not appear necessary, however. Data from several sources[10,23–25] show that the uranium

---

[17] P. R. Kasten *et al.*, *An Evaluation of Heavy-Water-Moderated, Organic-Cooled Reactors*, ORNL-3921 (January 1967).

[18] L. M. Ferris, *Possible Head-End Processes for Heavy-Water-Moderated Organic-Cooled Reactor (HWOCR) Fuels*, ORNL-4109 (July 1967).

[19] *Chem. Technol. Div. Ann. Progr. Rept. May 31, 1966*, ORNL-3945, pp. 40–42.

[20] G. Beone, *Dissolution of Fuel-Element Jackets of Aluminum and S.A.P. in a Recirculating Dissolver*, RT/CHI(65)1 (January 1965).

[21] M. J. Bradley, J. H. Goode, L. M. Ferris, J. R. Flanary, and J. W. Ullmann, *Nucl. Sci. Eng.* 21, 159 (1965).

[22] J. R. Flanary, J. H. Goode, M. J. Bradley, L. M. Ferris, and J. W. Ullmann, *Nucl. Appl.* 1, 219 (1965).

[23] A. M. Simpson and B. A. Heath, *Products of the Reaction Uranium Monocarbide–Nitric Acid*, IG Memorandum 464(D) (June 1959).

[24] *ORNL Status and Progr. Rept. Sept. 1966*, ORNL-4026 (Oct. 6, 1966) (official use only).

[25] F. Mannone, C. Stoppa, and G. Sanso, *Separation with Solvents of the Products of Nitric Acid Dissolution of Uranium Carbide*, EUR-1913-1 (1964).

and plutonium can be extracted (with TBP) from the product solution, leaving the organic compounds in the aqueous phase (Fig. 1.10). For efficient separation of uranium and plutonium from the organic compounds, the acid concentration in the aqueous phase should be 5 to 7 *M*, since emulsions can form at lower acid concentrations. Further purification of the uranium and plutonium can then be achieved in additional cycles of conventional solvent extraction. Alternatively, after the acid concentration of the solution has been adjusted to 5 to 7 *M*, the plutonium can be recovered selectively by an anion exchange process that leaves the uranium, organic compounds, and fission products in the waste solution (Fig. 1.10). This latter procedure appears highly attractive for SAP-clad UC (or UO_2) fuels because, after irradiation, plutonium is probably the only fissile material worth recovering.

The conceptual process for SAP-clad ThC-UC fuel would resemble the main process shown in Fig. 1.10 if the mixed carbide is found to be inert during decladding. Anion exchange would probably not be of value in separating the soluble organic compounds from the uranium and thorium since the distribution coefficients for uranium and thorium are much lower than that for plutonium. If irradiated ThC-UC hydrolyzes during decladding, the carbide carbon would be evolved from the system mainly as methane; the solid residue would be ThO_2-UO_2. The ThO_2-UO_2 would be dissolved in 13 *M* HNO_3–0.05 *M* HF, and the uranium and thorium would be recovered by conventional solvent extraction methods.

Obviously, further experimentation with irradiated fuel samples is required before the final selection of processing conditions can be made.

Decladding with Gaseous HCl

A hydrochlorination-oxidation head-end process (Fig. 1.11) appears applicable to most of the HWOCR fuels mentioned above. Initially, the fuel would be charged to a fluidized bed of inert alumina, and the aluminum matrix of the SAP would be removed as volatile $AlCl_3$ by reaction of the SAP with gaseous HCl at about 300°C. (Zirconium can be hydrochlorinated at 450°C, giving volatile $ZrCl_4$.) During hydrochlorination, most of the fuel

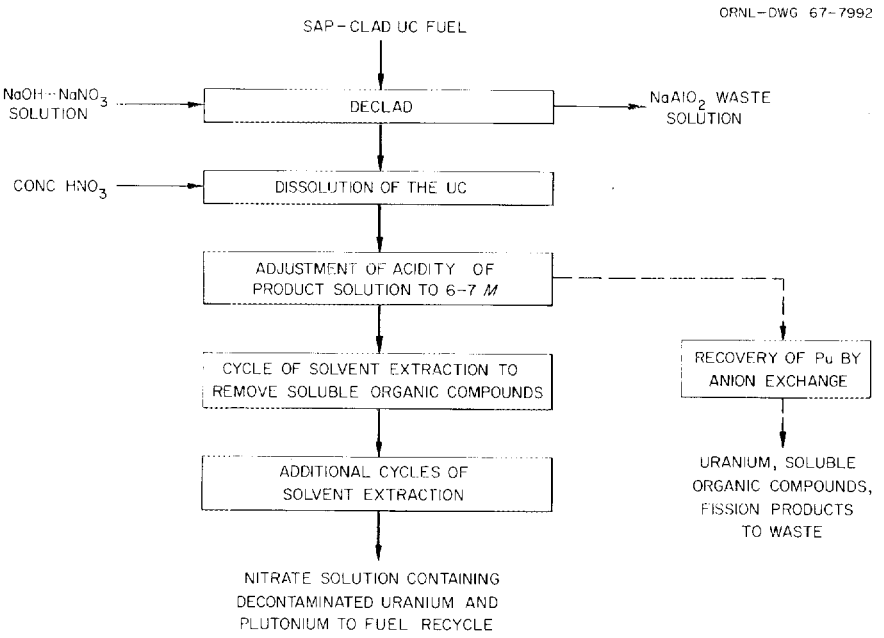

Fig. 1.10. Conceptual Caustic Decladding Processes for SAP-Clad UC Fuel.

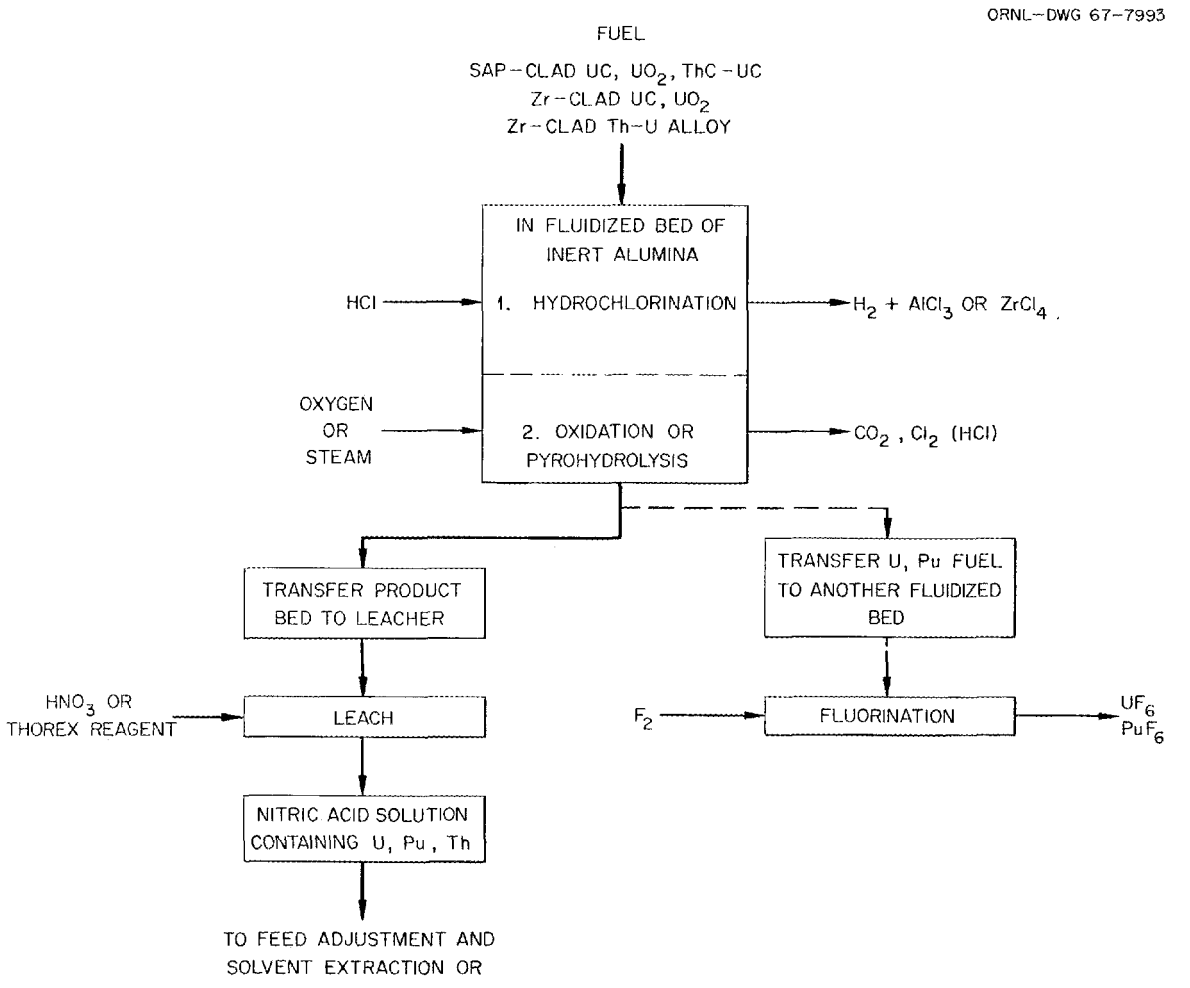

Fig. 1.11. Possible Fluidized-Bed Processes for HWOCR Fuels.

materials would be at least partially converted to their respective chlorides. For example, UC appears to react according to the equation

$$UC + 3HCl \longrightarrow UCl_3 + C + \frac{3}{2}H_2 .$$

Oxidation could be the second step of the process to convert the products from the hydrochlorination step to their respective oxides. Thus, with UC fuel, the UCl_3, free carbon, and any unconverted UC remaining from the hydrochlorination step would be oxidized to give a product composed mainly of U_3O_8 dispersed in the alumina bed; the free carbon would be removed as volatile CO_2 and CO. Pyrohydrolysis is an alternative to oxidation, particularly for carbide fuels.[22] Use of steam instead of oxygen would give UO_2 instead of U_3O_8. After oxidation (or pyrohydrolysis) the product bed could be leached with acid to provide a solution that is suitable as a feed for a solvent extraction purification process. Alternatively, fluoride volatility methods could probably be used to process fuels that did not contain thorium (Fig. 1.11). In this case the product bed after oxidation would be fluorinated to produce volatile UF_6 and PuF_6, which would be collected and purified.

1.6 DEVELOPMENT OF PROCESSES FOR FAST-BREEDER-REACTOR FUELS

This development, begun this year, has included studies of mechanical and chemical head-end processes for FBR fuel dissolution and of modified

solvent extraction processes for the recovery of plutonium and uranium. Mechanical processing work has included FBR fuel element disassembly studies and calculations of heat generation and dissipation in the various mechanical steps of the shear-leach process. Several methods were evaluated for the safe disposal of the sodium coolant adhering to the fuel assemblies and, more particularly, the sodium heat-transfer bond used with carbide fuels. The use of hydrogen and a platinized-alumina catalyst for reducing Pu(IV) to Pu(III) during solvent extraction partitioning of plutonium from uranium was also investigated.

Fuel Disassembly and Shear-Leach Studies

During the several visits made to a number of reactor designer and fuel fabrication companies to obtain up-to-date information on third-generation thermal reactor (LWR) fuel designs (see Sect. 1.1), data were also obtained on the general fuel element designs being considered for use in FBR's. This latter information was then evaluated in a cursory study to determine whether mechanical processing of FBR fuel will be more difficult than that of LWR fuel.

In general, the FBR fuel assemblies will have a hexagonal cross section approximately 7 to 8.5 in. across the flats and 10 to 15 ft long. The cladding will be stainless steel, and fuel rod diameters will be approximately $\frac{1}{4}$ in. A fuel rod will consist of upper and lower axial blanket sections and a central core section. The first cores will employ mixed oxides of plutonium and uranium and will use no internal sodium bond. Grids or wire wrapping will be used to separate fuel rods; in some assemblies the fuel rods will be enclosed in a sheath. Beryllium oxide rods may be interspersed with the fuel rods.

Preliminary studies of these data indicate that the FBR fuels are mechanically similar to thermal reactor fuels as far as the external hardware is concerned. It is expected that the early FBR fuels can be processed by the shear-leach process, as was developed for thermal fuels; however, some difficulty is anticipated from the decay heat owing to the very high burnup ($\sim$100,000 Mwd/ton), the high specific power (150 kw/kg), and the short preprocessing decay period (<60 days) proposed for FBR fuels.

Since the FBR fuels (and, to a lesser extent, third-generation LWR fuels) are expected to be irradiated to very high burnups, computer code BIGDEAL was used to calculate the temperatures that can be expected for these fuel assemblies during shear-leach processing. The reference fuel chosen was an 8.38-in.-square multitubular array containing 400 0.305-in.-OD by 102-in.-long UO_2-filled stainless steel fuel rods on 0.425-in. centers (Yankee Atomic). A burnup of 100,000 Mwd/ton (uranium) was assumed at specific powers of 75, 100, 125, and 150 kw per kilogram of uranium; cooling times of 30, 60, 90, 120, 150, 180, and 240 days were considered. Other assumptions were that (1) the baskets of sheared fuel are stored in a square array of 16 baskets on 12-in. centers, and (2) heat is dissipated during the various phases of processing by radiation, natural convection, or a combination of radiation and natural convection. The results are shown in the table below:

	Minimum	Maximum
Specific power, kw/kg	75	150
Cooling time, days	240	30
Temperatures, °F		
Fuel receipt in canal	111	231
Mechanical disassembly	1029	2012
Shear feed envelope		
Centermost rod	1128	2110
Center rod in outer row	753	1435
Sheared fuel stored in 5-in.-diam basket		
Center line of basket	828	2174
Surface of basket	533	1316
Sheared fuel stored in $7\frac{3}{4}$-in.-diam basket		
Center line of basket	1210	3095
Surface of basket	753	1740

These calculations indicate that heat dissipation from high-burnup and short-cooled fuel will be a serious problem and that forced cooling will be required during shearing and possibly for leach baskets whose inside diameters will otherwise be restricted to approximately 5 in.

Sodium Metal Deactivation Studies

The evaluation of methods for safely disposing of sodium in the processing of liquid-metal fast breeder reactor (LMFBR) fuels was begun during

the past year. Sodium will be used as the coolant and, possibly, as a heat-transfer bond in fast-reactor fuels. In the case of unbonded stainless-steel-clad UO_2-PuO_2 fuels, only sodium adhering to the external surfaces of the fuel elements poses a possible chemical problem during processing. This sodium can, however, probably be safely converted to oxide by a method similar to that used at the EBR-II Fuel Processing Facility.[26] The basis of this method is the controlled reaction of the sodium with oxygen and/or water vapor present at low concentrations in an inert gas such as helium.

Sodium disposal poses a major problem, however, in the processing of more advanced sodium-bonded UC-PuC fuels. To avoid the possibility of explosive vapor-phase reactions between hydrogen and nitrogen oxides,[27] the sodium must be destroyed or removed before the carbide can be dissolved in nitric acid. A possible head-end process that would circumvent this problem would involve shearing of the fuel in an inert atmosphere, followed by the simultaneous oxidation or pyrohydrolysis of the carbide and the sodium. In this connection, cursory studies were made of the reaction of sodium with air and water vapor. Thermobalance tests of the reaction of sodium (Baker Analyzed Reagent) with dry air gave inconclusive results. In some experiments the sodium was relatively inert in dry air at temperatures up to about 275°C, with controlled oxidation being achieved at about 300°C; in others, however, the sodium ignited at about 295°C and reacted very rapidly. Based on the weight change, the product of the reaction in all instances appeared to be Na_2O_2.

Sodium was nearly inert in a stream of 3% H_2O–97% He (H_2O partial pressure about 24 torrs) at temperatures up to about 275°C. At about 300°C, the sodium reacted at a controlled rate of about 2 mg/min, giving NaOH as the product. The results of these experiments suggest that the sodium bond could be safely destroyed at low temperatures; after reaction of the sodium, pure steam could be admitted to the system and could be allowed to react with the UC-PuC at about 750°C to give a UO_2-PuO_2 product.[22]

Other experiments showed that reaction with CO_2 was not an attractive method for the chemical destruction of sodium. Sodium was practically inert to CO_2 at temperatures below about 600°C; above 625°C, the sodium reacted rapidly, giving Na_2CO_3 and free carbon as the products.

Plutonium Reduction Studies

One of the principal problems that will emerge in the processing of FBR fuels is the partitioning of high concentrations of plutonium from uranium in an increased radiation field. Ferrous sulfamate has been used successfully to reduce plutonium to Pu(III) in the Purex process; however, this method was not satisfactory with FBR fuels (i.e., at Dounreay[28]). In several other laboratories, uranous nitrate is being studied as a reductant. We are developing a new partitioning process that uses hydrogen gas as the reductant for plutonium. In demonstrating this process, 4% H_2–argon and an organic solution that was 0.1 *N* in HNO_3 and contained about 80 g of uranium and 16 g of plutonium per liter were passed, cocurrent with an aqueous solution that was 0.5 *N* in HNO_3 and 0.02 *M* in hydrazine hydrate, through a column packed with 0.5% platinum on alumina pellets. The system operated satisfactorily at flows of 2 to 10 ml of total liquid flow and 100 to 600 ml of gas flow per minute through a 1-cm-diam, 22-cm-long column. When the organic extract did not contain plutonium, about 1% of the uranium was reduced to U(IV). Analytical problems have prevented the determination of uranium and plutonium valences when both plutonium and uranium were present; however, both the color of the solutions and the analyses for total uranium and plutonium have indicated satisfactory plutonium reduction and partitioning from uranium.

Extraction of Plutonium with Amines

We (and British workers[29]) are studying the use of amines as potential alternatives to TBP for use

---

[26] J. C. Hesson, M. J. Feldman, and L. Burris, *Description and Proposed Operation of the Fuel Cycle Facility for the Second Experimental Breeder Reactor (EBR-II)*, ANL-6605 (April 1963).

[27] K. S. Warren, *Survey of Potential Vapor-Phase Explosions in Darex and Sulfex Processes*, ORNL-2937 (Dec. 27, 1960).

[28] D. M. Donaldson, K. Hartley, P. Lees, and N. Parkinson, "Reprocessing of Fast Reactor Fuels at Dounreay," paper given at AIME meeting, Oct. 25, 1961; published in *Transactions*.

[29] E. S. Lane, A. Pilbeam, and J. M. Fletcher, *Reprocessing with Amine-Ether Systems*, AERE-R4440, Parts I, II, and III (1965).

Table 1.7. Extraction of Pu(IV) from Uranyl Nitrate–Nitric Acid Solution with Amines

Extractant: 0.3 *M* amine in diethylbenzene

Aqueous: 1 *M* $UO_2(NO_3)_2$–3 *M* HNO_3 solution containing tracer-level $^{239}Pu(IV)$ [about 10^5 counts (alpha) min^{-1} ml^{-1}]

Contact: 5 min at A/O phase ratio of 2.

Amine	Diluent	U Concentration in Organic (g/liter)	Extraction Coefficient, E_a°	
			Pu	U
Primary Amines				
Primene-JMT	Diethylbenzene (DEB)	4.2	0.5	0.018
1-Nonyldecyl	DEB	5.4	0.6	0.023
1-(3-Ethylpentyl)-4-ethyloctyl	DEB	5.4	1.0	0.023
Secondary Amines				
Di(tridecyl)	DEB	11.5	7.8	0.050
Di(1-nonyldecyl)	DEB	13.7	2.2	0.060
Amberlite LA-1	DEB	19.6	2.1	0.086
N-Benzyl-1-(3-ethylpentyl)-4-ethyloctyl		11.6	3.4	0.050
N-benzyl-(1-nonyldecyl)		12.3	3.1	0.053
Tertiary Amines				
Alamine-336	DEB	29.4	13	0.13
Adogen-363	DEB	35.0	16	0.16
Tri(2-ethylhexyl)	85% DEB–15% TDA[a]	23.3	12	0.10
N-Benzyl-di(2-ethylhexyl)	90% DEB–10% TDA	29.6	13	0.13
Dibenzyllauryl	95% *n*-dodecane–5% TDA	28.6	21	0.13
Di(2-ethylhexyl)lauryl	DEB	33.2	11	0.15
Di(2-ethylhexyl)hexyl	90% DEB–10% TDA	30.6	11	0.14
Benzyldilauryl	DEB	31.0	13	0.14
Quaternary Amine				
Aliquat-336	90% *n*-dodecane–10% TDA	57.5	59	0.28

[a]TDA = tridecanol.

in the recovery of plutonium from fast reactor fuels. It has been reported that the radiation degradation products from amines are less troublesome than those from TBP. Furthermore, since the amines extract plutonium much more strongly than uranium, they could provide separation from uranium in the first extraction cycle (and avoid a subsequent partitioning cycle), possibly after the fuel has been cooled for only a very short period. The uranium could then be recovered by extraction with TBP after extended cooling of the amine extraction raffinate to permit complete decay of ^{237}U. Amine extraction is also a potential alternative to ion exchange processing for final purification of the plutonium.[30–32]

[30]A. Chesne, G. Koehly, and A. Bathellier, "Recovery and Purification of Plutonium by Trilaurylamine Extraction," *Nucl. Sci. Eng.* **17**, 557–65 (1963).

[31]K. B. Brown, *Chem. Technol. Div. Chem. Dev. Sect. C Progress Report on Separations Process Research for Jan.–June, 1963*, ORNL-3496, p. 23.

[32]R. S. Winchester, *Aqueous Decontamination of Plutonium from Fission Product Elements*, LA-2170 (1958).

Present emphasis is on finding an amine of intermediate extraction power. This might allow stripping of the plutonium with dilute acid and avoid the addition of stripping agents (acetate, ferrous sulfamate, etc.) that would hinder close coupling of the recovery system with a sol-gel refabrication system. In an initial survey, coefficients for the extraction of tracer Pu(IV) from 1 *M* $UO_2(NO_3)_2$–3 *M* HNO_3 were obtained for a number of amines of different types and alkyl structures (Table 1.7). The extraction of plutonium varied with amine class in the order: quaternary > tertiary > secondary > primary. With some amines, particularly the quaternary amine and the tertiary amines, the plutonium extraction was appreciably depressed by uranium competition for the solvent. The plutonium extraction power of a secondary amine, di(tridecyl)amine, was of about the desired magnitude, whereas its uranium extraction power was relatively weak; therefore, this amine has been selected for more intensive study.

Figure 1.12 shows the effects of nitric acid and uranium concentrations on extractions of Pu(IV) with 0.3 *M* di(tridecyl)amine in diethylbenzene. With no uranium present, the plutonium extraction coefficient increased with increasing nitric acid concentration up to a maximum value of 26 at 7 *M* HNO_3 and then decreased. With 0.5 or 1 *M* $UO_2(NO_3)_2$ present, the maximum plutonium extraction coefficients were reduced by a factor of 2 to 3 and occurred at lower nitric acid concentrations (but at about the same total nitrate concentration).

In extractions of plutonium from nitric acid solutions containing macro amounts of plutonium but no uranium, 0.3 *M* di(tridecyl)amine in diethylbenzene was loaded with as much as 27 g of plutonium per liter without formation of a third liquid phase. A single contact of such an extract with an equal volume of 0.5 *M* HNO_3 stripped 95% of the plutonium.

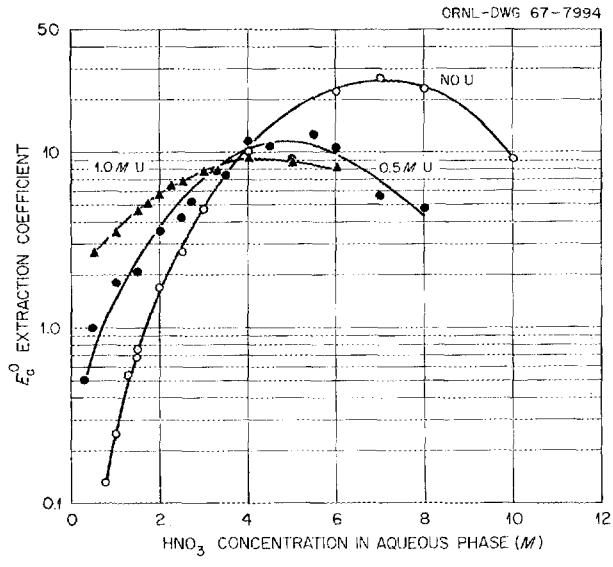

Fig. 1.12. Extraction of Pu(IV) with 0.3 *M* Di(tridecyl)amine in Diethylbenzene. *Aqueous phase:* HNO_3 *solutions with 0.0, 0.5, or 1.0 M* $UO_2(NO_3)_2$ *and tracer-level Pu(IV). Contact: 5 min at A/O phase ratio of 1/1.*

Conceptual Plant Study

A preliminary evaluation[33] was made of the processing of LMFBR fuel in the Nuclear Fuel Services (NFS) plant. The reference fuel used in this study consisted of stainless-steel-clad UO_2-PuO_2 [containing about 10% plutonium (heavy-metal basis)] that had been irradiated to an average core-plus-blanket burnup of 38,500 Mwd/ton. A throughput of 0.52 ton of LMFBR fuel per day was found to be compatible with existing operating license restrictions at NFS; however, a throughput of up to 1.4 tons/day is technically feasible. The solvent extraction flowsheet is based on the use of 15% TBP and feeds of subcritical concentrations (≤5.0 g of fissile plutonium per liter) in geometrically unrestricted equipment. Because of its limited capacity and lack of shielding, the existing plutonium system was replaced by a new shielded, high-capacity continuous anion exchange facility for purifying and packaging plutonium. The irradiation dose received by the solvent in the extraction section of the HA column was calculated, assuming 100% sorption of the beta energy and 40% sorption of the gamma energy, and was found to be 0.017 whr per liter of solvent per pass for fuel cooled 150 days and 0.043 whr/liter for fuel cooled 30 days. Processing after 30 days, or after even shorter cooling periods, was determined to be technically feasible. A brief cost study indicated that processing the fuel from ten 1000-Mw (electrical) fast reactors in the NFS plant would cost 0.11 mill/kwhr (electrical).

[33] E. L. Nicholson, *Preliminary Investigation of Processing Fast-Reactor Fuel in an Existing Plant*, ORNL-TM-1784 (May 8, 1967).

2. Fluoride-Volatility Processing

The present investigation of fluoride-volatility processing at ORNL is part of an intersite program; the aim of this program is to develop an alternative to the aqueous method for recovering valuable components that are present in spent UO_2 fuel from power reactors. The AEC's goals for this work, the responsibilities of other sites, and the possible advantages of volatility methods have been discussed in earlier progress reports. Our main contribution will be the installation and operation of a "hot" pilot plant (Fluidized-Bed Volatility Pilot Plant – FBVPP) in two of the shielded cells in Building 3019.

During this report period, the BrF_5-F_2 reference flowsheet was adopted for the FBVPP, thus eliminating the codistillation of UF_6 and PuF_6. Plans to install equipment for leaching waste solids from the primary reactor were abandoned. Nearly all the head-end equipment was fabricated, structural steel and much of the head-end shielding was installed, and installation of process equipment was initiated. Design of the distillation system for separating and purifying UF_6 was begun, and cell 2 was cleaned out in preparation for this equipment. A satisfactory method for purifying PuF_6 is not yet available.

We continued laboratory- and small-engineering-scale studies in support of the fluidized-bed volatility process. Laboratory work emphasized problems that are expected in conjunction with the use of bromine fluorides and sorption-desorption methods for purifying PuF_6. We developed a new laboratory method for decladding and oxidizing Zircaloy-clad UO_2 fuels by the use of hydrogen, oxygen, and HF-O_2 in sequence. This method has a very rapid rate of reaction; also, it would eliminate difficulties recently experienced with filtering $ZrCl_4$, which is produced in the HCl decladding step, and would tolerate higher fuel:alumina weight ratios than the HF-O_2 process. The effect on plutonium retention remains to be studied. The size range of U_3O_8 particles formed during the oxidation of UO_2 was determined, and problems of filtering U_3O_8 were studied. The effects of five process variables on the retention of uranium by alumina after treatment with fluorine were evaluated in a statistically designed experiment. Related studies indicated that fluorine apparently leaves less residual uranium with the alumina bed than BrF_5 does, particularly at temperatures above 300°C. A fluorine calorimetric reactor (FCR) was developed for determining concentrations of bromine and BrF_3 in the primary reactor off-gas by mixing the off-gas with fluorine and measuring the temperature rise.

Following further transpiration-type studies and simulated process flowsheet studies, attempts to purify PuF_6 by sorption-desorption using LiF were terminated in favor of the use of NaF as a sorbent. Low-surface-area LiF was found to have satisfactory sorption and desorption characteristics for PuF_6, and it satisfactorily separated UF_6 and PuF_6. However, low-surface-area LiF would require an excessively high bed volume. High-surface-area LiF, which could be used in reasonably low volumes, had satisfactory sorption characteristics but unsatisfactory desorption and disintegration properties. Separation of UF_6 from PuF_6 was inadequate at 175°C. Therefore the sorption of PuF_6 by NaF, and the subsequent dissolution of the NaF, was proposed as an alternative separation and purification method. Unfortunately, purification of the plutonium from the ruthenium and niobium fission products has, so far, been inadequate, and further studies have been abandoned.

More attempts were made to find a satisfactory metal fluoride sorption-desorption system for NpF_6. The sorbents MgF_2, LiF, CaF_2, and BaF_2 appear unsuitable; however, NaF sorbs NpF_6 effectively from 200 to 450°C, and the NpF_6 may be desorbed either with nitrogen or fluorine.

Equipment was installed in Building 4507 for hot-cell tests of the fluoride-volatility process. Emphasis will be on the effectiveness of the 400°C

NaF trap in decontaminating UF_6 during fluorination with BrF_5 and in developing purification methods for PuF_6. A scrubber was developed for the removal and disposal of gaseous fluorides and fluorine; the effectiveness of adding 0.2 *N* KI to 2 *N* KOH was demonstrated.

The subcontract with Battelle Memorial Institute – Columbus Laboratories (BMI) for corrosion studies was maintained. Workers at BMI reported data on intergranular modifications of nickel, examined specimens exposed during earlier HF-O_2 studies, exposed several metals to bromine at 300°C, and began assembling small-scale equipment for studying corrosion under fluidized-bed conditions. In addition, they determined the relative resistances of certain metals and alloys to HNO_3-HF solutions and subsequently recommended HAPO-20 as the most suitable material for leaching equipment.

The decision not to install equipment in the FBVPP for leaching waste solids from the primary reactor was based on results of laboratory studies. These studies indicated that a 13 *M* HNO_3–0.1 *M* HF solution is the most effective leachant. Uranium and plutonium recoveries were 85% or greater when the initial uranium or plutonium concentrations in the waste solids were 0.03% or higher; recoveries decreased rapidly below the 0.03% level, and reproducibility of data in this range was poor.

In small-scale engineering studies, work on the decladding and fluorination of stainless-steel-clad UO_2 was terminated; however, similar tests with Zircaloy-clad UO_2 were made. Use of HF-O_2 left relatively massive shards of ZrO_2, but the UO_2 pellets were apparently oxidized completely. Removal of Zircaloy cladding with HCl and subsequent conversion of the $ZrCl_4$ to ZrO_2 was studied by operating the primary reactor and pyrohydrolyzer in series. Difficulties were experienced with unsteady flows in the pyrohydrolyzer and plugging of either the primary reactor filters or the off-gas line between the primary reactor and the pyrohydrolyzer. These runs were interrupted by an accidental contamination of the equipment from an external source of radioactivity. Oxidation tests using untreated, as-received UO_2 pellets required a gradual increase in oxygen content of the oxidizing gas to avoid sintering. Pellets exposed to HCl were successfully oxidized with air.

We continued to investigate the problems involved in sampling solids from a fluidized-bed reactor. The design and the location of the gas-powered jet, which is used to withdraw solids from the fluidized bed for discharge into the external sample loop, were optimized during the period. A jet was designed for use in the FBVPP.

In-line instrumentation is now available for analyzing the hydrogen content of the pyrohydrolyzer off-gas stream, excess oxygen from the oxidation step, and the concentration of fluorine during the plutonium fluorination step. Work continues on the use of a gas chromatograph for analyzing off-gas from the BrF_5 fluorination step.

2.1 STATUS OF FLUIDIZED-BED VOLATILITY PILOT PLANT

The Fluidized-Bed Volatility Pilot Plant (FBVPP) is being designed for installation in Building 3019. Initial emphasis will be on the study of the processing of Zircaloy-clad UO_2 power reactor fuels at irradiation levels to about 30,000 Mwd/ton with 140-day cooling. Later, processing of stainless-steel-clad UO_2 may be studied.

In these studies we hope to develop data that are needed in the design of a full-scale commercial plant. Specific benefits to be derived were listed previously.[1]

In accordance with an agreement with project workers at ANL and ORGDP, and with the AEC, the flowsheet for the FBVPP was modified during the year, as described under "Process Description." Plans to install leaching equipment in the FBVPP were discontinued.

Nearly all the equipment required in the decladding, oxidation, and fluorination of cold uranium fuel has been fabricated. Structural steel and much of the shielding were installed in cell 3, where head-end process equipment will be located, and installation of equipment was begun. Purchasing and fabrication of mechanical handling equipment and instrumentation (including a computer-based data acquisition system) are progressing. Electrical gear and ventilation components are being installed.

The design of distillation equipment and traps for separating and purifying UF_6 was begun, and cell 2 was prepared for installation of that equipment. A satisfactory method for purifying PuF_6 is not yet available.

---

[1] *Chem. Technol. Div. Ann. Progr. Rept. May 31, 1966*, ORNL-3945, p. 54.

Studies of criticality problems and hazards evaluation were continued. A report on problems of handling plutonium in the FBVPP was issued.[2]

Arrangements were made to obtain all of the fuel (except nonirradiated PuO_2) that is needed for studies of Zircaloy-clad fuel processing.

Process Description

The FBVPP flowsheet initially consisted of the following discrete operations: decladding, oxidation, fluorination, and distillation for separating and purifying uranium and plutonium. Workers at ANL, however, had difficulty in obtaining high recoveries of plutonium from the fluidized-bed reactor during the fluorination step. Also, the likelihood of excessive thermal and radioactive decomposition of the PuF_6 in the still during rectification was recognized. The flowsheet was, therefore, changed from that described last year, hopefully to solve both problems.[1] A simplified version of the overall flowsheet as of May 31, 1967, is shown in Fig. 2.1.

In the revised flowsheet, as in the initial one, the Zircaloy cladding is removed from the fuel element by reaction with anhydrous HCl at a bed temperature of 400°C to form volatile $ZrCl_4$. The unreactive UO_2 pellets remain in the bed. The $ZrCl_4$ flows to a separate vessel and is converted to ZrO_2 by reaction with steam at 350°C in a fluidized bed of alumina.

Whereas previously UO_2-PuO_2 was oxidized to U_3O_8-PuO_2 in the lower part of the primary reactor while the oxides were being converted to the hexafluorides with fluorine in a higher zone, the new flowsheet includes an oxidation step followed by fluorination – first with BrF_5 at 350°C to form UF_6 and PuF_4 and then with fluorine at 350 to 550°C to produce PuF_6. This modification results in a complete and early separation of the uranium from plutonium, thus permitting simplification of the uranium decontamination process.

After decladding and pulverization of the UO_2 pellets by reaction with oxygen in nitrogen at 450°C to form U_3O_8, the uranium is converted to UF_6 by reaction with BrF_5 at or below 350°C. The PuO_2 is simultaneously converted to nonvolatile PuF_4 and remains in the reactor. The volatile UF_6, excess BrF_5, some volatile fission product fluorides, and the bromine or BrF_3 reaction byproducts pass out of the reactor to the recombiner, in which the bromine and BrF_3 are reacted with fluorine at about 700°C to re-form BrF_5. Then the gases, including an excess of fluorine, pass through a 400°C NaF trap for removal of much of the ^{95}Nb and ^{103}Ru fluorides. The remaining gases are cooled to about 60°C and are partially condensed in a cold trap at about –60°C. The UF_6, BrF_5, and volatile fission product fluorides in the cold trap are melted, weighed, sampled, and drained to a batch distillation column, where the UF_6 and BrF_5 are separated from each other and from most of the accompanying fission product fluorides. The still system operates at a pressure of 3 atm (abs) and a temperature of about 86°C, sufficiently above the UF_6 triple point (64°C) to prevent solidification of the UF_6. The low-boiling fission products are vented from the still overhead to the off-gas scrubber. The BrF_5 overhead, the initial still product, is held for reuse in subsequent runs. The BrF_5-free UF_6, the final still product, is collected separately and is subsequently vaporized through sorbent traps for final purification and then condensed in a product container. The high-boiling fission products remain in the still reboiler; they are eventually volatilized to sorbent traps and discarded.

Upon completion of the uranium volatilization step, the plutonium in the primary reactor is contacted with fluorine (at least 50 vol % in nitrogen) at temperatures that are progressively increased from 350 to 550°C; it is volatilized from the reactor as PuF_6 and collected. To date, however, the collection method and the purification flowsheet for the PuF_6 have not been selected.

Several additional items of equipment were required to accommodate the flowsheet changes, and some added safety precautions, such as the use of Monel pans under all equipment containing liquid BrF_5, were necessary to protect operating personnel and equipment. The following items of equipment were either modified or added: the BrF_5 vaporizer, the BrF_5 regenerator, the 400°C NaF trap, the cooler following the NaF trap, and the cold-trap sump. The system for withdrawing product from the distillation column was extensively revised.

The processing capacity of the facility was not changed. The pilot plant is sized to process a charge of about 40 kg of UO_2 and up to 2 kg of plutonium. The primary reactor will be 8 in. in inner diameter and about 12 ft high, and will accommodate a fuel element 60 in. high with a 5.4-in.-square cross section.

[2]F. W. Miles, *Plutonium-Related Safety Aspects in Designing the Fluidized-Bed Volatility Pilot Plant*, ORNL-TM-1593 (November 1966).

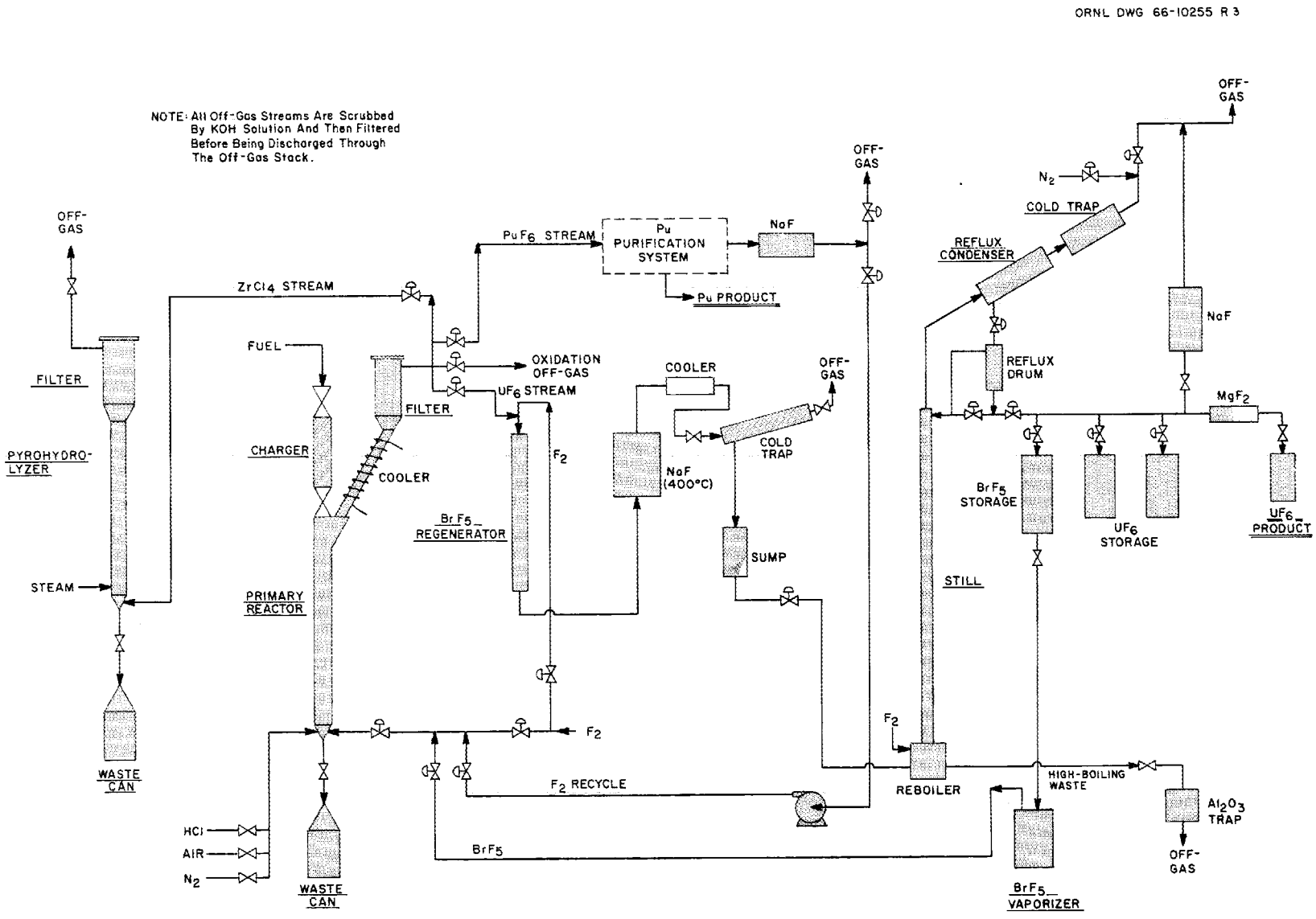

Fig. 2.1. Flowsheet for Fluidized-Bed Volatility Pilot Plant as of May 31, 1967.

Status of Design, Fabrication, Procurement, and Installation of Process Equipment

Engineering Flowsheets. – All engineering flowsheets except those for service equipment, plutonium fluorination, and plutonium purification were completed. The flowsheets show process equipment, flow paths, and instrumentation, and identify all process and instrument piping. Completed flowsheets and their drawing numbers are as follows:

Drawing No.	Flow Diagram
P-11080-XC-001-E	Head End Process
P-11080-XC-046-E	Uranium Fluorination
P-11080-XC-049-E	Uranium Purification
P-11080-EE-003-E	Off-Gas Scrubber
P-11080-XC-021-E	Utilities

Cell 3 Equipment. – Processing equipment to be located in cell 3 was designed, and approved drawings were issued for all items except the 400°C NaF trap. The conceptual design of this vessel was approved, and final design drawings are in preparation. The primary reactor, the pyrohydrolyzer, their filters, the reactor gas cooler, the primary cold trap, and the scrub tower demister were completed. The BrF_5 vaporizer and the BrF_5 regenerator are being fabricated. Wall thicknesses of the primary reactor and pyrohydrolyzer were measured using an ultrasonic technique (Vidigage) for later determinations of corrosion rates. The scrub tower and the scrub tank (previously fabricated), the primary reactor, and the primary cold trap were positioned in the cell.

Preliminary drawings for the piping associated with the decladding operation, the first step to be cold-tested in the pilot plant, were issued.

The cells in Building 3019 were prepared as required by the schedule. All curbing for shield supports, all sumps, a drain trap, all waste-liquid drain line block valves, and all floor gratings at three levels were installed in cell 3. Also, most of the shielding, cell ventilation ductwork, and cell lighting, all of the electrical junction boxes, and part of the electrical wireways were installed. Holes (6, 12, and 18 in. in diameter) were drilled in the 4- to 5-ft-thick concrete cell walls and ceiling.

Sections of the piping for the vessel off-gas scrubber were fabricated in ORNL shops; some have been installed in cell 3.

Cell 2 Equipment. – Conceptual design studies of the UF_6-BrF_5 still and UF_6 purification traps are proceeding. The UF_6 product station will also be located in cell 2. Preliminary design of the shielding and of the equipment layout was started.

All equipment remaining from the Molten-Salt Volatility Pilot Plant (MSVPP) was removed from cells 1 and 2. All surfaces of cell 2 were decontaminated and painted. In cell 1, the wall separating the waste station and the reactor room was removed preparatory to decontamination and subsequent installation of volatility waste processing equipment. The cell 2 off-gas duct was relocated and enlarged to allow passage of more air with a lower pressure drop; it extends into the sample gallery as before.

Exterior Construction. – The outside piping between the nitrogen trailer station and Building 3019 was installed. A platform to hold the new filters to be used in the building ventilation system was also installed. The Building 3100 ventilation duct was blanked off to minimize loss of vacuum. Stainless steel ductwork was received; however, installation will be delayed until all of the SGN caisson filter enclosures have been received.

Mechanical Equipment. – The overall design of mechanical handling equipment to be used for waste solids, excluding the plutonium phase of the project, is about 65% complete. Conceptual design of all in-cell mechanical handling equipment for cell 2 is virtually complete; detailed design is well advanced. The manipulator for all flanges between the solids outlet of the primary reactor and its waste can has been fabricated (Fig. 2.2). Other components and subassemblies are being constructed. Detailed design of the fuel-loading station is almost complete; part of the conceptual design and much of the detailed design of the fuel charger-carrier and the canal loading tools remain to be done. We are still studying a modification of the carrier that will allow it to serve as a means of handling both the fuel elements and waste-solids vessels. This change in the carrier concept was made possible by (1) a reduction of the reactor waste-can diameter to 14 in. and (2) a change in method for alpha containment during transfer of waste vessels between cell and carrier, namely, encapsulation of the vessel in a metal liner instead of plastic bags. Detailed design of the alpha-containment system for the waste vessel is essentially complete; after considerable study the same "canning" concept has been adopted for transferring porous metal filters from the filter enclosure to the carrier. Detailed design of the

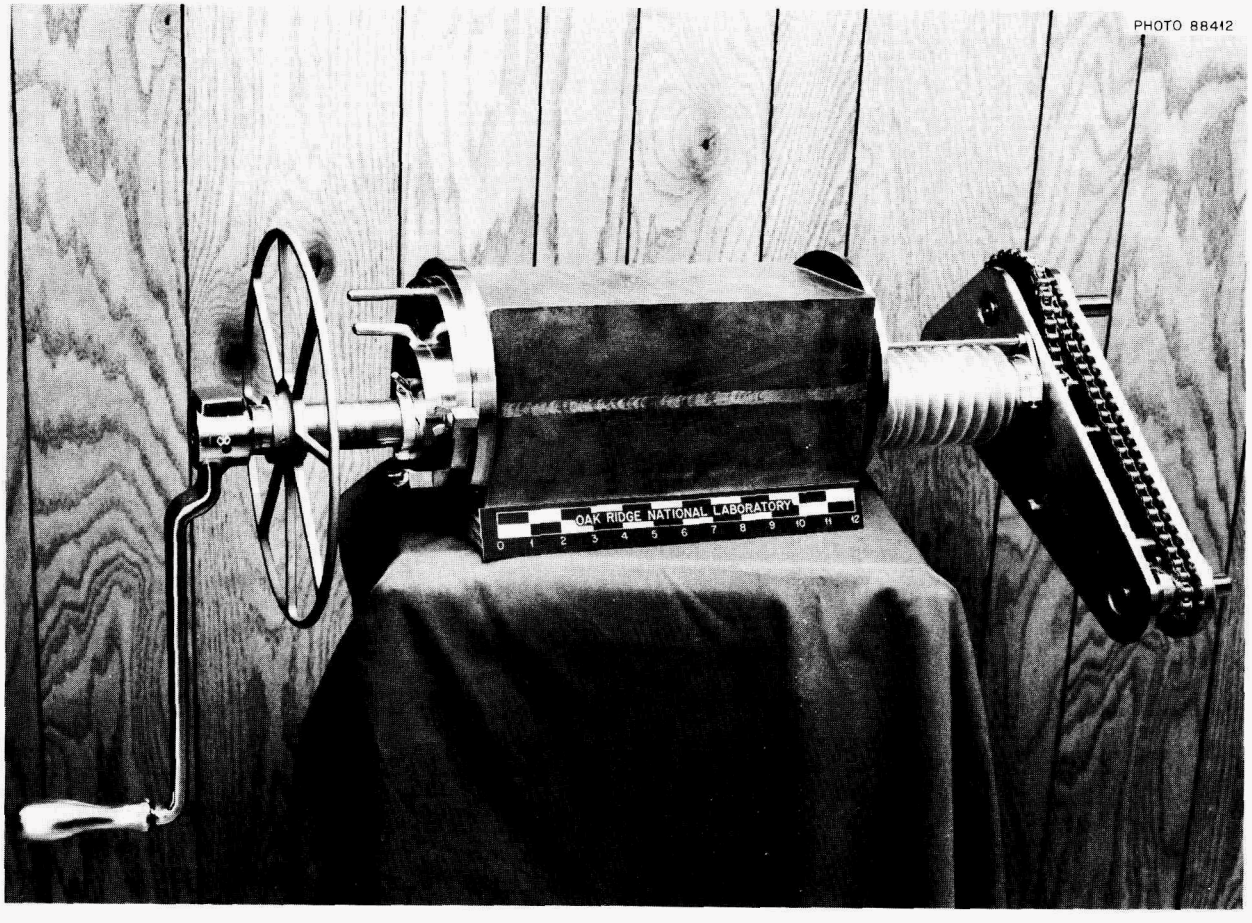

Fig. 2.2. Manipulator for Coupling and Uncoupling Flanges Between Solids Outlet of Primary Reactor and Its Waste Can.

filter removal system is now under way. Simplified views of the in-cell mechanical handling equipment, as it will be assembled, and the locations of the various solids waste cans and vessels are shown in Figs. 2.3 and 2.4. The pickup arm and elevator mechanism (Fig. 2.3) has three modes of movement: (1) rotation through 270° to positions for the primary reactor and pyrohydrolyzer waste cans and their storage racks, for the 400°C NaF (U-CRP) trap, and for the cell roof port at the carrier station; (2) extension and retraction of the pickup arm; and (3) elevator action of the pickup arm.

Figure 2.5 is a simplified view of the fuel element carrier and charging station. The station is in the penthouse directly above the primary reactor fuel chute. The main component is the shielded, alpha-contained glove box on which the charger-carrier is placed. A lead glass window is provided for viewing the passage of the fuel element, suspended by a zirconium wire, from the carrier through the glove box to the chute. A sliding section of the shield gives access to the glove port, when the radiation level is low, for operations such as opening and closing the fuel element ports, cleaning the interior of the glove box, and cutting the zirconium wire. The charger-carrier is provided with a position counter (a device for measuring revolutions of the cable on which the element is suspended) to track the movement of the element and a load indicator to detect any interference with free movement of the element. Alpha containment is provided at all stages for the carrier and also between the carrier and the glove box.

Material Procurement. – The furnace for the lower part of the primary reactor is expected to arrive from Marshall Products Company in mid-June 1967. Also,

ORNL DWG 67-5252

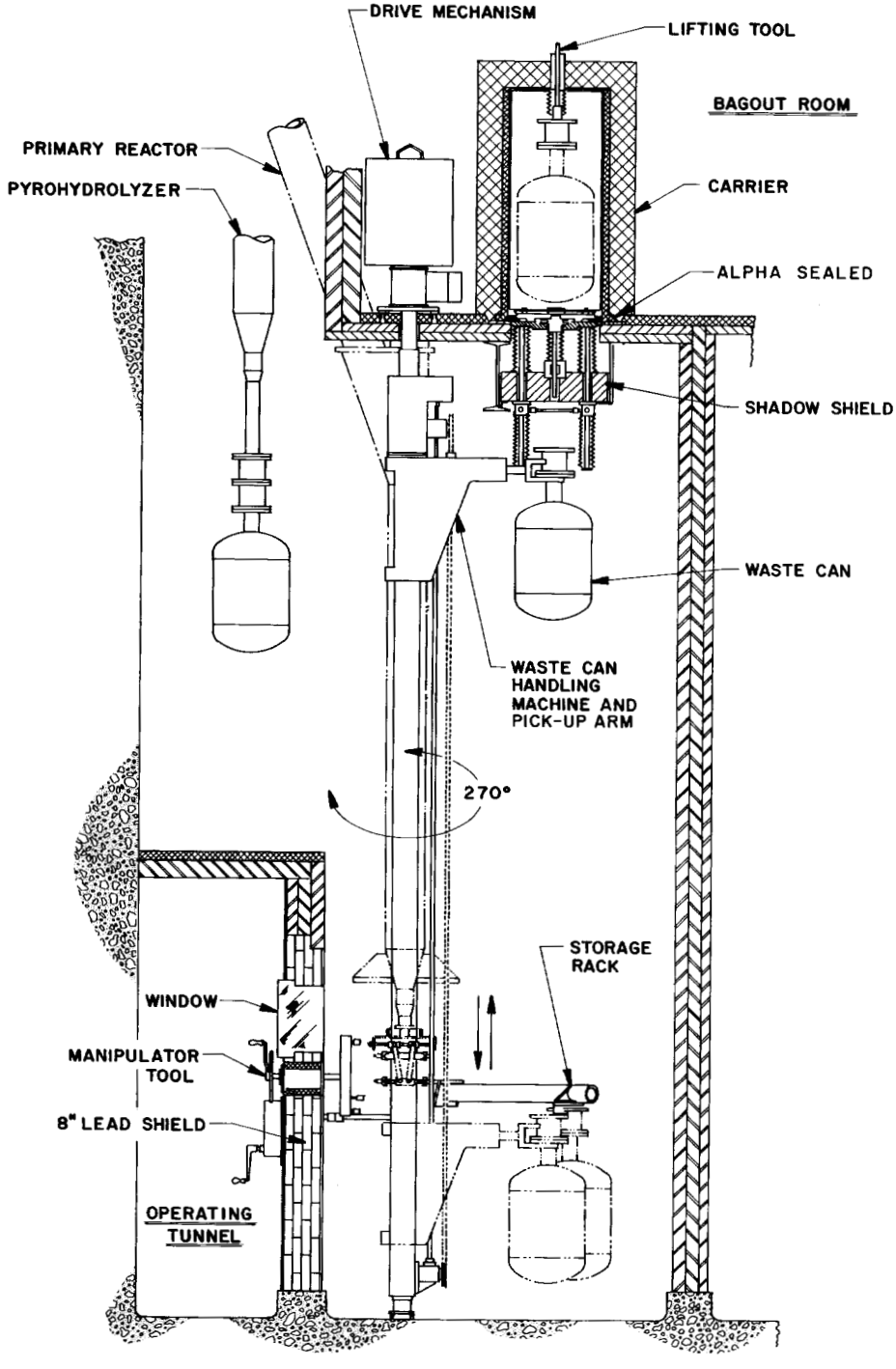

Fig. 2.3. Equipment for Handling Waste Solids in Cell 3 (Elevation View).

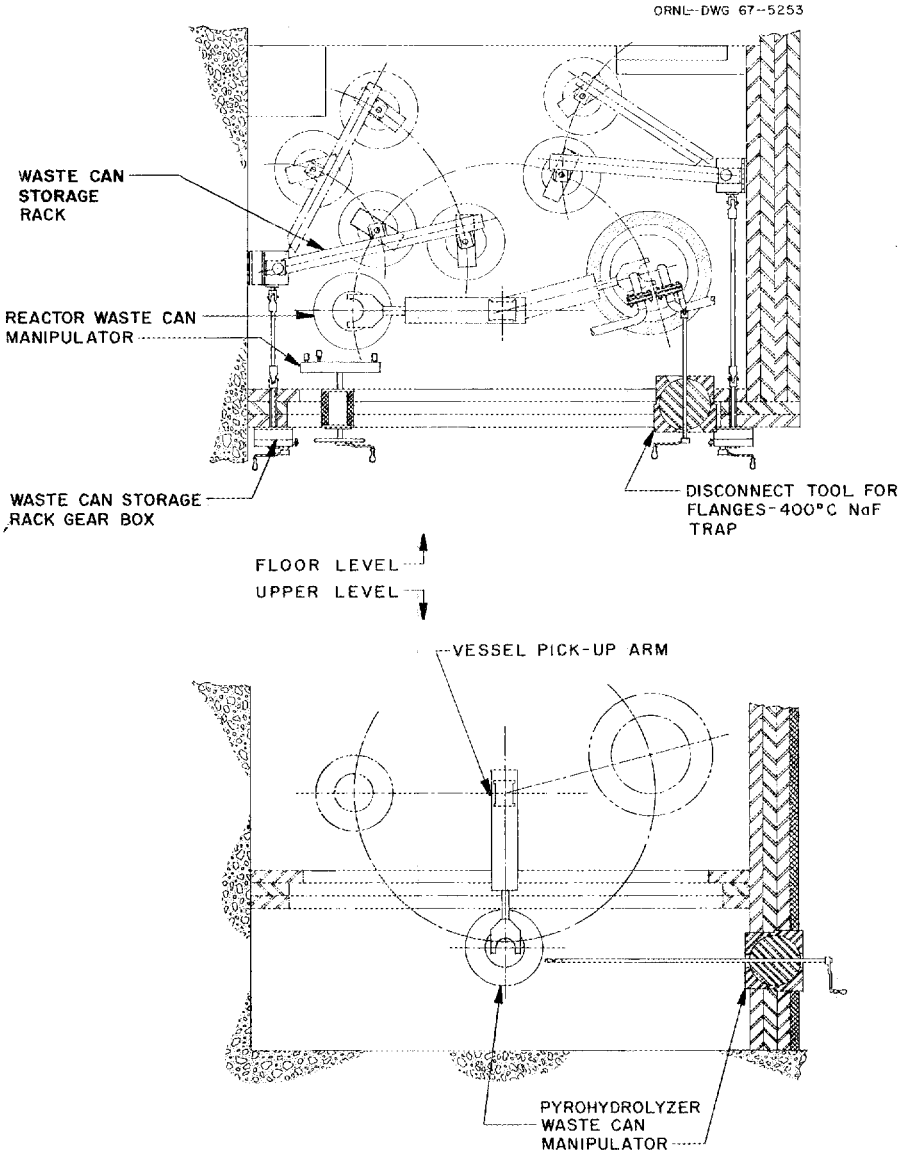

Fig. 2.4. Locations of Waste Solids Vessels and 400°C NaF Trap in Cell 3 (Plan Views).

ORNL DWG 66-6953RI

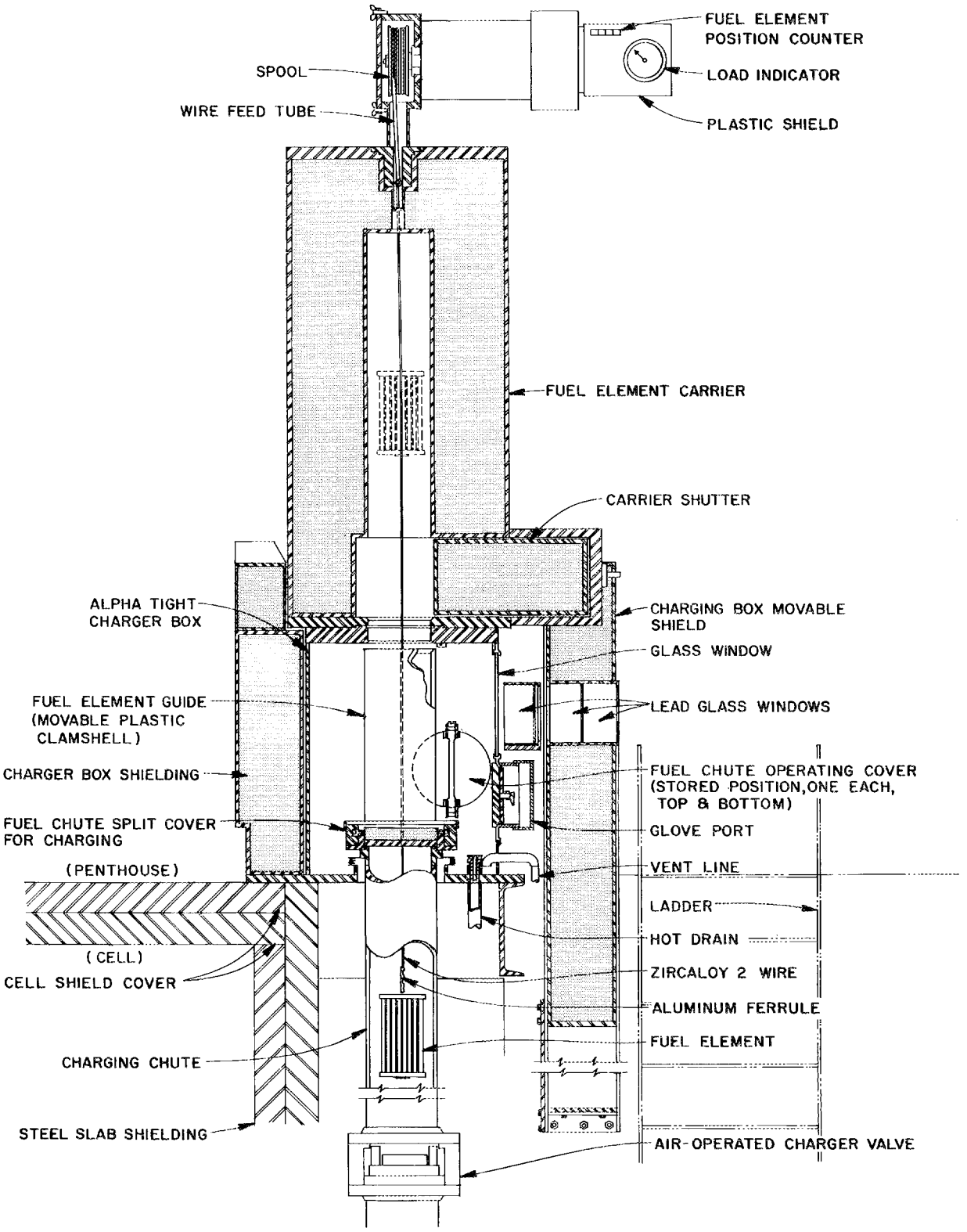

Fig. 2.5. Fuel Element Carrier and Fuel Charging Station.

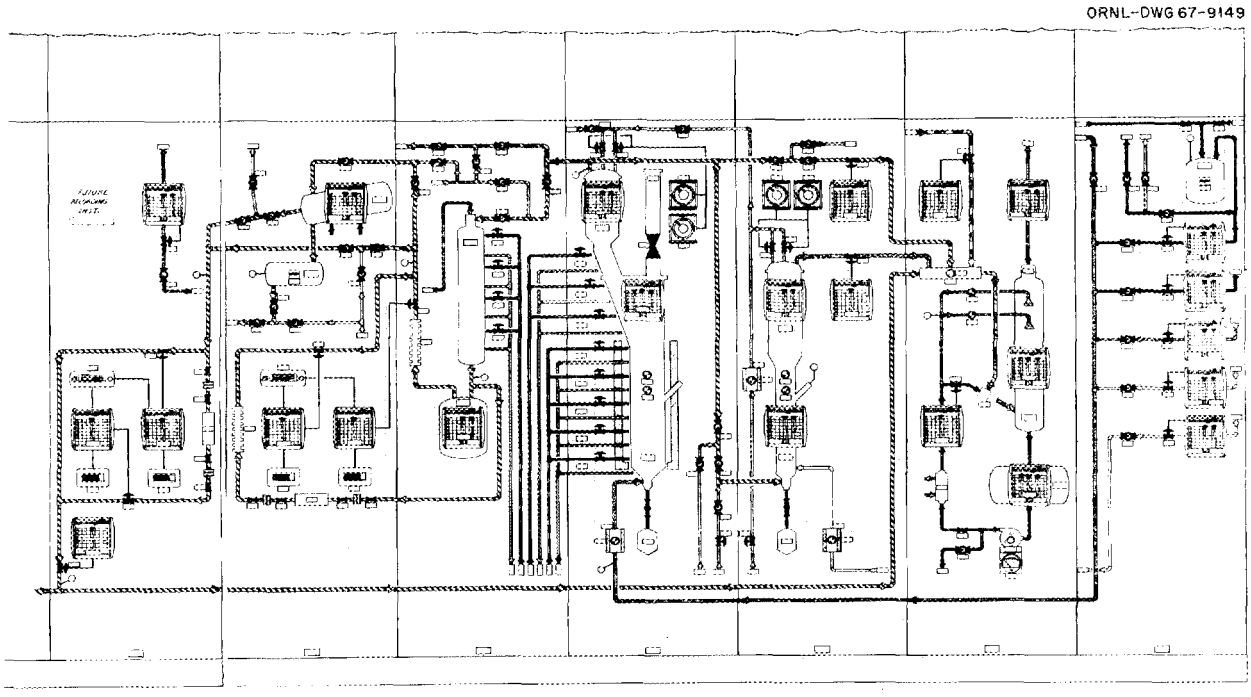

Fig. 2.6. Design of Graphic Panelboard for Decladding, Oxidation, and Uranium Fluorination Steps. Main vessels shown are, from left to right, UF_6-BrF_5 regenerator, primary reactor, pyrohydrolyzer, off-gas scrubber, and KOH tank.

the filter tubes for the primary reactor and the pyrohydrolyzer filters have been received and accepted. The filtration medium is nickel Feltmetal.[3] The 8-in. valve for the charging chute was received from Mill Lane Engineering Company. It was fabricated from stainless steel and was nickel-plated by the electroless process at ORGDP. The specially designed 3-in. stainless steel ball valves, for use at the bottom of the primary reactor and pyrohydrolyzer and for the waste cans, are being purchased from Worcester Valve Company and should be delivered late in June 1967. Numerous difficulties have been encountered in fabricating the finned gas coolers that are required before and between stages of the fluorine recycle compressor. These units are being fabricated by Wall Colmonoy Corporation and Oak Ridge Tool and Die Company and should be delivered in July 1967.

Instrumentation. – A graphic panelboard was designed for the decladding, oxidation, and uranium fluorination portions of the BrF_5-F_2 flowsheet (see Fig. 2.6). The panelboard is being fabricated in the ORNL shops. Essentially all of the process instruments and control valves needed for the cold decladding runs have been procured. Installation of the instrumentation in the pilot plant is scheduled to start early in fiscal year 1968. Only conceptual design work has been done on the instrumentation for the uranium purification and plutonium fluorination and purification portions of the process.

About 30 of the air-operated valves used in the MSVPP are being reconditioned for use in the FBVPP. An additional 25 Mason-Neilan valves, of Monel construction, and 8 Hammel-Dahl valves, of nickel construction, have been procured. Twenty Foxboro d/p cell transmitters, of Monel construction, have been obtained for pressure and flow measurements. The Foxboro transmitters were nickel-plated in the ORNL shops for additional corrosion protection. Some Bourdon-tube transmitters will also be used for pressure measurements in the FBVPP. Most of the temperature recorders, controllers, and autotransformers used in the MSVPP have been salvaged and will be used in the FBVPP.

The analytical instruments that will be used for continuous gas analysis in the FBVPP have been procured and are being tested in the Unit Operations Section. They include:

[3]Trademark for sintered metal fibers manufactured by Huyck Metal Co., Milford, Conn.

1. a Gow-Mac thermal conductivity gas analyzer to measure the hydrogen content of the off-gas during the HCl decladding step,
2. a Hays model 625 analyzer for measuring oxygen concentration during the oxidation and uranium fluorination steps,
3. a Du Pont photometric analyzer for fluorine analysis,
4. a Gow-Mac gas density detector to estimate the density (and possibly the uranium content) of the gas stream from the primary reactor during uranium fluorination,
5. an MSA Billionaire to detect chlorides and fluorides in the cell ventilation air.

The fluorine calorimetric reactor (FCR), developed by Chemical Development Section B and described in Sect. 2.6, will be used to give a continuous indication of the bromine-BrF_3 content of the primary reactor off-gas. Development work is also being done in the Unit Operations Section on a gas chromatograph that may be used to analyze the off-gas from the primary reactor.

Enclosures were designed for the main instrument transmitter rack in the penthouse and for the analytical instruments to be located in the cell 3 gallery. A mechanism was designed that will permit the transmitters and purges to be adjusted from outside the enclosure.

The number and types of radiation monitoring instruments that will be required for the FBVPP have been investigated. At present, we plan to use a gamma-ray spectrometer, consisting of an NaI scintillation crystal and multichannel analyzer, to identify fission products at various locations in the system. Ionization chambers (about ten) and electrometers will be used to measure the radiation level. Preliminary design work has been done on the shielding and the collimator for the gamma-ray spectrometer. Currently, we plan to use about four detectors for the gamma-ray spectrometer. Detection of neutrons from the (α, n) reactions with fluorine will be used as a means of determining the location of plutonium in the system.

The data handling requirements of the FBVPP have been reviewed, and a survey has been made of the commercially available equipment that might be used. As a result of this study we now plan to use a computer-based data acquisition system that will sample up to 298 electrical signals and 128 pneumatic signals at a rate of about 10 signals/sec. The system will convert raw data into engineering units for printout upon demand, limit check each signal, and write a magnetic tape for later analysis on an ORNL central computer. In addition, alarms will be actuated upon signal deviations, and periodic alarm summaries and up to six trend logs will be printed. The PDP-8 computer (Digital Equipment Corporation) and other components of the system are being purchased separately; they will be assembled at ORNL.

Instruments (e.g., air monitors, personnel monitors, and threshold detector units) to provide adequate radiation protection for personnel will be installed at strategic locations.

Electrical. – Electrical items for which the design is essentially complete include the junction boxes, wireways, and lighting for cell 3; and the wire and cable layouts, main vessel heaters, and process piping heaters for the head end of the FBVPP. Items for which the design is partially complete include the power distribution center and the bill of materials. Very little progress has been made on the design of cell 2 equipment.

In general, electrical designs are similar to those used in the MSVPP. Three differences are expected, however, to result in improved utility of power, plant operation, and safety for the FBVPP. First, a 10/20-v electrical system is being used to heat short pipelines to temperatures of 150°C or less. Use of this system is expected to result in a lower power requirement for these lines and, consequently, less overheating of the lines. Second, each 230- and 480-v compartment in the distribution center will obtain its control-circuit power from its own power leads, instead of from one of two control circuits as in the MSVPP. This arrangement will be safer, since activating the disconnect switch for a compartment will turn off both the control circuit and the load circuit. In addition, difficulty with any particular control circuit will affect only one compartment, instead of half of the compartments, as in the MSVPP. Finally, for increased safety 440-v autotransformers will be placed on a separate panelboard having an expanded-metal guard.

Ventilation and Containment. – The ductwork, filters, and an off-gas scrubber are the major components of the ventilation and containment system for the FBVPP. To ventilate the primary containment areas, 1500 cfm of air will be drawn from the penthouse, an existing secondary containment area in Building 3019, to both cells 2 and 3. The exhaust air streams from these cells will join and pass in series through an aqueous KOH scrubber and two

banks of high-efficiency particulate air filters (HEPA). Then this stream of air (3000 cfm) will mix with that (1500 cfm) from cell 1. The combined stream (4500 cfm) will flow through a second aqueous KOH scrubber and an HEPA filter bank (currently being modified) before joining the ventilation stream from other operations in Building 3019. This total ventilation stream will then flow through an exhaust fan and out of the Building 3020 stack. The first scrubber and the two banks of HEPA filters will be located in cell 2, while the other pieces of equipment mentioned will be situated outside the building. The outside ventilation scrubber was installed during the operation of the MSVPP to protect the downstream filters from damage by corrosive fluoride gases; this scrubber will remain in service.

A new filter system will allow air to be drawn through cells 1, 2, and 3 at the rate of 4500 cfm. Previously, the ventilation air from all of Building 3019 passed through only one set of filters. The new system will consist of three enclosures, each containing three $24 \times 24 \times 11\frac{1}{2}$ in. HEPA filters. The status of this installation is described under "Exterior Construction" above.

Items for which the design is complete are the new filter enclosures just mentioned and the ventilation system for cell 3. Design is partially complete for the ventilation system for cell 2 and the in-cell scrubber and filter installation in cell 2, which will clean the ventilation air from both cells 2 and 3.

Special features of the FBVPP ventilation system include its ability to:

1. Humidify the air streams in cells 2 and 3 to a dew point of 50°F to effect the removal of accidentally released PuF_6 and UF_6 as particles on HEPA filters.[2]
2. Provide shielded compartments in cells 2 and 3 for main equipment items and use enclosures and glove boxes in other areas to contain radioactivity in the event of an accidental release. All of these compartments are airtight and have ventilation systems equipped with filters and back-pressure dampers. Examples of enclosures are those used for the transmitter rack in the penthouse and the analytical sampling stations in the operating gallery opposite cell 3.
3. Scrub the ventilation air to prevent accidentally released fluoride gases from damaging the HEPA filter installations.

Some method is required for protecting the two-bank filter installation that is planned for cell 2. Before deciding to use an aqueous KOH scrubber, we made a study to determine whether a scrubber or a solid sorbent bed would be more suitable.[4] Results of the study showed the scrubber to be the obvious choice. The solid sorbent bed had some advantages, but it seemed more applicable to smaller-scale installations.

The above features are salient parts of the containment policy recommended for the design of the FBVPP[2] and were felt to be necessary to provide the degree of containment needed to safely handle plutonium isotopes and their daughters. Two of these measures are identical to two of the tentative ORNL containment criteria for processing cells[5] – item 2 is identical to criterion h and item 3 to criterion i of the reference.

The HEPA filters in cell 2 will be held within side-loading enclosures of special design. With these enclosures, filters can be changed without contaminating the surroundings or interrupting operations. This capability is thought to be essential in areas where plutonium is handled, in order to prevent the spread of radioactivity, the exposure of personnel to radioactivity, or both. Other filter enclosures in which plutonium may be collected will be of a similar design.

Project Planning, Scheduling, and Reporting. – Details of the cost reporting system and the critical path scheduling method used with this project were published during the year.[6]

The project plan was modified twice during this period. The first modification consisted in reconciling the plan with the schedule to November 1966. During March 1967, the project plan was completely revised as a result of the adoption of the BrF_5 flowsheet. The scope of each activity was reestimated, and the sequence of activities was, in many instances, changed. At that time, the project was reorganized along the lines of the major engineering flowsheets: head-end process, fluorination of uranium, purification of uranium, and processing of plutonium.

As of May 31, 1967, the project is estimated to be 54% complete, based on an estimate of labor and

---

[4] F. W. Miles and E. L. Youngblood, personal communication, May 22, 1967.

[5] *Radiation Safety and Control Manual*, sect. 6.2, Oak Ridge National Laboratory, 1961.

[6] W. W. Goolsby and F. T. Snyder, *Critical Path Time-Cost Scheduling for Management of Research and Development Projects*, ORNL-4112 (May 1967).

materials costs that include an assumed value for the processing of plutonium.

Miscellaneous Design Studies

Criticality. – From the standpoint of criticality, the only isotopes that will be present in sufficient quantities in the FBVPP to be important are ^{239}Pu and ^{235}U. Tentative limits of fissionable elements per run are 2 kg for plutonium (more than 40 wt % ^{239}Pu) and 40 kg of uranium (less than 2 wt % ^{235}U). The total allowable plant inventory for plutonium is, at present, considered to be 10 kg; the corresponding value for uranium is 200 kg.

Uranium-235 and plutonium-239 will coexist only in the primary reactor during decladding, oxidation, and uranium fluorination. Since these steps are performed in the absence of moderating materials, no criticality problem will exist for the per-run quantity of ^{239}Pu or ^{235}U or the combination of the two. In addition, no criticality problem will exist for a combination of the total-inventory quantity of ^{239}Pu and the per-run quantity of ^{235}U. However, the accumulation of ^{235}U in the primary reactor combined with the total inventory of ^{239}Pu could produce a criticality problem. Further investigation of the likelihood of such accumulations is needed to determine situations that are not critically safe.

No work relative to criticality has been done for any of the process vessels except the scrubber tank. In general, however, the absence of moderating materials in most of the other FBVPP vessels will eliminate the likelihood of a critical incident. Vessels that may contain moderators (and the possible moderators) are the uranium cold trap (HF), the NaF trap (HF), and the process and ventilation scrubber tanks (H_2O).

A suitable plan has been devised to prevent a critical incident in the process scrubber tank. It consists of the use of: (1) a soluble poison (B^{3+}) in the scrubber solution (4 *M* KOH), (2) a neutron absorptiometer, (3) a two-persons-per-batch-card makeup system, and (3) periodic boron analyses. Calculations indicated that a B^{3+} concentration of 20 g/liter is sufficient to ensure the critical safety of 10 kg of ^{239}Pu (the FBVPP inventory limit) in this tank.[7] The neutron absorptiometer and the other measures will be used as additional means for avoiding criticality. The absorptiometer will monitor the scrubber solution continuously to indicate any decrease in the B^{3+} concentration of the solution. The value of restricted solution makeup and periodic boron analyses is obvious.

Trivalent boron is added to the solution in the form of H_3BO_3. Since the reported solubility of B^{3+} in water is on the order of that needed for adequate criticality protection, solubility tests in 4 *M* KOH were made. These tests indicated that the solubility of B^{3+} in 4 *M* KOH is about 50 g/liter. Other tests in initial and spent scrubber solutions have indicated that values of 22 to 23 g/liter could be obtained at room temperature; no attempt was made to determine the saturation value.

Because precipitation of B^{3+} occurred in some of the simulated scrubber solutions when uranium was added as UO_2F_2, a difficulty in using the soluble poison appeared to exist. Precipitation occurred primarily in solutions containing free KOH and having uranium contents equal to or greater than 10 g/liter. Further tests indicated, however, that no precipitation occurred when an amount of uranium equivalent to 10 kg of plutonium was added to the solution. If plutonium behaves like uranium (as would be expected), protection against criticality is assured for 10 kg of plutonium. Since both uranium and plutonium are not expected to migrate to the scrubber solution at the same time, protection for all credible accidents in the pilot plant is felt to be adequate. In the event this unlikely migration does take place, however, adequate warning will be given by the neutron absorptiometer.

Hazards Evaluation. – The hazards evaluation of the FBVPP consists of two parts: (1) the preparation of a hazards evaluation report that will be presented to the ORNL Radiochemical Plants Committee for review and (2) the review of the system, as it is being designed, to ensure that desirable safety features are included. Preparation of the hazards evaluation report is in progress. A preliminary review of the FBVPP was made in October 1966 by the Chemical Technology Division Radiation Control Officer and several members of the Radiochemical Plants Committee. The purpose of the review was to acquaint the Committee with the layout, equipment, process, potential hazards, and safety features of the FBVPP.

Many factors are being considered in the hazards analysis of the FBVPP; those of primary importance are the containment of plutonium, fission products, and uranium; criticality control; and the hazards associated with the handling of highly reactive

[7] J. P. Nichols, personal communication, July 29, 1966.

chemicals such as fluorine and BrF_5. Safety features are being included in the system to eliminate potential hazards and to contain any material that may be accidentally released. In addition, written run sheets, which are checked during "cold" operation, will be followed during the runs with radioactive material. Some of the safety features being included in the system are discussed below.

Essentially all of the FBVPP process equipment that will contain radioactive material will be located in cells 2 and 3 of Building 3019. These cells are primary containment areas. Equipment that may become highly radioactive or may have external contamination will be located in shielded alpha enclosures within these cells. Equipment that may have internal contamination but that requires maintenance, such as valves, is being located in accessible areas in the cells. Air suits will be worn for maintenance operations; a change station has been installed at the lower entrance of cell 3 for washing down and changing these suits. Ventilation air from the FBVPP area passes through two caustic scrubbers and three sets of HEPA filters before being discharged to the 3020 stack. The caustic scrubbers serve to protect the filters from damage by corrosive gases, such as fluorine and BrF_5. They also ensure that any gaseous UF_6 or PuF_6 accidentally released is hydrolyzed to solid UO_2F_2 and PuO_2F_2, which can be effectively removed by the filters.

Trays will be placed under equipment, such as the BrF_5 vaporizer, that will contain large quantities of liquid BrF_5. Combustible materials will be excluded from the area. A satisfactory method for handling possible BrF_5 leaks in the FBVPP appears to be to collect the BrF_5 in trays and to allow it to evaporate and be neutralized in the ventilation scrubber. Consideration is also being given to the use of dry chemicals for neutralizing BrF_5 leaks. Tests are scheduled at ORGDP during the summer of 1967 to determine effective methods for handling such leaks.

Instruments attached to process equipment but located in secondary containment areas are being located in enclosures as a precaution against the spread of contamination during maintenance operations or in case leaks should occur in the instruments. Alpha-tight containers and bagging techniques will be used to provide continuous alpha containment during such operations as fuel charging, waste removal and burial, and filter replacement. Interlocks are being used to prevent the inadvertent mixing of incompatible process gases, such as oxygen or fluorine, with hydrogen; they are also being employed to automatically close valves to prevent backup of process material into supply lines in the event that the system pressure should exceed the gas supply pressure. A leak detection system is being used on important flanges in the system. In addition to detecting leaks, this system will maintain nitrogen pressure on the flanges to prevent external leakage of process material. Double valves, with nitrogen buffering, are being used in lines where valve seat leakage is particularly undesirable.

The safety of the FBVPP during emergencies such as power failures or abnormal operating conditions is being considered. Remotely operated valves will fail safe in the event of a power failure or loss of compressed air. The ventilation system for Building 3019 and the FBVPP area will switch to a steam-driven fan in the event of an electrical power failure; a study was made that recommends placing additional equipment on the existing system for supplying emergency power and providing additional generating capacity. We also plan to install a "scram" switch similar to the one now in use in the MSVPP. Actuating only one switch at the panelboard or at the entrance of the building will place the FBVPP in a safe standby condition during an emergency.

Laboratory-Scale Studies

2.2 NEW DECLADDING AND OXIDATION METHOD FOR ZIRCALOY-CLAD UO_2 FUELS USING HYDROGEN, OXYGEN, AND HF-O_2 IN SEQUENCE

The two current methods for processing Zircaloy-clad UO_2 have disadvantages. The better of these uses HCl to form volatile $ZrCl_4$. Recently, troublesome plugging of Feltmetal filters occurred when $ZrCl_4$ was being filtered at about 300°C. The second process uses HF-O_2 mixtures to form ZrO_2 in the primary fluidized-bed reactor. Here the acceptable fuel load is quite small because of lumping of the UO_2 when it is constricted in the presence of HF-O_2 mixtures. We have estimated that the fuel-to-bed area ratio should not exceed 0.1.[8] Since

[8] *Chem. Technol. Div. Ann. Progr. Rept. May 31, 1966*, ORNL-3945, p. 49.

neither of these processes is ideal, alternative methods of processing have been investigated.

One such alternative method consists in reacting zirconium with dilute hydrogen ("hydriding") at about 600°C in the presence of ZrF_4 to fracture the cladding, oxidizing at about 450°C to disperse the UO_2 as U_3O_8, completely pulverizing the cladding by treatment at 450°C with diluted $HF\text{-}O_2$ mixtures, and fluorinating with fluorine at 450 to 550°C to volatilize the uranium and plutonium. The use of BrF_5, BrF_3, or ClF_3 at lower temperatures would also be feasible for removing the uranium. The hydriding reaction is exothermic, and effective penetration rates of 80 to 160 mils/hr are attainable. The oxidation step, in which the UO_2 is oxidized to a fine U_3O_8 powder, has only a slight physical effect on the zirconium hydride. The subsequent reaction of zirconium hydride with an $HF\text{-}O_2$ mixture is very vigorous and exothermic but can be controlled by diluting the gas with nitrogen and by using only 5 to 10% HF in the mixture. The presence of ZrF_4 in the bed does not result in losses of uranium greater than those observed with an alumina bed. This method has been tested, using a 0.94-in.-ID fluidized-bed reactor, without serious difficulty.

The possible disadvantages of this method are those associated with plutonium retention and with the possible hazards of zirconium hydride. The amount of plutonium retention in the ZrF_4 produced by the hydride process has not been determined but would need to be defined before such a scheme could be seriously considered. Although zirconium hydride was handled successfully in these small-scale experiments, it should be recognized that, under some conditions, it could ignite during the oxidation step of the process. For example, a high radiation field might initiate the reaction. Further experiments, including hot-cell tests, would need to be made either to eliminate this possibility or to find ways to control and to take advantage of it.

2.3 PARTICLE SIZE AND FILTRATION OF U_3O_8 DURING OXIDATION

During the oxidation step of the fluidized-bed volatility process the UO_2 pellets are converted to a fine U_3O_8 powder. Photographic studies, using an electron microscope, revealed two distinct classes of U_3O_8 particles (Figs. 2.7 and 2.8). The larger particles were irregular in shape, with a number-average diameter of about 4.2 μ. The mass-average diameter of this group is estimated to be about 6 μ. The other class of particles consisted of spherical particles having a number-average diameter of about 0.6 μ. The mass-average diameter of this group is possibly 1.4 μ. Work done by an MIT practice school team gave further evidence about the size distribution of the U_3O_8 particles.[9] By using photomicrographs taken through an optical microscope at a magnification of 1000×, sizes of more than 900 particles were measured with a Zeiss particle analyzer; a log-probability plot of distribution is shown in Fig. 2.9. Since this plot shows only the number of particles determined by optical methods, most of the spherical particles were not included because they were too small to be counted. However, the plotted data agree well with the earlier approximations of average diameter. Since most of the particles are less than 10 μ in diameter, a distinct possibility exists that some of this U_3O_8 can pass through the process gas filters, which are rated to remove 100% of all 10-μ particles.

Experiments with a 0.94-in.-ID fluidized-bed reactor equipped with two filters, each with separate blowback pulsing, allowed approximately 1% of a U_3O_8 charge to pass through the filters during a 4- to 5-hr fluidization. Each of these filters consisted of a 1- by 4-in. flat piece of nickel Feltmetal, rated for 10 μ, that was edge-welded into a holder. Some welding damage to the filters was found in tests that were conducted after the completion of the MIT filtration studies described below. Because of the magnitude of the U_3O_8 loss, the MIT practice team studied U_3O_8 filtration. Their data showed that the Feltmetal filters, when operated properly, are capable of filtering out essentially all the U_3O_8. In fact, with a $1\frac{1}{2}$-in.-ID Pyrex column, a 3-in.-ID disengaging section, and a 3-in.-diam filter, less than 0.0002% of the U_3O_8 passed through the filter in 4 hr of fluidization. After obtaining these results, we made further tests with the 0.94-in.-ID reactor. We then found that, if the filters were operated without blowback, loss of U_3O_8 did not occur. Further, no loss of U_3O_8 was obtained by changing the temperature at which the UO_2 was oxidized from 450 to 525°C or by varying the temperature of the filter in the range of 50 to 275°C. Thus we conclude that the losses experienced earlier can be attributed either to welding damage

[9] D. D. Wilson and P. A. Tomlinson, *Filtration of U_3O_8 from a Gas Stream*, ORNL-MIT-5 (Nov. 9, 1966).

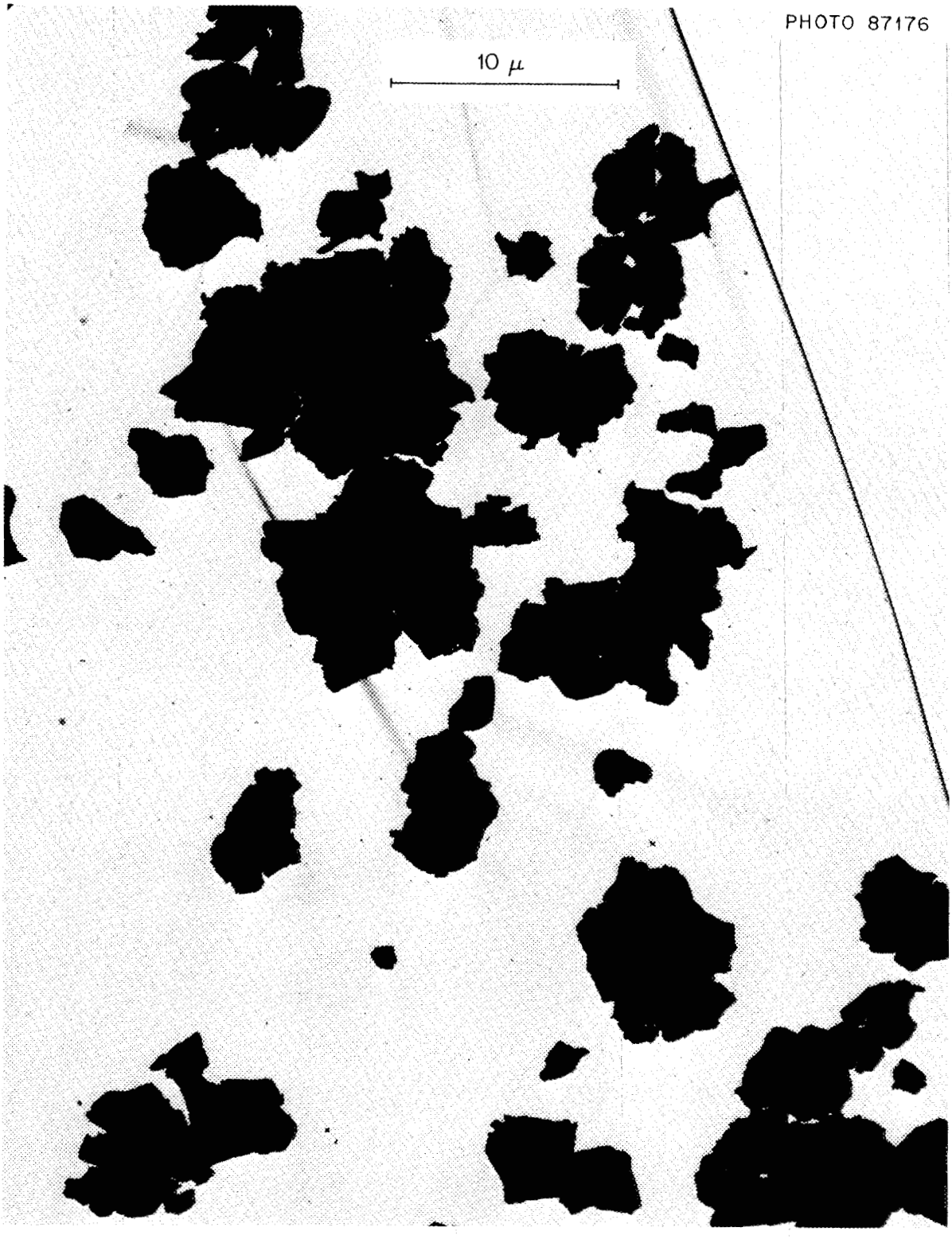

Fig. 2.7. Electron Photomicrograph of U_3O_8 Particles (High-Particle-Size Range). Particles formed in 2-hr fluidized-bed oxidation run at 525°C with 20% O_2–80% He.

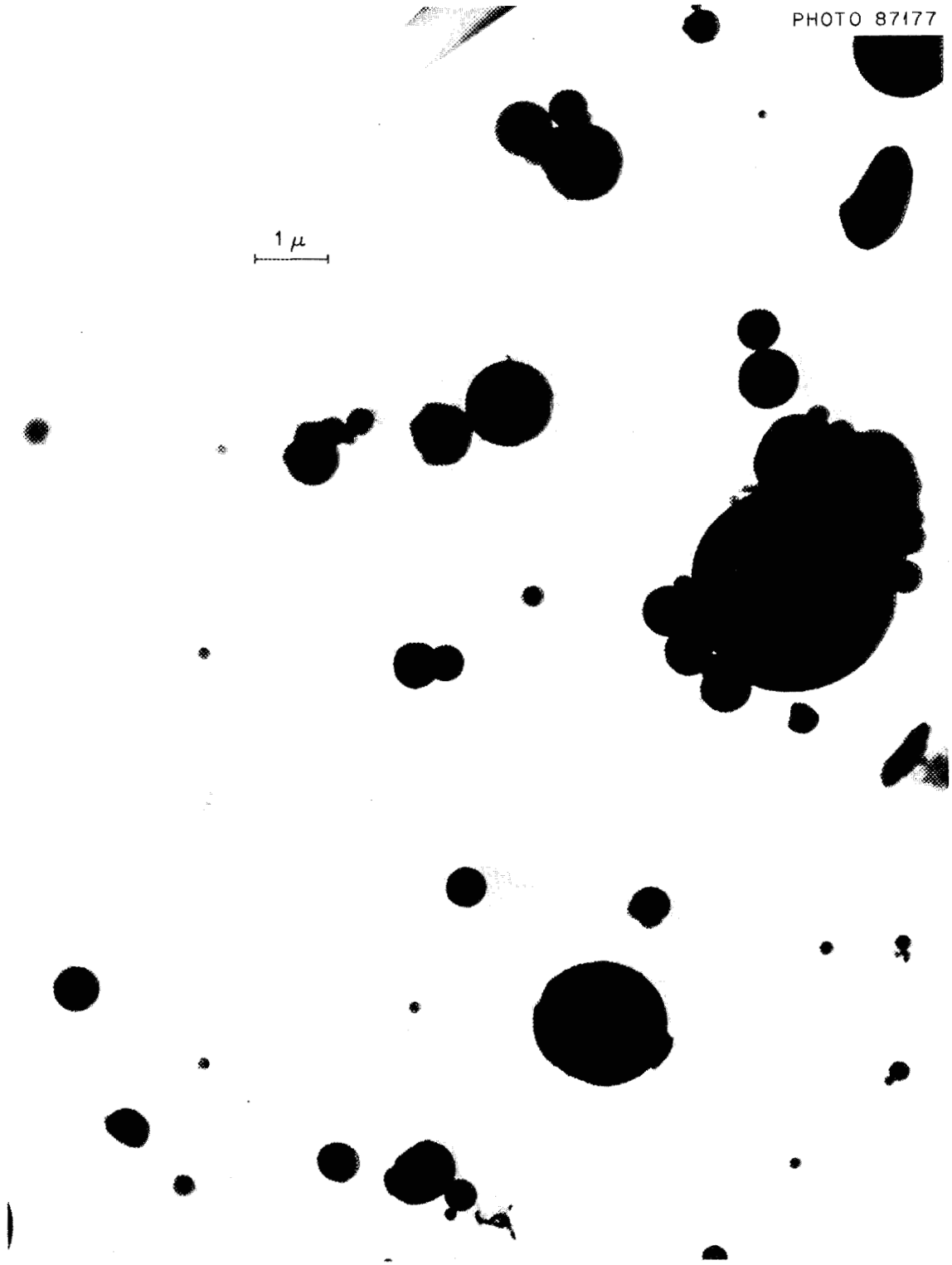

Fig. 2.8. Electron Photomicrograph of U_3O_8 Particles (Low-Particle-Size Range). Particles formed in 2-hr fluidized-bed oxidation run at 525°C with 20% O_2–80% He.

ORNL DWG 67-3631

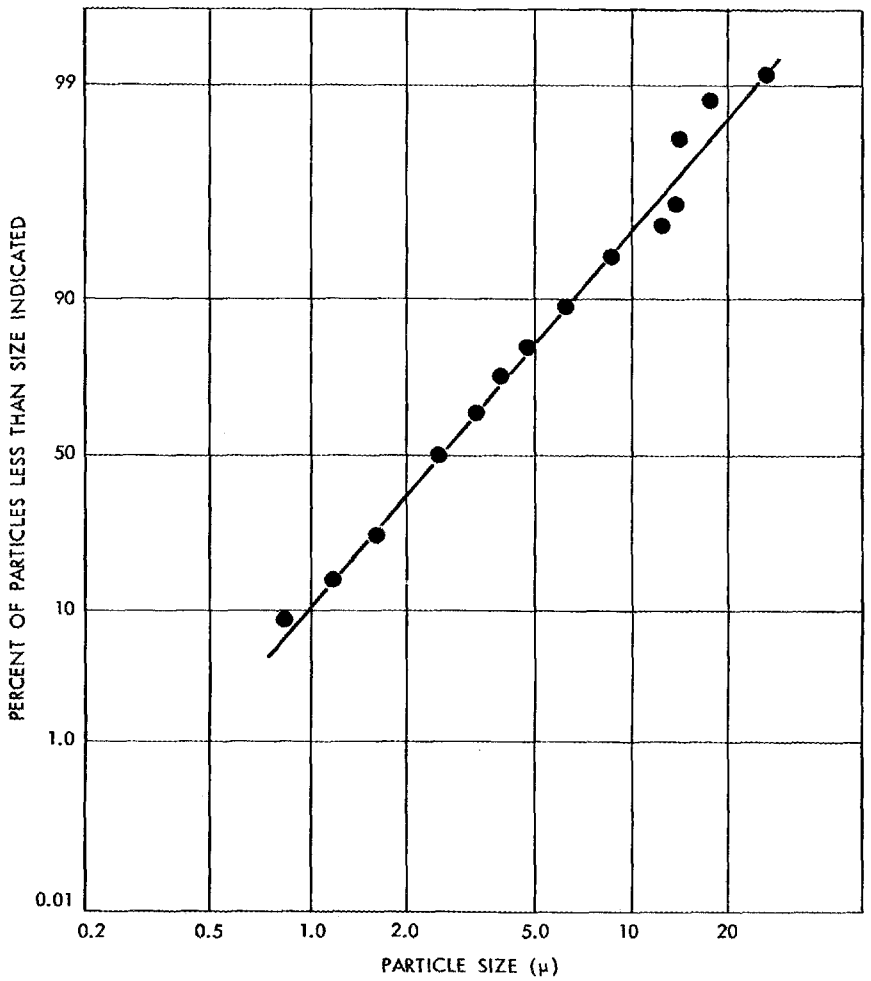

Fig. 2.9. U_3O_8 Particle Size Distribution.

to the filters or to the alternating blowback system used.

Another interesting observation made during the experiment with the $1\frac{1}{2}$-in.-ID Pyrex fluidized-bed reactor was that the major portion (possibly more than 90%) of the U_3O_8 powder was suspended in the lower part of the disengaging section by the fluidizing gas. This indicates that much of the subsequent fluorination reaction will take place in the bottom part of the disengaging section. The superficial gas velocity in the disengaging section was one-fourth of that in the fluidization section.

2.4 EFFECTS OF FIVE PROCESS VARIABLES ON RETENTION OF URANIUM BY ALUMINA AFTER TREATMENT WITH FLUORINE

A number of variables affect the extent to which UF_6 is volatilized from a fluidized bed in a given time. An attempt was made to evaluate the importance of some of these variables by using a rotating-bed technique to approximate the mixing action in a fluidized bed. Fluorine was used to react with the UF_4 in the experiments discussed in this section; however, BrF_5 and BrF_3 were also tested, as described in the next section.

The alumina and UF_4 charged to the reactor weighed about $2\frac{1}{2}$ g; of that amount, about 0.2 g was uranium (as UF_4). The flow rate of gas into the reactor was usually 200 ml/min (STP), which was sufficient to keep a nearly constant gas concentration in the reactor. The quantity of reacting uranium was insufficient to cause any significant variation in the temperature of the rotating reactor.

Of interest in these experiments were the effects of the following variables on final uranium concentration: the particle diameter of the alumina (Norton RR grade), the fluorination temperature, the concentration of the fluorinating gas, the time of reaction, and the initial concentration of uranium in the bed. A statistically designed experiment was performed to evaluate the effects of these variables.[10] A central composite design was used that consisted of the following 31 points: 16 points comprising one-half of a 2^5 factorial (the base design), 10 axial points, and 5 points all at the center of the design.

Results of the analysis indicated that, based on the first 16 experiments, the five variables, over the range studied, have no effect on uranium retention by the alumina.[11] Also, the expected retention of uranium over the range of variables studied is 0.010 wt %, with only one run in 40 expected to exceed 0.021 wt %.

2.5 RELATIVE EFFECTIVENESS OF FLUORINE, BrF_5, AND BrF_3 IN MINIMIZING RETENTION OF URANIUM BY ALUMINA

If uranium and plutonium are to be volatilized separately with BrF_5 and fluorine, respectively, as shown in the current flowsheet for the FBVPP, the quantity of uranium remaining in the bed after the BrF_5 step is of interest. If fluorine should volatilize some of this residual uranium in the subsequent step, then the plutonium stream will contain both uranium and plutonium, and further separation will be necessary. Experiments supplementing those described in the previous section were made to compare the relative effectiveness of fluorine, BrF_5, and BrF_3 in removing uranium from the alumina in the bed. The rotating-bed reactor was used.

Results of these experiments showed evidence that at all temperatures above 300°C fluorine leaves less residual uranium than BrF_5. For example, after 65 min of fluorination at 400°C with 15 vol % concentration of fluorinating agent, the residual uranium with BrF_5 fluorination was about 0.015 wt %, while with fluorine it was only about 0.007 wt %. More details have been reported elsewhere.[12] A possible solution is to treat the alumina with BrF_3 between the BrF_5 and fluorine steps. Treatment of a bed for 65 min with 16 vol % BrF_3 at 100°C resulted in a residual uranium content of only 0.0037 wt %. Treatment with BrF_3 could also serve as a method for completely removing uranium from disengaging section, filters, and lines; in several experiments, using a 0.94-in.-ID fluidized-bed reactor, BrF_3 was used successfully for this purpose.

Just as the residual uranium in the bed increases when the fluorination temperature is increased, the final fluoride content of the bed is higher at higher temperatures. The final fluoride content after fluorination at 600°C (1.5 wt %) is more than twice that after fluorination at 500°C (0.7 wt %). Fluorine and BrF_5 gave similar results. Minimizing the fluoride content of the discarded alumina could be important for subsequent disposal operations.

2.6 FLUORINE CALORIMETRIC REACTOR FOR DETERMINING BROMINE AND BrF_3 CONTENTS OF PRIMARY REACTOR OFF-GAS

In the FBVPP, continuous measurements of the BrF_5 utilization during the uranium volatilization would be desirable, both to allow periodic addition of the proper amount of makeup fluorine to the off-gas stream and to determine when the reaction is complete. One possible way to provide such a measurement involves the use of a fluorine calorimetric reactor (FCR), which is described below.

Description and Test Results

The FCR operates by reacting the exit gas stream, which consists of bromine, BrF_3, and BrF_5, with

[10] Experiment designed by D. A. Gardiner, Mathematics Division, ORNL.

[11] This analysis by L. B. Koppel, Associate Professor of Chemical Engineering, Purdue University, and consultant to the Chemical Engineering Division, Argonne National Laboratory. A summary of another analysis by W. Blot, Mathematics Division, ORNL, is presented in *Fluoride Volatility Processing Semiannual Progress Report for Period ending November 30, 1966*, ORNL-TM-1849, p. 27.

[12] R. P. Milford *et al.*, *Fluoride Volatility Processing Semiannual Progress Report for Period ending November 30, 1966*, ORNL-TM-1849, p. 29.

fluorine and measuring the increase in temperature. A schematic diagram of the FCR is shown in Fig. 2.10. The experimental model was about 6 in. long and $\frac{1}{2}$ in. in diameter. It was wrapped with resistance heating wire so that a temperature of about 200°C could be maintained. During testing the heater voltage was maintained at a constant value. The simulated off-gas flowed through the FCR at about 1500 ml (STP)/min and was mixed with fluorine near the midpoint of the reactor. Thermocouples upstream and about $\frac{3}{4}$ in. downstream of the mixing point were connected to give a differential signal. The thermocouples were positioned in the wells shown in Fig. 2.10. In tests thus far the quantity of fluorine supplied to the FCR has been exactly that required to react with the test mixture.

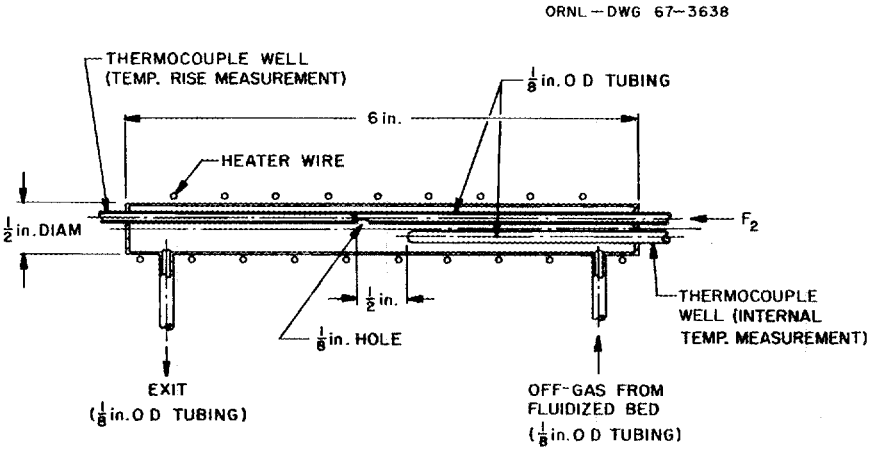

Fig. 2.10. Schematic Diagram of Fluorine Calorimetric Reactor (FCR) for Determining Bromine and BrF_3 Content of Gas Streams.

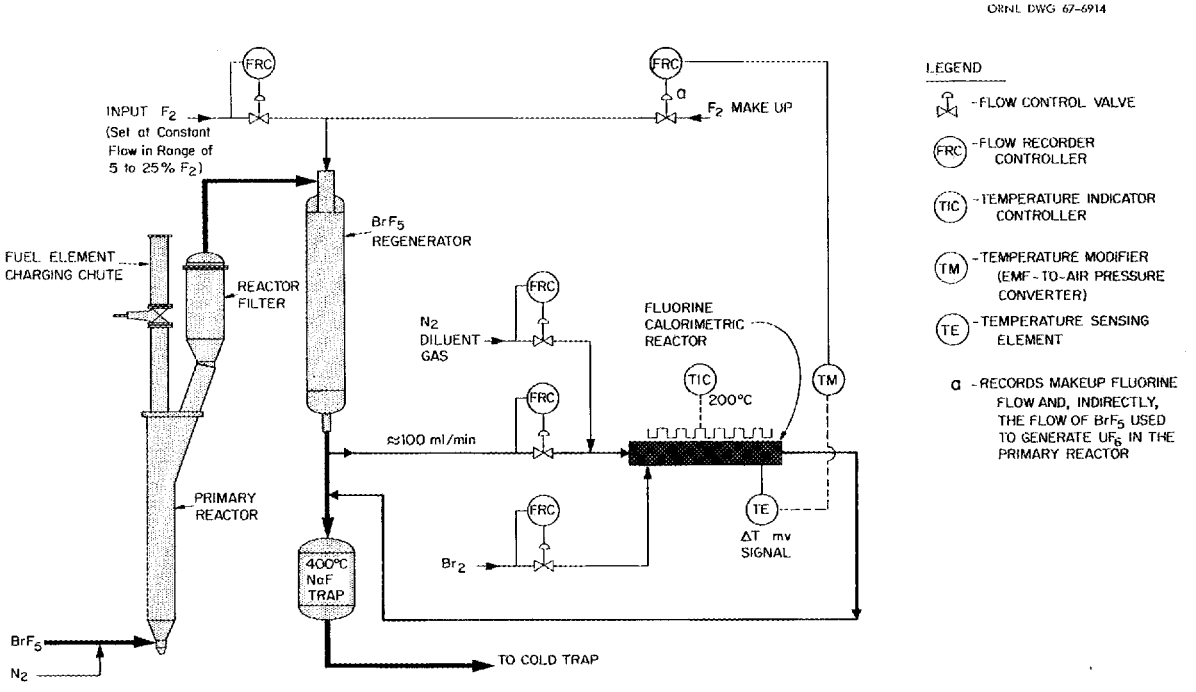

Fig. 2.11. Application of FCR to Process Control.

Operating with a constant fluorine flow is also possible, and this would probably be the best mode of operation for a large-scale installation.

A limited number of tests indicate that the experimental FCR should be able to measure as little as 5% utilization of the BrF_5 if the inlet gas to the fluidized-bed reactor contains 10 vol % BrF_5.

Another FCR, which is similar to the first model but longer to minimize end effects, has been constructed and is being given more extensive testing.

Application of the FCR to Process Control

Monitoring the flow of output, as well as input, streams is desirable in a process step. The FCR permits the monitoring of BrF_5 consumption or UF_6 generation in the fluidized-bed fluorination reactor. In addition, it provides means for controlling the amount of fluorine that must be added to the product gas (UF_6-BrF_5-BrF_3-N_2) to refluorinate BrF_3 or bromine to BrF_5. The gas entering the 400°C NaF trap must contain excess fluorine to prevent formation of $UF_5 \cdot xNaF$. If the main flow of fluorine to the BrF_5 regenerator is maintained as a fixed proportion, probably in the range of 5 to 25 vol %, of the gas leaving the primary reactor, then an FCR and appropriate instrumentation could be used to supply makeup fluorine at the rate required to keep the fluorine concentration in the gas entering the 400°C NaF trap at a constant value. This is illustrated in Fig. 2.11.

Process tests are being planned in order to study the above instrumentation while determining the optimum excess of fluorine for the BrF_5 regenerator and the 400°C NaF trap.

2.7 LiF AND FLUORINE AS A SORPTION-DESORPTION SYSTEM FOR PuF_6

A sorption-desorption system for PuF_6 comparable with the UF_6-NaF sorption-desorption system would be of value in volatility processing as a means for the recovery and purification of plutonium. Last year we found that, of 31 metal fluorides tested for possible use as sorbents, LiF was the only one on which PuF_6 could be sorbed to a useful extent and from which the PuF_6 could be refluorinated.[13] The sorption reaction involves formation of a PuF_4-LiF complex. The PuF_6-LiF system has now been characterized with respect to its potential usefulness. The oxidation-reduction chemical equilibrium has been determined by the transpiration method over a wide temperature range. The sorption reaction has been found to be dependent on the surface area of the LiF and on the sorption temperature. Separation of PuF_6 from UF_6 has been demonstrated, using LiF with a specific surface area of 1 to 3 m^2/g.

Use of high-surface-area LiF (20 to 37 m^2/g) resulted in over 99% sorption of PuF_6 at 175°C with a superficial residence time of 0.04 min. Use of low-surface-area LiF (1 to 3 m^2/g) required a temperature of 300°C to obtain a similar effectiveness with the same contact time. The recovery of PuF_6 from the PuF_4-LiF complex by refluorination at 450 to 600°C was shown to be more feasible with the low-surface-area LiF; the high-surface-area LiF degenerated during the desorption process, decreasing the efficiency of PuF_6 recovery.

To test the applicability of the proposed LiF sorption-desorption method for purifying PuF_6, studies that more closely simulated process conditions were made using a 0.94-in.-ID fluidized-bed reactor. Plutonium hexafluoride was fluorinated from fluidized beds of alumina, and the quantity of plutonium sorbed by LiF was determined as a function of such variables as fluorine flow rate, average $F_2 : PuF_6$ mole ratio, sorption bed temperature, and surface area of the LiF.

In this series, relatively poor plutonium retention was obtained in early tests using low-surface-area LiF. When LiF with a higher surface area was used, 9.1 vs 1.5 m^2/g, plutonium retentions of 96 to 97% were demonstrated at fluidizing velocities of 0.5 fps and average $F_2 : PuF_6$ mole ratios of 3800 : 1. Desorption of PuF_6 by refluorination has been shown to be feasible only with low-surface-area LiF; use of the latter, however, would require a 600% increase in bed volume. The need for a larger bed, coupled with the high volumes of fluorine required, made the use of LiF less attractive; therefore, the LiF studies were terminated. Experiments using NaF as a sorbent for PuF_6 are now under way.

Chemical Equilibrium in the Sorption-Desorption System

A dynamic gas refluorination procedure (analogous to a transpiration method) was used to measure

[13] *Chem. Technol. Div. Ann. Progr. Rept. May 31, 1966*, ORNL-3945, p. 66.

the equilibrium between PuF_6, fluorine, and the sorbed plutonium complex (probably Li_4PuF_8) over the temperature range 100 to 600°C. The test bed, consisting of about 300 mg of plutonium sorbed by 7.8 g of LiF, was used at different temperatures and fluorine flow rates to determine the desorption rate as measured by the amount of volatilized PuF_6 collected in an NaF trap at 300°C. The K value was found to be unchanged when the gas flow rate was varied by a factor of 2; this indicated that an equilibrium value was actually being measured. Similar results were obtained in sorption tests, that is, when the equilibrium was approached from the excess PuF_6 side of the reaction:

$$Li_4PuF_8 + F_2 \rightleftharpoons PuF_6 + 4LiF \ .$$

The data were found to be defined by the relationship

$$\log K = 2047/T(°K) + 0.827 \ ,$$

where $K = F_2 : PuF_6$ mole ratio. The data and the line representing the above equation are plotted in Fig. 17 in ref. 12. From this, the free energy–temperature relationship for the above reaction appears to be $\Delta F° = 9360 + 3.74T(°K)$ cal/mole.

Variables Affecting the Sorption of PuF_6 by LiF

The effects of gas flow rate, temperature, and surface area of LiF on PuF_6 sorption were investigated. The valence state of the sorbed plutonium was determined, and the manner in which sorption effectiveness varied with plutonium loading was studied.

Tests with gas flow rates of 10, 30, 60, and 250 ml/min (STP) demonstrated that sorption is only slightly affected by flow rates below 60 ml/min and that the effect at 250 ml/min is not large. For the low-surface-area LiF, a temperature of 275°C is required to achieve a PuF_6 retention comparable with that achieved with high-surface-area LiF at 175°C. Furthermore, partial sorption occurs at temperatures of 35 to 175°C with the high-surface-area LiF, in contrast to almost no sorption at temperatures up to 200°C for the low-surface-area LiF (see Table 3, ref. 12).

The plutonium that is sorbed by low-surface-area LiF at 300°C has previously been shown to be tetravalent, by use of the iodine liberation method.[13] Also, the x-ray pattern is similar in most respects to that of Li_4UF_8. The plutonium that was sorbed at 175 and 100°C by high-surface-area LiF was found by the iodine liberation method to have average valences of 4.21 and 4.55 respectively.

The sorption capacity of LiF for PuF_6 was studied in a series of 15 successive experiments involving cumulative sorptions on a single 7.8-g batch of low-surface-area LiF at 300°C. For each of the 15 sorptions, about 50 mg of plutonium as PuO_2 was added to the PuF_6 generator, and the NaF backup trap was renewed. A total of 0.76 g of plutonium as PuF_6 was passed into the sorbent bed; 0.71 g was retained. The specific loadings observed at the end of the series of tests varied from 0.1225 g of plutonium per gram of LiF near the entrance to 0.0309 g per gram of LiF at the exit.

Desorption of PuF_6 from LiF

Desorption tests with low-surface-area LiF provided results that were consistent with the equilibrium data presented in a previous section. The desorption rate increases with temperature up to approximately 550°C; here the relationship reverses, possibly as a result of sintering.

In a series of five cycles of sorption-desorption using the low-surface-area LiF, the quantity of residual plutonium on the LiF did not increase above that noted for one cycle (see Table 5, ref. 12).

The initial desorption from high-surface-area LiF appears comparable with that found with low-surface-area LiF. However, the tailing-out effect appears to be extended, and, at least at the relatively high desorption temperature of 475°C, it appears that some of the plutonium is not desorbable (see Table 6, ref. 12). Reduction of the surface area to about 3 m^2/g after attempts to desorb at 475°C indicated partial sintering of the sorbent. The use of high-surface-area LiF therefore appears to be limited to one cycle.

Separation of PuF_6 from UF_6

The separation of plutonium and uranium hexafluorides was demonstrated in duplicate sorption tests in which both PuF_6 and UF_6 were produced in the PuF_6 generator and two traps containing

low-surface-area LiF at 300°C were substituted for the single LiF trap (as described in ref. 12); gases from the LiF traps were finally passed through an NaF trap. No uranium was detected in the LiF traps, while 4.9 and 17.6 mg of uranium were found in the NaF traps. In the first test, the two LiF traps and the NaF trap contained 61.4, 3.0, and 0.3 mg of plutonium respectively; in the second test, corresponding values were 61.9, 4.5, and 0.4 mg of plutonium.

In similar experiments with the high-surface-area LiF as the sorbent at 175°C, a significant part of the UF_6 was cosorbed with the PuF_6 by the LiF bed. Independent tests confirmed the sorption of significant quantities of UF_6 by the high-surface-area LiF at 175°C.

Process Application Tests of PuF_6 Sorption by LiF

Process application tests of PuF_6 sorption by LiF were conducted, using a 0.94-in.-ID fluidized-bed reactor and two 25-g beds of LiF in series. The first two tests contained 7-g charges of 5.4% PuO_2–UO_2 (sol-gel-derived microspheres with diameters of about 300 to 450 μ), one with and one without the presence of stainless steel cladding. Fluorinations in each test were made at 550°C, using gas fluidization velocities of 0.55 fps [1200 ml/min (STP)]. The product gas streams of PuF_6-UF_6-F_2 (some CrO_2F_2-CrF_5 was present in the test that included stainless steel cladding) were passed through the LiF beds at 300°C. The respective overall sorptions of PuF_6 were 7 and 34%. The appreciable difference in retentions in the two tests was at first thought to be attributable to the presence of chromium fluorides; however, subsequent studies disclosed significant differences in the surface areas of various LiF batches that had been prepared under similar conditions. For batches that were prepared from fused Li_2CO_3 by reaction with fluorine at 400°C, the surface areas ranged from 1.3 to 3.4 m^2/g; at 200°C, 5.9 to 17.7 m^2/g; at 250°C, 6.5 to 36.8 m^2/g; and at 100°C, 3.5 to 9.1 m^2/g.

Based on determinations of the decomposition pressure of the PuF_4-LiF complex, described earlier in this section, a decision to lower the temperature of the LiF sorption beds from 300 to 250°C was made. In a test with the bed temperature at 250°C and with other conditions similar to those used previously, an overall PuF_6 sorption of 56% was achieved. This represents a definite improvement over the 34% that was obtained in the 300°C sorption test but is still not adequate for our purposes.

The importance of residence time and of the $F_2 : PuF_6$ mole ratio on the sorption of PuF_6 was demonstrated in a static bed test; a subfluidization velocity of 0.1 fps [240 ml/min (STP)] for 3 hr at 550°C was used. An overall sorption of 99.4% was achieved by a 50-g bed of LiF at 300°C. The low material balance for plutonium in this test (57.8% as compared with previous values of about 90 to 100%), in addition to the unusually high retention by the bed, suggested the possibility of some thermal decomposition. (The $F_2 : PuF_6$ mole ratio below which thermal decomposition occurs has been reported to be 396 : 1 at 300°C.[14]) In this test the mole ratio was 1270 : 1, based on a continuous evolution of PuF_6 over the 3-hr period. The actual mole ratio was determined in a similar test in which a neutron counting device, calibrated with a known amount of plutonium, was positioned adjacent to the LiF sorption bed. The neutron count during fluorination indicated that essentially all of the plutonium was removed from the fluidized bed within a period of about 30 min and that about 50 to 60% of it reached the sorption bed during that time (see Fig. 2.12). On this basis the actual $F_2 : PuF_6$ mole ratio was below the required value of 396:1 for a significant length of time. This evidence supports the previous tentative conclusion that thermal decomposition of PuF_6 was causing low material balances and high sorption.

The amount of PuF_6 not sorbed by LiF at the proposed sorption temperature was determined. Plutonium hexafluoride was formed by fluorination and sorbed by a 50-g bed of LiF at 300°C. Then fluorine was passed through the bed for 12 hr at a rate of 240 ml/min (STP). The amount of plutonium collected in a 10-g NaF backup trap at 300°C indicated an equilibrium constant of about 5×10^5 for $F_2 : PuF_6$.

A batch of LiF having a high surface area (9.1 m^2/g) was prepared by fluorination of Li_2CO_3 at 100°C and was used for sorbing PuF_6 (batches of lithium fluoride with surface areas between 1 and 2 m^2/g had been used previously in application

[14] M. J. Steindler, *Laboratory Investigations in Support of Fluid Bed Fluoride Volatility Process. Part II. The Properties of Plutonium Hexafluoride*, ANL-6753, p. 40 (August 1963).

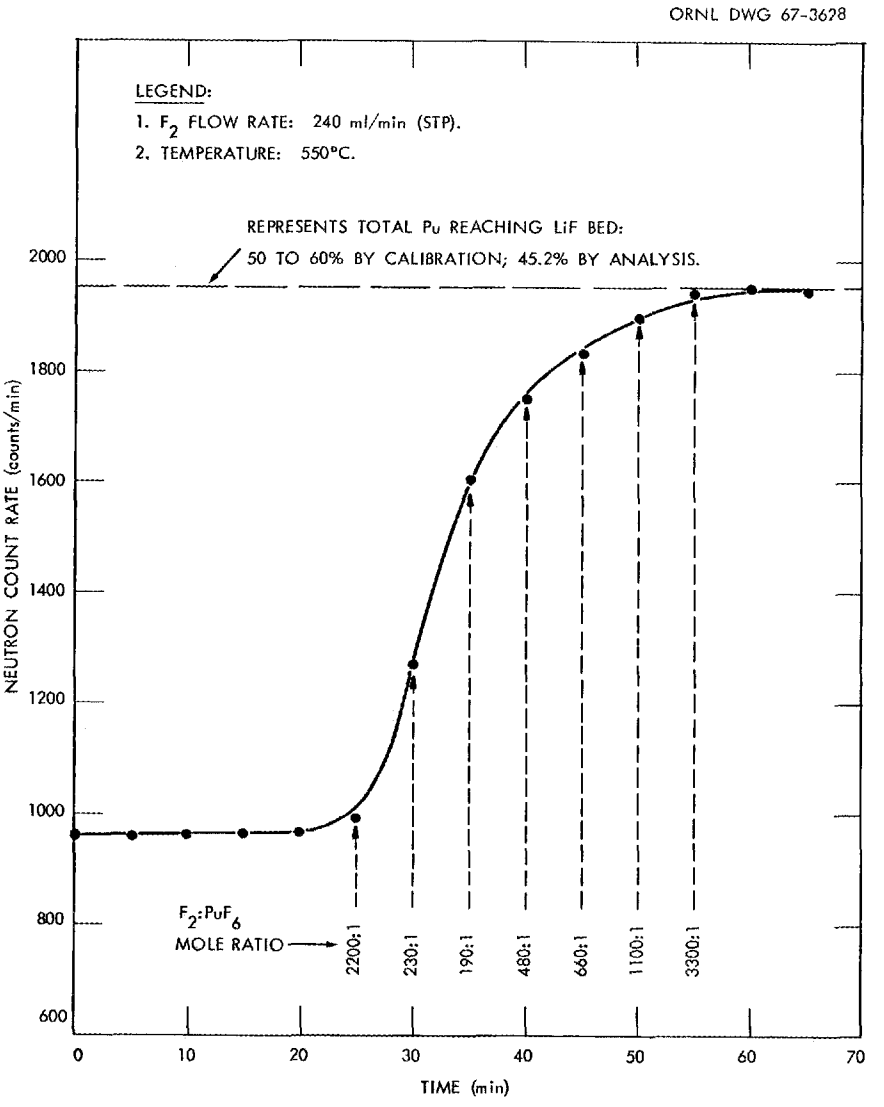

Fig. 2.12. Determination of Actual Fluorine:PuF_6 Mole Ratios by Neutron Counting (α-n Reaction) Method.

tests). In tests with this material, the PuF_6 sorption achieved under process flow conditions of 1200 ml/min (STP), using a 50-g bed at 250°C, was 96.1%.

2.8 SORPTION-DESORPTION SYSTEMS FOR NpF_6

A sorption-desorption system for NpF_6 comparable with the UF_6-NaF system would be advantageous in separating NpF_6 from either PuF_6 or UF_6, or both, in the volatility processing of nuclear fuels.

To date, the sorbents MgF_2, CaF_2, BaF_2, and NaF have been considered. Magnesium fluoride has been used previously to collect small amounts of NpF_6 from a UF_6 stream; however, our tests showed it to have several disadvantages: the necessary residence time is longer than 0.8 min, and the neptunium is not recoverable by fluorination. The sorbents LiF, CaF_2, and BaF_2 did not sorb NpF_6 satisfactorily at temperatures of 100 to 400°C. Sodium fluoride was found to sorb NpF_6 over a temperature range of 200 to 450°C; NpF_6 was desorbed readily by using either nitrogen or fluorine as a carrier gas at 500°C. Reduction of hexavalent neptunium to a lower valence state

occurs when the NpF_6-NaF complex is maintained at 400°C for 6 hr under nitrogen. The dissociation pressure of this complex appears to be about one one-hundredth of that for the comparable UF_6-NaF complex.

Sorption of NpF_6 by MgF_2 and Desorption with Fluorine

Only a partial sorption of NpF_6 by MgF_2 was achieved, even after long residence times. For the short residence time of 0.04 min, 15 to 20% of the NpF_6 in fluorine carrier gas was sorbed by MgF_2 at a bed temperature of 100 or 230°C. For longer residence times of 0.13 and 0.80 min, it was found that 23 and 79%, respectively, of the NpF_6 entering MgF_2 beds at 100°C was sorbed.

In 30-min desorption tests at temperatures of 235, 470, and 525°C and at a fluorine flow rate of 50 ml/min (STP), the amounts of neptunium desorbed, respectively, from an MgF_2 bed were 1.42, 0.81, and 0.78 mg; 21.3 mg (86%) remained on the bed.

Sorption of NpF_6 by LiF, CaF_2, and BaF_2

The sorption of NpF_6 varied from 20 to 35% over the temperature range of 100 to 400°C for both LiF and CaF_2 for 0.04-min residence times. In similar tests with BaF_2, amounts sorbed were about 35 and 60% at 125 and 230°C respectively.

Sorption of NpF_6 by NaF and Desorption with Fluorine or Nitrogen

Sorptions of NpF_6 by NaF were 17, 47, 94, 96, 86, and 9% for NaF bed temperatures of 100, 150, 250, 275, 300, and 450°C, respectively, at residence times of 0.04 min. The product was violet in color. The desorption of NpF_6 from a freshly prepared bed of NpF_6-NaF complex was accomplished with either fluorine or nitrogen; with fluorine, 21.1 mg (97%) of the neptunium was desorbed from the 500°C NaF bed in 1 hr, using a gas flow of 50 ml/min (STP); 0.57 mg was left on the NaF bed. With nitrogen, 21.60 mg (99%) of the neptunium was desorbed from the 500°C NaF bed in 4 hr, using a gas flow of 100 ml/min (STP); 0.19 mg remained on the bed. Preliminary dissociation pressure measurements indicated that the NpF_6 pressure over the NpF_6-NaF complex is about one one-hundredth of the observed value for the UF_6 pressure over the UF_6-NaF complex. Reduction of the hexavalent neptunium caused difficulties in dissociation pressure measurements when nitrogen was used as the carrier gas.

2.9 CORROSION IN VOLATILITY PROCESSES

The highly reactive nature of the principal reagents and the high temperatures (up to 550°C) that are used in fluidized-bed volatility processes could result in serious corrosion problems. Corrosion studies have had an immediate objective that is related to construction and operation of the FBVPP and a longer-range objective that is concerned with future commercial application. As part of the volatility development work, corrosion data have been gathered at each of the participating sites; during this period most of the ORNL work was performed at Battelle Memorial Institute – Columbus Laboratories (BMI) under a continuing subcontract.

Workers at BMI have completed their study of intergranular modifications of nickel exposed to alumina. Toward the end of the reporting period, the failures of several nickel pipes attached to the primary reactor in the small-scale engineering test facility (Unit Operations Section, ORNL) instigated more intensive studies of intergranular modifications; this work is nearing completion.

Nickel, several nickel alloys, and copper were exposed to gaseous bromine at 300 and 500°C. Corrosion of the nickel was insignificant, Monel corroded at rates of a few mils per month, and copper disintegrated rapidly.

Laboratory-scale fluidized-bed equipment is now being installed at BMI to study corrosion under dynamic conditions. In the first experiments with this unit, we shall attempt to determine the reason for the observed plugging of nickel Feltmetal filters during recent hydrochlorination runs.

Intergranular Modification of Nickel in the Fluidized-Bed Volatility Program

Last year we reported results of most of the work done at BMI to determine the cause of intergranular modifications sometimes found in nickel that had been exposed under conditions existing in the head-end step of the fluidized-bed volatility

process. To complement data previously reported, nickel specimens were exposed to Norton RR alumina in an evacuated Vycor capsule at 520°C for 200 hr. Data were also tabulated for 200-hr exposures (in 25-hr increments) of nickel 200 and 201 to Norton Regular, 38, and RR and to Alcoa T-61 aluminas; fresh charges of alumina were added every 25 hr. The report summarizing this project has been issued;[15] its abstract follows:

"Intergranular penetration could be produced in Nickel 200 or Nickel 201 specimens by exposure to static beds of the alumina used for the fluidized-bed material in the processing. Two of the four grades of alumina under consideration produced severe penetration when in contact with nickel at 520°C. Sulfur in the alumina is thought to cause the intergranular modifications. With the exception of one grade of alumina, chemical analyses confirmed this conclusion. A spot test sensitive to sulfur compounds showed a positive reaction to the grain boundaries of nickel coupons with modification present. Results of electron-beam microprobe analyses showed sulfur, iron, and oxygen at the surface of nickel specimens with intergranular modifications, but sulfur could not be detected to a significant depth at the grain boundaries.

"Bend tests indicated some damage to the material from the standpoint of strength. Tensile measurements made at room temperature and at 520°C showed that the ultimate tensile strength and the elongation of the nickel specimen were lowered appreciably by the intergranular modifications.

"The present practical means of alleviating the intergranular damage lies in bed-material selection."

Several years ago, when interest in the use of $HF-O_2$ for decladding and oxidation was at a peak, four corrosion tests were run in the Reactor Chemistry Division in a small fluidized-bed reactor.[16] During the current reporting period, BMI personnel examined these specimens metallographically to determine if intergranular modifications had occurred.[17] The specimens were INOR-8 and nickel 200 and had been exposed to: (1) oxygen at 800°C for 96 hr; (2) 60 vol % O_2–40 vol % HF at 625°C for 250 hr; (3) 60 vol % O_2–40 vol % HF at 625°C followed by fluorine at 500°C, cycled for 258 hr; and (4) oxygen at 550°C followed by fluorine at 550°C, cycled for 96 hr. The temperatures were nominal values, as variations occurred along the height of the bed.

Maximum depths of intergranular modifications (or pits) were as follows:

Test No.	Depth (mils)	
	Nickel	INOR-8
1	6	0
2	8	2.8
3	2.6	<0.5
	5.5[a]	
4	6	0.5
	8[a]	

[a]Depth of pits.

Corrosion Failures in the Engineering Test Facility

Shortly after the startup of the HCl decladding program in the small-scale engineering test facility (Unit Operations Section), several failures occurred in the HCl inlet pipe ($\frac{1}{2}$ in. nominal pipe size, sched 40) at the bottom of the reactor. Failure occurred in one instance after successive exposure to fluorine and oxygen for more than 100 hr and to HCl for 3 hr; during exposure, temperatures ranged from 400 to 500°C. The next two failures occurred after less than 5 hr of exposure to HCl; another failure occurred after less than 60 min of exposure to HCl. Other failures have occurred in $\frac{3}{8}$-in. nickel pipe and tubing, also attached to the bottom of the reactor, but without such clearly recorded history. Preliminary analyses and examinations at BMI indicate embrittlement, probably attributable to sulfur contamination, as the cause. The HCl being used was found to contain up to 4700 ppm of sulfur; however, a new supply, manufactured in the absence

[15]P. D. Miller *et al.*, *Intergranular Modifications in Nickel from the Fluidized-Bed Fluoride Volatility Process*, BMI-X-417 (Nov. 28, 1966).

[16]Tests performed by P. D. Neumann, Reactor Chemistry Division, ORNL.

[17]P. D. Miller, BMI, personal communication, Feb. 1, 1967.

of H_2SO_4 and containing less than 2 ppm of sulfur, was obtained. This corrosion problem is being studied intensively by BMI in cooperation with personnel of the Inspection Engineering Division, ORNL. There are indications that the attack is originating from the outside, as well as the inside, of the pipe – possibly from the asbestos tape used for insulation.

Corrosion of Nickel, Monel, and Duranickel in Bromine Vapor

With the adoption of BrF_5 as the reagent for fluorinating uranium, the possible corrosion effects of bromine (a reaction product) on nickel 201, Duranickel 301, and Huyck sintered nickel-fiber filters (Feltmetal) had to be considered. An experimental program was undertaken at BMI to supplement the meager information that was available in the literature.

In these experiments, bromine vapor flowed by the corrosion specimens in glassware at a rate of about 5 fpm. All runs were made at 300°C except one; it was made at 500°C.

When nickel 201, Duranickel 301, and Feltmetal were exposed individually or in various welded combinations (e.g., nickel 201 to Duranickel 301), weight losses were very small (see Table 2.1); these weight losses correspond to corrosion rates that are essentially negligible. When Monel and nickel 201 were exposed simultaneously in run 34, the weight loss of nickel, adjusted for exposure time, was ten or more times that of nickel exposed in the absence of Monel; nickel Feltmetal showed the same effect. The weight loss for Monel in run

Table 2.1. Corrosion of Nickel and Nickel Alloys in Bromine Vapor

Run No.	Material	Number of Specimens	Exposure Time (days)	Exposure Temperature (°C)	Weight Loss Range (mg)
1	Nickel 201				
	As received, unwelded	3	11	300	2.0–4.1
	As received, welded	3	11	300	2.6–5.8
2	Nickel 201				
	Surface ground, unwelded	3	10	300	1.8–4.0
	Welded, then surface ground	3	10	300	2.7–5.7
2	Huyck Feltmetal, nickel				
	As received	2	10	300	2.0–2.1
3	Duranickel 301				
	Surface ground, unwelded	2	10	300	1.2–2.8
3	Nickel 201 welded to Duranickel 301				
	Welded with nickel 201 filler metal, then surface ground	2	10	300	4.2–4.3
	Welded with filler metal 61, then surface ground	2	10	300	1.8–2.8
34	Monel (exposed in same run with nickel)				
	As received, unwelded	1	5	300	212.8[a]
	Welded, then surface ground	1	5	300	204.5
	Nickel 201 (exposed in same run with Monel)				
	Surface ground, unwelded	4	5	300	17.1–34.2
32	Nickel 201				
	Surface ground, unwelded	4	10	500	21.1–57.7

[a]Equivalent to a penetration rate of 3.3 mils/month.

34 was very high compared with nickel, indicating that Monel is not suitable for bromine service. The accelerated corrosion of nickel in the presence of Monel is believed to be caused by $CuBr_2$ that is formed by the reaction of bromine with copper from the Monel. Copper exposed alone dissolved rapidly in the bromine atmosphere.

Results of run 32 (Table 2.1) show that corrosion of nickel 201 at 500°C is higher than at 300°C by a factor of 10 or more; the same is true for Duranickel. However, this is not serious since the higher temperature conditions are not expected to be encountered in the FBVPP when bromine is present.

Nickel specimens exposed to a mixture of oxygen and bromine at 300°C for 11 days showed only a slight tarnish and negligible weight losses.

2.10 LEACHING OF URANIUM AND PLUTONIUM FROM PRIMARY REACTOR WASTE SOLIDS, AND RELATED CORROSION STUDIES

One of the objectives of the FBVPP is the demonstration of reliable accountability procedures for uranium and plutonium. Efficient solids-sampling methods will be required not only to meet this goal but also to determine the fate of fission products in the process and to provide other data necessary for the complete evaluation of the process. An accurate analysis of the waste solids from the primary reactor is of particular interest since it would give a direct measure of the amounts of uranium and plutonium that are not volatilized during the fluorination step. After each FBVPP run a small and, hopefully, representative sample of the fluorinator waste solids will be obtained and then analyzed for uranium and plutonium by standard procedures.

To test the effectiveness of solids sampling, the entire residue from each run would be leached; then the leachant would be sampled and analyzed, and the results would be compared with those obtained by analysis of the solids sample. The usefulness of such a procedure would depend upon our ability to quantitatively leach uranium and plutonium from the bed residue.

The program consisted of three phases: (1) laboratory and small-scale engineering studies to establish a flowsheet, (2) engineering flowsheet development and equipment design, and (3) corrosion studies (under subcontract with Battelle Memorial Institute – Columbus Laboratories) to aid in choosing a material of construction for the leacher and its associated piping. The design and the layout have been arranged, so far, to handle only fluidizable solids from the primary reactor or the pyrohydrolyzer; some alterations would be required if it were necessary to leach other solid wastes, such as NaF pellets. Laboratory studies of the chemistry of leaching were made, preliminary designs of the engineering flowsheet and equipment were prepared, and the corrosion experiments were concluded.

No further work is being done in view of our decision that leaching equipment will not be included in the FBVPP.

Description of Leacher Flowsheet

The leaching equipment (Fig. 2.13) is composed basically of an upflow leacher vessel, an overflow cooler, an air lift, and an elevated head-and-surge tank; the usual circulating lines, heaters, condensers, and off-gas separators are indicated. The direction of flow is indicated by the order in which the major vessels are listed above; circulation is obtained by means of the air lift and gravity flow to and from the head tank. The head tank has a nominal capacity of only 317 gal (1200 liters) because of space limitations and might require one or more solution changes during a run to maintain desired concentrations. The leacher is composed of a permanent top section and an interchangeable bottom section. The bottom section is actually a waste-solids can; it can be remotely disconnected from either the primary reactor or pyrohydrolyzer and clamped to the bottom of the leacher. Most of the leaching action takes place in the waste can, and any solids that are carried up into the top section return to the can when circulation stops. After draining and drying, the waste can is used as the burial container for the solids. The can and the part of the leacher immediately above it have inner diameters of 14 in.; circulation rates of about 5 gpm per square foot of cross section will be used.

Laboratory and Engineering-Scale Studies

Laboratory Studies. – Studies were conducted to determine how efficiently uranium and plutonium

could be leached from a variety of simulated primary reactor waste solids. Conditions for preparing the materials used in the leaching studies are outlined in Table 2.2. Each preparation was made in a fluidized-bed reactor similar to the FBVPP primary reactor. Most of the preparations simulated the wastes to be expected from the primary reactor after hydrochlorination, oxidation, and fluorination of zirconium-clad UO_2 fuel. One of the preparations (306-4) simulated the waste that is expected from a stainless-steel-clad UO_2 fuel after decladding by oxidative disintegration with $HF\text{-}O_2$ prior to fluorination. Analysis of a single sample did not accurately reflect the chemical composition of the preparation, even when the sample was obtained by riffling. In fact, the uranium and plutonium concentrations in "representative" samples obtained by riffling were found to vary as much as a factor of 5; the variation in the Pu : U atom ratios in the samples was even greater. Consequently, each sample was considered to have its own unique chemical composition, as determined from analyses of the leachates and the residue after leaching. This composition was used in the correlation of the data. In a typical experiment, a 2- to 5-g sample was leached once with about 25 ml of boiling reagent, using Teflon apparatus. After leaching,

ORNL DWG 67-5246

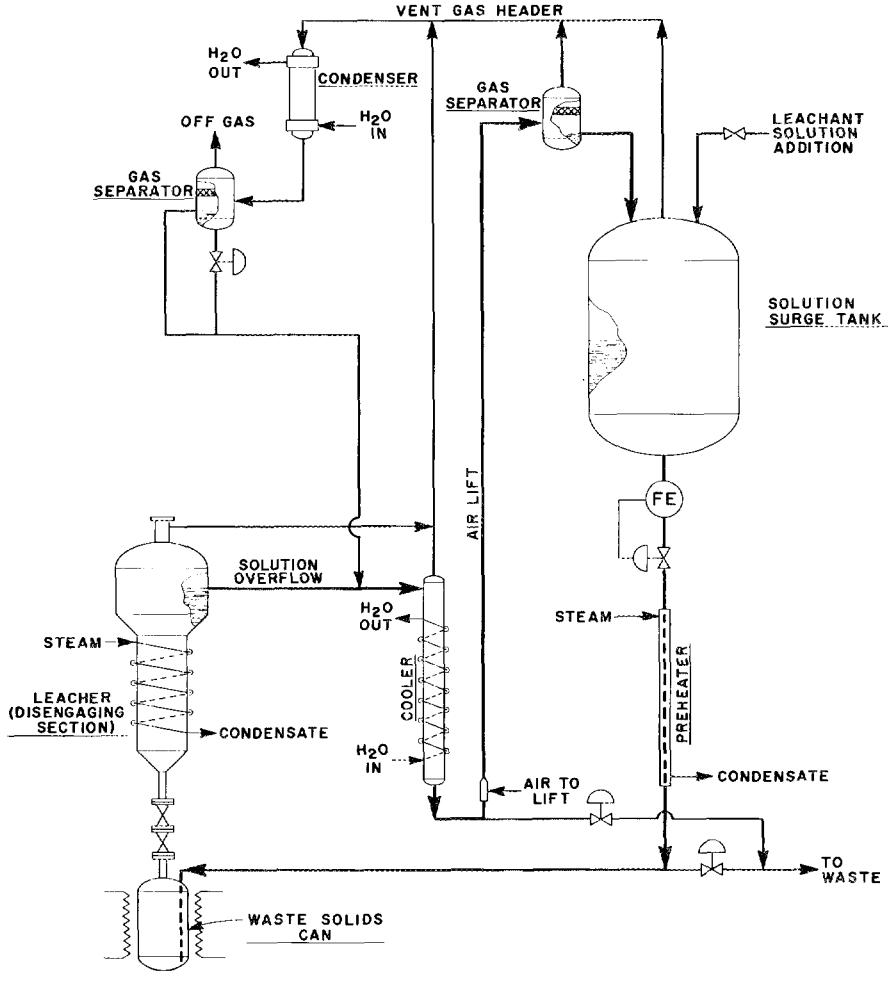

Fig. 2.13. Schematic Diagram of Equipment Required for Leaching Waste Solids.

Table 2.2. Conditions Used in Preparing Fluidized-Bed Samples for Leaching Studies

Initial charge was composed of about 7 g of 95% UO_2–5% PuO_2 microspheres (sol-gel-derived) and 40 g of −90 + 100 mesh Norton RR alumina; air was used in the oxidation step

Preparation	Oxidation Conditions		Fluorination Conditions					Analysis of Product[a] (wt %)		
	Temperature (°C)	Time (hr)	BrF_5 (%)	N_2 (%)	F_2 (%)	Temperature (°C)	Time (hr)	U	Pu	F
AFD-3[b]	461	5.5	0	74[c]	26[c]	450[d]	8.75	0.28	0	25.9
306-4[e]	650[f]	3.0[f]	0	90	10	450	0.25			
			0	80	20	450	0.25			
			0	60	40	450	0.25			
			0	0	100	450	2.25	0.051	0.0454	7.3
306-7	[g]	[g]	0	90	10	450	0.25			
			0	80	20	490	0.25			
			0	60	40	490–550	0.25			
			0	0	100	550	2.25	0.029	0.024	0.98
306-8	[g]	[g]	0	90	10	500	0.17			
			0	80	20	500	0.17			
			0	60	40	500	0.17			
			0	0	100	550	2.5	0.019	0.034	0.93
306-14	[g]	[g]	10	90	0	300	2.0			
			0	0	100	450	1.5	0.004	0.049	0.46
306-23	450	2.0	5	95	0	300–310	1.0			
			10	90	0	300–310	2.5			
			0	0	100	350	3.0			
			0	0	100	350–500	1.0			
			0	0	100	500	3.0	0.0038	0.036	0.44

[a]Based on single analysis of either "grab" sample or sample obtained by riffling the entire preparation.

[b]This bed was prepared at Argonne National Laboratory, starting with pure UO_2 pellets and −100 mesh Alcoa T-61 alumina.

[c]Average concentration during run; maximum fluorine concentration was 55%.

[d]Temperature actually varied from 420 to 480°C.

[e]This preparation simulated the residue from stainless-steel-clad UO_2 fuel. Product analyzed 0.47% Cr, 8.2% Fe, and 1.1% Ni.

[f]Oxidation step actually involved treatment with 20% HF–80% O_2 for 0.5 hr and then with 40% HF–60% O_2 for 2.5 hr.

[g]UO_2-PuO_2 was not oxidized before fluorination in these runs.

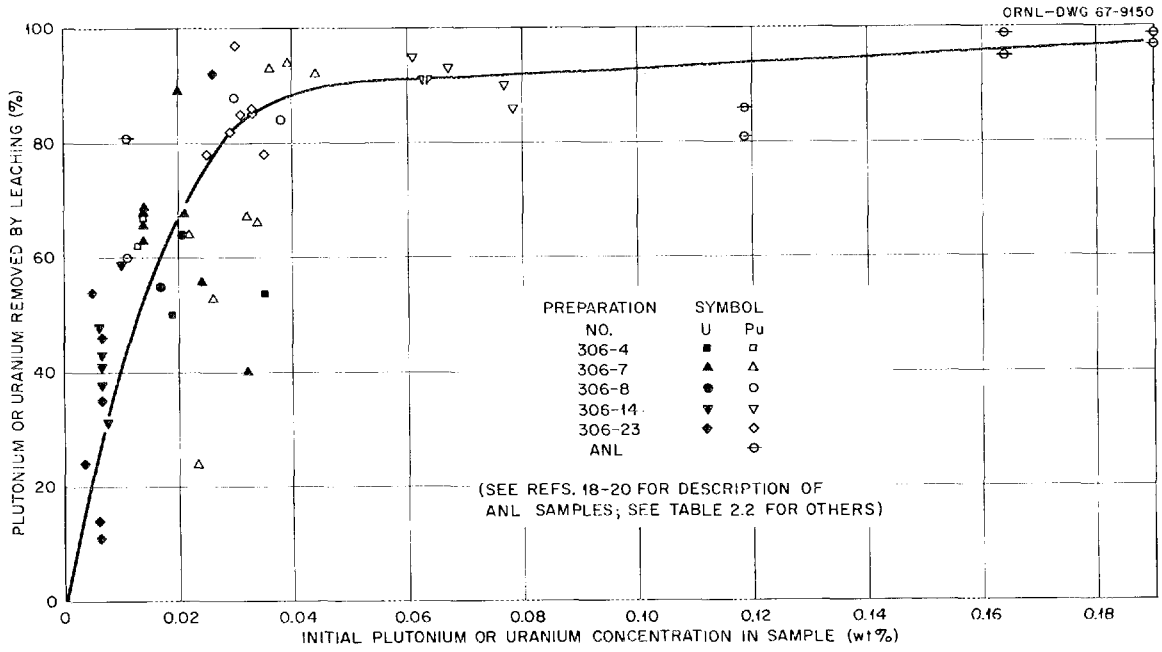

Fig. 2.14. Removal of Plutonium and Uranium by Leaching Samples of Fluidized-Bed Materials.

the residue was washed thoroughly with water. All solutions and residues were chemically analyzed.

In preliminary experiments with nitric acid solutions, we found that the amounts of uranium and plutonium leached increased with increasing acid concentration when the concentration was in the range of 0 to about 6 *M*. Therefore, most of the leaching tests were conducted with solutions having HNO_3 concentrations of 6 *M* or higher. Table 2.3 lists the data for 25 runs in which each sample was leached once for 5 hr with boiling reagent, using at least 5 ml of reagent per gram of sample. The data from Table 2.3, plus four other pairs of points for plutonium,[18–20] are plotted in Fig. 2.14 as the percentage of uranium or plutonium removed by leaching vs the initial concentration in the sample. From these data, the following general conclusions were drawn:

1. The leaching characteristics of uranium and plutonium are essentially identical. The leaching behavior of plutonium at a low initial concentration can, therefore, be predicted from that of uranium at a similar concentration. Based on results of the experiments just described, we can conclude that the leaching of plutonium, under the conditions used in these tests, will always yield a residue containing less than 12 mg per 100 g of waste alumina. This is equivalent to a plutonium loss of less than 0.5 to 1.5% in a typical pilot plant run with 1500 to 500 g of plutonium in the charge.

2. Agglomerates or sintered masses in the waste solids having high plutonium or uranium concentrations could probably be detected by leaching, but not necessarily by spot sampling of solids.

3. Successive leachings of a bed of waste solids would progressively decrease the plutonium content of the residue. The amount of decrease could be estimated by a stepwise calculation from the curve in Fig. 2.14.

4. Boiling 13 *M* HNO_3 is the preferred leachant; no significant benefit is derived from the addition of HF to levels up to 0.1 *M*.

---

[18] *Reactor Development Progr. Rept. Feb. 1965*, ANL-7017, p. 66.

[19] R. L. Jarry *et al.*, *Laboratory Investigations in Support of Fluid Bed Fluoride Volatility Processes. Part IX. The Fluid Bed Fluorination of Plutonium-Containing Simulated Oxidic Nuclear Fuels in a 1½-in.-Diameter Reactor*, ANL-7077, p. 37 (December 1965).

[20] M. J. Steindler, ANL, personal communication, Feb. 3, 1967.

Engineering-Scale Studies. – A limited amount of work was done by the Unit Operations Section to establish the feasibility of a circulation system as illustrated in the flow diagram (Fig. 2.13). Fresh T-61 Alcoa alumina, nominally −40 +100 mesh, was used to simulate reactor waste solids; water was used as the leachant. Tests were run first in a 1.5-in.-ID glass column and then in a 9-in. column at upflow "velocities" from about 2.5 to 6 gpm per square foot of cross section. The bed expansion (or fluidizing) and contacting were excellent when a bed support of coarse alumina (−4 +10 mesh) on a perforated plate with 62-mil holes was used; by contrast, use of a cone bottom with a tangential inlet and no bed support caused incomplete contact near the bottom. A small amount of the finest alumina remained in suspension as long as circulation continued but did not interfere with operability. Generally, results of this work followed closely the experience with similar liquid-solid contacting systems.

The design of the main vessels for the flowsheet was based on the laboratory- and engineering-scale data. Preliminary design drawings were completed,

Table 2.3. Results of Leaching Experiments with Fluidized-Bed Materials

Each sample leached once for 5 hr with boiling reagent, using at least 5 ml of reagent per gram of sample

Experiment No.	Preparation[a] (306-)	Concentration in Sample (wt %)		Concentration in Leachant (*M*)			Amount Leached (%)		
		Pu	U	HNO_3	HF	$Al(NO_3)_3$	Pu	U	F
1	4	0.013	0.035	8	0	0	62	54	59
2	4	0.014	0.019	8	0	0	67	50	66
3	7	0.022	0.032	4	0	0	64	40	88
4	7	0.023	0.020	6	0	0.1	24	89	14
5	23	0.025	0.0066	13	0.1	0	78	11	
6	7	0.026	0.024	8	0	0	53	56	91
7	23	0.029	0.0063	5	0	0	82	35	51
8	23	0.030	0.0069	13	0	0	97	46	40
9	8	0.030	0.017	13	0.05	0	88	55	
10	23	0.031	0.0060	13	0.05	0	85	14	
11	7	0.032	0.014	13	0.05	0.05	67	66	
12	23	0.033	0.0050	13	0	0	86	54	38
13	23	0.033	0.0036	13	0.05	0	85	24	
14	7	0.034	0.021	13	0	0	66	68	63
15	23	0.035	0.026	6	0	0.1	78	92	32
16	7	0.036	0.014	13	0.1	0	93	68	
17	8	0.038	0.021	13	0	0	84	64	26
18	7	0.039	0.014	13	0.05	0	94	69	
19	7	0.044	0.014	13	0.05	0	92	63	
20	14	0.061	0.0060	13	0.05	0	95	48	
21	14	0.063	0.010	13	0	0	91	59	41
22	14	0.063	0.0063	13	0.05	0	91	41	
23	14	0.067	0.0077	13	0.1	0	93	31	
24	14	0.077	0.0066	5	0	0	90	43	58
25	14	0.0785	0.0068	13	0	0	86	38	59

[a]See Table 2.2 for description of preparations.

and a preliminary layout was made. No further design work is intended since plans to install a leacher in the FBVPP have been abandoned.

Corrosion Studies to Aid in Choosing an Alloy for the Leacher

A corrosion program was completed under subcontract with Battelle Memorial Institute – Columbus Laboratories (BMI). Its purpose was to determine the most suitable material of construction for the leaching system.[21] This program included a survey of work by other investigators.

Welded and unwelded coupons of candidate constructional materials were exposed to a boiling solution (120°C) of 13 *M* HNO_3–0.1 *M* HF for times up to 240 hr. The addition of 0.1 *M* $Al(NO_3)_3$ to the leach solution greatly reduced the corrosion of the alloys during a 24-hr exposure.

HAPO-20 (50% Ni–25% Cr–16% Fe–6% Mo–1% Cu) was the most resistant of the materials that were studied from the standpoint of durability of both the welds and the base metal. Several other alloys showed fairly good resistance to the leach solution, but all were preferentially attacked near, or in, the welded areas; they were: Corronel 230 (nickel–36% Cr–5% Fe–1% Cu–1% Mn–1% Ti), 50% Ni–50% Cr, and Haynes 25 (50% Co–20% Cr–15% W–10% Ni–3% Fe–1.5% Mn). Earlier work conducted by investigators from BMI and the Hanford Laboratories had shown HAPO-20 to have superior fabrication properties compared with other high-nickel alloys.[22] An overall consideration of results leads to HAPO-20 as the preferred material and Corronel 230 as the second choice.

Small-Scale Engineering Studies

A small-scale fluidized-bed engineering test facility, located in a cell in Building 3503, contains a 2-in.-diam nickel fluidized-bed reactor and other process equipment that is required for decladding studies using either HCl-N_2 or HF-O_2, oxidation studies, and fluorination studies with BrF_5-N_2 or F_2-N_2. Since the primary purpose of this facility is to test instrumentation, controls, and sampling devices and to develop operating procedures for the FBVPP, the instruments and controls duplicate those to be installed in the FBVPP as closely as possible. The operations also simulate those planned for the FBVPP, except that irradiated fuel will not be used and no process step involving plutonium can be tested. Evaluation of the HF-O_2 flowsheet for stainless-steel-clad fuels was completed, and testing of the flowsheet for Zircaloy-clad UO_2 fuels was begun. Several instruments for the continuous in-line monitoring of gas streams were evaluated. The development of a gas-jet-powered system to obtain samples of the bed material from fluidized-bed reactors was continued.

2.11 PROCESS FLOWSHEET TESTS

Results of Decladding and Fluorination Tests with Stainless-Steel-Clad UO_2

The difficulties reported last year in decladding and fluorinating stainless-steel-clad UO_2 fuels[23] have now been resolved. Caking problems with the alumina bed can be avoided by using Alcoa T-60 alumina, nominally −48 +100 mesh, that contains less than 5% −140 mesh material. Using 40% HF–60% O_2 to initiate the decladding reaction and 20% HF–80% O_2 to complete the reaction ensured complete conversion of UO_2 to U_3O_8. Uranium losses in the bed material, in the filter residue, and on the primary reactor walls were consistently less than 0.2% in a series of tests using programmed flows of HF-O_2 followed by a fluorine-nitrogen mixture. Although the stainless steel cladding was completely reacted under these conditions, massive pieces of stainless steel were only partially oxidized. Operating characteristics of the sintered nickel (powder) filters appeared unchanged after six decladding-fluorination cycles. The pressure-, temperature-, and flow-measuring equipment performed satisfactorily in all tests.

Results of Decladding and Oxidation Tests with Zircaloy-Clad UO_2

The major experimental effort during this period was directed toward the decladding and oxidation

---

[21] P. D. Miller *et al., Corrosion of Construction Materials in Boiling 13 M Nitric–0.1 M Hydrofluoric Acids*, BMI-X-434 (Mar. 30, 1967).

[22] R. E. Burns *et al., Ind. Eng. Chem., Prod. Res. Develop.* 2(2), 163 (1963).

[23] *Chem. Technol. Div. Ann. Progr. Rept. May 31, 1966*, ORNL-3945, p. 53.

of Zircaloy-clad UO_2 fuel. Fuel assemblies were simulated by loading 1-ft-long Zircaloy tubes (0.4 in. OD, 30-mil wall) with $\frac{3}{8}$-in.-diam UO_2 pellets. Four tubes were arranged in a square array with tubes on 0.525-in. centers. The assembly was held together by two 20-mil-thick spacers made from stainless steel, each spacer being 1 in. from an end of the assembly. Alcoa T-60 alumina (nominally −48 +100 mesh) was used as the bed material.

Decladding with HF-O_2. – Two tests using HF-O_2 as the decladding reagent were made with a Zircaloy-clad fuel assembly to determine the nature of the residues. A programmed HF-O_2 flow (1 hr at 40% HF–60% O_2 followed by 2 hr at 20% HF–80% O_2) was used; reactor wall temperatures were held at 550°C. As expected, the bed residues contained relatively massive shards of ZrO_2. Although these pieces were not detrimental to bed fluidization, they would make the operation of any bed-sampling device difficult, and the time required for their conversion to ZrF_4 might be excessive due to a low surface-to-volume ratio. The UO_2 pellets appeared to be completely oxidized and partially fluorinated. The U^{6+}: U^{4+} ratio in all samples was greater than 2; one sample of oxidized pellets assayed 13.5% U^{4+}, 65.3% U^{6+}, and 12.8% F, with oxygen not determined.

Decladding with HCl. – The small-scale engineering test facility uses a 2-in.-ID primary reactor that is operated in series with a 2-in.-ID pyrohydrolyzer for HCl decladding flowsheet tests. In preliminary tests, trouble was experienced with operation of the pyrohydrolyzer bed due to unsteady flow.[24] Although the accumulation of ZrO_2 in the bed, as suggested by ANL, might modify the fluidizing behavior, we believe that extreme spouting conditions exist in the bed as a consequence of a high gas velocity that results from an increased volume of gas passing through the reactor, as illustrated in the following sequence of reactions:

1. Primary reactor:

$$Zr(s) + 4HCl(g) + 2.66N_2(g) \rightarrow ZrCl_4(g) + 2H_2(g) + 2.66N_2(g)$$

Total moles of gas into reactor per mole of zirconium reacted	6.66
Total moles of gas leaving reactor per mole of zirconium reacted	5.66

2. Pyrohydrolyzer reactor:

$$ZrCl_4(g) + 2H_2(g) + 2.66N_2(g) + 2H_2O(g) \rightarrow ZrO_2(s) + 4HCl(g) + 2H_2(g) + 2.66N_2(g)$$

(assuming only stoichiometric addition of steam)

Minimum total moles of gas into reactor per mole of zirconium reacted	7.66
Minimum total moles of gas leaving pyrohydrolyzer per mole of zirconium reacted	8.66

Since steam is always added in excess and the utilization of HCl is low, the volumes are actually higher than those shown above, and velocities greater than 2 fps can be expected.

During these "shakedown" tests an accidental contamination of the equipment from an external source of radioactivity occurred; a period of two months was required to decontaminate and rebuild the equipment. Following the cleanup, a series of tests was run using 60% HCl–40% N_2 in the primary reactor. Superficial velocities were 0.7, 1.0, and 1.25 fps; the reactor wall temperature was 450°C; and the UO_2 : Al_2O_3 mole ratio was 1 : 1.6. Although decladding was complete in 2 hr at velocities of 1 fps and above, the conversion of $ZrCl_4$ to ZrO_2 was not complete, and the $ZrCl_4$ either desublimed on the filters (if their temperatures were below 400°C) or passed through them to desublime in the cooler off-gas line; in both cases, plugs were formed. Uranium losses to the pyrohydrolyzer were about 0.2%; from 1 to 2% of the charged zirconium remained in the primary reactor bed. The chloride content of that bed (measured *after* the oxidation step) was about 0.1%.

UO_2 Oxidation Test. – Several oxidation tests using as-received and untreated UO_2 pellets were made at low fluidization velocities (0.7 and 1.0 fps) to minimize elutriation of fine U_3O_8 particles. The bed temperature was 450°C for the series, and the UO_2 : Al_2O_3 mole ratio was 1 : 1.6. When air was used as the oxidizing agent, sinters formed in the bed, and oxidation was incomplete after 2 hr with 20% to 50% of the uranium oxide in particles larger than 16 mesh. At the end of another test series using varying oxygen-nitrogen mixtures, the product beds flowed freely and contained no particles larger than 50 mesh. The oxygen content was initially 10%, then successively 20, 40, and 80%, followed finally by 100% oxygen for the

[24] R. P. Milford *et al.*, *Fluoride Volatility Processing Semiannual Progress Report Period Ending Nov. 30, 1966*, ORNL-TM-1849, p. 15.

final 30 min of a 2-hr run period. Oxidation of UO_2 to U_3O_8 was complete. From 1 to 2% of fine U_3O_8 remained with the filters.

In contrast to results of tests using untreated UO_2 pellets, no sintering was observed after air oxidation of pellets that had been exposed to HCl – either by special pretreatment or in a previous HCl decladding run. The product beds were free flowing, oxidation was complete, and the amount of fine U_3O_8 found on the filter was less than 2%.

2.12 SAMPLING OF SOLIDS FROM A FLUIDIZED-BED REACTOR

In the semiannual report we discussed the ideas and the preliminary experiments that led to the design of a system for obtaining samples of bed material from fluidized-bed reactors.[25] This system uses a gas-powered jet to withdraw solids from the fluidized bed and to discharge them into a sample loop for return to the reactor (see Fig. 2.15). When the circulation of solids has been established, the flow is stopped by operating valves, and the entire contents of the valved-off section of the sample loop are drained into a sample container. Most of the effort for this period was directed toward optimizing the design and the location of the gas-powered jet.

As originally conceived for the FBVPP, the jet was to be located outside the primary reactor furnace on a sample takeoff line oriented 45° downward from the horizontal; however, in-cell space considerations forced an orientation of 45° upward. Although circulating solids in a sample loop oriented 45° upward is possible, starting the flow of solids is very difficult when the jet is located more than 1 ft from the reactor walls, as would be the case if it were outside the furnace. This necessitated designing a jet that would fit inside the penetrations provided in the furnace for sample takeoff nozzles ($\frac{3}{4}$-in. sched 40 pipe). The current design, based on numerous experiments, is shown in Fig. 2.16. The outside diameter of the jet is the same as that of the sample nozzles. The jet will be installed with the face of the venturi section not more than 6 in. from the reactor walls. A jet made of nickel will be tested soon to determine the flow rates of solids at various bed fluidizing velocities, and, hopefully, to determine the correlation of the quantity of uranium in the sample with that in the entire bed.

ORNL DWG 67-1486R

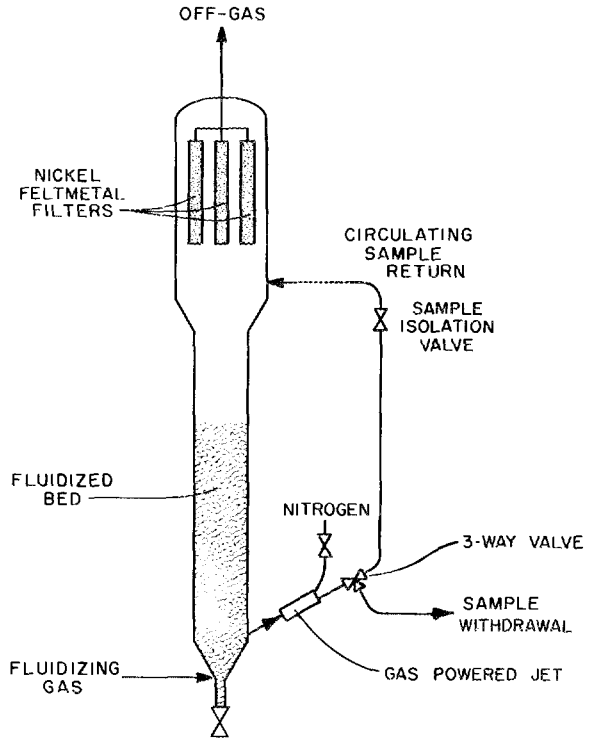

Fig. 2.15. Sample Circulating Loop for Fluidized-Bed Reactors.

2.13 CONTINUOUS IN-LINE MONITORING OF PROCESS GAS STREAMS

In-line monitoring of the change in concentration of one or more of the components in the off-gas stream is important in our work because, with the numerous gas-solids reactions involved and the difficulties of obtaining solid samples that are meaningful, it is the most practical way to follow the progress of the reaction. These gas stream analyses (preferably made continuously) can provide information on reaction rates, utilization of the reactants, and the end point of the reaction; and, if good stream flow information is available, a double check on process inventories may be possible.

The development effort has been directed toward choosing appropriate gaseous components whose

[25] R. P. Milford *et al.*, *Fluoride Volatility Processing Semiannual Progress Report for Period Ending Nov. 30, 1966*, ORNL-TM-1849, p. 62.

ORNL-DWG 67-6903

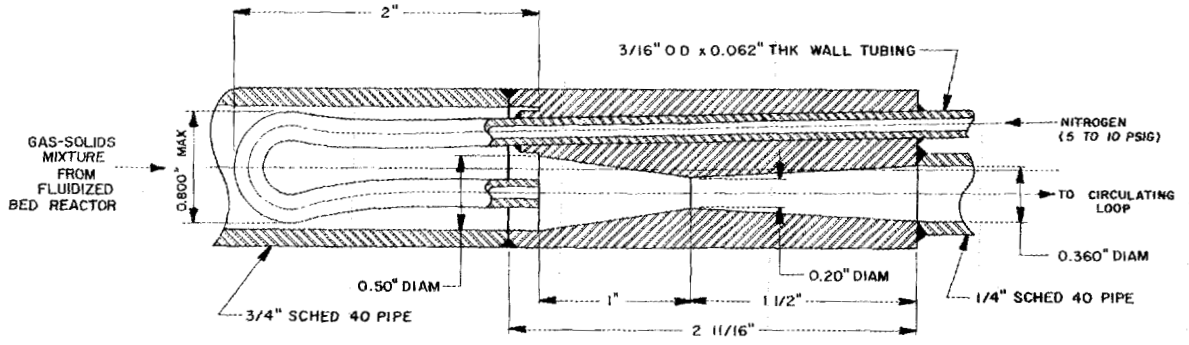

Fig. 2.16. Design of Gas-Powered Jet for Use in Solids Sampling Loop (see Fig. 2.15).

concentrations can be adequately measured with presently available instruments.

HCl Decladding Step

In the HCl decladding step the HCl reacts with the Zircaloy cladding to produce volatile $ZrCl_4$ and hydrogen. The $ZrCl_4$ is then reacted with steam to form solid ZrO_2 and to regenerate HCl. Thus, hydrogen is the only component in the pyrohydrolyzer off-gas stream that is a direct measure of the HCl-zirconium reaction. The relatively high thermal conductivity of hydrogen [0.108 Btu hr^{-1} ft^{-2} $(°F/ft)^{-1}$ at 80°F] as compared with that of nitrogen [0.015 Btu hr^{-1} ft^{-2} $(°F/ft)^{-1}$ at 80°F] suggests using a thermal conductivity cell to monitor the hydrogen. A sample loop was built to take a side stream from the pyrohydrolyzer off-gas stream, to remove the water and corrosive gases by means of appropriate traps, and to deliver to the thermal conductivity cell[26] a constant flow (about 50 cc/min) of the cleaned gas. The cell itself was placed in a constant-temperature bath held at 80°C. This equipment easily detected and continuously recorded hydrogen concentrations as low as 0.05% in the off-gas stream.

Oxidation Step

In the oxidation step the UO_2 pellets are oxidized to a fine U_3O_8 powder by oxygen in nitrogen (frequently air). Concentration of oxygen in the off-gas can be measured by taking advantage of its high magnetic susceptibility (paramagnetic effect) as compared with that of nitrogen. The Hays oxygen meter[27] easily detected changes in oxygen concentration of 0.25 vol %. The instrument is only useful in a qualitative sense because the oxidation reaction is characterized by an initial period where up to 10% of the oxygen is utilized, followed by a long tailoff period where oxygen utilization is less than 1%.

BrF_5 Fluorination Step

The current flowsheet uses BrF_5 as a fluorinating agent for uranium; the plutonium remains as nonvolatile PuF_4. The resulting off-gas stream is a rather complex mixture of nitrogen, bromine, BrF_3, BrF_5, UF_6, and oxygen. After leaving the reactor, this stream is reacted with fluorine in a regenerator to convert bromine and BrF_3 back to BrF_5. Minimizing the amount of fluorine fed to the regenerator can be done by (1) measuring the UF_6 concentration, (2) determining both the bromine and BrF_3 concentration, or (3) monitoring the oxygen concentration. The spectral characteristics of BrF_3 and BrF_5 rule out the use of ultraviolet and infrared absorption techniques for measuring concentrations of UF_6. To make use of oxygen concentration requires that the UF_6 and halogens be removed from the stream because of their corrosive nature. This

[26] Thermal conductivity cell, nickel, model SC-500, purchased from Gow-Mac Instrument Co., 100 Kings Street, Madison, N.J.

[27] Hays oxygen meter, model 635, purchased from the Hays Corp., Michigan City, Ind.

removal could be accomplished, but thus far no experimental work has been done toward that end.

Gas chromatographic techniques are probably the most effective means for resolving the off-gas composition. A system that uses columns packed with Kel-F 10 on an alumina support (Alcoa T-60, −60 +70 mesh) with Freon 114 as a carrier gas is currently being tested. Although complete resolution has not yet been obtained, this approach appears to offer several advantages over the conventional systems for corrosive gases. The tailing of the peaks is improved, and with light substrate loadings (typically 5% Kel-F 10 on alumina), it is possible that the analysis can be completed in an acceptable period of time. The Freon 114 carrier suppresses the BrF_5 signal because of their comparable densities (molecular weights of Freon 114 and BrF_5 are 171 and 175 respectively). Moreover, the use of the high-density carrier gas increases the sensitivity of the gas-density balance; the UF_6 response is increased about fivefold over that with an argon carrier despite the smaller density difference. Tests are continuing using other grades of alumina with various loadings and temperatures.[28]

Plutonium Fluorination Step

After the uranium has been volatilized with BrF_5, fluorine at a concentration of about 50 vol % in nitrogen will be used to volatilize the plutonium. No instruments have been proposed for monitoring the PuF_6, primarily because of its low concentration and the radiation problems. Monitoring the recycle gas stream, however, for fluorine concentration will be necessary. By use of a Du Pont photometric analyzer,[29] equipped with a capillary tube to control flow through the sample cell, we have been able to measure fluorine concentrations in the off-gas stream over a range of 0 to 90% with accuracies approaching ±1.0% fluorine.

2.14 ESTIMATION OF CRITICAL CONSTANTS FOR NbF_5

As an extension of previously reported experiments to determine vapor-liquid equilibria of the UF_6-NbF_5 system,[30] the pressure-density-temperature relationships of the liquid and vapor phases of NbF_5 were determined.[31] From these data the critical constants of NbF_5 were estimated using the law of rectilinear diameters. This law states that the orthobaric densities are a linear function of temperature up to the critical temperature. The critical constants were estimated to be: $\rho_c = 1.21$ g/cm^3, $V_c = 0.155$ liter/g-mole, $T_c = 737°K$, and $P_c = 62.0$ atm.

---

[28]Work done by A. S. Meyer and W. F. Peed, Analytical Chemistry Division, ORNL.

[29]Du Pont 400 split-beam photometric analyzer purchased from Instrument Product Div., E. I. du Pont de Nemours and Co., Inc., Wilmington, Del.

[30]*Chem. Technol. Div. Ann. Progr. Rept. May 31, 1966*, ORNL-3945, p. 69.

[31]W. W. Pitt, Jr., *Vapor Liquid Equilibria of the Binary System Uranium Hexafluoride–Niobium Pentafluoride* (thesis), ORNL-TM-1683 (January 1967).

3. Molten-Salt Reactor Processing

The development of a molten-salt breeder reactor (MSBR) is one of the long-range projects at ORNL. The Chemical Technology Division is participating by developing processes for continuously removing fission products from the core salt and for recovering the newly produced ^{233}U from the blanket salt. The reference reactor for this study, a 1000-Mw (electrical) MSBR, is a two-region system with an $LiF-ThF_4$ (71-29 mole %) blanket and an $LiF-BeF_2-UF_4$ (about 65.5-31.2-3 mole %) fuel stream.

The most attractive processing scheme would provide continuous removal of ^{233}Pa from the blanket, thereby keeping its concentration at a sufficiently low level to make its transmutation by neutron capture economically acceptable. The technology for achieving this is presently being explored by the Reactor Chemistry Division. The alternative method, removal of ^{233}U from the blanket by fluorination, is less attractive economically but is very much simpler to engineer. With this method, the ^{233}U concentration could be maintained below 0.012 mole %, which would allow removal of fission products by a small purge stream, resulting in complete replacement of the blanket volume every 40 years.

Fission products accumulate in the fuel salt at a much higher rate than in the blanket salt and must be removed on about a 39-day cycle. At present, the most attractive process for removing these contaminants consists in fluorination of the fuel salt to remove the uranium and subsequent distillation of the carrier salt to separate the valuable LiF and BeF_2 from the less-volatile fission products. The UF_6 from the fluorination is purified by sorption on NaF, desorption, and collection in a cold trap. It is subsequently combined with the purified carrier salt by simultaneously absorbing it in molten salt and adjusting the valence state of uranium by reduction with hydrogen. This processing scheme was previously described[1] and was subjected to a preliminary cost estimate that showed it to be economically feasible.[2] Advances in the technology this year include: the determination of the effects of operating variables on the recovery of uranium by continuous fluorination, and the completion of a facility to study the protection of the fluorinator walls by a layer of frozen salt. The relative volatilities of the rare-earth fluorides and zirconium fluoride are now known with good accuracy. Vaporization rates for the vacuum distillation of salts have been studied. Experiments have been planned in which 48 liters of fuel salt from the MSRE will be distilled; appropriate equipment to accomplish this work has been built. Plans have been formulated to provide the MSRE with a ^{233}U fuel charge; a facility to effect this is being provided. Alternative methods for fuel reprocessing have been studied. The most promising of these is the extractive reduction of the fission products.

3.1 CONTINUOUS FLUORINATION OF MOLTEN FLUORIDE MIXTURES IN 1-in.-diam COLUMNS

The recovery of uranium from molten salt by fluorination has been studied extensively in the development of the Molten-Salt Volatility Process. In this process, the uranium tetrafluoride in the salt is converted to volatile uranium hexafluoride by the reaction

$$UF_4 + F_2 \longrightarrow UF_6 .$$

The fission products and corrosion products that form volatile compounds during fluorination can be

---

[1] D. E. Ferguson, *Chem. Technol. Div. Ann. Progr. Rept. May 31, 1965*, ORNL-3830, pp. 301–2.

[2] C. D. Scott and W. L. Carter, *Preliminary Design Study of a Continuous Fluorination–Vacuum-Distillation System for Regenerating Fuel and Fertile Streams in a Molten-Salt Breeder Reactor*, ORNL-3791 (January 1966).

separated from the uranium by selective absorption on beds of NaF and MgF_2.

The removal of uranium from the fuel salt of a molten-salt breeder reactor (MSBR) requires the development of equipment that is suited to continuous operation and that will provide efficient removal of uranium and acceptably low corrosion rates. The attainment of a consistently high uranium recovery in a continuous fluorinator has been demonstrated, and the effects of some operating variables are reported here. We found that corrosion can be controlled by operation with a layer of frozen salt on the vessel walls (see Sect. 3.2).

Experimental studies of continuous fluorination of molten salt were made in a system consisting of a 1-in.-diam, 72-in.-long nickel fluorinator and auxiliary equipment (Fig. 3.1), which allowed the countercurrent contact of molten salt with fluorine. The fluorinator off-gas passed through a 400°C NaF bed for removal of chromium fluorides, a 100°C NaF bed for removal of UF_6, and a soda lime bed for F_2 disposal. A gas chromatograph was used to analyze the off-gas for F_2, UF_6, and N_2 just prior to its passage through the 100°C NaF bed. The uranium concentration in the salt after fluorination was determined from salt samples.

Fluorination tests were made in which molten salt (41.2-23.7-35.1 mole % $NaF-LiF-ZrF_4$) containing UF_4 was contacted countercurrently with a quantity of fluorine in excess of that required for conversion of UF_4 to UF_6. During a given experiment, salt and fluorine feed rates, operating temperature, and UF_4 concentration in the feed salt were maintained constant. However, these parameters were varied from one experiment to the next, as follows: operating temperature, from 525 to 600°C; salt feed rate, from 5 to 30 cm^3/min; fluorine feed rate, from 75 to 410 cm^3/min; and UF_4 concentration in the feed salt, from 0.12 to 0.35 mole % UF_4.

The effects of salt throughput, operating temperature, and initial UF_4 concentration on uranium removal during steady-state operation are shown in Fig. 3.2. The data are based on the average uranium concentration in the fluorinated salt, which was determined at 15-min intervals during 1- to 2-hr periods of steady-state operation. A salt depth of 48 in. was used in the fluorinator in all tests, and the fluorine feed rate was varied from 215 to 410 cm^3/min (STP). Removal of the uranium fed to the fluorinator ranged from 97.4 to 99.9%, with removal in most of the runs being greater than 99%.

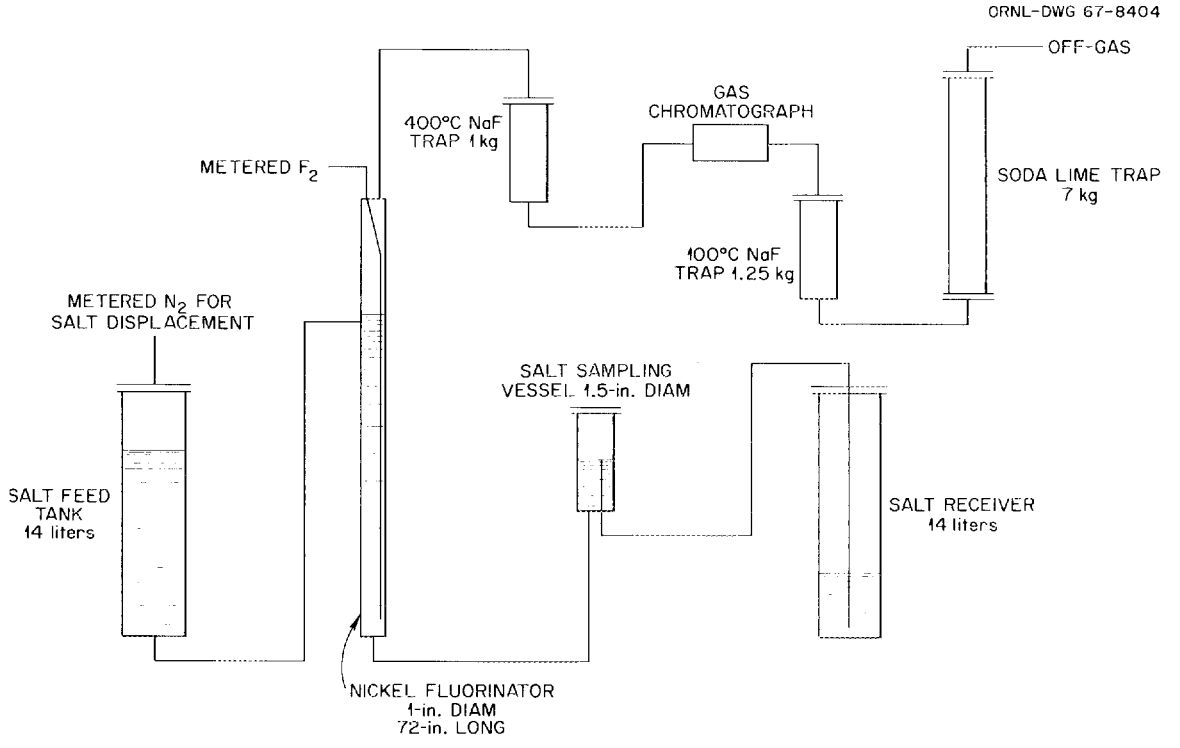

Fig. 3.1. Equipment for Removal of Uranium from Molten Salt by Continuous Fluorination.

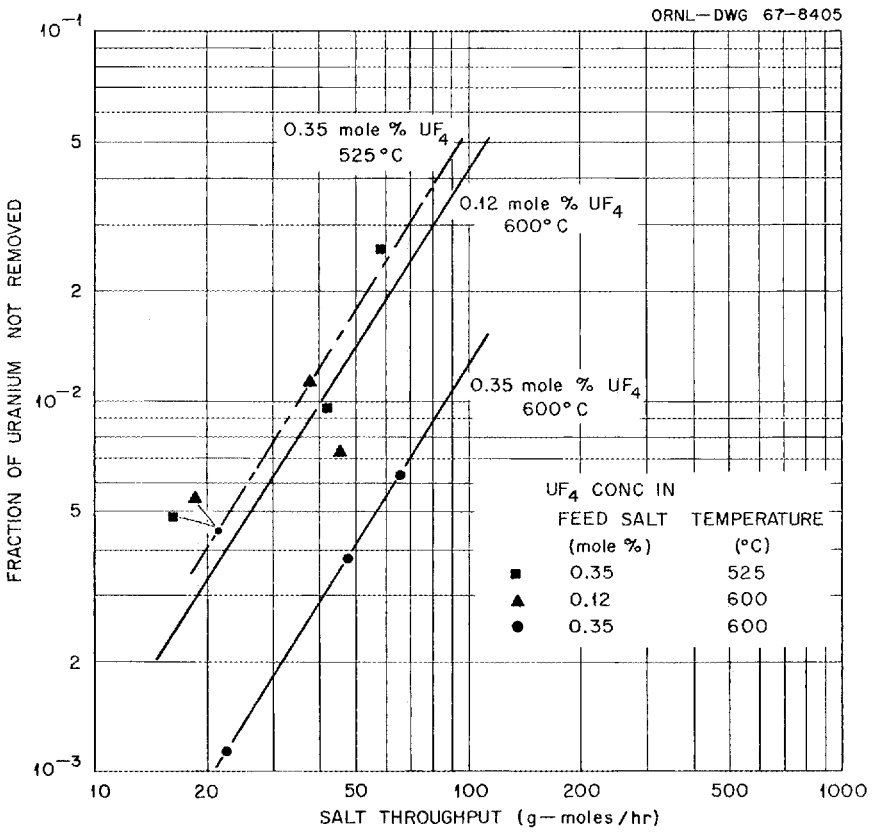

Fig. 3.2. Variation of Uranium Removal with Salt Throughput, Operating Temperature, and UF_4 Concentration in Feed Salt.

Uranium removal was observed to decrease as the salt throughput was increased, as the operating temperature was lowered, and as the UF_4 concentration in the feed salt was decreased. As long as the quantity of fluorine used was stoichiometrically adequate, no significant effect of fluorine feed rate was noted.

3.2 CORROSION CONTROL BY USE OF A FROZEN WALL

It is anticipated that a continuous fluorinator can be protected from corrosion by freezing a layer of salt on the vessel wall and that in processing the fuel salt of an MSBR the heat flux necessary for maintaining molten salt adjacent to frozen salt can be provided by the decay of fission products in the fuel salt. We are making preparations for the demonstration of frozen-wall protection. The experimental system will be operated with a frozen layer of salt on the fluorinator wall and will allow the countercurrent contact of an inert gas with molten salt in equipment of a design suitable for continuous fluorination.

The fluorinator is constructed from 5-in.-diam sched 40 nickel pipe and will provide a protected section about 6 ft long. Internal heat is supplied by Calrod heaters placed inside a $\frac{3}{4}$-in.-diam nickel tube along the center line of the vessel. The thickness of the frozen wall will depend on the radial heat flux and can be varied from $\frac{3}{8}$ to $1\frac{1}{2}$ in. The thickness will be determined from temperature gradients measured by two sets of four thermocouples located at different radii with respect to the center line of the vessel. A feed tank and a receiver vessel having salt volumes equivalent to approximately 10 fluorinator volumes are provided.

The experiment will use a salt mixture (66 mole % LiF–34 mole % ZrF_4) having a phase diagram similar to that of the LiF-BeF_2 fuel salt of the MSBR and will allow us to study the operating characteristics of a frozen-wall fluorinator.

3.3 RELATIVE VOLATILITIES OF RARE-EARTH FLUORIDES IN MSBR SALTS

The method currently proposed for processing the fuel stream of an MSBR includes a distillation step in which the major components of the stream, LiF and BeF_2, are vaporized from less-volatile fission product fluorides (primarily rare earths).[2] The design of equipment for this step requires vapor-liquid equilibrium data for the salt systems of interest. Vapor-liquid equilibrium data can be conveniently expressed as relative volatilities with respect to LiF, the less volatile of the two major components, and therefore an appropriate reference. The relative volatility of component A with respect to component B, α_{AB}, is defined as:

$$\alpha_{AB} = \frac{y_A/x_A}{y_B/x_B}, \qquad (1)$$

where A and B refer to the two components and x and y refer to the vapor-phase and liquid-phase mole fractions respectively.

Relative volatilities of a number of rare-earth fluorides (REF) with respect to LiF have been measured in the binary system LiF-REF and in the ternary system LiF-BeF_2-REF. Measurements were made using a recirculating equilibrium still (Fig. 3.3). Salt was vaporized in the $1\frac{1}{2}$-in.-diam still pot, condensed in the 1-in. condenser, and returned as liquid to the still pot. At steady state, the concentrations of liquid in the still pot and in the condenser will be equilibrium values from which relative volatilities can be determined if the liquid in the condenser and boiler is well mixed. Salt samples were taken after a run by freezing the salt and sectioning the still.

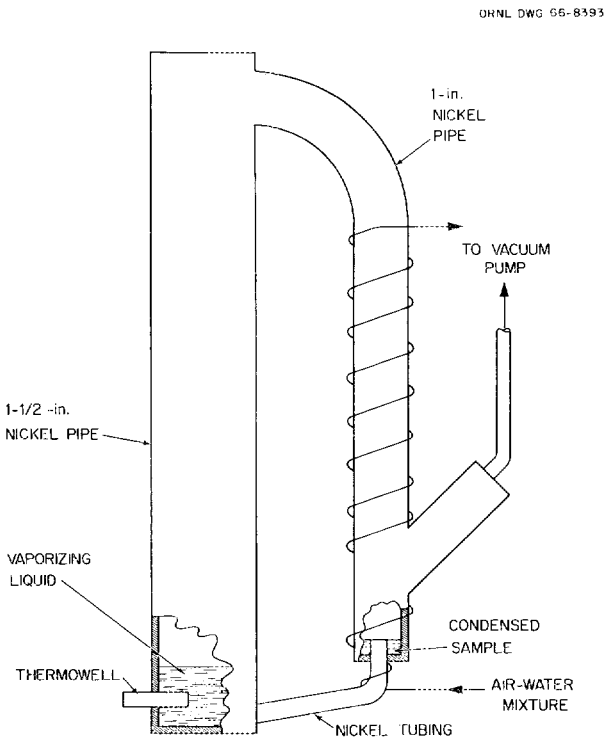

Fig. 3.3. Molten-Salt Still Used for Relative Volatility Measurements.

Approximately 30 experiments were made with the binary system containing LiF and the compound of interest, and 15 experiments were made with the ternary system, which was prepared by adding the compound of interest to an 88 mole % LiF–12 mole % BeF_2 mixture. The operating temperature was 1000°C in all instances. With the binary system, the operating pressure was 0.5 mm Hg; with the ternary system, it was 1.5 mm Hg. Data from these experiments are shown in Table 3.1.

Relative volatilities of the REF's appear to be slightly lower in the system containing BeF_2, although the differences are minor for all materials except CeF_3. These values indicate that the required REF removal efficiencies can be obtained in stills of simple design without rectification.

The relative volatility of ZrF_4 is approximately 1 in the LiF-BeF_2 system, which indicates that the removal of ZrF_4 by distillation will be negligible.

Table 3.1. Relative Volatilities of Several Components in LiF and LiF-BeF_2 Mixtures

Compound	Liquid-Phase Mole Fraction	Relative Volatility with Respect to LiF	
		In LiF	In LiF-BeF_2
LaF_3	0.02–0.05	3×10^{-4}	1.4×10^{-4}
CeF_3	0.01–0.02	3×10^{-3}	3.3×10^{-4}
PrF_3	0.055	6.3×10^{-4}	1.9×10^{-3}
NdF_3	0.05–0.06	6×10^{-4}	$<3 \times 10^{-4}$
SmF_3	0.05	2×10^{-4}	$<3 \times 10^{-4}$
ZrF_4	0.0003–0.01		1.1
BeF_2	0.10		4.73

3.4 VAPORIZATION RATES IN FLUORIDE SALT DISTILLATION

Data on the variation of vaporization rate with total pressure are necessary to predict vaporization rates in equipment that is suitable for MSBR fuel processing and to assess the error in relative volatilities that are measured in the recirculating equilibrium still. The equipment used for measuring the vaporization rates is shown in Fig. 3.4. The distillation unit was made from 1-in. nickel tubing bent into an inverted U. Salt was vaporized from a graphite crucible in the left leg of the still, and condensate was collected in a similar crucible in the right leg.

For operation of the still, an LiF-PrF_3 mixture containing 5 mole % PrF_3 was placed in a crucible in the vaporizing section of the still, and a second crucible (empty) was placed below the condenser. The system was purged with argon while being heated to the desired temperature. When the temperature in the vaporizing section reached 1000°C, the pressure in the still was reduced to the desired value and the temperature of the condenser was lowered to 500°C, which caused the salt vapor to solidify on the condenser walls. After a specified period of time, the still was pressurized with argon and the temperature of the condenser was raised to 1000°C; this allowed the condensate to melt and drain into the crucible below the condenser. Vaporization rates determined from the weight change in the vaporizing section of the still are given in Table 3.2.

ORNL DWG 67-1507

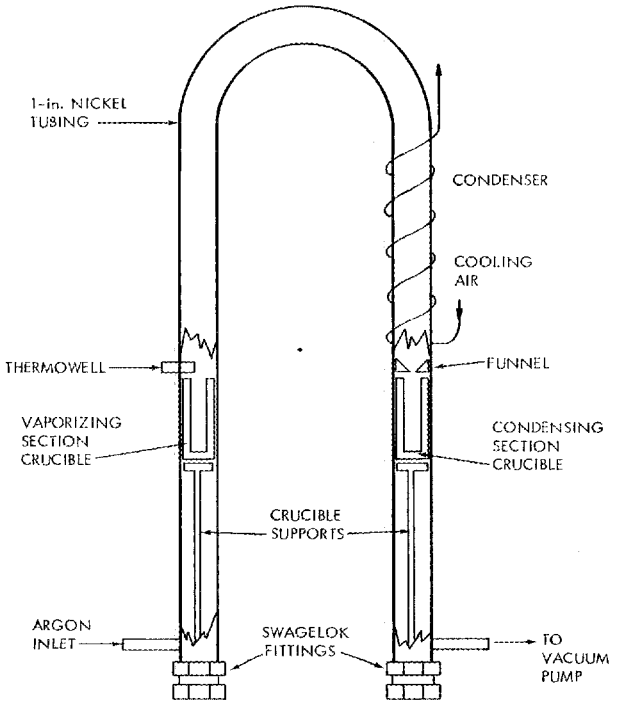

Fig. 3.4. Apparatus for Vaporization Rate Measurement.

Table 3.2. Variation of LiF Vaporization Rate with Total Pressure at 1000°C

Condenser Pressure[a] (mm Hg)	Vaporization Rate ($g\ cm^{-2}\ sec^{-1}$)
1.0	7.8×10^{-6}
0.50	3.3×10^{-5}
0.35	4.8×10^{-5}
0.1	2.4×10^{-4}

[a]The vapor pressure of LiF at 1000°C is about 0.53 mm Hg.

When the total system pressure is higher than the vapor pressure of the salt, the rate of vaporization should be controlled by the rate of diffusion of LiF and REF through the stationary argon present in the system; the measured rate at 1.0 mm Hg was comparable with that calculated by assuming the rate to be diffusion-controlled. The significant increase in vaporization rate as the condenser pressure was decreased indicates that the rate of vaporization is controlled at lower pressures by viscous drag in the passage to the condenser. Thus, the distillation rate at low pressures will be strongly influenced by the geometry of the equipment, as is normally the case for medium- and high-vacuum distillation. Plant-scale equipment to distill 15 ft^3 of fuel salt per day from a molten-salt breeder reactor would require about 43 ft^2 of distillation surface area if the highest experimentally observed distillation rate is achieved with the LiF-BeF_2 mixture. Conditions in the equilibrium still correspond to those at higher pressures; calculations showed that the error in relative volatility caused by the difference between the diffusivities of any rare-earth fluoride and LiF in argon is approximately 1%.

3.5 PREVENTION OF THE BUILDUP OF LOW-VOLATILITY MATERIALS AT A VAPORIZATION SURFACE

During the vaporization of a multicomponent mixture, materials that are less volatile than the bulk

of the mixture tend to remain in the liquid phase and are removed from the liquid surface by convection and molecular diffusion. Low-pressure vaporization does not generate deeply submerged bubbles and therefore provides little convective mixing in the liquid. The concentration of materials of low volatility at the vaporization surface may be appreciably higher than the average liquid concentration if these materials are removed by diffusion alone. An increase in surface concentration will result in the vaporization of a greater quantity of low-volatility material than would occur in a system having a uniform liquid-phase concentration and will decrease the separation efficiency for a still or will contribute to error in the measured relative volatilities of such materials.

The effect of surface buildup of materials having low volatilities on the separation efficiency has been considered for both transient and steady-state operation of several still types. For example, consider a still of the continuous type as shown in Fig. 3.5. Two molten salt streams are fed to the bottom of the still; one consists of a feed stream of LiF and REF, and the other results from circulation of molten salt from the vaporization surface to the bottom of the system. Part of the LiF fed to the still is vaporized, and the remainder is withdrawn continuously. The distribution of REF between the streams leaving the still depends on both the REF relative volatility and the variation in REF concentration between the vaporization point and the withdrawal point. The variation in REF concentration is dependent on: (1) the distance l that separates the vaporization point and the withdrawal point, (2) the diffusivity D of REF in molten salt between these points, (3) the velocity V of molten salt toward the vaporization surface, and (4) the fraction f of the salt moving upward which is vaporized.

The performance of a still having a nonuniform REF concentration can be conveniently expressed in terms of its performance under conditions resulting in a uniform concentration. The variation of ϕ, the ratio of the fractional removal of REF in a still having a nonuniform concentration to the fractional removal in a still having a uniform concentration, with the dimensionless group Vl/D is shown in Fig. 3.6 for several values of f, the fraction of salt vaporized per circulation cycle through the still. The REF relative volatility was assumed to be 5×10^{-4}, and 99.5% of the LiF fed to the system was assumed to be vaporized.

The value of ϕ is about 1 for $Vl/D < 0.1$ for any value of f. Within this region a nearly uniform concentration in the liquid phase is maintained by diffusion of REF within the liquid; liquid-phase mixing by external circulation is not required to prevent excessive vaporization of REF with the LiF. We

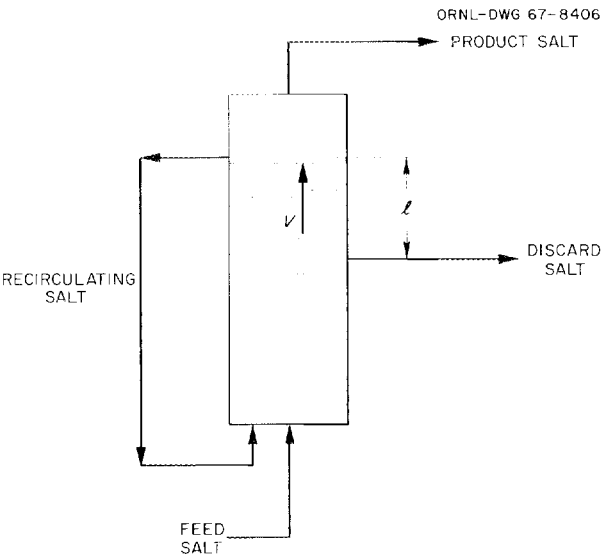

Fig. 3.5. Continuous Still Having External Circulation and a Nonuniform Liquid-Phase Concentration Gradient.

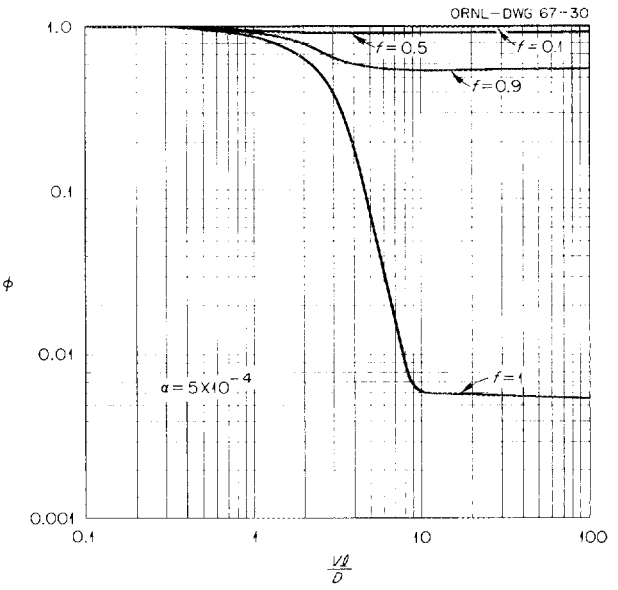

Fig. 3.6. Ratio of Fraction of Rare-Earth Fluoride Removed in Still Having a Nonuniform Concentration to That in a Still Having a Uniform Concentration for Vaporization of 99.5% of Salt Fed to System.

think an actual still will operate in the region of $Vl/D > 1$, where the distillation performance is strongly dependent on f. Within this region, a nearly uniform liquid-phase concentration can be maintained only if external circulation of the liquid is provided by mechanical or thermal methods. For $Vl/D = 100$, ϕ has a value of 0.0055 when circulation is not provided and a value of 0.99 if 90% of the salt is returned to the bottom of the still. Thus, the importance of the circulation of liquid cannot be overemphasized if good separation factors and highest distillation rates are to be obtained.

3.6 DEMONSTRATION OF FUEL-SALT DISTILLATION AT THE MSRE

Equipment has been designed and fabricated for a large-scale demonstration of the distillation of molten-salt reactor fuel. Distillation is carried out at ~1000°C and 1.5 mm Hg and results in volatilization and separation of the major components (LiF, BeF_2, and ZrF_4) from less-volatile fission product fluorides (primarily rare earths).

The system consists of a 48-liter feed tank, a 12-liter still pot, a condenser, a 48-liter condensate receiver, and associated auxiliaries required for removing condensate samples during operation and for maintaining desired operating conditions. All components that contact molten salt are fabricated from Hastelloy N. Provision is made for batch operation; also, salt can be fed to the still continuously.

The system will be operated for 500 to 700 hr using nonradioactive salt having the MSRE fuel carrier composition (65-30-5 mole % LiF-BeF_2-ZrF_4) and containing small quantities of rare-earth and/or other fluorides. During this period, data will be obtained on the variation of throughput with operating conditions and on the effective relative volatilities of components of the salt mixture. Corrosion data will also be obtained from test specimens of candidate materials of construction for future distillation systems.

The still and the condenser will be examined thoroughly after nonradioactive operation, using dimensional, radiographic, and ultrasonic methods. The system will then be installed in a cell adjacent to the fuel processing cell at the MSRE site and will be used to distill approximately 48 liters of radioactive MSRE fuel salt from which the uranium has been removed by fluorination. Additional data on the behavior and relative volatilities of various fission product fluorides will be obtained.

3.7 ALTERNATIVE PROCESSING METHODS

Methods other than distillation are being evaluated for the processing of MSBR fuel. Among these are reductive precipitation[3] and reductive extraction.[3–5] The first step in both of these methods would be removal of the uranium from the fuel salt by fluorination. In the reductive precipitation method a solid reductant such as beryllium would be added to the salt to precipitate the rare-earth fission products as insoluble, high-melting intermetallic compounds (beryllides), which would then be removed by filtration. Although this method appears to be chemically feasible,[3] its suitability for engineering-scale application is marginal because of the problems inherent in handling fission products in a concentrated form. A variation of this approach involves the addition of solid beryllium to the fuel salt while it is in contact with a liquid metal such as bismuth. The liquid metal would act as a solvent for the rare-earth fission product metals produced by the reduction reaction. Since it is possible that rare-earth beryllides could be formed as reaction intermediates and inhibit the transfer of rare earths from the salt phase to the metal phase, a general study of the stabilities of the rare-earth beryllides in contact with liquid bismuth was begun, using the system Be-La-Bi for the initial investigations.

Mixtures of $LaBe_{13}$ (1.05 g), beryllium powder (0.4 g), and bismuth (50 g) were heated in graphite crucibles for 20 to 115 hr at selected temperatures in the range 318 to 832°C. Fritted quartz samplers were used to obtain filtered samples (0.3 to 1 g) at temperature. The lanthanum and beryllium concentrations in these samples were determined by either neutron activation or emission spectroscopic methods. The lanthanum beryllide was prepared by sintering the appropriate mixture of the powdered elements in a closed tantalum crucible. Initially, the powders were sintered for about 3 hr at temperatures up to 1220°C under argon (pressures of

---

[3]D. E. Ferguson, *Chem. Technol. Div. Ann. Progr. Rept. May 31, 1966*, ORNL-3945.

[4]R. E. Briggs, *MSR Program Semiann. Progr. Rept. Aug. 31, 1966*, ORNL-4037.

[5]W. R. Grimes, *Reactor Chem. Div. Ann. Progr. Rept. Dec. 31, 1966*, ORNL-4076.

Table 3.3. Concentrations of Lanthanum and Beryllium Found in Bismuth After Equilibrating $LaBe_{13}$, Be, and Bi

Temperature (°C)	Concentration in Bismuth (ppm)		Be/La Atom Ratio in Bismuth
	La	Be	
318	440	<0.2	
357	15	<0.1	
428	10	0.15	0.23
547	1500	1.2	0.012
645	7600[a]	0.9	0.002
707	8100[a]	12.0	0.023
832	7500[a]	15.0	0.031

[a]These values approach the maximum concentration (11,300 ppm) attainable under the experimental conditions.

9×10^{-3} to 0.2 torr); then, the product was heated for 1 hr at temperatures up to 1455°C under argon at a pressure of 7 torrs. The only crystalline phase that could be identified in the product by x-ray diffraction analysis was $LaBe_{13}$. Chemical analyses, which gave a Be/La atom ratio of 12.57, indicated that the compound might have been slightly deficient in beryllium.

The results of the equilibration tests showed that $LaBe_{13}$ was not stable in the presence of liquid bismuth. At each temperature, both lanthanum and beryllium were transferred to the bismuth; however, the Be/La atom ratios in the bismuth were much too low for $LaBe_{13}$ to be considered the solute (Table 3.3). The extent of decomposition of the beryllide at each temperature appeared to be limited by the solubility of lanthanum in bismuth, which is markedly higher than the solubility of beryllium in bismuth.[6-8] In the tests at 318 to 547°C, the bismuth appeared to be saturated with both lanthanum and beryllium; however, under the conditions of the experiments, this did not cause complete decomposition of the beryllide. At 645°C and higher, the amount of lanthanum present in the system was insufficient to saturate the bismuth. The fact that most of the lanthanum from the beryllide was found in the bismuth phase indicates that nearly complete decomposition of the beryllide occurred.

The results of this work suggest that insoluble beryllides would not be formed in the reductive extraction method outlined above, provided that sufficient bismuth were present to satisfy the solubilities of the rare-earth fission products.

[6]D. G. Schweitzer and J. R. Weeks, *Trans. Am. Soc. Metals* 54, 185 (1961).

[7]J. R. Weeks, *Trans. Am. Soc. Metals* 58, 302 (1965).

[8]G. W. Horsley and J. T. Maskrey, *J. Inst. Metals* 86, 401 (1958).

3.8 PREPARATION OF ^{233}U FUEL FOR THE MSRE

Operation of the molten-salt reactor with ^{233}U fuel would provide valuable nuclear and chemical data for future molten-salt reactor research programs. Therefore, plans are now being made for refueling and operating the MSRE with this type of fuel early in 1968.

Approximately 71 kg of $^{233}UF_4$.^7LiF eutectic salt, containing 40 kg of ^{233}U, will be prepared for this refueling. Work with this material will require shielding because of the ^{232}U content (240 ppm) of the ^{233}U.

A simplified chemical flowsheet (Fig. 3.7) for $^{233}UF_4$.^7LiF eutectic salt preparation, involving simultaneous reduction and hydrofluorination of uranium oxide and lithium fluoride, was developed by the Reactor Chemistry Division. This flowsheet makes possible the design of simple equipment for economical remote operation in the TUFCDF, Building 7930.

Methods proposed for preparing the fuel concentrate are similar to those used for the routine preparation of UF_4 from oxides. Modifications of established processing methods include: (1) use of a vertical cylindrical reaction vessel for handling the molten fluoride product instead of trays or fluidized-bed reactors, (2) incorporation of LiF in the initial charge of starting materials, and (3) operation of the process at temperatures sufficient to maintain all LiF in its molten state. The mixture of starting materials will be heated to 900°C in helium to melt the LiF and to achieve some thermal decomposition of uranium oxides (to an overall composition of about $UO_{2.6}$). Subsequent

treatment with hydrogen will reduce this oxide mixture to near-stoichiometric UO_2. The conversion of UO_2 to UF_4 will be accomplished by hydrofluorination using an H_2/HF mole ratio of about 10 to maintain a highly reducing atmosphere to minimize corrosion during the conversion.

Development of the chemical flowsheet and the detailed design of processing equipment have progressed to the final stages. Construction and installation of the processing equipment in the TUFCDF are scheduled for completion so that salt production can start in January 1968.

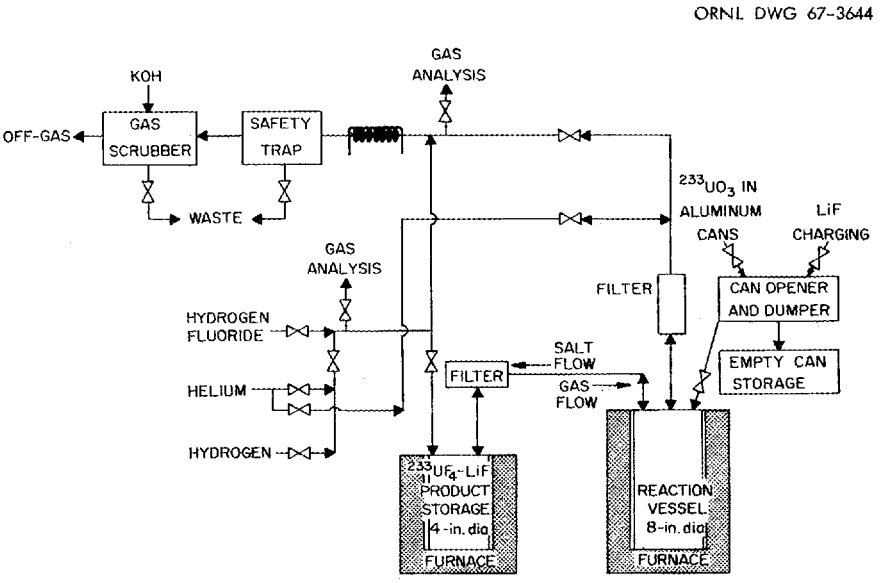

Fig. 3.7. MSRE ^{233}U Fuel Salt Preparation System.

4. Waste Treatment and Disposal

The objectives of the waste treatment and disposal development program are to develop a comprehensive waste-management system for nuclear wastes, including their final disposal, and to estimate the cost of this operation. Economical management of radioactive effluents is a prerequisite to the natural growth of a nuclear power industry. A comprehensive waste-management flowsheet, which was presented previously,[1] includes the following operations: High-level radioactive wastes (HLW), which contain nearly all the fission products, are converted to solids. Intermediate-level radioactive wastes (ILW), characterized by their generally high salt content, are incorporated in asphalt; any contained water is simultaneously volatilized. Low-level radioactive wastes (LLW) are treated to remove the radionuclides, and the decontaminated water is discharged to the environment or recycled for reuse. The recovered solids are combined with the ILW. Both the HLW and ILW solid products can be shipped to a final disposal site.

4.1 HIGH-LEVEL RADIOACTIVE WASTE

A process is being developed for preparing the waste powders from the Fluidized-Bed Volatility Process (FBVP) for final storage. The solids can be: (1) simply sealed in a stainless steel pot, (2) mixed with a "getter" to decrease the production of volatile components, or (3) dispersed in a glassy matrix. A pilot plant is being designed for testing these processes on radioactive wastes made in the ORNL Fluidized-Bed Volatility Pilot Plant (FBVPP, Sect. 2.0). Laboratory tests with nonradioactive simulated wastes showed that the addition of 10 wt % CaO to the fluidized-bed wastes reduced the weight loss at 850°C from 4.7 to 1.3%, or the weight loss attributable to moisture on the powder. Powders from aqueous wastes (produced in a spray calciner) were successfully dispersed in a glassy matrix in initial tests of a continuous process designed to immobilize all types of powdered waste products.

Chemical Development

Characterization of Waste Powders. – The principal effort in laboratory studies on the disposal of FBVP waste has involved the problems associated with canning (i.e., sealing in a stainless steel pot) the untreated powders for long-term storage. Since the waste powders consist of aluminum oxide plus aluminum fluoride, stainless steel fluorides, and a wide variety of fission product fluorides, the volatilization of fluorides presents a potential hazard at storage temperatures above about 250°C. Also, if moisture is present the hydrolysis of fluorides will cause corrosion.

Two arrangements of apparatus are used to determine the effects of time and temperature on the weight losses of waste powders and pure fluorides comprising the waste powder. In one, thermogravimetric methods are used to yield differential and integral weight losses of small samples ($\leq$1 g) as a function of time and temperature.[2] In the other, gross integral weight losses of large samples (several grams) are determined as a function of final temperature and time.

Thermogravimetric analyses (TGA) of waste powders from both the HF-O_2 and HCl processes have been made.[3] Weight losses obtained for

[1] *Chem. Technol. Div. Ann. Progr. Rept. May 31, 1965*, ORNL-3830, p. 96.

[2] W. W. Wendlandt, *Thermal Methods of Analysis*, pp. 53–55, Interscience, New York, 1964.

[3] J. C. Suddath and J. O. Blomeke, *An Economic Analysis of High Level Waste Management for Fluidized-Bed Volatility Processing of Power Reactor Fuels*, ORNL-TM-1441 (April 1966).

waste powder without stable fission products from the HF-O_2 method were 2.99% and 3.20% (see Table 4.1). Two experiments with waste powders without stable fission products from the HCl process gave weight losses of 0.998%. The weight losses of two samples of HCl-process material with stable fission products added to simulate a waste powder expected from processing five batches of fuel that had been irradiated to a burnup of 21,000 Mwd/metric ton were 2.02 and 2.20%. Each of the samples was heated at a rate of 4.7°C/min to 850°C and then either held at this temperature until an apparent constant weight was attained or for 3 hr – whichever came first. A flowing argon atmosphere was used; the off-gases were passed through two caustic scrubbers. Chemical analysis of the scrubber solutions of the experiments are not conclusive but indicate that hydrolysis of the fluorides is occurring at the elevated temperatures, giving HF as the primary off-gas.

Plots of differential weight losses with time (Δ weight/Δ time) vs temperature for the HF-O_2-process powder without stable fission products gave peaks at 130, 465, and 660°C in one instance and 475 and 675°C in the other. A typical plot is shown in Fig. 4.1. The 130°C peak corresponds to the dehydration of $Al_2F_6 \cdot 7H_2O$. The difference in weight loss between the two samples (0.21%) can be explained by the difference in amount of Al_2F_6 that is hydrated. The peaks at 465 and 475°C correspond to the dehydration of $Al_2O_3 \cdot H_2O$. The peaks at 660 and 675°C probably represent the sublimation of AlF_3. The peaks can be shifted slightly, depending on the amount of AlF_3 in the two samples. Plots of Δ weight/Δ time vs temperature for the HCl-process powder without stable

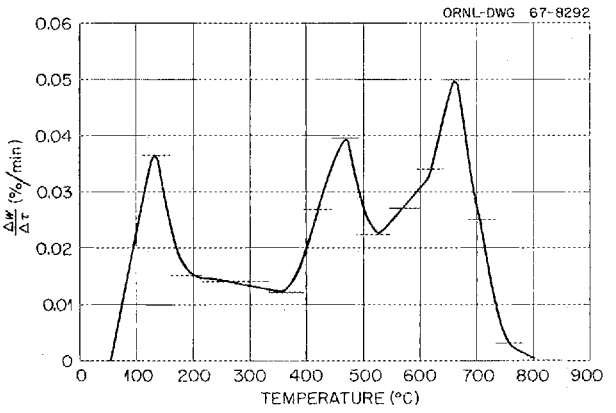

Fig. 4.1. Differential Weight Loss for HF-O_2 Flowsheet Waste Powder.

Table 4.1. Nominal Composition of Waste Powders from Fluidized-Bed Volatility Processes[a]

Component	Composition (wt %)		
	HF-O_2 Process	HCl Process	
	Without Stable Fission Products	Without Stable Fission Products	With Stable Fission Products[b]
Al	50.4	52.8	41.0
Cr	0.12		
F	11.8	2.23	16.8
Fe	0.97		
Ni	0.15		
Sn		0.024	0.04
U	0.11	0.015	0.22
Zr		0.12	0.3

[a]Flowsheets for these processes are given in *An Economic Analysis of High Level Waste Management for Fluidized-Bed Volatility Processing of Power Reactor Fuels*, by J. C. Suddath and J. O. Blomeke, ORNL-TM-1441 (April 1966).

[b]The fission product elements expected in a bed used to process five batches of fuel that had been irradiated to a burnup of 21,000 Mwd/metric ton were added. These elements, expressed as weight percent of the final bed, were: Se, 0.00567; Sr, 0.238; Rb, 0.212; Y, 0.1179; Zr, 0.805; Mo, 0.775; Ru, 0.315; Rh, 0.0747; Pd, 0.055; Ag, 0.00080; Cd, 0.00186; In, 0.00025; Sn, 0.00246; Sb, 0.00097; I, 0.0417; Cs, 0.484; Ba, 0.281; La, 0.227; Ce, 0.544; Pr, 0.217; Nd, 0.831; Sm, 0.1546; Eu, 0.00585; and Gd, 0.00229.

fission products gave peaks at 130 and 650°C. Again, the 130°C peak corresponds to the dehydration of $Al_2F_6 \cdot 7H_2O$, whereas the 650°C peak probably represents sublimation of AlF_3. TGA at 850°C of the pure anhydrous fluorides of rubidium, cesium, strontium, lanthanum, neodymium, aluminum, and cerium have been completed. A summary of the results is presented in Table 4.2. The experiments will also be run at intermediate temperatures (250 and 550°C), and the information obtained will be used to aid in interpreting the complex curves obtained by heating waste powders containing simulated fission products.

Integral weight losses as a function of time at temperature were determined using approximately 2-g samples. Each sample was placed in an alumina boat, which, in turn, was inserted in a 1-in.-diam nickel tube. Heating was done in a tube furnace. Flowing argon carried the off-gases into caustic scrubbers. In these experiments, the weight losses of pure anhydrous aluminum fluoride at 250°C were zero after heating periods of up to 74 hr. At 550°C, the weight loss of pure aluminum fluoride was 0.9% after 18.5 hr and 3.5% after 74 hr. Aluminum fluoride held at 850°C showed weight losses of 4.9 and 15.4% after heating periods of 18.5 and 74 hr respectively. These results agree with the high vapor pressures recorded in the literature for AlF_3 and lead to the conclusion that aluminum fluoride volatility can be a problem when waste is stored at high temperatures.

Waste powder without stable fission products from the HCl process (Table 4.1) was tested for fluoride volatility. Weight loss of the untreated powder was 0.91%, which agrees well with the TGA above, considering the differences in samples, sizes, and experimental conditions. The weight loss of HCl-process powder containing stable fission products (Table 4.1) was 7.35%. This result reflects the number of volatile compounds contained in the fission product spectrum.

Theoretical considerations indicate that the addition of alkaline-earth oxides should convert the metal fluorides in waste powder to stable metal oxides plus the more-stable alkaline-earth fluorides. Experiments were carried out in which calcium oxide and magnesium oxide were added to inhibit the fluoride volatility. When calcium oxide was added to the waste from the $HF\text{-}O_2$ process (Table 4.1) in 1:19 and 1:9 weight ratios, the weight losses were 2.4 and 1.3% respectively. Calcium oxide was added to the waste powder from

Table 4.2. Summary of Data Obtained by Thermogravimetric Analysis

Material	Heating Rate (°C/min)	Temperature (°C)	Time at Temperature (min)	Weight Loss (%)
$HF\text{-}O_2$ process powder:				
Without stable fission products	4.7	850	80	3.10
HCl process powder:				
Without stable fission products	4.7	850	160	1.00
With stable fission products	4.5	850	180	2.11
RbF	4.6	850	180	9.20
CsF	4.6	850	60	25.20
SrF_2	4.6	855	180	0.91
LaF_3	4.6	855	180	0.20
NdF_3	4.6	850	180	0.58
AlF_3	4.7	855	180	1.28
CeF_3	4.6	855	180	0.82

the HCl method (Table 4.1) in a 1:49 weight ratio, which resulted in a weight loss of 0.2%. As the calcium oxide: waste powder weight ratio was increased to 1:33, no further reduction in weight loss occurred. When magnesium oxide was added to the powder in a 1:49 weight ratio, the integral weight loss was 0.6%. Additional amounts of magnesium oxide to a 1:9 weight ratio did not further reduce the weight loss. These data lead to the conclusion that calcium oxide serves as an adequate fluoride getter. The weight losses observed, when calcium oxide is added in sufficient quantity to hold the fluoride present, correspond to the moisture content of the powders. When magnesium oxide is added to inhibit fluoride volatility, the magnesium fluoride formed probably reacts with moisture present on the powder and forms volatile hydrogen fluoride. Thus, calcium oxide appears to be a better stabilizer for the moist powders than magnesium oxide.

Samples (about 15 g) of HCl-process waste powder without stable fission products (Table 4.1) were heated to 250, 550, and 850°C. When each had reached a steady-state temperature, it was sealed in a nickel pot. After three months at temperature, the gage pressures, which were recorded continuously during this time, had decreased to −15, −25, and −60 in. H_2O respectively. As a part of the effort to understand and predict such behavior of the waste powders (which reflects the interactions between the powder, moisture, and the metal of the container), experiments to determine weight loss with temperature are being made; the pure fluorides (for example, see Table 4.2) and their hydrates, which are expected to be constituents of the waste, are used in these studies.

Dispersion of Powders in Glass. – Laboratory development work has indicated that some treatment of high-level radioactive waste powders may

Table 4.3. Summary of Laboratory Tests for Dispersion of Waste Powders in Glass

Experiment	Composition (wt %)		Maximum Temperature (°C)	Time at Maximum Temperature (hr)	Product Quality (% voids)
	Waste Powder	Glass			
1	35.4% Alcoa T-61	64.6% Corning #8463	770	1.5	40–50
2	36.6% Alcoa T-61	63.4% Corning #8463	925	3.5	40–50
3	38.5% Alcoa T-61	61.5% Pemco PB 41	935	3	40–50
4	34.5% Norton RR	65.5% Pemco 716	940	4	4–5
5[a]	33.0% FBVE No. 11, 3.7% CaO	63.3% Pemco 716	920	10	40–50
6	33.3% Purex calcine	66.7% Pemco 716	905	5.5	2–3
7	33.3% Purex calcine	66.7% Pemco 716	930	16	2–3
8[b]	32.9% Norton RR, 5.1% $Al_2F_6 \cdot xH_2O$	62.0% Pemco 716	950	18	20–25
9[b]	32.9% Norton RR, 5.1% $Al_2F_6 \cdot xH_2O$	62.0% Pemco 716	940	18	20–25
10[b]	32.9% Norton RR, 5.1% $Al_2F_6 \cdot xH_2O$	62.0% Pemco 716	930	18	20–25
11[b]	32.9% Norton RR, 5.1% $Al_2F_6 \cdot xH_2O$	62.0% Pemco 716	950	20	10–15
12[b]	32.9% Norton RR, 5.1% $Al_2F_6 \cdot xH_2O$	62.0% Pemco 716	900	24	10–15
13	34.2% Norton RR, 1.2% Al_2F_6	64.6% Pemco 716B	790	1.5	2–3

[a] FBVE No. 11 contained 1.7 wt % H_2O, and the CaO contained 1.1 wt % H_2O.

[b] $Al_2F_6 \cdot xH_2O$ contained 62 wt % Al_2F_6 and 38 wt % H_2O.

be required before they are sealed in a can. The instability, poor thermal conductivity, or solubility of these preclude safe interim storage or safe transport to final storage. Dispersion of the waste powders in a glass matrix will improve the physical and chemical stability and the thermal conductivity, as well as decrease the solubility of the powders. At present, no further work at ORNL is planned with this system since the responsibility for the dispersion of FBVP waste powders in glass has been assigned to Brookhaven National Laboratory.

Spray-calcined Purex waste powder (from Pacific Northwest Laboratories) and FBVP waste powders were successfully dispersed in lead silicate glass matrices. The stainless steel pots were sawed lengthwise to evaluate the products and the corrosion of the pots. All experiments (Table 4.3) yielded hard products; however, some of them contained too many (10 to 50%) voids. The presence of too many voids is undesirable, since they decrease the thermal conductivity and the volume reduction (volume of waste per volume of product) of the system significantly. Good products are considered to be those that are hard and strong and have only a low percentage of voids. Experiments 6 and 7 gave good products with spray-calcined Purex waste. These products represent a volume reduction of about 10, equal to that obtained in processes for forming ceramics or single-phase glasses with this waste. Experiment 13 gave the best product with FBVP powders (Fig. 4.2). This experiment also shows that a temperature less than 800°C is sufficient for operation with Pemco 716 glass and that the earlier use of temperatures greater than 900°C with this glass was not necessary to obtain a good product with this arrangement of equipment. This dense, hard, almost void-free product seemed to be the result of both zone heating and matching the particle sizes of the glass to those of the waste. Since the glass merely fills the interstices of the FBVP

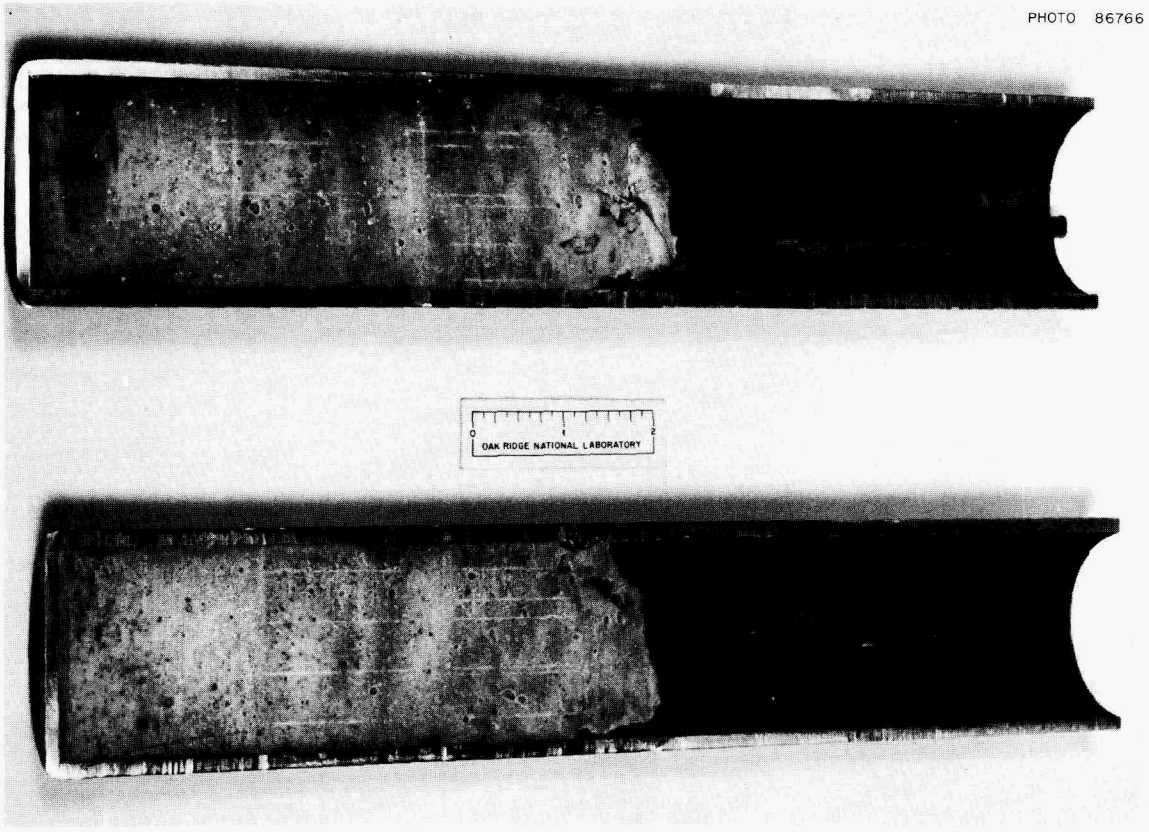

Fig. 4.2. Dispersion of Al_2O_3-AlF_3 Powder in Lead-Silicate Glass (Pemco-716B). Dispersion contains 35.4 wt % simulated waste powder and 64.6 wt % glass.

powder, the volume of waste to be stored is the same for the untreated powder and for the dispersion. Products with a very high percentage of voids – 40 to 50% – were made with glass powders that contained B_2O_3 (Table 4.3, experiments 1–3) or a waste powder plus additive that contained appreciable moisture (Table 4.3, experiment 5). Products with a moderately high percentage of voids – 10 to 25% – were made with powders that contained several percent moisture (Table 4.3, experiments 8–12). In earlier small-batch experiments with FBVP and glass powders, all mixtures (40 out of 130) with glasses containing B_2O_3 had a very high percentage of voids. Thus, B_2O_3 seems to cause excessive bubbling in this system. No apparent corrosion of the stainless steel pots was observed in any of the 13 experiments.

Thermal conductivities of a waste dispersed in glass and a waste powder were measured at 140°F. The conductivity of the dispersion was 1.22 Btu hr^{-1} ft^{-1} $°F^{-1}$, while that of the powder was 0.25.

To compare the solubility of the waste powders and the glass dispersions, leach tests were made. Cesium-137 was added to waste powder. A 50-g charge of the powder was dispersed in glass to give a 2.25-in.-diam, 0.5-in.-high right circular cylinder with a surface area of 11.49 $in.^2$. This glass sample and a 50-g powder sample were placed in separate 1-liter polyethylene bottles. Five hundred milliliters of distilled water was added to each bottle; then the bottles were placed on a mechanical shaker, which provided continuous mixing. The leachates were completely

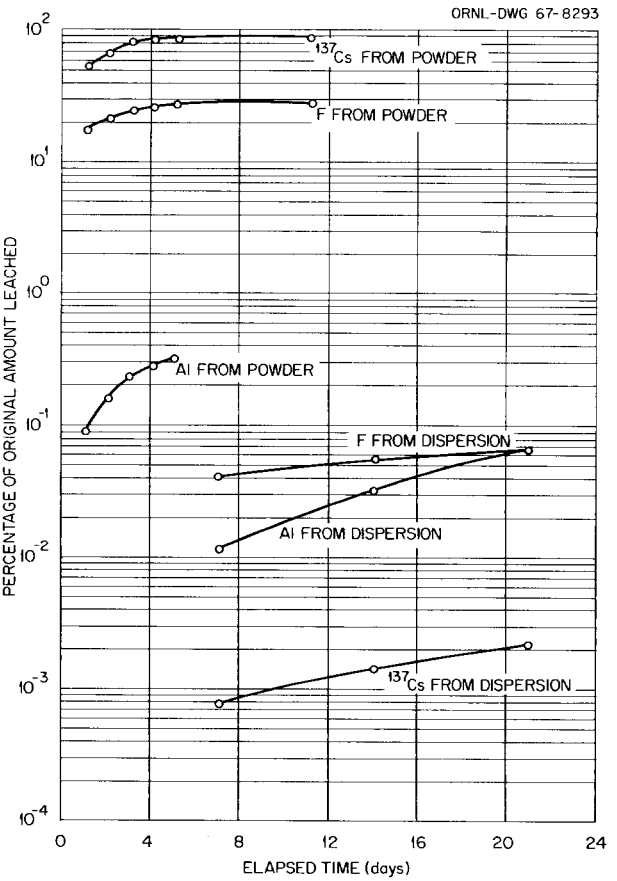

Fig. 4.3. Amount of Aluminum, ^{137}Cs, and Fluorine Leached from HF-O_2 Powder and from Powder Dispersed in Glass as a Function of Time.

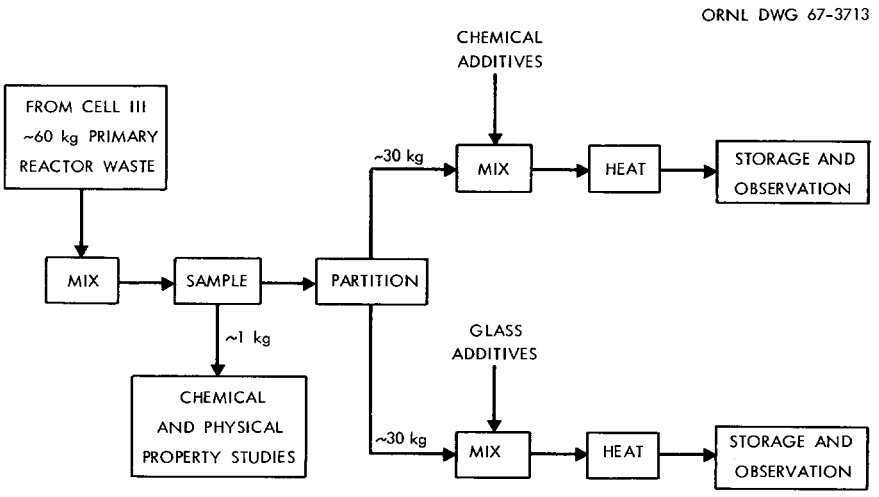

Fig. 4.4. Schematic Diagram of Operational Procedure for the Volatility Waste Pilot Plant.

removed from the powder sample daily and from the glass sample weekly and were replaced with fresh water. Each entire sample of leachate was submitted for chemical analysis. The solubility of the powder, as compared with the relative insolubility of the glass dispersion, is shown in Fig. 4.3. After 11 days of leaching, the percentage of original ^{137}Cs leached from the powder was about 8×10^4 times that leached from the dispersion (viz., 90 vs 0.0011%).

Pilot Plant Design. – The volatility waste plant (VWPP) will be located in Building 3019 in cell 1, adjacent to the Fluidized-Bed Volatility Pilot Plant (FBVPP). The wastes, which are principally Al_2O_3 containing up to 15% of the fluorides of aluminum and fission products, will be discharged from the primary reactor in the FBVPP and physically transferred to the waste processing cell. Here the waste will be converted into products that are suitable for permanent storage by the

ORNL DWG 67-5217

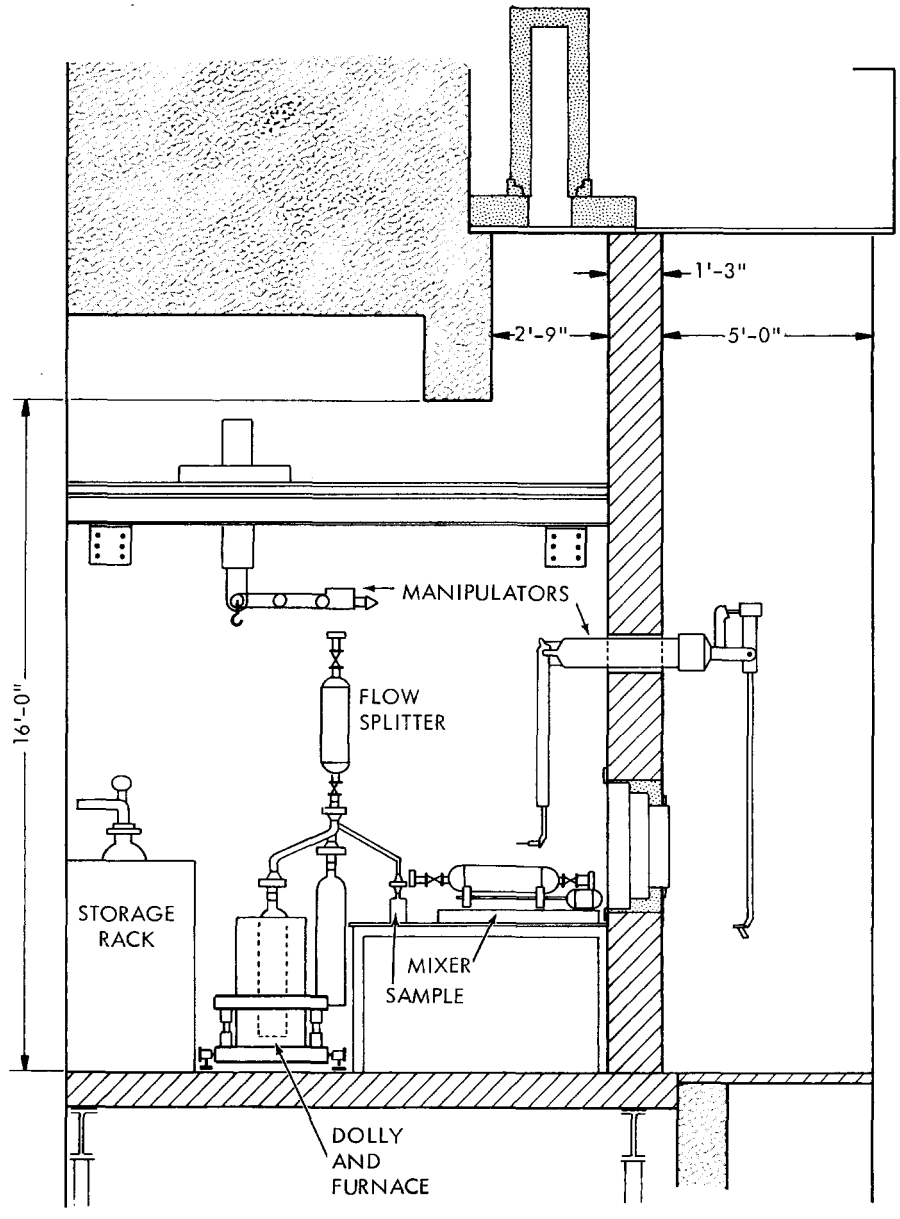

Fig. 4.5. Elevation Drawing of the Fluidized-Bed Waste Pilot Plant Equipment.

ORNL Powder Process and the BNL Glass Dispersion Process.

Conceptual design of the waste processing cell is complete. Facilities are being provided to permit evaluation of the chemical and physical properties of the waste powders concurrent with the processing of the waste for disposal. Briefly, the operational procedure will consist in mixing the waste powder to ensure homogeneity, sampling, adding powdered "fluoride getters" or glass frit, remixing, and then heating to temperature in a furnace (Fig. 4.4). After processing, the waste pots will be placed in temporary storage, where the temperature and pressure will be monitored and the off-gas will be sampled. Eventually, a few pots will be sent to Pacific Northwest Laboratories for long-term storage and observation in the environmental storage facility.

More-detailed plans include location of the process and laboratory data evaluation equipment in a steel-shielded, alpha-contained cubicle inside cell 1. Process operations will be performed remotely with a crane and manipulators from an operating area adjacent to the cubicle. Lead glass windows will permit direct viewing of all in-cubicle operations. An elevation drawing of the equipment in cell 1 is shown in Fig. 4.5.

4.2 INTERMEDIATE-LEVEL RADIOACTIVE WASTE

The intermediate-level wastes (ILW) generated in nuclear installations are usually stored in tanks or mixed with cement. These wastes include second- and third-cycle raffinates; solutions from decladding, solvent cleanup, and off-gas scrubbers; and slurries and solids from processes for decontaminating process waters. They are characterized by modest levels of radioactivity (heating and radiation dose levels are not serious problems) and by high salt or solids content, which prevents efficient treatment by a conventional method such as ion exchange or precipitation. Still, neither tank storage nor solidification in cement is completely satisfactory. Tank storage is only a temporary measure, and the products formed by mixing the waste with cement are only moderately insoluble and represent a volume increase. In addition, most operations with cement are dusty, good mixing is difficult to achieve, and the operations are cumbersome.

A promising recent development is the use of asphalt to solidify and insolubilize these wastes. Immobilization of wastes by incorporation in this cheap, insoluble material before burial or other storage can reduce not only treatment costs but also the flow of radioactivity to the environment. Plants for incorporating intermediate-level waste in asphalt are already in operation at Mol, Belgium,[4-6] and Marcoule, France,[7-9] while a plant similar to that in Belgium is being constructed at Harwell, England.[10]

In the process being developed at Oak Ridge National Laboratory (ORNL),[11,12] wastes are introduced into an emulsified asphalt at any convenient temperature below the boiling point of the solution, water is volatilized by heating, the temperature of the product is increased until the

---

[4] P. Dejonghe, N. Van de Voorde, J. Pyck, and A. Stynen, *Insolubilization of Radioactive Concentrates by Asphalt Coating*, Final Report No. 2, 1st Part, Concerning Proposal 167, April 1, 1961, to March 31, 1963, EURAEC-695.

[5] P. Dejonghe, L. Baetsle, N. Van de Voorde, W. Maes, P. Staner, J. Pyck, and J. Souffriau, "Asphalt Conditioning and Underground Storage of Concentrates of Medium Activity," in *Third United Nations International Conference on the Peaceful Uses of Atomic Energy*, A/CONF.28/P/774.

[6] N. Van de Voorde and P. Dejonghe, "Insolubilization of Radioactive Concentrates by Incorporation into Asphalt," SM-71/4, pp. 469–600, in *Practices in the Treatment of Low- and Intermediate-Level Radioactive Wastes*, IAEA, Vienna, 1966, STI/PUB/116 (ORNL-Tr-1431).

[7] J. Rodier, G. Lefillatre, and J. Scheidhauer, "Bitumen Coating of the Radioactive Sludges from the Effluent Treatment Plant at the Marcoule Center," *Review of the Progress Reports 1, 2, 3, and 4*, CEA Report 2331, 1963 (ORNL-Tr-202).

[8] G. Wormser, J. Rodier, and E. de Robien, "Improvements in the Treatment of Radioactive Residues," in *Third United Nations International Conference on the Peaceful Uses of Atomic Energy*, A/CONF.28/P/86 (May 1964).

[9] J. Rodier, M. Alles, P. Auchapt, and G. Lefillatre, "Solidification of Radioactive Sludges Using Asphalt," SM-71/52, pp. 713–29, in *Practices in the Treatment of Low- and Intermediate-Level Radioactive Wastes*, IAEA, Vienna, 1966, STI/PUB/116 (ORNL-Tr-1432).

[10] R. H. Burns, J. H. Clarke, T. D. Wright, and J. H. Myatt, "Present Practices in the Treatment of Liquid Wastes at the Atomic Energy Research Establishment, Harwell," SM-71/58, pp. 17–29, in *Practices in the Treatment of Low- and Intermediate-Level Radioactive Wastes*, IAEA, Vienna, 1966, STI/PUB/116.

[11] *Chem. Technol. Div. Ann. Progr. Rept. May 31, 1966*, pp. 88–93.

[12] H. W. Godbee, E. J. Frederick, R. E. Blanco, W. E. Clark, and N. S. S. Rajan, *Laboratory Development of a Process for Incorporation of Radioactive Waste Solutions and Slurries in Emulsified Asphalt*, ORNL-4003 (April 1967).

product flows freely, and, finally, the product is drained into a steel drum for preliminary storage and shipment. Attractive features of the process include: use of emulsified asphalt, which flows readily at room temperature; evaporation at low temperatures to minimize degradation of the asphalt; low agitation rates, which provide adequate mixing and keep the heated surfaces of the evaporator clean; operation in either a batch or continuous manner; and incorporation of soluble or insoluble solids with equal effectiveness.

Incorporating ILW in asphalt is a promising method for handling all wastes in this class. No serious problems have been observed in the incorporation procedure in laboratory, hot-cell, and nonradioactive pilot plant studies with alkaline solutions and slurries. The products show acceptably low leach rates in water over long periods of time, with no significant increase at radiation levels up to 10^9 rads (with external ^{60}Co irradiation). Hot-cell tests using samples that contained up to 52 curies of mixed radionuclides per gallon of asphalt product are in progress. No increase in leach rates of salts from the products, swelling of the product, or evolution of gases from the product occurred at doses up to 4×10^7 rads over a seven-month period.

A nonradioactive pilot plant was constructed to determine the feasibility of using a wiped-film evaporator for the incorporation of intermediate-level wastes in asphalt. The equipment operated for 62 hr at rates up to 11 gal of waste solution per hour and yielded a product that contained up to 64 wt % waste salts. No serious operating difficulties were encountered, and no appreciable wiper-blade wear was detected. The water that was distilled was decontaminated from sodium by a factor of greater than 4000 (based on comparisons with the original waste solution). The estimated capital cost of an asphalt plant for annually treating 400,000 gal of ORNL ILW containing 5 curies/gal was $330,500; the estimated unit operating cost, including amortization and burial at ORNL, was $0.37/gal.

Process Description

The emulsified asphalt process can be operated in either a batch or a continuous manner. In the laboratory, the batch process consists in adding the waste directly to emulsified asphalt in an evaporator which contains a stirrer and a bottom outlet, mixing at any convenient temperature up to about 100°C (with a low stirring rate of 100 to 300 rpm), evaporating the water, increasing the temperature to 130 to 160°C, and draining the product into a disposal container. In the continuous process, the waste and asphalt are introduced at the top of a wiped-film evaporator, and the mixture flows down the walls of the evaporator at about 160°C. Agitator paddles sweep the walls continuously at about 300 rpm and provide good mixing and heat transfer. This process has been demonstrated in the laboratory with nonradioactive waste, in hot-cell tests with waste containing up to 25 curies of mixed fission products per gallon in a 4-in.-diam, $6\frac{1}{2}$-in.-high evaporator, and on a pilot-plant scale with nonradioactive waste in a 12-in.-diam, 16-in.-high Pfaudler wiped-film evaporator having 4 ft^2 of heat-transfer surface.

The water vapor from the evaporator in either mode of operation is subsequently condensed and collected in a suitable receiver. In practice, this condensate would be sampled and sent to the plant LLW treatment system. Noncondensable gases from the condenser would be heated and passed through an absolute filter before discharge to the plant off-gas system.

Chemical Development

As reported previously,[11] asphalt products containing 10 to 80 wt % salts from waste have been prepared with ORNL ILW, an aluminum cladding solution (ACS), and a Purex second-plutonium-cycle waste (2CW) with and without added caustic (Table 4.4). No apparent difference, other than hardness, was observed in the product obtained with a given waste. Products made with 2CW are harder than those made with ILW or ACS at the same weight percent solids. Leaching tests with distilled water show that the rates at which strontium and ruthenium are leached from asphalt products are sufficiently low (0.1% or less leached out in 1.5 years). However, the leach rate of cesium is 50 to 100 times higher than this. Results of initial experiments with mineral additives to improve cesium retention indicate that the addition of Grundite clay should have the desired effect. Tests were made with ORNL ILW that contained 2 wt % Grundite clay and 2 wt % water glass (Na_2SiO_3). The purpose of the water glass is to hold or suspend the Grundite in the waste. An asphalt product containing 60 wt % solids from

this waste was prepared. After two months of leaching, the leach rate of ^{137}Cs from this product was about one-half of that of a similar product without Grundite, namely, 7×10^{-5} vs 1.4×10^{-4} fraction leached $(cm^2/g)^{-1}$ day^{-1}. At the end of the same time period, the leach rate of ^{137}Cs from a product containing 20 wt % salts (from ILW plus 2 wt % Grundite) was decreased by a factor of 10, that is, from 6.5×10^{-5} to 6.5×10^{-6}. Additional experiments are in progress to determine the effect of increased amounts of Grundite on cesium retention.

As part of a continuing program to evaluate the safety of asphalt–nitrate salts mixtures, large samples (150 g) of 60 wt % salts–asphalt products contained in stainless steel beakers were heated in air on a hot plate to about 400°C. Four out of five samples containing 2% Grundite and 2% water glass would not ignite under these conditions. The fifth only smoldered. Similar samples without the Grundite–water-glass additive ignited at about 335°C. This effect is being studied further as a function of the amount of Grundite, the amount of water glass, and the ratio of these additives.

We are investigating the feasibility of extending the emulsified asphalt process to the disposal of spent organic solvents generated in fuel processing. Asphalt products containing approximately 30 wt % asphalt, 10 to 30 wt % tributyl phosphate (TBP), and 40 to 50 wt % clay filler (bentonite or attapulgite) were prepared. The products containing 10 wt % TBP were too hard, whereas those containing 30 wt % TBP were too soft. The volume of the product containing 10 wt % TBP was about 50% greater than the original volume of 30% TBP–70% hydrocarbon waste treated. The volume of the product containing 30 wt % TBP was about 20% less than the original volume of organic waste

Table 4.4. Compositions of Simulated Wastes Used in Emulsified Asphalt[a] Incorporation Studies

	1 ILW[b]	2 ACS[c]	3 2CW[d]	4 2CW1[e]	5 2CW2[f]
Component (*M*):					
Na^+	6.61	4.16	0.64	6.64	7.01
NH_4^+	0.19				
H^+			6.2		
Al^{3+}	0.22				
Fe^{3+}			0.54	0.37	0.36
NO_3^-	4.64	2.2	6.2	4.26	4.14
OH^-	2.06	0.06		1.94	2.44
AlO_2^-		1.9			
Cl^-	0.056				
SO_4^{2-}	0.35		1.13	0.78	0.76
Density at 25°C, g/ml	1.34	1.21	1.31	1.33	1.34
Total solids in waste, wt %	39.1	28.5	38.8	39.4	39.9

[a]The emulsified asphalts used were those used in the surface treatment of roads (type RS-2, a rapid-setting, high-viscosity emulsified asphalt; type SS-1, a slow-setting, low-viscosity emulsified asphalt). Both types contained nominally 63 wt % asphalt, 35 wt % water, and 2 wt % emulsifying agent.

[b]ORNL intermediate-level waste solution (evaporator concentrates).

[c]Solution from dissolution of aluminum cladding with $NaOH$-$NaNO_3$.

[d]Purex second-plutonium-cycle waste.

[e]Purex second-plutonium-cycle waste with 455 ml of 51.5% NaOH added to each liter of 2CW.

[f]Purex second-plutonium-cycle waste with 497 ml of 51.5% NaOH added to each liter of 2CW.

treated. Studies are continuing to determine the effects of increasing the amount of TBP and decreasing the amount of thickener (clay) in the final asphalt product.

Radiation Stability

Hot-cell tests are being conducted in which three types of ILW (Table 4.4), along with large quantities of aged mixed fission products, were incorporated into asphalt to accelerate radiation effects. These effects are being measured by observation of swelling and/or radiolytic gas evolution from the asphalt products, and as a function of the rate of leaching of sodium and fission products from the mass. Samples of ORNL ILW (evaporator concentrate), ACS, and 2CW with added caustic (Table 4.4) were adjusted to four levels of radioactivity (nominal concentrations of 1, 2, 5, and 25 curies per gallon of waste) by adding a high-level waste concentrate, which contained a mixture of fission products that had decayed longer than two years. The wastes were then incorporated in asphalt, and the temperature was raised to 165°C. The final asphalt product had one-half the volume of the original waste and contained 60 wt % solids. Thus, the fission product concentration in the products was about twice that of the feed.

The condensates collected during the evaporation of the water from the asphalt product were slightly radioactive (9 μc to 0.7 mc/gal) because of entrained fission products. The laboratory-scale fixation apparatus, however, had no de-entrainment devices. The separation factor between the total beta-gamma activity in the wastes and that in the condensates ranged from 6.4×10^3 to 2.6×10^5, which is higher than earlier estimates based on nonradioactive tests. Essentially all the radioactivity in the condensates was due to ^{137}Cs. Ruthenium was almost nonvolatile, contributing less than 10% of the total gamma activity in the condensate from the most radioactive sample (52 curies per gallon of product). These condensates normally receive further treatment at a low-level waste treatment facility.

Fig. 4.6. Asphalt Product Prepared from Actual ORNL Intermediate-Level Waste Containing 26.1 Curies of Mixed Fission Products and Irradiated to an Absorbed Dose of 4×10^7 Rads.

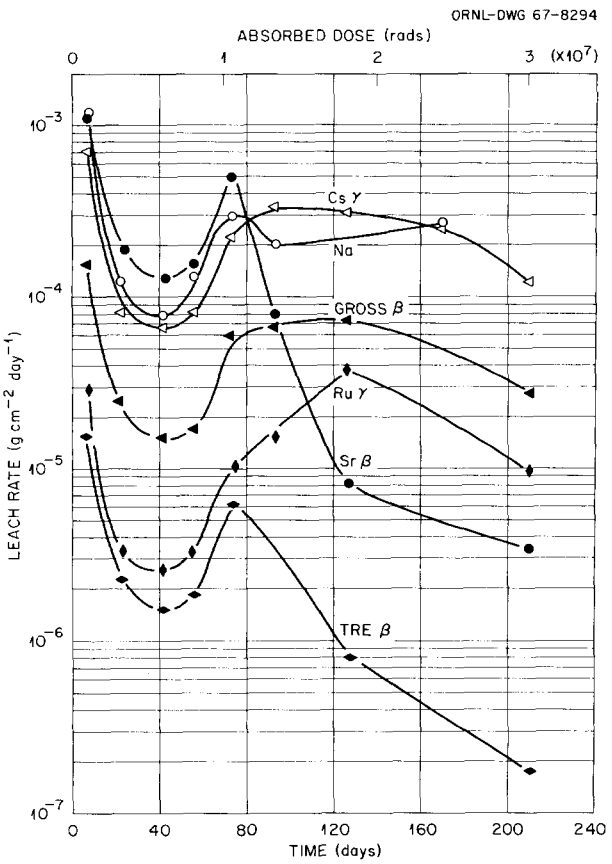

Fig. 4.7. Leaching of Fission Products from Intermediate-Level Waste Fixed in Asphalt.

Radiation degradation of the asphalt products appears almost negligible. No swelling or gas evolution from the samples has been observed during the past seven months. The maximum internal dose received by the most radioactive sample was about 4×10^7 rads (Fig. 4.6).

The static water leaching rates for sodium, gross beta activity, gross gamma activity, ^{90}Sr, ^{106}Ru, ^{137}Cs, and rare earths confirmed the results established in earlier tracer and nonradioactive[11] and hot-cell experiments at the 5-curie/gal level. Figure 4.7 illustrates typical rate curves for the leaching of evaporator bottoms in asphalt containing 61 wt % solids and 52 curies of activity per gallon of product. Sodium and ^{137}Cs were leached at a steady-state rate of 1 to 3×10^{-4} g cm^{-2} day^{-1}, while the rates for strontium, ruthenium, and the rare earths were orders of magnitude lower. Recent tracer experiments[12] have shown that the incorporation of Grundite clay into the asphalt-waste mix reduces the leaching of cesium by 1 to 2 orders of magnitude and, in turn, the gross gamma leaching rate to at least the range of that for ruthenium and rare earths.

Pilot-Plant Tests

A pilot plant was constructed to test the ORNL process for incorporation of intermediate-level wastes in asphalt by using synthetic nonradioactive waste solutions. A major objective of the pilot plant tests was to determine the applicability of a continuous wiped-film evaporator for the incorporation step. Other objectives were: (1) to verify the laboratory results, particularly the optimum content of salts in the final product and the operating temperature of 160°C; (2) to determine the operational characteristics of the evaporator for periods up to 100 hr; (3) to determine the capacity of the equipment; (4) to examine the effects of operating variables, particularly the speed of rotation of the wiper blades and the steam pressure in the evaporator jacket; and (5) to determine the amount of organic and inorganic materials entrained or volatilized in the vapors and appearing in the condensate.

The pilot plant was designed to yield approximately one drum (55 gal) per day of asphalt–waste-salts product formed by mixing emulsified asphalt and synthetic nonradioactive ILW in a wiped-film evaporator. The wiped-film evaporator, purchased from the Pfaudler Company, has 4 ft^2 of evaporating area (1 ft in diameter). The parts that contact ILW, emulsified asphalt, or a mixture of the two are made of austenitic stainless steel. The two feed streams (waste solution and asphalt emulsion) fall onto a spinning distributor plate, and from there they pass through weirs onto the heated surface. Four wiper blades continually smear the film, thus providing agitation. Grooves in the wiper blades assist gravity by impelling the product downward. The distributor plate supports the can that holds the wiper blades and also contains de-entrainment baffles for the generated vapor. At a rotational speed of 285 rpm, the wiper blades move at a peripheral speed of 15 fps (i.e., a wiper blade passes a given point on the circumference every 0.053 sec). Other equipment items include a 750-gal asphalt storage tank, a 120-gal ILW feed tank, a 75-gal emulsified asphalt feed tank, three pumps, a heat exchanger, and other related equipment. An engineering flowsheet of the ORNL Asphalt Process is shown in Fig. 4.8; a photograph of the

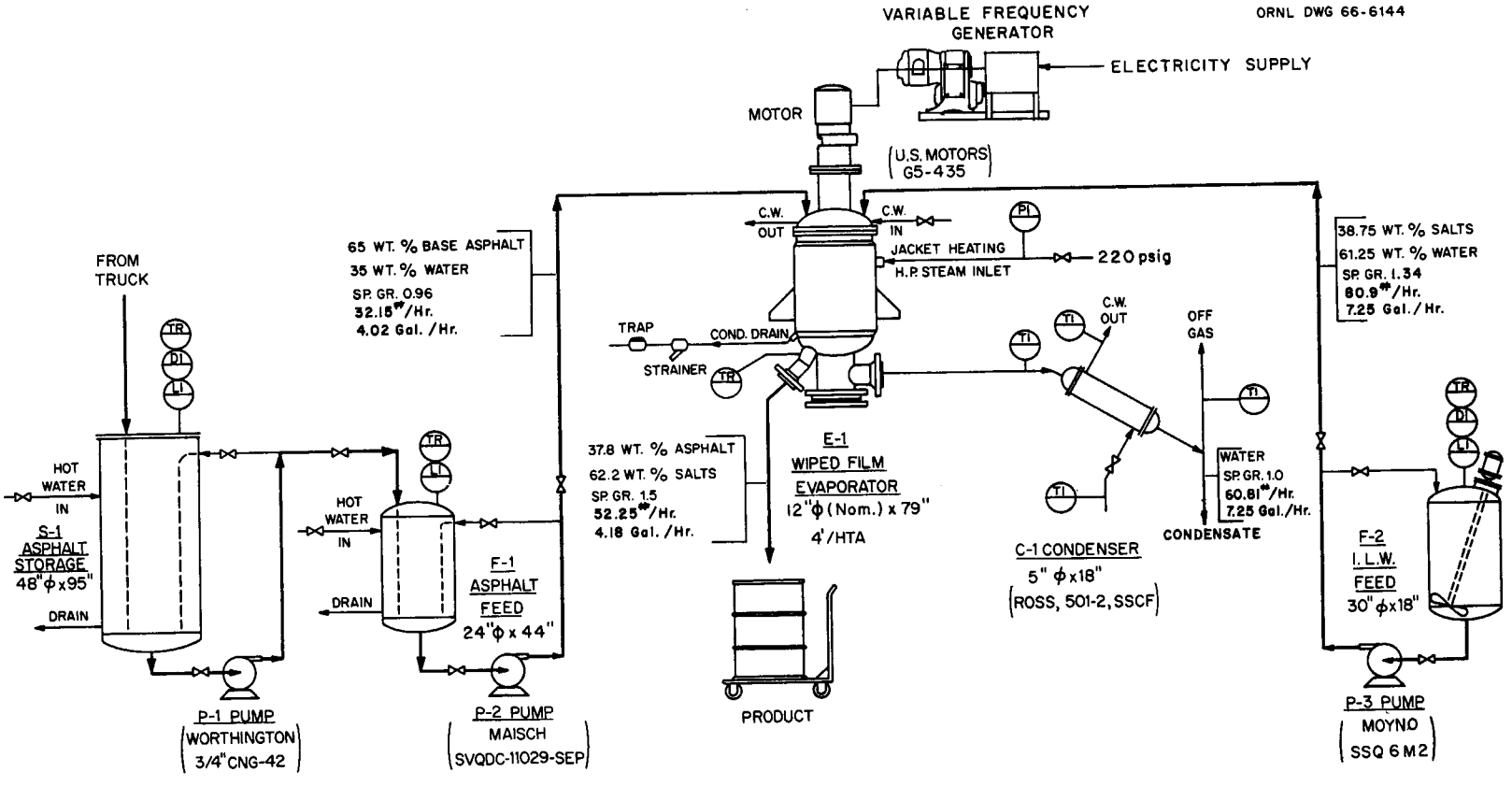

Fig. 4.8. Engineering Flow Diagram of the ORNL Asphalt Process.

installed equipment taken shortly after construction was completed is shown in Fig. 4.9.

Asphalt paving emulsion (Table 4.4, footnote *a*) was pumped into the feed tank from the storage tank as needed. Synthetic ILW (Table 4.5) was made up in 400-liter batches and pumped into the waste feed tank. The emulsion feed rate was controlled by the dc voltage on the drive to a gear pump and was monitored by measuring the pump rotation rate. The pump rotation rate was periodically compared with the actual flow rate as determined by the time needed to pump a measured amount into a graduated cylinder. The waste feed rate, which was controlled by a needle valve in the feed line, was measured by a calibrated rotameter. During startup and shutdown, only emulsion was fed to the evaporator. Thus, no waste salts were left in the evaporator body when it cooled off, or were added until it was again at operating temperature.

Since the temperature of the product is well above the atmospheric boiling point of water, failure to remove all the water can be detected by bubbles of steam breaking at the surface of the product or by flecks of salt left on the surface when the bubbles break. Unless the ratio of waste to emulsion was too high, or the capacity of the evaporator was exceeded, the product had a smooth, glossy appearance. Thus, the appearance of the product was a rapid and infallible indicator of the suitability of operating conditions. Because of the heat capacity of the equipment, about 30 to 60 min were needed to reach full operating temperature. However, the large heat capacity of the equipment and the small amount of material in the equipment were advantageous because any change in operating conditions caused only a momentary departure from steady state.

No problems were experienced in operating at feed rates that resulted in a product containing 60

PHOTO 84202A

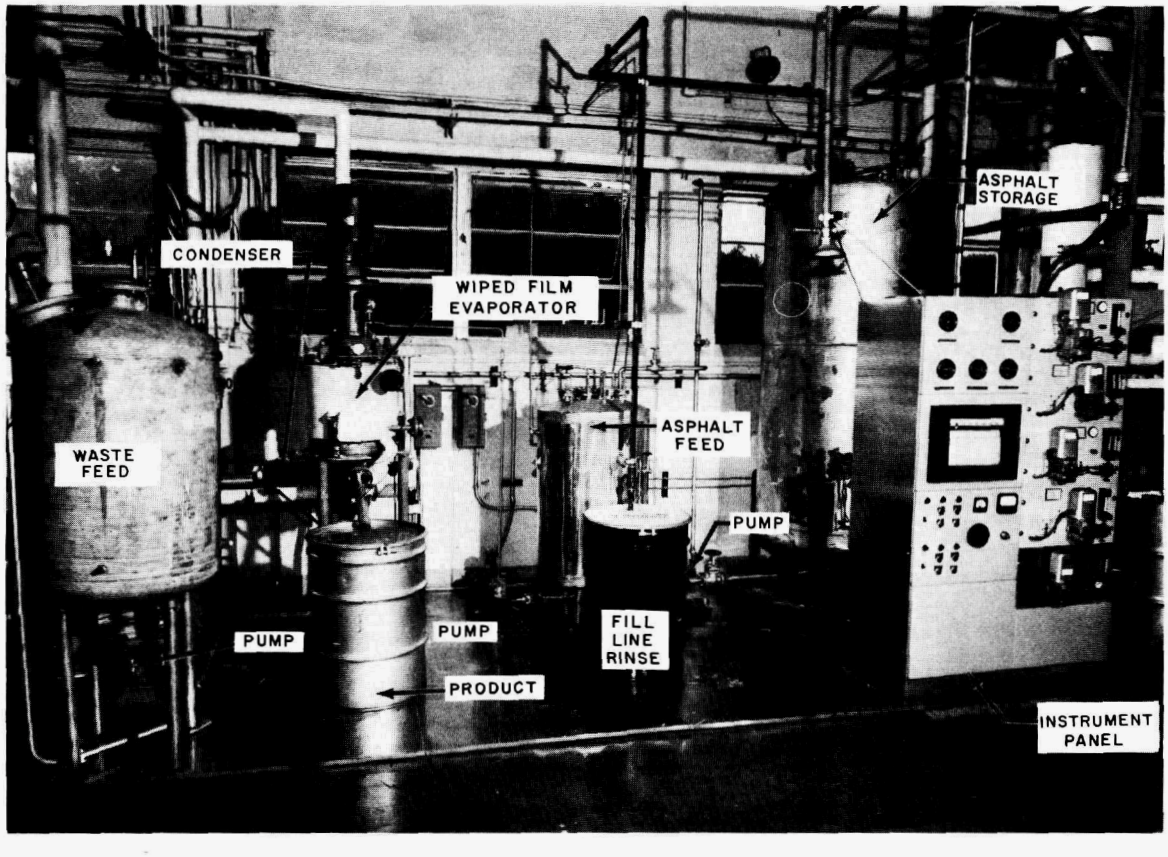

Fig. 4.9. Wiped-Film Evaporator as Installed for Development of the Waste-Asphalt Process.

Table 4.5. Routine Conditions for Waste-Asphalt Wiped-Film Evaporator Tests

	Design Conditions	Operating Conditions
ILW concentrate composition (mg/ml):		
Na^+	152	167
Al^{3+}	5.93	5.36
Cl^-	1.98	3.50
NO_3^-	276	288
OH^-	35.0	36.9
SO_4^{2-}	33.6	35.8
ILW feed rate, gph	7.25	7.75
Solids in asphalt emulsion, wt %	65	70
Waste salts in product, wt %	60	58
Wiper rotation rate, rpm		285
Steam supply pressure, psig	200	200
Temperature in evaporator body, °C	160	Unknown
Temperature in steam jacket, °C		192
Temperature of product outlet nozzle, °C		110–120
Decontamination factor for sodium		>4000

wt % waste salts. The equipment operated satisfactorily with up to 64 wt % salts in the product at waste feed rates up to 11 gph; however, this was very near the upper limit. At higher waste:asphalt ratios the salt particles were no longer infinitesimal but appeared as discrete crystals coated with asphalt. The product had a definite granular appearance or, in worse cases, was lumpy. Since the temperature of the mixture in the wiped film of the evaporator could not be measured, the desired temperature (160°C) set by laboratory tests could not be verified, but it was approximately in this range. The temperature of the steam jacket was about 190°C. After the product had partially cooled, the temperature of the outside of the product nozzle was 120°C; thus the temperature of the product must have been somewhat higher. The product flowed easily when it contained 64 wt % waste salts.

The equipment was operated for 62 hr at approximately the conditions shown in Table 4.5. No operating difficulties were encountered, and wear of the wiper blades was negligible. The equipment can be started up and stopped easily and, when disassembled, shows only an oily film on the evaporating surface. The limiting conditions are determined by both the rate at which water is evaporated (i.e., waste feed rate) and the ratio of waste to asphalt (i.e., the wt % solids) in the product (Table 4.6). Two ranges, 150 and 285 rpm, of wiper rotation rate can be used. Wiper rate appears to be unimportant at lower feed rates; however, the higher rate is required for operation at waste feed rates greater than 8 gph. The steam pressure could not be decreased below 185 psig, probably because of too low a temperature inside the evaporator body. Supply limitations prevented steam pressures greater than 200 psig. A trace of oil appeared in samples taken at the exit of the condenser, but the amount was too little for analysis. No oil appeared in the distillate leaving the knockout drum. Measurement of the decontamination factor (DF) for cesium was impractical, but the DF for sodium was readily obtained. In all tests the sodium DF between the waste feed and the distillate was greater than 3000; in most cases it was 6000 to 8000.

Table 4.6. Operating Limits for the Wiped-Film Evaporator

Waste Feed Rate (gph)	Percentage Waste Solids in Product		Water Evaporation Rate (gph)	
	Satisfactory Operation	Unsatisfactory Operation	Satisfactory Operation	Unsatisfactory Operation
11.1	64.5		10.0	
11.3	64.4	65.0	10.1	10.1
11.4	64.0		10.3	
11.6	62.6		10.5	
11.9	52.5	58.4	11.6	11.1
12.7	48.6	54.1	12.7	12.2
13.5		50.0		13.3

Economic Evaluation

A conceptual design and preliminary cost estimate were prepared for a plant[13] to immobilize the alkaline evaporator concentrate (ILW) produced at ORNL. Fundamental design considerations were: (1) The process would use a wiped-film evaporator with 50 ft^2 of heat-transfer area to produce one volume of homogeneous asphalt–waste-salts mixture when fed with two volumes of ILW and one volume of emulsified asphalt. The ILW would contain 0.1 to 5 curies/gal of radioactivity and up to 40% dissolved salts and would be processed at a rate of 60 gph for 278 days/year. The emulsified asphalt would be composed of 63 wt % base asphalt, 35 wt % water, and 2 wt % emulsifying agent. Asphalt–waste-salt product would be collected in 55-gal drums and would be composed of 62.5 wt % salts and 37.5 wt % asphalt. (2) A new building, conforming to ORNL double-containment standards, would be provided to house the process. The building would include a central cell ($10 \times 10 \times 16$ ft) and 3-ft-thick concrete walls, a shielding window, a pair of master-slave manipulators, a general shielded tunnel for handling product drums remotely, and a crane bay with a 5-ton bridge crane (Figs. 4.10 and 4.11).

The capital and operating costs were estimated for a plant with an ILW capacity of 400,000 gal/year. The total capital cost was $330,500 (Table 4.7). The unit operating cost was about 34¢ per gallon of waste, assuming 20-years amortization of capital without interest, or 37¢ per gallon with 20-years amortization and 4% interest. The plant was assumed to be operated three shifts/day, five days/week, and 52 weeks/year (Table 4.8).

Table 4.7. Capital Costs of Waste-Asphalt Plant

	Construction Costs	Total Costs
Improvements to land	$ 3,000	
Building	41,000	
Hot cell	74,300	
Process equipment and piping	69,400	
Carrier	10,000	
Process instrumentation	14,200	
Radiation monitoring instruments	10,500	
Outside utilities	7,500	
Total construction cost		$229,900
Engineering, design, and inspection (15% of construction cost)		34,500
Contingency (25% of construction cost and engineering, design, and inspection)		66,100
		$330,500

[13] A. M. Rom, *Incorporation of Intermediate-Level Waste in Asphalt: Preliminary Design and Cost Estimate of a Full-Scale Plant for ORNL*, ORNL-TM-1697 (January 1967).

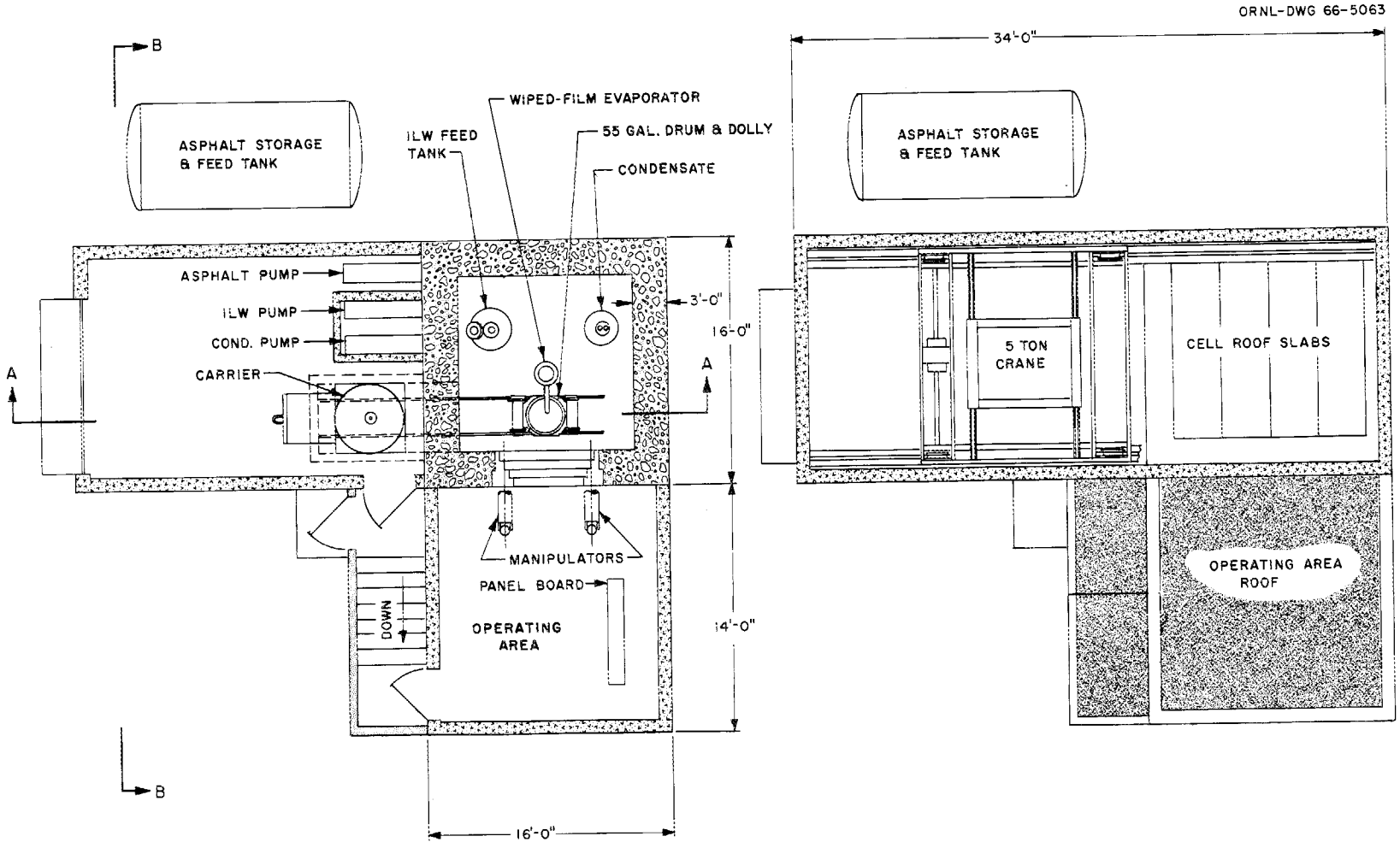

Fig. 4.10. Waste-Asphalt Building, Plan Views.

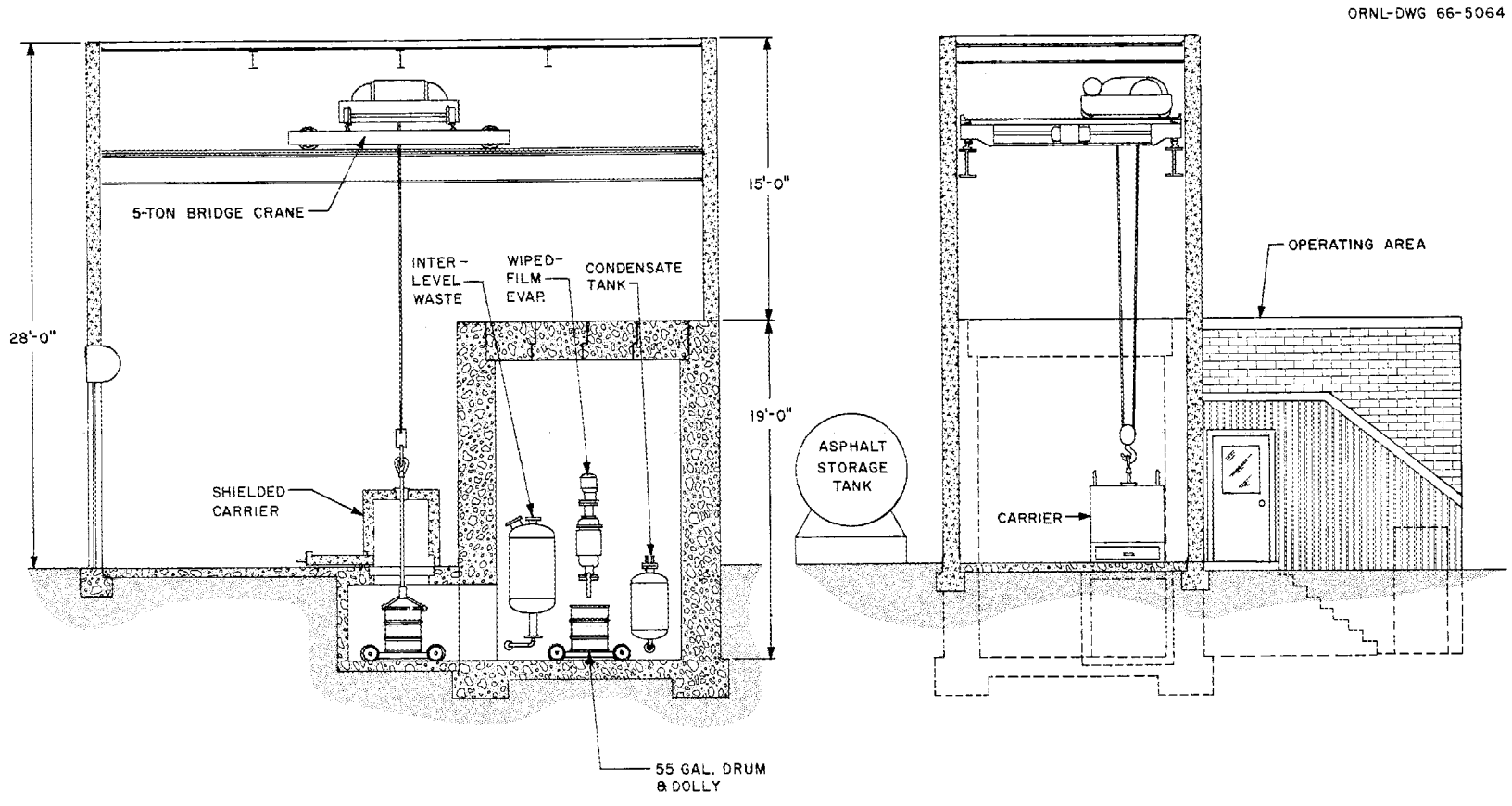

Fig. 4.11. Waste-Asphalt Building, Cross Sections.

Table 4.8. Operating Costs of the Asphalt–Waste-Salts Plant

	Annual Costs
Asphalt, 200,000 gal, at 12¢/gal (delivered)	$ 24,000
Steam, 586 lb/hr, at 97¢ per 1000 lb	3,550
Barrels, 4240, at $3.00 each	12,720
Burial ground storage space (includes transportation), 11.6 ft^3 per barrel, at 57¢ per cubic foot	28,000
Direct labor, 1 operator per shift, 3 shifts/day	20,500
Overhead (including supervision), 140% of direct labor	28,700
Maintenance of building, 1% of original cost	1,150
Maintenance of process equipment, 5% of original cost	5,200
Depreciation of capital by straight-line method, assuming 20-year life and no interest	16,525
	$140,345

4.3 LOW-LEVEL RADIOACTIVE WASTE

Introduction

Water reuse is the objective of the development of the Water Recycle Process (WRP) for treating low-level radioactive waste (LLW) solutions from fuel reprocessing plants. Conventional treatment involves only partial decontamination of these solutions and subsequent discharge to streams, relying on dilution to maintain radionuclide concentrations at levels below the required MPC_w; on the other hand, in the WRP, waste water containing low concentrations of dissolved solids is completely decontaminated and demineralized and then returned to the plant for reuse, thus providing a closed circuit. Also, fresh water is demineralized before entering the circuit.

Results of micro-pilot-plant tests employing low-salt-content recycle water have indicated that the WRP is a very promising process. For all major radioactive species, overall decontamination factors (DF's) of 1000 to 10,000 were obtained in tests treating up to 2400 volumes of waste per bed volume (BV) of cation resin. For the clarification of recycle water, it was found that samples having the same concentrations of dissolved solids (specific conductance of 50 to 60 micromhos/cm), but having either a low [5 Jackson turbidity units (JTU)] or a high (20 to 25 JTU) concentration of suspended solids, required the same amount of alum [2 to 3 ppm as $Al_2(SO_4)_3$] and activated silica (0.2 ppm as SiO_2). Low-turbidity water also required the addition of a nonionic organic polyelectrolyte during flocculation. When the two main components of synthetic detergents (syndets) were added in relatively high concentration [10 ppm each of tripolyphosphate (TP) and alkylbenzenesulfonate (ABS)], optimum clarification required a cationic organic polyelectrolyte as well as alum, activated silica, and a nonionic polyelectrolyte. Since the results obtained in small-scale laboratory work were verified in micro-pilot-plant tests, they will be used to predict the cost of processing and reusing water in a full-scale plant.

Experimental Work and Results

The Water Recycle Process consists in: (1) coagulating by zeta-potential- (ZP-) controlled additions of coagulant and coagulant aids, (2) clarifying by upflow through a fluidized bed of sludge (upflow clarifier) followed by filtering through a bed of anthracite coal and sand, (3) demineralizing by cation-anion exchange, and (4) sorbing the remaining radioactive and nonradioactive contaminants on granular activated carbon.

Laboratory work has included a study of important parameters that could significantly affect process operations in recycle water treatment, namely, the presence of turbidity and synthetic detergents. Optimum clarification does not appear to be attained simply by ZP control. This is indicated by micro-pilot-plant runs, using the following feeds (with the indicated specific conductances and suspended solids contents): (1) ORNL-LLW, ~15 JTU; (2) ORNL-LLW diluted fivefold with completely decontaminated and de-

mineralized LLW, 50 to 60 micromhos/cm, ~5 JTU; and (3) ORNL-LLW diluted as in run 2, 50 to 60 micromhos/cm, 20 to 25 JTU (achieved by adding LLW solids to increase the suspended solids concentration). The amounts of $Al_2(SO_4)_3$ necessary for clarification in these runs were as follows: run 1, ~20 ppm; run 2, 2 to 3 ppm; and run 3, 2 to 3 ppm. These data suggest that the required alum dose is proportional to the specific conductance (total dissolved solids) of the raw water and is not significantly affected by the degree of turbidity of the water. Further work on clarifying recycle water is needed in order to describe the system more precisely.

The feed used in one micro-pilot-plant run contained 10 ppm each of tripolyphosphate (TP) and alkylbenzenesulfonate (ABS), which is comparable with the maximum syndet concentration found in secondary effluent water, according to a U.S. Public Health Service survey.[14] In the coagulation step, ~20 ppm of Primafloc C-3 (a medium-long-chain cationic polyelectrolyte prepared by Rohm and Haas Company; molecular weight, 10^4) was used to lower the negative ZP of the suspended particles to the point where alum [~15 ppm as $Al_2(SO_4)_3$] and activated silica (0.2 ppm as SiO_2) were capable of neutralizing the surface charges to obtain optimum clarification. In the flocculation step, 0.2 ppm of Purifloc N-12 (a long-chain nonionic polyelectrolyte made by Dow Chemical Company; molecular weight, 5×10^6) was needed to increase floc size and to ensure proper upflow clarifier operation. The overall DF's were maintained (Table 4.9), but only for 1600 BV, because of the greater amounts of added coagulants, as well as early breakthrough of the radioactivity from the Dowex 1 anion exchanger.

Jar tests at pH 7, the optimum pH for alum floc formation, demonstrated that in the presence of a polyphosphate (the builder of a syndet), alum flocculation and clarification are difficult, particularly in water that has a low calcium content (e.g., recycle water). We studied the formation of alum floc in distilled water containing 25 to 30 ppm of ortho-, pyro-, tripoly-, or hexametaphosphate (as PO_4^{3-}). Alum floc was formed in orthophosphate (OP) solutions in the presence or absence of calcium, and the OP was removed (Fig. 4.12). In polyphosphate solutions containing 60 ppm of $Al_2(SO_4)_3$, no floc was formed in the absence of calcium. With the addition of 30 ppm of Ca^{2+}, alum floc formed immediately, and 80 to 95% of each of the polyphosphates was removed. Detailed column sorption tests with activated alumina, which is dehydrated alum floc (with less surface area), indicated that polyphosphate sorption was significantly higher when the calcium:phosphate molar ratio was 1.0 or higher; jar tests were made where these ratios were varied from 0 to 3.0. Thus, the implication is that when polyphosphates are present in recycle water, the calcium:phosphate molar ratio should be at least 1.0 to achieve optimum clarification with a minimum amount of alum.

Table 4.9. Water Recycle Process: Overall Decontamination Factors for Recycle Water Containing Synthetic Detergents[a]

	Feed Water Activity (dis/min)	Overall Decontamination Factor for Recycle Water
^{144}Ce	57	100[b]
^{106}Ru	166	615[b]
^{137}Cs	95	1,025
^{95}Zr-Nb	21	1,130
^{125}Sb	6.0	65[b]
^{60}Co	297	3,170
^{131}I	28	28[b]
^{90}Sr	63	63,000
TRE	28[c]	28,000
Specific conductance	75[d]	150

[a]1600 cation resin volumes of recycle waste treated. Recycle waste contained 10 ppm of tripolyphosphate and 10 ppm of alkylbenzenesulfonate.

[b]Treated effluent water decontaminated to limits of analytical detection.

[c]Counts/min.

[d]Units of specific conductance, micromhos/cm.

[14]J. H. Neale, "Advanced Waste Treatment by Distillation," U.S. Public Health Service Publication No. 999-WP-9 (AWTR-7), 5 (March 1964).

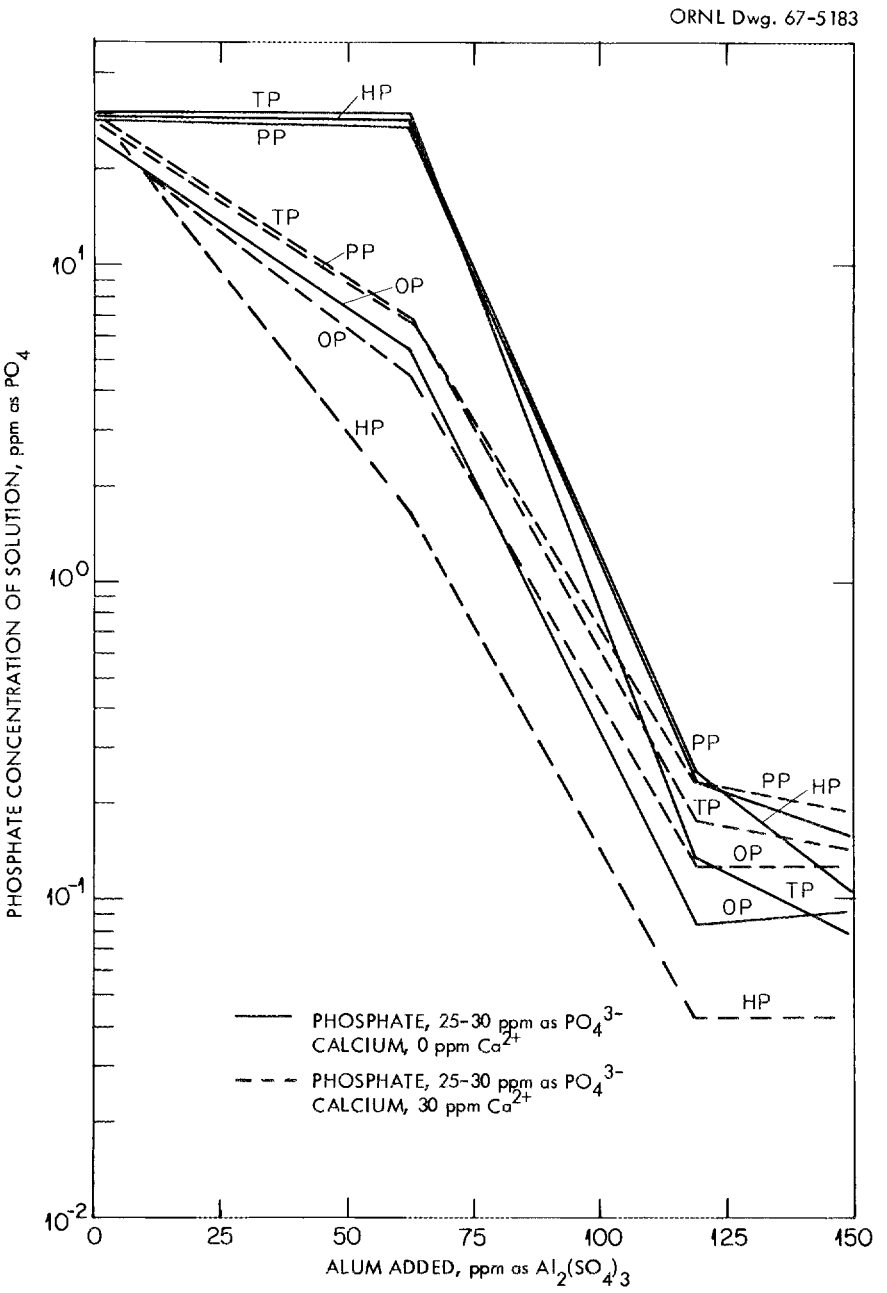

Fig. 4.12. Alum Flocculation. Effect of calcium ion on phosphate removal at pH 7. Orthophosphate (OP), pyrophosphate (PP), tripolyphosphate (TP), and hexametaphosphate (HP).

4.4 ENGINEERING, ECONOMIC, AND SAFETY EVALUATION

The management of wastes produced at nuclear power plants may become increasingly significant in an economy that is expected to grow to 50 times its present size within the next 13 years. As a preliminary step in assessing future implications, the operating experience in waste management at Dresden-I, Big Rock Point, Humboldt Bay, Elk River, Yankee, and Indian Point-I has been reviewed. In this study, to be published as ORNL-4070, the sources and characteristics of the wastes are reviewed, the waste management systems and techniques in use at the power stations are described, and the operating experience is analyzed from the standpoint of the radioactivity released to the environment.

4.5 SEPARATION OF NOBLE GASES FROM AIR USING PERMSELECTIVE MEMBRANES

The removal of krypton and xenon from off-gas during reactor emergencies and during normal fuel dissolution has been studied extensively in AEC-sponsored research. The processes currently in use or under development are based on adsorption techniques and either require operations at very low temperatures (less than −70°C) or facilities that occupy large volumes (where ordinary operating temperatures are used).[15] Recently, proposals have been made to achieve the development of processes based on permeability techniques. It is well known that the rate of permeability through semipermeable membranes is not equal for all gases;[16] however, separations became practical only after the development of thin plastic sheets that are free of holes.[17] Although all types of membranes separate gases, silicone rubber has a much higher permeability than any other material that has been tested.[18] The permeabilities of an unbacked dimethyl silicone rubber membrane (at room temperature) as measured for xenon, krypton, oxygen, and nitrogen at the General Electric Company were 203×10^{-9}, 98×10^{-9}, 60×10^{-9}, and 28×10^{-9}, respectively, where permeability is defined as gas flow (cm^3/sec) through a 1-cm-thick membrane per square centimeter of surface times the difference in pressure (cm Hg) across the membrane.[19] (These values are for the pure gases, not for mixtures.)

A joint program by the Oak Ridge Gaseous Diffusion Plant (K-25), the General Electric Company (GE), and Oak Ridge National Laboratory (ORNL) has been initiated to investigate the use of a cascade containing thin (~1 mil) silicone rubber membranes on a Dacron backing for removing xenon and krypton from a reactor containment vessel atmosphere following a reactor accident or from the off-gas generated during the dissolution of reactor fuel elements. Radionuclide decay data[20] indicate that one day after a reactor accident the containment shell may contain about 100 ppm of nonradioactive krypton, 650 ppm of nonradioactive xenon, and as much as 2×10^8 curies of activity that is associated with radioactive isotopes of krypton and xenon (Fig. 4.13). Calculations were made to determine the intervals of time that would be required at various processing rates to reduce the activity to 10^4 curies (allowing for radioactive decay and discharge to the environment) (Fig. 4.14).[21]

A preliminary cost study[22] was made, based on the reduction of the krypton activity in a 3×10^6 ft^3 containment shell by a factor of 100 in one week and the collection of the separated radionuclides in a 5×10^4 ft^3 volume. Based on the permeability data reported by GE, a minimum of 31,300 yd^2 of membrane allocated into 17 stages of various sizes would be required for this operation. The construction cost would be approximately

---

[15] G. W. Keilholtz, "Removal of Radioactive Noble Gases from Off-Gas Streams," *Nucl. Safety* 8(2), 155–60 (Winter 1966–67).

[16] J. K. Mitchell, "On the Penetrativeness of Fluids," *J. Roy. Inst.* 2, 101–18, 307–21 (1831).

[17] S. A. Stern, "Industrial Applications of Membrane Processes: The Separation of Gas Mixtures," *Proceedings of Symposium, Membrane Processes for Industry*, Birmingham, Alabama, May 19–20, 1966.

[18] Karl Kammermeyer, "Silicone Rubber as a Selective Barrier," *Ind. Eng. Chem.* 49(10), 1685–86 (1957).

[19] W. L. Robb, *Thin Silicone Membranes – Their Permselection Properties and Some Applications*, Report 65-C-031, General Electric Co. (October 1965).

[20] J. O. Blomeke and Mary Todd, *Uranium-235 Fission Product Production as a Function of Thermal Neutron Flux, Irradiation Time, and Decay Time*, ORNL-2127 (December 1957).

[21] R. H. Rainey, *Criteria for Noble-Gas Removal Using Permselective Membranes*, ORNL-TM-1822 (Apr. 3, 1967).

[22] S. Blumkin *et al.*, "Preliminary Results of Diffusion Membrane Studies for the Separation of Noble Gases from Reactor Accident Atmospheres," 9th AEC Air Cleaning Conference, Boston, Mass., September 13–16, 1966, CONF-660904, Harvard University, February 1967.

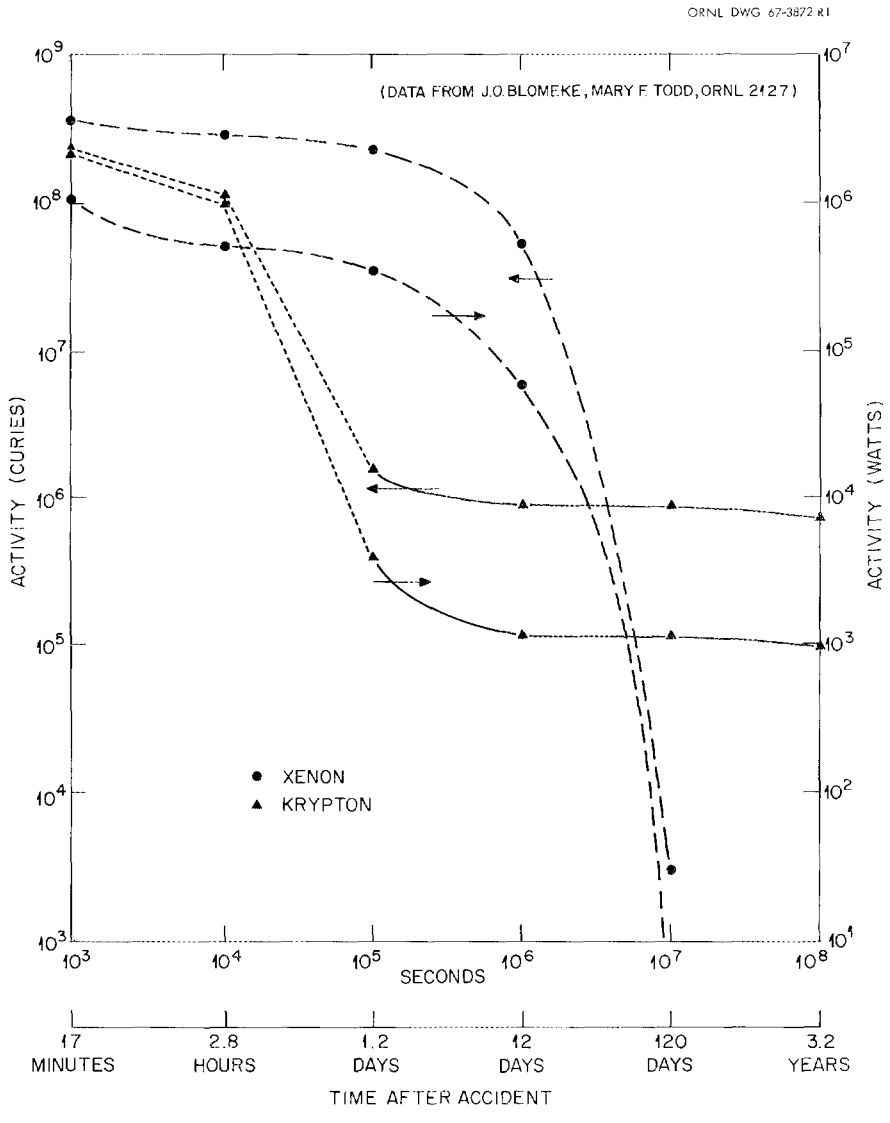

Fig. 4.13. Xenon and Krypton Activity in a Reactor Containment Shell Following an Accident.

$1.1 million; the power requirement would be about 2 Mw. This cascade would occupy about 6000 ft^3 and could be constructed in three semitrailers that could be air-lifted to the site of a reactor accident.

New permeability data obtained at GE, K-25, and ORNL in studies of a single Dacron-backed dimethyl silicone rubber membrane have revealed values for the pure gases that are approximately one-half those obtained previously with the unbacked membrane. The permeability of krypton, as determined by use of tracer ^{85}Kr, remained essentially constant, while the permeabilities of oxygen and nitrogen, as determined by volumetric measurements, decreased with increasing pressure (Fig. 4.15); however, this decrease as measured at ORNL was much less than that reported earlier by GE.[23] The lower permeability of the gases through this membrane has been attributed to the Dacron backing. The General Electric Company, under an ORNL subcontract, is continuing their membrane development program to improve the permeability of the membrane by the proper selection of backing materials and mounting procedures.

[23] A. Dounoucos and H. D. Briggs, *Evaluation of Silicone Rubber Permselective Membranes for Noble Gas Separation*, Research and Development Center, General Electric Company, September 1966 (personal communication).

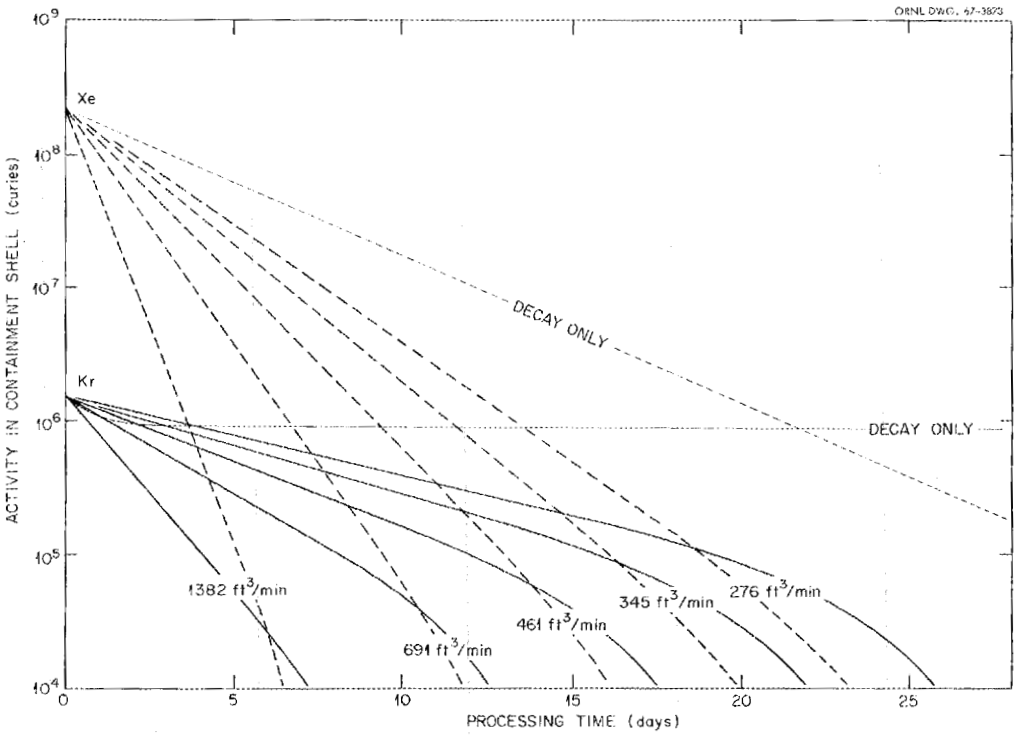

Fig. 4.14. Removal of Xenon and Krypton from a Reactor Containment Shell at Various Processing Rates.

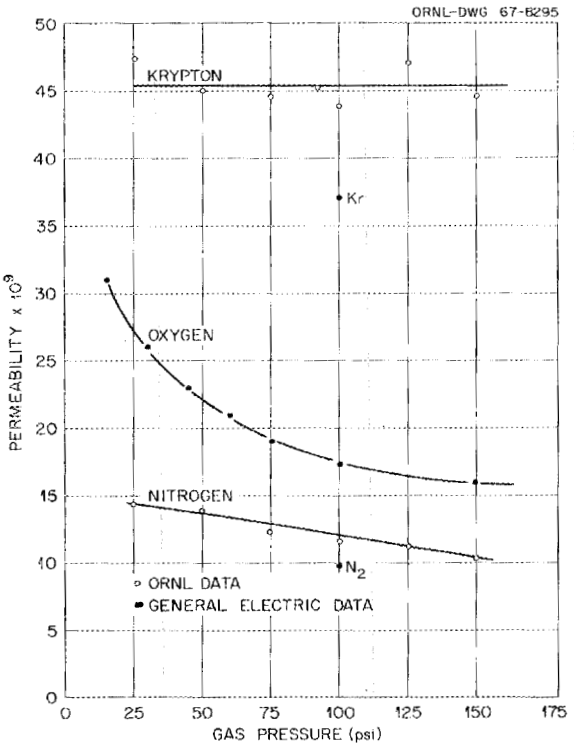

Fig. 4.15. Permeability of Gases Through Dimethyl Silicone Rubber Membrane vs Pressure.

In studies of pure gas samples, simple observations of volumes have been satisfactory for measuring permeabilities; however, in gas mixtures, precise analyses of the components are required. The analysis of gas samples by the mass spectrographic method was found to be unsatisfactory because of errors involved in the sampling technique, the process upset caused by the removal of samples, and the limited accuracy of the method. We have installed equipment that will be used to determine permeabilities by other methods that permit in-line analysis of mixtures of air and radioactive noble gases (Fig. 4.16).

Because of the comparatively low permeability of nitrogen, the noble gases and oxygen are quickly separated from the nitrogen in the cascade. The area of the membrane in all the later stages will therefore be determined by the permeability of the oxygen. Similarly, since the membrane is much more permeable to xenon than krypton, the number of stages required to concentrate the noble gases will be determined mostly by the separation factor of krypton from oxygen.

Using the permeability values determined at ORNL and a processing rate ($\sim$700 ft^3/min) that would decrease the activity in the containment

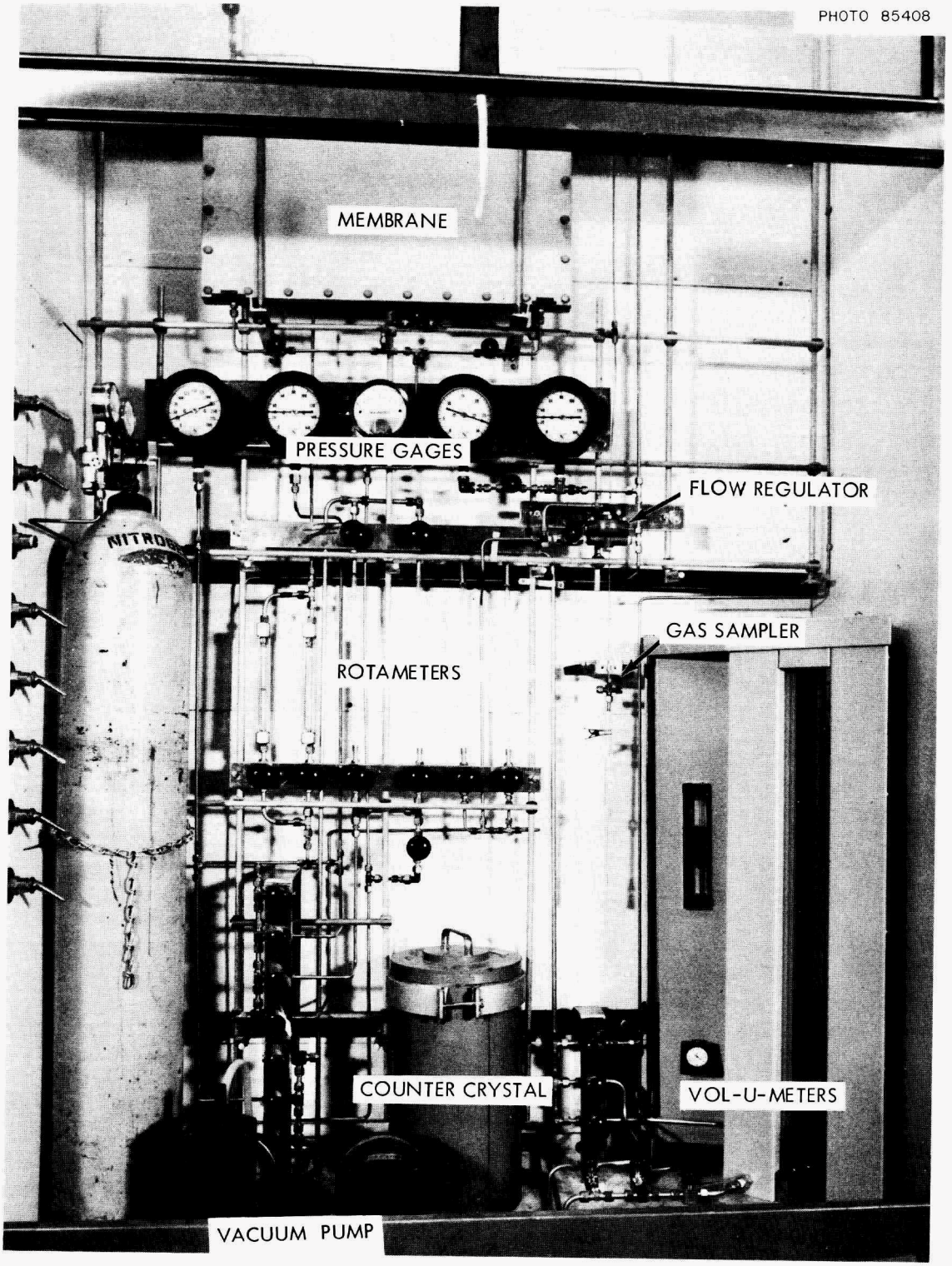

Fig. 4.16. Equipment for Measuring Permeabilities of Gases Through a Permselective Membrane.

shell to 10^4 curies in 12.5 days, the capital cost of such a treatment system would be approximately $940,000 and the power requirement would be about 1 Mw.

4.6 COMPUTER CODE FOR CALCULATING NUCLEAR PROPERTIES OF ACCUMULATED WASTES

Three computer codes for the CDC-1604 computer were written to calculate the buildup and decay of gross activity and heat production in a waste tank or waste system. The first two consider the buildup with a steady rate of addition of radioactive waste, while the third code will allow the waste to be added according to some programmed stepped function (such as one that approximates the rate of installation of power reactors of some given type).

These three codes were based on the activity functions that were used in PHOEBE (see Sect. 18.5). In fact, the calculational part of the PHOEBE code serves as an integral part of these waste programs. As in PHOEBE, a total of 14 group functions (12 gamma groups plus a beta activity group and a beta energy group) are used to describe the fission product activity. However, only in the Waste Tank-1 code are the individual gamma groups printed as part of the results. Codes designated as Waste Tanks-2 and -3 print only gross totals for beta curies, gamma curies, beta watts, gamma watts, total watts, and total Btu/hr. In most cases, the summary outputs of codes 2 and 3 are those generally used in waste tank or waste system calculations. Waste Tank-1 would only be used when a shielding analysis is required.

Three types of output may be selected in each case: (1) the activity and power in a single batch (the basic PHOEBE output); (2) the activity and power in a single tank or system in which the activity is accumulated for some specified filling period, followed by decay after filling (the results can be printed at several times during the filling as well as during decay periods following the filling); and (3) the total accumulated activity and power in a waste system composed of many individual units (tanks).

Codes 1 and 2 allow accumulation and/or decay for periods up to 10,000 years. Waste Tank-3 will only allow accumulation for 300 batches (100 years for all practical purposes) but will allow decay for 10,000 years.

These codes have been used in several economic evaluations of waste systems and in making an estimate of the accumulation of waste activity in an expanding nuclear economy.

5. Transuranium-Element Processing

The Transuranium Processing Plant (TRU) and the High Flux Isotope Reactor (HFIR) were built at ORNL to produce gram quantities of many of the transuranium elements and milligram quantities of some of the transcalifornium isotopes for use in research. This part of the USAEC Heavy Element Production Program began with the long-term irradiation of ^{239}Pu in a Savannah River production reactor. The initial irradiation, subsequent irradiation of some of the ^{242}Pu in a special high flux demonstration run in one of the Savannah River production reactors, and the processing of transuranium elements at ORNL prior to the startup of TRU were described in last year's annual report.

During the past year, TRU began "hot" operations; $^{242}PuO_2$ target irradiation was started in the HFIR; and isotopic enrichment of ^{244}Pu was achieved by the Isotopes Division. More than 40 shipments of transuranium elements were made to fulfill requests from national laboratories, universities, and industry in this country and in three foreign countries. Shipments included 7.4 mg of Pu (74.2% ^{244}Pu), 16.5 g of ^{243}Am, 22 g of ^{244}Cm, 18 μg of ^{249}Bk, and 100 μg of ^{252}Cf.

In TRU the first three processing steps [dissolution, plutonium recovery, and actinide purification (Tramex process)] were performed successfully, all at full levels of solution power density and alpha and beta-gamma radioactivity. The development of processes and equipment for subsequent steps was continued. The processing of ten irradiated targets, including laboratory-scale product cleanup and purification, is essentially complete. Products include about 50 g of ^{242}Pu, 10 mg of ^{244}Pu, 25 g of ^{243}Am, 80 g of ^{244}Cm, 200 μg of ^{249}Bk, and 2 mg of ^{252}Cf. This material was recovered from four HFIR prototype targets and six Savannah River reactor slugs that had been irradiated for about one year, in the High Flux Demonstration Run, at the Savannah River Plant. This report summarizes the production operations and the process and equipment development in the Chemical Technology Division during the past year. Development of procedures and equipment for remotely fabricating target rods is under the direction of the Metals and Ceramics Division and is reported elsewhere.

Some of the TRU target rods ruptured during irradiation in the HFIR. A general description of the failures and their possible effect on the program are included in this report.

5.1 TRU OPERATIONS

The Transuranium Processing Plant began operation this year; the first three processing steps – dissolution, plutonium recovery, and actinide purification – were performed successfully in plant equipment. Isolation and final purification of the actinide elements were accomplished in glass equipment that was installed temporarily in cell 5 of TRU (see Sect. 5.2).

Status and Progress

The HFIR became operational in June 1966. After being inspected and repaired in TRU, 18 targets that had been irradiated at the Savannah River Plant (SRP) for a year were transferred to HFIR for continued irradiation. Tracer-level runs were made in TRU process equipment in July; the first production runs were made in August. Four HFIR prototype targets were processed in the period from August through November. Six Savannah River reactor slugs were processed in the period from December 1966 through May 1967. The power densities of the solutions and the alpha and beta-gamma activity levels were as high as any we expect to handle. Feed preparation, plutonium recovery, and decontamination of transplutonium elements from fission products (Tramex) have been demonstrated in TRU.

The development of the steps that are to follow the Tramex process has been hindered by the lack of a usable method for partitioning the heavy elements. The original process for this step, the Pharex process, was found to be adversely affected by the presence of zirconium in the feed; extraction coefficients are changed in such a way that the separation factors are reduced to intolerable values. No alternative method has been developed sufficiently for use in TRU. Tests of the berkelium extraction process have not been successful in TRU, but the problems are fairly well known and can be circumvented. The process for separating californium, einsteinium, and fermium, using a chromatographic ion exchange technique, has not been attempted in TRU.

Materials Processed

Table 5.1 shows the amounts of transuranium materials recovered, using the main-line equipment, from the four SRP-irradiated HFIR prototype targets and from the six SRP reactor slugs.

Each of the prototype targets originally contained 9.57 g of ^{242}Pu in the form of calcined oxide and had been irradiated in the SRP reactors to about 73% burnup of the plutonium.

Each of the SRP slugs, which were about 1 in. in diameter by 6 in. long, originally contained about 34 g of ^{242}Pu and had been irradiated to about 75% burnup of the plutonium. Three of the slugs were processed after a cooling period of only 30 days.

Table 5.1. Materials Processed in TRU

Isotope	Half-Life	Quantity of Isotope Obtained from:	
		Four HFIR Prototypes	Six SRP Slugs
^{242}Pu	3.7×10^5 years	11 g	40 g
^{243}Am	7.65×10^3 years	5 g	20 g
^{244}Cm	18.1 years	13 g	70 g
^{249}Bk	314 days	30 μg	200 μg
^{252}Cf	2.6 years	130 μg	2 mg
^{253}Es	20 days		4 μg

Another product made available last year is plutonium that is highly enriched in ^{244}Pu. This enrichment was achieved by the Isotopes Division in their calutrons at the Y-12 Plant. The ^{244}Pu content in the plutonium that was processed (0.5% in the prototypes and 0.6 to 1% in the SRP reactor slugs) was five to ten times as high as that in any material previously available. About 8 mg of 73% ^{244}Pu and 3 mg of 31% ^{244}Pu have been isolated from the prototypes. Another batch of plutonium (15 g) is ready for isotopic enrichment in the calutrons. This material contains 96 mg of ^{244}Pu and, based on the previous 10% recovery, promises 10 mg of enriched product.

Process Flowsheet

Figure 5.1 is a block diagram showing the processing steps that are required for transuranium-element production; the steps are discussed individually in later sections.

The first step is the preparation of a feed solution by dissolving irradiated targets; the plutonium is then recovered, either by ion exchange (Plurix) or solvent extraction (Pubex); and, finally, all the transplutonium elements are decontaminated from fission products by countercurrent solvent extraction (Tramex). These three processing steps have been performed successfully in TRU. Following separation of the americium and curium from the transcurium elements, berkelium will be extracted using a batch solvent extraction process (Berkex), and the californium, einsteinium, and fermium will be separated by chromatographic ion exchange (Cefix). All the transuranium element products will be purified, if necessary, and stored either for future shipment to experimenters or for fabrication into targets for reirradiation.

Dissolving

Most of the feed material of interest can be dissolved in either 6 *M* HCl or fluoride-free 15.8 *M* HNO_3. Some low-burnup material (less than 70 to 75% conversion of the original ^{242}Pu) required nitric acid containing fluoride catalyst for complete dissolution. This necessitates a fluoride-removal step to prevent excessive corrosion of the Zircaloy-2 equipment. A dissolver made of stainless steel was installed temporarily for use in dissolving the prototype targets.

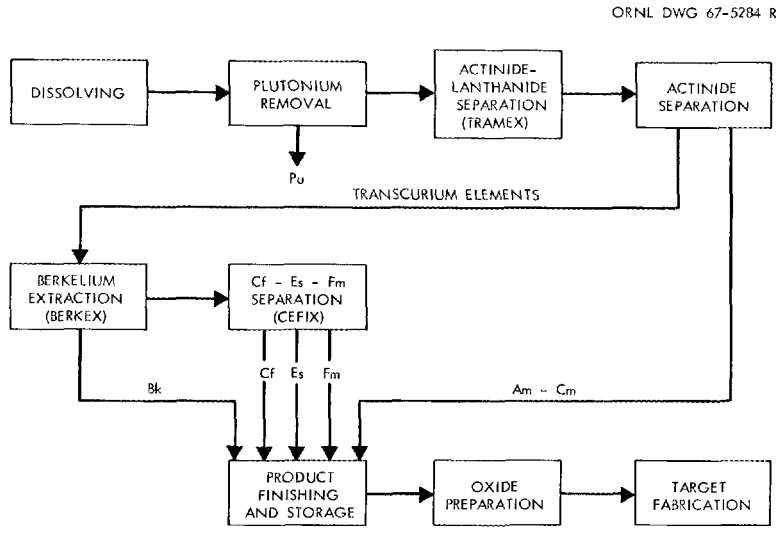

Fig. 5.1. Block Diagram of Operations Required in the Transuranium Processing Plant.

The dissolution method employing HCl is described below; the procedure is the same for HNO_3 or fluoride-catalyzed HNO_3 except that the use of fluoride would prohibit the use of a Zircaloy-2 dissolver.

The target rod is put into the Zircaloy-2 dissolver (T-70), a solution of 6 *M* NaOH–3 *M* $NaNO_3$ is added to dissolve the aluminum, and the dissolver is heated to initiate the dissolving, which then proceeds, exothermally, to completion. The aluminum-bearing solution is decanted from the dissolver through a filter and centrifuge, leaving undissolved particles of actinide oxides. The dissolver is flushed with LiOH to remove excess sodium. Less than 0.2% of the actinides has been lost during the aluminum removal and flushing, and no difficulty has been encountered in filtering the solutions. Finally, the oxides are dissolved in refluxing 6 *M* HCl, and the acidic solution of actinides is transferred to another tank for adjustment to feed for plutonium recovery.

Plutonium Recovery

When the processing equipment was being designed, an anion exchange process (Plurix) was developed and selected for use in recovering plutonium. Since then, a batch solvent extraction process (Pubex) has been formulated; although it is not fully developed, it appears to be promising and has been tested and used successfully in TRU.

The ion exchange processes that are used for plutonium recovery from nitrate and chloride feed solutions are similar. The nitrate-based process is well known; the plutonium is adjusted to Pu(IV) and loaded from a 7 to 9 *M* HNO_3 solution onto a strong-base anion exchange resin (Permutit SK), transplutonium elements and fission products are washed from the resin using 8 *M* HNO_3, and the plutonium is eluted using 0.7 *M* HNO_3. This process has worked very satisfactorily in TRU.

The chloride-based anion exchange process was investigated because the resultant curium product, which would be in the chloride form, could be readily converted to feed for the Tramex process. The process was satisfactorily demonstrated, using glass equipment, in the laboratory; however, it has not been used successfully in the metal equipment in TRU. The plutonium was apparently reduced to Pu(III), which does not load on the resin. Oxidants strong enough to keep the plutonium oxidized tended to cause excessive corrosion of equipment. This process is discussed further in Sect. 5.3.

The last attempt in TRU to recover plutonium by using the chloride-based ion exchange process was terminated immediately after it was started because the feed line failed. This occurred during a processing campaign that was being made to em-

phasize the recovery of einsteinium; the delay for equipment repair would have caused a drastic reduction (because of radioactive decay) in the yield of einsteinium. We, therefore, decided to try the simple batch solvent extraction process after only cursory tests.

The feed was made 5 *M* in HCl and 0.05 *M* in HNO_3 (oxidant). It was contacted with two volumes (feed solution, one volume) of 1 *M* di(2-ethylhexyl)phosphoric acid (HDEHP) in diethylbenzene (DEB) by air-sparging the tank. About 98% of the plutonium was extracted after 4 hr, and 99.5% was extracted after 8 hr. After a settling period the aqueous phase was jetted from the tank, and the organic was scrubbed by use of three one-volume contacts with a 5 *M* HCl–0.02 *M* HNO_3 solution. Essentially all the transplutonium elements reported to the aqueous phase, while the zirconium (from corrosion) remained in the organic phase. Stripping of the plutonium was effected, after modifying the organic by adding one-fourth volume of 0.2 *M* di-*tert*-butylhydroquinone in 2-ethylhexanol (this reduced the plutonium in the organic phase), by contacting with 1 volume of 8 *M* HCl solution containing 0.25 *M* hydroxylamine as a holding reductant. Essentially all the plutonium was recovered.

A key advantage of the batch extraction procedure over ion exchange is the removal of zirconium from both product fractions. As much as 50 g of zirconium has been introduced into dissolver solutions by corrosion of metal equipment; this contaminant forms solids that can plug equipment lines when the product streams are evaporated to small volumes. Also, subsequent operations of the Tramex process are adversely affected if the feed contains more than about 1 g/liter of zirconium.

Both the nitrate-based ion exchange process and the solvent extraction process provided good separation between plutonium and the other actinides, and the plutonium product from each process was decontaminated from gross gamma activity by a factor of about 150. The plutonium product must be further decontaminated before it can be moved from the processing cells to a laboratory glove box for final purification. A nitrate anion exchange technique has been used to accomplish this decontamination; a second extraction cycle will be investigated as an alternative method.

First-Cycle Solvent Extraction Process (Tramex)

The Tramex solvent extraction process (Fig. 5.2), used for separating the lanthanide rare-earth

ORNL DWG 67-5281

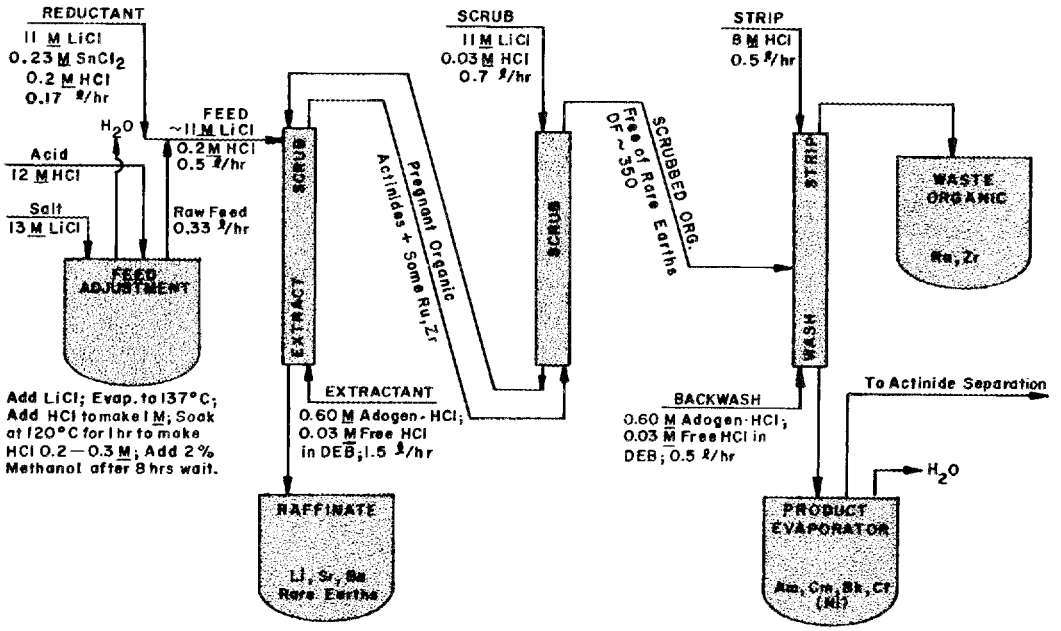

Fig. 5.2. Flowsheet for the Tramex Process for Separating Lanthanides from Actinides.

elements and other major fission products from the actinides or transuranium elements, is operational in TRU. Equipment operability still needs to be improved, and the flowsheet parameters need to be optimized. However, operation of the process is routine. Recovery of product is good, and the transplutonium elements are decontaminated from gamma activity by a factor of about 75, which is satisfactory.

The raffinate from the plutonium recovery step is adjusted so that it is 11 *M* in LiCl and 0.2 *M* in HCl, methanol is added to prevent loss of acid by radiolysis, and then this solution is fed to the Tramex process at the rate of $\frac{1}{3}$ liter/hr. A solution of 11 *M* LiCl–0.2 *M* HCl containing stannous chloride, which prevents oxidation of cerium to an extractable form, is added continuously to the feed stream at a rate sufficient to maintain an $SnCl_2$ concentration of 0.075 *M*. The total flow rate of 11 *M* LiCl–0.2 *M* HCl solution is 0.5 liter/hr. The transuranium elements are extracted into a solution of 0.6 *M* Adogen 364-HP (high-purity tertiary amine) – 0.03 *M* HCl, in DEB. The flow rate of the extractant is 1.5 liters/hr. Small amounts of extracted lanthanides are scrubbed out of the organic phase using a solution of 11 *M* LiCl–0.03 *M* HCl (flow rate, 0.7 liter/hr). The actinides are stripped from the solvent using 8 *M* HCl (flow rate, 0.5 liter/hr), and the aqueous solution containing the actinide product is backwashed with extractant to reduce the zirconium content.

The curium and the americium in the Tramex product will be suitable for recycle to the HFIR without further decontamination from fission products because remote refabrication techniques will be used in preparing the targets.

Treatment Subsequent to Tramex Processing

The first three processing steps – dissolution, plutonium recovery, and decontamination of actinides (by the Tramex process) – have been accomplished in TRU. Processes for subsequent steps have not been demonstrated in plant equipment. This year, the isolation and the final purification of actinide elements were accomplished in glass equipment that was installed temporarily in cell 5 in TRU (see Sect. 5.2).

The next step required in TRU is actinide partitioning, or the separation of americium and curium (which will be recycled to HFIR for reirradiation) from the heavier actinides. The latter will be separated from each other and recovered as purified products. The original flowsheet (Pharex) for this step can perform the required separation under ideal conditions; however, it was discovered this year that the presence of 100 ppm of zirconium in the feed reduced the separation factors to intolerably low values. Thus, Pharex is not a satisfactory process for use in TRU because much of the equipment is made of Zircaloy-2. We are developing a new process, Hepex, which is insensitive to the presence of corrosion products.

In tests of the berkelium extraction process in TRU, only about 30% of the berkelium was recovered. Apparently, the berkelium was rapidly reduced to Bk(III) in the concentrated nitrate system. If the entire extraction and stripping could be done in a few hours, the process would probably work; however, if it requires 16 hr, as in the tests in TRU, the reduction to Bk(III) will occur and the recovery of berkelium will be greatly decreased. The problem should be readily solved by shortening the processing time.

Demonstration of the Cefix process for the separation and purification of californium, einsteinium, and fermium has not been attempted in TRU.

The processes for oxide preparation have not been developed sufficiently for demonstration in TRU. The equipment to be used for remote target fabrication is now being installed in the processing cells.

Plant Shutdown and Maintenance Experience

TRU was shut down for an extensive program of equipment repair and replacement in February 1967, after about seven months of operation. Although several equipment problems had arisen during the seven months, none had been serious enough per se to force a plant shutdown; all of them had been circumvented or the equipment had been temporarily repaired. However, the combined effects had made plant operation inefficient. In addition to these repairs, several equipment modifications were made during this period.

The major repairs involved: (1) replacement of a bundle of process lines that connect equipment items located in cubicle 7 to tanks in the cell 7 tank pit, (2) replacement of the Plurix process ion exchange column, and (3) general overhaul of the cubicle 7 sampler station. Ten Zircaloy-2 lines in

the line bundle had corroded severely on the outside. Apparently, mixtures of HCl and HNO_3 had been allowed to stand in the disconnect well in which the lines terminated. The ion exchange column had collapsed, apparently because of excessive pressure that was applied to the water jacket.

Major equipment modifications included: (1) addition of a second tantalum-lined evaporator to the feed preparation system to provide for concentration of feed solutions, (2) installation of larger top sections on the Tramex solvent extraction columns to provide better venting and to improve the hydraulics of the system, and (3) installation of a new vacuum system for the plant.

The basic maintenance concept in TRU operations and design is that remote techniques will be required eventually; however, it has been possible thus far to use direct maintenance techniques in the cell tank pits. A total of 28 entries by personnel were made into tank pits 6 and 7 during this extended period of maintenance; the maximum radiation dose received per entry (average duration, about 20 min) was 150 millirems. No weekly doses exceeded 300 millirems. Although surface contamination in the tank pits was in excess of 10^5 alpha disintegrations per second per 100 cm^2 and a number of internally contaminated process lines were disconnected in the pits, the level of airborne contamination in the "limited access" area, into which the pits were opened, never exceeded normal tolerances. One entry (duration, 10 min) was made by an individual into cubicle 7. A dose of only about 100 millirems was received; very little contamination was found on the surface of the plastic suit worn.

Prediction of Heavy-Element Production in the HFIR

Accurate predictions of the compositions of HFIR targets, during and following irradiation, are vital to the transuranium-element production program. Such predictions are required to determine compositions that can be safely irradiated in the reactor, to plan irradiation and processing schedules, and to forecast the availability of various isotopes of the transuranium elements.

Two computer programs are used in making predictions of compositions of targets irradiated in the HFIR. The first of these is used to calculate production rates of the various isotopes during neutron irradiation. It is an extension of earlier programs that are based on the CRUNCH code. Two features distinguish it: it includes explicit contributions from epithermal neutron reactions, and it makes an approximate calculation of resonance self-shielding effects, which cause the effective neutron cross sections for particular nuclides to vary during irradiation as the concentrations of these nuclides change. Two ^{242}Pu targets, which were irradiated at the SRP to about 45% burnup and subsequently analyzed for heavy-element content, served as the first subjects for this code. Numerous calculations were made that involved the known irradiation histories of these targets and various assumed values for thermal-neutron cross sections.

The results of these calculations were then analyzed, using the second computer program, which interpolates and weighs the results by the least-squares method, to obtain the set of cross sections that most nearly results in the composition observed at the end of irradiation. This second program is capable of simultaneously considering the data for ten different targets.

In the analysis to date, resonance absorption has been based on literature values of infinite-dilution resonance integrals (1280 and 1500 barns for ^{242}Pu and ^{243}Am, respectively). For the purpose of estimating resonance self-shielding, a mathematical model that is appropriate to a single narrow resonance was assumed. The values for thermal cross sections (2200 m/sec) resulting from this analysis agree with the lower end of the range of values reported in the literature (see Table 5.2).

The results of the analysis of the SRP irradiations were used to predict the HFIR effective cross sections of ^{242}Pu and ^{243}Am, the first two members of the transuranium-element production chain (Table 5.3). Reactor effective cross sections vary during irradiation as target compositions change; this analysis was based on the target compositions at the end of one reactor-core lifetime in the HFIR.

HFIR target D-30 was irradiated for one reactor-core cycle at 90 Mw and dissolved, and the resulting solution was analyzed for transuranium elements; the results were then subjected to numerical analysis. Estimates of HFIR effective cross sections for ^{242}Pu and ^{243}Am are within 10% of the values previously calculated (see Table 5.3). This agreement is encouraging, indicating that there are no gross deficiencies in the mathematical model used to allow for resonance self-shielding for these two isotopes.

Table 5.2. Equivalent 2200-m/sec Cross Sections[a]

	^{242}Pu	^{243}Am
1. SRP slug	19.12	83.56
2. HFIR prototype	18.04	63.93
3. Combined analysis of 1 and 2	18.57	74.85
4. HFIR-irradiated target D-30	16.39	73.66
5. Combined analysis of 1, 2, and 3	18.00	73.74
Literature values[b]	17.5–30	73.6–183

[a]In barns.

[b]*Cross Sections for Transuranium Element Production*, BNL-982 (T-415), Neutron Cross Section Evaluation Group, Brookhaven National Laboratory (May 1966).

Table 5.3. HFIR Effective Cross Sections[a]

	Cross Section (barns)		Percentage Difference
	Predicted (from SRP Data)	Observed (D-30)	
^{242}Pu	22.1	20.3	−8.3
^{243}Am	99.6	98.6	−1.0

[a]Reactor effective cross sections vary during irradiation as target compositions change. These values are for the end of one irradiation cycle.

As larger quantities of the transuranium elements are produced, these two programs will be used repeatedly to reevaluate cross-section data and to make better predictions of the availability of various isotopes.

5.2 TRANSPLUTONIUM ELEMENT ISOLATION FROM TRAMEX PRODUCTS

Tramex processing in TRU provided products containing the transplutonium elements in chloride solution. Final purification and isolation of these elements were accomplished by additional processing, which was performed in glass equipment that was installed temporarily in cell 5 of the TRU facility.

Status and Progress

The generally accepted process methods that have been developed for isolating actinides from small-sized targets of highly irradiated plutonium, americium, and curium have been satisfactorily scaled up for processing Tramex products from TRU operations. The larger-scale processing has been accomplished in glass equipment with slightly modified process conditions. We have processed Tramex products from four prototype HFIR targets and three Savannah River slugs of $^{242}PuO_2$, all of which were irradiated to about 70% burnup. About 30 g of ^{244}Cm, 9 g of ^{243}Am, 600 μg of ^{252}Cf, and 50 μg of ^{249}Bk were isolated as products. Recovery of materials from the other three Savannah River slugs is essentially complete. The successful processing of these products has demonstrated the feasibility of separating significantly larger amounts of transplutonium elements than was previously considered possible.

Flowsheet

A flow diagram that indicates the four major processing steps required for transplutonium element isolation is shown in Fig. 5.3. After adjustment of the feed, the actinides were processed by an LiCl–anion exchange process. This not only provided additional decontamination from fission products and ionic contaminants but also separated the actinides into three intermediate product fractions that were subsequently processed for final isolation of the actinides. In the first fraction, most of the americium and curium was eluted with 9 *M* LiCl; continued elution with 8 *M* LiCl provided a second fraction, which contained the remainder of the curium and about 60% of the berkelium; and final elution with 8 *M* HCl provided a third fraction, which contained the remainder of the berkelium, all of the californium, and about 0.5% of the original americium-curium. Highly pure californium was recovered by chromatographic elution from cation exchange resin with ammonium α-hydroxyisobutyrate. The americium-curium-berkelium fractions from both columns were combined, and the berkelium was recovered by extraction of Bk(IV) with di(2-ethylhexyl)phosphoric acid (HDEHP) from 8 *M* HNO_3. Normally, the americium and curium were not separated from each other but were stored as a single product; they will be converted to a mixed oxide product for use in preparing HFIR targets. When separation was required, the americium was precipitated from potassium carbonate solution as a double potassium americium(V) carbonate.

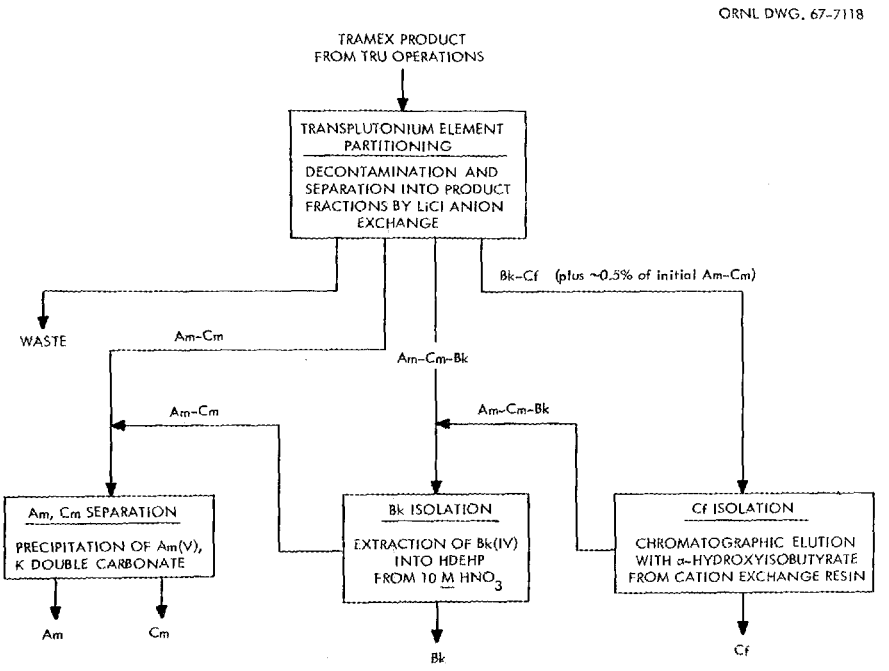

Fig. 5.3. Flow Diagram of Transplutonium-Element Isolation from Tramex Product.

Process Equipment

In-cell process equipment was constructed of glass and mounted on two standard TRU equipment racks for easy insertion into, and removal from, the cell bank, A photograph of the feed adjustment rack is shown in Fig. 5.4. The equipment consists mainly of 4-liter storage vessels, plus a precipitation vessel and a centrifuge. A feed adjustment evaporator is located on the right side in the middle tier of vessels. All vessels are closed and sealed; this permits transfer of solution by vacuum or pressure, which is generated by the small pump in the lower left corner. The ion exchange equipment rack is shown in Fig. 5.5. The 2-liter vessels are used to collect fractions from ion exchange runs. The LiCl–anion exchange column, located on the far left, is 2 in. ID by 16 in. high and has a resin capacity of 450 ml. The cation exchange column, located in the middle of the rack, is 1 in. ID by 30 in. high and has a resin capacity of 230 ml. Both columns have water jackets and are heated by the small water bath in the lower left corner. Solutions are fed to the column by a Sigma-Motor peristaltic finger pump located in the lower right corner.

The americium-curium and berkelium fractions were sufficiently decontaminated from fission products and californium by LiCl anion exchange that they could be removed from the TRU cell bank and processed in "junior caves" for berkelium isolation and for final separation of americium from curium.

The efficiency of in-cell ion exchange runs was greatly enhanced by the use of alpha detectors (to monitor column effluents) and neutron detectors (to determine the position of the californium on the column). This instrumentation allowed product fractions to be collected as desired.

LiCl–Anion Exchange Process

The Tramex product, which is supplied as an evaporated solution from the strip column, was adjusted to a suitable feed and processed by LiCl-based anion exchange, using the flowsheet shown in Fig. 5.6. The predominant radioactive contaminants in the feed were $^{103-106}Ru$ and ^{95}Zr-^{95}Nb; ionic contaminants included Zr, Cr, Fe, Ni, and Sn. Solids, primarily zirconia, were also present in the feed; they contained significant amounts of tin and nickel but not much radioactivity. These solids were difficult to filter; they were not readily soluble in concentrated HCl but could be dissolved in HNO_3-HF.

The Tramex product, which was 2 to 6 *M* in LiCl, was concentrated to 12.5 *M* LiCl by evaporating to a temperature of 137°C. After the HCl concentration was adjusted to 0.1 *M*, the feed had to be refiltered because of additional precipitation (zirconia) during concentration.

Feed containing 4 to 10 g of curium, plus lesser amounts of Am, Bk, and Cf, was passed through an anion exchange column of Dowex 1-X10 resin (200 to 300 mesh). The actinides and many of the contaminants load on anion resin from 12.5 *M* LiCl. In order to obtain satisfactory separation, the actinides had to be loaded in no more than the top 20% of the resin bed. The location of the actinides on the column was determined by means of an in-cell neutron detector. Curium losses in the feed effluent were less than 0.01%. Most of the rare earths and nickel was washed from the column with five to eight column displacement volumes of 10 *M* LiCl–0.1 *M* HCl–0.1 *M* $NH_2OH \cdot HCl$–5 vol % CH_3OH. (Hydroxylamine was used to maintain cerium in the trivalent state, and methanol was used to suppress radiolytic gas formation.) Elution with this solution was continued until the alpha activity in the effluent increased. Curium losses to this wash were less than 1.0%.

The profile of alpha activity in the eluate, as indicated by the in-line alpha monitor, for a typical run is shown in Fig. 5.7. As soon as an increase in alpha activity was detected in the eluate, the eluent was changed to 9 *M* LiCl–0.1 *M* HCl. Elution was continued until about 90% of the curium was eluted (see Fig. 5.7). The eluent was then changed to 8 *M* LiCl–0.1 *M* HCl. At the beginning of this elution, the californium band was determined, by a neutron detector, to be at the top of the column. Elution with 8 *M* LiCl was continued until the californium band approached the bottom of the column, at which point the eluent was changed to 8 *M* HCl, and the remaining actinides were stripped off the resin column. This elution sequence provided an americium-curium fraction that was nearly free of ionic and radioactive contaminants, with no detectable berkelium or califor-

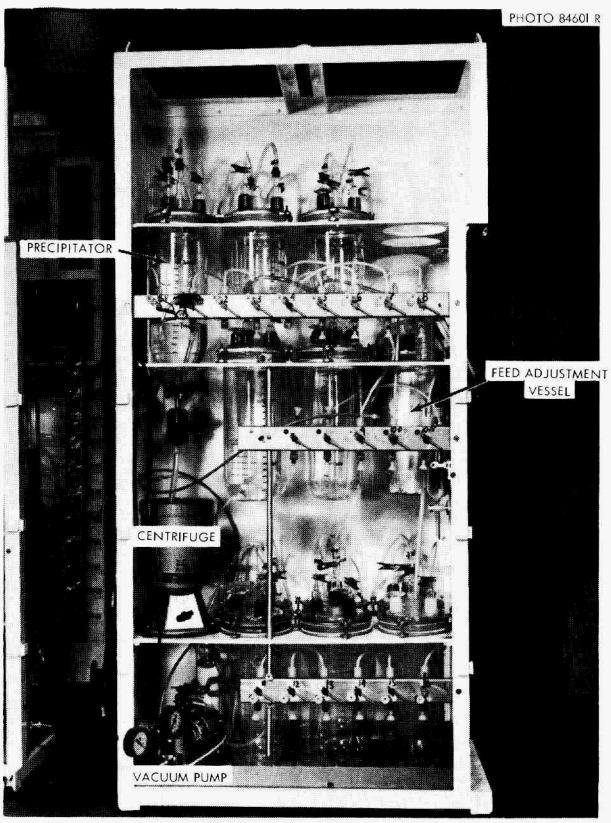

Fig. 5.4. Feed Adjustment Equipment for Final Transplutonium-Element Isolation.

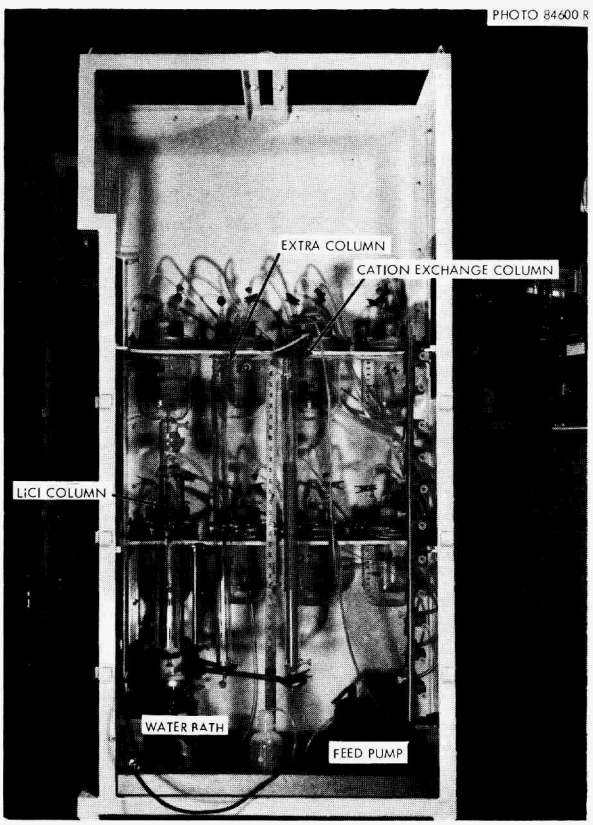

Fig. 5.5. Ion Exchange Equipment for Final Transplutonium-Element Isolation.

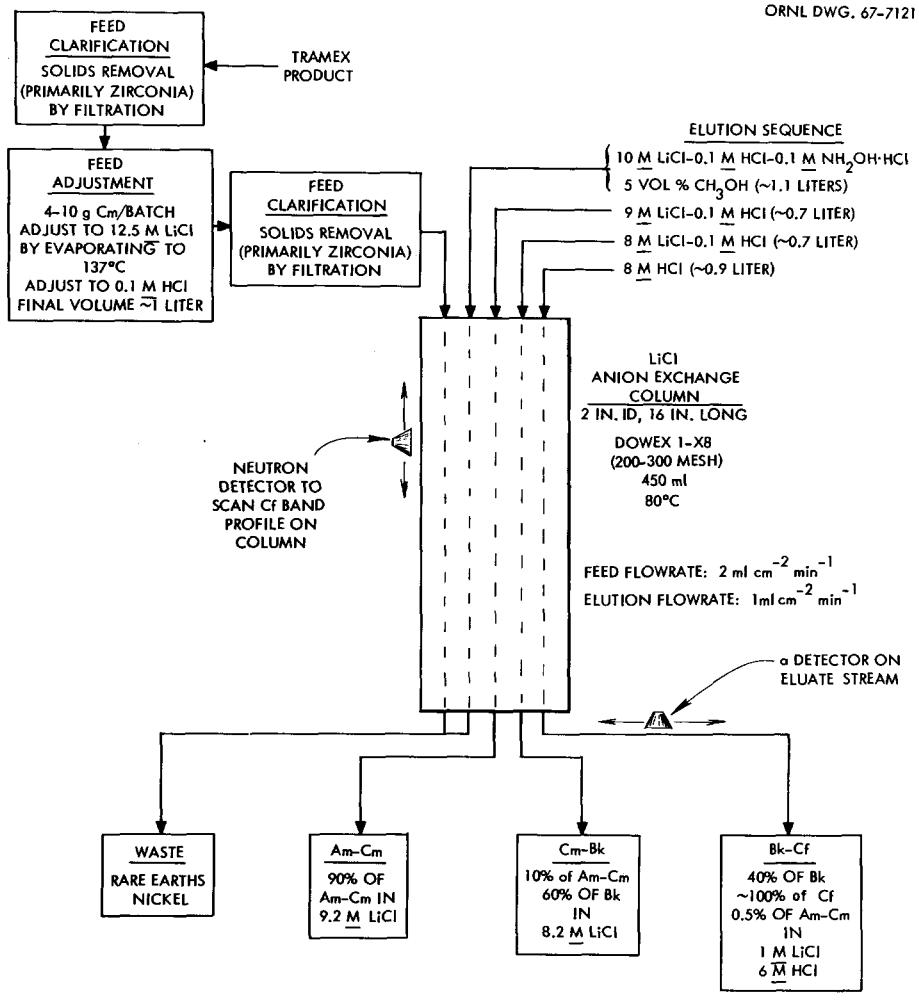

Fig. 5.6. Transplutonium-Element Partitioning of Tramex Product by LiCl-Based Anion Exchange.

nium. The americium-curium-berkelium fraction contained about 10% of the americium and curium and about 60% of the berkelium. The remaining berkelium, along with ~0.5% of the americium-curium, was eluted with the californium fraction. Although berkelium is not obtained in a single product fraction, this elution sequence gives product fractions that are amenable to final isolation of the elements in subsequent processing. In the original feed, the curium : californium mass ratio was about $2 \times 10^4 : 1$. This was reduced to about 100 : 1 in the californium fraction, providing a curium decontamination factor of about 200. Elution of californium with 8 *M* HCl afforded excellent decontamination from many contaminant ions that form chloride complexes. Contaminants such as Fe, Sn, Zr, and Pu(IV) remain on the column but can be stripped with 0.5 *M* HCl.

The anion resin was not adversely affected by a single run: three or four runs could be made before radiation-induced discoloration was detectable. At this point, the resin was changed, although a longer period of use might be possible.

Californium Isolation

The flowsheet for californium isolation from the berkelium-californium product fraction is shown in Fig. 5.8. This product, which contains HCl and LiCl, must be converted to a low-acid feed for the butyrate column. Lithium chloride is removed by

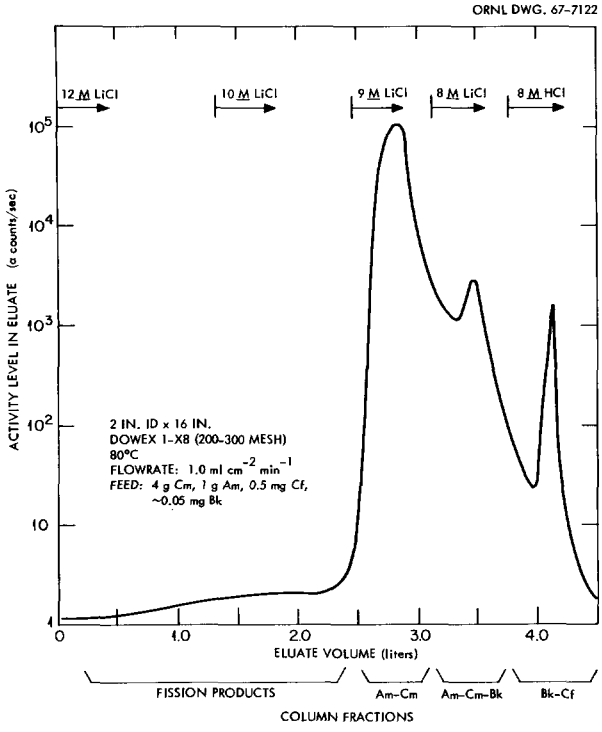

Fig. 5.7. Profile of Alpha Activity in Eluate from LiCl-Based Anion Exchange Column.

precipitating the metal hydroxides, washing them, and then redissolving them in hydrochloric acid. To ensure complete precipitation, about 50 mg of iron per liter of solution was added as carrier. The metal hydroxides were filtered, washed, and dissolved in a small volume (~25 ml) of 8 *M* HCl. Iron was removed by passing this solution through a small anion exchange column that preferentially sorbs iron but allows the actinides to pass through. The acid concentration of the column effluent was reduced by evaporating to a small volume and adding sufficient HCl to produce a final solution (~50 ml) having an acid concentration of 0.05 to 0.1 *M*.

This final solution, or feed, was passed through the 30-in. cation exchange column, which was packed with about 230 ml of Dowex 50-X12 resin (200 to 300 mesh) in the ammonium form. The actinides loaded in a narrow, dense band at the top of the column. Separation was obtained by chromatographic elution from the resin at 80°C with α-hydroxyisobutyrate solutions. The progress of the elution was followed by means of the neutron detector (to locate californium on the resin column) and by means of the in-line alpha detector (to properly select the product fractions). Initial elution with 0.4 *M* α-hydroxyisobutyrate at pH 4.2 was continued until the neutron activity reached the bottom of the column and alpha activity started to appear in the eluate. This required about 800 ml of solution. The elution was then continued with 0.4 *M* α-hydroxyisobutyrate at pH 4.8 until all the berkelium, americium, and curium were eluted. This required about 500 ml of solution.

The product fractions in butyrate solutions were converted to acid solutions by cation exchange. After adjustment of the pH to 1.0, these solutions were passed through small columns of Dowex 50-X4 resin to load the actinides. The resin columns were washed with 0.2 *M* acid to remove residual butyrate, and the actinides were stripped into 6 to 8 *M* acid. Californium, which is stripped into HCl, represents a purified product fraction. The berkelium-curium-americium fraction was stripped in 8 *M* HNO_3, which is convenient for subsequent berkelium isolation.

Berkelium Isolation

The process outlined in Fig. 5.9 was used to isolate pure berkelium from the americium-curium-berkelium fractions from both the LiCl–anion exchange columns and from the californium isolation column. Berkelium eluted from the LiCl column was precipitated as the hydroxide to remove residual LiCl. The curium in this fraction provided sufficient carrier to ensure complete precipitation. The precipitate was washed and dissolved in 8 *M* HNO_3, which is a suitable medium for oxidation and extraction of berkelium.

Berkelium was oxidized to the tetravalent state by the addition of 0.5 *M* $NaBrO_3$. The feed solution was allowed to stand 15 min to ensure complete oxidation, and the berkelium was then selectively extracted into 1 *M* di(2-ethylhexyl)phosphoric acid (HDEHP) in decane. The organic solvent was pretreated with 8 *M* HNO_3–0.5 *M* $NaBrO_3$ to remove all reducing impurities. The feed solution was contacted twice with equal volumes of solvent. The organic phases were combined and scrubbed twice with equal volumes of 8 *M* HNO_3–0.5 *M* $NaBrO_3$. Berkelium was stripped from the solvent by two consecutive contacts with half-volume passes of 8 *M* HNO_3–1 *M* H_2O_2, which reduced berkelium to Bk(III). Two solvent extraction cycles are required to produce a pure berkelium product. A curium decontamination factor of about 10^5

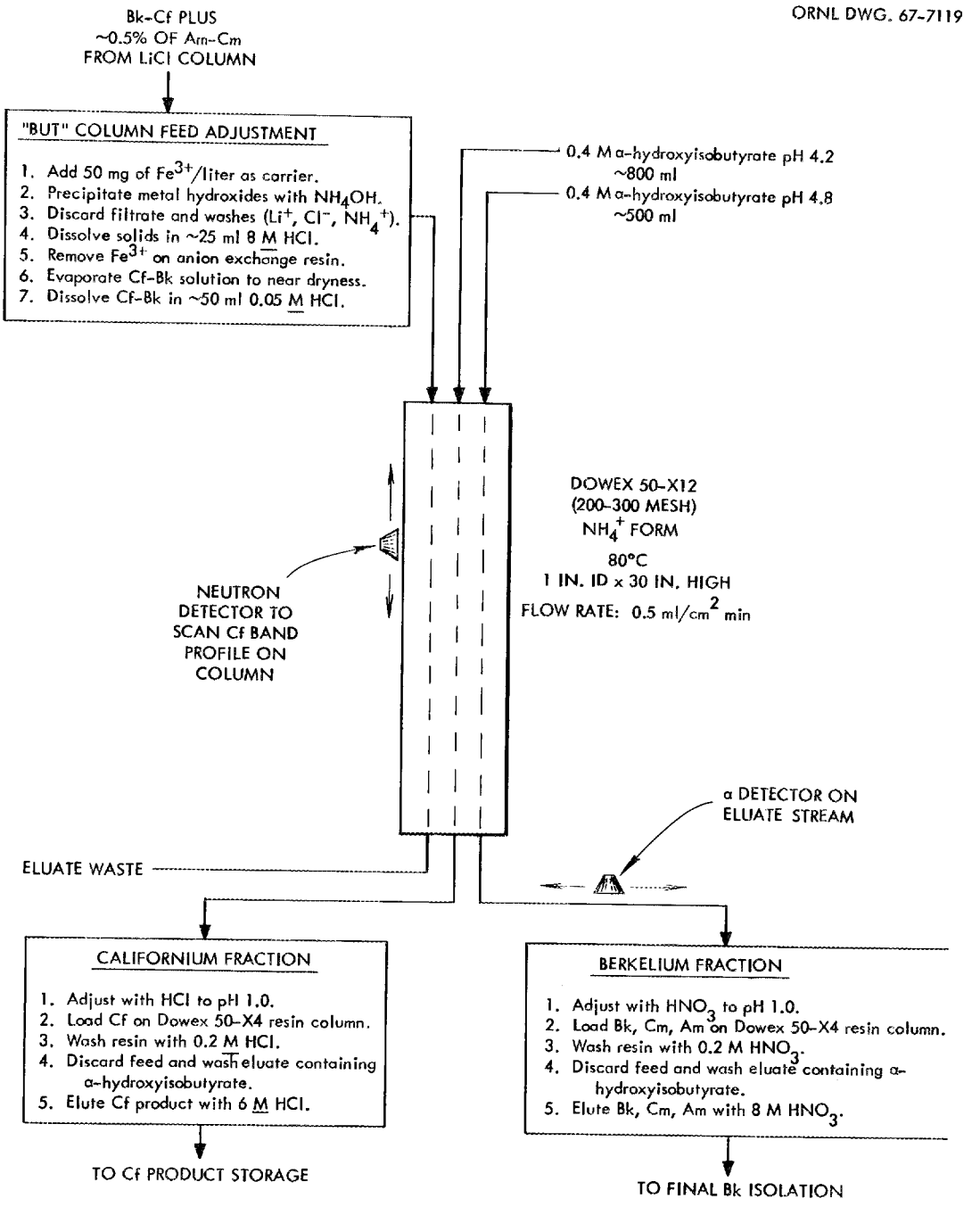

Fig. 5.8. Isolation of Californium by Chromatographic Elution with α-Hydroxyisobutyric Acid from Cation Exchange Resin. Feeds are kept as small as feasible (5 to 10 ml) and contain up to 0.5 mg Cf, 0.1 mg Bk, and 100 mg Am-Cm. The column is instrumented with neutron and alpha detectors in order to properly select product fractions with a minimum amount of cross contamination. Off-specification products are recycled through this process.

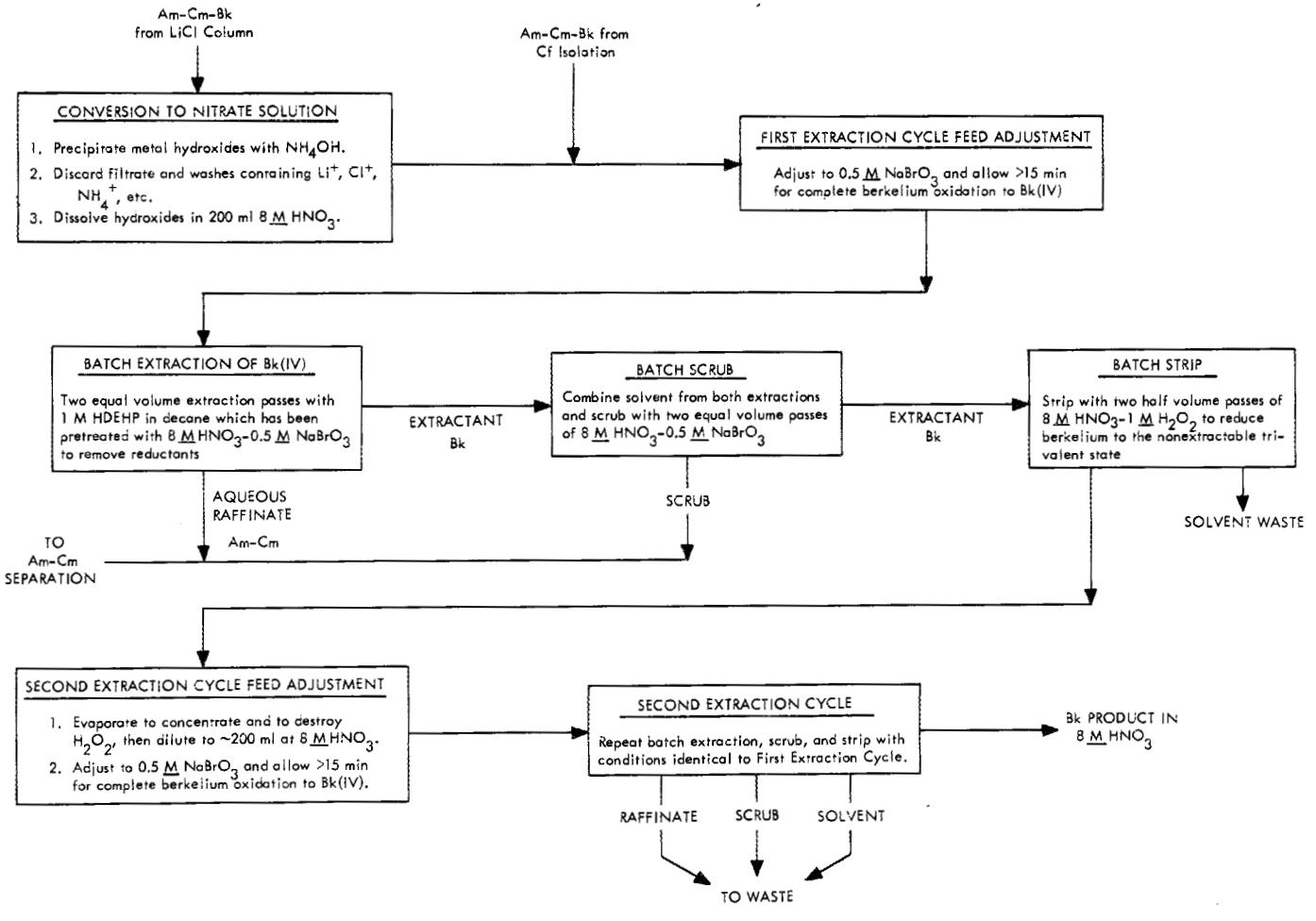

Fig. 5.9. Isolation of Berkelium by Selective Extraction of Tetravalent Berkelium. Typical feed contained ~1 g of Cm, ~1 g of Am, and 20 to 50 μg of Bk. Each extraction cycle gives curium and americium decontamination factors of $\sim 10^5$.

ORNL DWG. 67-7120 R1

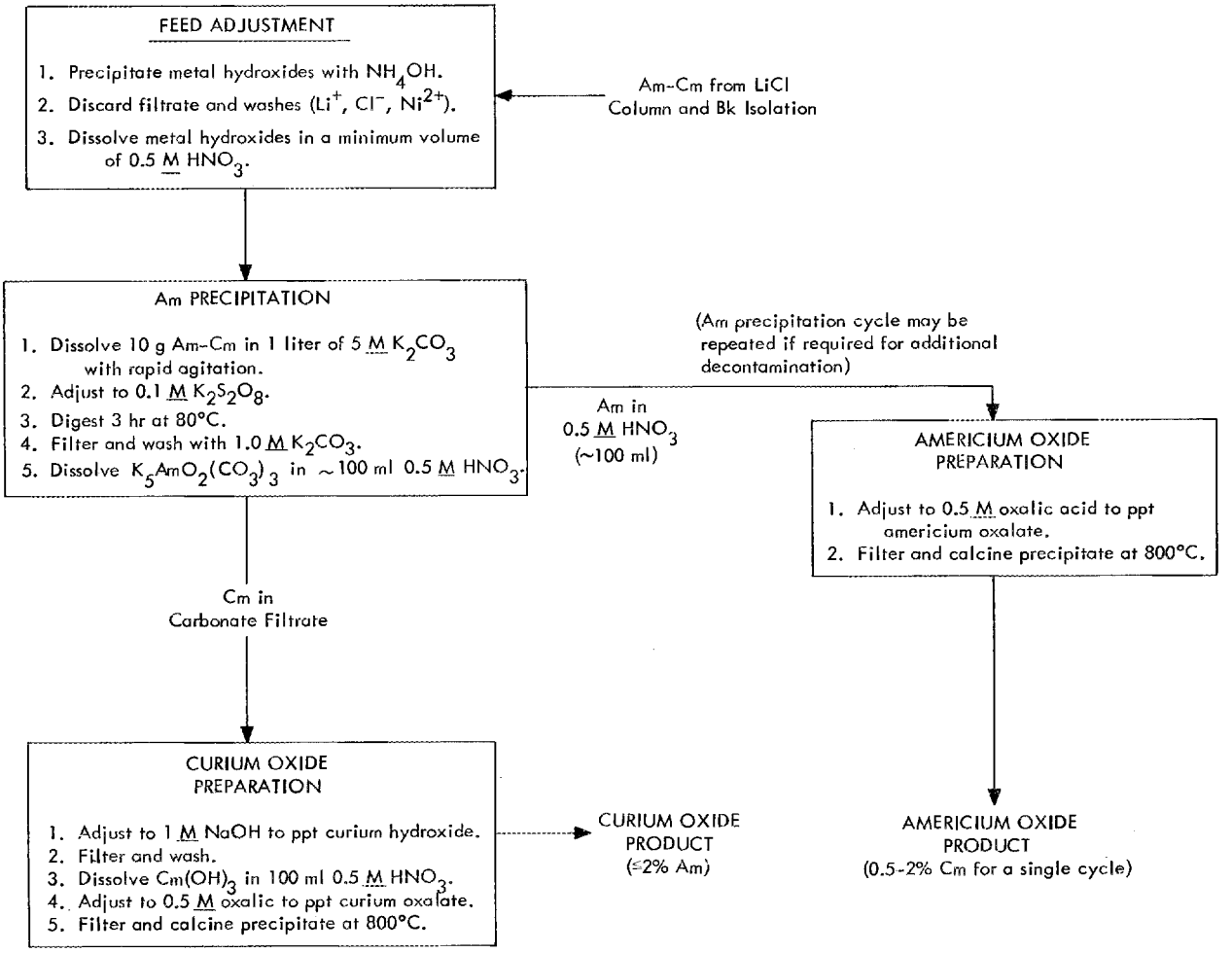

Fig. 5.10. Americium-Curium Separation by Precipitation of Americium Potassium Double Carbonate.

was accomplished in each extraction cycle; the final product was free of detectable alpha contamination.

Americium-Curium Separation

In TRU processing, a mixture of americium and curium is generally used for recycling to the HFIR. The process shown in Fig. 5.10 was used to separate some of the americium and curium for use in research. The mixed americium-curium was precipitated as hydroxide to remove lithium chloride. Ammonium hydroxide was used so as to obtain additional decontamination from nickel. The hydroxides were washed and then dissolved in a small volume of 0.5 *M* HNO_3. This solution, containing up to 10 g of americium plus curium, was added with vigorous stirring, to 1 liter of 5 *M* K_2CO_3. The trivalent actinides formed soluble carbonate complexes. By adjusting the solution to 0.1 *M* $K_2S_2O_8$ and digesting for 3 hr at 80°C, the americium was quantitatively oxidized to the pentavalent state, which forms an insoluble double carbonate, $K_5AmO_2(CO_3)_3$.[1] The precipitate was filtered, washed with 0.5 *M* K_2CO_3, and dissolved in 0.5 *M* HNO_3. This product contained 98% of the americium and about 2% of the curium. A second pre-

[1] L. B. Werner and I. Perlman, "The Pentavalent State of Americium," *J. Am. Chem. Soc.* 73, 495 (1951).

cipitation cycle was used if additional purification of americium was required. Americium oxide was prepared by precipitating the oxalate with oxalic acid and calcining at 800°C. Americium separated from curium by two successive precipitation cycles and converted to the oxide contained as little as 0.005 wt % curium and ~1 wt % calcium.

Curium in the carbonate filtrate was recovered by precipitation with 1 *M* NaOH. It was found that NH_4OH would not precipitate curium hydroxide quantitatively from K_2CO_3 solution. Curium losses in the filtrate following precipitation with excess NaOH were less than 0.1%. The curium hydroxide was filtered, dissolved in 0.5 *M* HNO_3, and reprecipitated with oxalic acid. The curium oxalate was calcined at 800°C to yield curium oxide, which contained ~ 2 wt % ^{243}Am and ~1 wt % Ca.

Table 5.4. Summary of Transuranium Elements Separated

Element	Quantity Isolated	Average Isotopic Composition	
		Isotope	%
^{244}Cm	29.35 g	^{244}Cm	93.8
		^{245}Cm	0.5
		^{246}Cm	5.4
		^{247}Cm	0.10
		^{248}Cm	0.12
^{243}Am	8.8 g	^{243}Am	99.8
		^{241}Am	0.2
^{249}Bk	54 μg[a]		
^{252}Cf	615 μg	^{249}Cf	7.3
		^{250}Cf	19.3
		^{251}Cf	4.4
		^{252}Cf	69

[a]The average time between the discharge of targets from the reactor and measurement of the amount of berkelium was six months.

Summary of Products

The total quantities of actinides isolated during this processing and their isotopic composition are shown in Table 5.4. Product purities and chemical forms are shown in Table 5.5.

5.3 DEVELOPMENT OF CHEMICAL PROCESSES

Laboratory support was provided to investigate chemical problems that arose during initial high-activity-level processing in TRU. We have continued process development of the recovery of plutonium by an HCl–anion exchange process, actinide partitioning by solvent extraction, Cf-Es-Fm separations, and americium-curium oxide preparation (for use in HFIR targets).

Table 5.5. Typical Product Purity

Element	Chemical Form	Radioactivity	Ionic Contaminants
^{243}Am	AmO_2	^{239}Np daughter activity; no fission products detected; 1 g measures ~50 r/hr gamma unshielded; with $\frac{3}{8}$-in. lead shielding the gamma activity is <50 mr/hr	~0.005% ^{244}Cm, ~1 to 2% Ca, <1% K
^{244}Cm	CmO_2	^{243}Cm gamma, spontaneous fission gamma; no fission product activity detected; 1 g measures ~1 r/hr of fast neutrons and ~200 mr/hr of gamma activity	~2% ^{243}Am, ~1% Ca, ~1% K
^{249}Bk	$Bk(NO_3)_3$ solution	^{249}Cf alpha and gamma; no other transuranium-element alpha activity; no fission product gamma activity detectable	None detectable
^{252}Cf	$CfCl_3$ solution	Spontaneous fission gamma and neutron activity; 1 mg of ^{252}Cf measures ~500 mr/hr of fast neutrons, ~300 mr/hr of gamma activity	None detectable

Status and Progress

Initial processing of prototype HFIR targets required HNO_3-HF for dissolution. Since fluoride is not compatible with main-line TRU process equipment, fluoride removal methods were studied. Hydroxide precipitation was determined to be the simplest method readily available, and process parameters for this procedure were evaluated. Highly burned plutonium targets can be readily dissolved in HCl media; also, it is convenient to isolate plutonium directly from HCl solution. Development of a process for recovering plutonium by chloride-based anion exchange was, therefore, continued.

We continued laboratory studies of the Pharex process, in which the heavy actinides are separated from americium and curium by preferential extraction into 2-ethylhexyl phenylphosphonic acid (HEH[ϕP]) from dilute HCl. In recent investigations, the presence of small amounts of zirconium was found to cause decreases in the curium-berkelium separation factors. In the present TRU process equipment, feed solutions for this separation are certain to contain zirconium. It was found that the deleterious effect of zirconium can be avoided by using di(2-ethylhexyl)phosphoric acid (HDEHP) as the extractant. Laboratory studies of this process are presently under way; details are reported in Sect. 8.9.

Chromatographic elution from cation exchange resin with α-hydroxyisobutyrate solutions will be used to separate californium, einsteinium, and fermium in TRU. Scale-up tests of this method were continued by separating americium from curium at high activity levels, and a high-pressure ion exchange system was evaluated. High-activity-level separations indicate that conventional columns can be scaled up sufficiently to process 100 to 150 mg of ^{252}Cf. The pressurized system appears to be well suited for this separation because it permits greater freedom in the selection of operating parameters, and objectionable radiation effects such as resin degradation and radiolytic gas formation are more readily controlled.

The sol-gel method for the preparation of 20- to 100-μ-diam particles of dense americium-curium oxide for incorporation into HFIR targets has several inherent advantages over alternative processes. A modified rare-earth sol-gel process, which appears to be convenient for in-cell operation, was reported previously. During the last year, major efforts have been concemed with the evaluation of equipment concepts for in-cell operations and with scouting experiments using ^{241}Am; results indicate that the modified procedure is amenable to actinide sol preparations. In-cell experiments with ^{244}Cm and mixed ^{244}Cm-^{243}Am are presently under way.

Methods for Dissolving Irradiated HFIR Targets and Recovering Plutonium

Two dissolution procedures and two plutonium recovery methods were used during the initial TRU processing of irradiated $^{242}PuO_2$ targets. Targets that still contain substantial amounts of PuO_2 (less than 70% plutonium burnup) require fluoride for complete dissolution. When HNO_3-HF is used, the fluoride must be removed prior to any recovery processes since plant equipment, which is fabricated from Zircaloy-2 and tantalum, is not compatible with this ion. Therefore, methods of removing fluoride were studied in the laboratory. When the burnup of the target is greater than 70%, dissolution in hydrochloric acid is preferred since chloride solutions are required for Tramex processing. Laboratory development of an HCl–anion exchange process for recovering plutonium from HCl solutions was continued.

Fluoride Removal from Target Dissolver Solution

Fluoride can be removed from nitrate dissolver solution by simply precipitating the metal hydroxides and leaving the fluoride in solution. However, laboratory experiments indicate that two or more precipitation-filtration cycles are required for complete removal unless very thorough washing of the hydroxide precipitate can be effected. Since HF is readily volatilized from concentrated boiling HNO_3, the distillation of fluoride from dissolver solution was also evaluated as a removal method. It was found that aluminum, an unavoidable constituent of plant dissolver solutions, prevented effective volatilization of fluoride.

Fluoride was removed from plutonium in HNO_3-HF solution by precipitating and filtering plutonium hydroxide. However, when appreciable amounts of aluminum were present, complete fluoride removal was not readily obtained. In typical experiments, sodium hydroxide was added to a nitric acid solution containing 1.5 g of plutonium and 0.6 g of

fluoride per liter, to precipitate the plutonium. A measured fraction of the total volume was removed as clear supernatant, and the residue was reacidified and adjusted to the original volume. This cycle was repeated three additional times. In each case, analysis of the supernatants indicated that essentially all of the fluoride was in solution, and hence the fraction of fluoride removed was equal to the fraction of solution removed. In similar experiments, the plutonium in nitric acid solutions containing 2.7 g of aluminum and 3.0 g of fluoride per liter was precipitated with excess sodium hydroxide, lithium hydroxide, or ammonium hydroxide. Analyses of the supernatants indicate that even with thorough washing only 82, 47, and 42% of the fluoride can be removed in a single sodium hydroxide precipitation, a lithium hydroxide precipitation, and an ammonium hydroxide precipitation respectively.

Fluoride can be removed from nitric acid solutions by distillation since HF is readily volatilized from boiling 8 *M* HNO_3; its volatility increases with increasing HNO_3 concentration. With boiling 15.8 *M* HNO_3, the mole fraction of HF in the vapor is approximately eight times that in the liquid. However, the presence of 0.1 *M* aluminum in nitric acid solution prevents complete removal of fluoride by distillation. A laboratory-scale run was made using a stainless steel evaporator to test the effectiveness of this method for fluoride removal. A 12 *M* HNO_3 solution that was 0.16 *M* in NaF and 0.10 *M* in $Al(NO_3)_3$ was distilled to one-half its original volume. Concentrated HNO_3 equal to the volume of the distillate was added to the evaporator, and the solution was again evaporated to half volume. This procedure was then repeated. After the third distillation the residual solution and the distillates were analyzed for fluoride. The first distillate contained 16% of the fluoride, the second 9%, the third 9%, and residue 60%. Neither the addition of 0.1 *M* boric acid nor the addition of glass beads to the evaporator enhanced fluoride removal.

Purification of Plutonium by an HCl–Anion Exchange Process

The feasibility of isolating plutonium from HFIR target dissolver solution by sorption on anion exchange resin from 6 to 8 *M* HCl was reported last year.[2] Under these conditions the trivalent actinides and rare-earth fission products do not load, and the HCl effluent from the column can readily be converted to feed that is suitable for Tramex processing. The first efforts to use this process in TRU were unsuccessful, primarily because of simultaneous corrosion of Zircaloy-2 equipment and reduction of plutonium to the trivalent state, which does not load on anion resin at these conditions. Laboratory experiments carried out with strips of Zircaloy-2 metal in the resin column produced similar results. A 6 *M* HCl solution containing 2 mg/ml of plutonium was prepared. Initially, the plutonium was essentially all Pu(IV), with only a trace of Pu(VI). A small piece of Zircaloy-2 was placed in the solution, and the spectrum was determined at intervals up to 24 hr. The Pu(IV) began to disappear very quickly, and Pu(III) began to grow in. At the end of the test, almost all of the plutonium was in the trivalent state.

By adding oxidants to the feed and wash solutions, the formation of Pu(III) can be prevented even in the presence of Zircaloy-2. Oxidants found to be effective in preventing plutonium reduction in 8 *M* HCl solution contacted with Zircaloy-2 were 0.001 *M* $K_2Cr_2O_7$, 0.015 *M* H_2O_2, 0.40 *M* HNO_3, and 0.10 *M* LiOCl. However, recent evidence indicates that corrosion of Zircaloy-2 by HCl is greatly increased with these oxidants present; hence the usefulness of this process in presently installed equipment is questionable.

Additional laboratory studies have been made to determine the effects of several variables on plutonium loading for three different resins. Distribution coefficients for Pu(IV) were determined as a function of HCl and LiCl concentration; also, the effect that the addition of ethanol had on plutonium sorption was investigated.

Distribution coefficients for Pu(IV) as a function of HCl concentration were essentially the same for Dowex 1 and Dowex 21K resins (Fig. 5.11). Substantially lower distribution coefficients were obtained for Permutit SK resin. A detailed study of the effect of LiCl in the HCl solution was made. The results show that for most LiCl-HCl solutions, the plutonium distribution coefficient is independent of the LiCl : HCl ratio but is a function of the total chloride concentration. However, at acid concentrations below about 2 *M*, the distribution coefficients decrease sharply with decreasing

[2] D. E. Ferguson *et al., Chem. Technol. Div. Ann. Progr. Rept. May 31, 1966,* ORNL-3945, p. 111.

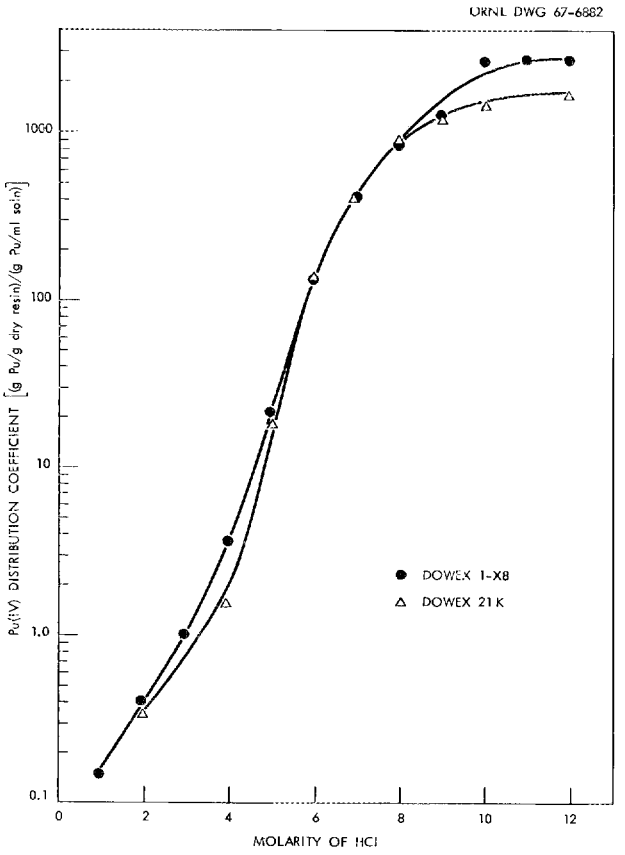

Fig. 5.11. Adsorption of Pu(IV) by Anion Exchange Resins Dowex 1 and Dowex 21K from Various Concentrations of Hydrochloric Acid. Resin was 50 to 100 mesh and in the chloride form.

acid concentration even at high LiCl concentrations (Fig. 5.12). Observations made during these studies show, qualitatively, that increasing the acid concentration of the feed while simultaneously decreasing the concentration of LiCl to maintain the same chloride concentration increases the kinetics for both loading and elution. The addition of a soluble alcohol, such as methanol or ethanol, to relatively low-acid feeds greatly increases the plutonium distribution coefficients. For example, the Pu(IV) distribution coefficient between Dowex 21K resin and 5 *M* HCl in water is 30; however, when the aqueous phase contained 40 vol % ethanol, the distribution coefficient was greater than 1000.

Plutonium elution from the anion exchange resin column can be accomplished either with dilute HCl or with concentrated HCl containing sufficient reductant to convert the plutonium from the tetravalent to the trivalent state. The latter method is desirable since the use of concentrated acid provides substantial decontamination from ruthenium and zirconium. Satisfactory elution of plutonium has been demonstrated with four to five column volumes of 5 to 8 *M* HCl containing 0.8% NH_4I, 0.1 *M* $FeCl_2$, or 0.5 to 1.5% ascorbic acid. Attempts to reduce the plutonium to the trivalent state in 5 to 8 *M* HCl by the addition of 1% NH_2OH, formic acid, or formaldehyde were unsuccessful. Although ammonium iodide satisfactorily reduces the plutonium, its use is not recommended unless the resin is discarded after each run, since the resin can not be satisfactorily regenerated.

When plutonium was eluted with 8 *M* HCl containing either 0.1 *M* $FeCl_2$ or 0.5 to 1.5% ascorbic acid, significant decontamination from both zirconium and ruthenium was obtained. Laboratory runs were made in which plutonium feeds contained macro amounts of these contaminants. Partial decontamination of both the curium fraction (which does not load) and the plutonium product was obtained. The results of several runs gave zirconium-niobium decontamination factors of 5 to 8 and ru-

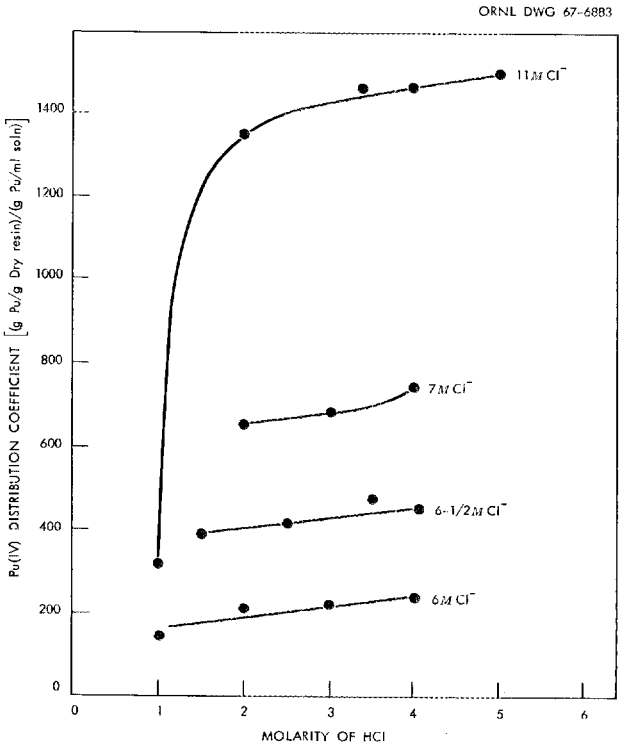

Fig. 5.12. Adsorption of Pu(IV) by the Anion Exchange Resin Dowex 21K from HCl-LiCl Mixtures.

thenium decontamination factors of 2.5 to 3 for the curium fraction. Decontamination factors of >100 for zirconium-niobium and 5 to 7 for ruthenium were obtained for the plutonium product.

Cf-Es-Fm Separations

Since the separation of Cf-Es-Fm and purification of some final products will be effected by ion exchange, column scale-up studies to high activity levels of ^{242}Cm were continued. The results confirm that this method can probably be used to process up to 100-mg batches of ^{252}Cf in conventional equipment. Very careful control of conditions and rapid processing are required in order to obtain satisfactory results. A new ion exchange technique that improves the control and decreases processing time has been tested with stable rare earths: Ion exchange resin of a very fine mesh size is used to increase the kinetics of ion exchange. A high-pressure feed pump makes it possible to maintain a constant, rapid flow through a long bed of this resin. The shorter processing time required with this system will decrease radiation damage to the resin, as well as the amount of radiolytic gas formed during processing.

Ion Exchange Separations at High Activity Levels

Several additional tests were made with macro quantities of ^{241}Am and ^{242}Cm to test the feasibility of chromatographic ion exchange separations at high activity levels. A glass column 1 in. in diameter and 28 in. long was packed with about 260 ml of Dowex 50W-X12 resin (200 mesh) in the ammonium form. Feed solutions that contained 125 to 250 mg of ^{242}Cm, 900 to 1700 mg of ^{241}Am, small amounts of Ni, Cu, Li, and Ca, and trace amounts of ^{106}Ru, ^{95}Zr-Nb, and rare-earth fission products in 0.1 *M* HCl were passed through the column at a flow rate of 3 ml cm^{-2} min^{-1}. Chromatographic elution was done at 80°C with 0.4 *M* α-hydroxyisobutyrate that had been adjusted to pH 4.6 with ammonium hydroxide.

These runs conclusively demonstrated that column design and flow rate characteristics are extremely important for satisfactory separations. In the first several runs the resin bed was compressed with a spring-loaded glass frit. Separations were adversely affected in these runs because of erratic flow rates; this behavior was due to partial plugging and apparent disintegration of the glass frit. In some runs the flow rate was reduced to such a low value that the resin charred; 15 to 20% of the curium was retained in the charred resin. The curium was recovered from this resin by leaching with 6 *M* HNO_3 for about 24 hr.

After the glass-frit retainer was replaced with a platinum screen, constant flow rates could be maintained during the elution. In a test using 125 mg of ^{242}Cm, resin degradation was not severe, even though the activity level of the loaded resin was ~1200 w/liter. The best separation demonstrated at this activity level gave one product fraction containing 80% of the ^{242}Cm and 10% of the ^{241}Am; the other fraction contained 90% of the ^{241}Am and 20% of the ^{242}Cm.

Evaluation of High-Pressure Ion Exchange Columns

We evaluated a high-pressure ion exchange system by determining its ability to separate Nd from Pr (a problem representative of those presented by the separation of trivalent actinides) by chromatographic elution with α-hydroxyisobutyric acid from Dowex 50 resin. A high-pressure pump was used to force solutions at a high flow rate through a column containing resin of small mesh size. The high-pressure feature permits greater freedom in the selection of operating parameters such as resin particle size, column length, and flow rate. The capabilities of this system are identical to those of a conventional ion exchange system, except that with the higher flow rates, results are obtained much more rapidly. Deleterious effects of radiation damage from high-activity-level materials are accordingly minimized. Operation has been unusually smooth, and essentially no problems have arisen.

Quantitative separations have been obtained routinely with flow rates up to 25 ml cm^{-2} min^{-1}. The experiments were done with ~100-mg quantities of rare earths. The degree of separation could be controlled from some overlap of the elution bands to complete separation, by regulating the eluent concentration. In one case, seven column volumes between the neodymium and praseodymium bands contained no detectable rare earths. With greater rare-earth loadings, a more-dilute eluent was required to yield the same degree of separation; alternatively, a larger column could be used with larger loadings. Operation at elevated temperature is generally desirable because the pressure drop

is less at a given flow rate, but temperature appears to have only a minor effect on kinetics over the range of conditions investigated.

In this system the resin column, 0.34 cm^2 in cross section and 150 cm long, was constructed from standard $\frac{3}{8}$-in. stainless steel tubing with a water jacket for temperature control. The column was packed with 50 ml of resin, which was retained at the bottom with a G-porosity stainless steel frit. It was used without difficulty at pressure drops in excess of 2000 psi, which were provided by a Beckman positive displacement pump. Connecting lines in the system were constructed of $\frac{1}{8}$-in. stainless steel (wall thickness, 35 mils).

The effects of eluent concentration, temperature, and flow rate were studied with this column. In general, decreasing the isobutyrate concentration of the eluent increases both the number of column volumes necessary to elute the sorbed ions and the separation between elements; decreasing the temperature during elution decreases both the quantity of elutrient required and the separations obtained. The effect of varying the flow rate was small over the range of 0.5 to 25 ml cm^{-2} min^{-1}.

An example of the excellent separation obtainable between neodymium and praseodymium at high flow rates is shown in Fig. 5.13. Figure 5.14 illustrates the increased separations obtained by decreasing the concentration of the eluent from 0.43 to 0.3 *M*. In this run, which was made at 80°C, about 26 column volumes of eluent were required before neodymium began to elute; this was reduced to six volumes by decreasing the temperature to 25°C. Complete separation of rare earths was still obtained.

Systems of this type have been installed in glove boxes, and testing with actinide tracers is in progress.

Preparation of Actinide Oxides for HFIR Targets

High Flux Isotope Reactor targets are made from pressed pellets of aluminum powder and actinide oxides, with the aluminum phase continuous to ensure satisfactory heat transfer during irradiation. To date, only $^{242}PuO_2$ has been used in these targets. Particles of the proper size were obtained

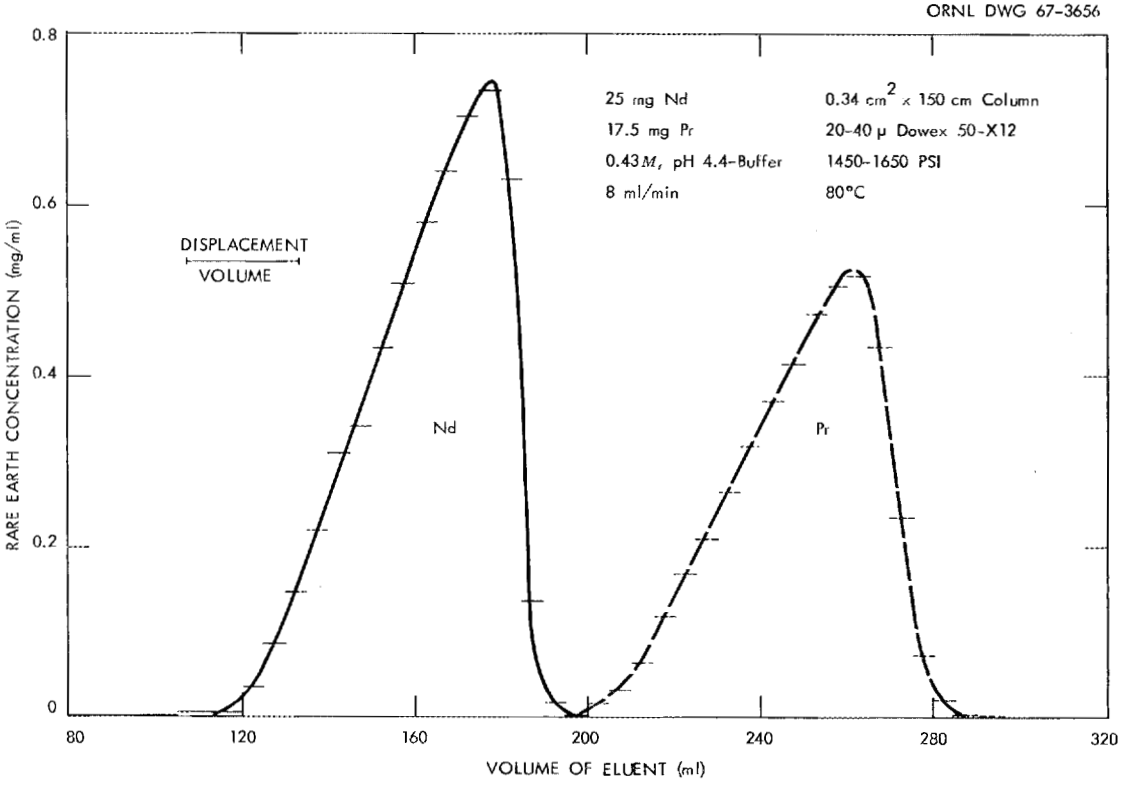

Fig. 5.13. Quantitative Nd-Pr Separation Is Obtained at High Flow Rate (23.5 ml cm^{-2} min^{-1}).

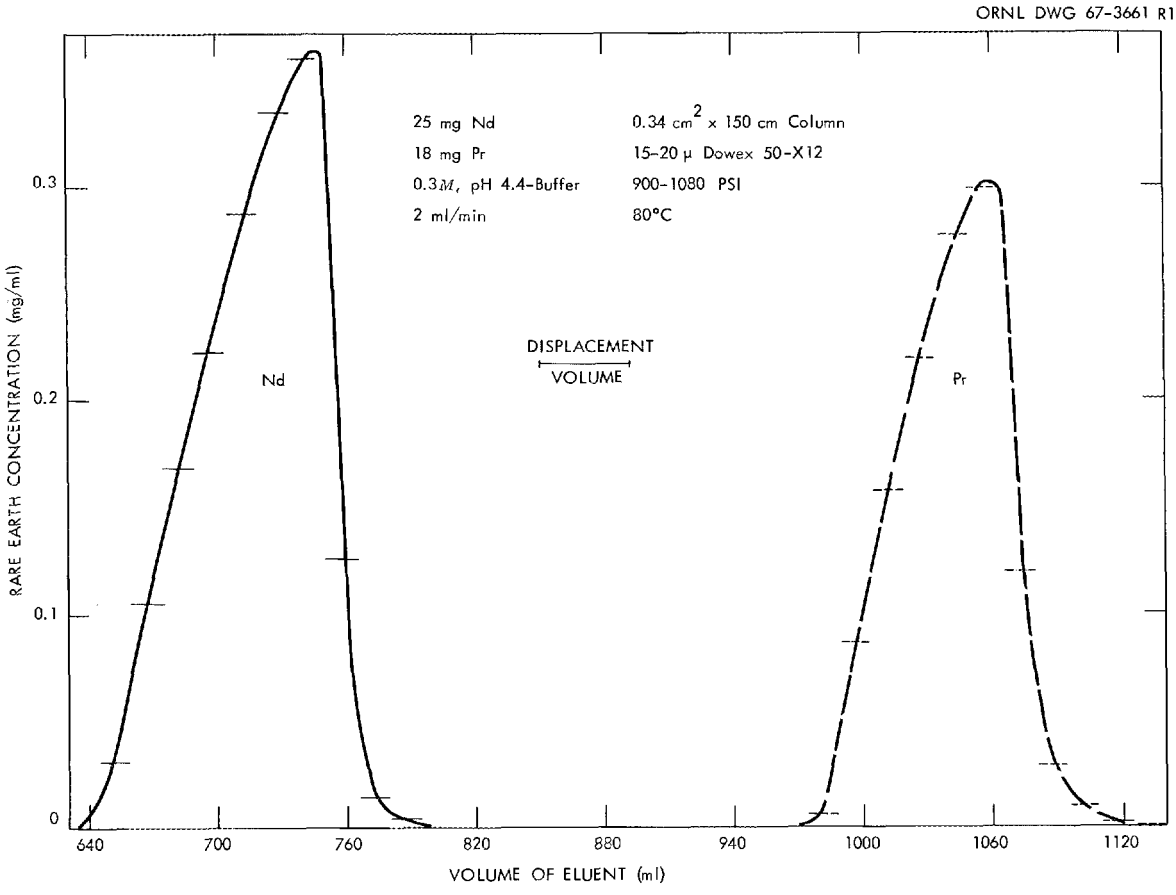

Fig. 5.14. Lower Eluent Concentration Yields Elution Bands That Are Sharp and Widely Separated.

by grinding and screening oxide prepared by a hydroxide precipitation method.[3] A sol-gel method that does not require grinding and screening appears to be suitable for the preparation of 20- to 200-μ-diam particles of dense americium-curium oxide. Last year[4] we reported the preparation of oxide microspheres of controlled particle size from rare earths (as stand-ins for americium and curium) by a modified procedure that is amenable to in-cell preparations. During the past year, two methods for preparing 10-g batches of sol were evaluated, and the modified sol procedure was tested with ^{241}Am.

The rare-earth sol process consists in precipitating the metal hydroxide by adding a dilute solution of rare-earth nitrate to a 20-fold excess of 8 *M* NH_4OH with stirring at 25°C, centrifuging the precipitate and washing it with water five or six times (the precipitate is reslurried and centrifuged, and the wash liquor is decanted, during each wash cycle), and heating the hydroxide for about 1 hr at 80°C (heating is not required for the light rare earths). During heating, the paste converts to a fluid sol that is about 0.5 *M* in metal; this sol can be formed into microspheres by standard procedures.

The two techniques investigated for the preparation of 10-g batches of sol are: filtration and washing in a jacketed filter funnel (which can be heated to convert the hydroxide paste to a sol), and filtration and washing in a sintered-metal bowl centrifuge (which can also be heated). Both procedures allow sol to be prepared in a single vessel and avoid handling and transfer of the hydroxide paste. After conversion to the sol, it can be collected by filtration through the filter medium.

Both these techniques appeared promising during initial evaluations in which europium hydroxide

[3] F. L. Culler, Jr., *et al., Chem. Technol. Div. Ann. Progr. Rept. May 31, 1964*, ORNL-3452, pp. 114–15.

[4] D. E. Ferguson *et al., Chem. Technol. Div. Ann. Progr. Rept. May 31, 1966*, ORNL-3945, pp. 111–16.

sols were prepared; however, additional development will be required before either can be considered operational. The optimum method for preparing sol requires efficient nitrate removal and a minimum of aqueous contact time during washing. To date, this has been best accomplished with the water-jacketed filter. Nitrate ratios of the product obtained with the centrifuge method have been somewhat high; a suitable method for heating the centrifuge cake without partially drying the hydroxide has not yet been developed.

The filter procedure was used to prepare 5-g batches of ^{241}Am hydroxide sol. In a typical experiment, 5 g of americium in dilute HNO_3 solution was precipitated with excess NH_4OH and filtered through a jacketed fritted-glass funnel. After water washing, the excess water was vacuumed through the filter, the filter was covered, and the moist filter cake was heated to about 85°C. The hydroxide paste was converted to a fluid sol in about 1.5 hr. This sol filtered readily; americium losses on the filter were estimated to be very low (1 to 2%). The final sol was 0.36 *M* in ^{241}Am, and the NO_3^- : Am mole ratio was 0.21. The sol was formed into microspheres by using standard tapered-column techniques, and the gel spheres were calcined to oxide spheres at 1150°C. These spheres were extremely uniform in particle size and would be suitable for incorporation into HFIR targets; however, surface blemishes, characteristic of microspheres prepared from dilute sols, were evident.

Preparations are presently under way for the in-cell preparation of CmO_2 and mixed CmO_2-AmO_2 microspheres using these procedures.

5.4 DEVELOPMENT OF PROCESS EQUIPMENT

Engineering studies in support of TRU are being continued. Emphasis has been on developing and testing solvent extraction flowsheets to be used in pulsed columns; tests were made both in prototype and in full-scale columns.

Hydraulic Testing of Pulsed Columns

"Cold" testing of proposed chemical flowsheets for separation of the heavy actinides from americium and curium has been continued in pulsed columns. Previously it had been shown that the Pharex flowsheet could not be operated in the TRU pulsed columns with the aqueous phase continuous. Severe wetting by the solvent of either tantalum or Zircaloy sieve plates caused flooding even at very low throughputs. Two alternative solutions to the problem are being investigated. One solution is to operate with the organic phase continuous; the other is to use ceramic sieve plates, which are preferentially wet by the aqueous phase. The first method was tested, using the Pharex flowsheet, with full-scale Zircaloy and tantalum TRU columns modified for operation with the organic phase continuous; satisfactory operation was achieved. In tests with ceramic pulse plates in a glass column and with the Pharex flowsheet, more than 400 hr of successful operation were obtained with the aqueous phase continuous. No wetting of the plates with organic was detected, even after the plates had been immersed in organic for 30 hr.

After these tests of equipment for the Pharex process were made, it was discovered that the presence of trace amounts of zirconium in the feed has a marked effect on the extraction coefficients for the actinides and reduces the separation factors to intolerably low values. A new process, Hepex, is being developed which uses di(2-ethylhexyl)phosphoric acid (HDEHP) as the extractant, instead of the 2-ethylhexyl phenylphosphonic acid (HEH[ϕP]) which is the Pharex solvent. Hepex is insensitive to the metallic impurities that adversely affect Pharex. However, Hepex exhibits similar hydraulic problems; it can be operated with the aqueous phase continuous with Zircaloy sieve plates (the extraction and scrub columns in the TRU equipment) but not with tantalum plates (the TRU stripping column) because of plate wetting. As with the Pharex process, operation with the organic phase continuous, or with the use of ceramic sieve plates, results in satisfactory operation of the Hepex process. One failure, due to organic wetting of the ceramic plates by the Hepex solvent, occurred when an aqueous feed containing hydrolyzed zirconium was tested; however, the plates were restored to good condition by cleaning with chromic acid.

The Tramex flowsheet was also operated successfully, with the organic phase continuous, in the prototype equipment that had ceramic plates. This showed that equipment for either mode of operation of the actinide separation step will be useful as standby equipment for the Tramex process.

From these studies it appears that operation with the organic phase continuous is the preferred method. If other aspects of the flowsheet are found to be favorable, the second-cycle equipment will be modified for this type of operation.

5.5 HFIR TARGET ROD FAILURES

In February 1967, it was observed that several TRU target rods had ruptured during irradiation in the HFIR. This was six to eight months before the processing of these targets had been scheduled. The Transuranium Element Production Program will not be seriously affected as a result of these premature target failures. It will be necessary to process and refabricate more targets than was originally planned; also, some reduction must be made in the estimated amounts of transuranium elements that will be made available next year.

The Failures

When the failures were detected, the target island in the HFIR flux trap contained 17 targets that had been irradiated for about a year in a reactor at the Savannah River Plant and 14 targets that had been irradiated only in the HFIR; each of the targets had been irradiated about 125 days in the HFIR. The total exposure to thermal neutrons (*nvt*) was 3.7×10^{22} neutrons/cm^2 at SRP and 2.6×10^{22} neutrons/cm^2 in the HFIR. The exposure to fast neutrons (1×10^{22} neutrons/cm^2) was essentially the same for all the targets because the SRP reactor has a very low fast-neutron flux.

The SRP-irradiated targets had been inspected and repaired in TRU prior to being put into the HFIR. Some of the targets had been damaged in the Savannah River reactor. Apparently the flow of coolant had caused the targets to flutter, and the spacer fins had beaten against the outer can, which directs coolant past the rod. This action of the fins had caused holes to form in some of the cans. New cans had been placed on nine of the targets, and a spacer (a "spider") had been put in each of the targets, near the top, to center the target rod in the can. Dimensional inspections and leak checks had assured the integrity of the targets prior to irradiation in the HFIR.

When the failures were detected, all rods were tested in the HFIR pool in flow loops with filters and ion exchange resin, which picked up residual activity. Suspect targets were transferred to TRU for further inspection. The cladding was found to be cracked on 5 of the 17 SRP-irradiated targets. The 14 targets that have been irradiated only in the HFIR have given no indication of leaking.

The failures consisted of cracks in the cladding near the centers of the target rods. Figure 5.15 is a photograph of the most severely damaged target. It was concluded that these failures occurred because the ductility of the cladding was reduced by the effects of irradiation, to the extent that the cladding was unable to deform to accommodate the normal swelling of the target material and the fission-gas pressures that were generated within the target pellet. The mechanism of the embrittlement has not yet been determined.

Effect on the Production Program

It is impossible to accurately predict the lifetime of the targets that have not failed. The following analysis, which includes a considerable amount of conjecture, is considered conservative.

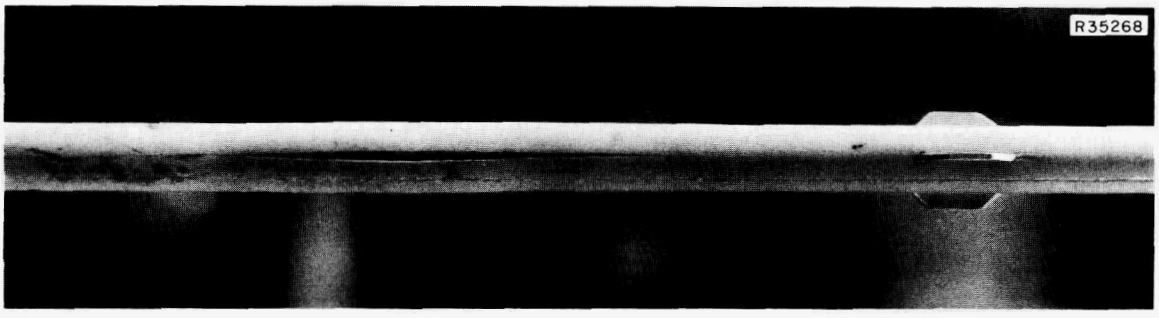

Fig. 5.15. SRP-Irradiated Target 56A Showing Crack in the Cladding. The hex can has been removed.

It is believed that the critical parameter is the total number of fissions that have occurred in the target. In very simple terms, we believe that the loss of ductility occurs very early but that the failure eventually occurs only after significant swelling of the cermet pellet. This latter effect is a function of total fissions. If this is correct, and if there are no mitigating effects, targets of the present design will begin to fail after about eight months of full-power irradiation in the HFIR. These targets have already been irradiated for nearly six months without any failures. Originally, plutonium-bearing targets were to be irradiated 16 to 18 months before being processed; recycle targets, most of which will contain americium and curium, were to be irradiated for periods of less than one year. For an equilibrium condition, which could occur after three years of operation of the HFIR, a typical loading of the target island would contain 20 of the first-cycle plutonium targets and 11 second- and third-cycle targets or targets for special irradiation. If the lifetime of a target proves to be eight months, about 30 target rods will have to be processed and fabricated per year to maintain 20 first-cycle targets in the target island. If the targets last for 16 months, which is the minimum life originally anticipated, only 15 will have to be processed and fabricated per year. Thus, if the target lifetime is only 8 months, each first-cycle plutonium target will have to be given an extra intermediate processing and refabrication. Subsequent cycles would not be affected significantly. The number of targets to be reprocessed and refabricated would be increased by about 50% (Table 5.6). TRU has sufficient capacity to accommodate this increase; therefore, the short target life should not have a substantial effect on the final rate at which transuranium elements can be made available to experimenters.

However, the failures will result in a reduction of the estimated amounts of transuranium elements that will be produced next year. It was planned that the 17 SRP-irradiated targets would be irradiated in the HFIR until September 1967, at which time they would have contained about 20 mg of californium, an order of magnitude more than is now available. The minimum time required to recycle the americium and curium in the failed targets will be six months; thus, the next significant increase in the amount of transuranium elements available may be deferred six months. Since contamination problems in HFIR have not been severe, the remaining SRP-irradiated targets will be irradiated in the HFIR either until they fail or until they have been irradiated as much as originally planned. The actual reduction in product availability will depend on how much longer these remaining targets can be irradiated.

Table 5.6. Modified Processing Requirements in TRU, Assuming Reduction in Lifetime of Target

Type of Target	Processing Requirement (targets/year)	
	Unlimited Target Life	Eight-Month Target Life
First-cycle plutonium	15	15
Intermediate-cycle plutonium		15
First recycle (americium-curium)	12	12
Other recycles	8	8
Total	35	50

6. Development of the Thorium Fuel Cycle

6.1 SOL PREPARATION BY SOLVENT EXTRACTION

A simple two- or three-stage extraction process was developed for the preparation of mixed ThO_2-UO_3 sols directly from solutions containing thorium and uranyl nitrates.[1] The nitrate (as nitric acid) is removed from the aqueous solution by extraction into an organic phase consisting of a long-chain amine extractant in an inert organic diluent. About 80 to 90% of the nitrate is extracted in the first stage. Subsequent heating of the aqueous phase converts it to sol and releases additional nitrate, which is extracted by amine in the second stage. This sol may be dried to gel fragments or evaporated to a concentration that is suitable for forming microspheres. In laboratory studies, sols were prepared from aqueous thorium nitrate solutions containing up to 68 mole % uranyl nitrate. Sols having compositions that are currently of interest for reactor fuels (22 to 25 mole % uranium) have been made in the engineering studies at the rate of 1 kg of oxide per hour.

Laboratory Studies

Typical flowsheet conditions used in preparing the sol (and, subsequently, oxide microspheres having a thorium : uranium atom ratio of about 3.5) are presented in Fig. 6.1. One volume of an aqueous solution about 0.21 *M* in $Th(NO_3)_4$ and 0.06 *M* in $UO_2(NO_3)_2$ is contacted in glass mixer-settler equipment for at least 2 min with about 1.9 volumes of an organic phase composed of 0.75 *M* Amberlite LA-2 (an extensively branched secondary amine, *N*-lauryltrialkylmethylamine) in *n*-paraffin, the commercial equivalent of *n*-dodecane.

To ensure rapid phase separation the extraction is made, with the organic phase continuous, at 50 to 60°C. The phases are separated, and the aqueous phase is heated for at least 10 min at 95 to 100°C. The aqueous phase changes from a yellow solution to a dark-red sol, indicating the further hydrolytic release of nitrate ions. This nitrate is then extracted when the aqueous phase is again contacted with the amine extractant in the second stage. Although the flowsheet in Fig. 6.1 is based on cocurrent flow, countercurrent or crosscurrent flows are equally effective. More than 98% of the extractable nitrate is removed in two stages, yielding a sol with a nitrate : metal mole ratio of about 0.2. The organic solvent containing amine nitrate from the second stage is scrubbed with water to remove entrained sol; the amine nitrate is then converted to free amine by contacting the organic phase with an aqueous phase containing sodium carbonate (at least 1.05 moles per mole of amine nitrate).

In this particular example, water was evaporated from the aqueous phase to provide a final sol having the following composition: 1.10 *M* in thorium, 0.32 *M* in uranium, 0.30 *M* in nitrate, and 0.01 *M* in carbon of an unspecified form. The crystallite size, according to x-ray analysis, was 35 to 40 A. Spheres were formed by injecting droplets of this sol into 2-ethyl-1-hexanol (2EH) containing 0.5 vol % H_2O and suitable surfactants. The gelled spheres were dried overnight at 100°C, held at 170 to 180°C for about 5 hr, and then calcined in air at 1150°C. Finally, the uranium was partially reduced by contacting the calcined spheres with Ar–4% H_2 for 4 hr at 1150°C. The resulting spheres were shiny black and had an oxygen : uranium atom ratio of 2.003. The measured porosity was less than 1%, and the density was equivalent to > 95% of the theoretical density of the oxide solid solution. Individual spheres 150 to 350 μ in diameter resisted crushing forces of 940 to 2000 g.

[1] J. G. Moore, *An Amine Solvent Extraction Sol-Gel Process for Preparing ThO_2-UO_3 Sols from Nitrate Solutions*, ORNL-4095 (in press).

The complete process was demonstrated, in batch operations on a laboratory scale, with thorium nitrate solutions containing 17 to 26 mole % uranyl nitrate. Stable sols that contained up to 68 mole % uranium were prepared by extracting the nitrate with Amberlite LA-2 (Table 6.1). A system employing approximately 1.5 moles of amine per mole of initial nitrate, four extraction stages, and three digestion stages was used to ensure that nearly all extractable nitrate was removed. The nitrate extraction was essentially complete (98 to 99.6%) after two stages.

The nitrate : metal mole ratio observed after the first extraction stage varied as a function of the uranium and thorium composition; the values decreased linearly from about 0.70 for pure thorium starting solutions to about 0.25 for thorium nitrate containing approximately 50 mole % uranium. The mole ratio in the sol product (after all extractions) also decreased linearly as the uranium content increased to about 25 mole % uranium. The nitrate/metal mole ratio then remained constant at about 0.16 for sol products containing 25 to 68 mole % uranium (Table 6.1).

Sols were prepared by use of similar extraction procedures employing primary, secondary, and tertiary amines such as Primene JM-T, 1-nonyldecylamine, ditridecyl P, and Adogen 364; however, most of the development work was done with Amberlite LA-2. Systems based on approximately 1.2 to 1.5 moles of amine per mole of nitrate were used to ensure complete removal of the extractable nitrate.

The use of several different diluents, including *n*-dodecane, *n*-paraffin, diisopropylbenzene, diethylbenzene, and Amsco 125–82, was studied. For convenience, most of the laboratory tests employed 0.6 to 0.75 *M* amine solutions in *n*-dodecane or *n*-paraffin.

The total metal ion concentration in the aqueous solution must be less than 0.6 *M* to prevent the formation of solids during the first extraction. Al-

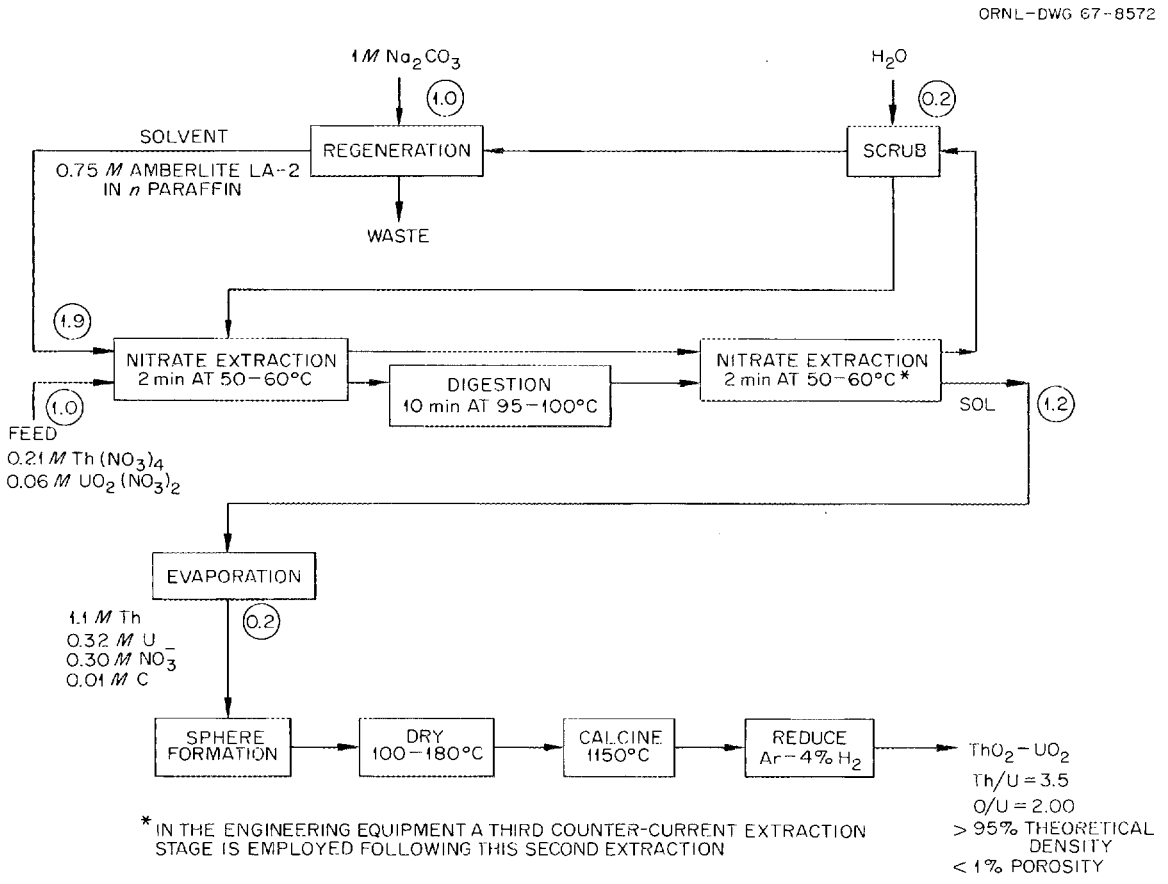

Fig. 6.1. Preparation of ThO_2-UO_2 Microspheres by the Amine Denitration Process.

Table 6.1. Preparation of ThO_2-UO_3 Sols

Procedure: 6C · 20D · 6C · 20D · 6C · 20D · 6C, where C = contact at 50 to 60°C, D = digestion at ~100°C, and numerals indicate time in minutes

Amine: 0.77 *M* Amberlite LA-2 in *n*-paraffin

Amine/NO_3^- mole ratio: 1.5

Flow: cocurrent

Aqueous concentration: 0.22 to 0.30 *M* (Th + U)

Mole Percent U	First Extraction		Second Extraction		Third Extraction		Fourth Extraction	
	NO_3^-/Metal Mole Ratio	pH	NO_3^-/Metal Mole Ratio	pH	NO_3^-/Metal Mole Ratio	pH	NO_3^-/Metal Mole Ratio	pH
0	0.73	4.46	0.31	4.33	0.28	4.99	0.28	4.31
2.5	0.68	4.24	0.30	3.93	0.28	4.74	0.26	4.47
5.3	0.67	5.00	0.28	4.09	0.24	4.57	0.25	4.65
9.4	0.62	4.71	0.25	4.61	0.24	4.84	0.23	4.88
18	0.55	4.84	0.21	5.02	0.20	4.38	0.19	4.46
26	0.45	4.13	0.19	4.27	0.16	4.46	0.16	4.50
35	0.39	4.76	0.23	4.67	0.19	4.67	0.16	4.77
53	0.26	4.92	0.20	5.12	0.20	5.14	0.18	5.06
68	0.25	5.06	0.16	5.46	Gelled			

though these solids liquefy on heating, they could become a source of difficulty in a continuous process; thus, their formation was avoided in the laboratory studies.

The aqueous phase must be digested for at least 8 to 10 min at 95 to 100°C after the first extraction step in order to achieve a nitrate : metal ratio of 0.2 or less in the final sol. The use of shorter digestion periods or lower temperatures will yield sols with higher nitrate : metal ratios; for example, values of these ratios for sols produced after digestion periods of 4 min at 100°C or 20 min at 80°C were each equivalent to about 0.4.

Sols prepared by the amine denitration process were found to be especially sensitive to the type and the concentration of surfactant used in operation of the sphere-forming column. For example, in the formation of microspheres from a ThO_2-UO_2 sol that had a thorium : uranium ratio of 3.5 and had been prepared by an alternative method (blending thoria and urania sols), 2EH containing 0.3 vol % Span 80 (sorbitan monooleate) and 0.5 vol % Ethomeen S/15 (the condensation product of a primary fatty amine with ethylene oxide) was used.[2] These same conditions and column operations resulted in severe cracking and/or "cherry pitting" of the microspheres that were formed from a sol prepared by the amine process. However, it was possible to produce good-quality spheres from the latter by reducing the concentration of each of the surfactants to about 0.1 vol % or less; up to 0.15 vol % of these surfactants could be used if the concentrated sols were refluxed for about 30 min or if the initial water content of the 2EH was increased to about 1.5 vol %. Other surfactants – Alkanol OD (a long-chain alcohol–ethylene oxide condensation product) and bis(2-ethyoxyethyl) phthalate – also produced satisfactory spheres; the concentration levels of these agents were not as critical, with regard to sphere formation, as those of Span 80 and Ethomeen S/15.

Engineering Studies

Based on the results of laboratory studies, equipment for continuous production of ThO_2-UO_3 sols was designed and built. Mixer-settlers constructed

[2] R. G. Wymer and D. A. Douglas (compilers), *Status and Progress Report for Thorium Fuel Cycle Development for Period Ending December 31, 1965*, ORNL-4001, p. 42.

of 3-in. glass pipe were selected as the contacting devices (Fig. 6.2). They are geometrically safe. Each mixer is divided into six compartments, each of which contains an agitator. The agitators are mounted on a single shaft, which is driven by a variable-speed motor. The solvent and the aqueous phase enter at the top and flow cocurrently through the mixer to the settler, which is a pipe tee located at the bottom of the mixer. The interface is maintained below the mixer to ensure an organic-continuous dispersion in the mixer. The position of the interface is controlled by a simple jackleg and an adjustable weir on the aqueous outlet of the settler. The digester is merely an enlargement of the aqueous jackleg of the first-stage settler. Temperature is controlled by circulating heated water through the baffles in the mixers and a coil in the digester. A large heat exchange area and low ΔT (temperature differential) are used to minimize local drying of the sol.

In this equipment three stages of extraction are used to ensure nitrate removal. Digestion takes place after the first stage. The second stage is cocurrent with respect to the first stage, primarily to remove the small amount of uranium that is extracted by amine in the first stage. The uranium is stripped by the low concentration of nitrate still remaining in the sol in the second stage. The third stage is countercurrent with respect to the first and second stages. This arrangement produces a lower nitrate content in the sol product because the equilibrium concentration is lower and vigorous mixing can be used without concern for entrainment in the solvent. The nitrate-loaded solvent leaving the second stage is scrubbed with water to remove entrained sol. The amine nitrate in the scrubbed solvent is regenerated to the free amine, by contacting the solvent with sodium carbonate solution, for recycle to the extraction section.

The equipment has been tested with the reference flowsheet (Fig. 6.1) at the design rate of 1 kg of ThO_2-UO_3 (mole ratio, 3 : 1) per hour. About 900 liters of 0.3 *M* sol was produced during the engineering study. The nitrate : metal mole ratio in the sol has been consistently below 0.10,

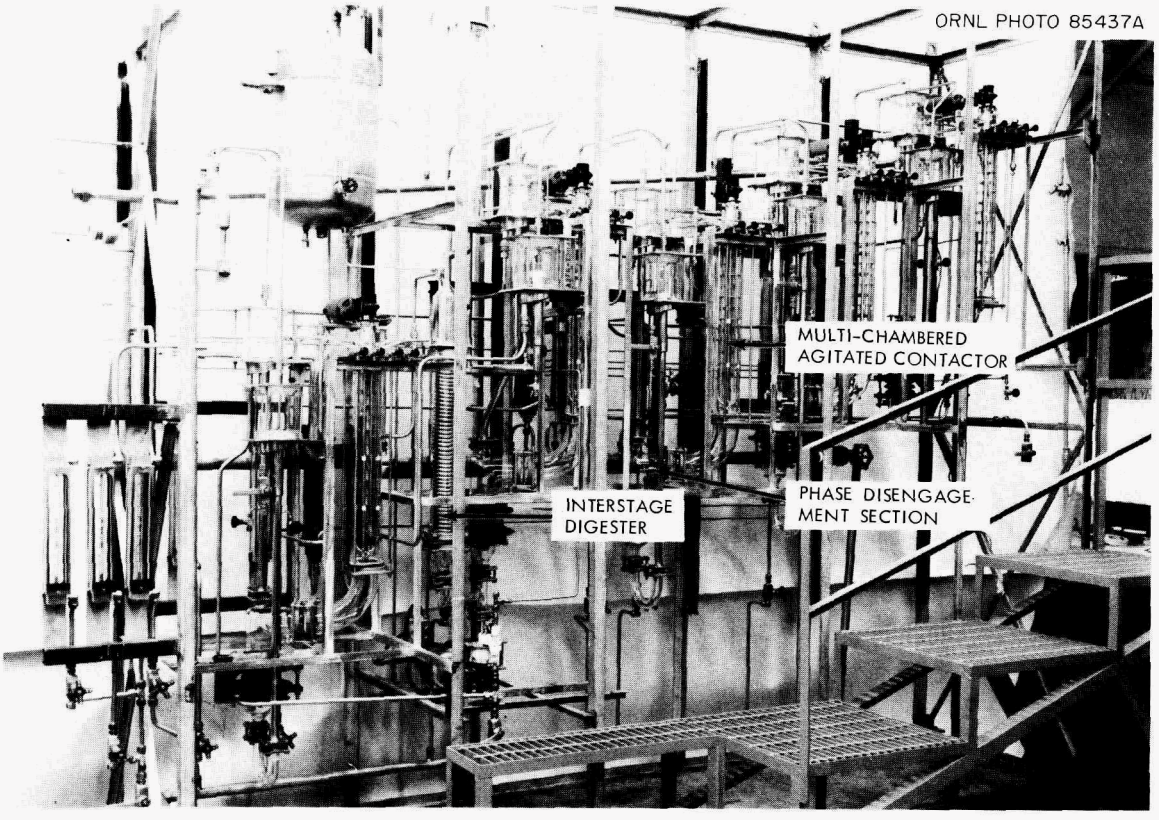

Fig. 6.2. Mixer-Settlers for Use in the Continuous Preparation of ThO_2-UO_3 Sols by Solvent Extraction.

about one-half of that obtained in the laboratory studies. The crystallite size of the sol is slightly larger (42 to 46 A) than that obtained in laboratory tests. Several batches of sol were concentrated to 1.5 *M* in a forced-circulating vertical-tube evaporator (Fig. 6.3). A high degree of turbulence and a large heat exchange area are maintained to minimize drying of sol on the heater tubes. The superheated sol is forced tangentially into the body of the evaporator to aid in deentrainment of the vapor. Very few solids were formed, and foaming did not occur even with operation at a vacuum of 25 in. Hg. The concentrate was very fluid and stable. Representative samples of the concentrated sol were formed into microspheres and fired to produce dense ThO_2-UO_2. This sol was not so sensitive to surfactant concentration in the forming column as was the laboratory-produced sol.

The equipment has operated very smoothly. No difficulty has been encountered in maintaining organic-continuous dispersions, and the interface control is very stable. Some emulsion accumulated in the first-stage settler during the early runs; however, most of it was broken in subsequent stages, so that the sol product contained less than 0.1 vol % solvent. During the latter runs the scrub was recycled to the first stage, and virtually no emulsion was formed. Entrainment of aqueous

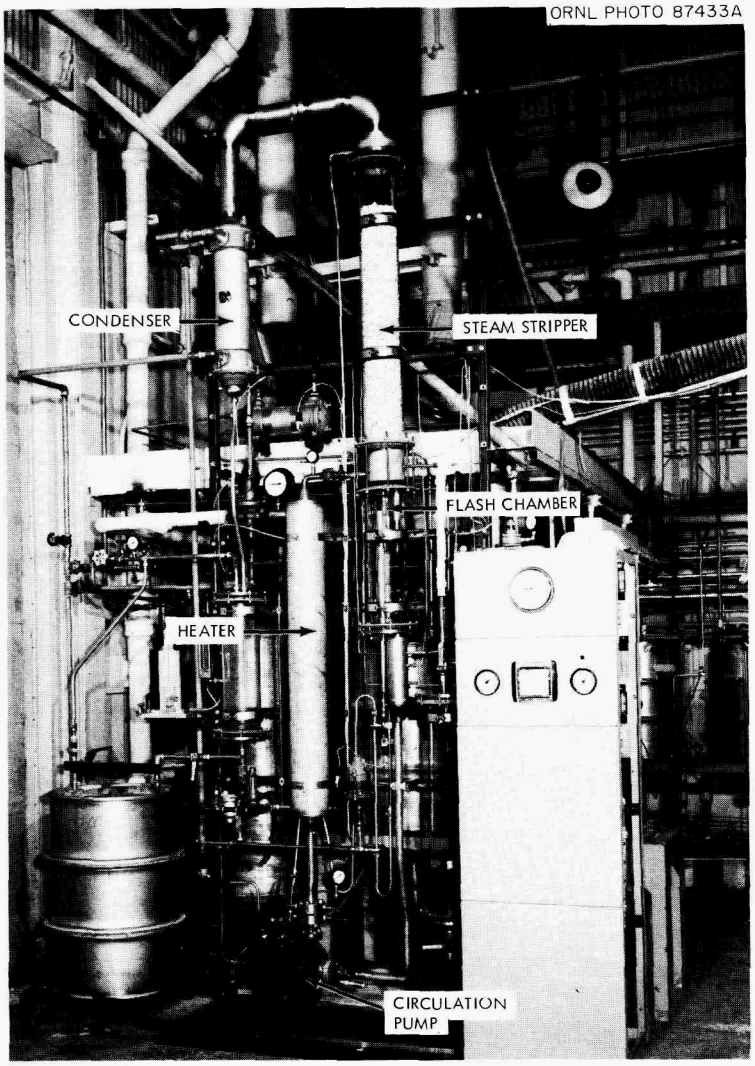

Fig. 6.3. Forced-Circulation Evaporator for Concentration of ThO_2-UO_3 Sols.

phase in the solvent was a problem only in the solvent stream leaving the extraction section. The entrainment was directly dependent on agitator speed in the mixer, ranging from 0.15% at 300 rpm to 0.8% at 600 rpm. Entrainment is the only significant cause of Th and U losses (about 0.1%). We believe that these losses can be reduced by improved scrubbing of the solvent before regeneration. Efficiencies of 90 to 95% have been obtained for the mixers at agitator speeds of 300 to 500 rpm.

6.2 SOL-GEL PROCESS: FURTHER DEVELOPMENT AND NEW APPLICATIONS

Preparation of Thorium Dicarbide by Sol-Gel Methods

We continued studies of a sol-gel process for preparing carbide fuels for nuclear reactors. Work to date has emphasized the preparation of thorium dicarbide, although we expect to extend this work to other carbides of nuclear interest, such as uranium carbide. The sol-gel approach involves preparation of a ThO_2-C sol, forming a ThO_2-C gel from the sol, and subsequently converting the gel to dicarbide in the firing step. Work performed during the past year was concerned mainly with studies of the basic properties of ThO_2-C sols, methods of preparation, and conversion of the ThO_2-C gels to thorium dicarbide.

Conversion of ThO_2-C Gels to Thorium Dicarbide. – The major problems involved in optimizing the sol-gel process for thorium dicarbide preparation include minimizing the free carbon content, reducing residual oxygen, and controlling porosity in the dicarbide product. We used gel fragments rather than microspheres in the initial work. These studies showed that gross porosity was the major problem (Fig. 6.4). A single-phase ThC_2 structure (by x-ray diffraction) was formed when the ratio of combined carbon to thorium was 1.85 or greater. The free carbon content of the product was about 400 ppm when there was a carbon deficiency (i.e., when ThC was also present) and up to 7000 ppm in the monophasic dicarbide product. The minimum conversion temperature in argon was 1800°C, whereas in vacuum it was 1500°C.

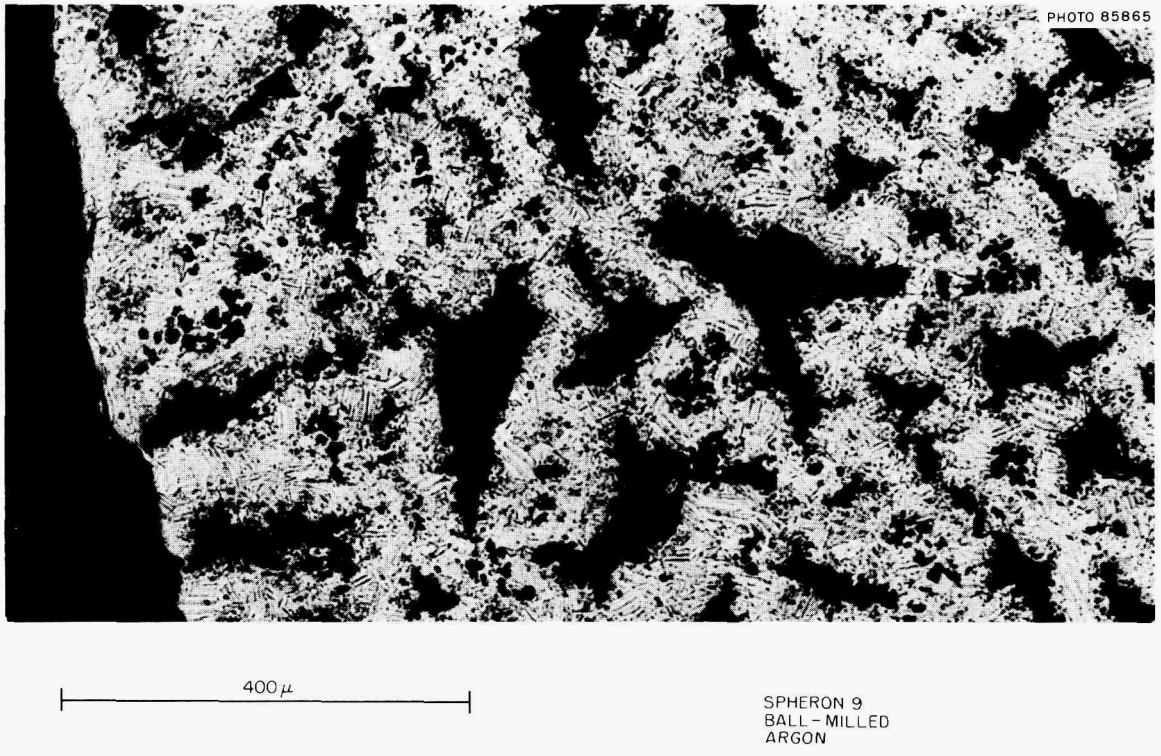

Fig. 6.4. Thorium Dicarbide Shard Showing Gross Porosity.

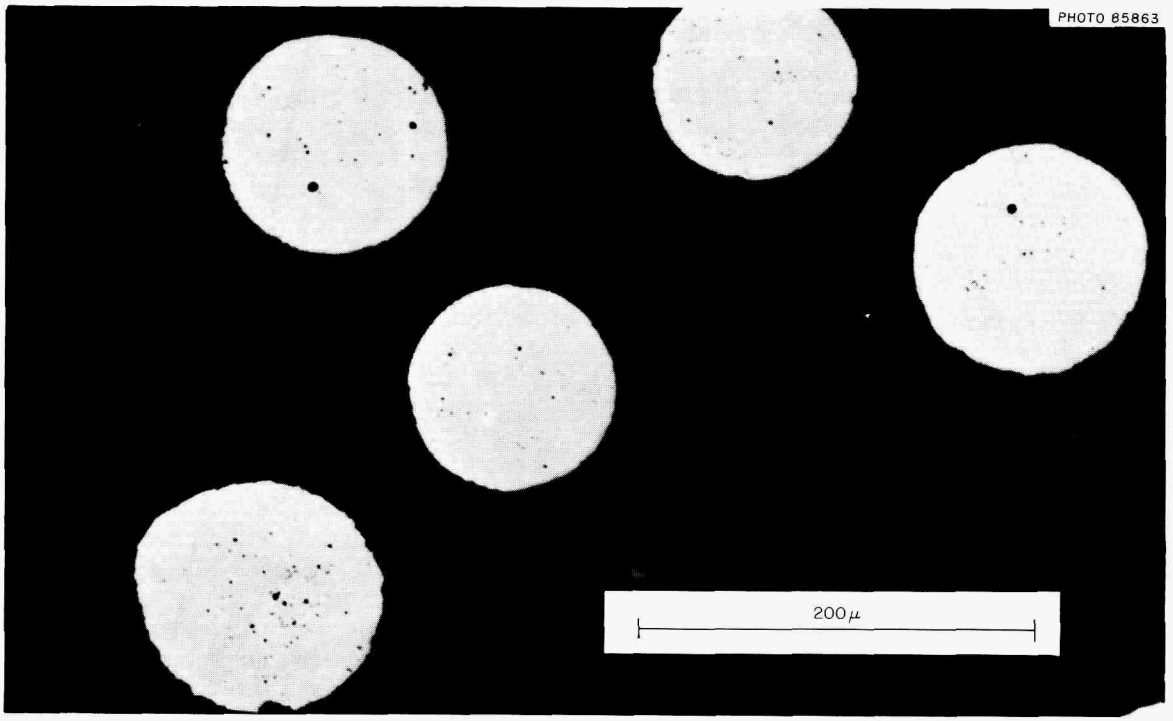

Fig. 6.5. Cross Section of ThC_2 Microspheres.

Results of several trial conversion runs that employed gel microspheres showed that less porosity was present in spheres than in shards and that the smaller spheres were the least porous. By firing the spheres in argon to retard the reaction rate, reasonably dense microspheres could be attained. An in-line infrared CO analyzer was used to monitor the reaction, which took 1 to 4 hr at 1850 to 2050°C. Near the end of the reaction, the CO concentration in the argon sweep gas dropped; vacuum was then applied to complete the conversion. Under the conditions of these experiments, the argon sweep gas contained about 4000 ppm of CO at steady state, which is controlled by diffusion of CO out of the sample crucible.

On six such runs, microspheres with densities greater than 90% of theoretical were obtained. Results are summarized in Table 6.2. The measured open porosities were about 1%; closed porosities were, therefore, about 6 to 8%. This is evident in the metallographic cross sections (Fig. 6.5). The crush resistance of these spheres is adequate for all anticipated requirements. The external appearance is not as uniform as would be desired (Fig. 6.6). Both oxygen and free carbon contents are reasonably low. In the five runs (Table 6.2) conducted at 1950° or above, the free carbon content ranged between 700 and 1900 ppm, and the oxygen content ranged between 300 and 1100 ppm. The extent to which these elements can be further removed is currently under study.

In general, the final firing method must be based on a critical balance between grain growth, sintering, and chemical conversion. The presence of the carbon greatly retards sintering of ThO_2; for example, Hamner's[3] work showed that the presence of small amounts of carbon in the starting material (ThO_2 microspheres) caused a permanent porosity to be left in the ThC_2 microspheres after conversion. If the temperature at which conversion to carbide occurs is too low, sintering of the grains establishes the outside dimensions and further heating simply consolidates the small pores into large internal pores. Under a CO overpressure of about 1 atm, conversion to carbide occurs at a temperature where grain growth is optimized and high-density spheres can be obtained,

[3]R. G. Wymer and D. A. Douglas (compilers), *Status and Progress Report for Thorium Fuel Cycle Development for Period Ending December 31, 1965*, ORNL-4001, pp. 70–74.

provided the shrinkage path is not too long. The presence of CO during this process may also facilitate grain growth by enhancing diffusion on the solid surfaces.

Preparation and Properties of Thoria-Carbon Sols. – In order to better understand the problems associated with the preparation of thoria-carbon sols, it was necessary to study the properties of these mixed sols. Electron microscopic techniques and viscosity and electrophoretic measurements were used in studying the interactions between thoria sols and carbon blacks. Examination of carbon-rich mixed sols by electron microscopy showed that the carbon black particles were coated by thoria particles; on the other hand, electron micrographs of thoria-rich sols suggested that the carbon blacks were dispersed to the individual crystallites. Other evidence of a carbon-thoria interaction is obtained from measured zeta potentials. The zeta potential of the ThO_2-C sol is +55 mv, which is about the same as that of a pure ThO_2 sol (+67 mv). In contrast, conventional aqueous carbon sols have a negative zeta potential.

Carbon blacks with widely varying surface areas and chemical activities have been tested; all are dispersed by ThO_2. To date, extension of this dispersion study to other oxide-type sols has shown that only urania sols behave like thoria sols; the behavior of silica, zirconia, europium hydroxide, and boehmite (AlOOH) sols is not similar.

Electron micrographs give no visual evidence of a well-defined "interaction ratio" between ThO_2

Table 6.2. Properties of Thorium Carbide Microspheres

Run No.	II-146	II-148	II-150	III-14	III-16	III-18
Maximum temperature, °C	2050	1950	1850	1975	1975	2030
Time at temperature, hr	1	2.5	4	2.5	2.5	4[a]
X-ray diffraction[b]						
ThO_2	?	ND	?	ND	ND	ND
ThC	v. wk.	ND	wk.	v. wk.	v. wk.	v. wk.
ThC_2	P	P	P	P	P	P
Thorium, %	90.93	91.25	90.88	91.23	91.23	91.45
Total carbon, %	9.09	8.74	8.85	8.57	8.52	8.65
Oxygen, %	0.096	0.045	0.360	0.033	0.032	0.106
Σ (material balance)	100.12	100.04	100.09	99.83	99.78	100.21
Free carbon, %	0.12	0.12	0.47	0.066	0.106	0.186
ThC_x (value of x)	1.92	1.83	1.83	1.81	1.79	1.80
Density,[c] g/cm^3						
Particulate	>8.75	8.83	8.75	>8.91	>8.76	>8.97
Hg intrusion	8.84	8.95	8.87	9.00	8.84	9.06
Helium				9.04	8.77	9.10
Open porosity,[c] %	<1	1.3	1.4	<1	<1	<1
Resistance to crushing,[d] g	700	790	940	800	700	

[a]Temperature was gradually increased from 1700 to 2030°C during the 4 hr.

[b]P indicates phase present; v. wk., very weak; ?, may be present; ND, not detected.

[c]"Particulate" density means the bulk density of single spheres; "Hg intrusion" density is the density after subtracting the volume occupied by Hg at 15,000 psi. The difference between these two values gives the "open porosity" for pores >120 A. The helium density subtracts all open pore volumes, including those <120 A.

[d]Corrected to 240-μ-diam sphere by assuming that resistance to crushing is proportional to the square of the diameter.

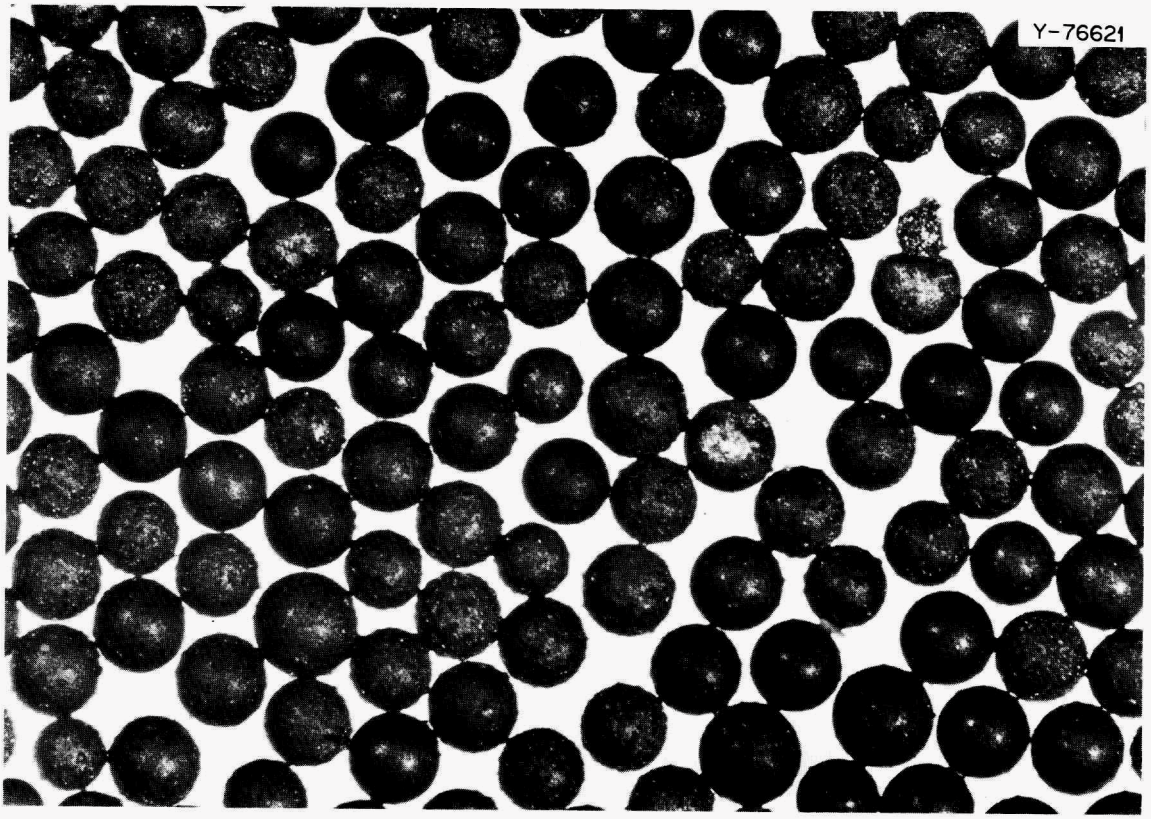

Fig. 6.6. External View of ThC_2 Microspheres

and carbon sols, but "viscosity titrations" indicate that there is a limiting value beyond which a given thoria sol will not suspend any additional carbon black. This value appears to be a function of surface area. As increasing amounts of carbon black are blended into thoria sol, the viscosity increases slowly from a few centipoises to about 50 centipoises. Beyond that value, additional carbon causes a very rapid increase in viscosity (up to hundreds of centipoises), thus providing a sort of titration end point. As the total available thoria surface is varied, either by changing the thoria concentration or by using a thoria sol of different crystallite size (i.e., different specific surface area), the carbon capacity at the end point changes in direct proportion to the surface area of the thoria. Thoria concentrations of 250 to 500 g/liter were used in these viscosity experiments. The carbon content at the end point was as high as 350 g/liter, depending on the surface-area relationships.

Although both acid and alkaline carbons are dispersed by thoria, the former yield a more permanent mixed sol. Preparations from acid carbons have been stored for one year without evidence of instability, whereas alkaline carbons give mixed sols that tend to gel and become lumpy within about a week. The surface area of the carbon black is important. If it is too high ($>1000\ m^2/g$), the mixed sol is too viscous; if it is too low ($<30\ m^2/g$), carbon dispersal is slow and difficult. For handling convenience, pelletized carbon black is much preferred over the fluffy form. Spheron 9 (Cabot Corporation) carbon black appears to be optimum for ThO_2-C sol preparation. This channel black has a specific surface area of $105\ m^2/g$, a volatiles content of about 5%, and a pH of 4.5 in water. Sols with good fluidity characteristics can be prepared easily, over the range of carbon : thoria ratios of interest, with this carbon black.

In the blending process the pelletized carbon black must be broken into its basic aggregates; after it is separated to this degree, the thoria sol itself acts as a dispersing and stabilizing agent. We have investigated ball milling, recirculation through a centrifugal pump recycle loop, and ultra-

Table 6.3. Properties of UO_2-ThO_2 Microspheres Prepared by Mixing UO_2 and ThO_2 Sols

Microsphere diameters: 250–297 μ; firing temperature: 1200°C

Preparation Code	Th/U Weight Ratio		Uranium Enrichment (% ^{235}U)		Density		Surface Area (m^2/g)	Carbon (ppm)	Gas Release to 1200°C in Vacuum (cm^3/g)
	Desired[a]	Measured	Desired	Measured	g/cm^3	Percent of Theoretical			
OL-2	0.3333	0.3337	43.5	43.3	10.34	96.5	0.004	<20	0.02
OL-3	1.000	1.005	65.3	65.04	10.31	98.3	0.006	30	0.01
OL-4	1.857	1.886	93.18		10.08	97.5	0.005	20	0.011

[a]The desired percentages of UO_2 (by weight) for OL-2, OL-3, and OL-4 were 75, 50, and 35 respectively.

sonic agitation as methods of preparation. Ultrasonic agitation was the most successful method tried.

Preparation of Mixed Oxide Sols

During the past year we have been studying methods whereby ThO_2-UO_2 sols may be prepared in any desired thorium : uranium atom ratio with good control of composition. Emphasis is being placed on attaining a thorium : uranium ratio of about 3 in the final oxide, since the most useful fuel for reactors utilizing thorium will probably have this thorium : uranium ratio. The original ORNL sol-gel process[4,5] is limited to sols having uranium contents of less than about 10%.

We have studied two approaches to the preparation of UO_2-ThO_2 sols. One method involves simply mixing UO_2 sols prepared by the formate method[6] with ThO_2 sols prepared from steam-denitrated thoria.[4,5] The other method involves sol preparation by coprecipitating thorium-uranium(IV) hydroxides and then peptizing the hydroxides to a stable sol. The latter approach was not studied beyond preparation of the sols. We have demonstrated the mixed-sol method through final product microsphere evaluation, and irradiation test specimens have been prepared from these materials.

It was previously thought that one of the major problems with the mixed-sol method would be close control of the thorium : uranium ratio. However, this was not the case (Table 6.3). Large (150-g) batches of mixed sol were prepared. Mixing of the sols was accomplished volumetrically by using calibrated glassware. Since the potential uses of these sols required different degrees of ^{235}U enrichment, the UO_2 sols to be mixed with the thoria sol were prepared by mixing a 93.18%-enriched UO_2 sol with a natural UO_2 sol. The mixed sols were formed into gel microspheres under standard operating conditions; about 40 to 60% of these microspheres were in the desired 210- to 297-μ-diam range (after calcination) and were of excellent quality. Also, they were characterized by high densities and low carbon contents.

We have prepared kilogram-sized batches of UO_2-ThO_2 microspheres in which the thorium : uranium atom ratios were 4.8 and 3.4.[7] These microspheres were prepared from fully enriched uranium and were used for irradiation tests of coated particles. The spheres were characterized by very high density, good resistance to crushing, and essentially "geometric" surface area (Table 6.4). X-ray diffraction measurements showed that solid solution was achieved. The spheres produced by

[4]J. P. McBride (compiler), *Preparation of UO_2 Microspheres by a Sol-Gel Technique*, ORNL-3784 (February 1966).

[5]D. E. Ferguson (compiler), *Status and Progress Report for Thorium Fuel Cycle Development for Period Ending December 31, 1962*, ORNL-3385.

[6]C. C. Haws, J. L. Matherne, F. W. Miles, and J. E. Van Cleve, *Summary of Kilorod Project — a Semiremote 10 kg/day Demonstration of $^{233}UO_2$-ThO_2 Fuel Element Fabrication by the ORNL Sol-Gel Vibratory Compaction Method*, ORNL-3681 (August 1965).

[7]W. D. Bond *et al.*, *Preparation of $^{235}UO_2$-ThO_2 Microspheres by a Sol-Gel Method*, ORNL-TM-1601 (August 1966).

Table 6.4. Analyses of UO_2-ThO_2 Microspheres (97.69% ^{235}U) After Firing

First firing – fired to 1100°C and reduced for 2 hr in Ar–4% H_2; cooled to 25°C in Ar
Second firing – the 210- to 297-μ-diam fraction from the first firing was fired to 1400°C and reduced 4 hr in H_2; cooled to 25°C in Ar

	Sample No.[a]		
	3371-78-1400[b]	3371-80-1400	3371-82-1400
Sol preparation No.	47-27-97	47-27-97	47-49A-97
Th/U atom ratio[c]	3.41	3.41	4.79
U, %	10.95	10.95	8.18
Th, %	37.3	37.3	39.2
Hg porosimetry			
Density, g/cm^3	10.13	10.17	10.11
Density, % of theoretical	99.3	99.7	99.6
Porosity, %	<1	<1	<1
Resistance to crushing, g	1152	1008	907
Surface area,[d] m^2/g	0.004	0.003	0.004
X-ray crystallite size, A	1537	1280	1348
Lattice parameter	5.5679	5.5680	5.5679
Carbon, ppm	<10	<10	<10
Aluminum, ppm	100	110	110
Gas release to 1200°C in vacuum			
Total volume, cm^3/g	0.011	0.007	0.007
Composition, vol %			
H_2	91.4	68.8	81.1
H_2O	0.69	5.24	2.16
N_2 + CO	7.92	13.4	16.2
Ar		0.26	0.27
CO_2		12.0	0.27
O_2		0.26	
Weight of 210- to 297-μ-diam fraction, g	439.2	539.3	1295.1
Screen analysis,[e] wt %			
>297 μ	20.6	9.2	15.5
249–297 μ	65.9	74.9	69.0
210–249 μ	0.6	1.7	3.2
<210 μ	12.9	14.2	12.2

[a]All analyses on 1400°C-fired material except as indicated.
[b]Contained some "cherry-pitted" spheres.
[c]Analysis on coated particles.
[d]Calculated geometric surface area of 210- to 297-μ-diam spheres is $2.0–2.8 \times 10^{-3}$ m^2/g.
[e]After 1100°C firing.

the 1400°C firing in H_2 were amber colored and transparent, an effect that was not produced in the 1100°C firings in Ar–4% H_2. Photomicrographs of typical metallographic sections of the 1400°C-fired spheres are shown in Fig. 6.7.

A number of interesting color effects were noted throughout the course of the firings; however, these effects are not understood at present. After the 1100°C firing the microspheres were not transparent and were composed of about equal numbers of pale-green and black microspheres. The density was 97 to 98% of theoretical, and the oxygen : uranium ratio was <2.006. These values are acceptable. However, it was decided to refire the spheres in pure hydrogen in the event that the colors were caused by minor variations in the oxygen : uranium ratio or the degree of solid solution among the individual spheres. A test batch of spheres was fired to 1150°C in hydrogen and held for 4 hr; spheres of three different colors resulted. In addition to the black and the pale green spheres, about half of the spheres were amber colored and transparent. The material was then refired to 1400°C in hydrogen, and all the spheres were converted to the amber-colored, transparent type.

A coprecipitation method was developed for the preparation of UO_3-ThO_2 sols and was demonstrated in the laboratory through the final calcination to obtain dense UO_2-ThO_2 microspheres having a thorium : uranium atom ratio of 3. Other precipitation methods were tried; these included (1) peptization of thorium hydroxide precipitates with uranyl nitrate and (2) addition of UO_3 to ThO_2 sols prepared from precipitated thorium hydroxide. Although sols could be readily formed by both of these methods, the nitrate : metal ratios of the sols were higher than those obtained by the coprecipitation method, and difficulty was encountered in the sphere-forming process. Preliminary work leading to the development of the coprecipitation process is the subject of a topical report that is currently in preparation.[8]

This method of sol preparation consists in coprecipitating the hydrous oxides in excess ammonia at 80 ± 5°C (i.e., a "reverse strike"), washing the hydrous oxide filter cake free of nitrate, boiling the aqueous slurry of the filter cake to remove residual ammonia, and then dispersing with nitric acid. In a typical laboratory-scale preparation of sol (0.5-mole batch of the mixed oxides), a 0.5 *M* $UO_2(NO_3)_2$–$Th(NO_3)_4$ solution was added at a nearly constant addition rate over a 20-min period to a 75% excess of 3 *M* NH_4OH; the precipitation temperature was maintained at 80 ± 5°C. The precipitate was then washed essentially free of nitrate with ten cake volumes of about 0.08 *M* NH_4OH at 80 ± 5°C. The washing procedure reduces the NO_3^-/(Th + U) mole ratio to about 0.003; the NH_4^+/(Th + U) mole ratio is 0.05. The NH_4^+ concentration is decreased to 10 to 30 ppm by boiling an aqueous slurry of the filter cake until the pH of the evolved steam is lowered from its initial value of 9 or 10 to about 6. The hydrous oxides have an x-ray crystallite size of <30 A.

A three-step process is used in dispersing the hydrous oxides to a sol in order to attain nitrate : metal mole ratios that are suitable for our sphere-forming process. The process used for the peptization is as follows:

1. One-third of the hydroxide slurry is boiled with sufficient nitric acid to give a nitrate : metal mole ratio of 0.40, and a clear, red sol quickly forms.
2. The second one-third of the slurry is added to the red sol and boiled for about 20 min; this treatment peptizes all the added hydroxides and provides a NO_3^-/(Th + U) mole ratio of 0.20.
3. The remaining slurry is then added, and boiling is continued at reflux temperature for about 8 hr or until the sol attains a clear, dark red color.

The sol is then concentrated by evaporation to 1.5 *M* (Th + U). The nitrate : metal-oxide mole ratio is about 0.13 with this process. X-ray measurements indicate that the crystallite size of the dispersed particles of the sol is 40 to 45 A.

The sol was readily formed into gel microspheres by the standard method (using 2EH containing 1.1% H_2O, 0.3% Span 80, and 0.5% Ethomeen S/15). The gel spheres were fired in air to 1200°C and then contacted for 4 hr with Ar–4% H_2 to yield a reduced product having near-theoretical density. Rates of temperature rise greater than 20°C/hr caused cracking during the heating to 300°C; however, the cracking could be eliminated entirely by using slower rates. Fired spheres 177 to 250 μ in diameter resisted crushing loads of about 1700 g.

[8] A. B. Meservey, *UO_2-ThO_2 and UO_3-ThO_2 Sols Prepared by Precipitation-Peptization Processes*, ORNL-TM-1782 (in preparation).

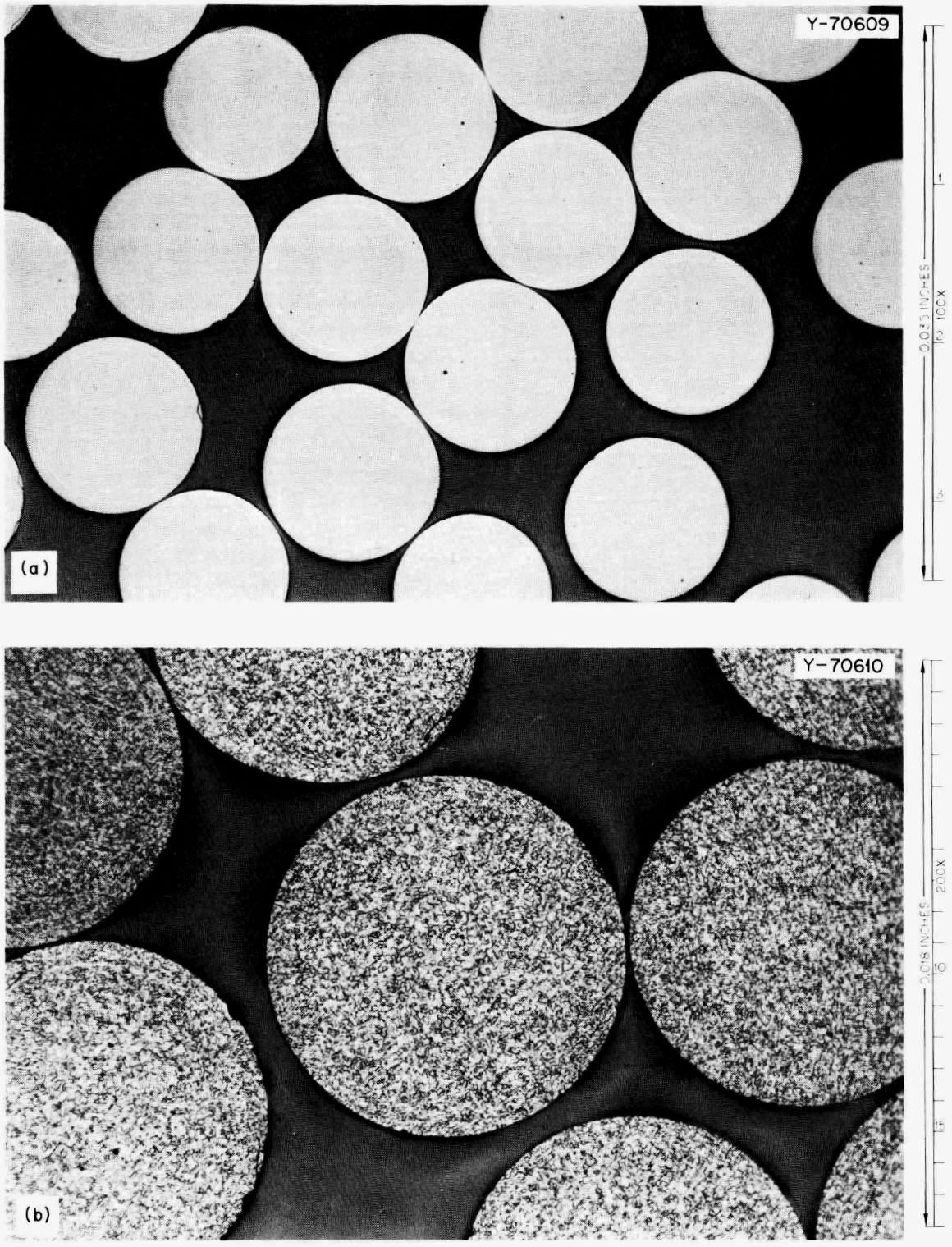

Fig. 6.7. Metallographic Sections of Sol-Gel UO_2-ThO_2. (*a*) Magnification 100X, as polished; the halos are light effects from the transparent spheres. (*b*) Magnification 200X, etched with H_3PO_4-HF; grain structure is visible.

Microsphere Preparation Column Chemistry

In the microsphere forming process, gel microspheres are formed by dispersing sol droplets into 2EH; water is extracted from the droplets, and gel microspheres are formed. To stabilize the droplets during water extraction, small amounts of two surfactants are used: Span 80 (Atlas Chemical Company's brand name for sorbitan monooleate) and Ethomeen S/15 (Armour Industrial Chemical Company's brand name for ethylene oxide condensation products with primary fatty amines). The organic solvent is recycled, after removal of water by continuous distillation at pot temperatures of 140 to 155°C, for use in column operations.

The chemical behavior of the various species in the solvent is not understood. Control of the microsphere forming has been obtained by empirical methods and has been very successful in most instances. The intended purpose of this investigation was to provide information that would be useful in attaining improved column operation and, in particular, improved long-term operation with the solvent. Since surfactants are depleted during operation and must be added periodically, the changes that occur were studied. We sought analytical methods that might be used to measure the surfactant concentrations, the changes that occur during solvent purification by distillation, and the equilibrium extraction of components from the organic medium.

Analytical Methods

We examined the use of surface tension and conductivity measurements as possible means for rapidly analyzing surfactant concentration during operation. These analyses, if successful, could be used to determine surfactant depletion and to show when additional surfactant was needed. Although surface tension measurements were not sufficiently sensitive to be useful, conductivity measurements proved to be sufficiently sensitive to Ethomeen S/15 concentration.

There was essentially no change in the surface tension, as measured against the air interface, of water-saturated 2EH containing 0 to 0.5 vol % of either Span 80 or Ethomeen S/15. Interfacial tension measurements for Span 80 were somewhat more sensitive (Fig. 6.8) but were not sufficiently sensitive to be useful. Similar results were obtained for Ethomeen S/15. Measurements were made by a ring tensiometer, and viscoelastic films were observed at all surfactant concentrations measured (0.05 to 2.0 vol %). With the Du Noüy ring method, the film does not break sharply but stretches considerably before the break occurs. The measured values were not very reproducible; the smoothed curve is an average of points.

Conductivity measurements provided a sensitive measure of Ethomeen concentration (Table 6.5). Ethomeen in water-saturated 2EH is essentially nonconductive (0.71 micromho/cm^2); however, when the 2EH solution is equilibrated with nitric acid, which is extracted by the Ethomeen, it is sufficiently conductive to provide a basis for measurement.

Solvent Changes During Distillation

To simulate the effects of distillation that occur during recovery of 2EH, dilute nitric acid (pH = 2.0) was continuously infused into boiling 2EH

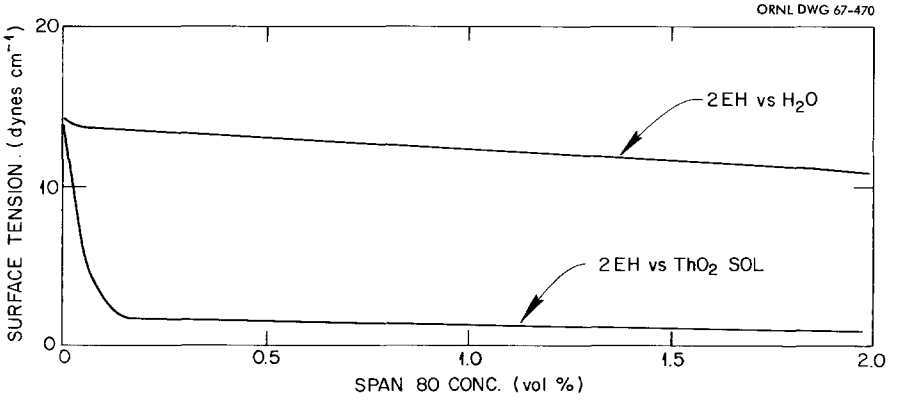

Fig. 6.8. Effect of Span 80 Concentration on Interfacial Tension in the Systems 2-Ethyl-1-hexanol–H_2O and 2-Ethyl-1-hexanol–ThO_2 Sol.

that contained Span 80 and Ethomeen S/15 surfactants. Nitric acid was added because it is known to be extracted into 2EH to a slight extent from the nitric acid–stabilized sols. The Span 80 concentration was determined by infrared analysis for its carbonyl group, and the amine and nitrate contents were determined chemically. The results showed that both the nitrate and the amine concentrations decreased (Table 6.6). The Span 80 concentration appeared to increase; that is, there were more carbonyl groups present in the 2EH after boiling than before. We interpret this result as evidence that oxidation of some organic species, probably the 2EH, is occurring. Since some oxidation may have been a result of failing to exclude air in this experiment, a second series of experiments was performed. In one of the experiments, the 2EH containing only Ethomeen S/15 was boiled in air; in another, the 2EH containing nitric acid and Ethomeen S/15 was boiled under argon. The results indicated that oxidation both by air and by nitric acid is occurring (Table 6.7). The Ethomeen S/15 in 2EH was stable in the absence of nitric acid. Analyses of the alcohol throughout the course of a continuous microsphere forming run during which the 2EH recovery still was operating showed the same general trends as our distillation experiments (Fig. 6.9). The implications of these results on long-term, continuous sphere-forming column operation are not clear; however, it is possible that better control of the composition of the 2EH phase will be necessary.

Table 6.5. Conductance of 2EH Solutions Containing Ethomeen S/15 After Equilibration with HNO_3[a]

Ethomeen S/15 Concentration (vol %)	Conductance (micromhos)
0	0.714
0.3	2.71
0.4	3.56
0.6	4.98
1.6	8.13

[a]Twenty volumes of 0.01 *N* HNO_3.

Table 6.6 Changes in Boiling 2EH During Continuous Infusion of Nitric Acid

Solution boiled in 140–160°C range

Boiling Time (days)	HNO_3 Added (millimoles)	Analysis (millimoles)		
		NO_3^-	Span 80	Ethomeen S/15
0	0.0	0.0	15.1	8.8
1	1.1	0.52	19.5	9.0
2	2.8	0.34	20.0	7.0
3	9.6	0.05	26.6	2.8
4	14.3	0.23	31.4	1.8
5	17.1	0.48	37.9	2.0

Table 6.7. Oxidation of 2EH

Boiling Time (days)	Atmosphere	HNO_3 Added (millimoles)	Analysis (millimoles)		
			NO_3^-	Carbonyl Group	Ethomeen S/15
0	Air	0.0	0.0	0.00	8.4
1.5	Air	0.0	0.0	0.00	8.4
2.5	Air	0.0	0.0	1.12	8.4
0	Argon	0.0	0.0	0.00	8.4
1.5	Argon	6.7	0.73	2.9	5.2
2.5	Argon	14.1	0.13	5.4	0.9

Equilibration Studies with ThO_2 Sols and Gels

Several experiments were made to determine if Span 80 or Ethomeen S/15 is sorbed on a ThO_2 surface. The results indicate that only very small amounts, if any, are sorbed. Span 80 in concentrations ranging from 0.13 to 2 vol % were equilibrated with sol and with dried gel for periods of one day. Within the limits of accuracy of the analytical method used (infrared absorption of the carbonyl group at 1727 cm^{-1}), no Span 80 was found to be adsorbed (Table 6.8). In similar experiments using Ethomeen, similar results were obtained (Table 6.9). Nitric acid extraction from the ThO_2 is a very slow process, as indicated by the nitrate : amine ratios.

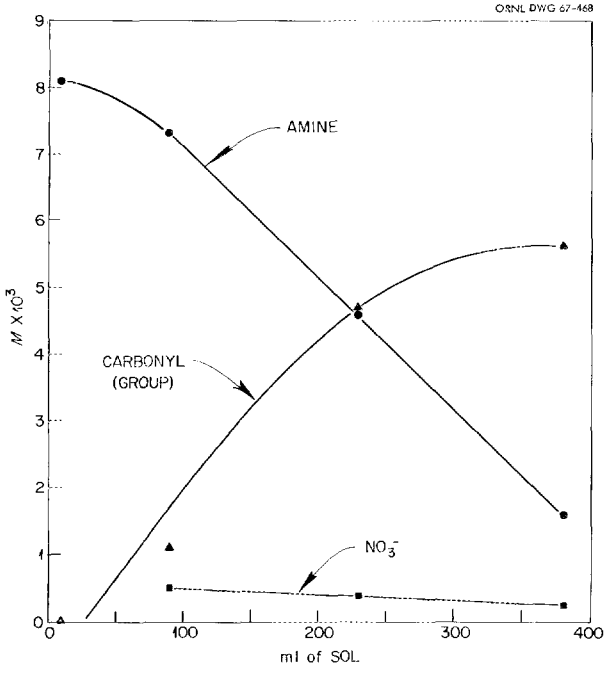

Fig. 6.9. Changes in 2-Ethyl-1-hexanol During Continuous Operation of a Sphere Forming Column. Flow rate of 2 *M* ThO_2 sol = 50 ml/hr.

6.3 DEVELOPMENT OF METHODS FOR PRODUCING MICROSPHERES

A process has been developed for converting sols into 10- to 1000-μ-diam spherical gel beads. In this process, droplets of sol are gelled by extraction of water from the droplet into an immiscible organic liquid such as 2-ethyl-1-hexanol (2EH).

Table 6.8. Equilibration of 2EH Containing Span 80 with ThO_2 Sols and Gels

Conditions: One-day equilibration with 2 *M* ThO_2 sol or 110°C dried gel

ThO_2	Span 80 Concentration in 2EH, vol %	
	Initial	Final
Sol	0.13	0.16
	0.80	0.81
	2.0	2.0
Gel	0.13	0.16
	0.80	0.87
	2.00	2.04

Table 6.9. Composition of 2EH Containing Ethomeen S/15 After Equilibration with ThO_2 Sols

Equilibration Time (days)	Molarity of ThO_2	Ethomeen Concentration (*M*)		Final Nitrate : Amine Ratio
		Initial	Final	
3.5	2.0	0.018	0.016	0.30
		0.019	0.019	0.18
		0.035	0.031	0.30
10	7.3	0.0086	0.0086	0.86
	8.6	0.0086	0.0085	0.61
	9.6	0.0086	0.0085	0.94

The following five operations are required:

1. disperse the sol into droplets,
2. suspend these droplets in the 2EH to extract water and cause gelation,
3. separate the gel microspheres from the 2EH,
4. recover the 2EH for reuse,
5. dry and calcine the gel microspheres.

The size of the product microsphere is determined in the first step. The maximum droplet size is limited since very large drops will be distorted. In the second (and key) step, the extraction of water causes gelation and thus converts the droplet of sol into a solid sphere. (Interfacial tension holds the drop in a spherical shape.) A surfactant must be dissolved in the immiscible liquid to prevent the coalescence of the sol drops with each other, the coalescence of the sol drops on the vessel walls, and/or the clustering of partially dried drops.

Microsphere-Preparation Pilot Plant

A system for carrying out the above five operations was built and was operated as part of the ORNL Coated Particle Development Laboratory (CPDL). A thoria sol feed rate of 25 cm^3/min or a ThO_2 microsphere product rate of about 1 kg/hr was selected as the design capacity for this equipment. This capacity was achieved, but it could not be exceeded because the steam supply to the distillation system was inadequate. The microsphere column system is operated to provide microspheres for other parts of the fuel cycle program and to develop equipment and procedures for remote operations of such a system.

The first four process operations are done continuously in a tapered glass column (Fig. 6.10). The sol is dispersed into droplets that are released into the enlarged top of the tapered column. These droplets are suspended or fluidized by a recirculated, upflowing stream of 2EH. As the water is

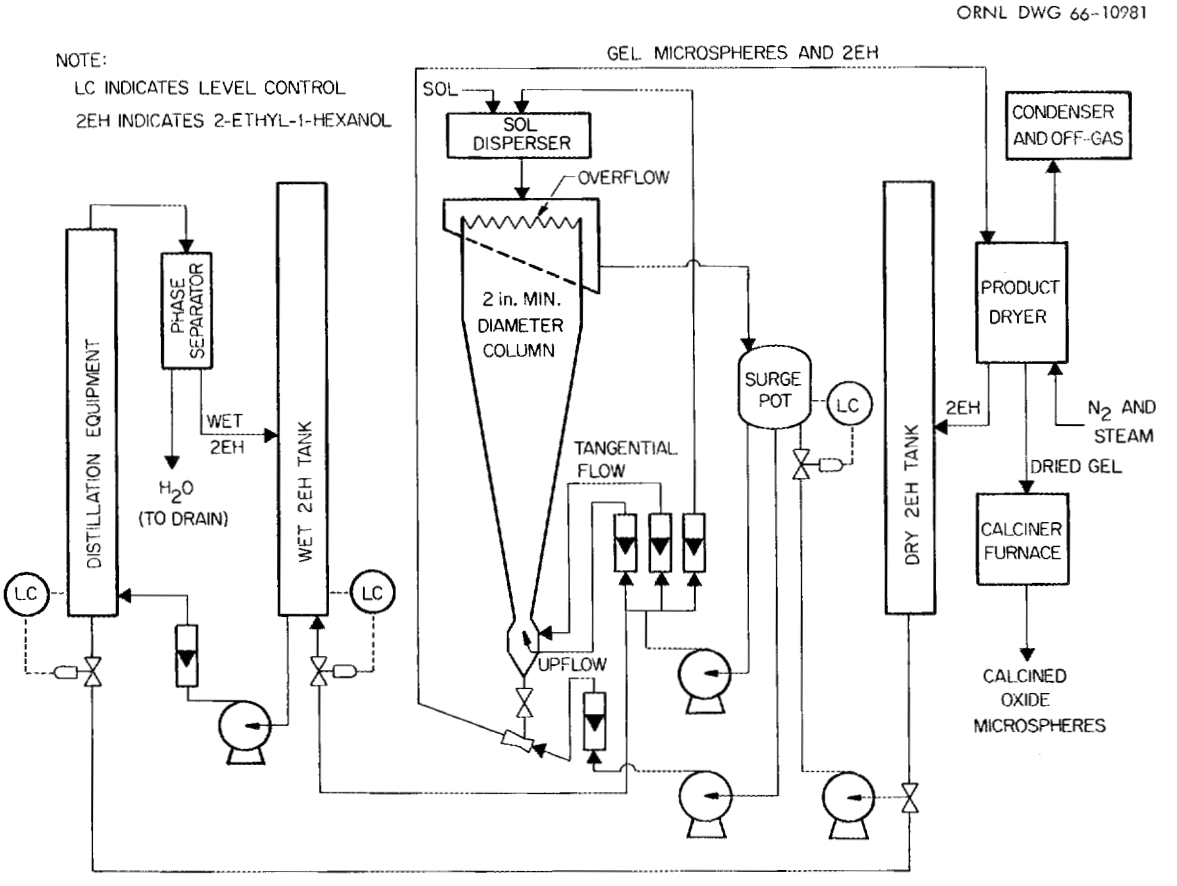

Fig. 6.10. Microsphere Preparation System for Coated Particle Development Laboratory.

extracted and the droplets gel into solid microspheres, the settling velocity increases. The column configuration and the fluidizing flow rates are selected to permit the gelled particles to drop out continuously while sol droplets are being formed in the top of the column. The gel spheres are transferred to a dryer, dried, and calcined batchwise. Fresh or purified 2EH is continuously added to the column and displaces a stream of wet 2EH to a recovery system. Water is removed from the 2EH by distillation.

We have demonstrated long-term, stable operation with respect to the 2EH and surfactant in the CPDL microsphere column. Single charges of 2EH were used for periods longer than six months. The coalescence and clustering problems associated with the thoria drops were effectively prevented with the use of about 0.3 vol % Ethomeen S/15 and 0.05 vol % Span 80 in the initial charge, plus 10 cm^3 of Ethomeen S/15 and 2.5 cm^3 of Span 80 added per liter of thoria sol fed to the column. When the system was drained in preparation for equipment changes, the only noticeable evidence of deterioration in the surfactant–2EH solution was a cloudiness, which resulted from accumulation of very small gel particles. Samples of the 2EH that was used for preparing thoria microspheres for a six-month period (a single charge of 2EH) were analyzed for NO_3^-, Th, total N, and amine. The results, neglecting one anomalous analysis for amine, for the final four months of operation were:

NO_3^-	$(1.5 \text{ to } 4) \times 10^{-4}$ *M*, no trend with time
Th	$(2 \text{ to } 7) \times 10^{-4}$ *M*, increasing with time
N	$(2 \text{ to } 5) \times 10^{-4}$ *M*, no trend with time
Amine	$(6 \text{ to } 10) \times 10^{-4}$ *M*, no trend with time

The distillation system for removal of water from 2EH was tested with a new high-pressure steam supply; it is now adequate for a sol feed rate of at least 50 cm^3/min. This is equivalent to about 50 kg of ThO_2 or 15 kg of UO_2 microspheres per 24-hr day.

A new gel dryer, for use in removing the residual water and alcohol from the gel spheres, was designed, installed, and operated successfully. A stream of 2EH from the column transfers the gel spheres from the column bottom to the dryer, where the spheres are collected on a filter of nonblinding wire cloth. After batch drying, the spheres are transferred pneumatically to the furnace for batch calcining. This new arrangement permits nearly continuous collection of the gelled spheres.

The problems of remote operation (necessary with highly radioactive materials) have been only partly solved. Gel spheres or calcined oxide spheres can be readily transferred, hydraulically or pneumatically, with 2EH or a gas. The inventory of sol drops or gel spheres in the column is adequately indicated by average bed-density measurements. However, we still need simple, remote techniques for determining the optimum fluidizing flow and for inspecting the gel spheres (to determine dryness and the absence of clustering and distortion).

Sol Disperser Development

Many column operating difficulties would be minimized if uniformly sized sol drops were formed; therefore, a variety of sol dispersion devices have been tested. Sol drops can be formed from a larger mass of sol by applying one or more forces, such as gravity, shear, inertia, interfacial tension, electrostatic repulsion, and centrifugal force. To obtain uniform drops and controlled diameters, the force, as well as the configuration of the sol where the force is applied, must be uniform; in addition, one or both of these factors must be controllable. For all the dispersers that were tested, a uniform configuration was obtained by feeding the sol through orifices or capillaries 0.004 to 0.030 in. in diameter.

Two-fluid nozzles have proved to be the most useful sol dispersion devices. They are reliable, give a uniform product, and are easily controlled for producing sol drops over the size range of interest (200 to 2000 μ diameter). In every case, 90 wt % of the product obtained from single two-fluid nozzles had diameters that were within ±15% of the mean diameter (Table 6.10). Since the capacity of single two-fluid nozzles was unacceptably low for pilot plant operations, multiple arrays of two-fluid nozzles, arranged in parallel, were tested. Two of these arrays consisted of 6 and 11 two-fluid nozzles, respectively, arranged in parallel. In these arrays the sol and the 2EH were fed to their feed locations from single pumps. Operations, over extended periods, with the 6-nozzle and the 11-nozzle arrangements provided acceptable products, of which 70 and 50 wt %, respectively, had diameters that were within ±10% of the mean diameter. Attempts to improve these yields will continue.

Table 6.10. Diameters of Calcined Thoria Microspheres from Three Dispersers

Sol feed: thoria sols 3.0 *M* in Th; sol drop diameters were 2.35 times those of theoretically dense ThO_2 product

Type of disperser	Two-fluid nozzle	Two-fluid nozzle	Vibrating capillary	Vibrating capillary	Vibrating capillary	Free-fall drop method
Number of feed capillaries	1	6	1	1	4	19
Capillary diameter, μ	250	425	425	480	480	400
Sol feed rate, cm^3/min	1.2	24.7	1.2	19.2	9.6	9.6
Vibration frequency, cps			40	200	50	
Predicted mean size, μ	270[a]	230[a]	330[b]	310[b]	390[b]	
Amount of sample, g	540	10,200		314	720	480
Weight per cent in:[c]						
30/35 or 500/590 μ						97.9
35/40 or 420–500 μ					0.1	0.8
40/45 or 350–420 μ			0.2		61.9	1.1
45/50 or 297–350 μ	2.9	0.2	98.3	30.4	37.6	
50/60 or 250–297 μ	92.0	3.0	1.5	62.6	0.4	
60/70 or 210–250 μ	0	85.8		7.0		
−70 or <210 μ	5.3	10.9				

[a]Calculated from equation developed for two-fluid nozzle.

[b]From number of drops per cycle and flow rate.

[c]From use of U.S. Sieve Series screens.

At optimum conditions, the most uniform sol drops are obtained by use of capillaries that are mechanically connected to, and vibrated by, an electrodynamic device (e.g., a loudspeaker) (Fig. 6.11). A simple sinusoidal displacement of the capillary tip appears to be the best vibratory wave shape. Secondary vibrations cause nonuniform drops. The best results are obtained with a continuous, approximately sinusoidal liquid stream that breaks at the midpoint position with respect to amplitude (Fig. 6.12). The amplitude for this type of operation varied from $\frac{1}{4}$ in. at 20 cps to $\frac{1}{32}$ in. at 200 cps and was obtained by 1.5- to 4.0-v inputs to commercial loudspeakers. Results for single capillaries were somewhat better than those for a multiple-capillary arrangement (Table 6.10).

The free-fall drop mechanism and the relationships between drop size, orifice size, and interfacial tension are well known. The use of plastic buckets with a large number of holes (Fig. 6.11) provides a practical capacity and avoids variations in drop size caused by variable wetting of the orifice by the sol. This disperser is useful for large drops only; the orifice sizes necessary to produce drops smaller than 1000 μ in diameter are too small to be practicable. The interfacial tension between the sol and the 2EH varies with the amounts of surface-active agents present and thus causes variations in drop size.

Gelation Development Studies

The choice of equipment that is most suitable for gelation by extraction of water in 2EH depends on the desired size of the spheres to be produced. A fluidized bed in a tapered column is preferred when the fired spheres are 150 μ in diameter or larger. The drops in this system can be fluidized long enough to be certain of gelation, while other types of apparatus permit discharge of wet drops or allow coalescence or breakup of the drops. Tests of several column tapers show that a small taper is not necessary when a swirl from a tangential 2EH inlet is used to aid fluidization. The early columns used $\Delta L/\Delta D$ ratios of 40 in./in., but columns of 20 in./in. and 12 in./in. have been used without difficulty (L is column length and D

ORNL DWG 66-10982

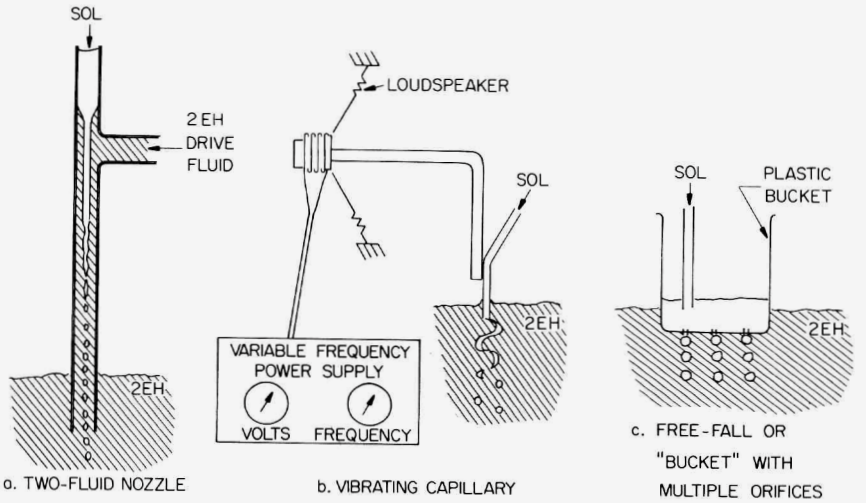

Fig. 6.11. Devices for Dispersion of Sol as Drops in 2-Ethyl-1-hexanol (2EH).

Fig. 6.12. Dispersion of a ThO_2–25% UO_3 Sol by a Vibrating Capillary Disperser. Four capillaries vibrated at 90 cps to form 950-μ-diam drops.

is diameter). If there is any tendency for sol drops to stick to the wall, the amount of sticking increases as the taper increases.

Microspheres of nonuniform diameters and less than 80 μ in mean diameter can be easily and efficiently prepared by using mechanical agitation to disperse and suspend the droplets in 2EH during extraction of water. The efficient collection of the gel spheres is more difficult for this type of operation than the dispersion and gelation operations. When a simple continuous inclined settler was used, the loss of very small microspheres by entrainment amounted to 2 wt % for product having a mean diameter of about 10 μ and 10 wt % for product having a mean diameter of less than 5 μ.

Alternatives to the fluidized-bed column were considered. A "fall-through" column that is long enough to give the required holdup time without fluidization is practical and attractive for small drops or microspheres. Such a "fall-through" column might be practical for 200-μ-diam thoria microspheres, but the maximum practical size would be smaller in the instance of other sols that are more dilute or that are slower to gel. Gel spheres were also produced in multiple column stages or coiled tubing with cocurrent flow of sol drops and 2EH. Both devices appeared less practical than the fluidized-bed column for large spheres or the "fall-through" column for small spheres.

A Study of Mass Transfer for Extraction of H_2O from Sol Droplets

The extraction of water from sol droplets by 2EH to cause gelation is a key step in the preparation of thoria microspheres. Information concerning the fundamental mechanisms of this gelation step would be a valuable aid in the selection of process conditions and equipment. The time required for gelling sols having different droplet sizes and molarities by suspension in an organic solvent has been estimated by visual observation; however, no attempt has been made to correlate the exact time required for gelation with the properties of the sol or the organic medium. We have begun an investigation to determine gelation times of single thoria sol droplets suspended in flowing 2EH by measuring changes in the droplet diameter until shrinkage no longer occurs. From a review of the literature we conclude that the mass transfer mechanism during gelation is somewhat different from any reported by other investigators. An experimental apparatus (involving optical and microphotographic equipment) was assembled and used to observe and photograph thoria sol drops, and drops of water, suspended in dry 2EH.

Thoria Microsphere Drying and Firing

Conditions that will prevent cracking of thoria gel microspheres during firing were investigated empirically. In general, the factors that minimize cracking are those that minimize composition gradients within the gel microspheres. The drying conditions were the important variables; the best drying conditions were found to include the use of superheated steam to a final drying temperature of 200°C. The principal observations for gel spheres produced from thoria sol were as follows:

1. The diameter is a major variable. Cracking increases as the diameter increases. If the calcined products are larger than 500 μ in diameter, the best drying conditions, namely, use of a superheated steam drying atmosphere to a final drying temperature of 200°C, are necessary to minimize cracking. To obtain calcined microspheres having diameters of less than 250 μ, the best drying conditions are not necessary. The amount of cracking that occurs in product having diameters of 250 to 500 μ is variable; drying conditions somewhat less than optimum can usually be used without causing excessive cracking.
2. The amount of cracking decreases as the maximum drying temperature increases from 100 to 200°C.
3. The presence of superheated steam in the drying atmosphere promotes the removal of 2EH from the gel and reduces the amount of cracking during firing. Use of an air atmosphere during drying may permit an exothermic reaction while relatively large amounts of 2EH remain on the gel and thus may result in very rapid temperature rises and excessive cracking. Inert atmospheres (Ar or N_2) without steam remove 2EH rapidly only at temperatures above 180°C, as compared with rapid stripping at 120 to 140°C by steam.

The currently preferred drying and firing conditions for ThO_2 microspheres are as follows:

Drying	Ar atmosphere	25 to 110°C in 1 hr
	Ar and steam atmosphere	110 to 200°C in 6 hr
Firing	Air atmosphere	100 to 500°C at 100°C/hr
	Air atmosphere	500 to 1150°C at 300°C/hr
	Air atmosphere	At 1150°C for 4 hr

6.4 THORIUM-URANIUM RECYCLE FACILITY

Design and Construction

A contract for the construction of the Thorium-Uranium Recycle Facility was signed with Blount Brothers Construction Company of Montgomery, Alabama, on May 6, 1965. One year later the building (which was estimated to be 60% complete) was enclosed, and the cell walls had been erected up to a point between the first- and second-floor levels.

During the past year, the portion of the work to be accomplished by the fixed-price contractor has been virtually completed. The procurement of special materials and equipment (exclusive of process equipment) to be installed in the building has been completed. An amount of work estimated to cost approximately $90,000 remains to be done by a cost-plus-fixed-fee contractor. This work consists mainly in installing the in-cell crane and manipulator system, plugs for the many points of cell access, and the viewing windows.

The Laboratory has procured equipment costing about $1,764,000 for the building. Except for three steel shielding doors, each item was received by the time it was needed. The doors, which with their housings weigh well in excess of 100 tons, arrived about three months later than specified by the contract. Excessive wear rate has been observed in the square-threaded jackscrew assemblies used to raise the two 25-ton doors. We have since learned that, in this type of application, ball screws have a life expectancy that is approximately 100 times that of square-threaded jackscrews.

The in-cell crane and manipulator system constituted the largest single procurement package; it involved intricate problems in both mechanical design and fabrication. In contrast to the experience mentioned above with the shielding doors, the crane and manipulator design proceeded smoothly and quite satisfactorily. Operational tests in the manufacturer's plant were successful.

Process Equipment Design

The main design effort during this report period was directed toward the design, fabrication, and, in some cases, testing of various items or assemblies of process equipment to be used by the development groups. In addition, sphere forming equipment that would be suitable for installation in TURF was designed.

Uranium Reduction. – Our evaluation and observation of the uranium reduction step have led to the conclusion that neither the atmospheric-pressure reduction procedure (as used by the chemical development group) nor the high-pressure reduction procedure (used in engineering development work to make significant quantities of reduced uranium) is suitable for use in a hot cell. The first procedure contains a difficult solids separation step, whereas mechanical and safety problems associated with high pressure make the latter method undesirable. We have proposed operation at atmospheric pressure, using a sufficiently large quantity of catalyst on a fixed, but removable, bed to accomplish the reduction. A trickle column system was designed and constructed; it is now undergoing tests. It consists of three water-cooled 1-in.-diam by 3-ft-long tubes filled with $\frac{1}{8}$-in.-diam by $\frac{1}{8}$-in.-long alumina cylinders coated with platinum.

Sol Preparation. – A bench-scale batch extraction unit was designed and constructed for laboratory use in the development of the amine extraction process as a method for producing urania sol (see Fig. 6.13). Also, a continuous extraction system was designed and constructed for the development of amine extraction as a means for producing both urania and urania-thoria sols. This latter unit was designed to have a capacity of at least 10 kg of mixed metal per day (see Fig. 6.2). Tests by the development groups have shown this process to be the method of choice for producing sol in the TURF.

Assistance was also provided in the operational tests and redesign of continuous process equipment that will be used for producing urania sol by precipitation. The gas-operated pumps were redesigned to handle the solids stream from the bot-

tom of a given settler as well as the clear, solute-poor stream that was mixed with it.

An evaporator is required for the concentration of sol product from both the amine extraction equipment and the continuous precipitation equipment. Two problems were expected in the evaporation operation: (1) fouling of heat transfer surfaces by deposition of solids and (2) foaming that would result from evolution of gas from a liquid containing finely divided solids. We designed a unit which would employ forced circulation of sol at relatively high velocity through heated tubes without boiling, and tangential entry of the slightly heated sol at high velocity into a tubular flash chamber (see Fig. 6.3).

Sphere Forming. – Adequate means for observation of the forming-column product have not yet been developed. One method that is to be tested utilizes a photoelectric cell and scaler combination to determine the size distribution of the product; another proposed method uses a telescope coupled with high-speed photography to obtain a picture of a very small sample of the spheres leaving the column.

When drops having diameters about one-fourth the intended size are formed in a sphere-forming column, they are carried overhead with the bulk flow of 2EH. They must be removed to avoid fouling the stream with very fine particles, which are formed when the already small drops or gel spheres are struck by the impeller of the centrifugal pump used to circulate the 2EH, and to avoid line plugging problems caused by solids settling out of the fluid. A filter presents problems in cleaning and plugging; thus preference has been given to use of a settler. One of these has been designed and constructed for testing; it has 20 parallel inclined decks on which the particles can settle by traveling not more than about 1 in. vertically through the suspending fluid. After reaching a deck the particles roll into a funnel and then into a conduit that conveys them to the bottom of the vessel, where they will be collected (see Fig. 6.14).

Drying and Firing. – Study of this problem has led to the conclusion that batch operation is preferable for the work to be performed in the TURF. We envision that both the dryer and the furnace will utilize fluidized transfer of particles into and out of the process vessel. It may be necessary to employ a translating product withdrawal tube to ensure removal of particles. Such a unit has

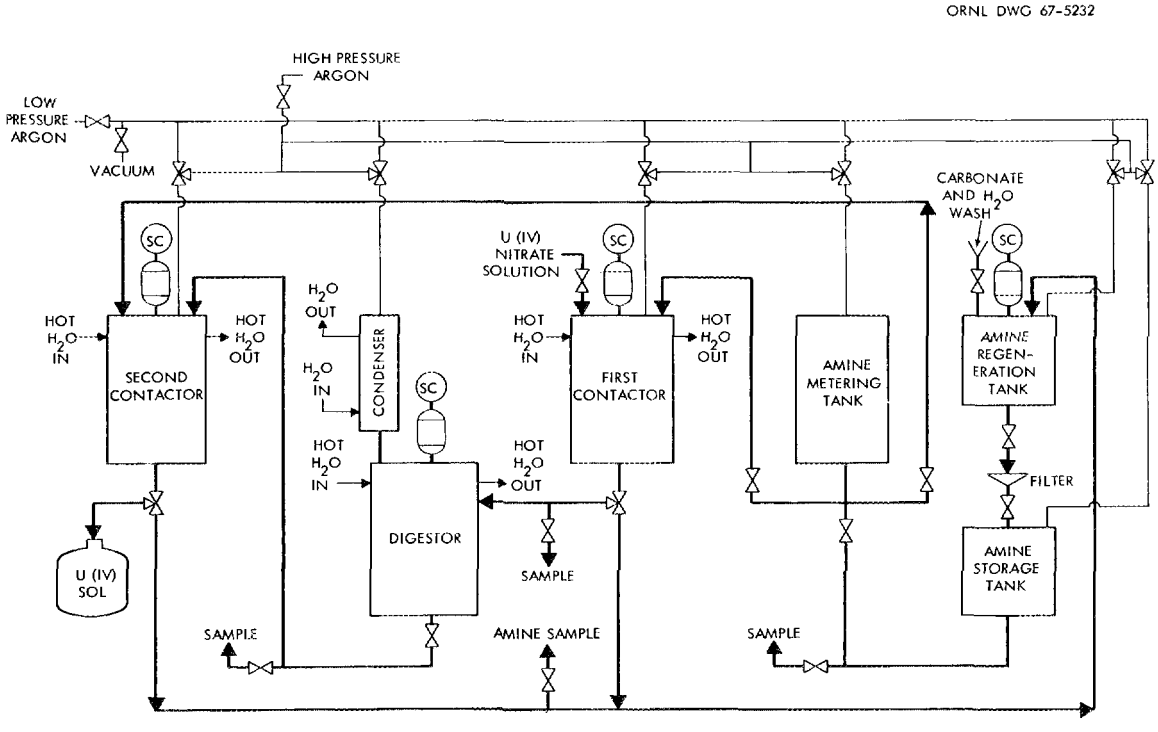

Fig. 6.13. Flow Diagram of Laboratory-Scale Amine Extraction Equipment.

been designed and constructed. It is so arranged that no contamination can be transmitted outside the equipment (there are no sliding seals). We have designed a dryer for use in the Coated Particle Development Laboratory which can attain a temperature of 260°C and process up to 15 kg of spheres per batch. This unit employs an integral electrically driven steam generator to supply heat at a known and controllable temperature. The furnace concept consists of an all-ceramic (alumina) vessel that is fitted with a number of nozzles and is heated by molybdenum resistors. The furnace is housed in a gas-tight insulated metal container. A prototype ceramic vessel has been procured and is being tested for leak rate and durability.

TURF Sphere-Forming Equipment Design. – The original sphere-forming equipment flowsheet was

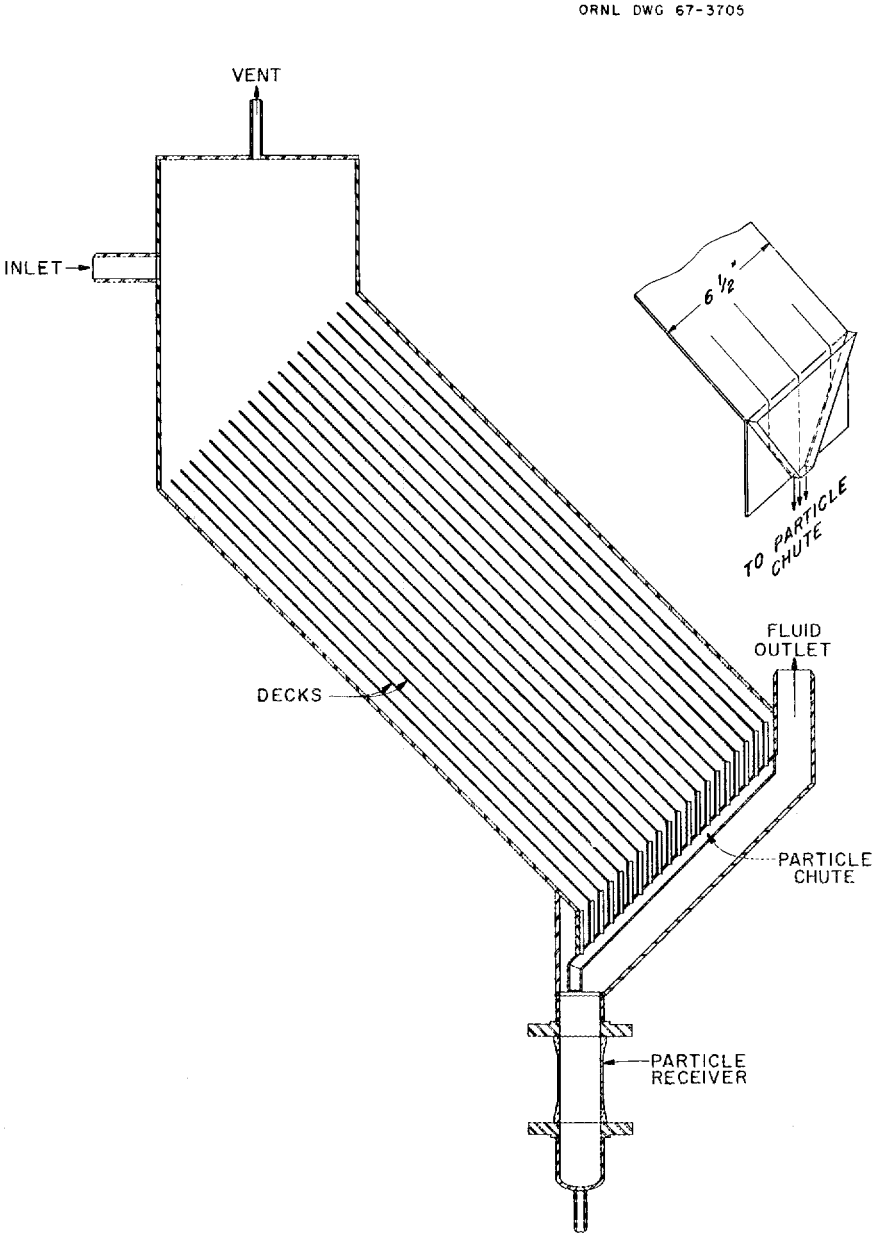

Fig. 6.14. Test Settler for CPDL Alcohol System.

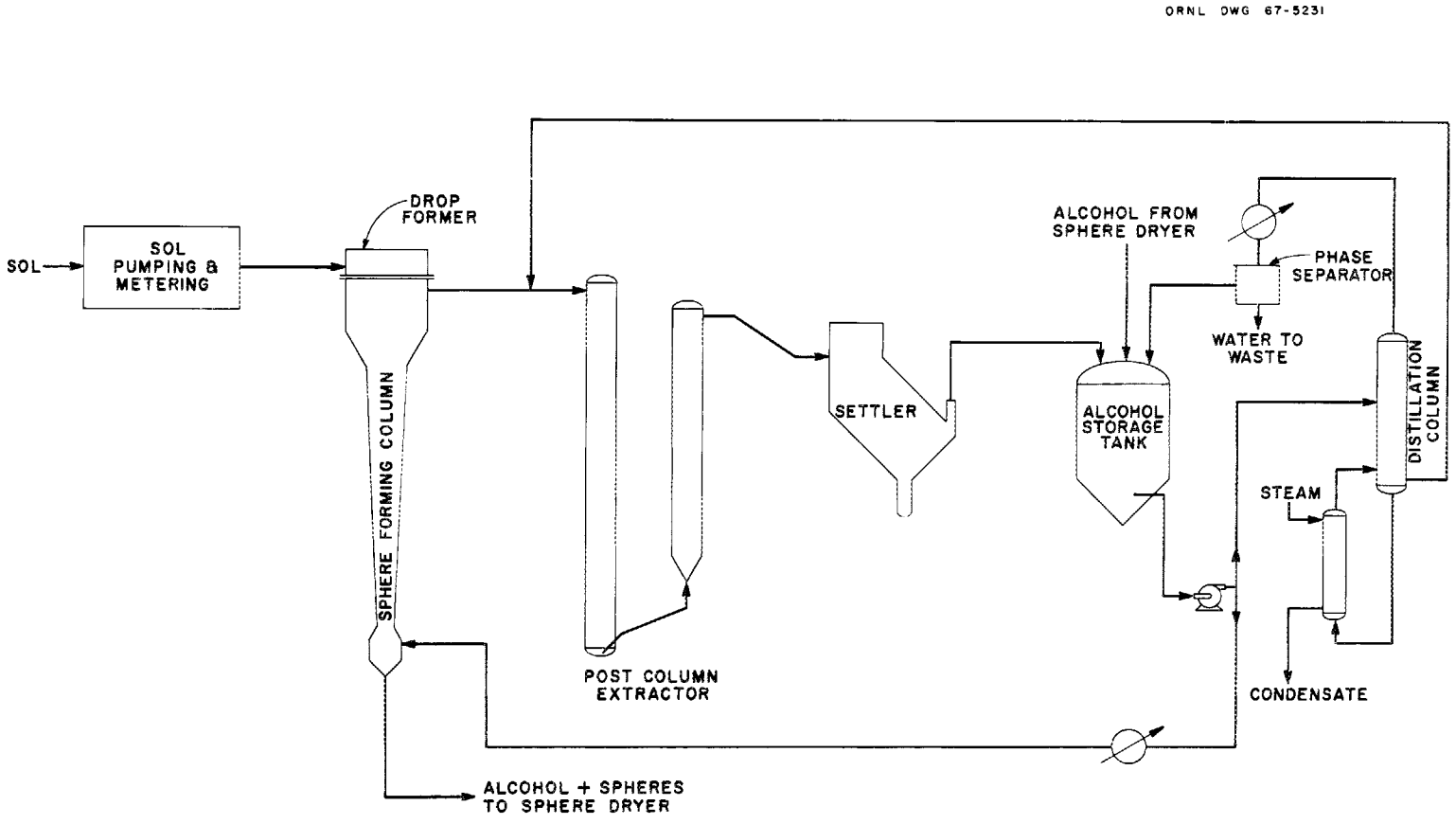

Fig. 6.15. Flow Diagram of TURF Sphere Forming Equipment.

simplified to minimize the number of equipment items and to reduce the space occupied by this process step (see Fig. 6.15). Only one mechanical pump is used to circulate alcohol for the entire system. This equipment is to be fitted within a framework which is $6 \times 6 \times 9$ ft high. The bulk of the equipment is considered nonvulnerable and will not be readily removable from the frame. Control valves, flowmeters, and the mechanical pump will be readily removable. Equipment design is under way and is scheduled for completion by June 30, 1967.

6.5 ^{233}U STORAGE AND DISTRIBUTION FACILITY

Oak Ridge National Laboratory serves as a storage, purification, and dispensing center for ^{233}U. Operations during the year, including uranium purification and transfers to and from the center, are summarized below. A study was made of the stability of uranyl nitrate solutions containing neutron poisons; the results of the study, indicating that the use of rare earths for criticality control in storage is feasible, are also presented.

Facility Operations Summary

During the past year, approximately 180 kg of ^{233}U (31 shipments) was received and 190 kg of ^{233}U (54 shipments) was transferred from the center. The bulk of the material had a low (<5 ppm) ^{232}U assay and was freshly purified at the production site. Approximately 73 kg of this material was exchanged with Nuclear Fuels Services (NFS), Erwin, Tennessee, for material of slightly lower purity (NFS is the fuel fabrication contractor for the Bettis Light Water Breeder Program). In addition, another 75 kg was transferred to the ORNL Neutron Physics Division for criticality experiments; this material will be returned to the center for storage.

Forty-six kilograms of ^{233}U was purified in five solvent extraction runs during the year.

The dissolver-leacher, described last year,[9] was placed in operation; performance during the year was satisfactory. The unit proved very efficient in the dissolution of high-fired ThO_2-UO_2 sol-gel material, attaining a dissolution rate approximately five times that observed in the batch dissolver. The dissolution rate of aluminum-canned UO_2 powder is limited to approximately 3 kg of ^{233}U per day.

Criticality Control in Storage

Facilities will be built for semipermanent storage of a large amount of mixed $^{233-235}UO_2(NO_3)_2$. Since geometrically safe facilities would be very expensive, calculations were made of the concentrations of samarium and gadolinium that would be required for criticality control. A solution that contains 150 g of U per liter and is 3.9 *M* in HNO_3, 0.05 *M* in $Sm(NO_3)_3$, and 0.05 *M* in $Gd(NO_3)_3$ would be both safe and stable. Stability was determined by storage in a stainless steel vessel at room temperature and at 90°C, by cooling until crystals formed, and by evaporation at room temperature until a precipitate formed.

No change was observed in the solutions at room temperature or at 90°C in stainless steel during a two-week period. Upon evaporation a precipitate was not formed until the solution was concentrated to 323 g of U per liter (a concentration factor greater than 2).

The solution could be cooled to between −25 and −30°C (−13 and −22°F) before crystals formed (they redissolved at about −18°C). A sample of the crystals was filtered from the solution. On heating, they liquefied, giving a solution of nearly the same composition as the supernatant liquid: supernatant – U, 121.6 mg/ml; HNO_3, 3.92 *N*; Sm, 8.2 mg/ml; Gd, 7.9 mg/ml; crystal solution – U, 165.5 mg/ml; HNO_3, 3.77 *N*; Sm, 7.9 mg/ml; Gd, 7.6 mg/ml.

---

[9] *Chem. Technol. Div. Ann. Progr. Rept. May 31, 1966*, ORNL-3945, pp. 141–42.

7. Sol-Gel Processes for the Uranium Fuel Cycle

7.1 URANIA

Chemical development of a urania sol-gel process was continued; further work was done to make the precipitation-peptization method of preparing urania sol more amenable to engineering scaleup. In addition, a laboratory-scale solvent extraction method for making urania sol was developed. Drying and firing conditions were established for preparing urania microspheres of near-theoretical density and low carbon content.

Work on the preparation of uranium(IV) solutions by catalytic reduction of uranyl(VI) nitrate with H_2 – a necessary first step in both urania sol preparation methods – included the development of a redox-potential measurement to determine the completeness of reduction, an investigation of possible slurry catalysts, and studies of the nature of the reduction process. A urania sol preparation method involving the direct reduction of U(VI) suspensions was developed on a laboratory scale; however, in considering engineering scaleup, this method was set aside in favor of the two sol preparation methods mentioned above. The urania sols were analyzed by means of chemical methods, pH and conductivity measurements, viscometry, electron microscopy, and x-ray diffraction techniques. Chemical development of zirconia sol preparation methods, the goal of which is the preparation of sols that are suitable for mixing with urania sols to prepare the mixed oxides, was continued. Urania-zirconia sols with a Zr/U mole ratio of 0.3 were prepared by an adaptation of the precipitation-peptization method of preparing urania sols.

Preparation of Urania Sols by Precipitation-Peptization

Chemical Development. – In the laboratory preparation of urania sol, the hydrous oxide was precipitated at pH 7.5 from a U(IV) nitrate-formate solution (NO_3^-/U mole ratio = 4.6; $HCOO^-$/U mole ratio = 0.6), collected by filtration, and washed in place until the NO_3^-/U mole ratio was at the level required for sol formation. The resulting filter cake was then heated at 60 to 65°C to produce a stable, fluid sol.[1,2] For engineering scaleup it was desirable to eliminate the filtration step, wash the precipitate completely free of electrolyte by decantation, and peptize the washed solids by the addition of peptizing electrolyte and heating. A tentative flowsheet for this procedure is shown in Fig. 7.1. A U(IV) solution is prepared by the catalytic reduction with hydrogen of a 0.5 *M* UO_2^{2+} solution 1 *M* in NO_3^- and 0.25 *M* in $HCOO^-$. After reduction and catalyst removal, concentrated formic acid is added to the reduced solution to give an $HCOO^-$/U mole ratio of 0.6 to 1.0. (This adjustment is necessary because part of the original $HCOO^-$ is destroyed in the reduction step.) The hydrous oxide is then precipitated by the addition of 3.5 *M* NH_4OH or 3.0 *M* NH_4OH–0.5 *M* $N_2H_4 \cdot H_2O$ to pH 9.0. The resulting precipitate is washed free of electrolyte by decantation, using either H_2O or 0.01 *M* $N_2H_4 \cdot H_2O$. The washed precipitate is resuspended, HNO_3 and HCOOH are added, and the suspension is stirred at 60 to 63°C until peptized.

The use of a U(IV) feed solution containing a much lower NO_3^-/U mole ratio than that used in the laboratory process was prompted by development studies which indicated that a stable U(IV) solution containing an NO_3^-/U mole ratio of 2 could be prepared if a small amount of formic acid were added prior to reduction.[2] It should be

[1] J. P. McBride *et al.*, *Preparation of UO_2 Microspheres by a Sol-Gel Technique*, ORNL-3874 (February 1966).

[2] *Chem. Technol. Div. Ann. Progr. Rept. May 31, 1966*, ORNL-3945, p. 157.

noted that when the uranium is completely reduced, the solution is acid-deficient. The use of hydrazine in the precipitation and washing steps and the addition of formic as well as nitric acid in the peptization step apparently control aging mechanisms in the precipitate and increase the sol yields. Initial laboratory studies of the engineering flowsheet, using NH_4OH as the precipitating agent, H_2O as the wash solution, and decantation washing (where the period between precipitation and subsequent peptization was as long as 48 hr), indicated that peptization was not always achieved and that sol yields were not as high as desired; these poor results were apparently associated with a precipitate aging effect. Out of ten preparation attempts, good-quality sols were produced in only six. The subsequently adopted use of hydrazine in the precipitation and washing steps and formic acid in the peptizing step has made the process more reproducible and increased the sol yields to more than 90%.

Table 7.1 shows the effects of the precipitating reagent and wash solution on sol yields and sol properties. The hydrous oxide precipitates were washed by decantation and peptized by the addition of HNO_3.

Table 7.2 shows the effect of the precipitating reagent and peptizing conditions on the sol yield and the sol properties.

Equipment Development and Sol Production. – The flowsheets derived from the laboratory studies were used in three routine developmental applications: (1) the preparation of UO_2 irradiation specimens, (2) the preparation of urania sol for

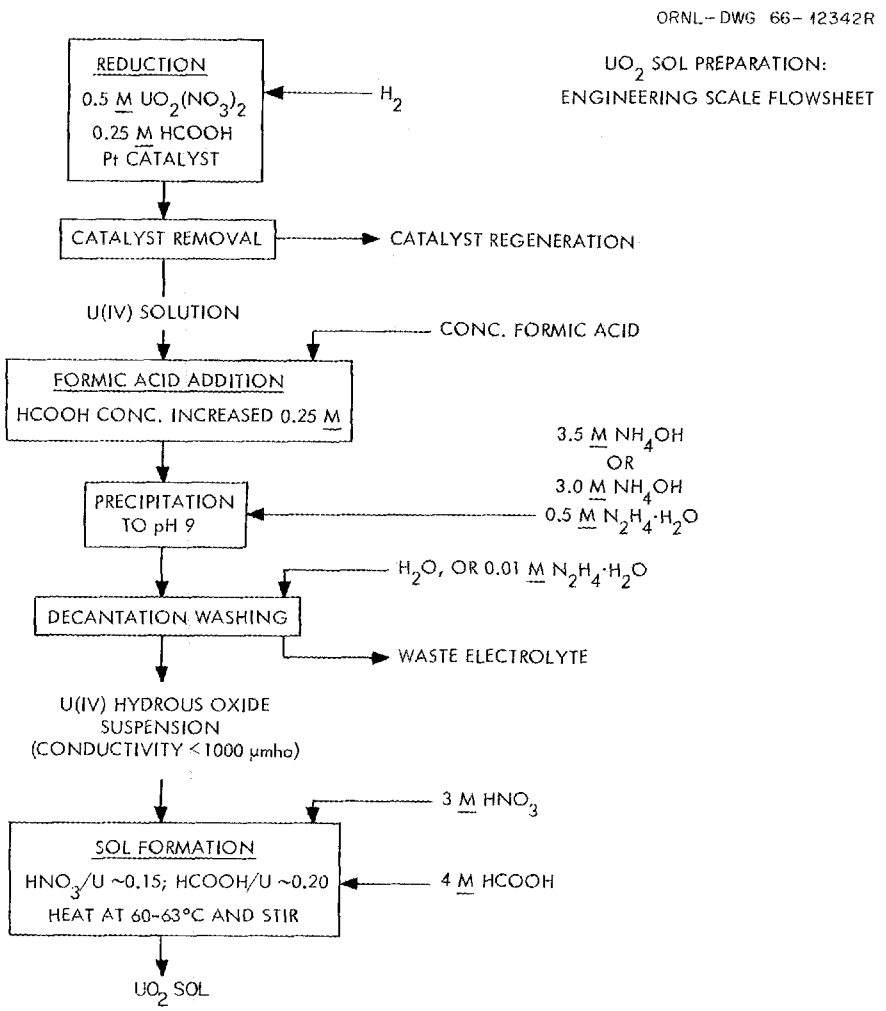

Fig. 7.1. Flowsheet for the Engineering-Scale Preparation of Urania Sol.

Table 7.1. Urania Sol Preparation Using Decantation Washing[a]

Preparation	Precipitation Conditions		Wash Solution	Sol Yield (%)	Sol Properties			
	Formate-to-Uranium Mole Ratio in Feed	Reagent			Uranium Concentration (*M*)	U(IV) Content (% of U)	Nitrate-to-Uranium Mole Ratio	Formate-to-Uranium Mole Ratio[b]
NUFD-13A	0.94	3.5 *M* NH_4OH	H_2O	72[c]	0.70	86	0.18	0.33
NUFD-13B	0.98	3.5 *M* NH_4OH	0.05 *M* HCOOH	69	0.87	84	0.22	0.50
NUFD-14A	0.87	3.5 *M* NH_4OH	0.013 *M* HCOOH	79	0.75	87	0.17	0.40
NUFD-14B	0.53	3.5 *M* NH_4OH	0.007 *M* HCOOH	59	0.45	88	0.29	0.30
NUFD-16A	0.79	3.5 *M* NH_4OH	0.01 *M* NH_4COOH	66	0.58	83	0.16	
NUFD-16B	0.77	3.5 *M* NH_4OH	0.01 *M* N_2H_5COOH	86	0.71	87	0.23	0.16
UNR-2	0.82	3.5 *M* NH_4OH	0.01 *M* N_2H_5COOH	84	0.74	88	0.23	0.19
UNR-5	0.59	3.5 *M* NH_4OH	0.01 *M* $N_2H_4 \cdot H_2O$	95	0.65	85	0.16	0.06
UNR-7	0.61	3.5 *M* NH_4OH, 0.2 *M* $N_2H_4 \cdot H_2O$	0.01 *M* N_2H_5COOH	92	0.85	87	0.16	0.13
UNR-9M	0.84	3.5 *M* NH_4OH, 0.2 *M* $N_2H_4 \cdot H_2O$	0.02 *M* N_2H_5COOH	94	0.88	87	0.11	0.29
UNR-6	0.61	2.5 *M* NH_4OH, 1.0 *M* $N_2H_4 \cdot H_2O$	0.01 *M* N_2H_5COOH	>90	0.62	84	0.16	0.12
UNR-1	0.79	3.0 *M* NH_4OH, 0.5 *M* $N_2H_4 \cdot H_2O$	0.01 *M* N_2H_5COOH	96	0.54	87	0.23	0.16

[a]Sol preparation conditions: 0.5 *M* U(IV) solution; NO_3^-/U mole ratio of 2.0; precipitate to pH 9, wash by decantation, peptize by addition of HNO_3(NO_3^-/U mole ratio = 0.14) and stirring at 60 to 65°C.

[b]Analyzed as carbon.

[c]Peptized with HNO_3 and HCOOH; NO_3^-/U mole ratio = 0.14; $HCOO^-$/U mole ratio = 0.20.

Table 7.2. Urania Sol Preparation Using Filtration Washing[a]

Preparation	Precipitating Reagent	Peptization Conditions		Sol Yield (%)	Sol Properties			
		Nitric Acid-to-Uranium Adjustment	Formic Acid-to-Uranium Adjustment		Uranium Concentration (*M*)	U(IV) Content (% of U)	Nitrate-to-Uranium Mole Ratio	Formate-to-Uranium Mole Ratio
A-3403-83[b]	3.0 *M* NH_4OH, 0.5 *M* N_2H_4OH	0.1	0	82[c]	1.13	84	0.13	0.05
A-3403-85	3.0 *M* NH_4OH, 0.5 *M* $N_2H_4 \cdot H_2O$	0.1	0	59[c]	0.95	86	0.12	0.01
A-3403-90	3.0 *M* NH_4OH, 0.5 *M* $N_2H_4 \cdot H_2O$	0.1	0.2	96	1.60	89	0.14	0.30
A-3403-96	3.5 *M* NH_4OH	0.1	0.2	72	1.26	88	0.13	0.24
A-3403-97	3.0 *M* NH_4OH, 0.5 *M* $N_2H_4 \cdot H_2O$	0.15	0.2	98	1.62	88	0.17	0.24
A-3403-100	3.0 *M* NH_4OH, 0.5 *M* $N_2H_4 \cdot H_2O$	0.15	0.2	99	1.40	85	0.15	0.23
A-3403-107	3.5 *M* NH_4OH	0.15	0.2	99	1.27	82	0.21	0.24
A-3403-111	3.5 *M* NH_4OH	0.19	0[d]	92	1.19	82	0.17	
A-3403-115[b]	3.5 *M* NH_4OH, 0.5 *M* $N_2H_4 \cdot H_2O$	0.15	0.2	96	1.04	79	0.15	0.008

[a]Sol preparation conditions: 0.5 *M* U(IV) solution; NO_3^-/U mole ratio = 2, $HCOO^-$/U mole ratio ~0.5; precipitate to pH 9; filter and wash in place; add HNO_3 or HNO_3–HCOOH and peptize by heating and stirring at 60 to 65°C. Time between precipitation and peptization <1 hr.

[b]0.5 *M* U(IV) solution; NO_3^-/U mole ratio = 4.6; $HCOO^-$/U mole ratio = 0.6.

[c]18 hr between precipitation and peptization.

[d]0.01 *M* N_2H_5COOH wash.

use in the development of processes for forming microspheres, and (3) the development of remotely operated equipment for possible use in the preparation of urania sols in TURF. The flowsheets had to be modified somewhat for each of these applications.

One of the flowsheets for urania sol preparation[1] was used in the preparation of microspheres for irradiation specimens; over 10 kg of enriched urania was used to form microspheres. Criticality control was maintained by limiting the batch size to 300 g of uranium. Hence, the enriched urania used in irradiation specimens was made in laboratory batch apparatus, using the flowsheet for precipitation at pH 7 to 7.5.

Most of the natural urania sols that were formed into microspheres during the year were prepared in a batch apparatus (1 kg of UO_2 per batch) using the engineering-scale flowsheet with precipitation at pH 9. The precipitation, washing, and dispersion were done in a single vessel that had a 12-in.-diam porous stainless steel plate as the bottom; it was equipped with a slow-speed paddle-type agitator. The supernatant was removed by filtration after precipitation and after each of four washing steps. The washing involved stirring 10 liters of H_2O with the 5 liters of filter cake. Peptization to sol was achieved by adding HNO_3 and HCOOH to the washed precipitate, and stirring and heating at ~60°C. Compositions typical of these sols are given for two of the last batches, F-31 and F-32, in Table 7.3.

A continuous urania sol preparation system (Fig. 7.2) was designed and fabricated to meet the requirements for both remote operation and large-scale critically safe operation with enriched uranium. This system consists of two continuous precipitators, six countercurrent mixer-decanter stages, and two continuous peptizers. The wash water flows by gravity, and the solids are transferred by gas-operated pumps. The initially installed precipitators, gas-operated pumps, and peptizers were inadequate for the transfer of precipitates and were replaced by units of modified design.

Two 70-hr runs, using the engineering-scale flowsheet and a natural-uranium feed rate of 0.5 mole/hr, were made in this system, which is called the P^2C^2D system (**P**recipitation-**P**eptization **C**ounter-**C**urrent **D**ecantation). The slurry pumped from the final settler was 0.2 to 0.4 *M* in U for most operating conditions. The sol products were dilute and had to be concentrated before they were suitable for the preparation of microspheres (Table 7.3). The operational data indicated that the P^2C^2D system satisfied the chemical flowsheet requirements. The mechanical operation of the system was marginal, with transfer of solids between stages and metering of flows into the peptizers being the principal problems. The results indicate that the P^2C^2D system as presently constituted would be acceptable for direct operation but not for remote operation. To obtain a system suitable for remote operation, more equipment development would be required.

A 12-ft-high, 4-in.-ID column was tested for countercurrent washing of the uranous hydroxide precipitate. Such a column might replace the mixer-decanters and solids-transfer pumps in the P^2C^2D system. The wash column tests showed good mechanical operation and adequately satisfied the washing requirements for either a batch precipitator or the P^2C^2D precipitators. The problems for peptization are approximately the same as those for the P^2C^2D system; however, the wash column has a shorter residence time and thus less holdup of precipitate. The wash column products were dewatered and peptized in the batch agitated filter apparatus. The sol compositions in Table 7.3 show the results that are possible with continuous operation of the wash column (WCT-1) and with a batch type of operation that is presently planned for the preparation of enriched uranium sols (WCT-8, -9, -10).

Preparation of Aqueous Urania Sols by Solvent Extraction

The preparation of aqueous urania sols by solvent extraction is being studied. In this process, sufficient nitrate ion is extracted in a stagewise fashion from an aqueous 0.2 *M* U(IV)–0.4 *M* NO_3^-–$HCOO^-$ solution to cause hydrolysis of the U(IV) and the production of a sol. The nitrate ion extraction is accomplished in mixer-settler equipment by contacting the aqueous phase with an immiscible organic phase containing 0.1 *M* Amberlite LA-2,[3] a long-chain secondary aliphatic amine, *N*-lauryltrialkylmethylamine, in *n*-paraffin.[4] The final NO_3^-/U mole ratio in the aqueous phase is

[3]Rohm and Haas, Philadelphia, Pa.

[4]South Hampton Co., Houston, Tex.

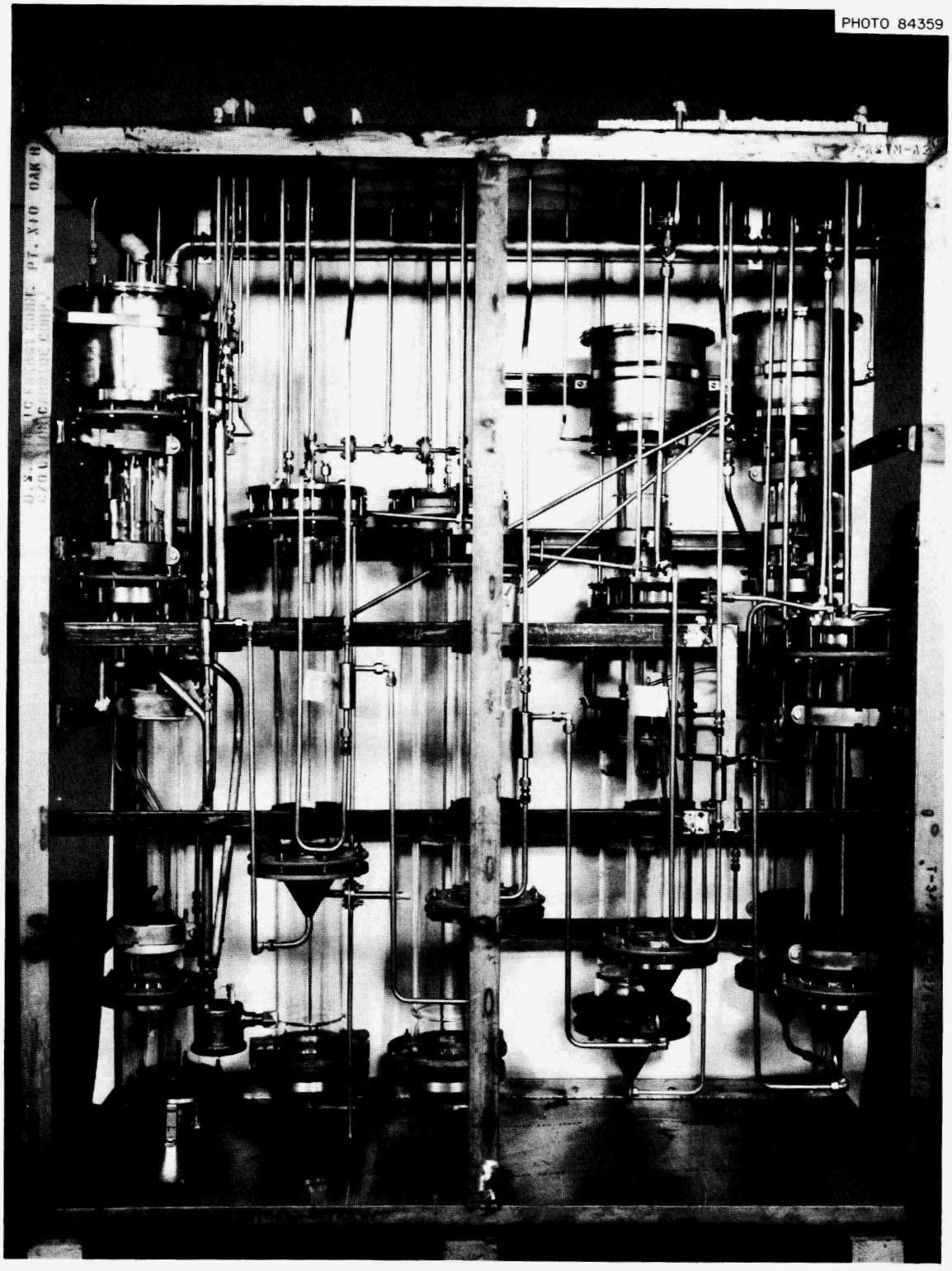

Fig. 7.2. Equipment Used for the Production of Urania Sol.

Table 7.3. Analyses of UO_2 Sols from Continuous or Large-Batch Equipment

Chemical flowsheets: Precipitation to pH 8 to 9; washing; addition of HNO_3 and HCOOH for peptization

Preparation System	Code No.	Precipitation pH	U Conc. (*M*)	U(IV) Content (% of U)	NO_3^-/U Mole Ratio	$HCOO^-$/U Mole Ratio	NH_4^+/U Mole Ratio
Batch agitated filter	F-31	9.0	0.75	86	0.168	0.26	
	F-32	9.0	0.84	88	0.159	0.41	0.026
P^2C^2D[a]	4-2	9.0	0.39	86	0.144		0.016
	4-3	9.0	0.49	87	0.120	0.17	0.018
	4-8	8.0	0.30	87	0.144	0.25	0.013
	4-9	8.0	0.31	87	0.154	0.29	0.013
Wash column	WCT-1	9.0	0.90	85	0.15	0.26	0.04
	WCT-8	8.4	0.91	87	0.22	0.30	0.002
	WCT-9	8.6	1.11	84	0.10	0.21	0.001
	WCT-10	8.6	0.97	80	0.20	0.14	0.001

[a]Precipitation-peptization countercurrent decantation method.

about 0.1. The overall chemical reaction is conveniently represented by the following equation:

$$U(NO_3)_4 + 4R_2NH + 4H_2O \rightarrow UO_2 \cdot 2H_2O + 4R_2NH \cdot HNO_3 .$$

The hydrated urania is obtained as a fluid, black sol that is stabilized in suspension by the residual NO_3^- and $HCOO^-$. Under the conditions of this process the $HCOO^-$ is not appreciably extracted.

The process consists in the preparation of the U(IV) solution by the catalyzed hydrogen reduction of $UO_2(NO_3)_2$, two extraction stages with a digestion period between, and concentration of the dilute sol by evaporation at reduced pressure (Fig. 7.3). In the laboratory, batchwise extraction is used, and an inert atmosphere is maintained during the operations.

Preparation of the U(IV) Solution. – The U(VI) in a solution containing 0.2 *M* UO_2^{2+}–0.4 *M* NO_3^-–0.1 *M* $HCOO^-$ is reduced to U(IV) by sparging with hydrogen (while stirring vigorously), at atmospheric pressure and ambient temperature, in the presence of a catalyst (we use 5% Pt on Al_2O_3 powder). The resulting solution contains > 99% U(IV) and a decreased $HCOO^-$ content due to losses in side reactions. The catalyst is removed by sedimentation and filtration; the resulting U(IV) solution is stored under argon.

Extraction and Digestion. – The NO_3^- extraction is carried out in two stages. In each stage, we used an amount of diluted amine that was stoichiometrically equivalent to one-half of the total NO_3^- present initially. In the first stage, 1.25 liters of 0.2 *M* U(IV)–0.4 *M* NO_3^- – ~0.075 *M* $HCOO^-$ aqueous solution is equilibrated with 2.5 liters of 0.1 *M* Amberlite LA-2 in *n*-paraffin by mixing for 10 min at ambient temperature (26°C). The aqueous phase is separated and then digested at 50 to 55°C for 0.5 hr. Its composition is approximately 0.2 *M* total U [90% U(IV)]–0.2 *M* NO_3^-–~0.075 *M* $HCOO^-$. The second extraction is made by equilibrating the digested aqueous phase with 2.5 liters of fresh 0.1 *M* Amberlite LA-2 solution for 10 min at the temperature that results from the mixing of the warm aqueous and the fresh, unheated organic phase (~30°C). The aqueous product of the second extraction is a dilute urania sol with the approximate composition 0.2 *M* total U [~90% U(IV)]–0.02 *M* NO_3^-–0.075 *M* $HCOO^-$. A turbine stirrer operating at 1000 rpm is used in the extraction stages, and the aqueous phase is stirred during digestion. In batch operation the aqueous phase is added to the stirred organic phase to obtain a water-in-oil type of emulsion to facilitate phase disengagement after equilibration.

The organic/aqueous volume ratio of 2 was chosen for this same reason. The used organic phases are washed with Na_2CO_3 solution; the recovered solvent can be recycled for process use.

Previous experience with urania sols[1] had indicated that the NO_3^-/U mole ratio should be about 0.1, but attempts to remove the necessary amount of NO_3^- from the aqueous phase in one extraction resulted in the formation of a black gelatinous precipitate. If aged for sufficient time at room temperature, the precipitate became liquid. The rate of liquefaction could be increased by warming the precipitate at 45 to 50°C. Precipitation also occurred when the NO_3^- extraction was carried out in two or three stages; however, the aqueous phase remained fluid if only 50 to 70% of the total NO_3^- was extracted. By interposing a digestion step (heating at 50 to 55°C for 0.5 hr) between the two extraction steps, it was possible to maintain the aqueous phase in a fluid condition throughout the extraction cycle. The process can be operated in a continuous manner. The temperature range for the digestion is important since lower temperatures would require longer digestion periods, while at higher temperatures the possibility of oxidation of the U(IV) is increased. The chemical changes occurring during the digestion step are not known; however, the aqueous phase, which is originally dark green and transparent, can be observed to change to a brown-black, opaque liquid. It may be surmised that further hydrolysis of the U(IV) and growth of urania crystallites occur.

When the first extraction is made at room temperature, some difficulties are encountered due to the formation of an unidentified voluminous, gray, stringy material that collects at the interface and distributes predominantly in the aqueous phase. The presence of this material increases disengagement time and interferes with the mechanical separation of the phases in the laboratory apparatus. It was found that a satisfactory way of solving this problem is to perform the first extraction at about 45°C. Although the troublesome material remains, it distributes predominantly in the organic phase; the phase disengagement time in the laboratory apparatus is decreased from about 4 min to about 1 min, and entrainment of the organic material into the aqueous phase is minimized. However, extraction at the elevated temperature results in some loss of U(IV) by oxidation. Increasing the total $HCOO^-$ concentration by a factor of 2 above its initial concentration by adding HCOOH after the reduction step is completed will also alleviate the phase separation

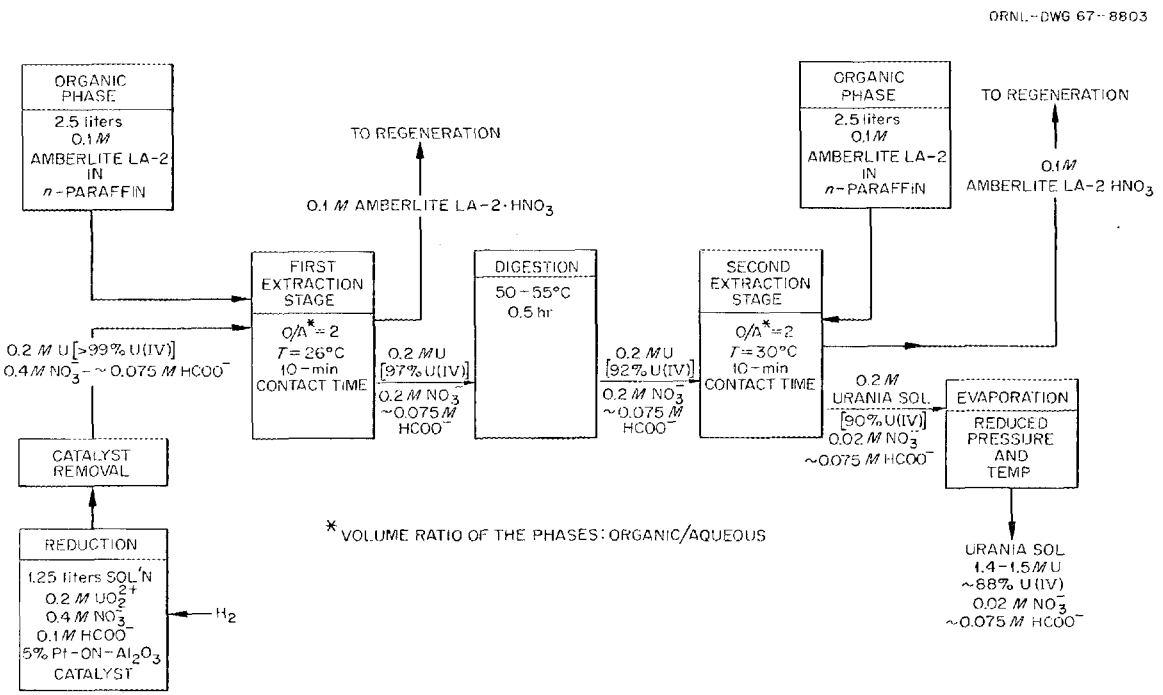

Fig. 7.3. Flowsheet for Preparation of Aqueous Urania Sols by Amine Extraction.

problem; however, use of this method will create other problems in the formation of microspheres. It should be emphasized that, while this unidentified material causes difficulties in the laboratory apparatus, the entrainment problem can probably be minimized in large-scale continuous operation by proper design of the phase separators. Formation of the troublesome material is not encountered in the second extraction stage.

Concentration of the Dilute Sol. – The urania sols produced by the process described above are about 0.2 *M* in total U, which is too dilute for use in producing urania microspheres by dispersion in 2EH in the usual manner.[1] For that purpose, the total U concentration in the sol should be about 1.0 *M* or higher. The dilute urania sols have been concentrated by evaporation at reduced pressure (31 torrs) and temperature (28 to 29°C) in a rotary vacuum evaporator to yield fluid sols with a total U concentration as high as 1.55 *M*.

Modifications to the Basic Process. – The basic solvent extraction process was modified to obtain information for continuous operation in large-scale extraction equipment. It was shown that the extraction process may be operated cocurrently, thus permitting simplification in equipment design. Increasing the organic/aqueous volume ratio to 2.1 while holding all concentrations fixed did not affect the sol, indicating that some excess amine is permissible in the extraction stages. This makes flow control less critical in the large-scale operation. Also, if needed, a third extraction stage may be added without deleterious effects on the product; it is possible that a third stage will be required to achieve the desired NO_3^- removal. The use of 1.5 times the stoichiometrically required amount of amine did not materially affect the final NO_3^-/U mole ratio, indicating that the NO_3^- extraction tends to be self-limiting. The effect of operating the extraction stages at elevated temperatures is now being studied; results are not yet available.

Chemical Analyses of Some Urania Sols. – Results of a group of experiments in which dilute urania sols were prepared under various conditions and then concentrated by evaporation at reduced pressure and temperature are given in Table 7.4.

Preparation of Urania Microspheres. – Experience in forming microspheres from urania sols and in the subsequent calcination of the spheres to dense UO_2 has been very limited since the quantities of

Table 7.4. Analyses of Aqueous Urania Sols Prepared by Amine Extraction

Aqueous feed: average composition, 0.2 *M* total U [>99% U(IV)]–0.4 *M* NO_3^-–0.075 *M* $HCOO^-$[a]
Organic phase: 0.1 *M* Amberlite LA-2 in *n*-paraffin

	Basic Process	High $HCOO^-$ Process[a]	Cocurrent Batch Process	"Excess" Amine Process	Three Extraction Stages
Volume ratio, O/A	2	2	2	2.1	2
Extraction stages	2	2	2	2	3
As-formed sol					
Total U, *M*	0.208	0.204	0.205	0.206	0.205
U(IV), %	89.96	98.25		89.56	92.49
Mole ratios:					
NO_3^-/U	0.12	0.10	0.095	0.074	0.085
$HCOO^-/U$	0.34	0.82	0.50	0.34	0.49
Concentrated sol					
Total U, *M*	1.39	1.44	1.58	1.44	1.55
U(IV), %	88.18	96.60	88.40	87.53	91.05
Mole ratios:					
NO_3^-/U	0.12	0.08	0.096	0.077	0.11
$HCOO^-/U$	0.37	0.44	0.28	0.26	0.38

[a]Total $HCOO^-$ concentration in sol with high $HCOO^-$ content was 0.173 *M*.

urania sols produced in the laboratory have been too small to permit extensive investigation. With urania sols prepared by the basic procedure as the starting material, large batches of microspheres have now been formed in the sphere-forming column using 2EH that contains 0.58 vol % Ethomeen S/15 and 0.48 vol % Span 80. These spheres were dried in steam and argon and then calcined to dense UO_2 by heating to 1250°C in Ar–4% H_2. The microspheres had the composition $UO_{2.006}$ and contained 0.091% carbon; measurements at 210 psi (Hg displacement method) showed the density to be 98% of the theoretical value.

Drying and Firing Studies on Sol-Gel Urania Microspheres

Drying and firing studies on sol-gel UO_2 microspheres are being made[1] to establish firing conditions that will yield products of low carbon contents (<50 ppm) and near-theoretical density. The major problem in firing UO_2 gel microspheres is the removal of carbon that is introduced during the microsphere-forming step as sorbed 2EH and surfactant.[1,2] Low-temperature drying methods such as steam drying to 200°C or washing at room temperature with acetone or methanol were unsuccessful in removing carbon to acceptably low levels. To remove carbon and to achieve high density, a mildly oxidizing gaseous atmosphere is necessary during the firing. Also, it appears that chemical reaction with either H_2O or CO_2 is required for removing the final traces of carbon compounds. Firing in an H_2O atmosphere has been far more successful than firing in a CO_2 atmosphere, although in many cases the latter has yielded adequate results. The difficulty in removing carbon with the CO_2 or H_2O atmosphere stems from the fact that the maximum shrinkage rate and pore closure occur between 400 and 600°C – the temperature range where carbon is oxidized. Carbon dioxide is more effective than H_2O in promoting sintering; this may be a disadvantage since it leads to trapping of the carbon compounds before they are oxidized, thus tending to inhibit densification. The enhancement of sintering may be due to oxidation of the UO_{2+x} by CO_2 or H_2O. Thermogravimetric analyses (TGA) show that oxidation of the UO_{2+x} by CO_2 or H_2O occurs at temperatures below those where carbon is oxidized. This result is in agreement with thermodynamic calculations.

The most effective atmosphere used to date for attaining low carbon content and high density has been Ar–4% H_2 saturated with water vapor at 90°C (H_2O/H_2 mole ratio, ≈40). Other compositions have not as yet been investigated. Thermodynamic calculations show that the composition of H_2-H_2O presently used is reducing with respect to UO_{2+x} up to 1000°C at all values of x of 0.05 or greater (x in our UO_{2+x} gels ranges from 0.1 to 0.35) but is oxidizing to carbon or hydrocarbons. On the other hand, Ar-H_2O or CO_2 atmospheres are oxidizing to the UO_{2+x} under the same conditions. Current work involves establishing the optimum kinetics for both carbon removal and densification using Ar-H_2-H_2O atmospheres.

In the past year, basic studies of the effect of various atmospheres on the sintering of UO_{2+x} gels were made in an attempt to gain information on both carbon removal and densification. Studies of shrinkage rate, crystallite growth, and surface area decrease were made. Differential thermal analysis (DTA), thermogravimetric analysis (TGA), and analyses of evolved gases were used to investigate phenomena that occur during the firing of UO_2 gels in various atmospheres. Low-temperature drying conditions were examined for their effectiveness in carbon removal. Firing procedures using a variety of atmospheres and soaking conditions were evaluated for their effectiveness in carbon removal and densification on a 10- to 300-g scale.

Low-Temperature Drying Studies

Low-temperature drying studies in Ar or in Ar-steam show[1] that carbon is not effectively removed by these atmospheres. Even after drying to 350 to 400°C, the gels still contained about ½% carbon. Argon-steam was slightly more effective than argon. The measured NO_3^-/U mole ratios indicate that nitrate removal is nearly complete at 180 to 200°C. The NO_3^-/U mole ratios were about 0.15 in the original sol. The O/U atom ratios were not affected by the drying. Amounts of steam above 2 g per gram of UO_2 gel did not significantly increase the rate of carbon removal below 200°C. The drying results indicate that the carbon-bearing materials are very strongly sorbed.

Oxidation Studies Using Thermogravimetric Techniques

Experiments in which oxidation was studied using TGA methods were reported previously.[1]

Additional studies made during this report period showed that the UO_{2+x} gels are readily oxidized by CO_2 or Ar-H_2O at 400°C or higher, but that the oxidation of carbon is not very rapid until a temperature of 500°C is reached. Weight changes at constant temperatures above 500°C indicated that simultaneous oxidation of the UO_{2+x} and the mixed carbon-bearing species was occurring. Initially, the rate of UO_{2+x} oxidation exceeded the rate of carbon oxidation, but after 2 to 5 min the rate of carbon oxidation increased. After treatment in CO_2 at temperatures as high as 650°C, the UO_2 sample lost 90% of its surface area. The oxidation of UO_{2+x} with CO_2 or H_2O is in agreement with thermodynamic calculations. Thermodynamic calculations also indicate that the oxidation of UO_{2+x} can be prevented during the carbon-removal step by using as little as 0.1% CO in the CO_2 or 0.1% H_2 in H_2O. The effect of the H_2-H_2O atmosphere will be evaluated in future TGA studies.

Firing Studies Using Various Atmospheres

In the firing of UO_2 gel microspheres, the gel is heated and soaked in atmospheres that can potentially react chemically with and remove the carbon and can then densify the gel. The final sintering is done in Ar–4% H_2 to reduce the UO_{2+x} to $UO_{2.00}$. Additional studies were made to determine the effects of CO_2 and Ar–4% H_2 atmospheres and room-temperature exposure to air followed by firing in Ar–4% H_2. In the present work with CO_2, a mixture of brown and black spheres is nearly always obtained (in earlier work, the fired spheres were always a uniform black color). The particle density of this mixture is frequently less than the desired 95% of theoretical. The brown spheres appear to be less dense than the black ones and generally contain fine closed porosity. This color effect is also observed when large batches (>100 g) of gel spheres are fired in Ar–4% H_2–H_2O atmospheres.

Table 7.5. Firing of UO_2 Gel Microspheres in Various Atmospheres to 1000 to 1200°C

Gel size: ~600 μ in diameter
Batch size: CO_2, H_2O atm: 100 to 300 g
Ar, Ar–4% H_2 atm: 10 to 25 g

Microsphere Preparation	Gel Analysis		Firing Code	Final Product Analysis[b]			
	O/U Atom Ratio	Net Carbon[a] (ppm)		Carbon (ppm)	Density[c] (g/cm^3) Hg at 210 psi	Hg at 15,000 psi	Helium
P-11-15-1550	2.37	0.50	Ar–4% H_2	70	10.83	10.83	10.94
			Air–(Ar–4% H_2)	30	10.90		
			Ar	<20	10.80		
			CO_2-1	<20	10.84		
			CO_2-B	<20	10.37	10.59	
P-11-10-1215	2.34	1.02	Ar–4% H_2	50	10.81		
			Ar	90	10.77		
			CO_2-1	<20	10.70		
			(Ar–4% H_2)–H_2O	60	10.6		10.8
P-10-20-1600	2.27	1.94	Ar–4% H_2	5500	10.4	10.6	10.6
			CO_2-1	120	10.70		10.81
			Ar–3% H_2O	110	10.72		10.90
P-11-7-1545	2.23	1.75	CO_2-1	160	10.90		10.94
			CO_2-B	50	10.79		11.02

[a] Formate-derived carbon is subtracted from the total carbon.

[b] O/U atom ratios for final material were 2.002 or less.

[c] Theoretical density is 10.97 g/cm^3.

Attempts are being made to determine the reason for this previously unobserved phenomenon.

Some typical results of the firings using various atmospheres are shown in Table 7.5. It is evident from the data that firing in Ar–4% H_2 is only effective for removing carbon from gels having O/U atom ratios of >2.3; moreover, this effectiveness may be dependent on the amount of excess oxygen in the UO_{2+x} relative to the amount of sorbed carbon compounds. Apparently, the excess oxygen can react with the sorbed organic materials. Exposure of the gel spheres to air at room temperature prior to firing in Ar–4% H_2 was effective only for spheres with the higher O/U atom ratios. Firing in argon rather than in Ar–4% H_2 seems to improve the carbon removal; however, it is also only effective for spheres with the higher O/U atom ratios, probably because excess oxygen is retained to higher temperatures in the argon atmospheres. With the use of Ar–3% H_2O, high-density spheres were always obtained, but the carbon contents were usually 100 to 200 ppm.

Preparation of U(IV) Solutions

The U(IV) solutions used in urania sol preparation by precipitation-peptization were prepared by the catalytic reduction with hydrogen of 0.5 *M* $UO_2(NO_3)_2$–0.25 *M* HCOOH solutions. In the laboratory the reductions are carried out in a stirred, baffled flask using finely divided palladium-on-thoria or platinum-on-alumina catalysts, and hydrogen is added through a sintered-glass gas diffuser tube. Solutions of U(IV) for the engineering-scale sol preparation are prepared in a stainless steel reactor constructed of 2-in. pipe containing a fixed bed of platinized-alumina catalyst. Solution and hydrogen are passed cocurrently through the reactor, which is maintained at a hydrogen pressure ≧300 psi.

Laboratory Development. – The apparatus shown in Fig. 7.4 was assembled to compare various catalysts for use in the reduction step and to provide information on the nature of the reduction process. Wet-test meters and rotameters installed on the gas input and outlet of the reduction flask were used to control the hydrogen flow rate and to measure the hydrogen consumption during reduction. Progress of the reduction was followed by measuring the redox potential with a platinum electrode and a silver–silver chloride reference electrode. As the occasion demanded, the solution was sampled, and the U(IV) and U(VI) contents were determined analytically.

Figure 7.5 shows the curve of the potential obtained during the preparation of a U(IV) solution of the composition 0.5 *M* U–1.0 *M* NO_3^-–0.25 *M* HCOOH. A sharp break in the curve is observed between 96 and 100% U(IV). If a saturated calomel reference electrode had been used, the potentials would have been more negative by about 44 mv. The presence of hydrogen has a marked effect on the potential observed at the platinum electrode. The potentials shown in Fig. 7.5 were measured while hydrogen flowed into the solution at a pressure of 1 atm (to keep the solution saturated with hydrogen). When hydrogen is removed and an argon blanket is substituted, the potential observed in a 100% U(IV) solution is about –100 mv. Measurements of potential were made repeatedly and reproducibly to follow the progress of the reduction during the laboratory-scale preparation of uranous nitrate-formate solutions; they were also used in estimating U(IV) concentrations in solutions that were prepared in stainless steel equipment. No special precautions were taken with the

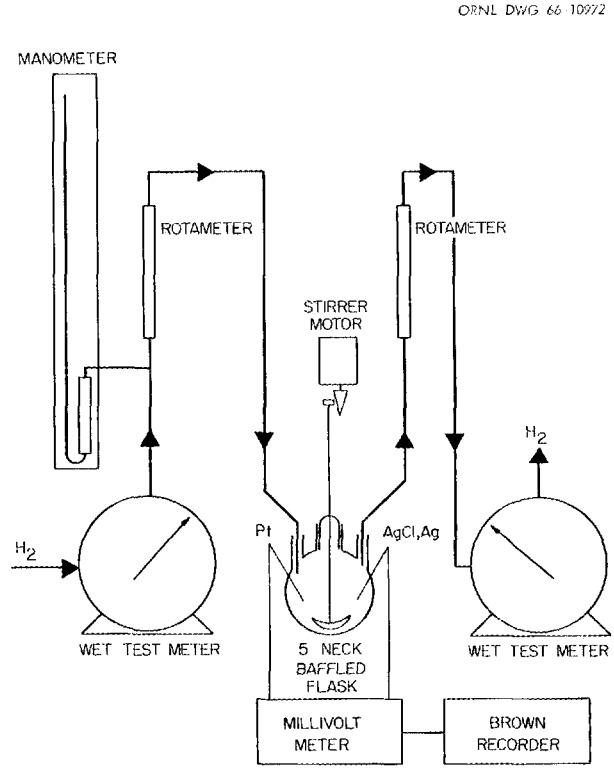

Fig. 7.4. Diagram of Reduction Apparatus.

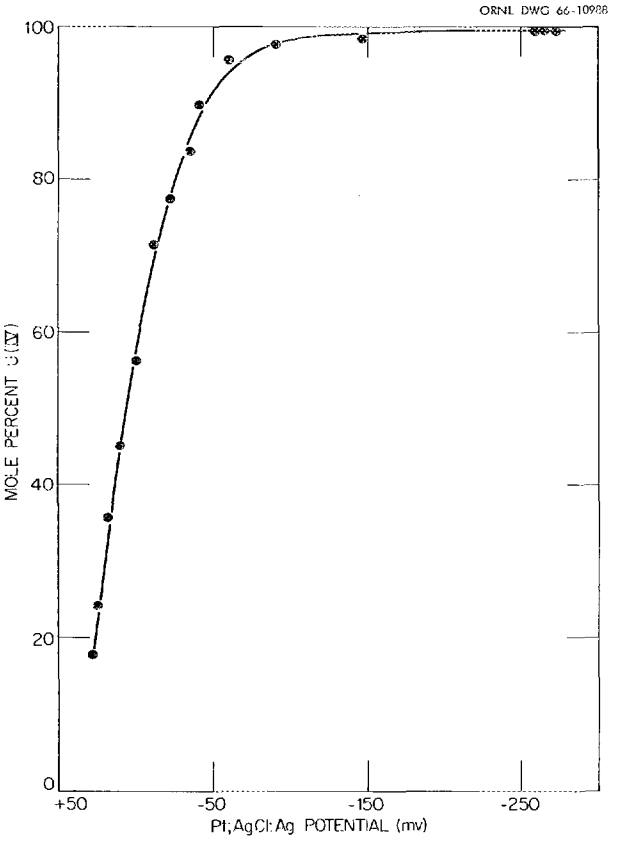

Fig. 7.5. Redox Potential Under Hydrogen at 1 atm Pressure During the Preparation of a U(IV) Solution of the Composition 0.5 *M* U–1.0 *M* NO_3^-–0.25 *M* HCOOH.

platinum electrode except to store it in distilled water when it was not in use.

Three slurry catalysts for possible use in the preparation of U(IV) solutions were evaluated using the laboratory reduction apparatus – Adams Catalyst (PtO_2), platinized-alumina powder (5 wt % Pt), and the palladium-on-thoria powder (2 wt % Pd) used in the early development work of the urania sol process.[1,2] In each experiment, 850 ml of 0.5 *M* $UO_2(NO_3)_2$–0.25 *M* HCOOH was reduced. Hydrogen flow rates were between 115 and 130 cm^3/min, and stirring speed was maintained at 600 rpm. Use of 2.58 g of the Adams Catalyst and 2.5 g of the platinized alumina permitted complete reduction in 3 hr. When the palladium-on-thoria catalyst, which contained an amount of palladium equivalent to the amount of platinum in the platinized-alumina powder, was used, reduction required about 6 hr. (In a previous similar experiment with the palladium catalyst, where the hydrogen flow rate and the stirring speed were not measured, reduction was complete in $3\frac{1}{2}$ hr.) All catalysts required settling overnight before the U(IV) solution could be decanted free of suspended catalyst. In view of the favorable results obtained with the platinized-alumina powder, further studies were carried out using this catalyst.

With both the palladium-on-thoria catalyst and the platinized-alumina powder, uranium reduction rates were linear with time (Fig. 7.6), indicating a zero-order dependence on U(VI) concentration. With the Adams Catalyst the rate was linear over most of the range, with a slight tailing-off near the end of the reduction. This was probably the result of flocculation of the catalyst and resultant loss of catalyst surface. In other experiments, gross flocculation of the Adams Catalyst was found to occur during the reduction. Hydrogen consumption rate was also linear with time (Fig. 7.7); however, the mole ratio of hydrogen consumed to uranium reduced (H_2/U) varied (using the platinized-alumina powder) from 1.0 to 1.4

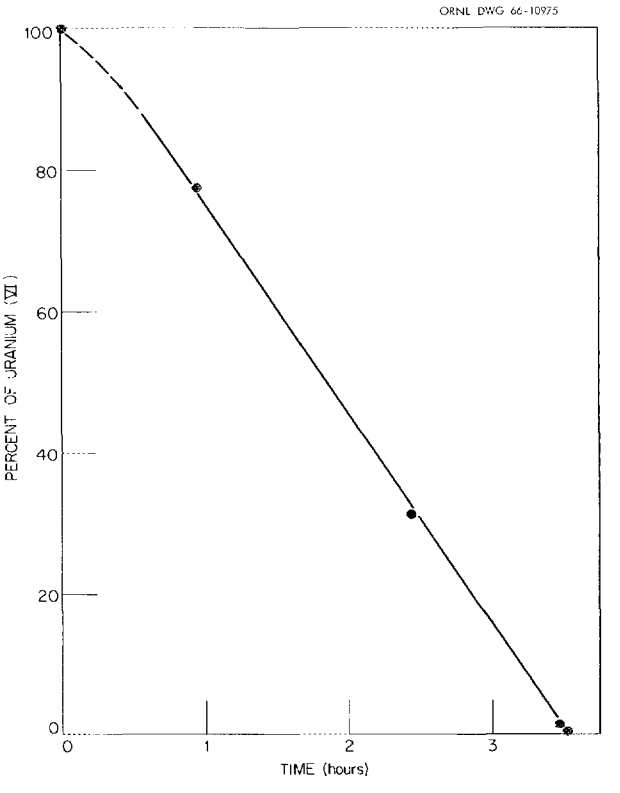

Fig. 7.6. Rate of U(VI) Reduction During the Preparation of a U(IV) Solution of the Composition 0.5 *M* U–1.0 *M* NO_3^-–0.25 *M* HCOOH.

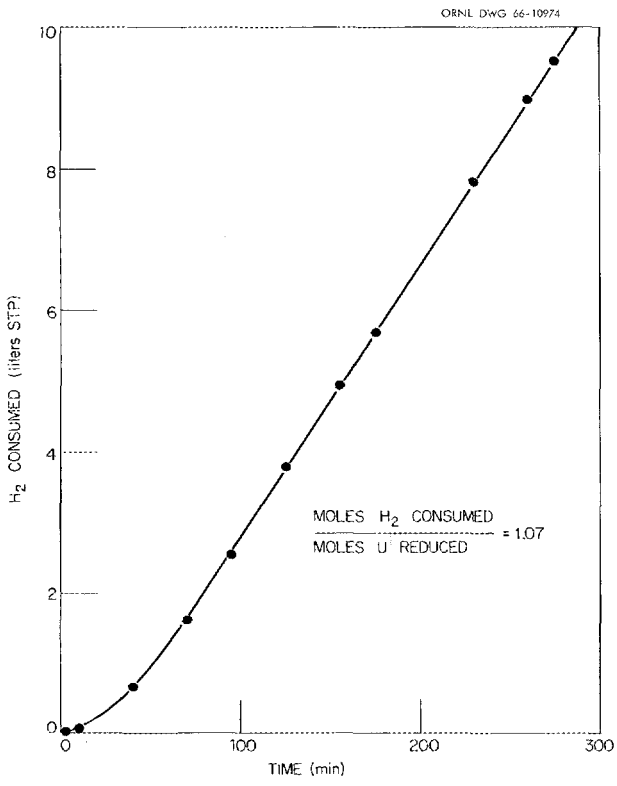

Fig. 7.7. Rate of Hydrogen Consumption During the Preparation of a U(IV) Solution of the Composition 0.5 *M* U–1.0 *M* NO_3^-–0.25 *M* HCOOH.

(see below). Analyses of the reduced solutions showed that a negligible amount of NO_3^- had been reduced but that about half the formate (and a corresponding amount of carbon) had been lost from the system during reduction. Presumably, the formate disappears by two processes: catalytic decomposition and catalytic reduction to volatile species that are sparged from the system by the hydrogen not consumed in the reduction processes.

Experiments on catalyst loading, using the platinized-alumina powder in the 0.5 *M* $UO_2(NO_3)_2$–0.25 *M* HCOOH solutions, were somewhat inconclusive. Variations in rate were observed, depending on whether the catalyst was added to the solution before or after the addition of formic acid (faster rates were observed if the formic acid was added first); for given conditions, rates were not always reproducible. In addition, the amount of hydrogen required to reduce a given amount of uranium was not constant, as indicated above. Figure 7.8 shows the maximum reduction rates obtained for the given catalyst loadings, using 850 ml of the 0.5 *M* uranium solution.

To determine possible poisoning effects on the platinized-alumina catalyst, the U(VI) in 850 ml of a 0.5 *M* $UO_2(NO_3)_2$–0.25 *M* HCOOH solution was reduced to U(IV) using 3.5 g of the catalyst; the catalyst was then allowed to settle. After standing two days under argon, 600 ml of the solution was removed and replaced with fresh U(VI) solution; then the uranium in the solution was again reduced at the same hydrogen flow rate and stirring speed used initially. This experiment was repeated several times over a period of 19 days. Table 7.6 shows the time required to complete the reduction, the mole ratio of hydrogen consumed to uranium reduced, and the catalyst activity (based on the hydrogen consumption rate). It is seen that the time required for reduction increased by 36% after the catalyst had been in contact with the reduced solution for 19 days. The number of moles of hydrogen consumed relative to the number of moles of uranium reduced, however, varied from experiment to experiment and, in general, increased with time. The loss in catalytic activity, based on the hydrogen consumption rate, was only about 20%.

The platinized-alumina powder used in the various experiments was recovered by filtration and washed first with 1 to 2 *M* nitric acid and then

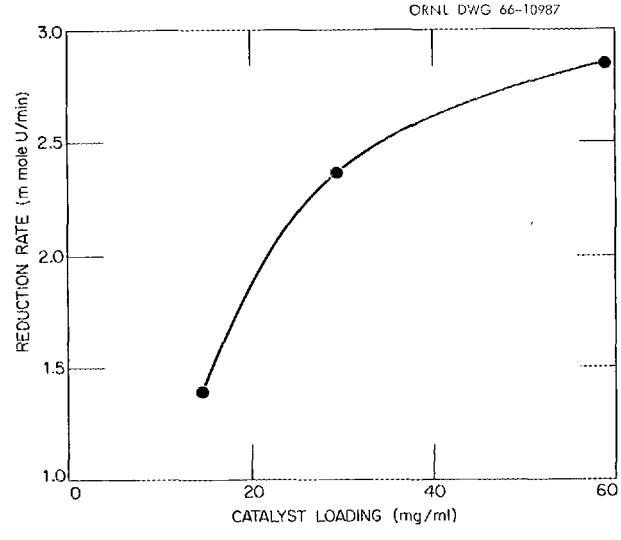

Fig. 7.8. Maximum Uranium Reduction Rates Observed for Given Catalyst Loading of Platinized-Alumina Powder in a Solution of the Composition 0.5 *M* U–1.0 *M* NO_3^-–0.25 *M* HCOOH.

with water. The washed powder was dried in air at ~100°C and reused. No significant loss in specific catalytic activity was observed.

Continuous Production of U(IV) Solutions. – For engineering-scale urania sol preparation, U(IV) solutions were prepared continuously in a stainless steel reactor constructed of 2-in. jacketed pipe containing a 3-ft-high bed of platinized-alumina catalyst (0.5 wt % Pt) in the form of $\frac{1}{8}$- by $\frac{1}{8}$-in. right cylinders. Figure 7.9 is a schematic of the reduction system. The 0.5 *M* $UO_2(NO_3)_2$–0.25 *M* HCOOH solution is fed continuously to the bottom of the reactor, and hydrogen flows concurrently with the solution through the reactor, which is maintained at a hydrogen pressure of $\geq$300 psi. Operation of the reduction reactor is monitored by measuring the redox potential of the reduced solution, using a platinum electrode and a saturated calomel reference electrode. More than 99% reduction is achieved at solution flow rates up to 2 liters/hr. As with the laboratory reductions, approximately half the formic acid is lost from the solution during the reduction cycle.

Table 7.6. Effect of Aging Time in the U(IV) Solution on the Catalytic Activity of the Platinized-Alumina Powder

Catalyst Aging Time (days)	Reduction Time (min)	H_2/U Mole Ratio	Rate of H_2 Consumption (millimoles/min)
0	164	1.05	1.92
2.0	197	1.19	1.81
5.1	197	1.19	1.81
7.0	177	1.13	1.92
13.0	216	1.24	1.72
19.1	223		

The reduction system has operated continuously for periods of over 100 hr without apparent loss of catalytic activity. Mass transfer of the hydrogen into the solution is apparently rate controlling, and successful operation depends upon having a hydrogen flow rate sufficient to give agitation of the liquid in the catalyst bed. A precipitate forms during shutdown, resulting in a loss of catalytic activity, when the uranium solution is allowed to stand, that is, with the catalyst and hydrogen being present. Either the uranium solution must be removed from the system, or an argon blanket must be substituted for the hydrogen in order to prevent this loss in catalytic activity. If precipitation is allowed to occur, the catalyst may be regenerated by washing first with HNO_3 (to dissolve the precipitate) and then with water.

ORNL DWG 67-3664

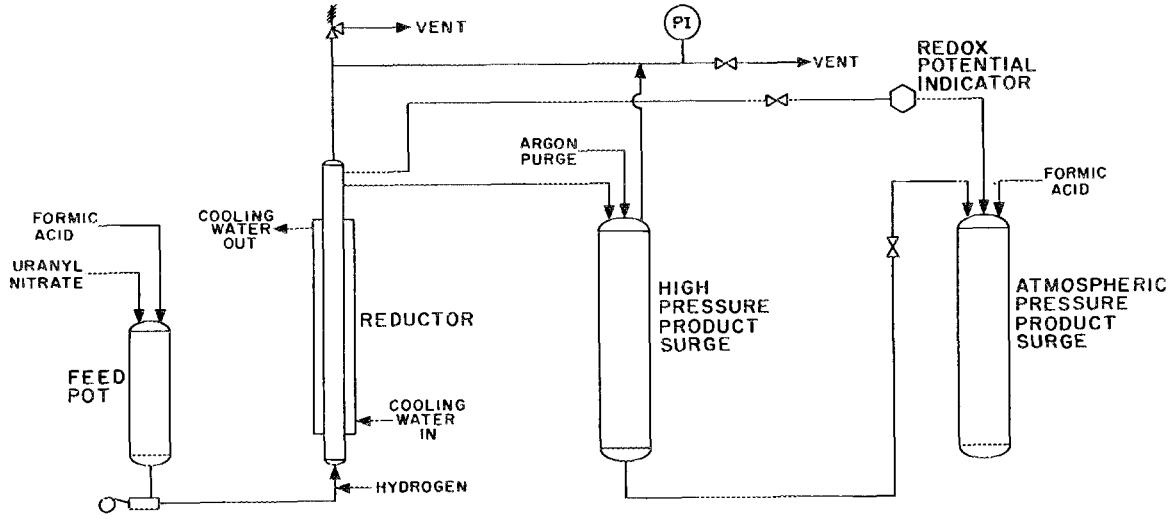

Fig. 7.9. Apparatus for the Continuous Production of U(IV) Solutions.

Preparation of Urania Sols by the Direct Reduction of UO_3 Suspensions

Although the major effort is now concentrated on the precipitation-peptization and the solvent extraction methods of UO_2 sol preparation, we have developed a method of UO_2 sol preparation that involves direct reduction of UO_3 suspensions in nitric acid–formic acid solutions in which the nitrate/uranium and formate/uranium mole ratios are comparable with those obtained in the final sols prepared by the other methods. In the initial work, UO_3 was added directly to a well-stirred nitric acid–formic acid solution in a baffled flask, palladium-on-thoria catalyst was added, and hydrogen was bubbled through the suspension by means of a gas-diffuser tube. Using 2.0 *M* UO_3 suspensions and NO_3^-/U and $HCOO^-/U$ mole ratios of 0.2 and 1.0, respectively, more than 90% conversion to sol was achieved in about 20 hr at 30 to 40°C. In some experiments the suspension was then heated to 45 to 75°C for 1 to 3 hr to enhance the catalytic destruction of formate, but this treatment was not effective. Later investigation showed that converting the UO_3 to a basic formate by stirring it in the formic acid solution prior to the addition of nitric acid and catalyst and the hydrogen treatment shortened sol formation time and, in general, produced higher yields of sol. Such a procedure necessitated the use of a higher nitric acid concentration (NO_3^-/U mole ratio = 0.25) to produce a fluid sol. In the final development work, it was demonstrated that a uranyl nitrate solution could be converted to a dilute uranyl formate solution by an ion exchange method, and the resulting solution could be concentrated by heating to give a "creamy" suspension of the basic formate. Nitric acid and catalyst were then added, and the system was treated with hydrogen as before.

Zirconia and Urania-Zirconia Sol Preparations

Development of methods for preparing concentrated zirconia sols of low electrolyte content continued. The objective is to produce zirconia sols that can be mixed with urania sols in all proportions and to form these mixed sols into dense microspheres. Two methods were used in previous attempts to prepare zirconia sols: destruction of the nitrate in zirconyl nitrate solution with formaldehyde, and precipitation of hydrous zirconia and subsequent peptization with nitric acid.[2] Neither approach was successful in producing concentrated sols of low nitrate content. During this report period we attempted sol preparation by removal of nitrate ion from an aqueous zirconyl nitrate solution by multistage solvent extraction, employing an amine extractant in an inert organic diluent; the aqueous phase was digested at 100°C between extraction stages. Satisfactory sols were not produced. However, it was possible to prepare concentrated zirconia sols having low nitrate content by autoclaving zirconyl nitrate solutions at 200°C to promote crystallite growth and zirconia precipitation, removing the bulk of the nitrate by centrifugation and decantation, peptizing the recovered solids by addition of water, and finally decreasing the nitrate content of the zirconia sol to the desired level by a solvent extraction technique.

Urania-zirconia sols with a Zr/U mole ratio of 0.3 were made by an adaptation of the laboratory method for preparing urania sol by precipitation-peptization.[1] Strong, dense microspheres of urania-zirconia were prepared from the sols on a laboratory scale. In the sol preparation, zirconyl nitrate or zirconia sol is added to the uranium solution prior to the precipitation of the hydrous oxide.

7.2 PLUTONIA

A plutonia sol-gel process for the preparation of dense forms of PuO_2 and homogeneous mixtures of PuO_2-UO_2 and PuO_2-ThO_2 was reported last year.[2] The objective of this work was to develop processes for preparing plutonia sols which (1) could be used to prepare dense PuO_2, (2) would be compatible with other oxide sols, and (3) would afford versatility in forming techniques already developed at ORNL. To meet these requirements, a stable plutonium colloid with a low nitrate content is required. The current process utilizes the polymerization behavior of tetravalent plutonium to maintain valence stability and to produce colloidal particles of PuO_2. The sols produced by this procedure are 1 to 3 *M* in plutonium and have NO_3^-/Pu mole ratios of 0.1 to 0.15. They are stable for several months and are compatible with both the thoria and urania sols that are produced at ORNL. The ability to produce dense plutonia microspheres as well as homogeneous plutonia-urania or plutonia-thoria microspheres at desired heavy-metal ratios has now been demonstrated on an engineering scale. Equipment for thermogravimetric and differential thermal analyses was

installed in a glove-box facility, cold-tested with europia gel, and used to analyze plutonia sol-gel materials.

Status and Progress

The successful processing of 560 g of plutonium into plutonia sol in small equipment was reported last year.[2] During this report period the operability and the reproducibility of the basic flowsheet were further demonstrated by the production of 20 additional sol batches (50 to 150 g of Pu per batch) containing over 1500 g of plutonium. During sol preparation, engineering efforts were concentrated on developing essential equipment components with increased reliability and ease of operation. Engineering-scale equipment (installed last year) to produce oxide microspheres from plutonia sols and mixed sols was successfully used to prepare 865 g of PuO_2, 4 kg of PuO_2-UO_2 containing 5 to 20 wt % PuO_2, and 1.5 kg of PuO_2-ThO_2 containing 5 wt % PuO_2. Densities were generally greater than 95% of the theoretical crystal density.

We continued laboratory efforts to optimize variables in the plutonia sol process, to delineate the nature of the colloidal plutonia particles, to examine alternative procedures for preparing plutonia sol, and to characterize microsphere products. During this work, plutonia sols, sol intermediates, and sol-gel products were studied by use of spectrophotometry, x-ray line broadening, powder camera techniques, electron microscopy, metallography, mercury porosimetry, electron microprobe analysis, and surface area measurements. Several critical parameters in the plutonia sol process were elucidated. Gel microspheres of europia and plutonia and gel products formed by drying the oxide sols were examined using thermogravimetric and differential thermal analyses.

Sol Process

The flowsheet for the plutonia sol process is shown in Fig. 7.10. Hydrous plutonia is precipitated from a plutonium nitrate solution that is 1 to 3 *M* in excess HNO_3 by slow addition of the plutonium solution to a 100% excess of NH_4OH, with simultaneous rapid stirring. The plutonia is recovered by filtration, the filter cake is resuspended in water, and the suspension is filtered. Three washings are usually sufficient to reduce the pH of the filtrate to less than 8.0, which indicates satisfactory removal of contaminant ions. The freshly precipitated plutonia is then aged by refluxing in water for 1 to 2 hr. It is peptized by digestion with dilute HNO_3. Complete peptization, which is characterized by a change from an opaque light-green slurry to a nearly transparent dark-green suspension, requires a minimum NO_3^-/Pu mole ratio of 1. At this HNO_3^-/Pu ratio, a digestion time of about 4 hr at 80°C is necessary. Higher nitrate concentrations, however, can be used to reduce the digestion time and temperature; for example, at NO_3^-/Pu mole ratios of 2 or more, digestion requires only 10 to 15 min at room temperature.

The plutonia sol produced during digestion is a stable colloidal dispersion but is not suitable for fuel-particle preparation until the NO_3^-/Pu mole ratio has been reduced. This is accomplished by evaporating the sol to produce a gel and then baking the gel at 250°C for about 2 hr. Nitrate removal is a function of both time and temperature, and excessive baking will result in material that cannot be redispersed. For this reason, very uniform heating of plutonia solids is required during nitrate removal. The final sol is prepared by resuspending the baked gel in water and evaporating to the desired plutonium concentration. Sols with plutonium concentrations in excess of 2 *M* and with NO_3^-/Pu mole ratios between 0.1 and 0.15 are obtained.

Demonstration of the Process on an Engineering Scale

Sol Preparation. – Twenty plutonia sols (50 to 150 g of Pu per batch) containing more than 1500 g of Pu were prepared using the flowsheet described above except that the hydroxide was not aged prior to peptization. These preparations demonstrated the operability of newly developed equipment and the reproducibility of the standard flowsheet (Fig. 7.10) and provided sol for the preparation of microspheres of plutonia, plutonia-urania, and plutonia-thoria. Data for the last six runs, which were made in recently developed engineering-scale equipment, are presented in Table 7.7.

Thermal denitration continues to be the step of major concern. There appears to be some correlation between the molarity of nitric acid used in peptization and the baking time required. As acid concentration increased from 0.4 to 0.9 *M* (runs PS-23–25, Table 7.7), the total baking time required to produce comparable NO_3^-/Pu mole ratios in the final sol decreased from 2 to <1 hr.

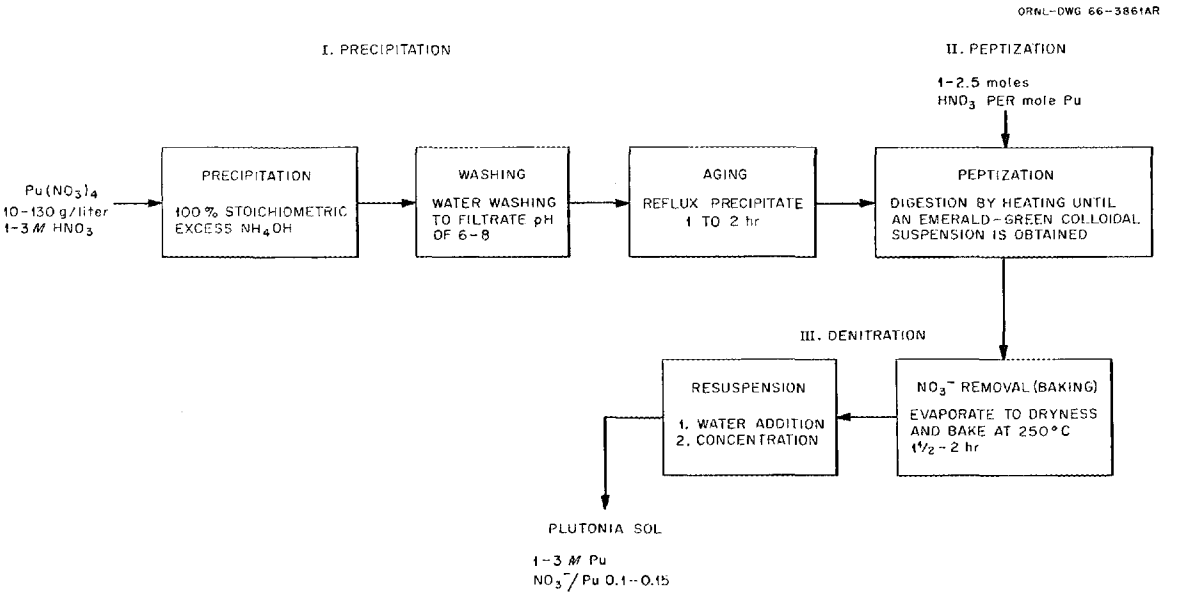

Fig. 7.10. Flowsheet for Plutonia Sol-Gel Process.

Equipment Development. – Equipment development work was primarily devoted to the construction of a new precipitation-filtration vessel and a separate baking unit to replace the original sol-forming vessel, which was designed to perform all functions required for sol preparation. The new precipitation-filtration vessel (Fig. 7.11) features an 8-in.-diam porous stainless steel bottom. Filtration time is reduced to about 20 min per wash with this vessel, and fewer washes are required for adequate NH_4NO_3 removal. The baking unit (Fig. 7.12) provides uniform temperatures (within ±1°C) over the entire surface of both heated elements.

Microsphere Preparation. – Sphere-forming equipment was successfully operated to produce PuO_2-UO_2, PuO_2-ThO_2, and PuO_2 microspheres in 50- to 100-g batches. The equipment is installed in two 6-ft glove boxes; the first is used for sol mixing and microsphere forming and drying, while calcination and classification are accomplished in the second.

Mixed oxides were prepared by mixing the respective sols to obtain desired compositions. Microspheres were formed by a standard technique, which employs a fluidizing column and a glass two-fluid nozzle. The drying alcohol was 2EH in all cases. Gel spheres were dried in argon at 150 to 170°C and calcined at 1100 to 1200°C. The primary variables in the formation process were the type of surfactant used in the drying solvent and the type of atmosphere control required. Satisfactory microspheres were readily formed from plutonia and PuO_2-ThO_2 sols by using 0.3 to 0.5 vol % Ethomeen S/15. The 20% PuO_2–UO_2 spheres were formed using a mixture of 0.3 to 0.5 vol % Ethomeen S/15 and 0.3 to 0.6 vol % Span 80; however, it was found later (during the preparation of 15% PuO_2–UO_2 spheres) that a less-concentrated surfactant system (0.1 vol % Ethomeen S/15 and 0.4 vol % Span 80) was more satisfactory. Plutonia and ThO_2 sols and their mixtures require no atmospheric protection; therefore, gel spheres of this composition are fired in air. Urania-containing sols and gels, on the other hand, require an inert blanket at all times; thus firing is carried out in Ar–4% H_2 with a CO_2 cycle at an intermediate temperature to oxidize residual carbon. After being cooled to room temperature in argon, these calcined materials may be handled in air.

The types of material produced, size ranges, total weights, number of batches prepared, and physical properties are shown in Table 7.8. Table 7.9 shows the disposition of the products. No significant differences were observed in gel microsphere forming characteristics during the preparation of PuO_2-UO_2 spheres varying from 5 to 20 wt % in PuO_2 content; the preparation of 5% PuO_2–ThO_2 microspheres was similar to that of thoria. Product diameters were varied from $<44\ \mu$ (fines) to $>600\ \mu$. Densities of all the types of materials were $\geq 95\%$ of theoretical except for the fines. Analytical data (Hg porosimetry) for fines were variable and subject to question.

Table 7.7. Plutonia Sol Preparations by the Standard Flowsheet[a]

Batch No.	Plutonium Content (g)	Composition of $Pu(NO_3)_4$ Feed		NH_4OH[b] Concentration (*M*)	Peptization Conditions		Denitration Conditions		Properties of Final Sol	
		Plutonium (g/liter)	HNO_3 (*M*)		NO_3^-/Pu Mole Ratio	HNO_3 (*M*)	Temperature (°C)	Time (min)	NO_3^-/Pu Mole Ratio	Plutonium Content (g/liter)
PS-23	56	56	1.4	4.5	2.9	0.40	200 → 240	35	0.15	306
							240	85		
PS-24	100	68	1.7	4.5	2.5	0.59	200 → 240	20	0.14	380
							240	60		
PS-25	150	79	2.0	4.5	2.5	0.87	200 → 240	25	0.16	305
							240	30		
PS-26	100	58	1.5	4.0	2.4	0.50	200 → 225	25	0.10	273
							225	50		
							200 → 240	40		
							240	45		
PS-27	100	58	1.5	4.0	2.4	0.50	200 → 230	30	0.13	359
							230	160		
PS-28	130	50	3.0	4.5	2.0	0.35	200 → 230	35	0.15	318
							230	120		
PS-29	100	58	1.5	4.0	2.0	0.35	200 → 220	26		
							220	120		

[a] No hydroxide aging (digestion) step prior to peptization; see Fig. 7.10.
[b] Precipitant.

Properties of the 5% PuO_2–UO_2 spheres and the PuO_2 fines were not determined. Carbon levels were less than 100 ppm in all cases, and specific surface areas of all material except fines were generally ≤ 0.03 m^2/g.

Laboratory Studies and Product Evaluation

We continued laboratory studies to improve and optimize the plutonia sol preparation process and to delineate the nature of colloidal plutonia. Areas of study were:

1. investigation of process variables that affect the nature of the colloidal aggregate that is obtained after denitration,
2. preparation of low-nitrate plutonia sol that does not require denitration,
3. evaluation of plutonia sols prepared by peroxide precipitation,

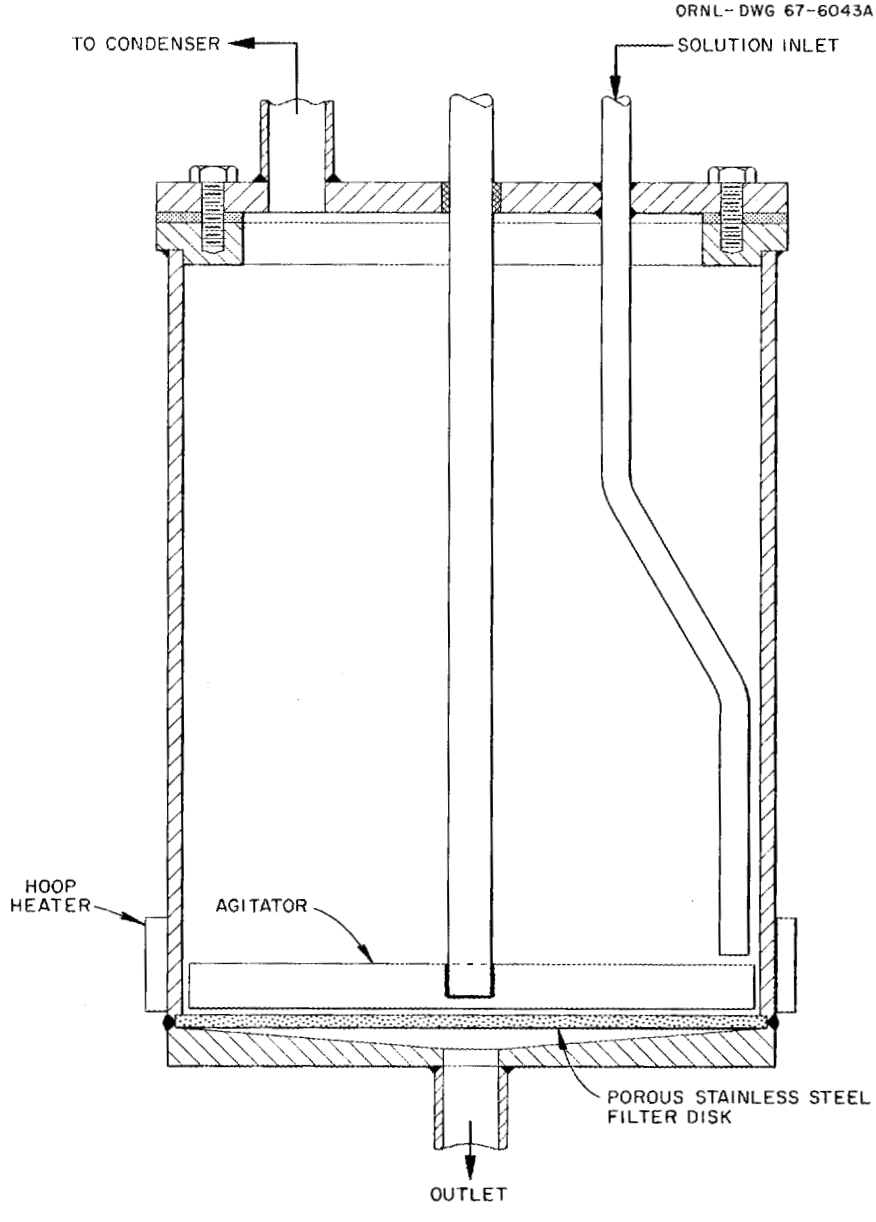

Fig. 7.11. Vessel for the Precipitation, Filtration, and Peptization of PuO_2 Sol.

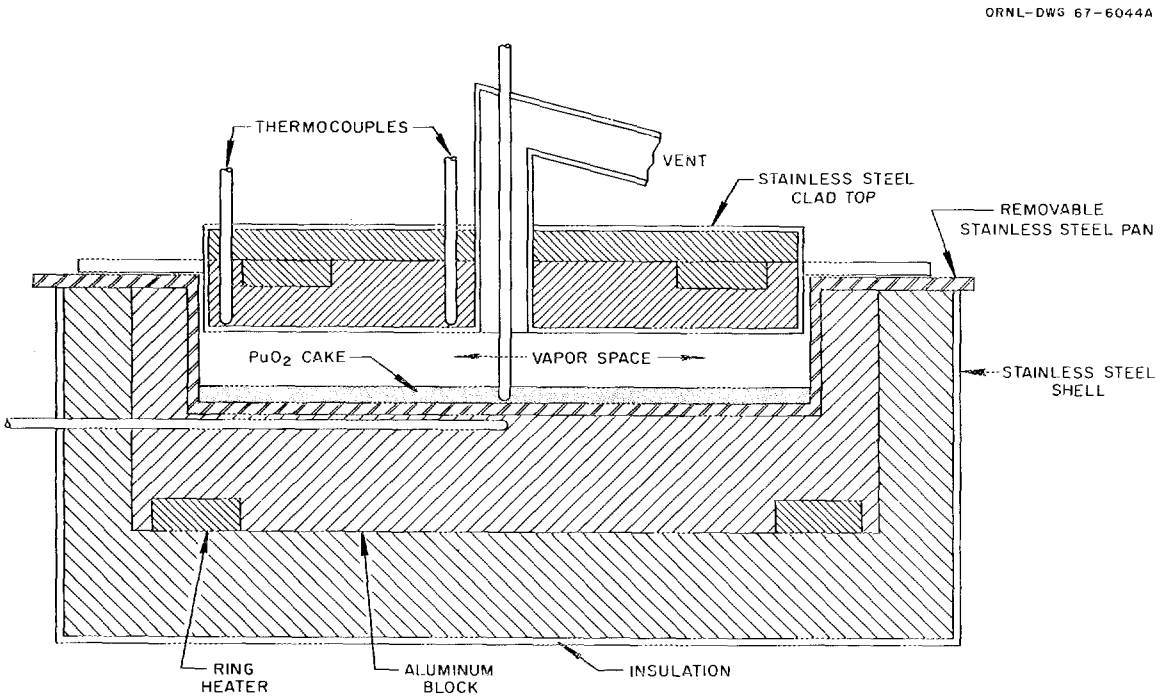

Fig. 7.12. Vessel for the Thermal Denitration of PuO_2 Sol.

Table 7.8. Properties of PuO_2-Containing Microspheres Prepared in Glove-Box Facility

Composition of Microspheres	Size Range (μ)	Total Weight (g)	Number of Batches	Bulk Density (g/cm^3)	Hg Density[a]		Carbon (ppm)	Specific Surface Area	
					g/cm^3	Percent of Theoretical		Measured[b] (m^2/g)	Calculated (m^2/g)
20% PuO_2–$^{235}UO_2$	300–600	1900	23	10.3	10.5	95	<10	0.02	
	<44	340	5	~6	9.0	82	<10	0.04	0.08
15% PuO_2–$^{238}UO_2$	300–600	970	11	10.5	10.6	97	<90		0.06
	<44	234	4	5.6	~9.2	~84	<100		0.5
5% PuO_2–$^{238}UO_2$	300–600	496	3						
5% PuO_2–ThO_2	300–600	1148	5	9.48	9.84	97	<10	0.02	
	<44	403	4	~6	~9.5	~94		0.17	
PuO_2	250–600	251	4	11.13	11.22	98	<30	0.02	0.03
	50–250	571	7	11.06	11.19	98	<70	0.01	0.02
	<44	43	1						

[a]By Hg porosimetry at 10,000 psi.
[b]By gas adsorption.

4. evaluation and characterization of oxide microsphere products.

Investigation of Process Variables. – As previously reported, it was established by spectral analysis that the high-nitrate sol (NO_3^-/Pu mole ratio ≥ 1) formed during digestion of the hydroxide consisted of polymerized tetravalent plutonium. During denitration by baking, crystallite growth and crystallite agglomeration were shown to occur; these phenomena appear to be intimately associated with the preparation of stable plutonia sol at desirably low nitrate concentrations.

It was previously demonstrated in development studies that relatively dilute HNO_3 must be used when precipitated plutonium is peptized. An acid

Table 7.9. Distribution of Plutonia and Mixed Oxide Microspheres to Various Facilities

Date	Type of Material	Weight (g)	Size Range (μ)	Destination
7/5/66	20% UO_2–PuO_2	330	300–600	ANL
7/5/66	20% UO_2–PuO_2	110	<44	ANL
8/5/66	20% UO_2–PuO_2	144	300–600	ANL
8/5/66	20% UO_2–PuO_2	48	<44	ANL
9/8/66	5% ThO_2–PuO_2	1122	350–600	ORNL
9/8/66	5% ThO_2–PuO_2	389	<44	ORNL
9/9/66	20% UO_2–PuO_2	81	300–600	ORNL
9/9/66	20% UO_2–PuO_2	24	<44	ORNL
9/29/66	20% UO_2–PuO_2	282	300–600	ANL
9/29/66	20% UO_2–PuO_2	94	<44	ANL
10/4/66	PuO_2	12	50–250	ORNL
10/11/66	5% UO_2–PuO_2	496	300–600	ORNL
10/31/66	PuO_2	26	88–210	Mound Laboratory
11/16/66	PuO_2	40	88–177	BNW
1/6/67	15% UO_2–PuO_2	664	300–600	ORNL
1/6/67	15% UO_2–PuO_2	214	<44	ORNL
1/30/67	PuO_2	9	300–600	Savannah River
1/30/67	PuO_2	8	Uncalcined	Savannah River
2/9/67	PuO_2	2	Uncalcined	ORNL
2/15/67	PuO_2	320	50–500	BNW
3/8/67	20% UO_2–PuO_2	8	44–350	NUMEC
3/8/67	20% UO_2–PuO_2	10	<44	NUMEC
3/8/67	PuO_2	9	88–350	NUMEC
3/8/67	PuO_2	42	<44	NUMEC
3/16/67	PuO_2	28	177–300	ORNL
4/12/67	PuO_2	69	50–250	Mound Laboratory

concentration in excess of 1 *M* resulted in product with undesirable characteristics. Results of recent studies established that the acid concentration of the plutonium feed and the molarity of the NH_4OH used for precipitation are also critical. A high electrolyte concentration in either step (precipitation or peptization) appears to result in a rapid nitrate loss during baking and high product losses due to material that will not resuspend. Final sols prepared in this way are very opaque, are light green in appearance, and show solids separation. They are very difficult to form into satisfactory microspheres (in extreme cases, microspheres cannot be formed at all).

One factor that is at least partly responsible for this behavior was indicated by the spectrophotometric analysis of high-nitrate sols prepared from plutonium stock containing excessive amounts of HNO_3. Depolymerization of Pu(IV) polymer occurred during evaporation, giving rise to ionic forms of Pu(IV) and Pu(VI) [Pu(VI) results from the oxidation of ionic Pu(IV) under these conditions]. On evaporation to dryness and subsequent baking, both the ionic Pu(IV) and Pu(VI) yield an undesirable form of plutonium. Although exact limits have not been established, it was shown that precipitation from feed solution with an HNO_3 concentration as high as 8 *M*, using 5 *M* NH_4OH, results in greater depolymerization during concentration of the high-nitrate sol than when the plutonium feed solution was less than 3 *M* in HNO_3. The present indication is that a high nitrate content promotes a polymer form that is less resistant to depolymerization. This situation is further complicated by indications that the precipitates of plutonium that are immediately peptized in dilute HNO_3, rather than stored for short periods in water, also exhibit a greater degree of depolymerization during subsequent evaporation and baking steps.

A recent extension of these observations gave rise to a simple process modification that appears to result in improved sol product. It involves "aging" precipitated washed hydroxide by boiling for 1 to 2 hr in water prior to peptization. Several product sols prepared in the laboratory by using this technique were characterized by high yields, improved colloidal stability, and good handling and sphere-forming characteristics. This modification will be additionally evaluated on an engineering scale.

Direct Preparation of Low-Nitrate Plutonia Sol. – Previous efforts to make plutonia sols by methods not requiring a denitration step were reported last year; however, in these cases, it was found that an NO_3^-/Pu mole ratio of 1 or greater was required to form a stable sol. Recently, by use of a modified procedure, plutonium sols having intermediate NO_3^-/Pu mole ratios have been obtained directly from plutonium precipitates. The procedure involves forming plutonium polymer prior to precipitation by adding plutonium nitrate solution to NH_4OH to a selected pH in the range of 1.5 to 2. The polymer is aged by digestion at an elevated temperature until it precipitates (pH above 3.5). The precipitate forms a sol when sufficient NH_4NO_3 and NH_4OH have been removed by washing. Two types of sol – a translucent emerald-green sol and an opaque light-green sol – can be obtained by this procedure, depending primarily on the final pH selected for precipitation. The first type appears to be superior but requires more careful control during its formation. Both types of sol are characterized by a very small crystallite size (20 to 30 A or less) and NO_3^-/Pu mole ratios ranging from 0.4 to 0.8. If excess NH_4OH is used, a precipitate is obtained that requires the addition of approximately 1 mole of nitrate per mole of plutonium to attain a stable sol. This behavior is consistent with that of sols studied last year.

Evaluation of these sols is presently under way. It is felt that, while these sols might have special application because of simplified equipment requirements, sols produced by the standard flowsheet are superior and have a more universal applicability. The relatively high nitrate content of these special sols enhances instability and resultant precipitation when they are mixed with low-nitrate thoria and urania sols. Also, these sols are not reversible (i.e., they cannot be evaporated to dryness and then re-formed to sol by resuspension in water). Microspheres not only are more difficult to form from these sols but also have a strong tendency to crack and disintegrate during calcination.

Characterization of Calcined Microspheres. – Plutonia and PuO_2-UO_2 microspheres that have been calcined at 1150°C are characterized by high density, low surface area, and high resistance to crushing. Photographs of polished metallographic sections of PuO_2 and PuO_2-UO_2 microspheres are shown in Fig. 7.13. Mercury porosimetry measurements indicate densities of 95 to 99% of the theoretical crystal density for typical products. Specific surface areas of 0.02 m^2/g were obtained for 300- to 600-μ-diam microspheres. Calcined (at 1150°C

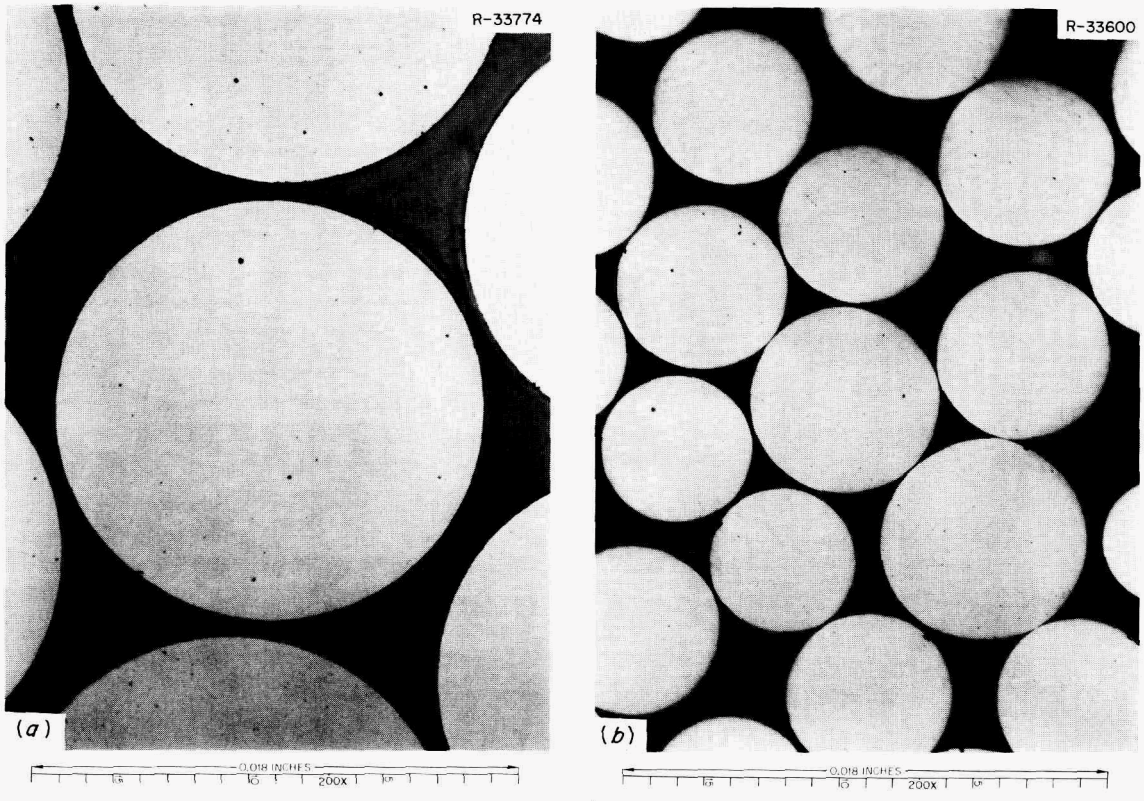

Fig. 7.13. Polished Metallographic Sections of Calcined UO_2–20% PuO_2 Microspheres (*a*) and PuO_2 Microspheres (*b*).

and at 1600°C) 250-μ-diam microspheres resisted an average crushing load of about 550 g; 500-μ-diam microspheres resisted loads greater than 1 kg.

Crystallite size, as measured by x-ray diffraction line broadening, was 1000 A for PuO_2 spheres calcined in air at 1150°C. Crystallite size increases with firing temperature; for example, 1700-A crystallites were found in material calcined for 0.5 hr at 1550°C.

It was found that $^{239}PuO_2$ microspheres can be washed free of transferable alpha contamination. Calcined spheres were water-washed, dried in air, and smeared. Extensive contact with 50 to 100 spheres produced counts on the order of 20 dis/min per smear.

The homogeneity of urania-plutonia microspheres was investigated by the electron microprobe technique. The analysis of microspheres containing 20 wt % PuO_2 indicated a homogeneous mixture with a uniform distribution of urania.

Thermal Analysis of Plutonia Gels

As a result of continued efforts to produce transplutonium elements by irradiating targets in the high neutron flux of thermonuclear devices, there is a need to investigate the thermal stability of actinide compounds of interest for use as targets. To obtain information of this kind, equipment for thermogravimetric and differential thermal analyses was acquired for use in an alpha-contained facility. The thermogravimetric balance, furnaces, and associated parts that could become contaminated were installed in glove boxes; the supporting and control instrumentation was assembled adjacent to the glove boxes.

The thermogravimetric balance is an Ainsworth semimicro vacuum balance with a recorder span that corresponds to a weight change of 10 mg. The differential thermal analyzer (DTA) unit is built as a part of the baffle-plate assembly. Separate DTA sample holders are used to permit complete recovery of the sample material and also to prevent contamination of the differential thermocouples. Three types of DTA sample holders can be employed: a large sample cup that permits the use of up to 150 mg of sample, a small cup that serves for samples in the 5- to 20-mg range, and a type of dish that is useful for 1 to 10 mg. The combined system permits

simultaneous thermogravimetric and differential thermal analyses of alpha-active materials up to 1600°C in vacuum, air, or various atmospheres up to pressures slightly above atmospheric. Baffle-plate assembly units can be interchanged to optimize conditions for a particular temperature range. In addition, the existing baffle-plate assembly design can be temporarily removed, and other assemblies or designs can be used for special experiments or applications.

Thermal Analysis of Europia Sol-Gel Material. – The equipment described above was cold-tested with europia gel because of the known similarity between lanthanides and actinides and the related interest in the actinide and rare-earth sol-gel processes.[5] The TGA-DTA study of europia gel was limited to temperatures below 1100°C by the construction material used for prototype baffle-plate assemblies.

Two types of colloidally dispersed hydrous oxides (sols) can be made with rare earths: one crystalline and one amorphous (which slowly crystallizes upon aging in aqueous media). The thermal analysis of gel microspheres prepared from both types of sol suggests a difference in chemical forms. Thermograms for europia gel microspheres prepared from crystalline sol exhibit a rapid weight loss, accompanied by a sharp endothermic DTA peak, at 250 to 300°C. The weight change corresponds to a loss of 1 mole of water per mole of europium, indicating the empirical formula $Eu_2O_3 \cdot 2H_2O$. Thermograms of microspheres made from an amorphous sol show only a gradual weight loss, with no detectable endothermic DTA peak in the 250 to 300°C region.

Analysis of the thermograms of microspheres is complicated by the presence of organic residues from the drying solvent used in forming the gel microspheres. Oxidation of this carbon residue either by residual nitrate and/or oxygen from the air results in an exothermic DTA peak in the region of 300°C. Material from amorphous and crystalline sol that gelled by evaporation (instead of by use of solvents) was examined to aid the interpretation. Thermograms for gels made by evaporating both amorphous and crystalline sols at 60°C were identical, indicating that the amorphous sol was converted to the crystalline form during evaporation. Gels obtained by vacuum evaporation (at 25°C) of an amorphous sol gave a thermogram that appeared to be a mixture of the amorphous and crystalline materials. Thermograms of evaporated gels were the same in oxygen, argon, or vacuum, but thermograms of microspheres were different in different atmospheres. The height of the exothermic DTA peak at 300°C was greatly enhanced by an oxygen atmosphere and the weight change in this region was more abrupt. This is as expected if these effects result from the oxidation of organic material in the microspheres.

The weight changes and the endothermic DTA peaks are tentatively considered to result from loss of water below 300° and nitrate decomposition in the 350 to 500° region. The sharp weight change and the endothermic peak at approximately 250 to 300°C correspond to a loss of 1 mole of water per mole of europium. Further work is planned to completely define the system.

Thermal Analysis of Plutonia Sol-Gel Materials. – After alpha containment of the TGA-DTA system was complete, the equipment was used to examine several plutonia sol-gel compounds. In the plutonia sol-gel process there are two steps that involve solid-state reactions at temperatures above ambient: (1) denitration of high-nitrate plutonia gel, which is then redispersed into plutonia sol; and (2) calcination of gel microspheres formed from such a sol.

High-nitrate plutonium gel was studied by TGA and DTA methods in vacuum, argon, and oxygen atmospheres up to 1600°C. The decomposition reaction of this material (Fig. 7.14*a*) did not vary with atmosphere and consisted of two weight loss steps (total loss, 32%) accompanied by corresponding endothermic DTA peaks. The decomposition mechanism has not been completely elucidated, but nitrate is lost in both steps. Decomposition products in the first step appear to consist of water and oxides of nitrogen, while the second weight loss corresponds to the measured loss in nitrate.

Thermograms for plutonia gel microspheres and for gel prepared by drying plutonia sol are shown in Figs. 7.14*b* and 7.14c. The thermogram for plutonia microspheres was again complicated by the presence of organic residue, as evidenced by an exothermic DTA peak at about 230°C. The TGA plot for gel microspheres shows several inflections rather than well-defined weight loss regions; evaporated gel not exposed to organic solvents produced a thermogram similar to that for high-nitrate gel, except that the two weight loss steps extended to higher temperatures. The total weight loss was 6.5% (constant after 700°C) for evaporated gel and 7.5% for micro-

[5] C. J. Hardy, S. R. Buxton, and M. H. Lloyd, *Preparation of Lanthanide Oxide Microspheres by Sol-Gel Methods*, ORNL-4000 (Aug. 8, 1967).

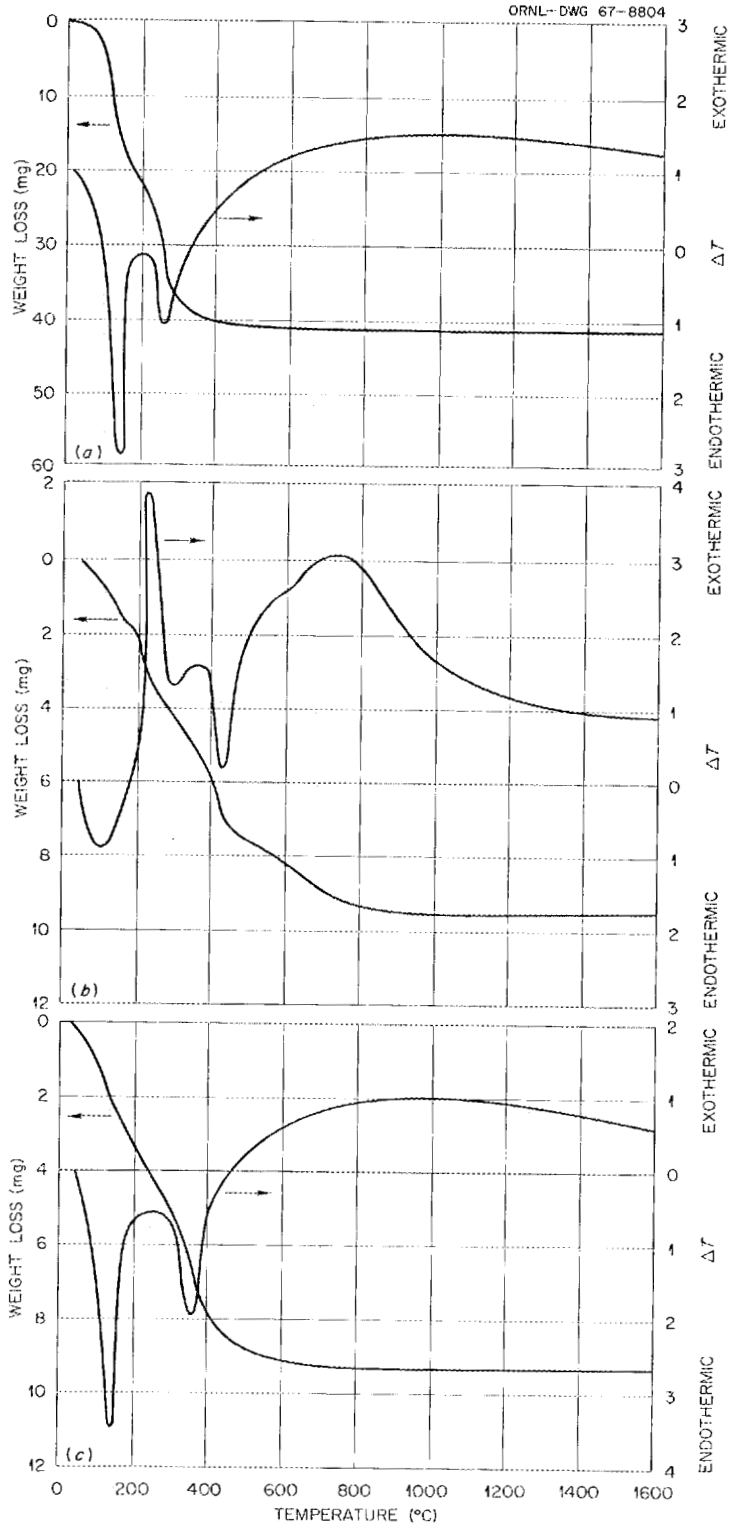

Fig. 7.14. TGA-DTA Curves for (*a*) High-Nitrate Plutonia Gel, (*b*) Plutonia Gel Microspheres, and (*c*) Evaporated Plutonia Gel.

spheres (constant after 900°C). There were no detectable TGA or DTA changes in the 1200 to 1600°C temperature range. Essentially no difference was noted in thermograms obtained in oxygen, argon, or vacuum except for increased height of the exothermic peak at 230°C in oxygen atmosphere. X-ray analysis showed all the products to be PuO_2.

7.3 OXIDES OF CONTROLLED POROSITY

Porosity in sol-gel fuel particles may be desirable as traps for fission product (and other) gases. It may also be useful as a source of "sinks" for relief of strains generated by thermal and irradiation-induced stresses.

The production of sol-gel ThO_2 and UO_2 having controlled porosity was attempted by incorporating, in the oxide sols, materials that volatilize when gels prepared from the sols are fired. In the preparation of porous ThO_2, carbon black was dispersed in ThO_2 sols, gel spheres were prepared from the sols, and the carbon was removed by firing the gels in air.[6] The usual techniques of sol preparation and gel microsphere forming were used.[7] Porous UO_2 was prepared by volatilizing either chloride or molybdic oxide (MoO_3) from the urania gel.[8]

Special techniques were required for preparation of the sol and for formation of microspheres of porous UO_2.[7,9] Sols containing molybdenum were made by mixing 1 *M* $(NH_4)_2MoO_4$ sols with 1 *M* U(IV) chloride sols. [Uranium(IV) chloride sols were prepared by bubbling NH_3-Ar into 1.0 to 1.7 *M* U(IV) chloride solutions until the solutions gelled, and then liquefying the gels at about 50°C.] Gel microspheres were formed by injecting sol from a syringe onto a layer of 2EH floating on 15 *M* NH_4OH. The sol dispersed into droplets in the alcohol, and the droplets fell into the NH_4OH, where they gelled.

The primary variables studied in the preparation of porous thoria were the C/ThO_2 mole ratio and variations in the firing cycle. The best control and maximum porosity for a given carbon content were obtained if the mixed gel was first densified at about 1400°C and the carbon was burned out later. This method gave porosities up to 64%, with pore sizes in the 120- to 2000-A range (Fig. 7.15).

In the studies of the preparation of porous UO_2, the effects of incorporating either chloride (present initially as UCl_4) or molybdic oxide into the gel microspheres were examined. Urania microspheres with porosities between 1 and 44% were made by firing gel microspheres containing chloride. The porosity was found to be dependent on the chloride content. Most of the pores were about 1 μ in diameter at porosities above 25% (Fig. 7.16). At a lower volume percentage of porosity, the pore sizes were distributed over a range from 0.01 to 10 μ.

Urania microspheres of 20 to 35% porosity were prepared by volatilizing MoO_3 from the gels during firing. The porosity could be controlled empirically by varying the Mo/U atom ratios in the sols from 0.1 to 0.8. The fired products closely resembled the products obtained by chloride volatilization, except that the pore sizes tended to be larger and increased as the porosity increased (Fig. 7.17).

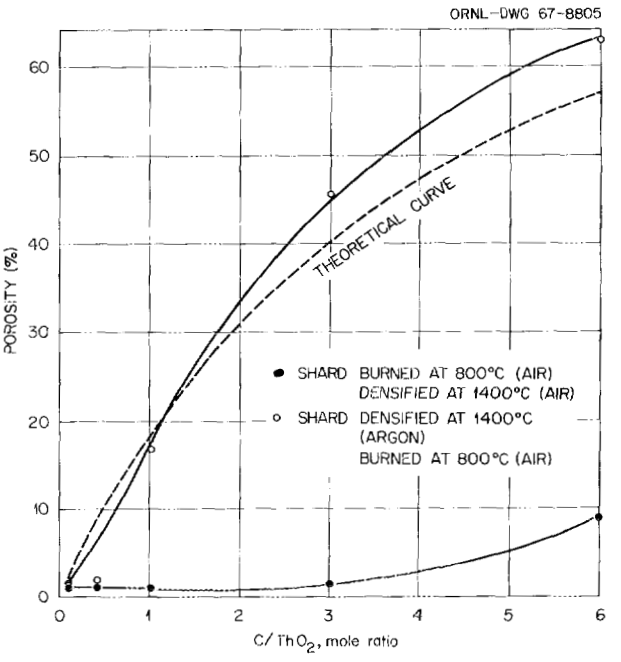

Fig. 7.15. Porosity of Sol-Gel Thoria from Which Incorporated Carbon Was Burned Out.

[6] K. J. Notz, *Preparation of Porous Thoria by Incorporation of Carbon in Sols*, ORNL-TM-1780 (in press).

[7] D. E. Ferguson, O. C. Dean, and D. A. Douglas, "The Sol/Gel Process for the Remote Preparation and Fabrication of Recycle Fuels," *Proc. Intern. Conf. Peaceful Uses At. Energy, Geneva, 1964* 10, 307–15 (1965).

[8] T. A. Gens, *Preparation of Uranium and Thorium Oxide Microspheres with Controlled Porosity by a Sol-Gel Process*, ORNL-TM-1530 (May 31, 1966).

[9] T. A. Gens, *Formation of Uranium, Zirconium and Thorium Oxide Microspheres by Hydrolysis of Droplets*, ORNL-TM-1508 (July 10, 1966).

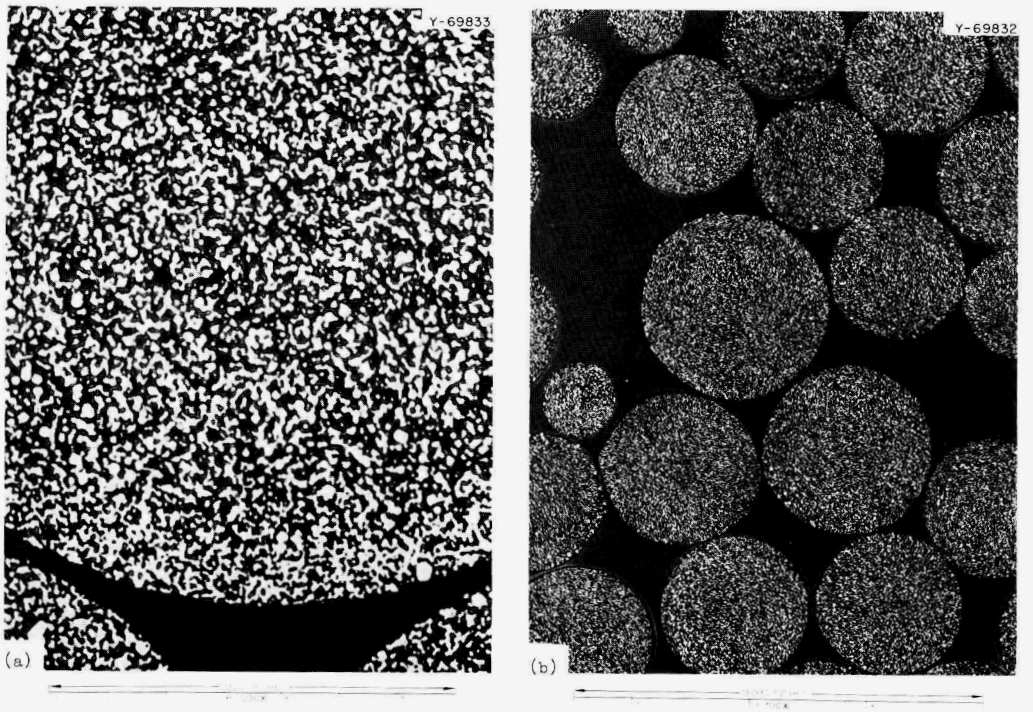

Fig. 7.16. UO_2 Microspheres with 44% Porosity. The pores are uniformly distributed throughout the microspheres.

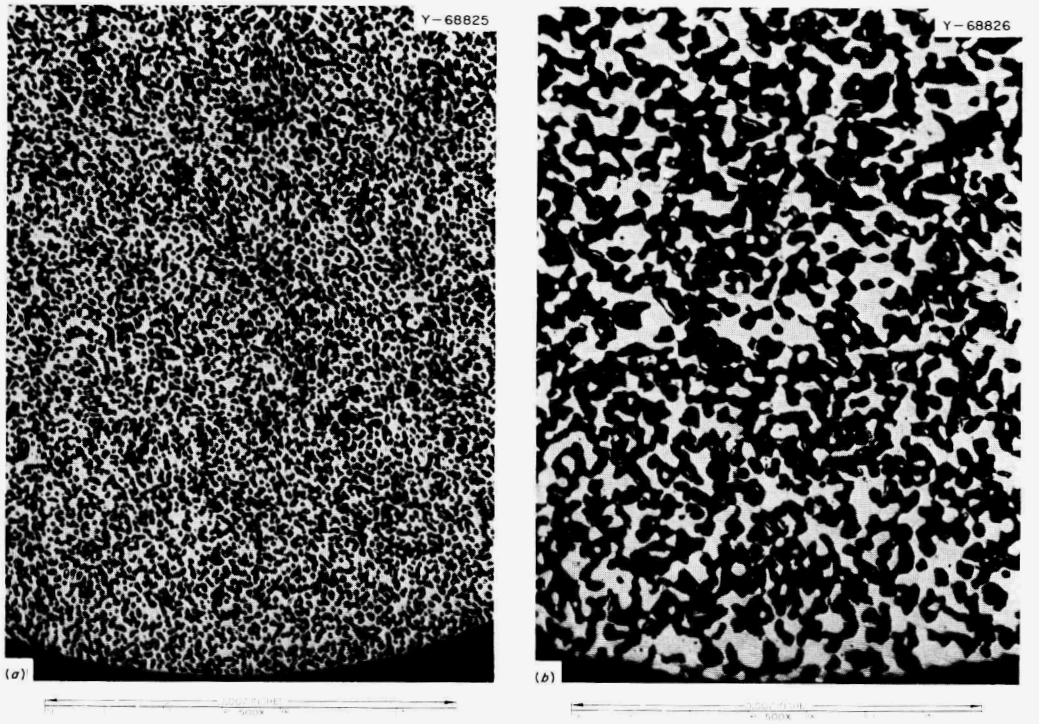

Fig. 7.17. Porous UO_2 Microspheres Made from U^{4+} Chloride Sols. Porosity is 19.2% in (*a*) and 29.7% in (*b*). The Mo/U atomic ratios in the respective sols were 0.10 and 0.29.

8. Separations Chemistry Research

8.1 EXTRACTION OF METAL SULFATES AND NITRATES BY AMINES

In view of the potential for increased use of amine extractants, a systematic survey is being made of the extraction characteristics of many metals from various acid and salt solutions with representative amines. The study of metal chloride extractions from hydrochloric acid and acidified lithium chloride solutions has been completed and reported.[1] Data now have been obtained for extraction of 16 metals from acidified lithium nitrate solutions (0.5 to 10 N NO_3^-) and 12 metals from acidified lithium sulfate solutions (0.3 to 0.5 N SO_4^{2-}).

Figure 8.1 shows data for the extraction of Sc, Fe(III), and Tc from nitrate solutions, and for the

[1] F. G. Seeley and D. J. Crouse, *J. Chem. Eng. Data* 11(3), 424 (1966).

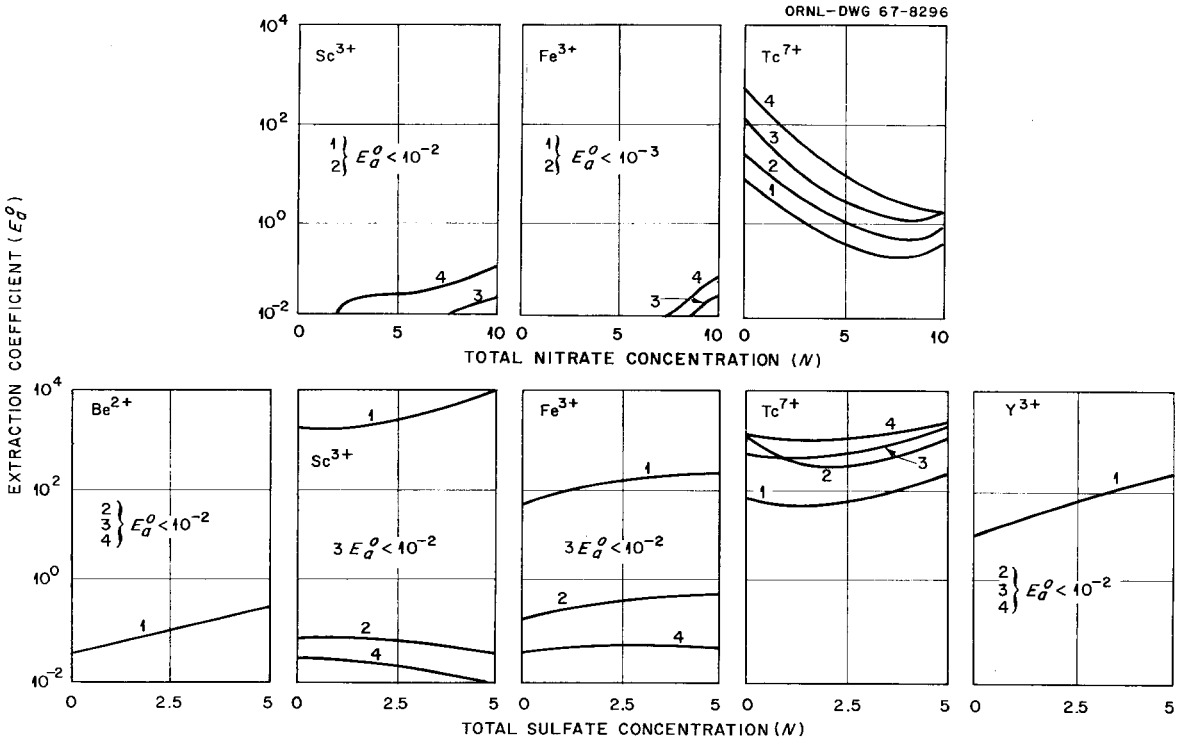

Fig. 8.1. Extraction of Metals from Nitrate and Sulfate Solutions with Amines. Organic phase: 0.1 M solutions of (1) Primene JM ($RR'R''CNH_2$, 18 to 24 carbon atoms); (2) Amberlite LA-1 ($RR'R''CNHC_{12}H_{23}$, 24 to 27 carbon atoms); (3) Adogen 364 (R_3N, R = *n*-octyl, *n*-decyl mixture); (4) Adogen 464 [$R_3(CH_3)N^+$, R = *n*-octyl, *n*-decyl mixture] in diethylbenzene. With Adogen 464, 3 vol % of tridecanol was added to the solvent phase to prevent the formation of a third phase. Amines were in the nitrate or sulfate form. Aqueous phase: 0.01 M metal ion in either $LiNO_3$–0.2 N HNO_3 or Li_2SO_4–0.2 N H_2SO_4. Contact time: 10 min at a phase ratio of 1:1.

extraction of Sc, Fe(III), Tc, Be, and Y from sulfate solutions with 0.1 *M* solutions of representative primary, secondary, tertiary, and quaternary amines in diethylbenzene. In the sulfate system, the primary amine extracted Sc, Fe(III), and Y strongly, and Be weakly, the extraction coefficients in all cases increasing with increasing sulfate concentration. Very slight, or negligible, extraction of these elements was obtained with the other types of amines in the sulfate system and with all types of amines in the nitrate system. Technetium was extracted strongly in both systems. Besides the results shown in Fig. 8.1, extraction coefficients were less than 0.05 over the total range of salt concentrations for Li, Na, K, Rb, Cs, Be, Mg, Ca, Sr, Ba, Al, Y, and Zn from nitrate solutions, and for Li, Na, K, Rb, Cs, Al, and Zn from sulfate solutions.

8.2 NEW SEPARATIONS AGENTS

We are continuing to investigate, for potential utility in solvent extraction or other separations methods, compounds that are: (1) newly available commercially, (2) submitted by manufacturers for testing, or (3) specially procured for testing of class or structure.

Sulfonic and Carboxylic Acids

A supply of didodecylnaphthalenesulfonic acid (HDDNS) was prepared for use in cation exchange and synergistic extraction tests. This compound is $\geq$98% pure and has a neutral equivalent of 534 (theoretical, 545); we assume, from the method used for its synthesis, that the material has only one structure, 3,7-di-*n*-dodecylnaphthalene-1-sulfonic acid. As expected, it is a strong acid and is effective as a cation exchanger for metals from concentrated acid (aqueous) solutions. It is 30% converted from the hydrogen to the sodium form (0.05 *M* DDNS) by contact with 2 *M* HNO_3–1 *M* $NaNO_3$, while more than 50% conversion is achieved by contact with 1 *M* HNO_3–2 *M* $NaNO_3$. Extraction coefficients for strontium and europium (cf. Sect. 8.13) are much lower than with dialkylphosphoric or carboxylic acids and lack the prominent maxima in the *E* vs pH curves that are characteristic of those complexing acids. These data suggest that the extractions occur through cation exchange alone, with little or no coordination being observed. This is consistent with the earlier observation that adding phosphoryl compounds to a sulfonic acid (dinonylnaphthalenesulfonic acid plus phosphonate ester or phosphine oxide) synergizes the extraction of various metal ions.[2] In preliminary tests with HDDNS, europium extraction was synergized by trioctylphosphine oxide (TOPO) but not by TBP; strontium extraction was not synergized by TOPO.

Two new branched carboxylic acids, of higher molecular weight than those previously available, have been obtained for testing solubility and extraction properties. They are a "neo" acid mixture, $R\text{-}C(CH_3)_2\text{-}CO_2H$, containing 15 to 19 carbon atoms, and 3,7,11,15-tetramethylhexadecanoic acid.

Aminopolycarboxylic Acids

Three aminopolycarboxylic acids, needed in the investigation of the effects of structure on their formation of complexes with trivalent actinides (Sect. 8.11), were synthesized by reaction of sodium chloroacetate with the appropriate polyamine under reflux. The aminopolycarboxylic acids were liberated from the resultant salts by hydrochloric acid (pH 1.0), precipitated by adding an equal volume of ethanol, and purified by successive recrystallizations from water-ethanol mixtures. The purities were verified by elemental analysis, and the successive pK_a's of each were determined by potentiometric titration (Table 8.1).

β-Diketones

Sterically hindered β-diketones have been reported as complexers for lithium ion.[3–5] However, the lithium complexes with the reagents used in those studies (dipivaloylmethane, dibenzoylmethane) had either significant solubility in the alkaline aqueous solution or low solubility in common organic diluents. The data suggest

---

[2] *Chem. Technol. Div. Chem. Dev. Sect. C Progr. Rept. for October, 1959*, CF-59-10-101, pp. 22–24.

[3] G. A. Guter and G. S. Hammond, *J. Am. Chem. Soc.* **78**, 5166 (1956).

[4] T. V. Healy, *Chem. Div. Progr. Rept. for 1 Nov. 1964 to 30 Apr. 1965*, AERE-PR/Chem 8, p. 13 (May 1965).

[5] D. A. Lee, Abstracts of Papers, 153rd Meeting Am. Chem. Soc., April 10–14, 1967, Div. Nucl. Chem. and Technology.

Table 8.1. Aminopolycarboxylic Acids: Determination of Purities and Dissociation Constants

Acid	Elemental Analysis (%)								Acid Dissociation Constants						
	C		H		O		N								
	Theor.	Found	Theor.	Found	Theor.	Found	Theor.	Found	pK_{a_1}	pK_{a_2}	pK_{a_3}	pK_{a_4}	pK_{a_5}	pK_{a_6}	pK_{a_7}
Triethylene-tetraamine-hexaacetic	43.72	43.7	6.11	6.0	38.83	39.0	11.33	11.3	2.46	2.52	4.00	5.98	9.35	10.33	
Tetraethylene-pentaamine-heptaacetic	44.37	44.4	6.26	6.2	37.61	37.6	11.73	11.8	1.99	2.19	2.55	3.19	5.80	9.46	11.11
2-Hydroxy-1,3-diaminopropane-tetraacetic	41.12	40.9	5.33	5.2	44.82	45.2	8.72	8.7	~1.60	2.65	6.98	9.50			

that a hindered diketone of suitable size and structure should give improved solubility properties while retaining its ability to extract lithium. Synthesis of sterically hindered diketones is difficult; however, a new method was developed that enhances the reactivity of the intermediate compounds. By use of this method, 2,2,6,6-tetramethylpentadecanedione-3,5,

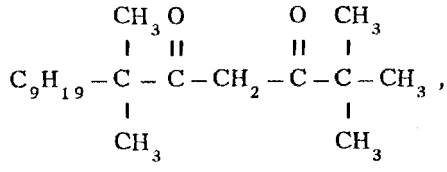

was prepared and subsequently distilled to a purity of 98.8%. In preliminary tests this reagent extracted lithium from concentrated potassium hydroxide solutions. A 1.0 *M* reagent solution in hexane gave extraction coefficients for lithium and potassium of 2.7 and 0.014, respectively, from 0.1 *M* LiCl–1 *M* KOH solution. The solubility of the reagent will be examined, and its extraction ability will be compared with that of other diketones.

Dialkyl Sulfoxides

As was previously noted,[6] several symmetrical dialkyl sulfoxides extracted only a few metal ions (Hg^{2+}, Ag^{+}, Pt^{2+}, Cu^{2+}) from chloride or nitrate solutions, which suggested coordination with the sulfur rather than the oxygen. This has now been confirmed with seven different symmetrical dialkyl sulfoxides, the alkyls being *n*-butyl, isobutyl, isoamyl, 2-ethylhexyl, *n*-decyl, *n*-tetradecyl, and *n*-octadecyl. It was also found that both (organic) solubility of the reagent and extraction power at corresponding concentrations decreased as the size of the alkyl groups increased. Since the water-soluble dimethyl sulfoxide forms complexes with a wide range of metal ions, an unsymmetrical methyl alkyl sulfoxide was tried in the expectation that it might more closely resemble dimethyl sulfoxide.

Methyl 2-ethylhexyl sulfoxide was successfully prepared by the reaction of methyl iodide with 2-ethylhexyl mercaptan or of methyl mercaptan with 2-ethylhexyl iodide, followed by oxidation of the resulting sulfide with 30% hydrogen peroxide in glacial acetic acid. The distilled products boiled at 135°C, 12 mm Hg. The undiluted compound dissolves water to 57 wt % and dissolves in water to 1.7 wt %. The sulfoxide-in-water concentration decreases both with dilution by diethylbenzene and with ionic solutes in the aqueous phase (not measured quantitatively); the water-in-sulfoxide concentration decreases to 0.8% when the sulfoxide is diluted to 0.1 *M* with diethylbenzene.

In contrast to the extractions cited above, this sulfoxide extracts the metals that suggest association with the sulfinyl oxygen rather than with the sulfur, for example, uranium as uranyl chloride and uranyl nitrate, and iron(III) as chloride but not as nitrate (Table 8.2). Higher-molecular-weight methyl alkyl sulfoxides will be prepared for comparison.

Primary Amine

As previously mentioned, 1-(3-ethylpentyl)-4-ethyloctylamine (3,9-diethyltridecyl-6-amine, "heptadecylamine," "HDA," "Amine 21F81") is an excellent extractant for many purposes but is no longer available from the original source. We have prepared small amounts of this amine at ORNL,[7] but until recently had not been able to find a commercial source. We have now obtained a 1-kg batch on special order from the Midwest Research Institute of Kansas City, Missouri. It assays 93.8% primary amine, 4.8% secondary and tertiary amines, and 1.4% inert material. Its beryllium extraction properties are consistent with those of previous batches from the original source as well as with those of the material prepared at ORNL.

8.3 SELECTIVITY OF POLYACRYLAMIDE GELS FOR CERTAIN CATIONS AND ANIONS

Polyacrylamide gels are used primarily for separating macromolecules of different size and for desalting solutions of macromolecules. However, we have now found that these gels also exhibit selectivity for certain small cations and anions, indicating a separation mechanism that is not

[6] *Chem. Technol. Div. Ann. Progr. Rept. Sept. 1966*, ORNL-3945, p. 177.

[7] H. L. Holsopple and F. G. Seeley, *Synthesis of 3,9-Diethyltridecyl-6-amine*, ORNL-TM-1314 (Nov. 5, 1965).

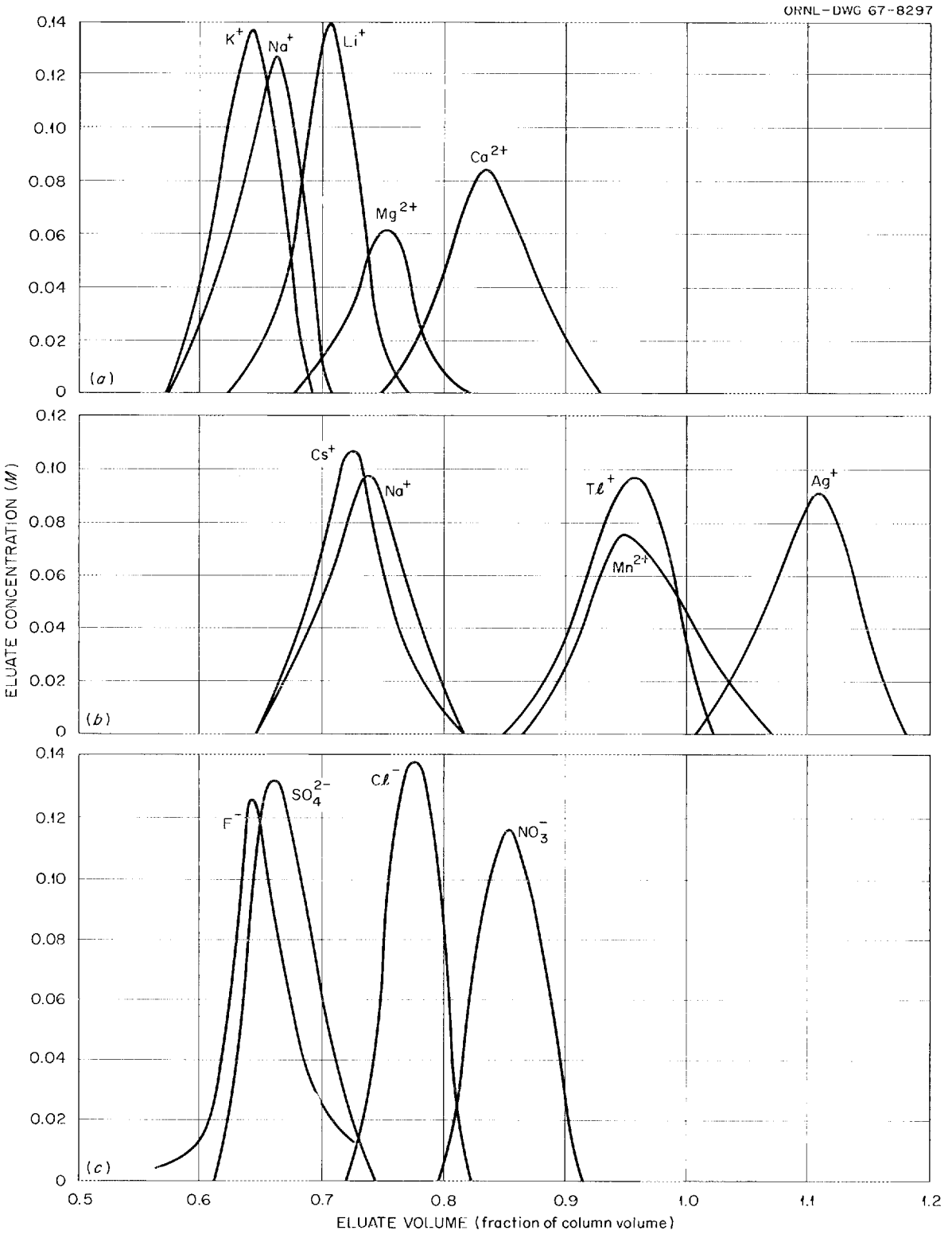

Fig. 8.2. Polyacrylamide Gel Chromatography of Simple Ions. Bio-Gel P-2, eluted with water. (*a*) 0.05 *M* Mg^{2+}, 0.1 *M* each K^+, Na^+, Li^+, Ca^{2+}, as chlorides, in 100 ml of feed; elution rate, 2 ml/min at 5°C; column, 2.5 × 223 cm. (*b*) 0.1 *M* each Cs^+, Na^+, Tl^+, Ag^+, Mn^{2+}, as nitrates, in 100 ml of feed; elution rate, 2 ml/min at 5°C; column, 2.5 × 223 cm. (*c*) 0.1 *M* each F^-, Cl^-, NO_3^-, SO_4^{2-}, as sodium salts, in 14 ml of feed; elution rate, 0.5 ml/min at 23°C; column, 1.0 × 235 cm.

Table 8.2. Extraction of Various Metals by Methyl 2-Ethylhexyl Sulfoxide[a]

Metal Salt[b]	Extraction Coefficient from:			
	0.2 *M* HX[c]	6 *M* HX[c]	6 *M* LiX,[c] pH 1–2	5.8 *M* LiX[c]–0.2 *M* HX[c]
$AgNO_3$	<0.001	0.01	0.03	0.01
$FeCl_3$	<0.001	21	19	25
UO_2Cl_2	0.04	2.0	7.1	7.4
$UO_2(NO_3)_2$	0.09	1.4	>2000	>10,000
$Co(NO_3)_2$, $Fe(NO_3)_3$, $CoCl_2$, $CuCl_2$, $ZnCl_2$, $ScCl_3$, YCl_3			All <0.01	

[a]0.1 *M* methyl 2-ethylhexyl sulfoxide in benzene.

[b]Initial metal concentrations 0.01 *M*.

[c]X = Cl^- or NO_3^-, corresponding to metal salt shown.

based solely on matching the size of the solute species to the size of the gel pores.

A solution containing Li^+, Na^+, K^+, Mg^{2+}, and Ca^{2+} chlorides was chromatographed on a 2.5- by 223-cm column of Bio-Gel P-2, an extensively cross-linked polyacrylamide with a pore size that excludes molecules above a molecular weight of 1600. When the cations were eluted with water, the order of appearance in the effluent fractions was K^+, Na^+, Li^+, Mg^{2+}, Ca^{2+} (Fig. 8.2*a*). The same elution order, but poorer separation, was observed on a column of Bio-Gel P-100, a polyacrylamide with a lower degree of cross-linking and larger pores that exclude molecules above a molecular weight of 100,000. Similar treatment of a solution containing Na^+, Cs^+, Mn^{2+}, Ag^+, and Tl^+ nitrates on a Bio-Gel P-2 column separated these into three groups (Fig. 8.2*b*). Anion selectivity was demonstrated by chromatographing a solution containing F^-, Cl^-, SO_4^{2-}, and NO_3^- (as sodium salts) on a Bio-Gel P-2 column (Fig. 8.2*c*).

The chemical basis for these separations presumably includes association with the amide groups and perhaps also ion exchange on ionizable groups arising from hydrolysis and/or impurities.

8.4 PERFORMANCE OF DEGRADED REAGENTS AND DILUENTS

In radiochemical processing by solvent extraction, degradation of the solvent phase can cause unsatisfactory operation. The amount of degradation varies with the types of solvents used and with the extent of their exposure to radiation and reaction chemicals during the processing of the aqueous feed.

Progress and Status

Studies of several aspects of diluent and reagent degradation have been made at ORNL, and summaries of prior work have been published.[8,9] This year a study of the role of iodine in solvent extraction processing was initiated. Information from this program will be applicable to the processing of high-burnup, short-cooled reactor fuels, which contain significant amounts of ^{131}I. In the processing of feed solutions containing iodine, it has been found that the element accumulates in the organic phase; therefore, our objectives are to determine what types of organic iodine compounds are formed with the common aliphatic and aromatic diluents and organic complexing agents, to determine the effects of their presence on the extraction process, and to establish methods for separating them from the solvent phase, if necessary.

[8]C. A. Blake, W. Davis, Jr., and J. M. Schmitt, *Nucl. Sci. Eng.* 17, 626–37 (1963).

[9]C. A. Blake and J. M. Schmitt, *Solvent Extraction Chemistry of Metals*, pp. 161–86, Macmillan, London, 1965.

When solutions of sodium iodide in 3 *M* HNO_3 were stirred with 1.0 *M* TBP in a hydrocarbon diluent (e.g., *n*-dodecane or diethylbenzene), the iodide was rapidly oxidized to elemental iodine, which reported to the extractant phase. Oxidation was slower when no extractant phase was present, even when the acid phase was aerated with moist air. However, when the iodide concentration was low (10^{-4} *M*), approximating a level that could result from dissolution of a short-cooled fast-reactor fuel, 75% of the iodine was sparged with air from the 3 *M* HNO_3 in about 3 hr, and the remainder was removed in less than 24 hr. This suggests that the addition of suitable oxidizing agents to the aqueous feed while maintaining a gas sparge could effect removal of iodine from the feed before it enters the solvent extraction cycle and, subsequently, the extractant phase. When a stirred two-phase system (1 *M* TBP in diluent vs 3 *M* HNO_3 containing 0.4 *M* iodine) was irradiated (by a ^{60}Co gamma source) to an absorbed dose of 100 whr/liter (approximately 1500 times that expected in a single cycle of extraction from a high-burnup, short-cooled fast-reactor fuel solution), about 2% of the solvent molecules were converted to iodine-containing compounds. The organic-phase iodine analyses were as follows:

	TBP in *n*-dodecane	TBP in diethylbenzene
I_2, *M*	0.235	0.223
I^-, *M*	0.002	0.006
Hydrocarbon iodide, *M*	0.114	0.086

Total iodine concentrations in the aqueous phases were less than 0.0004 *M*. The elemental iodine was completely removed from the organic extracts by scrubbing with dilute aqueous sodium thiosulfate. Gas-liquid chromatograms of the irradiated organic phases after I_2 removal showed the presence of new components that could not be ascribed to nitration. These new species have not yet been identified.

8.5 RECOVERY OF BERYLLIUM FROM ORES

The apparent scarcity of high-grade beryllium ores has increased the need for recovery processes that are capable of treating low-grade domestic ores in order to meet the increasing demand for beryllium metal and compounds. A tentative solvent extraction process was previously outlined[10,11] for recovering beryllium from low-grade ore sulfate liquors by extraction with a primary amine, scrubbing with dilute sulfuric acid, and stripping with either dilute sulfuric acid or dilute fluoride solutions. The primary amine that continues to show superiority to all others tested is 1-(3-ethylpentyl)-4-ethyloctylamine (HDA).

Status and Progress

Further testing of the process was encouraging. Recent results showed sulfuric acid stripping to be superior to fluoride stripping. Optimum conditions were established for stripping the beryllium with sulfuric acid and for recovering a beryllium oxide product from the strip solution. The process has been applied successfully in bench-scale batch countercurrent tests to the recovery of beryllium from Spor Mountain, Utah, ore leach liquors and to synthetic leach liquors of similar composition.

In addition to the amine extraction studies, a few beryllium extraction tests were made with di(2-ethylhexyl)phosphoric acid (D2EHPA); they showed that extractions of beryllium with this reagent, usually very slow, can be accomplished rapidly under certain conditions.

Beryllium Product from the Amine Extraction Process

The beryllium product recovered from a synthetic leach liquor (similar in composition to leach liquors obtained by the U.S. Bureau of Mines in leaching Utah ores and containing, in g/liter: 0.65 Be, 6.0 Al, 7.5 Mg, 2.3 Fe(II), 0.44 Mn, 0.08 Zn, 0.4 Ca, 7.8 F, 1.0 Cl, and 95 SO_4) analyzed greater than 99% BeO. Spectrographic analysis showed, in %: 0.2 Al, 0.03 Mg, 0.3 Fe, 0.03 Mn, 0.07 Ca, 0.02 Cu, 0.02 Pb, 0.2 Cr, 0.005 B, and 0.1 Si (the last five were not present in the original liquor). In this test the beryllium was batch-extracted at pH 2.5 with 0.3 *M* HDA in Solvesso 100, the extract was scrubbed with

[10] *Chem. Technol. Div. Ann. Progr. Rept. May 31, 1966*, ORNL-3945, p. 182.

[11] D. J. Crouse, K. B. Brown, and F. G. Seeley, "Primary Amine Extraction of Beryllium from Sulfate Liquors," pp. 237–341 in *Solvent Extraction Chemistry of Metals*, Macmillan, London, 1965.

0.01 *M* H_2SO_4, and the beryllium was stripped with sulfuric acid using 9 lb of H_2SO_4 per lb of BeO. Beryllium was precipitated from the strip solution with NH_4OH at pH 8 and redissolved in caustic solution. This solution was filtered to remove insoluble metal hydroxides, and the beryllium was precipitated, presumably as the β form of beryllium hydroxide, by heating. This precipitate was washed and calcined to yield the final product.

Extraction of Beryllium with D2EHPA

Extractions of beryllium from acid solutions with D2EHPA are extremely slow, and, in process application, contact times of 20 min or longer, usually at elevated temperatures, are used to obtain high beryllium recoveries. Both the beryllium extraction coefficients and the extraction rate increase as the acid concentration of the aqueous phase decreases. The acid released to the aqueous phase on extraction of beryllium with D2EHPA therefore lowers the beryllium extraction efficiency. However, by extracting with reagent that is all, or partly, in the form of the sodium salt (rather than in the acid form), the acid concentration during extraction can be maintained at a level where the extraction of beryllium is efficient and rapid. This is shown in Fig. 8.3 for the extraction of beryllium at room temperature with 0.3 *M* D2EHPA (50% in the sodium salt form) from beryllium sulfate–sodium sulfate solutions that were initially adjusted to pH 2.0, 3.0, or 4.0. With all three solutions, the pH, after a 15-min contact, was only slightly different from that of the original solution. At an aqueous/organic (A/O) phase ratio of 2/1, the amounts of beryllium extracted in 1 and 15 min were 42 and 72%, respectively, at pH 2, and 81 and 94%, respectively, at pH 3. By contrast, more than 99.5% of the beryllium was extracted in 1 min at pH 4 with an A/O phase ratio of 2/1 (and at pH 3 with an A/O phase ratio of 1/1).

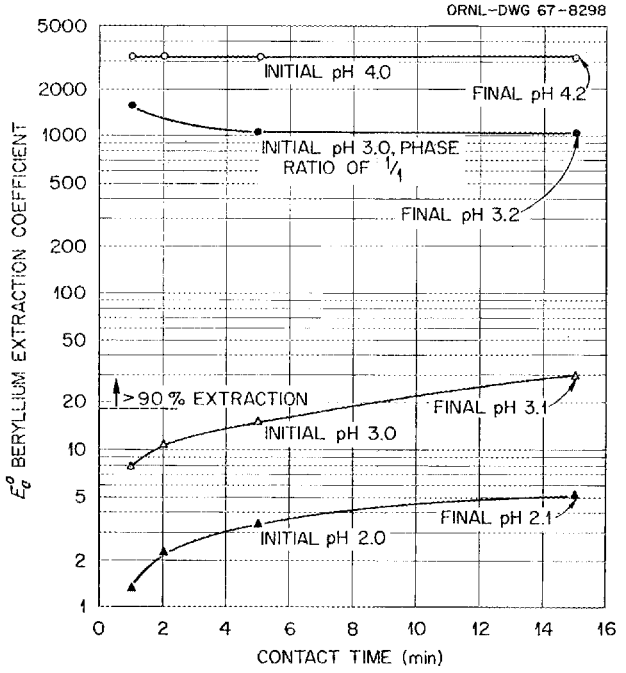

Fig. 8.3. Rate of Beryllium Extraction with Di(2-ethylhexyl) Phosphoric Acid. Aqueous phase: 0.5 g of Be per liter, ^7Be tracer, 1 *M* SO_4^{2-}; organic phase: 0.15 *M* D2EHP–0.15 *M* TBP–Amsco 125-82; A/O phase ratio: 2/1; temperature: ~23°C except where noted.

Attempts to extract beryllium rapidly with Na-D2EHP from leach liquors containing an aluminum : beryllium weight ratio of 9/1 were not successful since the rate and extent of aluminum extraction were also increased. The procedure may be useful, however, for treating liquors with low aluminum : beryllium ratios.

8.6 BERYLLIUM PURIFICATION BY SOLVENT EXTRACTION

New and potentially less-expensive methods are being studied for preparing high-purity beryllium compounds for reactor use, starting with high-grade beryllium concentrates such as those obtained by amine extraction of low-grade beryllium ore leach liquors (see Sect. 8.5). We have found that quaternary ammonium compounds extract beryllium efficiently from carbonate solutions. This appears to be an attractive extraction system since the beryllium can be stripped readily from the solvent phase with an aqueous solution of a volatile stripping agent (ammonium bicarbonate) from which beryllium can be recovered by heating.

Preparation of Feed Solutions

Impure, freshly precipitated beryllium hydroxide is dissolved readily in sodium or ammonium car-

bonate-bicarbonate solutions, provided that sufficient bicarbonate is supplied to satisfy the reaction

$$Be(OH)_2 + 2HCO_3^- \longrightarrow Be(CO_3)_2^{2-} + 2H_2O .$$

The dissolution is more rapid if the initial solution contains some normal carbonate. Feed solutions about 0.4 *M* in beryllium have been prepared by digesting beryllium hydroxide with 0.15 *M* Na_2CO_3–0.85 *M* $NaHCO_3$ for 1.5 hr at about 55°C.

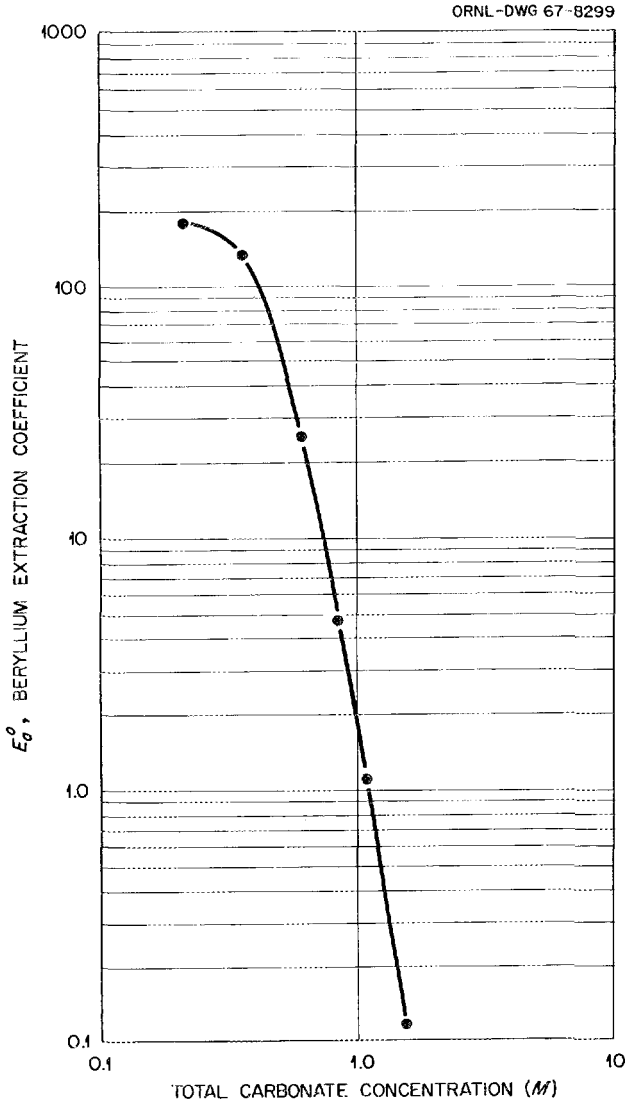

Fig. 8.4. Effect of Total Carbonate Concentration on Beryllium Extraction. Organic phase: 0.1 *M* Adogen 464 (carbonate form) in diethylbenzene; aqueous phase: 0.02 *M* Be with ^7Be tracer; initial carbonate/bicarbonate mole ratio of 1/1; contact: 10 min at an O/A phase ratio of 1/1.

Beryllium Extraction

Adogen 464, the quaternary ammonium compound used in this study, has the general structure $R_3(CH_3)N^+$, where R is 5% *n*-hexyl, 60% *n*-octyl, 33% *n*-decyl, and 2% *n*-dodecyl.

The efficiency of beryllium extraction increases rapidly with decreasing total carbonate concentration. In tests with 0.1 *M* Adogen 464 in diethylbenzene, the beryllium extraction coefficients decreased from about 60 at a total carbonate concentration of 0.5 *M* to 0.1 at 1.5 *M* (Fig. 8.4). The initial aqueous solutions in these tests contained an equimolar mixture of sodium carbonate and sodium bicarbonate. In tests with a constant total carbonate concentration (1 *M*), the beryllium extraction coefficients increased with increasing carbonate/bicarbonate ratio (Table 8.3). In other tests, increasing the pH of a 0.02 *M* solution of beryllium in 1 *M* NH_4HCO_3 from 8.8 to 10.0 by adding ammonia increased the beryllium extraction coefficient from 0.8 to 90.

Addition of a long-chain alcohol as a diluent modifier to Adogen 464–diethylbenzene solutions improves phase separation and prevents formation of a third liquid phase at high extractant concentrations. Also, addition of the alcohol can increase the beryllium extraction coefficient. In

Table 8.3. Effect of Carbonate/Bicarbonate Ratio on Beryllium Extraction

Aqueous phase:	0.01 *M* Be with ^7Be tracer, 1 *M* total carbonate
Organic phase:	0.12 *M* Adogen 464 (bicarbonate form) in 97% diethylbenzene–3% tridecanol
Phase ratio:	1/1

Initial Aqueous Phase		Beryllium Extraction Coefficient, E_a^o
Carbonate Concentration (*M*)	Bicarbonate Concentration (*M*)	
0.0	1.0	0.35
0.2	0.8	0.39
0.4	0.6	0.73
0.6	0.8	1.4
0.8	0.2	2.5
1.0	0.0	3.9

extractions with 0.27 *M* Adogen 464, the coefficient increased from 7.1 with 1.2 vol % tridecanol in the diluent to 13.3 with 10 vol % tridecanol (tridecanol/quaternary amine mole ratio, 1.5/1) and then decreased on further addition of tridecanol.

Extraction isotherms obtained with 0.5 *M* Adogen 464 in 95% diethylbenzene–5% tridecanol diluent at pH 9 and pH 10 showed poor loading of the solvent at pH 9. At pH 10 the solvent loaded to 2.3 g of beryllium per liter (0.5 mole of beryllium per mole of quaternary amine), which is consistent with extraction of a divalent anion:

$$(R_4N)_2CO_3(org) + Be(CO_3)_2^{2-}(aq) \rightleftharpoons (R_4N)_2Be(CO_3)_2(org) + CO_3^{2-}(aq) .$$

Beryllium Stripping

Because of the strong dependence of beryllium extraction on aqueous-phase carbonate concentra- (Fig. 8.4), beryllium can be stripped efficiently with relatively concentrated sodium or ammonium carbonate or, preferably, bicarbonate solutions.

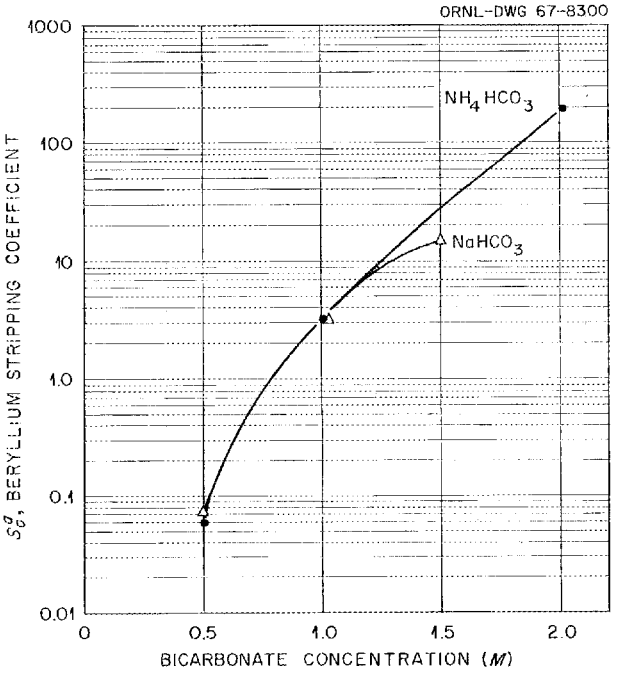

Fig. 8.5. Stripping of Beryllium with Bicarbonate Solutions. Organic phase: 0.1 *M* Adogen 464 in diethylbenzene loaded with 0.36 g of Be per liter. Contact: 10 min at an O/A phase ratio of 4/1.

Ammonium salts are preferred since they are more soluble than the sodium salts and, because they are volatile, are more readily separated from the beryllium product obtained by heating the strip solution. Coefficients for stripping beryllium from 0.1 *M* Adogen 464 at an organic/aqueous phase ratio of 4/1 increased from about 2 with 1 *M* NH_4HCO_3 to 200 with 2 *M* NH_4HCO_3 (Fig. 8.5). Beryllium was recovered almost quantitatively from both ammonium and sodium bicarbonate strip solutions by heating for 1 hr at 80°C to form a rapid-settling precipitate, which was probably the β form of beryllium hydroxide.

Tests to determine the purity of product obtainable in this system are not yet complete. Many potential metal contaminants are not appreciably soluble in carbonate solutions, and efficient separation from at least the bulk of these metals is obtained in the dissolution step. Preliminary extraction tests with Adogen 464 showed no significant extraction of calcium and magnesium from carbonate solutions, indicating that a highly efficient separation of beryllium from these contaminants can be expected.

8.7 SEPARATION OF ZIRCONIUM AND HAFNIUM WITH AMINES

In preliminary extraction tests made several years ago, the amine extractants showed some promise for the separation of zirconium and hafnium in the sulfate system; however, no attempt was made at that time to evaluate the possibilities of process application. We are briefly reexamining this system to determine if it represents an attractive alternative to present commercial processes for purifying zirconium. Initial results have been encouraging.

Batch Extraction Tests

The Zr/Hf separation factors are strongly dependent on the type of amine and the alkyl structure (Table 8.4). In extractions from pure sulfate solutions containing 19.4 g of zirconium and 0.3 g of hafnium per liter, the separation factors (Zr/Hf) were highest (6 to 8) for two of the tertiary amines and for S-24 amine (an extensively branched secondary amine) and lowest (0.6 to 0.8) for two primary amines. Separation factors for three less

Table 8.4. Extraction of Zirconium and Hafnium with Amines

Organic phase: 0.2 *N* amine (sulfate salt form) in 95% Varsol–5% tridecanol
Aqueous phase: 19.4 g of Zr and 0.3 g of Hf per liter, 0.7 *M* SO_4^{2-}, pH 0.5
Contact: 1 hr at an aqueous/organic phase ratio of 1/1

Amine	Type	Zirconium Loading of Solvent Phase (g/liter)	Separation Factor (Zr/Hf)
Amberlite XLA-3[a]	Primary	2.2	0.6
Heptadecyl[b]	Primary	2.7	0.8
Di(tridecyl)[c]	Secondary	12.0	1.4
Amberlite LA-2[d]	Secondary	7.2	1.1
S-24[e]	Secondary	4.2	8.4
N-Benzylheptadecyl[b]	Secondary	5.0	1.1
Adogen 364[f]	Tertiary	4.3	5.8
Tri(isooctyl)[g]	Tertiary	4.0	6.9
Di(2-ethylhexyl)hexyl	Tertiary	1.8	1.9
Tri(2-ethylhexyl)	Tertiary	0.4	2.0
Adogen 464[h]	Quaternary	14.5	1.3

[a]Branched primary amine.
[b]Heptadecyl = 1-(3-ethylpentyl)-4-ethyloctyl.
[c]Tridecyl chain branched no closer than the third carbon.
[d]$C_{12}H_{25}$–NH–CRR′R″; R's contain 12 to 14 carbon atoms.
[e]Bis(1-isobutyl-3,5-dimethylhexyl)amine.
[f]Mixed *n*-octyl and *n*-decyl alkyls.
[g]Branching no closer than the third carbon.
[h]Trialkylmethyl where alkyls are mixed *n*-octyl and *n*-decyl.

extensively branched secondary amines, a quaternary amine, and two tertiary amines with branching close to the nitrogen were in the range of 1.1 to 2.0. The quaternary amine and di(tridecyl)amine loaded with zirconium to a level about three times that for S-24 amine and for some of the better tertiary amines; this is surprising since the zirconium extraction coefficients for all these amines are high at low loadings (and the loadings achieved in these tests should be near the maximum attainable). Some additional extraction tests were made from feed solutions prepared by fusing zircon sand with caustic, washing with water to dissolve sodium silicate, and dissolving the zirconium and hafnium in sulfuric acid. Extractions of zirconium from this solution (28 g of zirconium per liter, pH 0.15) with 0.4 *M* solutions of tri(isooctyl)amine or S-24 amine in 95% Varsol–5% tridecanol diluent were effective, and Zr/Hf separation factors were in the range of 8 to 10. Phase separation was rapid with each solvent.

8.8 SEPARATION OF RARE EARTHS

The large recent increase in demand for certain rare earths has increased the need for more efficient separation methods. Present emphasis in our studies is on the use of solvent extraction with di(2-ethylhexyl)phosphoric acid (D2EHPA). Coefficients for the extraction of the rare earths with this reagent increase with increasing atomic number.[12] The separation factor between adjacent rare earths varies appreciably with position in the series but has an average value of about 2.5. In separating a mixture of rare earths by solvent extraction in a conventional countercurrent system, a number of runs must be made. First, the most (or least) extractable member of the series is separated from the others, then the adjacent member of the series is separated from the remaining

[12]D. F. Peppard, G. W. Mason, J. L. Maier, and W. J. Driscoll, *J. Inorg. Nucl. Chem.* 4, 334 (1957).

members, etc. To achieve efficient separations, each of the countercurrent runs must be very carefully controlled with respect to aqueous acid concentration and solvent loading. Since this is very difficult and cumbersome, we are examining other systems using D2EHPA, for example, extraction chromatography, that will separate the rare earths in a single run.

Extraction Chromatography

A number of investigators have demonstrated efficient separation of rare earths by sequential elution from columns containing D2EHPA supported on an inert material such as diatomaceous earth. Since the primary objective of these studies was to develop improved separation methods for analytical purposes, very small columns were used. We are now examining the system to determine if it shows promise as a large-scale separation method. Several runs were made to determine the effect of increasing the diameter of the columns, with other critical variables being held constant.

The column packing was prepared by slurrying 100- to 200-mesh acid-washed Chromosorb P (diatomaceous earth) with D2EHPA and acetone and air-drying. The dried packing contained 0.4 meq of D2EHPA per gram. The concentration of D2EHPA in the packed columns was 0.22 mole per liter of wet-settled bed. Rare earths were loaded onto the top of the bed from a nitrate solution containing 10 g of Ce, 22 g of Pr, 1.1 g of Eu, 2.0 g of Sm, and 9.6 g of Nd, and 0.1 *M* H^+ per liter and were removed from the column by gradient elution with nitric acid. Tracer cerium and neodymium were also added to simplify the analyses for these elements.

Figure 8.6 shows results of runs in 0.9-, 2.5-, and 5.0-cm-diam columns. The experimental conditions were not optimum for producing the most efficient separation of the rare earths, but the test results are useful for comparing the effect of change in column diameter on separation efficiency. The heights of the peaks and the widths of the bands were almost identical for the runs in the 0.9-cm- and 2.5-cm-diam columns. With the 5.0-cm-diam column, however, the peak heights were lower and the bands were wider, indicating a partial loss of resolution. The distance between the peaks was almost the same for all three runs. The somewhat poorer results with the largest column may have been caused by the increased

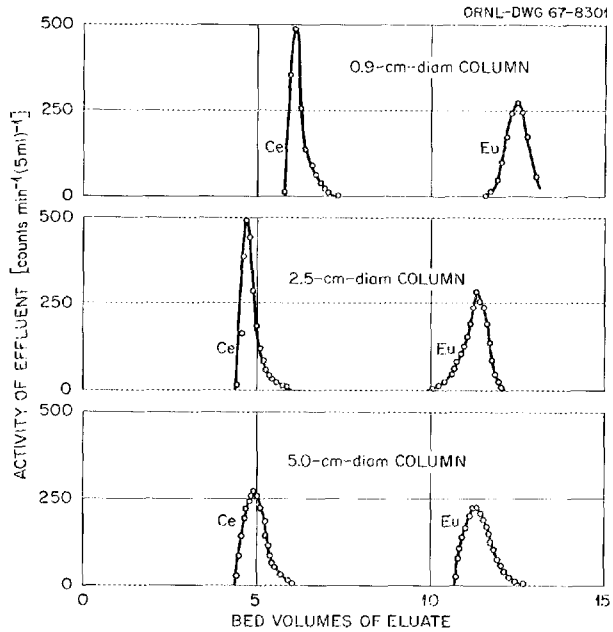

Fig. 8.6. Effect of Column Diameter on Separation of Rare Earths. Column packing: 50-cm-deep bed of Chromosorb P + D2EHPA. Loading: 0.04, 0.31, and 1.21 g of total rare earths in the respective runs. Elution: approximately linear (slightly concave) gradient; HNO_3 concentration in the eluting solution varied from 0.15 *M* to about 0.7 *M* during the run; flow rate of 0.9 ml cm^{-1} min^{-1}.

difficulty of distributing the eluting solution uniformly over the total cross section of the column. Tests with even larger columns are needed to determine if this separations system is potentially attractive for the large-scale separation of rare earths.

Separations in a Mixer-Settler System

Sequential stripping of the rare earths in a chromatographic manner was obtained in a mixer-settler system with a static solvent phase (0.5 *M* D2EHPA in Amsco 125-82). It should be possible to scale up such a system to any desired size without loss of separation efficiency. The procedure consisted in placing solvent loaded with rare earths in the first mixer-settler stage (and barren solvent in the remaining stages) and then stripping by passing acid through the system. The mixer-settlers are designed to minimize holdup of the aqueous phase.

Figure 8.7 shows results of preliminary tests in a ten-stage system. A sharp separation of neo-

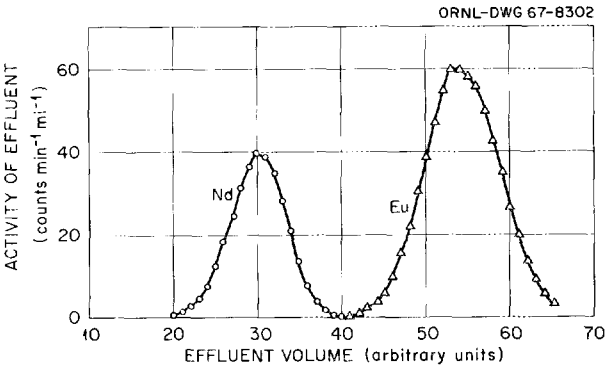

Fig. 8.7. Separation of Rare Earths in a Liquid-Liquid Stream with a Static Organic Phase. *Organic phase:* 0.5 *M* D2EHPA in Amsco 125-82; solvent in the first stage initially contained 5.7 g of Pr, 2.7 g of Nd (and Nd tracer), and 0.2 g of Eu (and Eu tracer) per liter. *Aqueous phase:* HNO_3 of gradually increasing concentration (approximately linear gradient) from 0.1 to 1.9 *M*. *Stages:* 10.

dymium from europium was obtained; a much larger number of stages would, of course, be needed for efficient separation of adjacent rare earths. A device with about 25 stages is being assembled to better define the potential of this method.

8.9 COMPARATIVE CHEMISTRY OF LANTHANIDES AND TRIVALENT ACTINIDES

Order of Extractability of Lanthanides and Actinides

In extractions of lanthanides by di(2-ethylhexyl)-phosphoric acid (HDEHP) and 2-ethylhexyl phenylphosphonic acid (HEH[ϕP]) from mineral acids, distribution coefficients are not rectilinear with respect to atomic number. The difference between cerium and lanthanum is much greater than the differences between other pairs of adjacent lanthanides, although there is a continual increase in extraction as the atomic number increases. However, in extractions from carboxylic acids, relative extractabilities may be altered so that neodymium, instead of lanthanum, becomes the least extractable lanthanide. The addition of aminopolyacetic acids, especially diethylenetriaminepentaacetic acid (DTPA), further alters the order so that lanthanum is the most extractable of the light lanthanides and the extractabilities of all the lanthanides are greatly decreased. Figure 8.8 shows specific examples of the behavior of the lanthanides from lanthanum to europium and of the actinide americium. Figure 8.9 shows that extractions of americium and californium are inversely proportional to the first power of the concentration of DTPA over a wide range of concentrations. In contrast, dependences for the lanthanides are similar at high DTPA concentrations but tend to level off at low DTPA concentrations.

Extractions of Trivalent Actinides from Pure Aqueous Solutions of Mineral Acids

Distribution coefficients for the extraction of americium and californium by HEH[ϕP] in both aliphatic and aromatic diluents from both hydrochloric and nitric acids have an approximately second-power dependence on extractant concentration, rather than the previously reported third-power dependence. At acid concentrations less than about 5 *N*, the dependence of extraction on

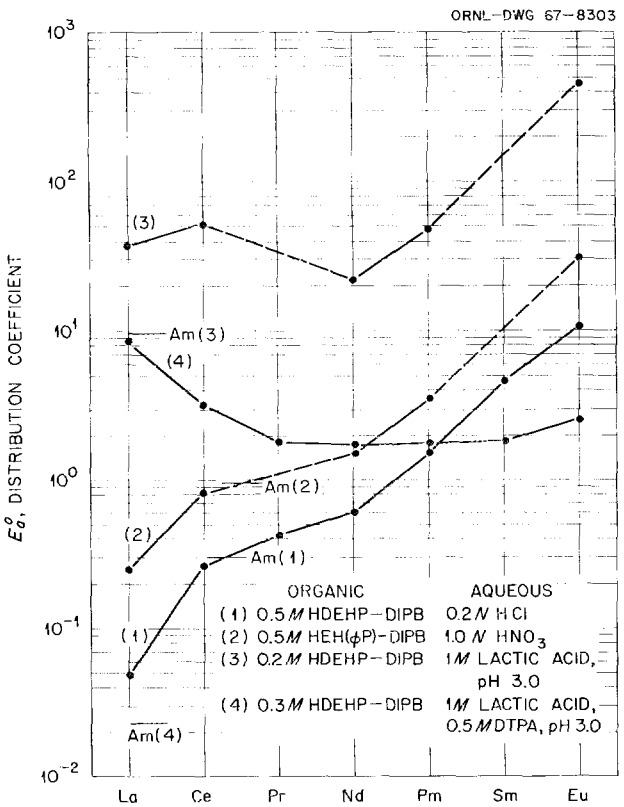

Fig. 8.8. Order of Extractability of Some Lanthanides and Americium with HDEHP and HEH[ϕP] from Various Aqueous Solutions.

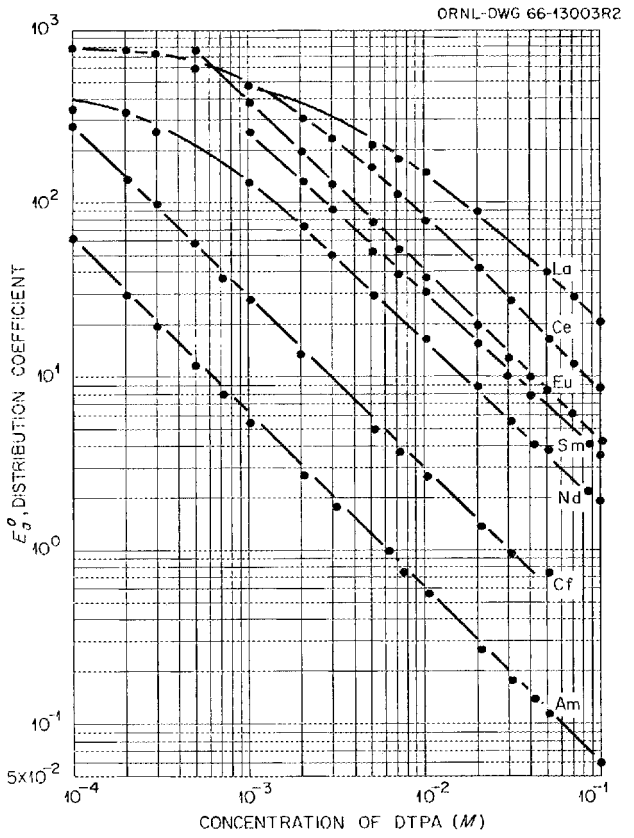

Fig. 8.9. Dependence of Extraction of Some Lanthanides and Actinides on Concentration of DTPA. Organic phase: 0.5 *M* HDEHP-DIPB; aqueous phase: 1 *M* lactic acid, variable DTPA concentration, pH 3.0.

acid concentration is greater than inverse third-power, and is higher for californium than for americium. Californium/americium separation factors are about half as large in extractions from HNO_3 as from HCl. Distribution coefficients are about 1.5 times as high with diisopropylbenzene as with diethylbenzene for diluent. Distribution coefficients are several times higher with aliphatic diluents than with aromatics, but Cf/Am separation factors are smaller with aliphatics because californium coefficients increase less than do americium coefficients. Separation of phases is considerably more rapid with aliphatic diluents. The maximum practicable Cf/Am separation factors in extractions by HEH[ϕP] in aromatic diluents are about 80 from HCl and 40 from HNO_3, while the corresponding values for aliphatic diluents are 50 and 25. Higher separation factors, up to 100, can be attained but only under conditions where distribution coefficients are too low to be of practical use.

Since HDEHP is so much weaker than HEH[ϕP] as an extractant, an aliphatic diluent is necessary in actinide separations. Contrary to predictions based on published data, maximum practicable separation factors between the actinides are about the same with both extractants in aliphatic diluents. Dependence of extraction on the concentration of HDEHP is also about second power – slightly lower for californium than for americium. Dependence on acid concentration is about inverse third power up to about 5 *N*, with a reversal at about 6 *N*. This reversal also occurs in lanthanide extractions. Maximum Cf/Am separation factors under useful conditions are about 50 from HCl and 20 from HNO_3. For the separation of greatest interest, that of berkelium from curium, the HCl system gives factors of 12 to 14, which are at least as high as can be obtained with HEH[ϕP].

Commercial HDEHP contains impurities that decrease separations between lanthanides and between actinides. The major impurity, mono(2-ethylhexyl)phosphoric acid, is readily removed by a single contact of the diluted reagent with an excess of a dilute solution of NaOH or Na_2CO_3. An additional interfering impurity, of unknown composition, requires numerous further alkali treatments for removal. It is more easily removed by two half-volume contacts with ethylene glycol after the single alkali treatment and reacidification.

Effects of Metallic Cations on Extraction of Lanthanides and Actinides

Synergism by Cations of the Type MO^{2+}. – We observed a remarkable enhancement of the extraction of some lanthanides and actinides by HEH[ϕP] from both HCl and HNO_3 solutions containing zirconium or hafnium, probably present as ZrO^{2+} and HfO^{2+} (see Fig. 8.10). Titanium did not cause any enhancement; however, the aqueous solutions tested were unstable. There was no enhancement by thorium or uranyl ions. The maximum enhancement factor was greater than 100 when the MO^{2+} concentration was only 0.01 *M*. The effect was much greater in HNO_3 than in HCl solutions. It was independent of the concentrations of extractant and acid but was greater with an aliphatic than with an aromatic diluent. It decreased with increasing atomic number in both the lanthanide and actinide series. Thus, only a small amount of zirconium as

an impurity can effectively prevent the separation of californium from americium (and berkelium from curium) by this means. This bimetallic synergism does not occur in extractions by HDEHP.

Effects of Other Cationic Impurities. — Lithium chloride in HCl solutions at concentrations 1 *M* and 2 *M* decreased distribution coefficients of trivalent actinides with both HEH[ϕP] and HDEHP by factors of approximately 2 and 4 respectively. Iron(III) decreased distribution coefficients for the HEH[ϕP] extraction of lanthanides and actinides by factors up to 4 when present in concentrations up to 1 g/liter. The Fe(III) was extracted slowly and formed precipitates at concentration levels of 0.4 g/liter or more. Chromium(III) had no apparent effect on extractions.

Coprecipitation of Berkelium(IV) and Cerium(IV)

Berkelium and cerium in solutions 0.05 *M* in HIO_3 and up to 0.5 *N* in HNO_3 may be oxidized by bromate and coprecipitated. Precipitation of

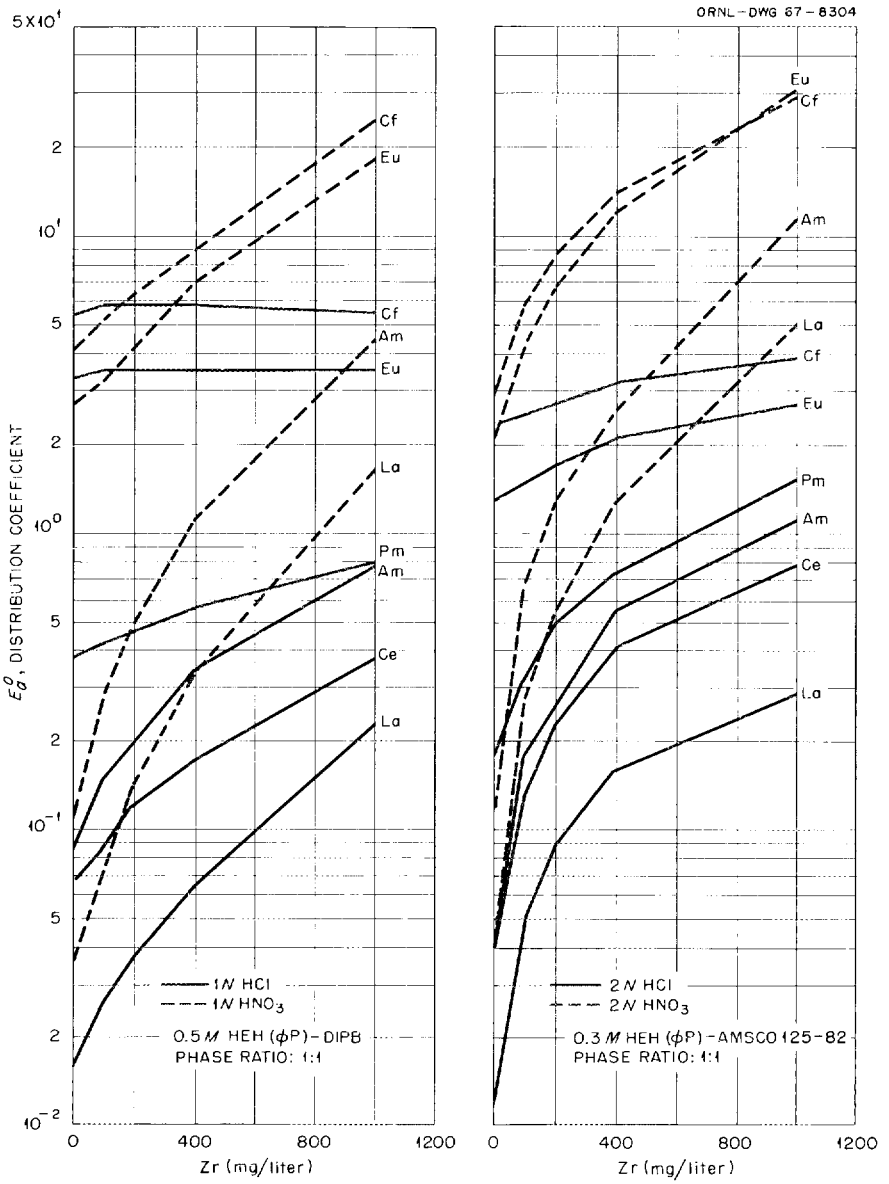

Fig. 8.10. Effect of Zirconium on Extraction of Lanthanides and Actinides with HEH[ϕP].

trace amounts of berkelium with 1 mg of cerium in 10 ml was >99.8% complete when precipitation of the cerium carrier was only 95 to 99% complete.

8.10 TRANSPLUTONIUM ELEMENT COMPOUND PREPARATION AND X-RAY CHARACTERIZATION

Preliminary preparations of various oxides of berkelium were made as a part of the program to prepare and characterize compounds of the transplutonium elements. We were able to prepare these oxides from only microgram quantities of the element by using the single ion exchange bead technique of Cunningham and Green.[13-15] This technique consists in loading a single ion exchange resin bead to saturation (using a highly purified solution of berkelium) and then destroying the resin matrix by calcination. A coherent particle of the element oxide remains.

The berkelium was purified by a series of solvent extraction and ion exchange techniques. Analysis of the berkelium oxide by the neutron activation method showed $\leq$1.3% Ce, <0.5% Nd, 0.008% La, and <0.005% Eu. No other impurities were detected.

The air-stable form of berkelium oxide is BkO_2, which has a face-centered cubic structure with lattice parameter $a = 5.334 \pm 0.005$ A. The hydrogen-reduced oxide is Bk_2O_3, which has a body-centered cubic structure with $a = 10{,}880 \pm 0.005$ A.

We are planning additional work on the oxide system and on berkelium halide preparations and characterizations; also, we plan to extend the use of these techniques to similar studies of ^{249}Cf.

8.11 AMINOPOLYCARBOXYLIC ACID COMPLEXES OF TRIVALENT ACTINIDES

It is anticipated that the determination of stability constants of a variety of transplutonium actinide chelate compounds will contribute to formulation of a theory regarding stability trends and will lead to improved separation methods. Ion exchange and spectrophotometric techniques are being used. Initial work has been centered on complexes with aminopolycarboxylic acids, which are already important in processing. In addition to stability constants, the type of complexes formed and the effects of structural changes on their formation are being determined.

Spectrophotometric Determination of Americium Complexing with Aminopolyacetic Acids

The complexing of americium with aminopolyacetic acids was studied by absorption spectrophotometric analysis in an effort to ascertain the type of complexes formed, and also to provide an alternative method for determining stability constants. The presence of complexing agents displaces the absorption spectra of americium to longer wavelengths. With successive complexing, new absorption bands are formed, which makes it possible to study the complexes in solution and the conditions under which they are formed.

The aminopolyacetic acids examined have two to seven carboxylic acid groups. The experiments were carried out in series at constant Am^{3+} (0.001 *M*) and ligand (0.005 *M*) concentrations. The ionic strength was held constant with 0.1 *M* NH_4ClO_4, while the pH was varied from 1 to 9 by small additions of $HClO_4$ or NH_4OH. The optical densities were measured with a Cary 14 spectrophotometer. A second isomolar series of experiments at constant pH and varying metal-to-ligand ratios was used to determine the composition of the complexes. An example of the spectral shift of the americium complex with diethylenetriaminepentaacetic acid (DTPA) is shown in Fig. 8.11. With increasing pH, the band at 502.7 mμ disappears and a new absorption band at 507.6 mμ is formed. A single complex was found with this ligand; the isomolar series showed it to be a 1 : 1 complex. Two or three complexes were found between each of the other ligands and americium (Table 8.5).

Ion Exchange Behavior with 2-Hydroxy-1,3-diaminopropanetetraacetic Acid (HPDTA)

HPDTA differs from the foregoing aminopolycarboxylic acids in having a hydroxy group. The effect of this hydroxy group on aminopolycarboxylic acid complexing of the transplutonium elements is

---

[13] B. B. Cunningham, *Microchem. J., Symp. Ser.* 1 (1961).

[14] B. B. Cunningham, *Proceedings of the Robert A. Welch Foundation Conferences on Chemical Research. VI. Topics in Modern Inorganic Chemistry, 1962.*

[15] J. L. Green, *The Absorption Spectrum of Cf^{+3} and Crystallography of Californium Sesquioxide and Californium Trichloride*, UCRL-16516 (November 1965).

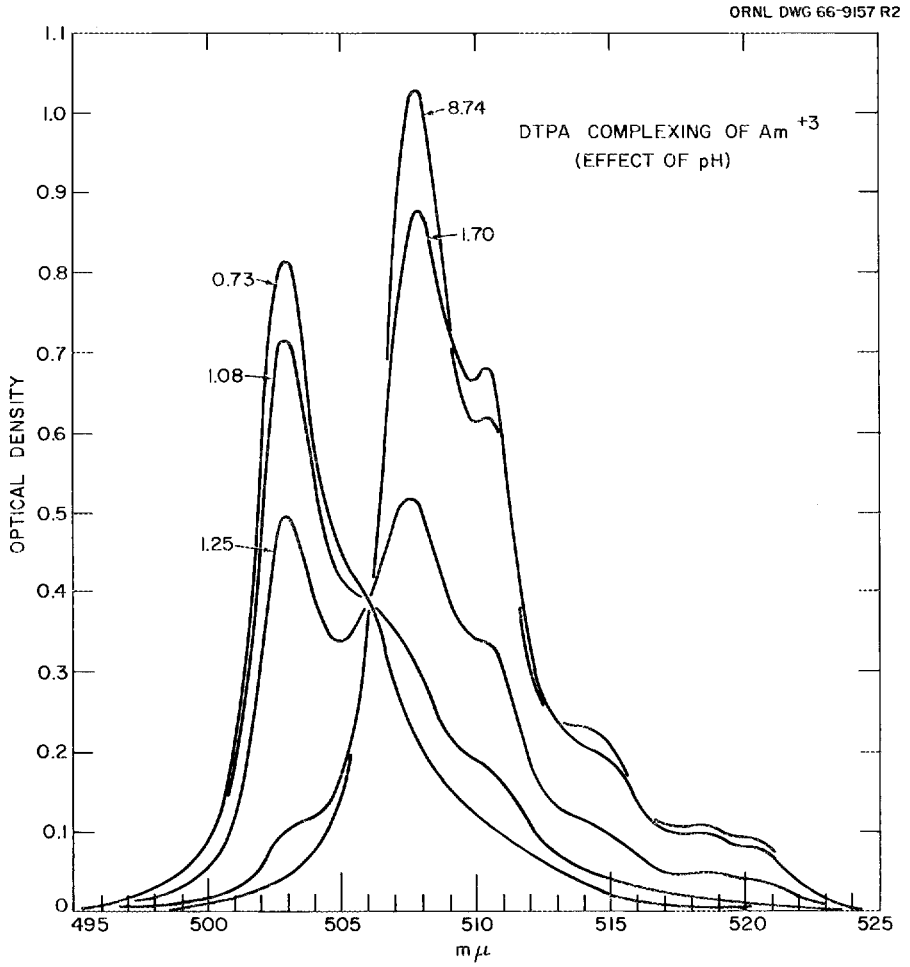

Fig. 8.11. Effect of pH on the Spectrum of Americium Complexed with Diethylenetriaminepentaacetic Acid. Composition: 0.001 *M* Am^{3+}, 0.005 *M* DTPA, ~0.10 *M* NH_4ClO_4 (ionic strength = 0.10).

Table 8.5. Americium Complexes with Aminopolyacetic Acids

Ligand	Number of Complexes	pH Range of Formation	Am: Ligand Ratio in Complex	pK_s	Reaction
Imidodiacetic acid	3	(1) 2.5–5.4 (2) 4.0–7.0 (3) 5.0–8.0	1 : 1	6.1	
Hydroxyethylimidodiacetic acid	2	(1) 1.3–2.8 (2) 1.7–6.0	1 : 1 1 : 2	10.44 7.4	$Am^{3+} + H_2Y \rightarrow AmY^+ + 2H^+$ $Am^{3+} + 2HY^- \rightarrow AmHY_2 + H^+$
Ethylenediaminetetraacetic acid	2	(1) 1.0–2.0 (2) >3.5–9.0	1 : 1	18.15	$Am^{3+} + H_4Y \rightarrow AmY^- + 4H^+$
Diethylenetriaminepentaacetic acid	1	(1) 0.9–1.6	1 : 1	24.6	$Am^{3+} + H_5Y \rightarrow AmHY^- + 4H^+$
Triethylenetetraaminehexaacetic acid	2	(1) 1.0–2.2 (2) 3.0–5.5			
Tetraethylenepentaaminoheptaacetic acid	3	(1) 1.0–2.0 (2) 2.0–2.5 (3) 2.5–4.0			

being examined by ion exchange distribution. The stability constants (pK_s) for Am, Cm, Cf, and Eu have been calculated for the complex with HPDTA, as follows:

Am	12.14 ± 0.05
Cm	12.30 ± 0.05
Cf	13.18 ± 0.05
Eu	12.21 ± 0.05

These values were calculated from the variation of ion exchange distribution coefficients of the metals vs pH (Fig. 8.12). The method for calculating pK_s was previously described.[16] The acid dissociation constants used for the HPDTA are $pK_1 = 1.60$, $pK_2 = 2.60$, $pK_3 = 6.96$, and $pK_4 = 9.49$ (ref. 17).

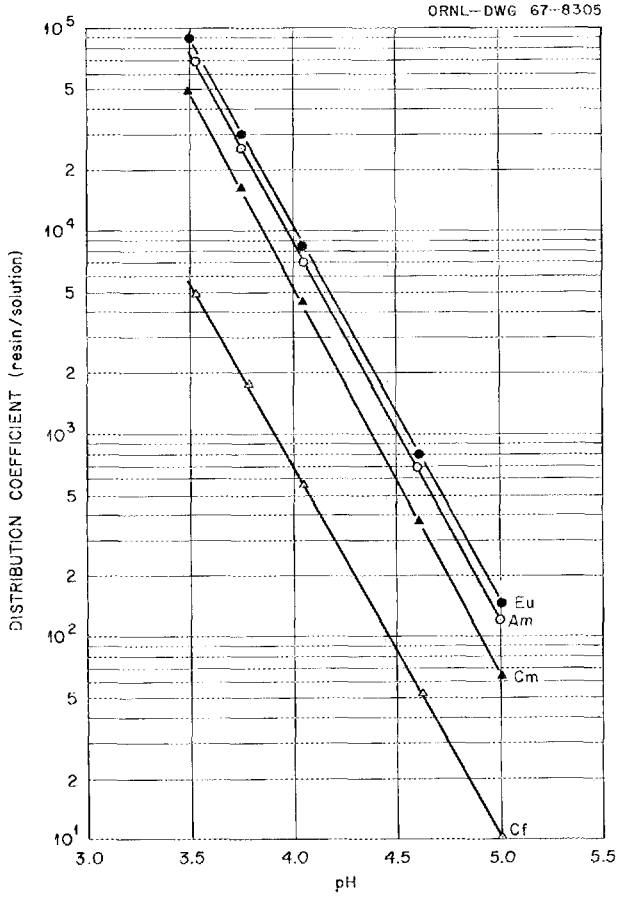

Fig. 8.12. Effect of pH on Sorption of Trivalent Metal Ions in Competition with Complexing by 2-Hydroxy-1,3-diaminotetraacetic Acid. Dowex 50-8X (100 to 200 mesh); $<10^{-6}$ *M* metals, 0.001 *M* HPDTA, ~0.10 *M* NH_4ClO_4 (ionic strength = 0.10).

The presence of the CHOH group between the two aminopolyacetic acid groups decreased the strength of the complex as compared with the ethylenediaminetetraacetic acid (EDTA) complex.[18] The suppression of stability constants was much greater than expected, that is, from EDTA, $pK_s \approx 18.2$, to HPDTA, $pK_s \approx 12.1$, for Am. However, the difference in pK_s between americium and californium is considerably greater than with other ligands. This unusually strong differentiation between the transplutonium elements is being further investigated in an attempt to develop improved separation techniques for the inner group of actinide elements.

8.12 LANTHANIDE AND ACTINIDE SULFATE COMPLEXES

Several workers have studied the formation of lanthanide and trivalent actinide sulfate complexes at sulfate concentrations up to about 0.3 *M* by means of chelate or cation exchange extraction.[19] Their data on formation constants for the mono- and disulfate complexes MSO_4^+ and $M(SO_4)_2^-$ agree fairly well. Only in one case was a trisulfate complex detected, $Lu(SO_4)_3^{3-}$. We previously showed that liquid anion exchange (amine extraction) has some advantage in detecting and evaluating formation of anionic complexes, and we used it to study the anionic sulfate complexes of uranyl and of thorium.[20] We have started a similar investigation of the sulfate complexes of europium; this will be extended to americium and eventually to other lanthanides and actinides.

Essentially, in this method we determine the compositions of a series of aqueous phases such that they are in equilibrium with organic phases of a single composition. The activity of each extractable species is accordingly constant throughout the series of aqueous solutions, being propor-

---

[16] R. D. Baybarz, *J. Inorg. Nucl. Chem.* **27**, 1831 (1965).

[17] L. C. Thompson and S. K. Kundra, *J. Inorg. Nucl. Chem.* **28**, 2945 (1966).

[18] J. Fuger, *J. Inorg. Nucl. Chem.* **18**, 263 (1961).

[19] P. G. Manning and C. B. Monk, *Trans. Faraday Soc.* **58**, 938 (1962); B. M. L. Bansal *et al.*, *J. Inorg. Nucl. Chem.* **26**, 993 (1964); Tatsuya Sekine, *Acta Chem. Scand.* **19**, 1469 (1965); R. G. de Carvalho and G. R. Choppin, *J. Inorg. Nucl. Chem.* **29**, 725 (1967).

[20] K. A. Allen, *J. Am. Chem. Soc.* **80**, 4133 (1950); K. A. Allen and W. J. McDowell, *J. Phys. Chem.* **67**, 1138 (1963).

tional to its constant activity in the organic phase. These are composed of various combinations of sulfuric acid and sodium sulfate, all adjusted to one sulfuric acid activity.[21] The actual concentration of sulfate ion[21] and the ionic strength are calculated for each. The extraction coefficient of the metal is a function of the actual sulfate ion concentration, and, since the organic-phase concentration of the metal is held constant, the aqueous-phase concentration varies inversely with the extraction coefficient. The required activity coefficient ratios are estimated by means of a Debye-Hückel expression. According to this, the activity coefficient of a neutral species does not change with changing ionic strength. Hence, the concentration, as well as the activity, of a neutral complex is constant throughout the series. The concentration of each of the other possible species can be expressed as the concentration of the real or hypothetical neutral species times the appropriate formation constant and activity coefficient ratio. Their sum is equated to the measured total aqueous metal concentration, and the resulting series of equations is solved for the formation constants by simultaneous least-squares analysis.

The secondary amine (didecyl) used to extract uranyl and thorium sulfates is a poor extractant for lanthanide sulfate. Several primary amines have high extraction coefficients for europium. Of these, nonyldecylamine normal sulfate, which is both sufficiently soluble in benzene and negligibly soluble in the aqueous phase, was selected for the present extraction tests. Two series of extractions (see Fig. 8.13) have been completed, at sulfuric acid activities of 3.58×10^{-10} and 6.45×10^{-5} M^3. The data are now being analyzed; the actual sulfate ion concentrations have been calculated for the set at the higher acid concentration (open circles in Fig. 8.13). Here the positive slope indicates that more of the negative than of the positive species is present, and the increasing slope suggests that more than one negative species is involved, that is, that a significant amount of $Eu(SO_4)_3^{3-}$ exists at the highest sulfate concentrations. Similarly, the region of negative slope at the lowest sulfate concentrations indicates that here more of the positive (Eu^{3+}, $EuSO_4^{+}$) than of the negative [$Eu(SO_4)_2^{-}$, etc.] species are present.

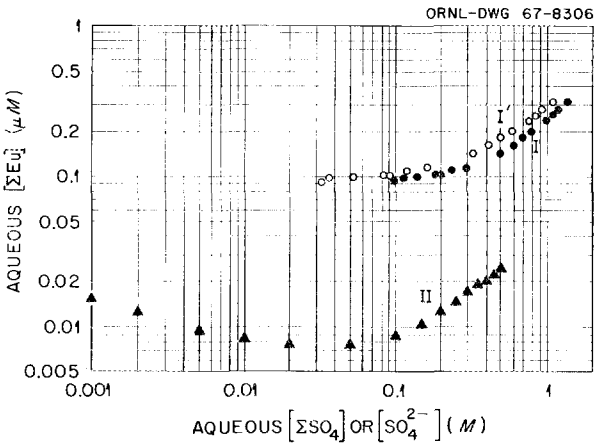

Fig. 8.13. Variation of Aqueous-Phase Europium with Sulfate Concentration. 0.1 *M* Nonyldecylamine in benzene containing 5×10^{-3} *M* Eu + $^{152-154}$Eu tracer.

I: $a_{H_2SO_4} = 6.45 \times 10^{-5}$ M^3, pH 1.0 – 1.3, ionic strength 0.17 to 3.9 *M*; [Eu] vs total sulfate concentration.

I′: Same; [Eu] vs actual SO_4^{2-} concentration.

II: $a_{H_2SO_4} = 3.58 \times 10^{-10}$ M^3, pH ≈ 3; [Eu] vs total sulfate concentration.

8.13 EQUILIBRIA AND MECHANISMS OF EXTRACTIONS

Synergistic Extraction of Strontium by Di(2-ethylhexyl)phosphoric Acid and Tributyl Phosphate

The previously reported studies of synergistic strontium extraction[22] indicated that the synergistic enhancement of extraction was the result of replacement of molecular di(2-ethylhexyl)phosphoric acid (HDEHP, HA) by TBP in coordination with the extracted strontium to form $SrA_2 \cdot 2HA \cdot 2TBP$ or $SrA_2 \cdot 2HA \cdot TBP$ and $SrA_2 \cdot 4TBP$. The experimental, derived dependences of extraction on DEHP concentration and on pH were consistent with formation of those species, but the dependence on TBP concentration appeared to be perturbed by some unidentified variable. This variable was suspected to be aggregation of TBP (in the presence of some water) in dilute hydrocarbon solution.

[21] C. F. Baes, *J. Am. Chem. Soc.* **79**, 5611 (1957).

[22] *Chem. Technol. Div. Ann. Progr. Rept. May 31, 1965*, ORNL-3830, p. 213.

The study of synergistic strontium extraction has now been completed with a continuous-variations examination of the effect of the TBP:A ratio on the extraction and a brief direct test of the suggested TBP-H_2O aggregation. The results are shown in Fig. 8.14. The ordinate is the synergistic enhancement of the extraction coefficient, ΔE_{Sr} = (E_{Sr} with the combined extractants) minus (E_{Sr} with DEHP alone); E_{Sr} with TBP alone is zero throughout. The maximum occurs near 60% TBP–40% ΣA and 0.3 NaA/ΣA. The relative maxima remain fairly constant at 60% TBP as NaA/ΣA increases above 0.3, but decrease linearly as NaA/ΣA decreases below 0.2 (Fig. 8.15). This is consistent with the formation of $SrA_2 \cdot 4TBP$, as previously deduced, when NaA/ΣA is 0.2 or higher, with the TBP content decreasing to perhaps as low as ½ TBP (average) per Sr at NaA/ΣA extrapolated to zero (i.e., all DEHP as HA).

The previously observed power dependence of E_{Sr} on TBP concentration was 0.25.[22] This is too low to be consistent with an average of 1 TBP per Sr, as in $SrA_2 \cdot 2HA \cdot TBP$, or even ½ TBP per Sr, unless the TBP is aggregated. It is conceivable that such aggregation does occur, in association with water molecules, in the dilute hydrocarbon solutions. Whitney and Diamond[23] postulated that 3 or 4 TBP molecules associate with a hydronium ion. Brief tests of water extraction as a function of TBP concentration in HDEHP–TBP–*n*-octane suggested association of up to 3 TBP per H_2O; however, these measurements were close to the limits of the infrared absorption method used for analysis.

The final conclusions from these and the previously reported results are that diluents (and organic additives) have two distinct effects on strontium extraction by DEHP: (1) a shift of the E_{Sr} vs pH curve along the pH axis, reflecting a shift in the apparent acid strength of HDEHP due to the (Lewis) acidity or basicity of the diluent or additive, and (2) a synergistic enhancement of E_{Sr} due to direct association of the additive with the extracted strontium, or an antagonistic depression of E_{Sr} due to competitive association of the additive with DEHP. With TBP (synergist) and dodecyl alcohol (antagonist), the latter effects are marked when the diluent is an aliphatic hydrocarbon but negligible when it is benzene. TBP interacts with both sodium and strontium DEHP salts but not with the free acid alone. We believe that the strontium species result from replacement of HA by TBP in $SrA_2 \cdot 4HA$ to give $SrA_2 \cdot 2HA \cdot TBP$ when nearly all of the DEHP is present as HA, and $SrA_2 \cdot 4TBP$ when NaA/ΣA is 0.2 or greater.

[23] D. C. Whitney and R. M. Diamond, *Inorg. Chem.* 67, 209–16 (1963).

Alkaline-Earth and Rare-Earth Extraction by Sulfonic and Carboxylic Acids

Extractions of strontium and europium by the newly available didodecylnaphthalenesulfonic

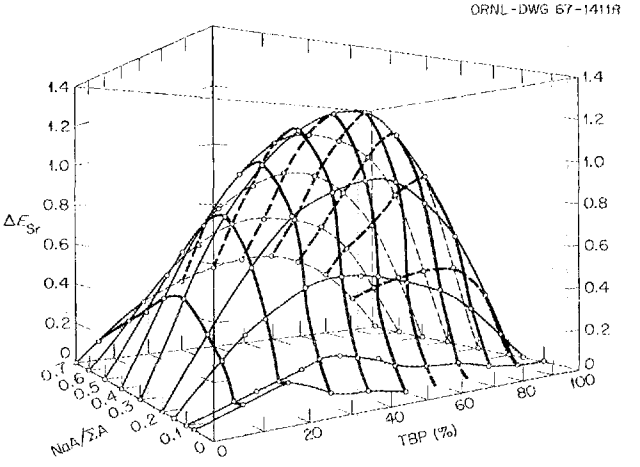

Fig. 8.14. Three-Dimensional Plot of the Continuous-Variations Results of the TBP-DEHP Synergistic Extraction of Strontium at Several NaA/ΣA Values.

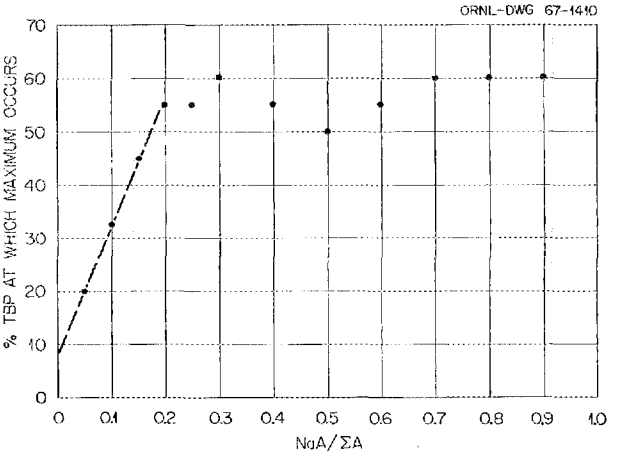

Fig. 8.15. TBP Concentration at Which ΔE_{Sr} Maximum Occurs as a Function of NaA/ΣA.

acid (HDDNS) confirm the expectation that this strong acid functions as a liquid cation exchanger in concentrated acid solutions (Fig. 8.16). One-third of the hydrogen ion (of 0.05 *M* HDDNS in benzene) present is replaced by sodium ion in equilibration with 1 *M* $NaNO_3$–2 *M* HNO_3 solution, while more than half is replaced in equilibration with 2 *M* $NaNO_3$–1 *M* HNO_3 solution. The extraction of both strontium and europium (0.001 *M*) increases with decreasing acid concentration in nearly direct proportion to the NaDDNS/ΣDDNS ratio. The absence of any extraction maximum, in contrast to the prominent maxima in the corresponding extraction curve for a dialkylphosphoric acid, indicates that the salts $Sr(DDNS)_2$ and $Eu(DDNS)_3$ do not coordinate with any additional HDDNS. This further suggests (as also does the low level of the extraction coefficients) that little or no coordination may be involved in the formation of these salts, that is, that they may be simply ion groups. In any case, the apparent absence of coordination with additional HDDNS should provide opportunity for extensive synergism by organic additives that coordinate with the extracted metal ions. Synergistic extraction of several metals was previously noted when either phosphonate or phosphine oxide was added to dinonylnaphthalenesulfonic acid;[24] preliminary tests showed synergistic enhancement of europium extraction by HDDNS upon addition of trioctylphosphine oxide.

Extraction coefficients of strontium and barium (0.001 *M*) from acid sodium nitrate solutions with three carboxylic acids (0.1 *M*) were an order of magnitude higher than those with di(2-ethylhexyl)-phosphoric acid at pH's corresponding to the same extraction of sodium, that is, at the same NaA/ΣA extractant compositions. These acids are: neotridecanoic acid, a "Koch" acid (molecular weight of about 300), and monoheptadecyl tetrapropenylsuccinic acid. The log *E* vs pH curves showed maxima very similar to those found with dialkylphosphoric acids. It has been shown that, for the latter, the NaA/ΣA ratio giving the maximum extraction indicates the composition of the principal extraction species.[25] We expect the same relation to hold in the carboxylic acid extractions. If so,

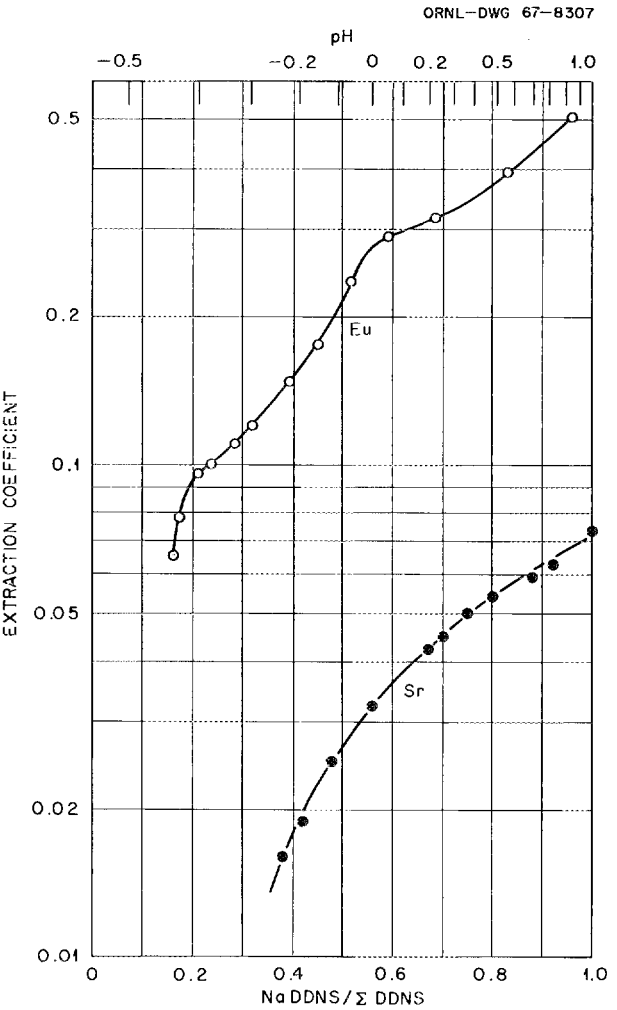

Fig. 8.16. Extraction of Strontium and Europium by Dodecylnaphthalenesulfonic Acid. 0.05 *M* HDDNS in benzene; HNO_3-$NaNO_3$ at ionic strength = 3.0 *M*; pH and resulting NaDDNS/ΣDDNS ratio as indicated.

the maxima measured thus far indicate formation of $SrA_2 \cdot 4HA$ with neotridecanoic acid, $BaA_2 \cdot 3HA$ with the "Koch" acid, and $BaA_2 \cdot HA$ with the heptadecyl tetrapropenylsuccinic (ester) acid. The last probably functions as a bidentate complexer, filling 6-coordination for the barium.

Uranium Extraction by Amine Sulfate at Low Water Activity

In the continued studies in which we are attempting to resolve apparent deviations of amine extraction equilibria from the mass action law, the

[24] *Chem. Tech. Div. Chem. Dev. Sec. C. Progr. Rept. October 1959*, ORNL-CF-59-10-101, pp. 22–24.

[25] W. J. McDowell and C. F. Coleman, *J. Inorg. Nucl. Chem.* 28, 1083 (1966).

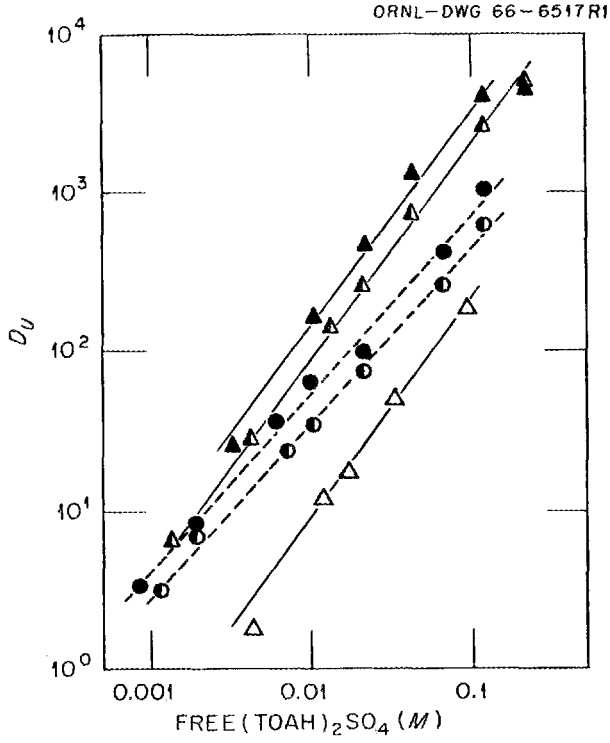

Fig. 8.17. Reagent Concentration Dependence on Uranyl Sulfate Extraction by TOA at Different Water Activities. 0.1 *M* TOA in benzene; equilibrium-free $(TOAH)_2SO_4$ concentration calculated from analyses and material balance.

- ● pH 1.0 1 *M* Na_2SO_4, $a_w = 0.96$
- ▲ pH 2.0
- ◐ pH 1.0 Saturated Na_2SO_4, $a_w = 0.93$
- ◭ pH 2.0
- △ pH 2.0 Saturated $(NH_4^+)_2SO_4$, $a_w = 0.80$

activity and lack of aggregation of the normal sulfate of tri-*n*-octylamine (TOAS) were determined as a function of water activity[26] up to $a_w = 0.90$. Since the uranyl sulfate extractions of concern were at $a_w \geq 0.95$, a small but conceivably important gap remained to be investigated. This gap has now been bridged by comparing uranyl extractions at $a_w = 0.80$ (saturated ammonium sulfate) and $a_w = 0.93$ (saturated sodium sulfate) with extractions at $a_w = 0.96$ (1 *M* sodium sulfate). The log-log extraction plots are parallel, at each of two pH levels (Fig. 8.17), which eliminates the possibility that the deviations from mass action behavior depend on some abrupt change at high water activities.

8.14 KINETICS OF METAL-ION EXTRACTIONS BY DI(2-ETHYLHEXYL)PHOSPHORIC ACID (HDEHP)

Iron Extraction

In the continued study of the kinetics of the slow extraction of iron(III) by HDEHP, we found a detailed explanation, consistent with the general explanation previously suggested,[27] that appears to account for the increase of extraction rate with decreasing acidity. Thus far it is supported by the experiments designed to test it.

The kinetics of iron extraction from acid perchlorate solution are well summarized by two proportionalities for the first-order rate constant $k = -d \log [Fe]/dt$:

$$k \propto [Fe^{3+}][HA]^{0.5}/[H^+] \quad \text{at } [HA] < 0.2\ M\ , \quad (1)$$

$$k \propto [Fe^{3+}][HA]^{1.5}/[H^+]^2 \quad \text{at } [HA] > 0.5\ M\ , \quad (2)$$

for the *net* reaction

$$Fe(H_2O)_6^{3+} + \underset{\cdots\cdots}{3(HA)_2} \rightleftharpoons \underset{\cdots\ \cdots}{FeA_3 \cdot 3HA} + 3H^+ + 6H_2O\ , \quad (3)$$

at least at the lower HA concentrations.[28] Here, HA is HDEHP; dotted underlines designate the organic phase or the interface; and reaction occurs essentially only at the interface. Eigen[29] has demonstrated that in the formation of, for example, ferric chloride complexes, a two-step reaction,

$$Fe(H_2O)_6^{3+} + Cl^- \longrightarrow FeOH(H_2O)_5^{2+} + H^+Cl^- \longrightarrow FeCl(H_2O)_5^{2+} + H_2O\ ,$$

actually occurs instead of the direct substitution

$$Fe(H_2O)_6^{3+} + Cl^- \longrightarrow FeCl(H_2O)_5^{2+} + H_2O\ .$$

[26] *Chem. Technol. Div. Ann. Progr. Rept. May 31, 1965*, ORNL-3830, p. 218.

[27] *Chem. Technol. Div. Ann. Progr. Rept. May 11, 1966*, ORNL-3945, p. 185.

[28] C. F. Baes, Jr., and H. T. Baker, *J. Phys. Chem.* **64**, 90 (1960).

[29] M. Eigen, "The Kinetics of Fast Solvent Substitution in Metal Complex Formation," *Advances in the Chemistry of Coordination Compounds* (ed. by S. Kirschner), p. 371, Macmillan, New York, 1961.

Whereas the spontaneous ionization of one of the waters of hydration (leaving a hydroxyl complex) is slow, the direct substitution would be much slower still. The direct substitution of chloride for hydroxyl, on the other hand, is fast. In the analogous slow first step of the iron extraction,

$$Fe(H_2O)_6^{3+} + \underset{\cdots}{A^-} \longrightarrow FeOH(H_2O)_5^{2+} + \underset{\cdots}{HA}\ , \quad (4)$$

the concentration of A^-, and hence the rate of reaction, will vary inversely with the acid concentration since HDEHP is a moderately weak acid. If this reaction (limited to the interface) is correct, we expect the rate of extraction to be increased by the addition of aqueous-soluble proton-accepting complexers:

$$Fe(H_2O)_6^{3+} + X^- \longrightarrow FeOH(H_2O)_5^{2+}$$

$$+ HX \longrightarrow FeX(H_2O)_5^{2+} + H_2O\ , \quad (5)$$

$$FeX(H_2O)_5^{2+} + \underset{\cdot\cdot}{HA} \rightleftharpoons \underset{\cdot\cdot\cdot\cdot\cdot\cdot\cdot\cdot\cdot\cdot}{FeA(H_2O)_5^{2+}} + HX\ , \quad (6)$$

followed by further fast reactions to yield $FeA_3 \cdot 3HA$. (Competition by the aqueous complex should decrease the *equilibrium* concentration of $FeA_3 \cdot 3HA$ slightly, but the resulting small decrease in the driving force will have only a small effect on the net *rate* in the early stages of extraction.) Addition of several aqueous complexers to the perchlorate solution did indeed speed up the extraction, some by large factors (Table 8.6). While it is not yet feasible to try to distinguish the effects of the proton-accepting and iron-complexing affinity of X^- in Eq. (5) and the iron-complexing affinity of X^- vs A^- in Eq. (6), the greater effectiveness of nitric than of hydrochloric acid, and of acetic than of dichloroacetic acid, suggests that the proton-accepting affinity (acid weakness) is important.

Beryllium Extraction

We have begun to study the kinetics of the slow extraction of beryllium from acid perchlorate solutions by HDEHP. (Brief preliminary measurements of the beryllium extraction rate, showing that the rate is inversely proportional to the acidity, were previously made for comparison with iron extraction rates.)[27] Over the range of conditions examined to date, the extraction rate does not fit well to any order, integral or fractional, although it comes closest to fitting first order. Instead, the plots of log $([Be]_0/[Be]_t)$ vs t are curved, concave downward. This could result from rate control by two extraction reactions in parallel; however, it is more likely to result from a slow first-order step in the extraction of a particular beryllium species, accompanied by slow reequilibration to replenish that species from other aqueous beryllium species. If the latter is correct, we expect to find that the slow extraction step is similar to that proposed for iron (above), since the extraction rate for both increases with decreasing acid concentration.

Table 8.6. Proton-Accepting Complexers Increase the Rate of Iron Extraction by HDEHP

0.1 *M* HDEHP; 2 *M* $NaClO_4$–$HClO_4$ at pH 1, 0.002 *M* Fe(III), 0.1 *M* complexer; 25°C

Complexer	Rate Constant (cm/min)
	$\times 10^{-4}$
None	6
Cl^-	9
NO_3^-	30
Ethylenediamine	35
Dichloroacetate	85
Acetate	105
Citrate	110

8.15 AGGREGATION AND ACTIVITY COEFFICIENTS IN SOLVENT PHASES

Association of Tributyl Phosphate with Sodium Di(2-ethylhexyl)phosphate in *n*-Hexane

Information on the association between TBP and NaDEHP is needed in the interpretation of synergistic extractions by their mixtures (cf. Sect. 8.13). Dielectric measurements[30] previously demonstrated that TBP does not associate significantly with HDEHP alone in dilute solution but that it does

[30] W. J. McDowell and C. F. Coleman, *J. Tenn. Acad. Sci.* 41, 78 (1966).

Table 8.7. Determination of the Association of Tributyl Phosphate with Di(2-ethylhexyl)phosphate, Using 0.2 $M \Sigma$ DEHP in *n*-Hexane

Average aggregation measured by isopiestic vapor-pressure balancing vs azobenzene

[TBP] (M)	Measured Average Aggregation	Calculated Average Aggregation, Assuming —			
		TBP; NaA and HA Unaffected[a]	NaA · 3TBP; Rest of NaA and HA Unaffected[a]	TBP; NaA · 2HA · TBP; $(HA)_2$	TBP; NaA · HA · 2TBP; $(HA)_2$
0[b]	3.9[a]				
0.15[b]	2.08	1.75	2.80	2.00	2.33
0	7[a]				
0.05	4.16	3.16	3.90	4.72	7.10
0.10	3.24	2.33	4.22	2.91	5.20
0.20	2.55	1.74	4.70	1.97	4.00
0.40	1.75	1.39	3.00	1.48	3.00

[a]Average aggregation of NaA + HA from *J. Inorg. Nucl. Chem.* **26**, 2005 (1964).

[b]$NaA/\Sigma A = 0.25$; for all others $NaA/\Sigma A = 0.50$.

associate with NaDEHP and/or HDEHP when NaDEHP is present. The latter has been confirmed by isopiestic measurement of the average aggregation number (Table 8.7) resulting from adding various concentrations of TBP to 0.2 *M* DEHP in *n*-hexane. Comparison of the aggregation numbers measured with those to be expected from the various likely formulations suggests that the principal adduct may be NaA · 2HA · TBP, where A = DEHP.

Techniques for Measuring Vapor-Pressure Depression

To determine solute activity coefficients and aggregation numbers by measuring the diluent vapor-pressure depression, we generally use either isopiestic vapor pressure balancing (as above) or direct differential manometric measurements. We repeated some previous measurements on typical solutions with a commercial matched-thermistor osmometer to evaluate its usefulness for our purposes. It is convenient and rapid, and operates in a lower concentration range (0.005 to 0.1 *m* reference solute) than the isopiestic method. However, the reproducibility above 0.01 *m* was not as good as desired for the calculation of activity coefficients.

The matched-thermistor osmometer is essentially a revised application of the principles of the porous-disk (nonequilibrium) osmometer,[31] using calibrated temperature difference instead of calibrated rate of travel of a meniscus to measure the rate of distillation and thus estimate the equilibrium conditions. Review of the principles of the porous-disk osmometer suggested that a still different system might incorporate the same principles to provide a sensitive absolute measurement of vapor-pressure depression as a function of very low solute concentrations. Results of a few preliminary tests are promising. Briefly, solution and pure diluent are equilibrated at a constant temperature through the vapor phase in a sealed container, as in isopiestic vapor-pressure balancing, but across a pressure gradient obtained by holding the solution at a higher elevation than the pure diluent. Diluent will distill from one liquid to the other, changing the concentration of the solution until its vapor pressure is less than that of the pure diluent by ρ_1, the product of the height separating the two liquids and the vapor density. Then the osmotic pressure (g/cm^2) of the solution is ρ_1, the same height (cm) times the density of the pure liquid diluent, from which it can be shown that the solute concentration $c(M) = 3.96 \times 10^{-5} \rho_1$. Tests with triphenylmethane in benzene gave the following average results:

Height (cm)	TPM Concentration (M)	
	Calculated	Observed
12.5	5.6×10^{-4}	5.2×10^{-4}
25	1.13×10^{-3}	1.15×10^{-3}

[31]A. T. Williamson, *Proc. Roy. Soc. (London)* **195**, 97 (1948).

Equilibration was slow but required no attention during the test period. These results suggest that the method may be useful in studies involving very low concentrations of solutes (or moderate concentrations of highly aggregated solutes), much lower than can be measured in our direct differential manometer system.

Water Solubility in Diluents

Accurate values for the solubility of water in various organic diluents are often needed. We have recently determined these values for several common diluents (Table 8.8) by liquid-liquid equilibration, using tritiated water as analytical tracer. The precision of the results is better than we have been able to obtain by Karl Fischer titration or to find in the literature. For five of the eight diluents, water contents were determined at water activities a_{H_2O} from 0.1 to 1 (mole fraction scale). All five conformed to Henry's law ($X_{H_2O} = ka_{H_2O}$) over the entire range. Thus the Henry's law constants in Table 8.8 also represent the water solubilities ($a_{H_2O} = 1$) on the mole fraction scale.

Activities in the TBP-H_2O and TBP-D_2O Systems

Water contents and TBP activities as functions of water activity in the TBP-H_2O system were previously measured by isopiestic vapor-pressure balancing.[32] The results were verified and extended to a TBP-D_2O system by liquid-liquid equilibration with tritium as analytical tracer. Both systems conform reasonably well to Henry's law over a considerable range:

$$a_{H_2O} = (2.09 \pm 0.04)X_{H_2O}, \quad a_{H_2O} < 0.7,$$

$$a_{D_2O} = (2.03 \pm 0.06)X_{D_2O}, \quad a_{D_2O} < 0.6.$$

At saturation, $a_{TBP} = 0.519 \pm 0.005$ at $X_{H_2O} = 0.510$ and $a_{TBP} = 0.508 \pm 0.008$ at $X_{D_2O} = 0.517$. The TBP-H_2O system values are in good agreement with the isopiestically determined values[32] of $a_{TBP} = 0.514 \pm 0.001$ at $X_{H_2O} = 0.511$.

The activity of TBP was calculated (with pure TBP as the standard state) as previously described. Water activities (with pure water as the standard state) were fixed by means of lithium chloride and potassium acetate solutions. We did not find any D_2O activities reported for these salt solutions; hence we estimated the values by assuming that the osmotic coefficients for corresponding D_2O and H_2O solutions are the same at the same compositions, expressed as moles of solute per 55.51 moles of solvent.[33]

Table 8.8. Solubility of Water in Common Diluents at 25°C

Diluent	Solubility (M)	Henry's Law Constant (mole fraction scale)
Chloroform[a]	7.40×10^{-2}	
Carbon tetrachloride	9.20×10^{-3}	8.89×10^{-4}
Benzene	3.43×10^{-2}	3.05×10^{-3}
Toluene	2.46×10^{-2}	2.62×10^{-3}
o-Xylene	1.92×10^{-2}	
Cyclohexane	2.77×10^{-3}	3.00×10^{-4}
n-Hexane	3.00×10^{-3}	
n-Octane	2.60×10^{-3}	4.25×10^{-4}

[a]Measured immediately after scrubbing stabilizing alcohol from the chloroform.

Tri-*n*-octylamine–Sulfuric Acid–Water

The average aggregation numbers of tri-*n*-octylamine bisulfate (TOAHS) at concentrations from 0.007 to 0.5 *m* in benzene were reported previously.[34] A computer program was prepared to represent these aggregation numbers up to 0.4 *m* in terms of various continuous polymerization models. The best fit, especially at the low concentrations most important for calculating activity coefficients, was obtained with a model including monomers, dimers, and tetramers, with the following formation concentration quotients:

$$2R_3NH \cdot HSO_4 \rightleftharpoons (R_3NH \cdot HSO_4)_2, \quad Q_{12} = 11.7;$$

$$2(R_3NH \cdot HSO_4)_2 \rightleftharpoons (R_3NH \cdot HSO_4)_4,$$

$$Q_{24} = 2.99 \times 10^5.$$

[32]J. W. Roddy and J. Mrochek, *J. inorg. Nucl. Chem.* **28**, 3019 (1966).

[33]R. E. Kerwin, "The Osmotic and Activity Coefficients of Some Alkali Halides in Heavy Water at 25°C," thesis, Univ. of Pittsburgh, 1964.

[34]*Chem. Technol. Div. Ann. Progr. Rept. May 31, 1966*, ORNL-3945, p. 186.

The resulting distributions among these species and the comparison of the calculated with the experimental aggregation numbers are shown in Table 8.9.

With the aid of this model, extrapolation of the osmotic coefficients to infinite dilution was improved to give a more complete evaluation of the stoichiometric activity coefficients. Previously, only the ratios between activity coefficients, at concentrations above 0.1 *m*, were considered reliable. Those ratios remain unchanged, but the absolute values are corrected to $\gamma = 0.060$ instead of 0.05 at 0.1 *m*, 0.151 instead of 0.12 at 0.02 *m*, etc.

The effects of varying water contents on the infrared absorption spectra of the normal sulfate TOAS and the bisulfate TOAHS, in benzene and in carbon tetrachloride, were examined for information concerning the type of association between water and the amine salts. For both TOAS and TOAHS, two absorption bands in the OH stretching region result from water-salt association. The higher-frequency band is narrow and is slightly shifted (3680 cm^{-1}) from the position of the antisymmetric ν_3 stretching mode (3705 cm^{-1}) of free water. Its intensity increases with increasing water content. The lower-frequency band (3420 cm^{-1}) that characterizes this association is broad and considerably displaced to a frequency lower than the range of free OH stretching modes (3500 cm^{-1}). Bending-mode bands are also present in the 1600 to 1750 cm^{-1} region.

The water-CCl_4 spectrum in the OH stretching regions shows two bands, at 3705 and 3614 cm^{-1}, which can be identified as ν_3 and ν_1, the antisymmetric and the symmetric OH stretching modes.

The two bands found in the salt-diluent system show the characteristics expected for a species of the type H-O-H—TOAS. The sharp, high-frequency band can be attributed to stretching of the free OH band, and the broad low-frequency band, to the hydrogen-bonded OH group. A third band (at about 3200 cm^{-1}), which is also observed in some of the spectra of solutions containing higher water concentrations, can be attributed to the overtone of the bending vibration. A very small band at 2720 cm^{-1} is probably due to chelate-type hydration.

Although the species to which the water molecules are attached are ion pairs, no evidence exists that any direct interaction occurs between the oxygen of the water and the alkylammonium ion. If the water molecules were to enter the ion pair between the anion and cation, some spectral changes might reasonably be expected. All the spectra, however, suggest hydrogen bonding to the sulfate ion, as exhibited by the decrease in the number of bands in the antisymmetric valence vibration ν_4 at ~1100 cm^{-1} as the water content increases from zero to saturation, and by the almost complete disappearance of the harmonics of the antisymmetric distortion vibration ν_3 at 1280 and 1220 cm^{-1}.

Table 8.9. Calculated Distribution of Trioctylamine Bisulfate in Benzene Among Consecutively Aggregating Species

[TOAHS] (*m*)[a]	Monomer (%)[a]	Dimer (%)[a]	Tetramer (%)[a]	$\bar{n}$, Average Aggregation	
				Calculated	Found
0.001	88.3	1.8	9.9	1.09	1.10
0.004	47.2	2.8	50.0	1.64	1.40
0.01	25.8	1.6	72.6	2.24	2.07
0.1	4.9	0.6	94.5	3.47	3.35
0.4	1.7	0.3	98.0	3.80	3.83

[a] In terms of contained stoichiometric TOAHS.

9. Chemical Applications of Nuclear Explosions

The purpose of this program is to provide research and development in selected areas of the Plowshare Program, especially those areas requiring knowledge of chemistry or metallurgical engineering to determine feasibility. Areas in which research was performed last year included:

1. studies of the distribution and possible fate of radionuclides formed during the use of nuclear devices to aid in the recovery of copper from ore deposits;
2. measurement of the rate of exchange of tritium and hydrogen in water and natural gas under conditions that may be encountered in the stimulation of gas production from wells by nuclear explosives;
3. studies of the distribution and possible fate of radionuclides formed during the use of nuclear devices to aid in the recovery of oil from shales;
4. hypervelocity jet sampling as a means of removing a specimen after irradiation in the neutron flux of a detonation, but ahead of the detonation shock wave.

Knowledge of the thermal stability and high-temperature reactions of actinide compounds is pertinent to their possible production through the use of thermonuclear devices. A description of related studies to determine some of these data by differential thermal analysis and thermogravimetric analysis techniques appears in Sect. 7 of this report.

9.1 COPPER ORES

Fracturing of copper ores with nuclear explosives, followed by leaching in place, is being studied for the AEC by Lawrence Radiation Laboratory (LRL) and by the U.S. Bureau of Mines at Tucson, Arizona. The Oak Ridge National Laboratory is cooperating in this program by studying potential problems that might arise from the presence of radioactive contaminants in the processing cycle. The proposed flowsheet for recovering copper includes percolating a leaching solution of dilute sulfuric acid down through the nuclear-broken ore to dissolve the copper, collecting the leach liquor at the bottom of the ore body and pumping it to the surface, recovering a copper concentrate from the solution by cementation on iron, and returning the barren solution, after fortifying it with acid, for reuse in the leaching step.

Status and Progress

Recent studies continued to support the earlier observation[1] that ^{106}Ru is probably the only radioisotope of importance with respect to radiocontamination of the cement copper. Ruthenium and copper are not separated when the cement copper is smelted into a consumable anode, but they are separated efficiently during electrolytic purification of the anode. The final copper product should contain only trace amounts of radiocontaminants and thus should not be hazardous to the user. Some method for decreasing ruthenium contamination of the cement copper would be desirable, however, in order to minimize contamination of the electrolytic processing facility. Several potential methods have been studied, but none of these have been acceptable.

Factors Affecting Ruthenium Cementation

Of the variables that affect the amount of ruthenium cemented with the copper, the initial ruthenium concentration in the liquor was the most

[1] *Chem. Technol. Div. Ann. Progr. Rept. May 31, 1966*, ORNL-3945, p. 189.

important. Doubling the initial ^{106}Ru concentration within the range studied (1000 to 40,000 counts min^{-1} ml^{-1}, equivalent to about 0.001 to 0.05 $\mu c/ml$) caused the ruthenium concentration in the cement copper to increase by a factor of about 2.5 (Fig. 9.1). This increase was due to increased ruthenium cementation, since the amount of copper cemented was about the same in all tests. The ruthenium contamination of the cement copper also increased slightly with increasing temperature and with increasing pH but was not significantly affected by changes in the rate of agitation, the salt content of the liquor, or the amount of iron used for cementation.

In a test with a copper-barren liquor, about the same amount of ruthenium cemented with the iron as usually cemented with the copper under the same conditions. When copper was present, essentially all the cemented ruthenium was found with the cement copper; only a negligible amount was found with the residual sheet iron. On the other hand, ruthenium could not be removed from solution with cement copper or other forms of copper metal in the absence of iron. These results suggest that the ruthenium actually cements on the iron, but is cleaned off and occluded with the cement copper when it flakes off the surface of the iron.

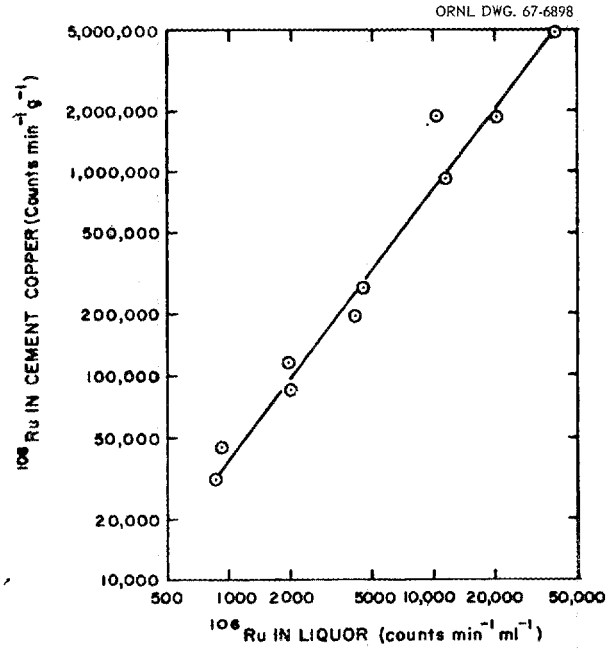

Fig. 9.1. Effect of Initial Ruthenium Concentration on ^{106}Ru Contamination of Cement Copper. Solutions: synthetic leach liquor (pH 2.0) containing 0.15 *M* SO_4^{2-} and, in grams per liter, 2.0 Cu^{2+}, 1.0 Fe^{3+}, 3.0 Fe^{2+}, and 0.5 NaCl spiked with 1000 to 40,000 counts min^{-1} ml^{-1} of ^{106}Ru. Procedure: 200 ml of solution stirred at ~25°C with 0.7 g of detinned cans for 45 min.

Studies of methods for minimizing ruthenium contamination of the cement copper were only partially successful. In a cyclic column leaching test the addition of lime to increase the pH of the solution to 4 to 5 removed ruthenium effectively from the recycle liquor following removal of copper by cementation. This treatment lowered the ruthenium concentration in subsequent batches of leach liquor. The ruthenium concentration increased rapidly, however, when the lime treatment was discontinued. Evidently, continuous treatment of the recycle liquor with lime would be needed; however, this would be too expensive. Lime treatment of the liquor prior to cementation of the copper was not practical since copper losses to the precipitate were excessive. More than 20 organic and inorganic materials, mostly ion exchangers, were tested as ruthenium adsorbents, but none of them adsorbed ruthenium effectively from leach liquors.

Attempts to preferentially dissolve ruthenium from cement copper were not very successful. Some ruthenium was dissolved in 1.0 *M* HCl and in 1.0 *M* NaOH, but part of the cement copper was also dissolved in these reagents.

Behavior of Ruthenium in Smelting and Electrolysis

Cement copper is usually smelted to produce impure copper metal in the form of consumable anodes, which are then converted to pure copper by electrolysis. Small-scale tests simulating the smelting and electrolysis operations showed no significant separation of copper from ruthenium in smelting. However, an efficient separation occurred in electrolysis; the electrolytic copper contained only 1 to 2% of the ruthenium present in the cement copper.

In the smelting tests two small copper anodes were prepared from cement copper that contained 99.4% copper and about 0.7 μc of ^{106}Ru per gram. The cement copper was heated at 1350°C in a graphite crucible with a flux of CaO and SiO_2, cooled, separated from the slag, and then remelted

and cast. In each case about 95% of the copper and 93% of the ruthenium were recovered in the anode. About 4% of the ruthenium was found in the slag. The ruthenium material balances of 97 to 98% indicate that little, if any, of the ruthenium was volatilized.

The anodes were electrolyzed in consecutive runs in the same cell electrolyte (45 g of copper and 200 g of H_2SO_4 per liter) at a current density of about 13 amp/ft^2 and a cell voltage of about 0.2 v. The current efficiency was >90%. The ruthenium concentration in the cell electrolyte increased at a uniform rate throughout the runs, indicating that the ruthenium was uniformly dispersed (alloyed with the copper) in the anode (Fig. 9.2). About two-thirds of the ruthenium released from the anodes was found in the cell electrolyte, and one-third was found in the "anode mud" that settled to the bottom of the cell. Only 1 to 2% was found in the cathode copper product.

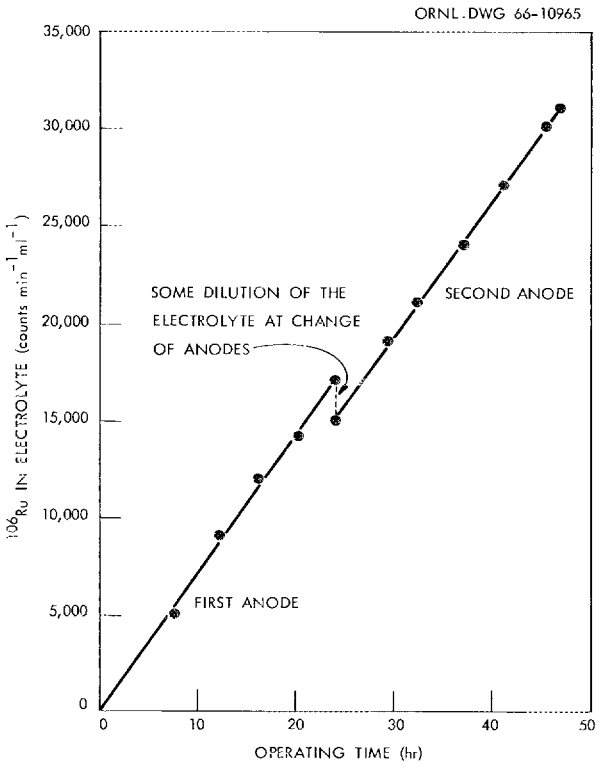

Fig. 9.2. Accumulation of ^{106}Ru in the Cell Electrolyte. Anodes containing 8.23×10^5 counts of ^{106}Ru per gram were electrolyzed in a solution containing 45 g of copper and 200 g of H_2SO_4 per liter.

Solvent Extraction of Copper

LIX-64 is a copper extractant that was developed[2] specifically for treating dilute acid liquors of the type that would be obtained by in-situ leaching of copper ore. It is a cation exchanger and is highly selective for copper ions. The use of LIX-64 for copper recovery is a potential alternative to cementation.

The indicated molecular weight of LIX-64 is about 300 as determined by measuring the freezing point depression of benzene. A direct method is not available for analyzing the LIX-64 concentration in organic solvents. Consequently, its concentration has been estimated from uv absorption measurements or by determining the copper capacity of the solvent phase. The uv spectra for LIX-64 in Varsol and in Amsco 125-82 have well-resolved peaks at 320 mμ. At this wavelength the LIX-64 solutions obey Beer's law; the absorptivity [(wt/vol)% LIX-64/absorbance] is 0.0285 in both diluents. This method cannot be used with diluents such as kerosene, which strongly absorb at 230 mμ. The copper saturation method, although less convenient, does not limit the choice of diluent. On contacting a copper sulfate solution containing 40 g of copper per liter at pH 2, the copper loading of the extract was directly proportional to the LIX-64 concentration. The LIX-64 concentration, in (wt/vol)%, was three times the copper loading, where copper loadings are expressed in grams per liter.

Isotherms for the extraction of copper with 10 (wt/vol)% LIX-64 in kerosene or Varsol diluents from a synthetic leach liquor, initially at pH 2 and containing 2 g of copper per liter, showed a maximum copper loading of the solvents of about 3 g/liter. Recovery of 99% of the copper could be obtained in five ideal extraction stages while loading the organic phase to 2.4 g of copper per liter. Copper was stripped efficiently from the extract with 1.8 *M* H_2SO_4 to yield a relatively concentrated copper solution (>50 g of copper per liter), which could be fed directly to an electrowinning system for the recovery of copper metal.

The relative extractability of copper and some of the radionuclides that might be present in the copper recovery system was measured between pH 1.5 and 2.5, the range of interest in copper ore processing. In 5-min extractions with 10 (wt/vol)%

[2] D. W. Agers *et al.*, *Mining Eng.* 17, 76–80 (1965).

LIX-64 in Varsol from a synthetic leach liquor containing 0.2 g of copper per liter and tracer amounts of the radiocontaminants, the extraction coefficients for copper were 10 at pH 1.6 and greater than 50 at pH 1.9 and above. Ruthenium-106 (the most troublesome contaminant in the cementation process), ^{134}Cs, ^{85}Sr, ^{60}Co, ^{46}Sc, ^{65}Zn, and ^{144}Ce each had an extraction coefficient of less than 0.005 over the pH range studied. However, significant amounts of ^{95}Zr-Nb, ^{59}Fe, and ^{110}Ag were extracted; extractions of the first two were strongly rate dependent. In 5-min contacts the ^{95}Zr-Nb extraction coefficients were 1.4 and 0.7 at pH 1.5 and 2.5 respectively. At either pH the coefficients were more than 50 for a contact time of 1 hr. There was no extraction of ^{59}Fe at pH 1.5 in 1 hr, but at pH 2.0 the extraction coefficient increased from 0.05 at 5 min to 0.16 at 1 hr. Extraction coefficients for ^{110}Ag were 0.2 and 0.6 at pH 1.5 and 2.4 respectively. Essentially all the ^{59}Fe but only about 30% of the ^{110}Ag and 20% of the ^{95}Zr-Nb were stripped from the extracts with 2 M H_2SO_4 in 10-min contacts at a phase ratio of 1 : 1. Fortunately, it is anticipated that the concentrations of ^{95}Zr-Nb, ^{59}Fe, and ^{110}Ag in the leach liquors will be very low. Solvent extraction with LIX-64, therefore, should produce a copper product solution that is nearly free of radionuclides.

9.2 STIMULATION OF NATURAL GAS WELLS

In feasibility studies of the stimulation of gas production from wells by nuclear devices (Project Gasbuggy), it is important to consider the relative distributions of tritium gas (produced by the device) to the groundwater, to the natural gas (e.g., methane) initially present in the cavity, and to the gas that enters the well after gas production has started. Because of the extreme temperatures and pressures at the instant of detonation and shortly thereafter, the tritium distribution occurring during this phase can be measured realistically only in an actual nuclear test. However, laboratory measurements have been made that provide an indication of the tritium exchange to be expected during the gas-production phase.

Such tests have shown that the formation of tritiated methane from contact with tritiated water will be low, provided that the tritium concentration in the gas phase is low and provided that there is no catalytic effect from the cavity medium. Specifically, the rate of tritium exchange with hydrogen in methane–water-vapor mixtures at room temperature and atmospheric pressure in a 1-liter glass vessel is

$$R \sim 2.3 \times 10^{-8} [\mathrm{HTO}]^2 ,$$

where R is the rate of exchange in mc liter^{-1} day^{-1} and the tritium (as HTO) concentration is in the range of 10 to 50 mc/liter. In a test performed last year at 100°C the exchange rate was equal to, or less than, 2.2×10^{-6} mc liter^{-1} day^{-1} when the tritium concentration was 1 mc/liter.

It is possible that the exchange rates within the nuclear cavity can be different from those reported above as a result of effects from the large surface area of the crushed rock within the cavity. Laboratory experiments with crushed shale (from the gas-producing geological formation) in the exchange vessel were inconclusive. Although the shale had been exposed to water vapor for several days prior to its addition to the tritiated-water–methane mixture, a large portion of the tritiated water was absorbed by the shale as the experiment progressed. Within 30 days, for example, the gas-phase tritium concentration decreased from 20 to 2 mc/liter. The measured exchange of tritium with hydrogen in the methane during the same period was about equal to that which would have been observed if all the tritium had remained in the gas phase.

9.3 RECOVERY OF OIL FROM SHALE

The AEC and its contractors, along with the U.S. Bureau of Mines and a private company named CER Geonuclear, are studying the feasibility of using nuclear explosives to fracture oil shale for an in-situ retorting process (Project Bronco). ORNL has been asked to assist in the project by studying the possible fate of radionuclides in the process operations. It is known from earlier Plowshare experience that most of the fission products and radionuclides formed by neutron activation during the nuclear blast will be trapped fairly efficiently in the fused rock (puddle glass) that accumulates at the bottom of the nuclear chimney. The crushed shale, however, will be contaminated with fusion product tritium (presumably as tritiated water) and fission products having gaseous precursors, for

example, ^{90}Sr and ^{137}Cs, and volatile radionuclides, for example, ^{106}Ru. In addition, the void space in the chimney will contain krypton and tritium (assumed to be mostly tritiated water vapor). Without actually performing a nuclear test, it is impossible to assess accurately the potential problems involved in producing and handling the oil. Conceivably, the product shale oil can be contaminated with radionuclides at several points in the process, for example:

1. exchange of tritium and hydrogen between water and shale oil during the retorting phase,
2. dissolution of oil-soluble fission product compounds present in the shale rubble and puddle glass,
3. inclusion of tritiated hydrocarbons that may be produced in the fireball and that will be dispersed in the chimney.

Also, the gases emerging from the retort will be contaminated with krypton and tritium. The relative amounts of the various fission products and tritium in the system will depend on the type of device used and the elapsed time following the shot. Assuming the use of a predominantly fusion device and a delay of at least a year prior to the start of retorting, tritium will be, by far, the predominant radionuclide present.

The nuclear blast will produce an underground chimney that is several hundred feet high and filled with several million tons of broken shale. The proposed in-situ retorting process is designed to operate as follows: Air is forced down through the broken shale, and the top is ignited. As the combustion front moves very slowly down through the chimney, the gas (CO_2, N_2, H_2O) from the combustion transports heat from the combustion front to the shale below. This maintains a temperature gradient that moves with the combustion front in a fixed relationship. The temperature limits of this gradient are the temperature of the flame at the top and that of the much cooler shale at the bottom of the chimney. When the shale temperature is about 400°C, the kerogen destructively distills, producing natural gas (CH_4, C_2H_6) and oil vapor. These products are swept down by the hot gas stream, thereby leaving depleted shale, which is similar to charcoal and serves as the fuel when the combustion front reaches it. The oil condenses in the lower range of the gradient and drains to the bottom of the chimney, where it is collected and withdrawn as product. It is hoped that 50 to 70% of the oil can be recovered from shale by this method. Recoveries of about 70% have been obtained by mining and burning the shale in distillation retorts at ground level.

Laboratory-Scale Retorting Studies

To obtain some understanding of the type and degree of radiocontamination of the oil that may occur, we are retorting shale spiked with radionuclides in small-scale equipment and are leaching nuclear-test-shot debris with shale oil.

Green River oil shale from the Piceance Basin, Colorado, was crushed and sized as follows:

Sample	Size Range (in.)	Percentage of Total Sample
Coarse	−0.31 +0.19	71
Medium	−0.19 +0.05	20
Fine	−0.05	9

Samples of each of the fractions were analyzed by the U.S. Bureau of Mines at Laramie, Wyoming. They varied only slightly in composition (Table 9.1). The coarse fraction was used in our experiments.

A laboratory retort was constructed in which several of the steps in the sequence of in-situ oil recovery can be simulated. Essential features of the system are a heated shale furnace (to which

Table 9.1. Analysis of Sized Oil Shale

Analysis	Fractions of Shale Sample		
	Fine	Medium	Coarse
Oil, wt %	10.7	11.8	12.1
Water, wt %	1.0	1.2	1.0
Spent shale, wt %	85.8	84.5	84.4
Gas + loss, wt %	2.5	2.5	2.5
Specific gravity of oil	0.919	0.918	0.914
Oil, gal/ton	28.0	30.8	31.7
Water, gal/ton	2.2	2.6	2.5

CO_2, N_2, H_2O, oil, CH_4, and air can be added in sequence or in a mixture), an oil condenser at 38°C, and a water condenser at 0°C. By controlling the composition of the inlet gases and the temperatures, the shale can be first retorted and then burned.

Samples (100 g) of shale were retorted successfully in this unit. Distillation of the oil began when the shale temperature was about 300°C and was essentially complete at about 430°C. The oil yield was 12 to 13 g, the approximate amount present in the sample as determined by Fischer analysis (see Table 9.1).

When the shale was wetted with tritiated water prior to retorting, the product oil contained tritium compounds that were not removed by washing the oil with water. The shale had been moistened with 4.5 mc of ^3H per ton of shale; this is about ten times the maximum level anticipated in Project Bronco, assuming uniform distribution throughout the rubble and the use of a predominantly fusion device. The washed oil contained about 1 mc of ^3H per gallon of oil, which is equivalent to about 0.5% of the tritium originally added to the system.

In other tests, samples of shale oil were heated with test-shot debris in the form of rubble (broken rock from up in the chimney) and puddle glass (material from the bottom of the chimney which was melted by the blast and then cooled into a glass). After being heated at 220°C for 4 hr, the oil contained about 0.2% of the gross gamma activity initially present in the rubble and about 0.02% of that originally present in the puddle glass. More than 85% of the total radioactivity of the oil that was heated with the rubble was due to ^{106}Ru; about 10% was due to ^{137}Cs. The gamma activity of the oil sample from the test with the puddle glass was mostly due to ^{106}Ru (56%) and ^{60}Co (42%). Only 1.5% of the ^{90}Sr was dissolved from the rubble; less than 0.01% was dissolved from the glass.

9.4 DEVELOPMENT OF HYPERVELOCITY JET SAMPLERS

Tests to demonstrate a jet-sampler method for recovering a target located and irradiated at about 1 m from a detonating nuclear device were completed. The tests were conducted at the Frankford Arsenal, Vincentown, New Jersey, in an evacuated (1 mm Hg) flight chamber that is 18 in. in diameter and 55 ft long. In the final tests five copper cones were machined to provide a high degree of symmetry, and gold, simulating transplutonium targets, was plated in the cones. These were jetted at the test range. The wood that was used to catch the jetted targets has been received at ORNL, where the gold will be recovered from the wood to determine the efficiency with which the jetted target was focused within the flight chamber.

10. Recovery of Fission Products by Solvent Extraction

The objective of the fission product recovery program is to develop processes that are applicable to large-scale recovery and purification of fission products from reactor-fuel-reprocessing wastes. Since the inception of this program the principal emphasis has been on the development of solvent extraction methods, because they are particularly versatile and readily adaptable to large-scale operations. A solvent extraction process using di(2-ethyhexyl)phosphoric acid (D2EHPA) has been successfully developed for recovering ^{90}Sr and mixed rare earths. A modification of this process has been developed and operated on a plant scale at Hanford. New processes have also been developed in the laboratory for recovering cesium with substituted phenols and for recovering zirconium-niobium and ruthenium. The combination of these processes with previous methods for separating rare earths and recovering technetium, neptunium, and plutonium affords a possible integrated solvent extraction flowsheet for recovering nearly all the valuable components from waste solutions.

The experimental work planned for this program is nearly complete. Recent studies have included the bench-scale demonstration of a simplified flowsheet for isolating strontium, mixed rare earths, and cesium from each other and from other fission products and bulk contaminants.

10.1 NEW FLOWSHEET FOR RECOVERING STRONTIUM, RARE EARTHS, AND CESIUM

The proposed process (Fig. 10.1) provides less-pure rare earths and strontium concentrates than processes developed earlier; however, it requires less equipment and does not use large amounts of aqueous-phase complexing agents (e.g., tartrate or citrate). In this flowsheet the rare earths, as well as nearly all the iron and ^{95}Zr-Nb and most of the aluminum, are extracted in a single stage from Purex sugar-treated waste (STW) solution with the sodium salt of di(2-ethylhexyl)phosphoric acid (Na-D2EHP) in normal paraffin hydrocarbon (NPH)--tributyl phosphate. The amount of Na-D2EHP fed to the system is regulated to provide a final extraction pH of 2 to 2.5. Iron extraction, which is very slow at higher acid concentrations, is rapid under these conditions. The rare earths are selectively stripped from the extract with dilute nitric acid, after which the solvent is prepared for recycle by a single-stage contact with dilute NaOH. The raffinate from the rare-earths recovery operation is adjusted with NaOH to a pH of about 6, where the bulk of the contaminant metals, but only a small fraction of the strontium and essentially none of the cesium, precipitates. The resulting supernatant solution constitutes a feed from which the recovery of strontium with D2EHPA, and then the recovery of cesium (at pH 12) with a substituted phenol, can be easily accomplished.

Estimates of the distribution of the more important fission products and bulk metal contaminants in the various process streams are given in Fig. 10.1, and estimates of the decontamination factors obtainable by the process are given in Table 10.1. These values should be considered as tentative since they were made on the basis of very limited process testing with simulated Purex STW feeds at tracer level. Recoveries of more than 90% of the rare earths, strontium, and cesium are indicated, with each of the concentrates being relatively free of contaminants.

The first-cycle extraction of rare earths and metal contaminants was demonstrated successfully in continuous runs in equipment that included two cocurrent mixers (to improve the stage efficiency) and a settler. The residence time of the phases in the mixers, which were operated at 50 to 60°C,

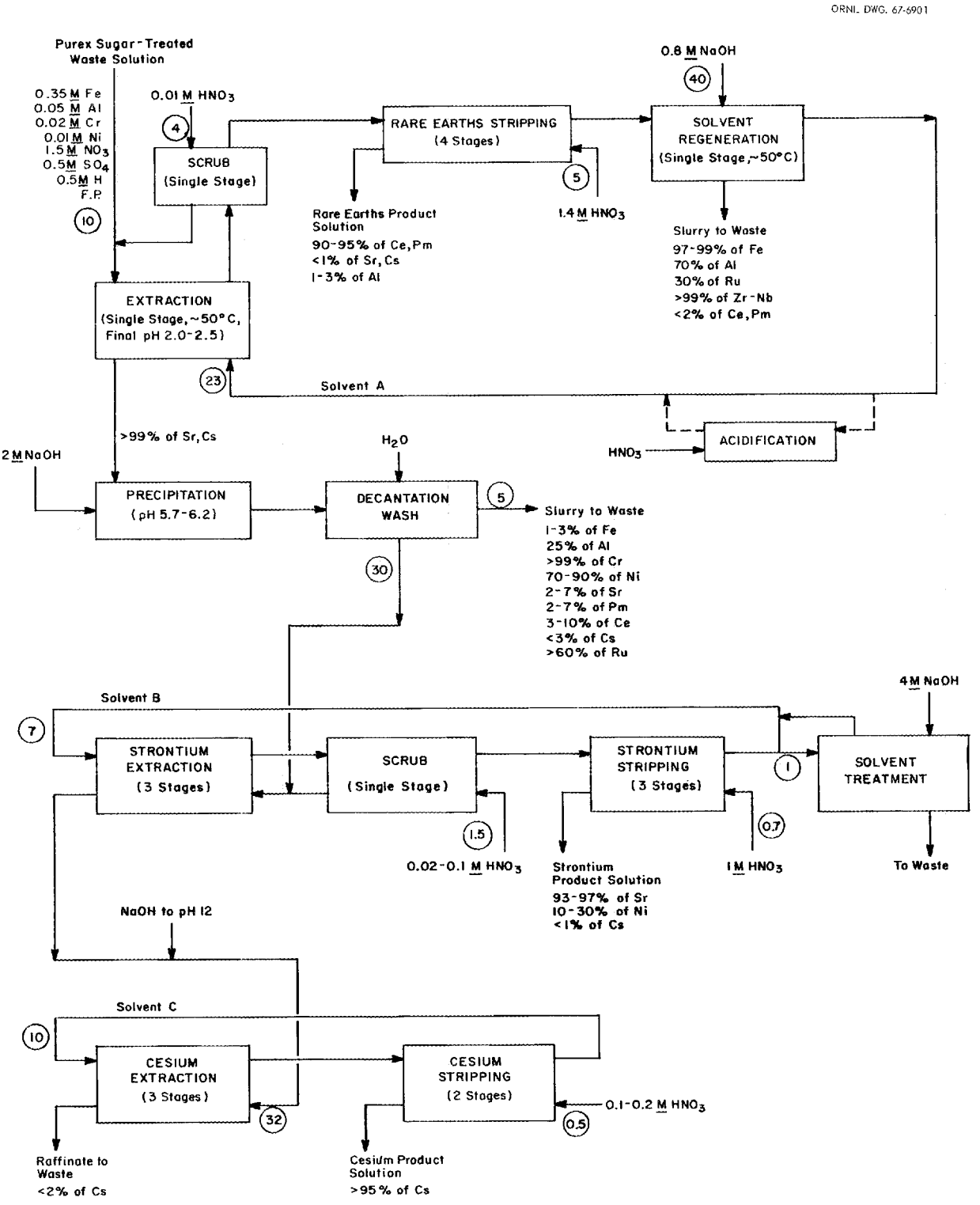

Fig. 10.1. Fission Product Recovery Flowsheet. Organic solvents: *A* – 0.75 *M* D2EHPA (80–100% in sodium salt form)–0.3 *M* TBP-NPH; *B* – 0.3 *M* D2EHPA (10–20% in sodium salt form)–0.15 *M* TBP-NPH; *C* – 1 *M* BAMBP in NPH. Numbers in circles show the relative solution flow rates.

Table 10.1. Estimated Decontamination Factors[a] for Fission Product Recovery Process

Product	Estimated Decontamination Factors from —								
	Fe	Al	Cr	Ni	Sr	Cs	RE	Zr-Nb	Ru
Mixed rare earths	>1,000	>30	>100	>100	>100	>100		>1,000	>50
Strontium	>5,000	>500	>100	3–10		>100	>200	>5,000	>100
Cesium	>10,000	>1000	>1000	>1000	>1000		>1000	>10,000	>100

[a]Based on flowsheet conditions shown in Fig. 10.1.

was about 10 min. The raffinate from this operation was adjusted continuously with dilute NaOH to a pH of about 6 to precipitate the residual iron, aluminum, etc., and then passed to a decanter. The precipitate settled fairly rapidly, giving a clear solution overflow.

When the first-cycle solvent is regenerated with NaOH solution prior to solvent recycle, the mixer-settler is operated at 40 to 50°C, and the organic phase is maintained as the continuous phase to avoid formation of stable emulsions. Two volumes of caustic solution per volume of extract provides sufficient aqueous volume to accommodate the large volume of precipitate formed in the regeneration step. Regenerated solvent is recycled from the settler to the mixer to provide the organic : aqueous ratio (>2 : 1) needed to maintain the organic phase continuous. With these operating conditions, phase separation in this system is acceptable.

11. Biochemical Separations

11.1 DEVELOPMENT OF PROCESSES FOR MACROMOLECULAR SEPARATIONS

Separation of Transfer Ribonucleic Acids

In the last annual report we described a reversed-phase chromatographic system that employed a quaternary ammonium extractant dissolved in an isoamyl acetate diluent. It was useful for the preparation of highly purified samples of phenylalanine transfer ribonucleic acid (tRNA) and a leucine tRNA from *E. coli*. During this report period we developed a new reversed-phase chromatographic system that yields superior chromatographic resolution of *E. coli* transfer nucleic acids (tRNA's). The system is similar in principle to the previous reversed-phase chromatographic system; however, use of a new diluent and a different quaternary amine, as well as a concave-gradient elution method, produced sharper tRNA chromatographic peaks and better separation of the tRNA's in the front region of the chromatogram. In this separation method a solution of tricaprylylmethylammonium chloride in a water-insoluble Freon, tetrafluorotetrachloropropane, is immobilized as a film on a hydrophobic diatomaceous earth support. After the treated solid (an organic anion exchanger) has been packed in a glass column, the crude tRNA is absorbed on the exchanger from a dilute sodium chloride solution. Chromatograms are then developed by use of the sodium chloride gradient elution technique.

The effects of flow rate, temperature, and the shape of the gradient elution curve (concave or linear) were investigated; these conditions were then optimized for the best distribution of *E. coli* B tRNA's throughout the chromatogram. Chromatograms were run at two pH levels, 4.5 (Fig. 11.1) and 7.0 (Fig. 11.2), to investigate the distribution, the positions, and the heterogeneity of 14 tRNA's. These experiments, employing the NaCl gradient, were performed at 37°C with the additional presence of 0.01 *M* $MgCl_2$ (and either 0.05 *M* Tris buffer at pH 7.0 or 0.01 *M* sodium acetate buffer at pH 4.5). An elution flow rate of 0.5 ml/min and a concave gradient were employed.

Twelve of the fourteen tRNA's were found to be heterogeneous (i.e., they had multiple elution peaks). For example, at pH 7.0, five leucine tRNA's were found, while at pH 4.5, three peaks were detected for each of the following: alanine, arginine, phenylalanine, and methionine tRNA's. A greater degree of heterogeneity for many tRNA's was obtained with the Freon diluent reversed-phase system than with the previous system using isoamyl acetate. Heterogeneous tRNA's could result from subtle differences in chemical composition and/or physical conformation.

The special advantage or usefulness of the Freon reversed-phase chromatographic system lies in the sharpness of the individual tRNA elution peaks that are obtained and in the capability of the system with regard to separation of tRNA's from sources (other than *E. coli*) for which methods have not previously been available. For example, this system has been used by investigators in the Biology Division to fractionate tRNA's from rat liver, mouse liver, and two different types of mouse plasma cell tumors.

Isolation of Phenylalanyl-RNA Synthetase from *E. coli* B

To investigate the interaction between tRNA's and the enzymes that recognize the tRNA's and catalyze the attachment of the correct amino acid (RNA synthetases), it is desirable to be able to prepare purified synthetases that correspond to the purified tRNA's. A method for the preparation of small amounts of highly purified phenylalanyl-RNA synthetase from *E. coli* B has been developed by

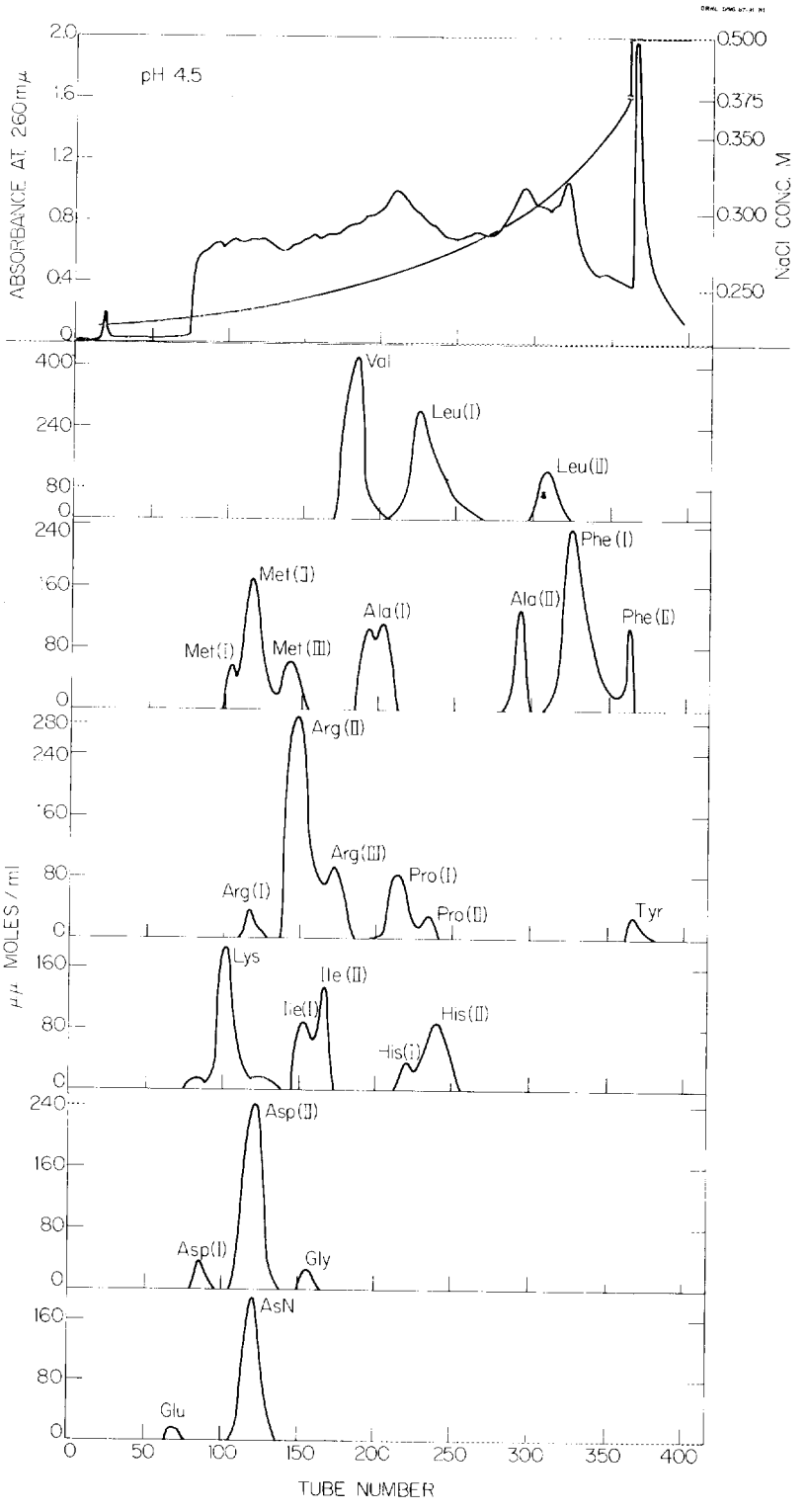

Fig. 11.1. Chromatograms at pH 4.5 with Freon Reversed-Phase Column.

M. P. Stulberg in the Biology Division; however, it could not be used for the preparation of larger-sized samples because of limitations of some of the techniques. Therefore, a laboratory development effort was undertaken to scale up the procedure so that purified phenylalanyl-RNA synthetase could be prepared in larger quantities. This involved the substitution of streptomycin sulfate precipitation for high-speed centrifugation (for ribosome removal), utilization of commercial centrifuges instead of laboratory centrifuges for removal of cell debris, and substitution of gel filtration techniques for dialysis (for salt removal).

The revised procedure (Fig. 11.3) was used to process 4.3 kg of *E. coli* B cells, which were found to yield 110 g of protein mixture after removal of broken cells and nucleic acids. From this product 22.4 mg of highly purified phenylalanyl-

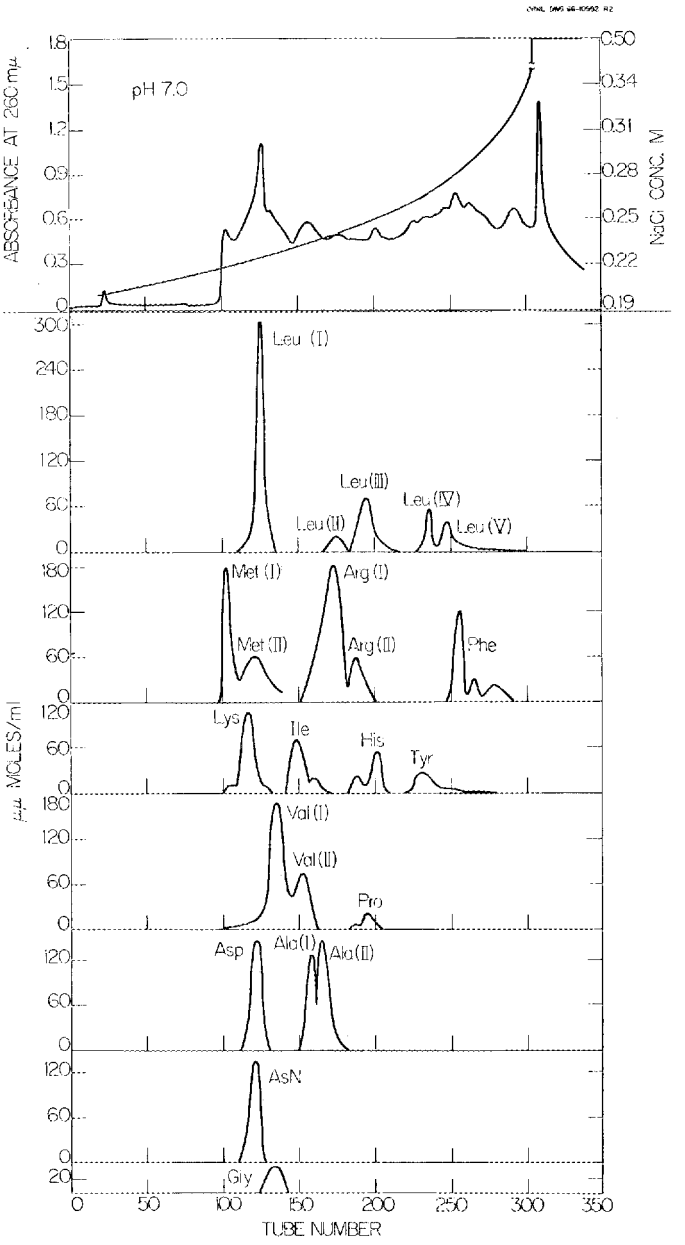

Fig. 11.2. Chromatograms at pH 7 with Freon Reversed-Phase Column.

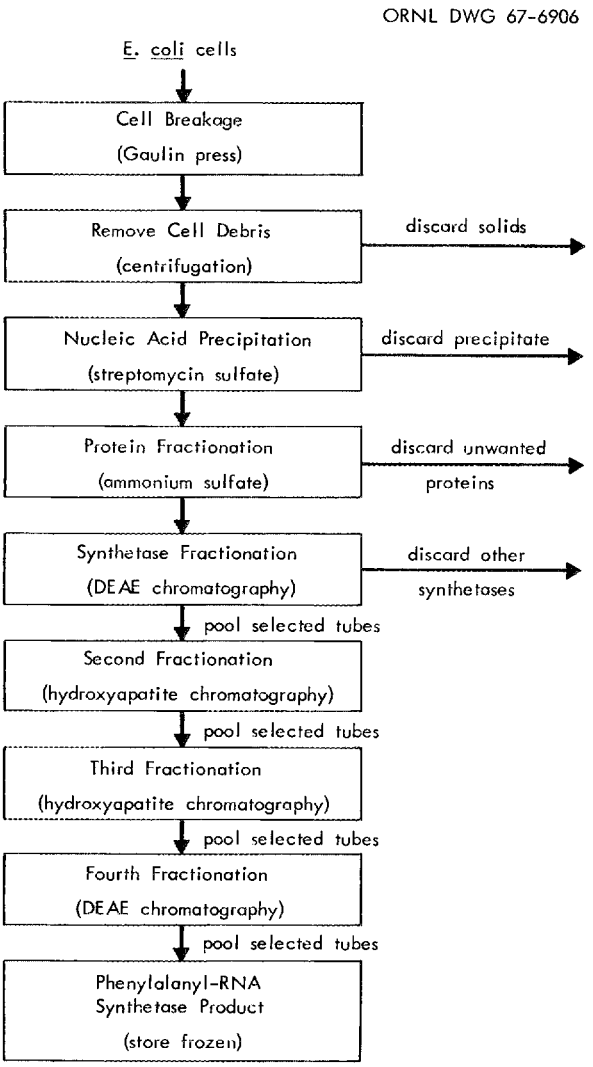

Fig. 11.3. Flowsheet for Recovery of Purified Phenylalanyl-RNA Synthetase.

RNA synthetase was obtained, representing a fourfold increase over the yield obtained by the previous method. The revised procedure contains no steps that are limited with regard to capacity; thus greater quantities of phenylalanyl-RNA synthetase can be prepared as needed. With appropriate changes in the ammonium sulfate fractionation and column chromatographic steps, the method should also be useful for the recovery of a number of other RNA synthetases.

11.2 SCALEUP OF PROCESSES FOR MACROMOLECULAR SEPARATIONS

The activities of the Unit Operations section have been expanded to provide engineering-scale research and development aimed at larger-scale capabilities for the preparation of purified tRNA's. The emphasis of the program is centered on research and development; however, the demonstration of successful scaleup is expected to yield, periodically, gram-sized samples of specific tRNA's. As agreed with the sponsoring agency, the National Institute of General Medical Sciences (NIGMS), these samples will be shared between ORNL and the scientific community at large.

The laboratory-scale preparation of highly purified phenylalanine tRNA and a leucine tRNA from *E. coli* B were described in the previous report.[1] The method involved production of a crude tRNA mixture from *E. coli* cells, fractionation of the mixed tRNA's by reversed-phase chromatography utilizing the isoamyl acetate system, desalting and concentration of selected chromatographic fractions, and final purification by gel filtration chromatography. Engineering efforts were initiated to define and evaluate the critical parameters of these steps so that a substantial scaleup of the laboratory method could be made. During the latter half of the year, at the suggestion of the NIGMS, engineering research was curtailed, and an intensive development program was undertaken to prepare a gram-sized sample of phenylalanine tRNA from *E. coli* B. The results of this campaign are described in the following sections.

Crude tRNA Production

A flow diagram showing the method for producing crude tRNA from *E. coli* cells is presented in Fig. 11.4. This procedure and the successful preparation of 630 g of crude tRNA from *E. coli* W that had been grown by continuous fermentation techniques were described in the previous annual report.[1]

For this campaign we decided to grow *E. coli* B cells rather than to use the crude tRNA from *E. coli* W (that was on hand) since the laboratory sample of phenylalanine tRNA had been prepared from *E. coli* B. However, despite extensive attention to fermentation conditions (medium composition, cell density, culture techniques, and sterilization procedure), *E. coli* B could not be grown by

[1] *Chem. Technol. Div. Ann. Progr. Rept. May 31, 1966*, ORNL-3945.

continuous fermentation techniques. Within 2 to 4 hr after harvesting was initiated, the cells lysed, and the remainder of the material in the fermenter had to be discarded because large quantities of DNA were released on lysis. Lysis was found to be due to T2 phage infection, probably caused by inadequate isolation of the fermenter. Another possibility is that this strain of *E. coli* B carried a prophage of T2.

It was expedient to revert to batch fermentation in order to grow *E. coli* B. Four weeks of intermittent three-shift operation were required to grow 390 kg of cells. The harvested cells were carried batchwise through the phenol step to the first ethanol precipitation (see Fig. 11.4) as rapidly as possible (4 to 8 hr) to minimize losses from degradative reactions. The precipitates were combined and stored frozen until after completion of the cell-growing step. The precipitate was then processed batchwise through the isopropanol and DEAE-cellulose steps to yield approximately 500 g of crude tRNA.

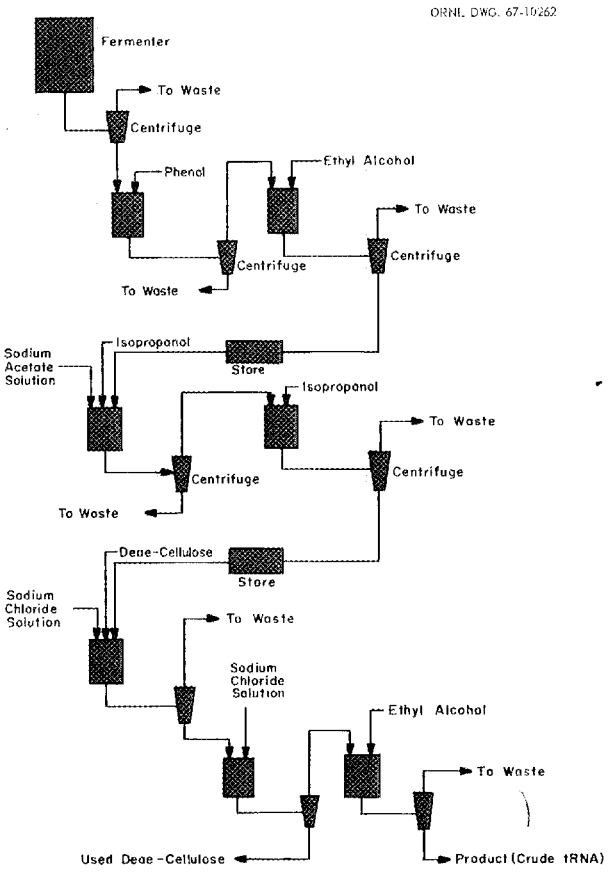

Fig. 11.4. Flow Diagram for Production of Crude tRNA.

Separation of Phenylalanine tRNA

Research activities designed to produce scaleup information on the isoamyl acetate reversed-phase chromatographic system uncovered several problems that were only partially solved when the phenylalanine tRNA production campaign was undertaken. The qualitative effects of flow rate and column length upon batch resolution (separation of the phenylalanine and leucine tRNA peaks) and recovery were evaluated. Varying the column length from 4 to 24 ft in 1-cm-, 1-in.-, or 2-in.-diam columns did not appreciably affect separation, other variables being equivalent. The greatest separation was achieved by the use of a more gradually increasing concentration of eluent (sodium chloride). It was found that the flow rate could be increased from 0.8 to 9.5 ml cm^{-2} min^{-1} without loss of resolution or recovery. The higher flow rate represents a twelvefold increase (over that in the initial laboratory work) in the throughput attainable with a given set of columns. Another important finding was that the quaternary ammonium chloride was dispersed off the column into the mobile aqueous phase at 37°C when the NaCl concentration was less than 0.45 *M*.

In the production campaign, fractionation of the crude *E. coli* B tRNA was accomplished with two sets of coupled columns at 37°C, each set comprising a 2-in. by 8-ft column feeding a 1-in. by 8-ft column. In a typical run, approximately 20 g of crude tRNA was applied to the 2-in. column; the crude tRNA was contained in 100 to 200 ml of a solution that was 0.50 *M* in NaCl, 0.01 *M* in $MgCl_2$, and 0.01 *M* in sodium acetate buffer (pH 4.5) and that contained 0.5 ml of isoamyl acetate per liter. The column was then washed at a rate of 3 liters/hr with 24 liters of 0.58 *M* NaCl solution containing other constituents as listed above. An eluent with concentrations of NaCl varying linearly from 0.58 to 0.72 *M*, and containing the other constituents listed above, was then used to elute the phenylalanine and final leucine tRNA's in a total volume of approximately 50 liters. The product from the phenylalanine peak was obtained in a volume of approximately 10 liters.

Twenty such runs were required to process the crude *E. coli* B tRNA. A typical chromatogram is shown in Fig. 11.5. The material eluted during the 0.58 *M* NaCl wash contained the bulk of the tRNA's other than phenylalanine, leucine, and tyrosine. It was collected and precipitated with ethanol; the precipitate was then stored frozen for future use. A number of chromatographic peaks were developed by the gradient elution. The positions of the phenylalanine and leucine tRNA's are shown in the figure. The other peaks observed in the ultraviolet absorbance trace did not accept any amino acid.

The specific activity (a measure of relative purity) of the phenylalanine tRNA peak was initially greater than 500×10^3 counts (^{14}C-phenylalanine) per minute per optical density unit (ODU), as measured by the amino acid acceptance assay. The specific activity of the leucine tRNA was much lower, and a leucine tRNA product was not obtained. Column performance deteriorated after several runs, and the specific activity of the phenylalanine tRNA peak decreased to the range of 300 to 400×10^3 counts/min per ODU, indicating that the product was contaminated with other material. Concurrently, analyses of concentrated samples indicated the presence of tryptophan tRNA. Tryptophan tRNA had not been detected in previous runs; it is assumed that differences in the crude tRNA or differences in column operating variables resulted in the cochromatography of tryptophan and phenylalanine tRNA's in this instance.

The recovery of phenylalanine tRNA averaged 23% (See Table 11.1). Loss of phenylalanine tRNA during reversed-phase chromatography remains a serious problem. Experiments to investigate the effects of chemical or physical factors on recovery have not yielded useful information. These experiments have included studies of temperature, flow rate, column geometry, packed column density, solution composition, oxidation, metal contamination, and exposure to ultraviolet light.

Desalting and Concentration

Pooled fractions of phenylalanine tRNA from the reversed-phase columns were desalted by gel filtration on a 4-in. by 7-ft column of Sephadex G-25. Polyacrylamide P-2 gel columns had been used in the laboratory-scale work; however, the batches of Bio-Gel P-2 obtained for this campaign were different in that, after several desalting runs, large losses of phenylalanine tRNA were incurred. In a typical run, 4 liters of phenylalanine tRNA solution were desalted in one batch, and two batches were processed per 8-hr shift.

The desalted solutions were concentrated in a wiped-film evaporator. This evaporator operated at a pressure of 17 torrs and had an evaporation

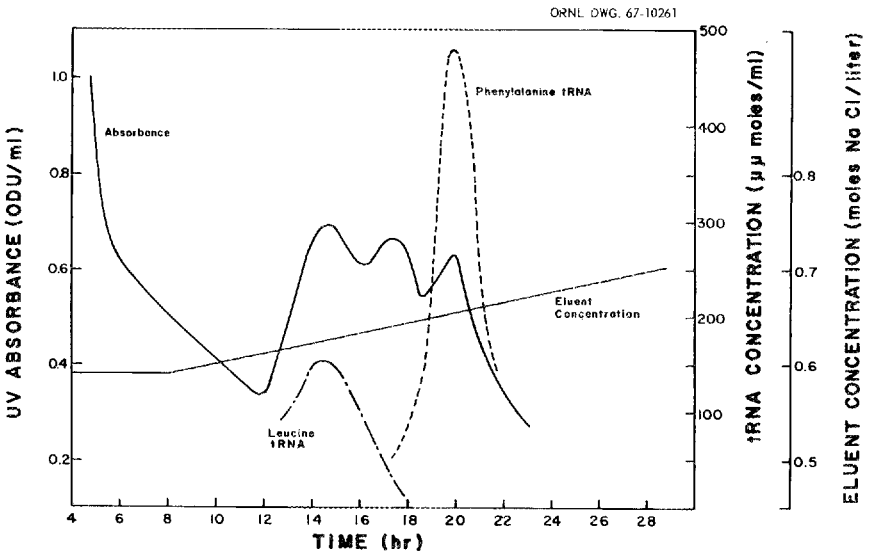

Fig. 11.5. Elution Curve for a Typical Production Run.

Table 11.1. Recovery of Phenylalanine tRNA

	Total Counts per Minute per ODU[a]	Percentage Recovery
	$\times 10^9$	
Crude tRNA	54	100
After reversed-phase chromatography	26	48
Before desalting on G-25 column	20	37
After desalting on G-25 column	18	32
After concentration	17	31
Pooled after G-100 column chromatography	12	23

[a]Phenylalanine tRNA followed by calculating total ^{14}C-phenylalanine-accepting activity.

rate of approximately 3 liters/hr. A four- to sixfold concentration of a 10- to 12-liter batch was obtained in two or three passes. The residence time of the solution was 6 min per pass, and the temperature was about 21°C. The phenylalanine tRNA was further concentrated to about 25 ODU/ml (1 ODU is approximately equivalent to 0.05 mg of tRNA) in a rotating flash evaporator. At this point it was precipitated by ethyl alcohol and recovered by centrifugation.

Gel Filtration

Final purification was achieved by gel filtration on 2.4- by 240-cm columns of Sephadex G-100. The Sephadex G-100 gave substantially better chromatographic resolution than the polyacrylamide Bio-Gel P-100 that was previously used. A total of 21 batches of phenylalanine tRNA were processed in lots containing 1000 to 5000 ODU each. In a typical run the solid phenylalanine tRNA from the concentration step was dissolved in 4 ml of a solution that was 0.4 *M* in NaCl, 0.01 *M* in $MgCl_2$, and 0.05 *M* in Tris buffer (pH 7.0) and that contained 0.5 ml of isopentyl acetate per liter. The capacity of the column was increased to the 5000-ODU level by operating at 37°C. A typical chromatogram is shown in Fig. 11.6. Selected fractions were pooled on the basis of phenylalanine-accepting activity to yield two product samples of different purities.

The amino acid acceptance and terminal adenosine nucleoside assays are shown in Table 11.2. The better-grade material (~1 g) assayed 64% phenylalanine tRNA, 2% leucine tRNA, and 8% tryptophan tRNA. These percentages are based on the terminal adenosine content (all tRNA's terminate with an adenosine nucleoside). If all the tRNA's were active, each terminal adenosine would accept an amino acid, and the total amino-acid-accepting ability would equal the terminal adenosine content. In Table 11.2 the terminal adenosine content is thus taken as 100% accepting activity. No other amino acids were accepted. Since these tRNA's total only 74%, the remainder of the sample was assumed to be inactive, possibly denatured, tRNA's. The balance of the product (~0.5 g) assayed 51% phenylalanine tRNA, 3% leucine tRNA, and 15% tryptophan tRNA.

The 1-g sample of phenylalanine tRNA will be distributed by NIGMS. A preliminary release of portions of this sample will be made to selected investigators, and information that they accumulate concerning the physical and chemical properties of the sample will be added to the data obtained here. Then a public announcement of the availability of phenylalanine tRNA will be made, and the remaining portions will be distributed.

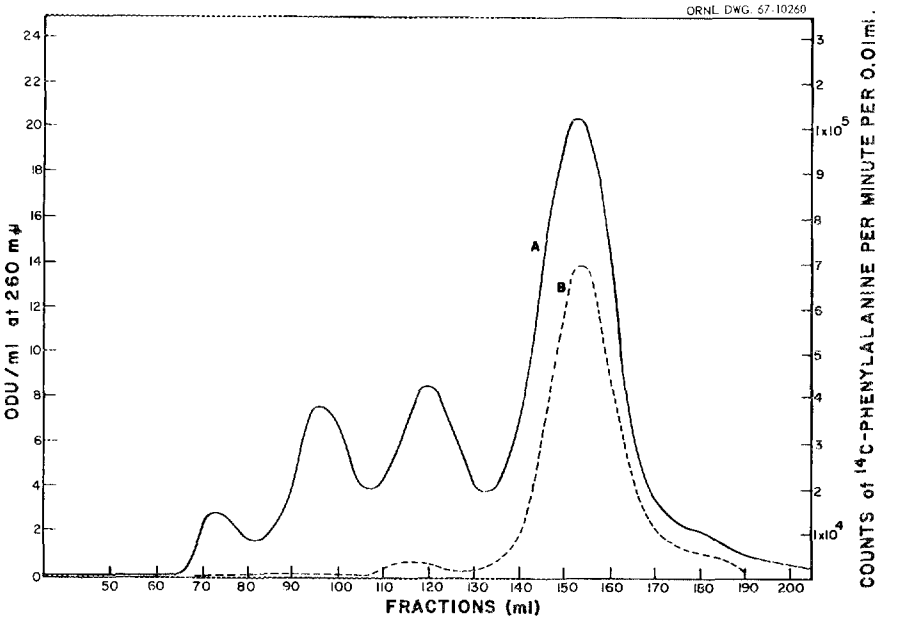

Fig. 11.6. Sephadex G-100 Chromatography of Phenylalanine tRNA. Curve *A* shows ODU/ml at 260 mμ; curve *B* shows counts of ^{14}C-phenylalanine per minute per 0.01 ml.

Table 11.2. Analyses of Phenylalanine tRNA Products

	Better-Grade Material	Less-Pure Material
Yield, ODU	17,700 (~1 g)	9040 (~0.5 g)
Amino acid acceptance		
Phenylalanine, micromicromoles/ODU	882 ± 67	667 ± 41
Phenylalanine, %	64	51
Leucine, micromicromoles/ODU	33 ± 2	38 ± 3
Leucine, %	2	3
Tryptophan, micromicromoles/ODU	105 ± 10	200 ± 10
Tryptophan, %	8	15
Serine, micromicromoles/ODU	~8	~13
Serine, %		1
Others, micromicromoles/ODU	<5	<5
Terminal adenosine, micromicromoles/ODU	1380 ± 14	1305 ± 21
Terminal adenosine, %	100	100

11.3 MOLECULAR WEIGHTS OF TRANSFER RIBONUCLEIC ACIDS

Since tRNA is frequently contaminated with higher-molecular-weight components, molecular weight measurements can serve as a measure of the purity of a tRNA sample. Also, the separation of specific tRNA's is known to be dependent on variables such as pH, temperature, and Mg^{2+} concentration. It is desirable, therefore, to determine the effects of these variables on the apparent molecular weight of tRNA in solution. Membrane

osmometry has proved to be a very useful method for this purpose.

For a given set of conditions, osmotic pressure measurements were made at several tRNA concentrations. The results were extrapolated to zero concentration from a plot of π/c (osmotic pressure divided by concentration) vs c. The molecular weight was calculated from this limiting value of π/c by using the van't Hoff equation.

The molecular weight of crude, mixed tRNA obtained from the General Biochemicals Company was compared with that of a sample prepared at ORNL (Table 11.3). The samples were dried in a vacuum desiccator over P_2O_5 and were used without further purification. The solutions were 0.1 *M* in NaCl, 0.01 *M* in $MgCl_2$, and 0.05 *M* in Tris-HCl buffer (pH 7.0, measured at 25°C). The molecular weight of the crude tRNA from General Biochemicals was also determined at 25°C with no $MgCl_2$ added; a value of 41,800 was obtained.

The tRNA mixture obtained from the General Biochemicals Company was further purified by gel permeation chromatography, using a column of Bio-Gel P-100 polyacrylamide gel. A high-molecular-weight component eluted separately ahead of the tRNA. The fractions containing the tRNA were pooled, desalted on a Bio-Gel P-2 column, concentrated by evaporation at 37°C, and dried in a vacuum desiccator over P_2O_5. The molecular weights of this purified, mixed tRNA under various conditions are summarized in Table 11.4.

Purification of the crude tRNA by the method just outlined significantly reduced the apparent molecular weight to values that are consistent with those obtained by investigators using nucleotide and end-group analyses. The higher values obtained at lower pH's suggest aggregation or association of tRNA, probably involving hydrogen bonding.

The addition of 0.01 *M* Mg^{2+} to the purified tRNA solutions under the conditions studied does not significantly affect the apparent molecular weight. The extent of the effect of varying the temperature is difficult to assess because of simultaneous pH change. The pH of the buffers is temperature-dependent, decreasing with increasing temperature. Nevertheless, the apparent molecular weight appears to decrease slightly with increasing temperature.

Table 11.3. Apparent Molecular Weights of Crude, Mixed tRNA

Source	Temperature (°C)	Apparent Molecular Weight[a]
General Biochemicals Company (lot 642574)	10	45,600
	25	46,200
ORNL (RG-B3)	25	41,300
	60	44,100

[a]All tRNA samples were in the sodium salt form.

Table 11.4. Apparent Molecular Weights of Purified, Mixed tRNA

Solution	Temperature (°C)	Apparent Molecular Weight[a]
0.1 *M* NaCl; 0.05 *M* Tris-HCl, pH 7.0 (25°C)	15	31,500
	25	30,800
	35	30,700
0.1 *M* NaCl; 0.05 *M* Tris-HCl, pH 7.0 (25°C); 0.01 *M* $MgCl_2$	10	32,800
	15	32,800
	25	31,700
	35	30,100
0.1 *M* $NaC_2H_3O_2$; 0.01 *M* $Mg(C_2H_3O_2)_2$; $HC_2H_3O_2$, pH 4.1 (25°C)	25	38,400
	50	35,200

[a]All tRNA samples were in the sodium salt form.

11.4 BEHAVIOR OF TRANSFER RIBONUCLEIC ACIDS ON POLYACRYLAMIDE GEL COLUMNS

Polyacrylamide gel chromatography is a technique used for purifying tRNA by removal of higher-molecular-weight components (Sect. 11.3). This technique also results in partial separation of certain specific tRNA's.

A 250-mg sample of crude tRNA was chromatographed on a 2.5- by 238-cm column of Bio-Gel P-100 at 5°C and eluted with a solution that was 0.4 *M* in NaCl, 0.01 *M* in $MgCl_2$, and 0.05 *M* in Tris-HCl (pH 7.0). The effluent fractions were

assayed for amino-acid-accepting ability. There appeared to be two tRNA's for each of the following: arginine, alanine, glycine, lysine, proline, phenylalanine, valine, and serine. The tRNA's were separated into two major groups, with a minor group between. Overlapping of the peaks was fairly extensive. The group near the front of the tRNA peak contained 10 tRNA's – phenylalanine, glutamic acid, alanine, asparagine, lysine, proline, tyrosine, valine, tryptophan, and serine – plus small amounts of arginine and glycine tRNA's. The middle group contained isoleucine, histidine, and serine tRNA's. The group near the end of the chromatogram contained alanine, glycine, arginine, methionine, proline, and valine tRNA's plus a small amount of lysine tRNA. Leucine tRNA gave a broad peak covering all groups.

On a 2.3- by 118-cm P-100 column, five samples of crude tRNA were chromatographed under the following conditions:

Run	tRNA Load (mg)	Eluent	pH	Temperature (°C)
1	49	0.4 *M* NaCl 0.01 *M* $MgCl_2$ 0.05 *M* Tris-HCl	7.1	5
2	50	0.4 *M* NaCl 0.01 *M* $MgCl_2$ 0.01 *M* $NaC_2H_3O_2$	4.3	5
3	20	0.01 *M* $MgCl_2$ 0.05 *M* Tris-HCl	7.1	5
4	20	0.05 *M* Tris-HCl	7.2	5
5	25	0.4 *M* NaCl 0.01 *M* $MgCl_2$ 0.05 *M* Tris-HCl	7.0	37

Run 3 gave the best separation of tRNA's from high-molecular-weight components, as measured by the absorbance of the fractions at 260 mμ. The fractions were assayed for phenylalanine tRNA and leucine tRNA. Runs 1 and 3 gave the best separation of these tRNA's. The relative amounts of tRNA and high-molecular-weight components also changed under the different conditions.

In another experiment, 250 mg of crude tRNA was chromatographed on a 2.5- by 237-cm P-100 column at 5°C and was eluted by gradient elution; the NaCl concentration was decreased continuously from 0.1 *M* to zero, while the $MgCl_2$ concentration was increased from zero to 0.01 *M*. The buffer concentration was maintained at 0.05 *M* Tris-HCl, pH 7.0. The fractions were assayed for accepting ability with 17 amino acids. The phenylalanine tRNA was eluted at the front of the tRNA peak and was partially separated from the other specific tRNA's.

Separations on a gel column are generally considered to occur on the basis of size differences of the solutes; however, charge effects cannot be ruled out (see Sect. 8.3).

11.5 BODY FLUID ANALYSIS

Over 400 molecular constituents of human urine have been reported.[2-6] These include inorganic compounds, organic acids and amino acids, sugars, purines and related compounds, hormones, vitamins, estrogens, enzymes and other proteins, and many others. Knowledge of the quantities of many of these constituents of urine represents a wealth of information that can be used to evaluate body function. This is particularly true of many of the organic chemicals of low molecular weight (less than 1000) since more than 200 such constituents have been reported to have pathological significance.

An automatic, high-resolution analytical system is being developed to quantitatively determine many of the low-molecular-weight constituents in human urine. The present approach is to modify and expand the capabilities of an existing nucleotide analyzer[7] for this use. Initial results indicate that this concept is feasible; that is, a high-pressure, high-resolution modification of the nucleotide analyzer has resolved over 100 chromatographic peaks of uv-absorbing constituents from a 2-ml urine sample.[8]

---

[2]P. L. Altman and D. S. Dittmer, *Blood and Other Body Fluids*, Federation of American Societies for Experimental Biology, Washington, D.C., 1961.

[3]P. L. Altman and D. S. Dittmer, *Biology Data Book*, Federation of American Societies for Experimental Biology, Washington, D.C., 1964.

[4]H. C. Damm (ed.), *Handbook of Clinical Laboratory Data*, The Chemical Rubber Co., Cleveland, 1965.

[5]C. Long (ed.), *Biochemists' Handbook*, E. and F. N. Spon, Ltd., London, 1961.

[6]S. A. McKee, Oak Ridge National Laboratory, unpublished data, 1966.

[7]N. G. Anderson *et al.*, *Anal. Biochem.* **6**, 153 (1963).

[8]C. D. Scott, J. E. Attrill, and N. G. Anderson, *Proc. Soc. Exptl. Biol. Med.* **125**, 181 (1967).

For purposes of a logical presentation, the program can be divided into several specific areas of interest: (1) operation of prototype systems, (2) a literature search for pathological urine constituents and analytical techniques, (3) urine processing methods, (4) high-resolution separation systems, (5) detection and monitoring devices, (6) identification of the separated molecular constituents, and (7) data acquisition and analysis. Some of these areas are interconnected and can be investigated simultaneously, while others must be studied individually.

Prototype Urine Analyzer

Experimental System. – The present prototype system for urine analysis is composed of a heated high-pressure anion exchange column (typically 0.62 cm ID × 200 cm, filled with Dowex 1-X8 resin, and operating at 40°C) and a recording ultraviolet (uv) spectrophotometer that operates alternately at two to four wavelengths (see Fig. 11.7). There are also provisions for volumetric measurement and collection of the column effluent.

The chromatogram, which shows the uv absorbance of the column effluent as a function of time, is developed by introducing a urine sample (0.5 to 2 ml) into the eluent stream just ahead of the ion exchange column by use of high-pressure valves and eluting it from the column with a sodium acetate–acetic acid buffer solution (pH 4) having a concentration that gradually increases from 0.015 to 6 *M* and a flow rate of 30 to 60 ml/hr. In the usual chromatogram, 80 to 100 peaks are resolved in about 48 hr (see Fig. 11.8).

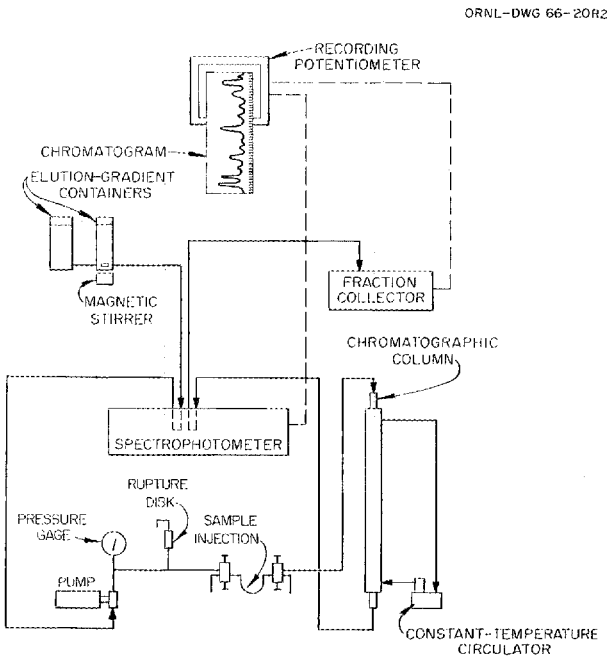

Fig. 11.7. High-Resolution Urine Analyzer for the Ultraviolet-Absorbing Constituents of Urine.

Comparison Between Pathological and Normal Urine. – Several pathological urine samples have been run to determine if the system is capable of differentiating between normal and abnormal urine. Significant differences have been observed between normal samples and samples from subjects with acute lymphocytic leukemia[9] and schizophrenia[10] (see Fig. 11.8). The urine from four leukemics showed a notable decrease in hippuric acid content as well as an increase in the ratio of uric acid to xanthine and hypoxanthine. The chromatograms of urine from three schizophrenics had two very large unknown peaks that we have not previously seen in normal urine.

Literature Search

A survey of the literature concerning the pathological significance of low-molecular-weight organic compounds present in human urine has been completed; the search primarily included *Chemical Abstracts* and *Biological Abstracts* for 1964 through 1965. Also, *Index Medicus* was searched for 1965; however, it yielded only 20% as many references as either of the other two for the same time period. More than 800 literature citations from these three sources, coupled with data from handbooks, yielded information on 312 urinary organic constituents of low molecular weight; more than 200 of these are thought to be pathologically significant.

An automated bibliographic search was also made by the MEDLARS computer search facility at the National Library of Medicine. This search of literature for 1966 was not as complete as the manual searches have been.

---

[9]Urine samples from subjects with leukemia were obtained from Dr. C. L. Edwards of the Medical Division of Oak Ridge Associated Universities, Oak Ridge, Tenn.

[10]Urine samples from subjects with schizophrenia were obtained from Dr. C. F. Mynatt of Eastern State Psychiatric Hospital, Knoxville, Tenn.

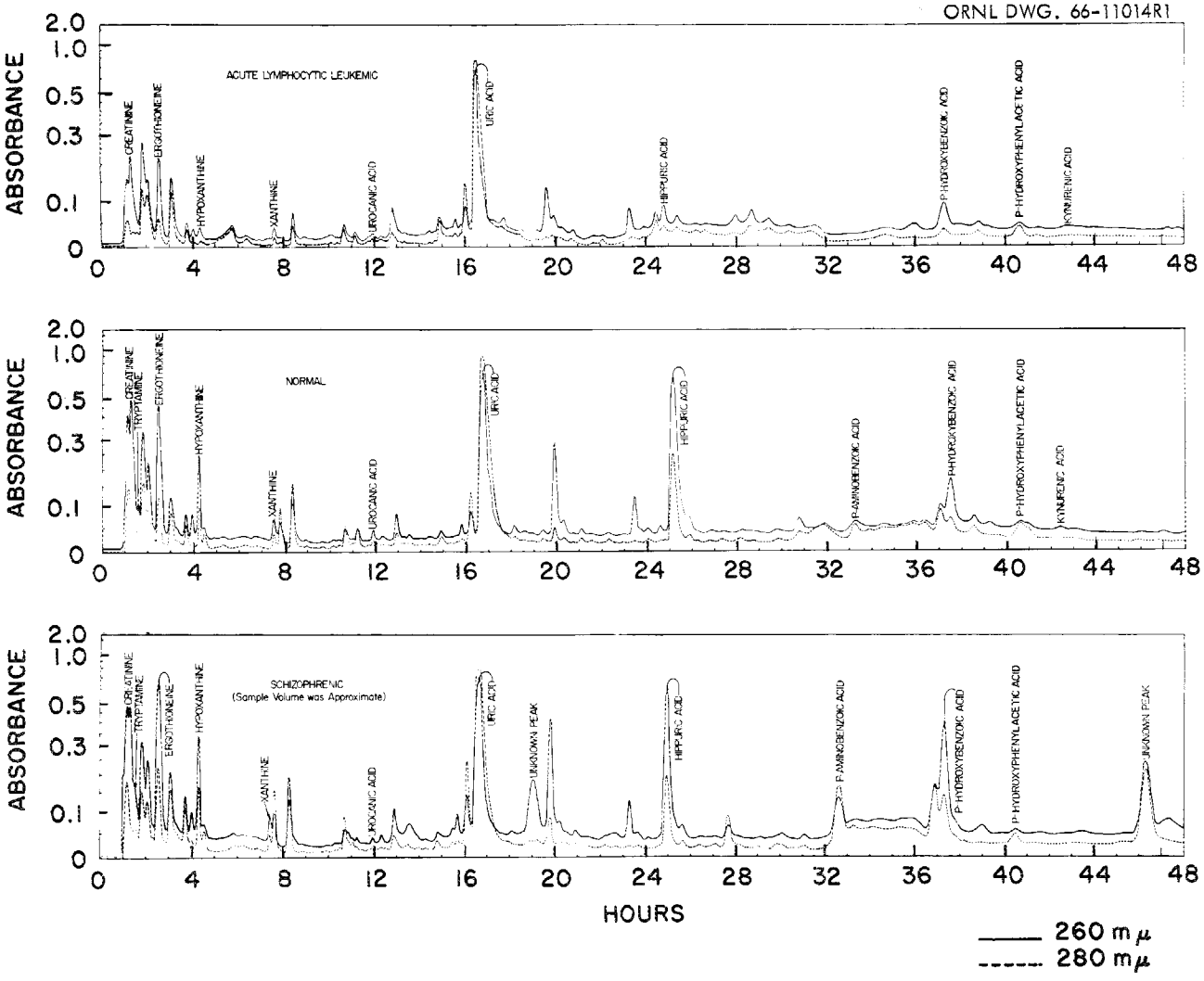

Fig. 11.8. Typical Chromatograms from the Urine Analyzer Showing Reproducibility and the Comparison Between a Normal Chromatogram and Chromatograms from Typical Acute Lymphocytic Leukemics and Schizophrenics. Run conditions: stainless steel column, 0.62 cm ID × 200 cm, with 5- to 10-μ-diam Dowex 1-X8 resin; urine sample, equivalent to 0.05 kg of body weight for a 24-hr collection period; temperature, 40°C; pressure, 1000 to 2200 psig; eluent, ammonium acetate–acetic acid buffer, pH 4.4, varying in concentration from 0.015 to 6 *M*; average flow rate of eluent, 28 ml/hr.

Urine Processing Methods

Until additional tests can be made, it has been assumed that, since many components vary as a function of the daily cycle, quantitative evaluation of urinary components requires a sample from a composite of urine that has been collected over a period of at least 24 hr. For example, urines from diabetics characteristically show the highest concentration of glucose after meals, etc. It may be possible that a single sample, such as that collected on arising in the morning following a prescribed regimen of intake, can eventually be considered as acceptable for a screening test.

To prevent bacterial action and degradation by chemical reaction, prompt refrigeration of the urine specimen is desirable. If this is impractical, an antibacterial agent may be added to the collection vessel. Of the agents considered, formaldehyde appears to be the most useful. After collection, filtration of the specimen through a membrane filter having a pore size of less than 0.5 μ satisfactorily removes bacteria.

Urine specimens often contain a fairly heavy sediment even in the absence of significant bacterial growth. This sediment is apparently composed of material that has precipitated due to decreased solubility at lower temperatures. In acid urines the precipitates consist of organic compounds such as uric acid, tyrosine, hippuric acid, etc., while alkaline precipitates are likely to be inorganic. These can probably be dissolved by heating to above 37.5°C and diluting with distilled water. Our present procedure includes diluting the urine with distilled water, buffering to the pH of the chromatographic system (4.4), heating the urine sample to approximately 40°C, and filtering through a 0.5-μ membrane filter. After processing, the urine samples are frozen to −20°C.

High-molecular-weight compounds such as mucopolysaccharides and proteins probably will not be eluted from the chromatographic column and may tend to foul the ion exchange resin. To circumvent this problem, pressure filtration of the urine sample through dialysis tubing has proved to be effective.

Separations Systems

A large number of separations media have been evaluated by scouting tests for use in separating the uv-absorbing constituents of urine. These included inorganic materials, activated charcoal, various organic anion and cation exchange resins, and a polyacrylamide gel (Table 11.5). Resolution was defined as the number of separate uv chromatographic peaks detected in the column effluent. These scouting tests were made at conditions that produced good results for a Dowex 1 type of ion exchange resin; therefore, they may not have utilized the best conditions for each particular medium.

The best separations media were found to be organic ion exchange resins, of which Dowex 1 resin was the most satisfactory. As reported earlier,[11] resolution of the Dowex 1 resin is very dependent on particle size; for example, 5- to 10-μ-diam resin provides 50% more chromatographic peaks than 20- to 40-μ-diam resin.

The effect of nominal degree of cross-linkage of Dowex 1 resin has also been investigated. (Dowex 1 resins are formed from styrene polymers that are cross-linked with divinylbenzene; the degree of cross-linkage is indicated by the percent of divinylbenzene used.) Resin of low cross-linkage (2 to 4%) gives better separation in the beginning of the chromatogram, whereas resin of high cross-linkage (10 to 12%) gives better separation in the latter part of the chromatogram. A resin of medium (8%) cross-linkage is superior in overall performance. Initial tests where resins of varying cross-linkage were used either mixed or in series gave results inferior to those from any of the separate tests. Additional tests will be made with both anion and cation exchange resins.

Although it is possible to operate a single ion exchange column with reasonable reproducibility, it is difficult to obtain reproducible results from multiple columns packed with the same type (even from the same batch) of resin. Moreover, if different batches of resin (same nominal type) are used, the experimental data are frequently very different. Some of this difference can be attributed to varying particle sizes or degrees of cross-linkage; however, some of the more fundamental properties of the resin, such as the amount and type of porosity or the type and quantity of charged functional groups, are also probably important. In the future, an attempt will be made to more fully characterize the ion exchange resins

[11] *Chem. Technol. Div. Ann. Progr. Rept. May 31, 1966*, ORNL-3945, p. 206.

Table 11.5. Resolution of a Standard Urine Sample for UV-Absorbing Constituents by Different Separations Media

Operating conditions: Column, 0.62 cm ID × 150 cm long, stainless steel; elution system, three series-connected chambers containing 330 ml of 0.015 *M*, 330 ml of 3 *M*, and 1000 ml of 6 *M* acetic acid–sodium acetate solution buffered at pH 4.4; temperature, 40°C; average flow rate, 30 to 35 ml/hr

Material	Particle Size Range (μ)	Initial Operating Pressure (psig)	Total Number of Chromatographic peaks	Comments
Biorad AG-1-X8, anion exchange resin	10–20	370	68	All Biorad AG-1 resin is spherical.
Biorad AG-1-X8, anion exchange resin	20–40	220	53	
Biorad AG-1-X8, anion exchange resin	40–60	170	41	
Biorad AG-1-X10, anion exchange resin	20–50	240	50	
Biorad AG-1-X4, anion exchange resin	20–50	140	44	
Biorad AG-1-X2, anion exchange resin	20–50	250	37	Resin tended to compress with higher flow rates to give an increased pressure drop.
Biorad AG-1-X2, AG-1-X4, AG-X8, AG-X10 (an equal-volume mixture of four)	20–50	290	35	Resin tended to compress with higher flow rates to give an increased pressure drop.
Bio-Rex 5, anion exchange resin	40–70	120	24	Resin tended to compress with higher flow rates to give an increased pressure drop.
Amberlite CG-400, anion exchange resin	10–20	2500	34	Ground resin of irregular shapes.
Amberlite IRA-900, anion exchange resin	>100	800	32	This resin has very large pores, and it compresses with high flow rates.
Biorad AG-50w-X8, cation exchange resin	10–40	400	30	Some absorbing material did not leave the column.
Bio Gel P-2, acrylamide gel	75–150	60	6	
Zehlon-H, synthetic zeolite	10–70	350	15	Ground material.
Activated alumina	5–70	450	6	Ground material. Pressure became very high before end of run.
Activated charcoal	20–70	100	14	Ground material. Some uv-absorbing material did not leave the column.
Silica gel	20–70	140	7	Ground material.

in an attempt to predict the behavior of different batches of the same type of resin.

Detection Systems

The detection system that is being used in conjunction with the present model of the urine analyzer is a modified continuous-flow uv spectrophotometer which monitors the column effluent stream alternately at two to four different wavelengths every 5 sec. A continuous-flow uv spectrophotometer that uses solid-state detectors and is capable of automatic operation at two wavelengths is being developed for use as the column effluent detector. Such a detector will be less expensive and will require less maintenance than the present modified spectrophotometer.

A continuous-flow ratio refractometer with a sensitivity of 10^{-7} refractive index units has been tested as the detector for the column effluent. At the beginning of the chromatogram this instrument produced results that were comparable with those obtained with the uv detector and showed a much greater sensitivity; however, it was not usable during the latter part of the chromatogram because of a large amount of material that was apparently eluted from the ion exchange column and subsequently prohibited the measurement of refractive index differences.

Other detectors that are being considered are a continuous-flow fluorometer and a continuous-flow polarograph.

Identification of Separated Urinary Constituents

Urine constituents that are indicated by the chromatographic peaks are being tentatively identified by determining the position and the absorbance ratio (at two or more different wavelengths) of the chromatographic peaks of known chemicals and comparing them with similar information for unidentified peaks in the urine chromatogram. Standard mixtures of known chemicals are also being combined with urine samples to enlarge suspected chromatographic peaks. Chromatographic position and absorbance ratios give two independent means of comparison, both of which should be characteristic of specific urinary constituents or small groups of constituents. Fifteen urinary components, many of which have pathologic significance, have been tentatively identified in this manner. They are: creatinine, tryptamine, ergothioneine, hypoxanthine, xanthine, urocanic acid, uric acid, hippuric acid, *p*-aminobenzoic acid, *p*-hydroxybenzoic acid, *p*-hydroxyphenylacetic acid, kynurenic acid, vanillic acid, homovanillic acid, and salicylacetic acid.

A more definite identification is being made by isolating and analyzing specific eluate fractions associated with a chromatographic peak. We are investigating several methods for possible use in the analysis of these fractions.

Thin-Layer Chromatography. – Thin-layer chromatography is a potential method for identification since the mobility in a thin-layer chromatogram is specific for an individual compound or a small group of compounds and this value will be different from that in ion exchange chromatography. The chromatographic mobility is described as the partition R_f value, which is the ratio of the distance traveled of a solute zone to the distance traveled

Table 11.6. Migration Rates[a] of Some Urinary Compounds on Nonactivated Silica Gel

Compound	R_f Value[a]
1. Arginine	0.06
2. Creatinine	0.06
3. Indican	0.11
4. Ergothioneine	0.17
5. Cytosine	0.18
6. Tryptophan	0.30
7. Xanthine	0.43
8. 3-Methoxy-4-hydroxymandelic acid	0.44
9. Urocanic acid	0.45
10. Kynurenic acid	0.48
11. Maleuric acid	0.52
12. Adenine	0.58
13. Riboflavin	0.60
14. Hypoxanthine	0.71
15. Homovanillic acid	0.75
16. Hippuric acid	0.81
17. 5-Hydroxyindoleacetic acid	0.85
18. 3-Hydroxyanthranilic acid	0.89
19. Uric acid	0.92
20. *p*-Hydroxybenzoic acid	0.93
21. *p*-Hydroxyphenylacetic acid	0.94
22. *p*-Aminobenzoic acid	0.95

[a]Referred to the solvent front during development with $CHCl_3$–CH_3OH–acetic acid (75 : 20 : 5).

of the solvent front; R_f values for 22 different urinary constituents that are present in urine in relatively large amounts have been determined for a chloroform–methanol–acetic acid (75 : 20 : 5) solvent on thin layers of unactivated silica gel (Table 11.6). These compounds were visualized on the developed chromatogram by using either uv light or iodine vapor.

UV Spectrophotometry. – Since the present analytical systems use a uv spectrophotometer as a detector, comparison of the uv spectra of known urinary constituents with those of the components of the eluate fractions will be useful in identifying the peaks.

A large number of the organic compounds reported to be present in urine have been obtained from commercial sources, and the uv spectra (220 to 340 mμ) of standard buffered solutions (pH 4.4) of these compounds have been determined. The location of inflection points in the spectra, as well as the general shapes of the curves, will be useful in identification. Maxima and minima have been tabulated for 60 compounds. Thus the maxima and minima of the eluate fraction representing a chromatographic peak can be compared with the tabulated values. Five of the chromatographic peaks have been further identified in this manner. These are: creatinine, hypoxanthine, xanthine, uric acid, and hippuric acid.

Changes in the shape of the uv spectral curve with varying pH have been used by Cohn[12] and others to establish the identity of unknown biochemicals; it is possible that this technique may also be applicable to this program.

Computer Resolution of Complex UV Spectra. – A significant development in the field of radiochemical analyses consists in using computers to resolve the spectrum of a mixture of ten or more gamma-ray-emitting nuclides to determine the quantity of each nuclide present.[13–15] The spectra of individual components serve as a library in the linear least-squares resolution performed by a high-speed digital computer. This technique is being extended for use in the resolution of the uv spectra of aqueous mixtures of biochemicals. It may ultimately be a valuable means of identifying unknown urinary compounds in the column effluent, especially when the eluate fractions contain more than one compound.

The effects of the number of species present and their individual concentrations on the accuracy of this method of uv-spectrum resolution are currently being studied. In investigations of simulated spectra, each of which is composed of the summation of two bands having a Gaussian distribution about the wavelength of maximum absorption, a spectrum composed of six to eight separate spectra can be resolved (that is, the concentrations of six to eight separate chemicals can be determined).

When the wavelength region of spectra determined for standard biochemicals in solution was extended from 220–340 mμ to 190–400 mμ, 16 of the 17 materials tested showed structure (in the region 190 to 220 mμ) that has not been reported previously. For example, vanillic acid has two absorption maxima between 250 and 300 mμ and an additional two maxima between 200 and 220 mμ. The presence of these additional maxima in the extended spectral range means that more than the six to eight components can be resolved by the computer resolution technique.

For this technique to be generally useful, identification of all of the uv-absorbing urinary constituents in a particular column eluate fraction would be necessary. Since this information is not currently available, the identification problem may have to be solved by another method. Thus the computer resolving technique is not expected to be advantageous in the initial identification problem; however, it should have utility in analyzing chromatograms after peak identification is completed.

Other Identification Methods. – Many other techniques may aid in the identification of unknown chromatographic peaks.[16] To a limited extent, spot testing may be conducted directly on the eluate fractions or concentrated portions of them. The following reagents identify classes or groups of compounds: periodic acid, phosphomolybdic acid, diazotized sulfanilic acid (Ehrlich), HCl + $KClO_3$ (Colmant), thio-Michler's ketone, dimethyl oxalate, and hexamethylene tetramine.

---

[12] W. E. Cohn, *J. Biol. Chem.* **235**, 1490 (1960).

[13] E. Schonfeld, A. H. Kibbey, and W. Davis, Jr., *Nucl. Instr. Methods* **45**, 1 (1966).

[14] J. S. Eldridge and A. A. Brooks, *Nucleonics* **24**(4), 54 (1966).

[15] G. D. O'Kelley (ed.), *Applications of Computers to Nuclear and Radio-Chemistry, Proceedings of a Symposium, Gatlinburg, Tennessee, October 17–19, 1962*, NAS-NS 3107.

[16] K. S. Warren, Oak Ridge National Laboratory, unpublished data, 1967.

Additional techniques include melting point determination after purification of the solute in the column eluate, x-ray powder diffraction, infrared spectroscopy, mass spectroscopy, and nuclear magnetic resonance spectroscopy.

Data Acquisition

A data acquisition system for digitizing the output of the recording spectrophotometer that monitors the column effluent has been designed and should be available by the summer of 1967. This system includes a digital voltmeter (that digitizes the analog signal from the spectrophotometer), a paper-tape punch and a typewriter printer (that record the digitized data), and the necessary control circuitry. The resulting punched tape will be used as the input to a computer program that will analyze the urine chromatogram to quantify the separated urinary constituents.

12. Chemistry of Protactinium

The purpose of this program is to study the chemistry of protactinium, particularly in systems that are potentially applicable to separations processing, and to elucidate the relationship of the properties of protactinium to those of the other actinides. In most aqueous systems, protactinium does not behave in a simple or reproducible manner; its chemistry, therefore, cannot be predicted with certainty. During the past year this program was extended to the study of heavier actinides and to the development of new experimental techniques for use in this study.

12.1 CHEMICAL BEHAVIOR OF PROTACTINIUM IN SULFURIC ACID SOLUTIONS

The study of the preparation and properties of solid protactinium sulfate was continued,[1] partly in the hope of obtaining a more definite and reproducible starting material than the oxide or hydroxide for preparation of protactinium sulfate solutions. However, attempts to measure the solubility of the solid protactinium sulfate in sulfuric acid continued to give results that vary with the conditions. In one experiment we observed reasonably constant solubilities until a fresh portion of solid protactinium sulfate was added to the mixture; this caused an increase in the concentration of dissolved protactinium. Two more additions were made, each of which caused a further increase in the apparent solubility. The solubility remained fairly constant after each addition and was relatively unaffected by heating to about 200°C.

Since the apparent solubility depends on the amount and the nature of the solid equilibrated with the solution, we have not been able to obtain meaningful solubility data for this system. It is possible that solid protactinium compounds (oxide or sulfate, for example) develop a surface layer that differs from the bulk of the material and is substantially more soluble. The first addition of hydrochloric or sulfuric acid to a given sample of solid has repeatedly been observed to dissolve much more material than did subsequent additions, even after prolonged mixing. The results, which suggest that more than one species is present in these solutions and that equilibrium between these species is extremely slow, even in very high acid concentrations and after heating to about 200°C, are in agreement with the conclusions previously reached on the basis of spectral measurements. It is very doubtful that any useful thermodynamic data can be obtained from studies of the solubility of protactinium in sulfuric acid solutions because of the complexity and the nonreproducibility of the system. If more than one species exists in these solutions and if the species are not in equilibrium with each other (as indicated by all work to date), then thermodynamic data can be obtained only if some means is found to distinguish between the different species.

12.2 ABSORPTION SPECTRA OF PROTACTINIUM IN SULFURIC ACID SOLUTIONS

Absorption spectra were measured for sulfuric acid solutions of the protactinium sulfate. In general, they were similar to spectra previously obtained for protactinium hydroxide dissolved in sulfuric acid. The relatively sharp band near 2000 A, observed in solutions that had been heated to fuming,[2] was not obtained when the protactinium sulfate was dissolved in either concentrated or

[1] *Chem. Technol. Div. Ann. Progr. Rept. May 31, 1966*, ORNL-3945, p. 209.

[2] *Chem. Technol. Div. Ann. Progr. Rept. May 31, 1966*, ORNL-3945, p. 211.

dilute sulfuric acid. This indicates that the species remaining in solution when the solid protactinium sulfate is prepared by precipitation from fuming sulfuric acid are different from those obtained by redissolving the solid and provides additional evidence that several species, all quite persistent, are present in these solutions.

Unambiguous, quantitative information is clearly difficult to obtain from such a complex system, but there is some hope that the spectra can be resolved into individual bands by computer methods. Possibly, each individual band could be associated with a particular species in solution. This approach has been postponed until a newly purchased digital output can be installed on the Cary model 14 spectrophotometer. Conversion of data from strip chart to digital form was not only time consuming but also somewhat inaccurate.

12.3 ANION EXCHANGE BEHAVIOR OF PROTACTINIUM IN HYDROCHLORIC ACID SOLUTIONS

We have demonstrated a novel anion exchange protactinium purification procedure that, although slow, works well on a small scale. Although protactinium oxide is soluble (about 30 mg/ml) in 10 *M* HCl, dissolution is slow. Protactinium will load on anion exchange resin from 10 *M* HCl with a very high distribution coefficient. In these studies, solid pieces of fired Pa_2O_5 and of Dowex 1 resin were placed in a bottle of 10 *M* HCl solution and tumbled continuously. Samples of the resin were removed at intervals and analyzed to determine the amount of sorbed protactinium. At room temperature the amount increased uniformly for 35 days until the system was loaded to the extent of approximately 1 g of protactinium per liter of resin. Subsequently, the rate slowed, and in the next 31 days the amount sorbed increased only 10%.

The same scheme was tested in a closed loop in which 10 *M* HCl was pumped slowly through a bed of 100 mg of impure, ignited Pa_2O_5 and then through a 20-ml Dowex 1 anion exchange column. After one month the column was removed and eluted with HCl-HF solution. A total of 15 mg of highly pure protactinium was recovered.

These observations support the previous conclusions from dissolutions in sulfuric acid, namely, that the dissolution of protactinium from a solid is fairly rapid initially but subsequently becomes very slow.

13. Irradiation Effects on Heterogeneous Systems

13.1 RADIOLYSIS OF WATER IN THE ADSORBED STATE

The study of the radiolysis of adsorbed water was continued in an effort to determine the mechanism by which the adsorbent influences the yield of molecular hydrogen. Results previously reported[1,2] showed that a wide variety of adsorbents enhance the yield of hydrogen and that the magnitude of the effect depends on the nature of the adsorbent, its specific surface area, and the water content. For a given type of material, the effect also appears to be related (with few exceptions) to the surface acidity, which is, in turn, frequently related to the catalytic properties of the solid adsorbents. Recent advances in the use of molecular sieves as catalysts suggested that an investigation of the radiolysis of water adsorbed on the surfaces of these materials might be worth while. The fact that the surface properties can be drastically altered by changing the cation associated with the sieve without appreciably affecting the surface area or the bulk crystal structure offers a method of investigating surface effects essentially independent of bulk effects. This was not possible in earlier studies with silica gels.

Experimental

Measurement of the Rate of Radiolysis of Water. – The experimental technique and the beta radiation source used in most of the work have been previously described.[1-3] Briefly, the method consists in periodically measuring the amount of hydrogen gas that accumulates in a thin-windowed chamber containing the water-adsorbent sample in the radiation field. Hydrogen is usually the only gaseous product observed; however, in some instances, involving specific molecular sieves, substoichiometric amounts of oxygen have been observed. Further investigation of the latter phenomenon will require special experiments, which will be performed in the future. For the present work, the gaseous hydrogen yield is assumed to be a measure of efficiency of the use of the radiant energy.

Surface Area Measurements. – Surface area measurements were made after outgassing at 120°C, using standard BET techniques, with nitrogen gas as the adsorbate. The results are given in Table 13.1. It is recognized that the values obtained in this manner for molecular sieves are probably in

Table 13.1. Specific Surface Areas of Adsorbents

Material	Cation	BET Surface Area[a] (m^2/g)
Linde SK-40[b]	Na^+	620
Linde SK-40[b]	Ca^{2+}	720
Linde SK-40[b]	H^+	442
Linde SK-40[b]	La^{3+}	686
Linde La-Y[c]	La^{3+}	740
Linde Di-X[c]	Mixed rare earths	603
Linde Di-NH_4-Y[c,d]	Mixed rare earths and H^+[d]	642

[a]Accuracy of values obtained by BET method is questionable for molecular sieves.

[b]Commercial Y zeolite.

[c]Research samples provided by the Linde Division of Union Carbide Corporation.

[d]Fired at 400°C to destroy NH_4^+.

[1]*Chem. Technol. Div. Ann. Progr. Rept. May 31, 1965*, ORNL-3830, p. 233.

[2]*Chem. Technol. Div. Ann. Progr. Rept. May 31, 1966*, ORNL-3945, pp. 218–20.

[3]N. A. Krohn, *Nucleonics* 23(5), 83 (1965).

error; however, in the absence of a better technique, they at least provide gross comparisons among the various materials.

Determination of Surface Acidity. – Previously reported results indicated a relationship between surface acidity and the efficiency of utilization of the radiant energy for the decomposition of adsorbed water. Attempts were made to quantitatively measure the surface acidity of some of the tested adsorbents; the method involved titration of the surface with *n*-butylamine in dry benzene, using butter yellow (*N,N*-dimethyl-*p*-phenylazoaniline) as the indicator, according to the method described by Johnson.[4]

Preparation of Materials. – All the adsorbents were pretreated by soaking in distilled water and drying at 150°C in air overnight; the residual water content was estimated by determining weight loss on ignition to 1000°C. Samples of varying water contents were prepared by absorbing water vapor at room temperature. For experiments in which it was desired to use materials containing less water than that remaining after the 150°C treatment, the given adsorbent was heated to 300 to 400°C for a suitable period of time and the additional water loss was obtained by weight change. All subsequent operations on these samples were performed in a dry argon atmosphere to prevent readsorption of water. The different forms of the Y zeolite (Linde SK-40) were obtained by ion exchange methods; the original sodium form was treated with aqueous solutions (~1 *M*) containing $CaCl_2$, $La(NO_3)_3$, or $NH_4C_2H_3O_2$. After extensive washing with distilled water, they were dried overnight. The ammonium-exchanged sieve was then fired at ~300°C to drive off NH_3 and thereby convert the sieve to the hydrogen form. BET surface area measurements indicated a partial collapse of the sieve structure as a result of this treatment.

The extent of exchange was found, by analyses for sodium, calcium, and lanthanum, to be 75% for the Ca^{2+} form and 69% for the La^{3+} form. The extent of exchange for the hydrogen form was calculated to be 72% from sodium analyses before and after treatment; no nitrogen was found by a special micro-Kjeldahl analysis of the fired material.

Results and Discussion

The results are shown in Figs. 13.1 and 13.2. The indicated values are maximum observed hydrogen yields per 100 ev of energy absorbed by the water-adsorbent system. The yields varied with total radiation dose, as noted in earlier studies of silica gel and other tested adsorbents. Figure 13.3 shows some examples of this behavior for the Linde SK-40 sieve after exchange with various cations. The electron fraction of water in the SK-40 molecular sieves was calculated by using a nominal formula of $Na_{56}(AlO_2)_{56}(SiO_2)_{136}$ for the Y zeolite and making appropriate corrections for the ion exchanged materials. The electron fractions of water for the research samples obtained from the Linde Division of Union Carbide Corporation were calculated from actual analytical data supplied with the samples. The water contents for the Ca^{2+} form of the SK-40 sieve in Fig. 13.1 are different from those presented in a preliminary report because of an error found in the measurement of the residual water content of the stock material.

The data in Fig. 13.2 indicate reasonable agreement in behavior between the La-Y zeolite sample obtained from Linde and the lanthanum form of the Linde SK-40 sieve that was prepared in our laboratory. Nothing can be said about the didymium-X sieve since no data were obtained on X-type sieves exchanged with other cations. Why the Di-NH_4-Y material did not show a larger effect is not known. It might have been anticipated that its behavior would be similar to that of the hydrogen and lanthanum forms of the SK-40 material; its unusually high $SiO_2 : Al_2O_3$ mole ratio (5.1) compared with that for SK-40 material (~2.4) may be a factor.

The data shown in Fig. 13.1 reveal the effect of the nature of the surface on the hydrogen yield. Since the crystalline structure and the surface area of the SK-40 molecular sieve are common to all these cases, except for the hydrogen form (where a partial collapse of the sieve structure apparently occurred), the amount of absorbed beta energy transferred from the adsorbent to the adsorbed water should be about the same. Yet, the hydrogen yields vary greatly, indicating that the nature of the surface (i.e., the cation present in this case) affects the efficiency of the conversion of the reactive species to molecular hydrogen. If correction is made for the differences found in surface area by the BET method, the efficiency is inversely related to the charge-to-ionic-radius ratio. However, the BET method for obtaining the

[4] O. Johnson, *J. Phys. Chem.* **59**, 827 (1955).

surface area of molecular sieves is not strictly applicable because of the nature of the porosity of the sieves, which leads to abnormally shaped isotherms. On the other hand, relative values, all of which are obtained in the same manner, can probably be utilized for comparative purposes.

Analysis of previously reported data obtained using silica adsorbents[5] with specific surface areas ranging from 65 to 227 m^2/g showed that, for coverages of water up to ~0.5 mg of water per square meter of surface, the yield of hydrogen, and hence the amount of energy transferred per unit of surface, was constant.

Comparison of this result with the data given in Fig. 13.1 indicates that beta-ray energy absorbed in these solids is transferred to the surface, probably by the migration of displaced electrons. At the surface they react with the adsorbed water molecules, resulting in the formation of H atoms

[5] *Chem. Technol. Div. Ann. Progr. Rept. May 31, 1965*, ORNL-3830, pp. 233–35.

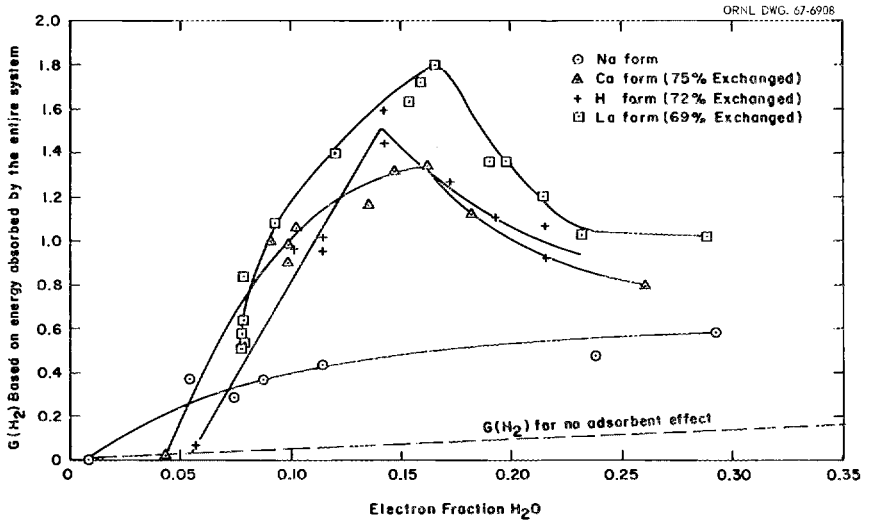

Fig. 13.1. Hydrogen Yields for the Radiolysis of Water Adsorbed on Linde SK-40 Molecular Sieves.

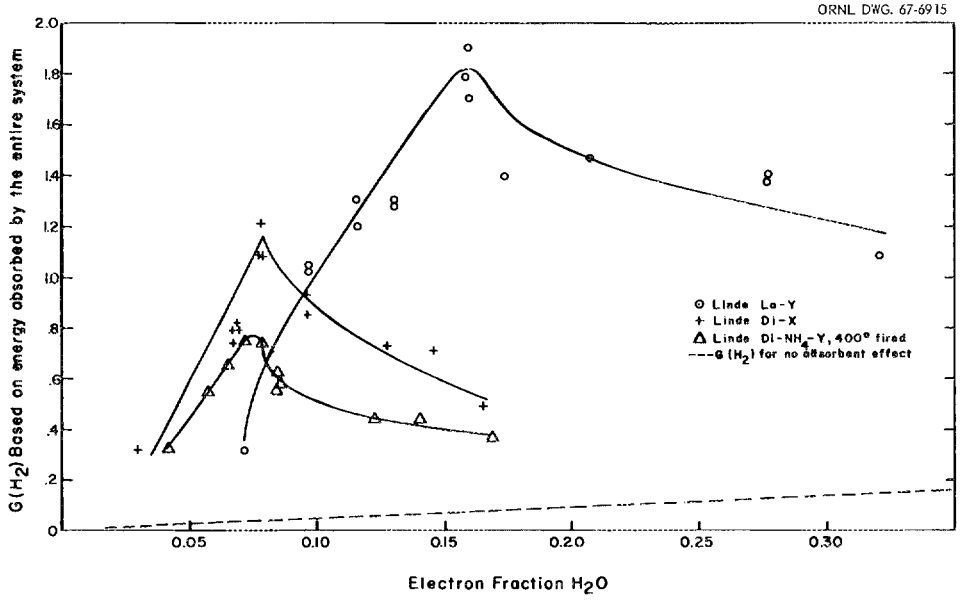

Fig. 13.2. Hydrogen Yields for the Radiolysis of Water Adsorbed on Some Molecular Sieves.

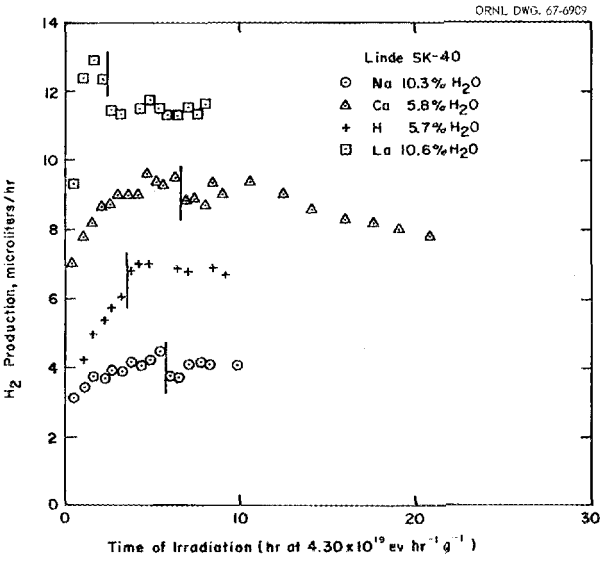

Fig. 13.3. Effect of Irradiation Time on Hydrogen Yields from the Radiolysis of Adsorbed Water. Vertical lines indicate overnight stand out of radiation source.

or solvated electrons. If the surface is extensively degassed, the H atoms formed (by scission of residual silanol groups) are not very mobile and no gaseous hydrogen is detected.[6] However, if adsorbed water is present, proton transfer can occur across the surface and the radicals can unite to release hydrogen gas. Under certain conditions of surface and water content, the highest observed yield of hydrogen, $G(H_2) = 1.8$, is half that for electrons plus H atoms in water; this shows essentially 100% efficiency of utilization of the radiant energy. As the surface is altered by the addition of more water, this efficiency declines because of competing reactions with oxidizing species formed by that fraction of the radiation absorbed by the water. The yield varies with total dose by at least two mechanisms: it may increase initially because of the filling of radiation-induced H_2 adsorption sites;[7] and it may then decline because of the buildup of relatively slow-moving, positively charged species that are left within the adsorbent, which then also compete for electrons. The effect of changing the cation may be related to charge effects or to the heats of hydration of the various ions.

[6] P. H. Emmett *et al.*, *J. Phys. Chem.* **66**, 921 (1962).

[7] Sh. A. Ablaev *et al.*, *Proceedings of the Tashkent Conference on the Peaceful Uses of Atomic Energy*, vol. 1, AEC-tr-6398, p. 222.

14. Spectrophotometric Studies of Solutions of Alpha-Active Materials

The objective of this program is to develop spectrophotometric techniques for the study of the properties of aqueous solutions of the actinide and lanthanide elements over wide ranges of experimental conditions. Efforts thus far have been concentrated principally on the uranyl ion; some preliminary work has also been done on U(IV) in perchlorate media. To permit the study of the more highly alpha-active actinides, a specially modified Cary model 14 spectrophotometer system[1-3] has been built and is being tested. In addition to providing safe containment for highly radioactive materials, this system is designed to operate at temperatures up to the critical point of water (372°) and at pressures up to 10,000 psi.

14.1 SPECTRAL STUDIES OF URANIUM SOLUTIONS

A comprehensive theory of the uranyl ion with respect to its spectroscopic properties has not yet been fully developed. Until the new spectrophotometer system (see Sect. 14.2) is available for high-temperature work, experiments at temperatures up to about 95°C are being performed with other spectrophotometric equipment. We have developed ancillary equipment to aid in these studies. Several computer techniques and programs have been developed and evaluated specifically for the analyses of certain types of spectroscopic data. We plan similar studies with the lanthanides for comparison with the actinides.

Absorption Spectra of the Uranyl Ion in Perchlorate Media

Descriptions and results of most of the work in this part of the program have been recently published[4,5] or submitted for publication;[6] therefore, only a brief summary is presented here.

The ultraviolet and visible spectra of the aqueous uranyl ion in a perchlorate medium have been resolved into 24 absorption bands of Gaussian character; this resolution included the first detailed analysis of the complete ultraviolet spectrum (1795 to 3565 A) for any actinyl type of ion in an aqueous "noncomplexing" medium. The 24 bands have been grouped into 7 major absorption bands with an average spacing of 6137 cm^{-1} and progressively increasing oscillator strengths or transition probabilities (Table 14.1). A linear relationship between the band energies and the logarithms of the oscillator strengths was noted.

The first two major bands are in agreement with the two triplet excited states proposed by other authors.[7] The lower-lying triplet is composed of 12 vibrationally perturbed bands and has a center at 24,107 cm^{-1}; the second triplet, which has not been previously observed, is located at 31,367 cm^{-1} and is composed of 7 vibrationally perturbed bands. We believe that the five remaining bands represent electron transitions from the ground state

[1] *Chem. Technol. Div. Ann. Progr. Rept. May 31, 1966,* ORNL-3945, pp. 221–27.

[2] *Chem. Technol. Div. Ann. Progr. Rept. May 31, 1965,* ORNL-3830, pp. 236–47.

[3] R. E. Biggers and R. G. Wymer, *Design and Development of a High-Temperature, High-Pressure Spectrophotometric System: Status Report,* ORNL-CF-60-11-96 (Nov. 12, 1960).

[4] J. T. Bell and R. E. Biggers, *J. Mol. Spectry.* **18,** 247 (1965).

[5] J. T. Bell and R. E. Biggers, *J. Mol. Spectry.* **22,** 262 (1967).

[6] J. T. Bell and R. E. Biggers, "The Absorption Spectrum of the Uranyl Ion in Perchlorate Media. Part III. Resolution of the Ultraviolet Band Structure; Some Conclusions Concerning the Excited State of UO_2^{2+}," *J. Mol. Spectry.* (in press).

[7] S. P. McGlynn and J. K. Smith, *J. Mol. Spectry.* **6,** 164–87 (1961).

Table 14.1. Properties of the Seven Major Absorption Bands of the Aqueous Uranyl Ion

Band	Subbands	Band Center (cm^{-1})	Oscillator Strength	Log Oscillator Strength	Band Spacing (cm^{-1})
A	1–12	24,107	0.000117	−3.943	7260
B	13–19	31,367	0.000513	−3.290	5506
C	20	36,873	0.00329	−2.483	5944
D	21	43,817	0.0235	−1.630	6112
E	22	48,930	0.0669	−1.175	6020
F	23	54,950	0.112	−0.9523	5979
G	24	60,930	0.635	−0.1970	

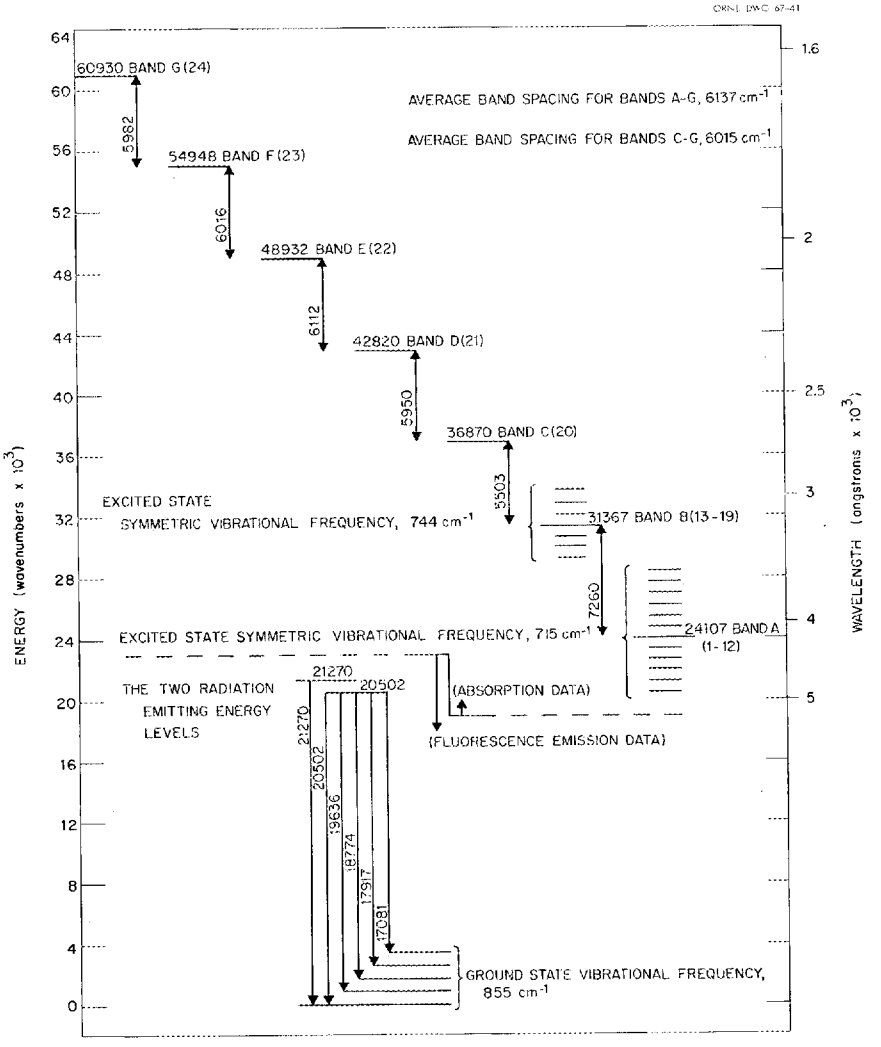

Fig. 14.1. Energy Levels of the Aqueous Uranyl Ion in Perchlorate Media as Determined from the Resolved Absorption and Emission Spectra.

to five excited states that are characterized by regular energy increments.

The fluorescence emission spectrum is shown to result from two excited levels to five vibrational levels in the ground state; however, only 4.66% of the emitted energy is from the higher of the two excited levels. An energy-level diagram in Fig. 14.1 depicts the relative energy levels for the complete ultraviolet and visible absorption spectra and fluorescence emission spectra, as determined from resolution of the bands.

Studies of U(IV) in Perchlorate Media

This work is complicated by the oxidation of U(IV) to U(VI); thus far we have not been able to solve this oxidation problem.

The spectrum (2000 to 13,000 A) of U(IV), in perchloric acid solution is composed of 23 absorption bands of varying intensities and widths. Most of the bands seriously overlap with two or more adjacent bands, and the changes in the observed spectrum cannot be directly associated with particular transitions. The resolved spectra of U(IV) at various stages of hydrolysis can be related to changes in the nature of the U(IV) species that occur as a direct result of hydrolysis. Also, the association between U(IV) and U(VI) can be determined at these stages.

We are trying to obtain a pure $U(ClO_4)_4$ solution from which the hydrolyzed samples can be prepared. Preliminary results show very marked changes in the absorption bands when the $HClO_4$ concentration of a 0.006 *M* U(IV) solution is reduced from 1.2 *M* to 0.045 *M*.

14.2 INSTALLATION AND TESTING OF THE SPECTROPHOTOMETER SYSTEM FOR HIGH ALPHA LEVELS

The modified spectrophotometer, which is installed in a "cold" laboratory for testing, is now operating satisfactorily. This instrument, with its larger scale and specially designed optics, provides about twice the resolution of a standard Cary model 14 spectrophotometer.

Special cell cradles, which have been fabricated for the large cell supports in the cell compartment, permit the placement of standard absorption cells in-beam in the spectrophotometer. These devices allow servicing, calibration, and standard spectrophotometric operations to be carried out. Automatic programmer operations have been checked out, and a Sun-Gun light source unit, Variacs, and lapsed-time meters were added to the ultraviolet and infrared source systems. Initial checkout of the equipment is more than 90% complete. The system is undergoing thermally hot operations with dummy cells prior to operation with uranium and lanthanides. After sufficient testing with the latter, it will be relocated in a high-level alpha laboratory for work with the transuranium elements.

15. Chemical Engineering Research

15.1 PERFORMANCE OF A PROTOTYPE STACKED-CLONE CONTACTOR WITH INTEGRAL PUMPS

The stacked-clone solvent extraction contactor has been developed to perform at relatively high mass-transfer efficiencies at high flow rates with a small volume per stage, which results in extremely short contact times. The device consists of a cascade of liquid cyclones, or hydroclones, each operating with countercurrent flow of the two liquid phases. Since the establishment of an optimum geometrical design, the contactor has been tested with many chemical systems having a broad range of physical properties. It has also been operated with the light phase continuous, although in normal usage a continuous heavy phase is employed. The eventual application of this device to the processing of highly radioactive solutions, where short contact times are desirable, has been the ultimate objective of development. Ease of cleanout and the rapid attainment of steady-state operation are features that make the contactor uniquely attractive for use in short, or varied, processing campaigns (e.g., in a multipurpose plant that is designed for processing a wide variety of fuel elements of different compositions).

This year's efforts have included a study of contactor scaleup. We have also continued to test and evaluate a stainless steel prototype model

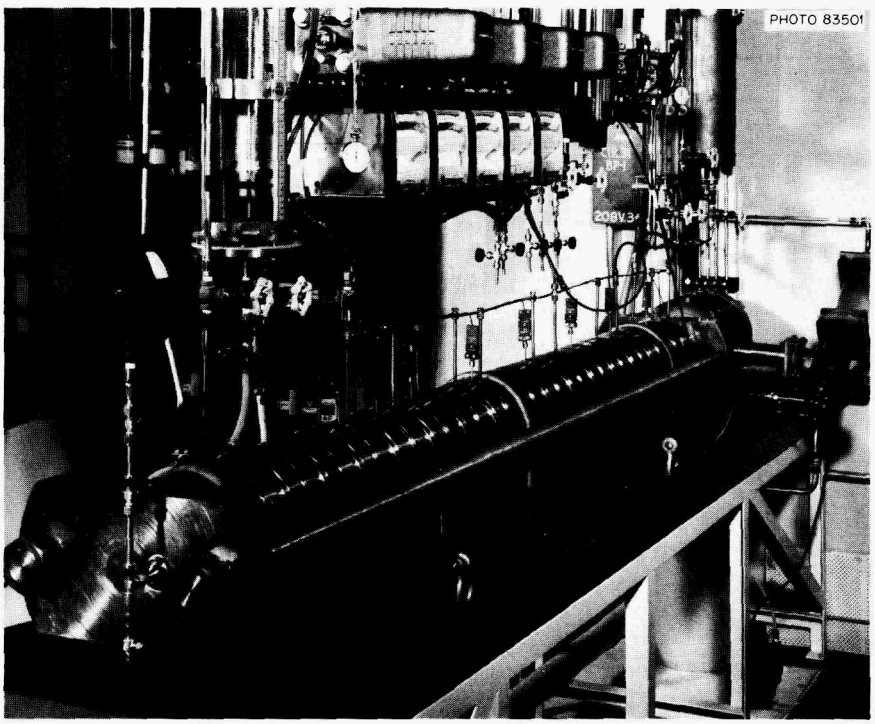

Fig. 15.1. Prototype Stacked-Clone Contactor.

Table 15.1. Performance and Flow Capacity Data for Four Stacked-Clone Contactors

Continuous Phase	Dispersed Phase	Distributing Solute	Physical Properties of Solute-Free Aqueous and Solute-Free Organic Solutions				Mass Transfer Efficiency (%)	Flow Capacity (liters/min)					
			Density Difference (g/cm^3)	Viscosity of Continuous Phase (centipoises)	Viscosity of Dispersed Phase (centipoises)	Interfacial Tension (dynes/cm)		A/O = 1/2	A/O = 1	A/O = 2	A/O = 3	A/O = 5	A/O = 10
One-Half-Scale Experimental Contactor													
1 *M* $NaNO_3$, 0.08 *M* H^+	18% TBP–Amsco	$UO_2(NO_3)_2$	0.255	0.73	1.19	13.5	85.5	0.67	0.84	1.09	1.25	1.44	1.67
0.8 *M* $Al(NO_3)_3$	40% TBP–Amsco	HNO_3	0.305	1.24	1.46	8.9	81.4	0.47	0.58	0.76	0.89	1.08	
Full-Scale Experimental Contactor													
1 *M* $NaNO_3$, 0.08 *M* H^+	18% TBP–Amsco	$UO_2(NO_3)_2$	0.255	0.73	1.19	13.5	65.1	1.72	2.08	2.65	3.08	3.66	4.42
0.8 *M* $Al(NO_3)_3$	40% TBP–Amsco	HNO_3	0.305	1.24	1.46	8.9	47.4	1.28	1.46	1.71	1.86	2.05	
0.1 *M* HNO_3	Diethylbenzene		0.143	0.66	0.73	23.4			1.13	1.38			
1.4-Scale Experimental Contactor													
1 *M* $NaNO_3$, 0.08 *M* H^+	18% TBP–Amsco	$UO_2(NO_3)_2$	0.255	0.73	1.19	13.5	73.9	2.03	2.46	3.16	3.67	4.39	5.35
Full-Scale Stainless Steel Prototype Contactor													
1 *M* $NaNO_3$, 0.08 *M* H^+	18% TBP–Amsco	$UO_2(NO_3)_2$	0.255	0.73	1.19	13.5	64.5	1.67	2.00	2.50	2.85	3.33	3.93
2 *M* HNO_3	30% TBP–Amsco	$UO_2(NO_3)_2$, HNO_3	0.246	0.75	1.37	10.2	*a*	0.75					
0.01 *M* HNO_3	30% TBP–Amsco	$UO_2(NO_3)_2$	0.186	0.75	1.37	10.2	*b*		1.64	2.02			
0.5 *M* $Al(NO_3)_3$, 0.3 *M* H^+	20% TBP–Amsco	$UO_2(NO_3)_2$	0.273	0.94	1.28	12.6	51[c]		0.96				
2 *M* HNO_3	20% TBP–Amsco	$UO_2(NO_3)_2$	0.265	0.66	1.28	13.1	72[d]		(1.20 liters/min at A/O = 0.75)				
0.01 *M* HNO_3	20% TBP–Amsco	$UO_2(NO_3)_2$	0.205	0.66	1.28	13.0	33[e]		1.48				
0.5 *M* $Al(NO_3)_3$, 0.3 *M* H^+	20% DSBPP–DEB	$UO_2(NO_3)_2$	0.180	0.94	0.93	14.5	56[f]		(0.69 liter/min at A/O = 0.75)				
0.03 *M* HNO_3	20% DSBPP–DEB	$UO_2(NO_3)_2$	0.210	0.67	0.93	13.0	27[g]		1.31				
0.5 *M* $Al(NO_3)_3$, 0.1 *M* H^+	Diethylbenzene		0.203	0.94	0.73	27.4		0.97	1.05	1.19	1.36		
Diethylbenzene	0.5 *M* $Al(NO_3)_3$, 0.1 *M* H^+		0.203	0.73	0.94	27.4		2.31	2.06				
0.1 *M* HNO_3	Diethylbenzene		0.143	0.66	0.73	23.4			1.25	1.65			

[a] More than 99.93% extraction in 7 stages.
[b] More than 99.98% stripping in 13 stages.
[c] 99.16% extraction in 7 stages.
[d] 99.83% extraction in 7 stages.
[e] More than 99.99% stripping in 14 stages.
[f] 99.98% extraction in 7 stages.
[g] More than 99.97% stripping in 14 stages.

that is suitable for actual radiochemical in-cell operation.

The 14-stage prototype stacked-clone contactor shown in Fig. 15.1 has undergone continued testing this year. The principal advantage of this unit is the incorporation of all pump impellers on a single shaft. Only one seal is required, and pump-clone transfer ports are very short. The Graphitar shaft bearings also serve as interstage seals. Since there are no gaskets, the individual stainless steel clone modules will be sealed together by welding prior to use with radioactive materials. A two-stage pump having the same design as that of the prototype has operated for more than 16,000 hr without significant wear of the bearings. The contactor itself has operated for about 400 hr. Tests with Purex-type solutions and 30% tributyl phosphate (TBP) in Amsco have been made; five extraction runs (featuring separate aqueous feed and scrub streams) and six stripping runs were concluded. Results showed that the performance of this device (Table 15.1) is comparable with that of the previous standard experimental contactor. The unit is currently being evaluated for use with a ^{233}U recovery scheme involving either 20% TBP in Amsco or 20% di-sec-butyl phenylphosphonate (DSBPP) in diethylbenzene (DEB). Data accumulated from 13 extraction-scrub runs and 9 stripping runs are included in the table.

Operation of the prototype contactor with the light (organic) phase continuous was achieved by employing stage pump pressures to sense an internal interface. This type of operation does not require an external settling section and thus reduces solution inventory. The tests made with 0.5 *M* aluminum nitrate and DEB showed that higher flow capacities are obtained at the lower flow ratios (A/O) when the organic phase is continuous. The capability for handling this mode of operation greatly expands the operating range of the contactor.

15.2 SCALEUP OF THE STACKED-CLONE CONTACTOR

Scaleup of the stacked-clone contactor was studied by evaluating the performance of 0.5- and 1.4-scale experimental units with a sodium nitrate–tributyl phosphate–Amsco system using uranyl nitrate as a distributing solute. Results were compared with those obtained with the standard experimental contactor and the prototype contactor (see Table 15.1). Flooding data for the above-mentioned system are shown in Fig. 15.2.

Since hydroclone flow capacities depend, to some extent, on the cross-sectional area, one would expect the 0.5-scale contactor to permit a flow of only 25% of that for the standard device. However, we obtained a flow capacity of 40% of that of the larger unit, which indicates that the 0.5-scale contactor must be more effective in the separation of small drops. On the other hand, the flow capacity of the 1.4-scale device is only 20% higher, instead of the expected 100% increase over that of the standard contactor. Since solution contact times are determined by stage volumes as well as flow rate, the advantages of the small-scale clones are quite evident. Whereas the contact time per stage was about 3 sec in the standard experimental contactor at flows near flooding and at a flow ratio (A/O) of 3, the contact time in the 0.5-scale contactor was <1 sec for the same conditions. It is apparent that the most effective technique for scaleup will involve manifolding several small clones in each stage.

Mass transfer efficiencies for uranium were somewhat higher in the 0.5-scale contactor than in any of the other units. In a study of 80 mass transfer runs made with a four-stage 0.5-scale contactor, the average efficiency was 85.5%. Comparative data were obtained from 36 runs with a four-stage 1.4-scale contactor, 40 runs with the standard seven-stage experimental contactor, and 78 runs with the prototype contactor.

The impressive performance of 0.5-scale clones was verified by tests made using an alternative chemical system that was characterized by somewhat different physical properties. For instance, from 21 mass transfer runs that demonstrated nitric acid transfer between 0.8 *M* aluminum nitrate and 40% TBP in Amsco, the efficiency was markedly higher (81%) than in the standard contactor (48%).

The results of scaleup studies and of the prototype tests will have a substantial impact on future stacked-clone contactor technology; for example, an array of multiclone stages is envisioned for future prototype models. The existing prototype contactor, which is 8.5 in. in diameter and about 9 ft long and has a nominal flow capacity of 3 liters/min, may be scaled up to a unit having nine 0.5-scale clones per stage and operating at more than 10 liters/min but measuring only 10 in. in diameter and 4.5 ft long.

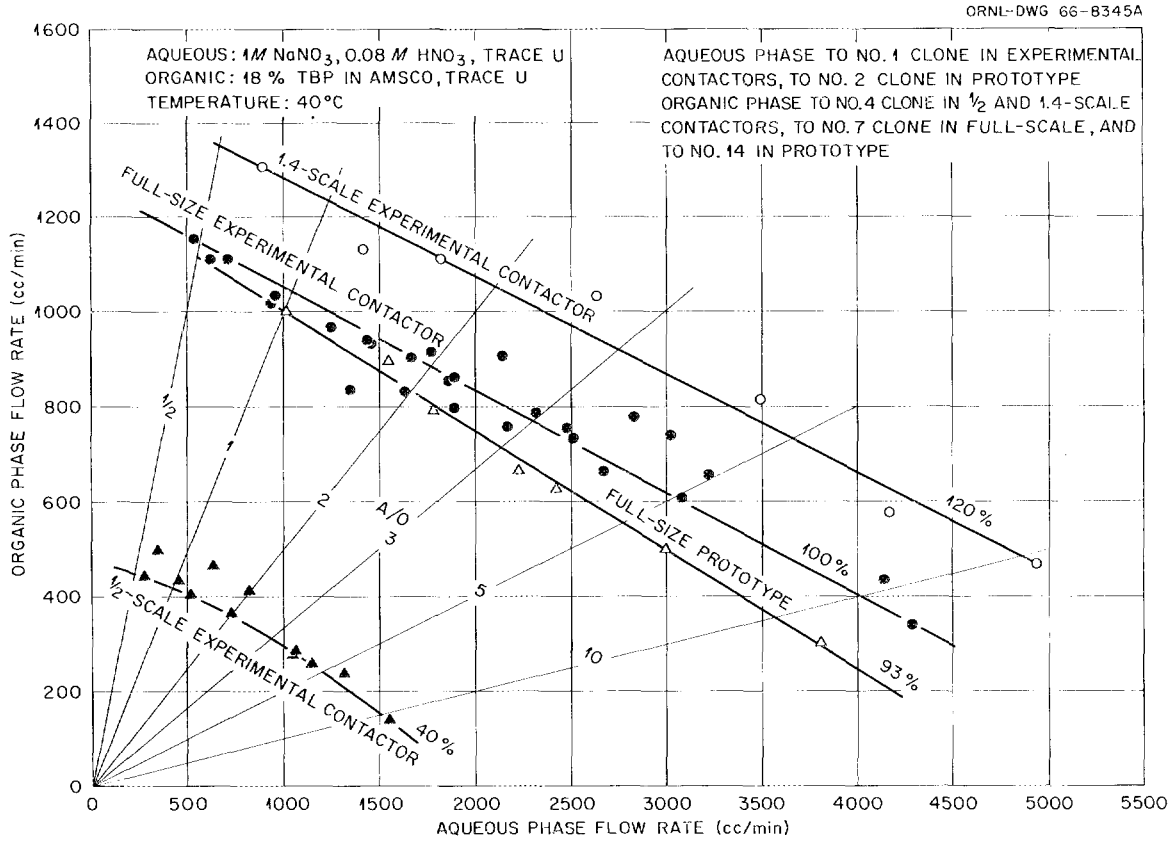

Fig. 15.2. Comparison of Flow Capacities of Four Stacked-Clone Contactors.

15.3 MASS TRANSFER OF WATER FROM SOL DROPLETS DURING MICROSPHERE GELATION

The sol-gel process, developed at ORNL, is a method of preparing a wide variety of ceramic fuel materials for nuclear reactors. Compared with more conventional preparation procedures, this method has the advantage of requiring a much lower calcination temperature for particle densification. Recently, the sol-gel program has emphasized the preparation of spherical particles (microspheres) of thorium-uranium oxides. Pyrolytic-carbon-coated microspheres of this type in the diameter size range of 200 to 400 μ are the proposed fuel materials for certain high-temperature gas-cooled reactor designs.

The microspheres are prepared by dispersing the appropriate sol at room temperature in an immiscible organic liquid that extracts small amounts of water. The sol droplets must be suspended in the organic phase until enough water is extracted from the aqueous sol to cause gelation. After drying, the gelled spheres are calcined at 1150°C to achieve oxides having densities within 1% of theoretical; these spheres are then coated with pyrolytic carbon.

The time required for the gelation of sol droplets suspended in an organic solvent has been estimated by visual observation; however, no attempt has been made to correlate the exact time with the concentration of the sol, or droplet size, or organic-phase properties. A basic program has been undertaken to study the mechanism of mass transfer from single thoria droplets suspended in flowing 2-ethyl-1-hexanol. The principal variables in the initial stages of investigation will be the diameters of the sol drops (0.05 to 0.2 cm), sol molarity (0 to 3 *M*), and water concentration in the bulk solvent (0 to 0.02 g/cm^3). Later, mass transfer studies may include the effects of different sol preparations (urania and thoria-urania sols), and surfactant concentrations in the organic phase.

An 8-in.-long tapered column (machined from a block of Plexiglas) with a convergent-divergent

flow channel has been employed in these studies. In experimental operation a vertical velocity profile is developed and held stationary along the central axis of the flowing divergent channel; the sol droplets that form are observed to maintain near-spherical shapes during the gelation process, and they exhibit no detectable horizontal motion. Observation of the forming process with photographic equipment and with optical magnifications of 20 to 40× is feasible; thus, through the use of photographs, the amount of water transferred from the sol droplet to the organic phase can be determined by measuring changes in drop diameters with time. (The reverse process, transfer of 2-ethyl-1-hexanol into the sol droplet, will be neglected since the solubility of organic in water is an order of magnitude less than the solubility of water in organic.) As the droplet shrinks and densifies, the fluidizing flow is steadily increased to maintain horizontal alignment between the droplet and the optical system.

From the decrease of droplet diameter with time, mass transfer coefficients can be calculated for bulk solvents with varied water contents. It has been shown that the experimental data can be correlated by a model which assumes that the mass transfer rate is controlled by the diffusion of water through an organic film surrounding the drop. At some stages of the gelation process the diffusion of water within the drop itself may contribute a significant resistance to mass transfer; however, the relative effect of these different mechanisms can be analyzed by studying separately the rates of water extraction from sol droplets and from pure-water droplets.

15.4 HYPERFILTRATION OF SPENT SULFITE LIQUOR WITH A SELF-REJECTING MEMBRANE[1]

Hyperfiltration using dynamically cast membranes is a new technique that is potentially useful for various radiochemical applications such as concentration of low- and intermediate-level wastes. We have been participating in its development by assisting in programs with similar applications, for example, the concentration of dissolved solids in paper-mill wastes.

In the pulp and paper industry one of the principal chemical pulping processes is the sulfite process, in which the wood is cooked in sulfurous acid and a salt (usually the calcium salt) of this acid. If the dissolved substances could be separated from the spent sulfite liquor, the water could be recycled and the concentrated liquor could be prepared for disposal by evaporation and burning, thereby eliminating one industrial source of water pollution.

Hyperfiltration experiments by the Pulp Manufacturers Research League, using spent sulfite liquor and cellulose acetate membranes, resulted in excellent separation of dissolved solids (mostly lignin) and water, with a solids rejection of 97.5 to 99%. However, product fluxes were rather low.[2]

Dynamically formed "membranes," under study at ORNL,[3] have the potential advantage of high production rates. Usually these are formed by forcing feeds containing additives of a colloidal nature through porous bodies. Instances have been observed where no additive was required to obtain rejection. Examples of such self-rejecting systems are Th(IV), Fe(III), and humic acid in aqueous solutions.[3]

A self-rejecting membrane was formed with calcium-base spent sulfite liquors supplied for this study by A. J. Wiley and B. F. Lueck of the Pulp Manufacturers Research League. The concentration range of interest is 1 to 10 wt % dissolved solids. The porous support structures used were two different types of carbon tubes, which were manufactured for use as electrodes, and three grades of ceramic tubes, which are sold commercially as polishing filters.

When the type 03 ceramic tube (median pore diameter 0.9 μ) and type 6C carbon tube (median pore diameter 0.4 μ) were operated continuously with 1% liquor for 340 hr, permeabilities decreased and rejections increased significantly. For the ceramic tube, the permeability and the rejection were 6.5×10^{-3} cm min^{-1} atm^{-1} and 86% (400 psig and 35°C) at the beginning; after 300 hr they had leveled off at 1.8×10^{-3} cm min^{-1} atm^{-1} and

[1] Members of the Director's and Chemistry Divisions, the MIT Practice School, and Fida Butt, guest scientist from Pakistan, also participated in this work.

[2] A. J. Wiley, A. C. F. Ammerlaan, and G. A. Dubey, "Application of Reverse Osmosis to Processing of Spent Liquors from the Pulp and Paper Industry," Research Conference on Reverse Osmosis, sponsored by the Office of Saline Water, San Diego, Calif., Feb. 13–15, 1967.

[3] K. A. Kraus, H. O. Phillips, A. E. Marcinkowsky, J. S. Johnson, and A. J. Shor, *Desalination* 1, 225 (1966).

96% respectively. Corresponding values for the carbon tube were 2.7×10^{-3} cm min^{-1} atm^{-1} and 70%, and 1.2×10^{-3} cm min^{-1} atm^{-1} and 90% at the same pressure and temperature. During this period, conditions were not held constant; pressure, temperature, and feed circulation rate were varied. These final permeabilities correspond to product rates of 17.5 gal day^{-1} ft^{-2} for the ceramic tube and 12 gal day^{-1} ft^{-2} for the carbon tube at 400 psig. After 300 hr of operation, the temperature was increased to 60°C, and product rates increased to 29 and 19 gal day^{-1} ft^{-2} for the ceramic tube and the carbon tube, respectively, at 400 psig. Rejections were not affected.

16. Reactor Evaluation Studies

This program, supported jointly by the Reactor Division and the Chemical Technology Division, consists of studies of various advanced reactor and fuel-cycle systems to determine engineering and economic feasibility. The work in this Division during the past year included cost studies of shipping fresh and spent nuclear fuel, processing spent fuel (including final waste disposal), and preparing various virgin and recycle fuel materials (oxides, metals, fluorides, etc.). In addition, computer codes were developed for estimating and analyzing the overall cost of nuclear power, for calculating decay characteristics of fission products in spent nuclear fuel, and for optimizing the size, date of construction, and location of processing plants in an expanding nuclear economy. We have prepared formal cost estimates in conjunction with evaluations of the HWOCR (Heavy-Water-Moderated, Organic-Cooled Reactors) and several desalination reactor proposals,[1,2] and in support of the evaluation programs assigned to the USAEC Fuel Recycle Task Force and the Systems Analysis Task Force.[3]

16.1 STUDIES OF THE COST OF SHIPPING REACTOR FUELS

Shipping costs for various fresh, spent, and recycled reactor fuels were estimated during the year. This was done as part of a continuing effort to develop fuel cycle cost estimates for reactor evaluation purposes. The estimating methods used, based on computer programs MYRA and NORA, have been described in previous reports.[4,5] Basic changes in the AEC shipping regulations took place in July 1966.[6] The new regulations are generally more lenient with regard to the "loss of coolant" condition and the setting of temperature restrictions on the cask; this has eased the problem of heat removal from the cask for some irradiated fuels, notably fast-breeder fuels. For most other fuels, the change in shipping cost resulting from the new regulations is negligible when compared with the uncertainties in the estimate.

Summary of Estimates of Shipping Costs

Table 16.1 summarizes some of the shipping costs that were estimated for some of the reactors that are being evaluated in the current AEC reactor systems analysis study.

Table 16.2 shows the shipping costs that were estimated for irradiated HTGR fuel elements of the hexagonal block type, 31.2 in. long and 14.2 in. across flats.

A shipping cost of about $11 per kilogram of uranium plus plutonium was estimated for the spent fuel from a liquid-metal-cooled fast breeder reactor of the type designed by the General Electric Company.[7,8] This cost is based on the assumption that the fuel elements are disassembled prior to

---

[1] P. R. Kasten *et al., An Evaluation of Heavy-Water-Moderated, Organic-Cooled Reactors*, ORNL-3921 (January 1967) and ORNL-3921 Supplement (to be issued).

[2] R. P. Hammond *et al., Nuclear Desalination Program Annual Progress Report for Period Ending October 31, 1966*, ORNL-4087 (March 1967).

[3] *Civilian Nuclear Power — the 1967 Supplement to the 1962 Report to the President*, USAEC (February 1967).

[4] R. Salmon, *A Computer Code for Calculating the Cost of Shipping Spent Reactor Fuels as a Function of Burnup, Specific Power, Cooling Time, Fuel Composition, and Other Variables*, ORNL-3648 (August 1964).

[5] R. Salmon, *Estimation of Fuel-Shipping Costs for Nuclear Power Cost-Evaluation Purposes*, ORNL-3943 (March 1966).

[6] Title 10, Part 71 in *Federal Register*, July 22, 1966.

[7] M. J. McNelly, *Liquid Metal Fast Breeder Design Study (1,000 MWe UO_2-PuO_2 Fueled Plant)*, GEAP-4418.

[8] K. P. Cohen and G. L. O'Neill, *Proceedings of the Conference on Safety, Fuels, and Core Design in Large Fast Power Reactors, October 11–14, 1965*, ANL-7120, pp. 185–204.

Table 16.1. Summary of Costs for Shipping Spent Fuel, Fresh Fuel, and Recycled Fuel

Reactor	Fuel Element Design	Burnup (Mwd/metric ton)	Year	Cooling Time (days)	Shipping Cost (dollars per kilogram of heavy metal)		
					Spent Fuel	Fresh Fuel	Recycled Fuel
PWR	204-rod cluster	33,000	1970	150	4.01	0.65	1.10[a]
		33,000	1980	150	3.37	0.50	0.95[a]
BWR	49-rod cluster	27,500	1970	90	3.23	0.65	1.10[a]
		27,500	1980	90	2.90	0.50	0.95[a]
HWOCR – UC (slightly enriched)	37-rod cluster	17,000	1975	120	2.80	0.50	
		17,000	1980	120	1.50	0.40	
HWOCR – ThO_2	37-rod cluster	20,000	1975	120	3.30	0.50	1.80[b]
		20,000	1980	120	2.91	0.40	1.40[b]
HWOCR – Th metal	4-ring nested cylinders	20,000	1975	120	4.30	0.50	2.00[b]
		20,000	1980	120	3.77	0.40	1.60[b]
HWOCR – U (natural U metal)	Nested cylinders	8,200	1975	120	1.25	0.50	
		8,200	1980	120	1.12	0.40	
HWBLWR[c]	19-rod cluster	9,100	1975	120	1.80	0.45	
		9,100	1980	120	1.67	0.40	

[a]Pu recycle.

[b]^{233}U recycle.

[c]Boiling-light-water-cooled, heavy-water-moderated, natural-uranium-fueled reactor.

Table 16.2. Spent-Fuel Shipping Costs – HTGR Backup Design

Casks shared among 15 reactors

Cooling time, days	40	60	90	120
Weight, thousands of pounds	240	229	219	213
Shipping cost, dollars per kilogram of uranium plus thorium	27.89	26.61	25.49	24.89

shipment; however, since the cost of disassembly has not yet been evaluated, it has not been included in the estimated cost.

Shipping costs of $18 to $20 per kilogram of uranium plus plutonium were estimated for this same spent fuel without disassembly, assuming that the complete fuel assembly is "canned" in a welded steel container filled with sodium. This shipping concept has been discussed with the AEC Division of Materials and Licensing.

All costs shown in this section are based on a round-trip shipment, 1000 miles each way.

16.2 COMPUTER CODE FOR STUDIES OF OVERALL POWER COSTS

Previous reports[9–11] described a computer code (POWERCO) for calculating the cost of electricity that is produced by nuclear power stations. In

[9]*Chem. Technol. Div. Ann. Progr. Rept. May 31, 1965*, ORNL-3830, pp. 268–69.

[10]*Chem. Technol. Div. Ann. Progr. Rept. May 31, 1966*, ORNL-3945, p. 240.

[11]R. Salmon, *A Procedure and a Computer Code (POWERCO) for Calculating the Cost of Electricity Produced by Nuclear Power Stations*, ORNL-3944 (June 1966).

writing this code it was assumed that all the cash expenditures of the project were known, except for the Federal income tax, which was calculated by the code. Annual cash expenditures for state and local taxes, interim replacements, and property insurance were required as input. The code also calculated fixed charge rates on depreciable and nondepreciable capital; these were defined in accordance with the Oyster Creek report[12] to include only recovery of investment, return on investment, and Federal income tax. State and local taxes, interim replacements, and insurance were accounted for as expenses in the calculation of the power cost but were not included in the fixed charge rates. However, because fixed charge rates given in various sources frequently include these items, it was felt that POWERCO should be able to display fixed charge rates calculated on this basis. This capability has now been incorporated into the code. The revised code (POWERCO-35) will permit a critical evaluation of the breakdown of fixed charge rates into their components and will facilitate the setting of appropriate fixed charge rates for evaluation studies.

As an example of the results observed thus far, the 3.0 to 3.4% that is conventionally charged to Federal income tax for investor-owned power companies[13] was found to be too high for new projects; the proper value, using sum of the years' digits depreciation, is about 1.0 to 1.8%, depending on the rates of return, debt structure, and other factors.

A report covering this work is in preparation.[14]

16.3 PHOEBE FISSION PRODUCT CODE

A computer code, PHOEBE, was written to calculate the decay properties of mixed fission products resulting from the fission of ^{235}U.[15] Fission product beta and gamma activity and spectra are calculated for these fission products as a function of power, irradiation time, and decay time. Either constant or variable power may be specified for the reactor operation period.

A total of 12 gamma energy groups are used to describe the gamma spectra. The computer output is in terms of gamma photon emission rates for each group, gamma energy emission rates for each group, total gamma emission rate, total gamma energy emission rate, beta particle emission rate, total average beta energy emission rate, and total energy release rate.

The code contains a permanent data section that describes the release rates as a function of time after fission. The report[15] presents a discussion of these data functions and describes how they were obtained, how they are used, and how they may be modified for use in specific instances. It also presents other detailed discussions that include: gamma photon and energy release; beta particle and energy release; the fission rate function for variable power operation; the data library; input preparation, operation, and output; sample problems; and a FORTRAN list of the code.

An earlier version of this code was released on a temporary, unpublished basis several years ago. However, the variable-power section has been completely rewritten, and those who have been using the old form of the code should either replace their old decks with the new version or recompile any programs that use PHOEBE as a subroutine.

16.4 COST STUDIES OF FUEL PREPARATION AND PROCESSING FOR NEW AEC CIVILIAN NUCLEAR POWER EVALUATION

Cost estimates for fuel-material preparation (chemical conversion) and for spent-fuel processing were made in support of the Fuel Recycle Task Force, the Systems Analysis Task Force, and the various reactor task forces taking part in the USAEC study whose purpose is to update the 1962 assessment of civilian nuclear power and to extend it beyond the year 2000.[3] Our previous estimates of fuel cycle costs for advanced converter reactors[1,9,10,16] were revised to reflect the change from a ground rule which specified the use

[12] *Report on Economic Analysis for Oyster Creek Nuclear Electric Generating Station*, Jersey Central Power and Light Company (February 1964).

[13] *Costs of Nuclear Power*, USAEC Report TID-8531 (Rev.) (January 1961).

[14] R. Salmon, *A Revision of Computer Code (POWERCO) (Calculation of Cost of Electricity Produced by Nuclear Power Stations)*, ORNL-4116 (April 1967).

[15] E. D. Arnold, *PHOEBE – a Code for Calculating Beta and Gamma Activity and Spectra for ^{235}U Fission Products*, ORNL-3931 (July 1966).

[16] M. W. Rosenthal *et al.*, *A Comparative Evaluation of Advanced Converters*, ORNL-3686 (January 1965).

of single-purpose plants that are designed to match an economy of 15,000 Mw (electrical) of the particular reactor type being evaluated; under the new rule it is necessary to consider that the size of the nuclear economy, as well as the relative number of various reactor types, changes with time. This new basis calls for prediction of fuel-cycle costs as a function of time, and thus presents a complex and controversial task. We have made estimates of capital and operating costs for single-purpose plants with daily processing capacities of up to 30 metric tons/day for HWOCR-U and HWBLWR fuels, up to 15 metric tons/day for BWR-PWR and HWOCR fuels, and up to 10 metric tons/day for HTGR and FBR (mixed core-plus-blanket) fuels.

Thus the largest-size processing plants would service the equivalent of 60,000 to 120,000 Mw (electrical) of a given reactor type. These estimates must be converted into predictions of costs vs time by making assumptions concerning: how the fuel loads will increase with time; how the preparation and processing industries will expand with time (whether many small plants or fewer large plants); and what the costs of investment capital will be for these industries. This work is not yet complete; however, it is expected that the results will be published as a report of the AEC Fuel Recycle Task Force by the end of 1967. Our cost optimization studies in support of this work are reported in Sect. 16.5.

16.5 OPTIMIZATION OF THE SIZES, DATES OF CONSTRUCTION, AND LOCATIONS OF PROCESSING PLANTS IN AN EXPANDING ECONOMY

The projected growth of nuclear electric power production to a very large scale, 150,000 Mw (electrical) by 1980 and on the order of 10^6 Mw (electrical) by 2000, creates a need for a mathematical model to evaluate growth patterns for nuclear fuel-cycle systems in the interest of cost minimization. We are currently using a simplified mathematical model and are developing more sophisticated models, as described below.

Linear-Growth-Rate Model

For the present we are using a simplified linear-growth-rate model of the spent-nuclear-fuel processing economy to guide our thinking on plant sizing and timing. This model, an improvement of the one described in last year's report,[10] assumes that fuel is backlogged for y years (incurring storage and inventory costs), at which time a plant of capacity mx comes on stream. The cycle is repetitive, with plants of size mx coming on stream every x years starting at y. For this model the total present-worth-levelized processing cost, including fuel inventory costs, per unit amount of fuel is given by Eq. (1):

$$C_p = g + \frac{(kr^2/m)\,(my^2/2)^b + (Kr^2/m)\,(mx)^a\, e^{-ry} - (V_s - g)\,(2rye^{-ry} + e^{-2ry} - 1)}{(1 - e^{-rx})}, \quad (1)$$

where

C_p = total processing cost per unit of production,

g = that part of unit processing cost which is constant (e.g., expendable materials proportional to production rate),

k = capitalized cost of building and operating a fuel-receipt-and-storage (backlogging) facility of unit capacity, such that $k(my^2/2)^b$ is the capitalized cost of building and operating (indefinitely) a backlogging facility that accumulates fuel for y years before processing begins,

m = rate of growth of spent-fuel production, units per year per year,

r = cost of money, the effective discount (continuous) interest rate for the present-worth calculation, fraction per year,

b = cost-scaling factor for backlogging facility, dimensionless fraction,

K = capitalized cost of building and operating a processing plant of unit annual capacity, such that $K(mx)^a$ is the capitalized cost of building, operating, and replacing (indefinitely) a processing plant of throughput capacity mx,

a = cost-scaling factor for processing plant,

V_s = unit sale value of recovered fuel.

Table 16.3. Processing Costs,[a] in Dollars per Kilogram, for Selected Values of Backlogging Time (y) and Plant Size (mx)

x (years)	$\frac{y}{x}$ = 0	0.05	0.10	0.15	0.20	0.25	0.50
1	30.42	31.04	31.37	31.62	31.83	32.02	32.75
2	20.71	21.16	21.35	21.49	21.60	21.69	22.12
3	16.94	17.29	17.41	17.49	17.54	17.59	18.01
5	13.67	13.90	13.93	13.92	13.93	13.96	14.84
10	11.34	11.37	11.24	11.19	11.26	11.49	15.43
15	10.96	10.81	10.60	10.64	11.00	11.73	20.64
16	10.96	10.78	10.56	10.64	11.09	11.95	22.00
17	10.98	10.76	10.54	10.66	11.20	12.21	23.44
18	11.02	10.76	10.54	10.71	11.35	12.51	24.95
19	11.06	10.77	10.55	10.77	11.53	12.85	26.53
20	11.12	10.78	10.57	10.85	11.74	13.23	28.16
25	11.49	10.96	10.81	11.51	13.14	15.64	36.90

[a]Basis: $a = 0.35$; $b = 0.35$; $r = 0.12$/year; $m = 300$ metric tons/(year)^2; $V_s = \$100{,}000$/metric ton; $g = \$500$/metric ton; $k = 2.66 \times 10^6$ \$/(metric ton)$^{0.35}$; $K = 9.58 \times 10^6$ \$/(metric ton/year)$^{0.35}$.

Table 16.3 shows the results of a typical calculation. It is based on light-water-reactor fuel value and processing-cost estimates, with a growth rate of 300 metric tons/(year)^2 (predicted for the 1970's), and a discount rate of 12%/year (applicable to common ownership of fuel, backlogging facility, and processing plant by a fuel-cycle corporation with a "medium" cost of money). This growth rate is approximately equivalent to 1.0 metric ton per day per year, so that in this case x is equal to the processing plant capacity in metric tons/day. In this model the value of y cannot exceed 0.5x. The cost drops from about \$31/kg in a 1.0-metric ton/day plant (relatively independent of backlogging time) to less than one-half of that in a 5.0-metric ton/day plant (still relatively insensitive to backlogging time in this case) and to little more than one-third of the 1-metric ton/day cost at the optimal conditions of $y = 1.7$ to 1.8 years and $x = 17$ to 18 years (= 17- to 18-metric ton/day plant). The optimum is quite "flat"; for example, a 10.0-metric ton/day plant with 1.0 year of backlogging gives a levelized unit cost only 6% higher than the minimum, and might be preferable from the risk point of view.

Linear and Dynamic Programming Models

We are developing a linear-programming model that will allocate spent fuel from H sources to reprocessing plants to be constructed at K potential sites so as to minimize present-worth expense, if the following are specified:

1. a forecast over T time periods of the power demands to be placed on the reactors that generate the spent fuels,
2. the processing and capital economies that result from the construction of fewer and larger reprocessing plants,
3. the transportation economies that result from construction of numerous reprocessing plants.

The basic information to be obtained from the model consists of the optimal sizes, dates of construction, and locations of reprocessing plants.

In considering the trade-off between the sizes of plants and the number of plants necessary to meet demand, the model will:

1. recognize the nonlinearity between the capital required to construct a plant and the size of the plant;

2. recognize the individual unit costs for shipping fuel between each of the H sources and the K potential plant sites;
3. allow fuel to be inventoried, as optimal, at sources and reprocessing sites; this, of course, allows plant construction to be deferred until a larger and more efficient plant can be used at an economical percentage of capacity;
4. accept the existence of initial and final inventories;
5. readily permit a respecification of the number of spent fuel sources, the number of potential reprocessing sites, and the number of time periods in the planning horizon;
6. be limited, in at least its initial formulation, to regarding all spent fuels as a homogeneous entity no matter what types of reactor might actually be in service;
7. treat unit direct processing costs and unit inventorying costs as independent of volume but not necessarily independent of location. It is probable that this restriction will be eliminated after some use of the model.

There are a number of optimization techniques that could have been used as the basis of the model. One of these is dynamic programming, which is particularly well suited to a problem, such as this, containing nonlinearities and even discontinuities.[17] L. Thiriet and co-authors, in particular, have made extensive use of dynamic programming in the analysis of fuel reprocessing plants in France.[18] However, dynamic programming suffers from two disadvantages: (1) any problem except the smallest requires the use of a computer for solution, which in turn requires the writing of a custom program for each type of problem, and (2) the dimensionalities of "real-world" problems often exceed the memory capacity of even the largest computers. The U.S. spent-fuel problem falls in the latter category; moreover, the results are needed quickly. For these reasons, dynamic programming was not chosen as the basis of the present model.

Another technique that could have been used as the basis of the optimization is the simulation of the fuel reprocessing facilities as a stochastic system. Such simulations have become very extensively used in recent years because they allow systems to be treated on a probabilistic, rather than a deterministic, basis. Certainly the probabilistic assignment of demands, shipping costs, capital costs, processing costs, and inventorying costs would be appropriate amidst all the uncertainties in the spent-fuels problem. Again, however, the development of a custom simulation algorithm for this problem might well be prohibitive with respect to elapsed time, computer hardware, and programming and execution time.

The third optimization technique considered (the method chosen) was linear programming. A major factor in the decision for its selection was the present existence of computer programs that would handle problems of the magnitude of the spent-fuels problem. A second factor was that, in any event, the technique used would have to contain an embedded transportation linear program (LP) to handle the fuel movements between sources and reprocessing sites. A conventional LP will not, however, handle the nonlinearities that must be recognized between plant capital and size. Two modifications of a conventional LP are possible in order to cope with nonlinearities. One of these is separable programming, which interpolates on line segments that approximate the nonlinear function.[19] The other modification involves solving a conventional LP where capital cost coefficients are assigned initially, based on guesses as to what the plant sizes will be. The resultant plant sizes are used to determine new capital cost coefficients from the cost-size function, and the new coefficients are used in the LP to get revised values for plant size, etc., until the plant sizes are identical in two successive linear programming solutions.

The linear programming model contains three types of constraints: material balances at spent-fuel sources, material balances at reprocessing sites, and reprocessing capacities at sites The

[17] R. E. Bellman and S. E. Dreyfus, *Applied Dynamic Programming*, Princeton University Press, Princeton, N.J., 1962.

[18] L. Thiriet and J. Gaussens, "A Method for the Choice of Allocations and Capital Investments," paper presented at Fourth Operational Research Conference, Massachusetts Institute of Technology, Boston, Mass., Aug. 29–Sept. 2, 1966.

[19] C. E. Miller, *The Simplex Method for Local Separable Programming*, ed. by Graves and Wolfe, McGraw-Hill, New York, 1963.

model has five types of activity vectors: (round-trip) shipments between sources and sites, amounts of fuel inventoried at sources, amounts of fuel inventoried at sites, reprocessing rates at sites, and capacity increases at sites. Our reference runs of the LP will be made using eight spent-fuel sources, eight potential reprocessing sites, and a planning horizon of 60 one-year time periods. These parameters are selected to fit a 60-year projection of power demand made by the USAEC and the Federal Power Commission which assumes that the United States is comprised of eight regions. The model will consider each region as a single source and allow no more than one reprocessing site per region. These parameters, in conjunction with the use of three line segments in the plant capital-cost–size function, lead to a model having 1920 row constraints and 7184 column vectors. We are using the IBM-MPS package for the IBM-360 computer, with a capability of 4000 constraints.

17. Preparation and Properties of Actinide-Element Oxides

The purpose of this program is to determine the microstructural, surface-chemical, and colloidal-chemical properties that control the behavior of thoria, urania, and other metal oxides of importance in the development of sol-gel processes. Techniques that were developed for thoria were also used for urania; in the future they will be extended to plutonia and other actinide oxides.

17.1 FUNDAMENTAL STUDIES OF THORIA SOLS AND GELS

Electrophoretic Studies

Studies of the electrophoretic behavior of five different thoria sols (Table 17.1), using a moving boundary apparatus, showed at least two different electrophoretic bands at ionic strengths of the intermicellar fluid ($HNO_3 + NH_4NO_3$) of 3×10^{-4} and 3×10^{-3}; however, only one band is observed at an ionic strength of 0.01. Both the shape of the electrophoretic pattern and the mobilities of the bands were essentially independent of pH between 2.0 and 3.5. An increase in thoria concentration caused an increase in the area under the secondary electrophoretic peak (as observed by schlieren optics). It was shown that the multiple bands observed are not due to any inhomogeneity of the thoria sol particles. Instead, the results are explained in terms of moving-boundary theory for strong electrolytes; that is, the true boundary gives the correct mobility for thoria, while the additional "false" boundaries are attributed to Th^{4+}

Table 17.1. Sol Preparation Procedures

Sol Designation	Particle Radius (A)	Procedure
OXO-500	35[a]	Precipitated as oxalate from $Th(NO_3)_4$ solution, calcined to the oxide by heating in air at 500°C for 4 hr, peptized in HNO_3 to adjust nitrate ratio and to remove possible CO_2 contamination, and finally dispersed in H_2O and dialyzed
OXO-650	58[a]	Same procedure as above, except calcined at 650°C for 4 hr
SDN	35[a]	Thoria prepared by steam denitration of thorium nitrate
NH_3	18[a]	Precipitated as the hydrous oxide by NH_4OH addition to $Th(NO_3)_4$ solution, peptized and aged in concentrated NH_4OH to facilitate crystal growth and remove possible CO_2 surface contamination, washed by centrifugation, and dialyzed
NH_3-R	10[b]	Precipitated as the hydrous oxide by the addition of 2 *M* $Th(NO_3)_4$ to concentrated NH_4OH, washed by centrifugation, and dialyzed

[a]Determined by x-ray line broadening.

[b]Determined by electron photomicrographs.

and other charged thoria species that are present in the intermicellar fluid.

All operations following the initial precipitation of the thoria, including the loading of the electrophoresis cell, were conducted in a glove box filled with dried argon. Moving-boundary electrophoresis studies were made using a standard Tiselius cell and a Beckman model H electrophoresis-diffusion instrument. Combined schlieren and Rayleigh interference optics were used for observing the boundaries. In general, the displacement of each boundary was found to be linear with time, and the displacement per coulomb appeared to be independent of electrical field strength.

Table 17.2 gives the apparent mobilities of the five thoria sols as determined in these experiments. Increasing the ionic strength decreased the resolution of both the descending and the ascending boundaries, as is normally found in electrophoresis of mixtures. However, the reduction in the mobilities of both the faster-ascending and -descending boundaries was greater than would be expected from the usual effect of ionic strength on electrophoretic patterns. At an ionic strength of 0.01, only one boundary was observed in the descending limb for all five thoria sols studied. In three of the sols the faster-ascending boundary was reduced such that it contained $\leq$3% of the total area; in the other two it was absent. A number of minor bands, particularly in the ascending limb, were observed at the lower ionic strengths.

Measurement with varying pH (3.5 to 2.0) indicated that ionic strength, rather than pH, is the important variable controlling the electrophoretic behavior. An increase in thoria concentration caused a marked increase in the relative area of the faster-descending boundary; however, the relative area of the faster-ascending boundary decreased.

Table 17.2. Apparent Mobilities of Thoria Sols[a] at pH 3.5

Sol	Ionic Strength[a]	Apparent Mobilities ($cm^2\ v^{-1}\ sec^{-1}$)			
		Descending Boundaries		Ascending Boundaries	
		Main	Secondary	Main	Secondary
		$\times 10^{-4}$		$\times 10^{-4}$	
OXO-500	1.01×10^{-2}	2.9	*b*	3.0	3.3
	3.16×10^{-3}	2.9	3.5	3.6	4.1
	3.17×10^{-4}	2.5	8.9	8.4	*d*
OXO-650	1.01×10^{-2}	3.0	*b*	3.0	*b*
	3.16×10^{-3}	3.2	4.1	3.1	3.9
	3.17×10^{-4}	3.5	7.2, 2.6	5.6	~5.5
SDN	1.01×10^{-2}	2.9	*b*	2.6	2.8
	3.16×10^{-3}	3.1	4.0	3.4	3.9
	3.17×10^{-4}	3.7	7.7	5.2	5.8[d]
NH_3	1.01×10^{-2}	2.5	*c*	2.5	*c*
	3.16×10^{-3}	2.4	*c*	2.4	*c*
	3.17×10^{-4}	2.4	*c*	2.3	*c*
NH_3-R	1.01×10^{-2}	2.9	*b*	4.0	3.8
	3.16×10^{-3}	3.0	3.4	6.8	6.7
	3.17×10^{-4}	1.1	7.8	19.1	*d*

[a]Intermicellar fluid is $HNO_3 + NH_4NO_3$.

[b]None observed.

[c]None observed, but electrophoretic pattern very poor.

[d]Several minor bands observed.

We were not able to account for the multiple boundaries by assuming inhomogeneity in the sol (i.e., mixtures either of different crystallite habits or of different sizes or shapes of aggregates). The cubic and octahedral faces of thoria crystals have comparable energies[1] but different spacings between thorium atoms; hence cubic and octahedral crystallites might have different charge densities. However, this explanation would not suffice to account for the ionic strength dependences; moreover, electron photomicrographs showed similar sizes and predominantly similar cuboctahedral habits in separated electrophoretic fractions. Different sizes and shapes of colloidal aggregates could cause different electrophoretic velocities;[2] however, these velocities would differ only by a factor of ≤ 2 in the case of nonconducting particles, whereas our observed mobilities differed by factors as great as 3. In addition to the electron photomicrographs, x-ray line broadening and BET area measurement, which use different averaging techniques, gave essentially identical values, thereby indicating a narrow size distribution.

The moving boundary theory of Svensson[3] and Dole[4] for strong electrolytes can account for the additional moving boundaries if an additional charged species (besides the charged particles, H^+, and NO_3^-) is present. We found that small amounts of Th^{4+} ($\sim 10^{-4}$ *M*) in the intermicellar fluid fulfill this requirement. Calculated mobilities for the faster-descending boundaries, using Svensson's equation,[3]

$$V = \frac{C_1\mu_2\mu_3 + C_2\mu_1\mu_3 + C_3\mu_1\mu_2}{C_1\mu_1 + C_2\mu_2 + C_3\mu_3},$$

where C is equivalent concentration and μ is mobility of these indexed ions, agreed reasonably well with the mobilities that were observed, even though the effect of the charged particles was neglected (Fig. 17.1). The additional minor boundaries at high pH are possibly due to other thorium species[5] that are in solution in the intermicellar fluid.

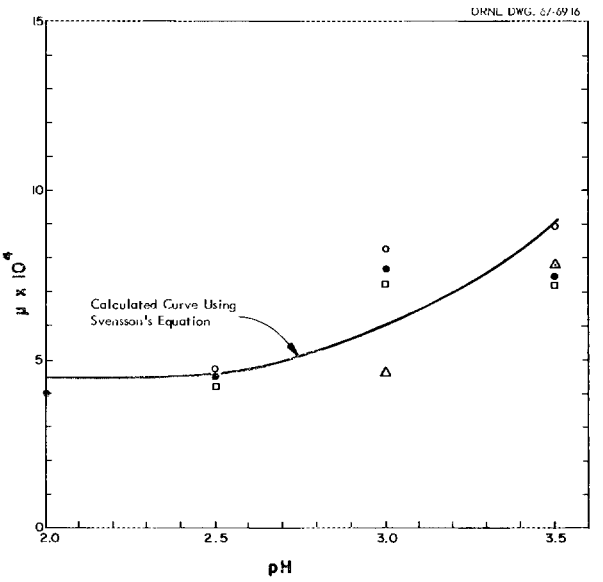

Fig. 17.1. Electrophoretic Mobilities of the Fast-Descending Boundary Compared with the Theoretical Curve from Svensson's Equation. Ionic mobilities: H^+, 33.6×10^{-4}; NO_3^-, 6.66×10^{-4}; Th^{4+}, 4.25×10^{-4} (see ref. 5); sols (see Table 17.1): ○, OXO-500; □, OXO-650; △, SDN; ●, NH_3-R.

Properties of Iron-Thoria Cermets

Two iron-thoria cermets that were prepared by mixing sols of thoria and α-Fe_2O_3, drying to gels at 80°C in air, and reducing in hydrogen at ~700°C as previously reported[6] were submitted to the Metals and Ceramics Division for further testing. The nominal composition of one sample was 98% ThO_2–2% Fe; the other was 2% ThO_2–98% Fe. The materials were cold pressed into pellets, sintered in hydrogen, encapsulated in iron, and extruded in an effort to obtain dense, workable material for thermal conductivity and hardness tests. When the iron jackets were removed (by machining), the specimen containing 98% ThO_2 was brittle and could not be machined. A test specimen successfully machined from the other sample showed that,

[1] J. M. Bannister, Australian AEC, Lucas Heights, personal communication (Sept. 27, 1965).

[2] D. C. Henry, *Trans. Faraday Soc.* **44**, 1021 (1948).

[3] H. Svensson, *Arkiv Kemi* **22A**, 1 (1946).

[4] V. P. Dole, *J. Am. Chem. Soc.* **67**, 1119 (1945).

[5] K. H. McCorkle, Ph.D. dissertation, University of Tennessee (1966); K. A. Kraus and R. W. Holmberg, *J. Phys. Chem.* **58**, 325 (1954).

[6] *Chem. Technol. Div. Ann. Progr. Rept. May 31, 1966*, ORNL-3945, p. 243.

compared with Armco iron, its thermal conductivity was reduced about 10% by the 2% ThO_2:

	Thermal Conductivity $[w\ cm^{-1}\ (°C)^{-1}]$	
	47°C	98°C
98% Fe–2% ThO_2	0.634	0.600
Armco iron	0.702	0.670

17.2 SURFACE AND SINTERING PROPERTIES OF SOL-GEL-DERIVED THORIA

The work reported in this section was done under subcontract with the University of Utah, under the direction of M. H. Wadsworth.

Sintering and Grain Growth of Thoria Gels Containing Calcium Oxide

The effect of a calcium impurity on the sintering of thoria gel compacts was studied by measuring shrinkage and grain growth. Thoria gels with calcium concentrations as high as 1% were obtained by adding calcium nitrate. Both grain growth and sintering were greatly enhanced by the additions.

Computer analysis of the shrinkage data showed that the sintering rate increased as the calcium concentration was increased. The average activation energy observed, 45 kcal/mole, was virtually the same as that observed by Daniels and Wadsworth[7] for plain gel.

The average initial grain sizes of the thoria gels were 60 to 85 A; the maximum average grain size during sintering at 850°C was 300 A.

The effects of air and hydrogen atmospheres on grain growth during sintering were examined. In air the grain growth rate increased with increasing calcium concentration. Above 850°C, abnormal grain growth was observed when 1% calcium was present.

Grain-boundary diffusion was found to provide a satisfactory explanation for the sintering data up to 850°C. Correlation of the sintering data with grain growth indicated that the rate of sintering was normal (i.e., the grain-boundary-diffusion model was obeyed) only in the range of normal grain growth (below approximately 850°C for the 1% Ca–ThO_2 gels). The activation energy for grain growth was essentially the same as that for sintering.

Shrinkage Measurements of Thoria Compacts Containing Impurities

Sintering studies were made of several thoria samples that were prepared at ORNL. These samples contained various impurities (Table 17.3). To obtain well-dispersed sols, several dispersion and drying cycles were required.

[7] A. U. Daniels and M. H. Wadsworth, *Sintering of Thoria Gel*, University of Utah technical report No. XXIII (Jan. 10, 1964).

Table 17.3. Properties of Thoria Samples

Sample No.	Impurity	ppm	Number of Dispersing Cycles	Approximate Degree of Dispersion (%)
DT-1A	PO_4	3,260	8	Excellent
DT-1B	PO_4		20	~90
DT-2A	SO_4	3,640	9	Good
DT-2B	SO_4	18,600	20	~60
DT-4A	Fe	4,694	20	~80
DT-4B	Fe	20,300	20	~50
DT-5A	F	4,700	20	~80
DT-5B	F	16,700	20	~50

Table 17.4. Percentage Shrinkage of Thoria Compacts Sintered at 700 and 900°C for 300 min

$(L_{ps} - L_f)/L_{ps} \times 100$[a]

Temperature (°C)	Plain gel	DT-1A	DT-1B	DT-2A	DT-2B
700	4.85	5.63	5.38	4.59	3.08
900	12.72	10.82	8.40	9.08	6.80
700–900	7.87[b]	5.19[b]	2.02[b]	4.49[b]	2.79[b]

[a] L_{ps} represents the length of the sample after pretreating at 560°C for 30 min, and L_f represents the length of the sample after sintering.

[b] Percentage increase in shrinkage.

The sols thus prepared were dried, crushed, and sized to −100 +400 mesh. This material was then pressed into 0.5-in.-diam compacts under 20,000 psi pressure. Attempts to prepare pellets from sols containing iron or fluoride were unsuccessful. Shrinkages of pellets containing other impurities at 700 and at 900°C were compared with the shrinkage of a plain gel compact (see Table 17.4). Shrinkage was rapid for the first 50 to 100 min but was relatively slow after 300 min. At both temperatures DT-2B (the sol having the highest sulfate content) exhibited the least amount of shrinkage. The shrinkage at 900°C, and also the increased shrinkage from 700 to 900°C, decreased as the concentration of sulfate or phosphate in thoria gel was increased.

Gas Evolution from Pyrolysis of Thoria Gel

Gas chromatographic measurements of the gases evolved from thoria in the temperature range 50 to 460°C revealed rather surprising results, namely, the predominance of CO_2 in the adsorbed gases.

The analysis of the desorbed water was made with a 361-mg sample of pressed thoria using a $\frac{1}{8}$-in.-diam by 12-in.-long gas chromatograph column packed with Carbowax 1500 on glass beads. Nitrous oxide, if present, should have been detected with this system. Another sample consisting of three pressed pellets (total weight, 1333 mg) was analyzed in a series column arrangement with dimethylsulfoxide on Gas Chrom RZ as packing for the first column and Linde 13X molecular sieve as packing for the second column. This arrangement should have allowed the detection of CO, CO_2, NO, NO_2, and N_2; only NO_2 and CO_2 were found. Measurements were made at 50°C intervals from 50 to 460°C. Before each temperature rise the sample was evacuated; after each temperature rise, when the pressure had reached equilibrium, the total pressure was measured and a portion of the desorbed gases was analyzed.

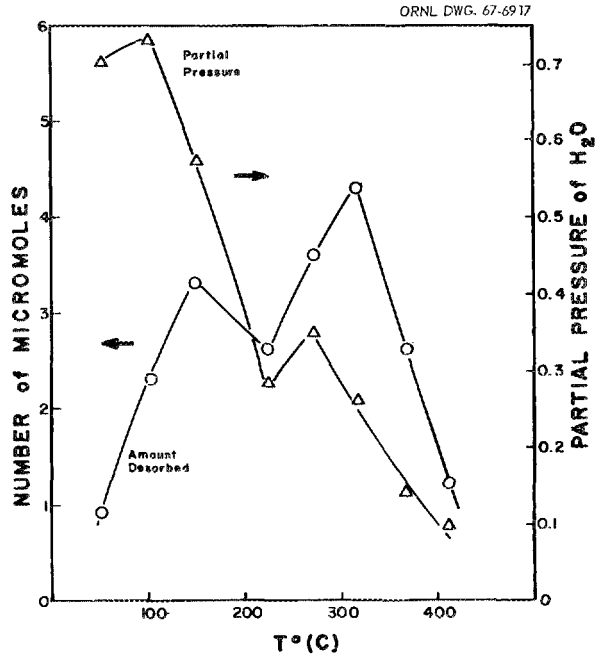

Fig. 17.2. Incremental Water Desorption from Thoria.

The total incremental pressure rose almost linearly to 17.5 mm Hg at 340°C and then dropped to 16 mm at 390°C. The corresponding total incremental moles of evolved H_2O and incremental partial pressures of H_2O (Fig. 17.2) show that, on a mole ratio basis, the predominant chemisorbed species is not water. The H_2O peak at 150°C undoubtedly corresponds to physically adsorbed water, while that at 320°C corresponds to chemisorbed water. Above 220°C, where the chemisorbed H_2O is being evolved, the partial pressure of water was less than one-third that of the total gases.

The shrinkage model previously proposed[8] is based on the weight of the gaseous species evolved, according to the equation

$$\Delta W = S\,\Delta V\,, \qquad (1)$$

[8] *Chem. Technol. Div. Ann. Progr. Rept. May 31, 1966*, ORNL-3945, p. 245.

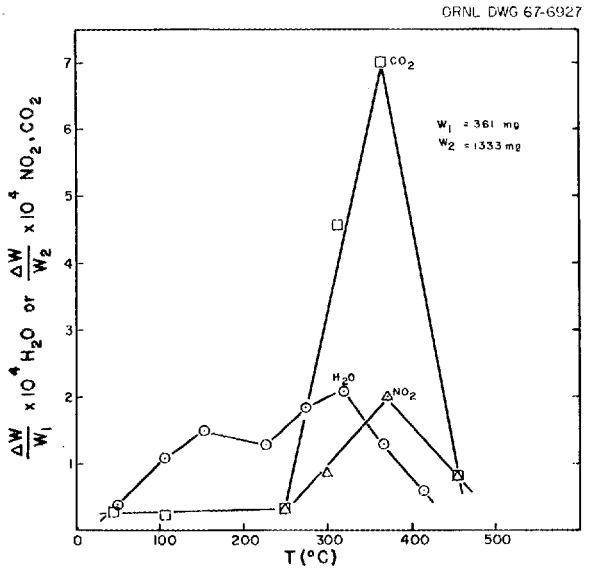

Fig. 17.3. Normalized Incremental Weight Loss from Thoria Due to H_2O, NO_2, and CO_2 Desorption.

where ΔW = weight loss of gases at $T > 200°C$, ΔV = volume decrease, and S = a constant. Accordingly, the incremental weight losses due to H_2O, CO_2, and NO_2 are compared in Fig. 17.3. The dominance of CO_2 was not expected. These results, together with Eq. (1), imply that CO_2 predominates in the shrinkage mechanism and that the effective volume ratios with regard to shrinkage are 1, 2.55, and 2.44 for H_2O/H_2O, NO_2/H_2O, and CO_2/H_2O respectively. Unfortunately, CO_2 adsorption by thoria from the air is of such concern that these measurements must be repeated to properly assess the importance of CO_2.

17.3 STUDIES OF URANIA SOLS AND GELS

Electrophoretic Studies of Urania Sols

The electrophoretic mobilities of a few UO_2 sols were measured. These sols are difficult to prepare reproducibly, and gradual oxidation invariably occurs in spite of all precautions. Ordinarily, UO_2 sols are stabilized by formic and nitric acids. In attempts to obtain lower U(VI) contents, we prepared sols that were stabilized by hydrochloric acid; results showed the U(VI) content to be as low as 1.5 to 2%. Because of the opacity of these sols, it was necessary to dilute them to ~ 0.02 *M* and to use the 2-ml electrophoresis cells to obtain sufficient light transmission for observation of the Rayleigh fringe pattern. Schlieren patterns were weak or absent; thus it is not certain whether multiple boundaries were present. However, the ascending boundary did move somewhat faster than the descending one, which would indicate nonideal behavior. Electrophoretic mobility data for the descending boundary, which should represent more accurately the true mobility of the colloidal particles, showed no trends with the type of electrolyte, the pH of the solution, or the U(VI) content of the sol.

Preparation and Viscometry of Concentrated Chloride-Stabilized Urania Sols

The preparation of aqueous UO_2 sols that are stabilized by chloride is based on the precipitation of hydrous UO_2 from a uranous chloride solution which is, in turn, prepared by catalytic re-

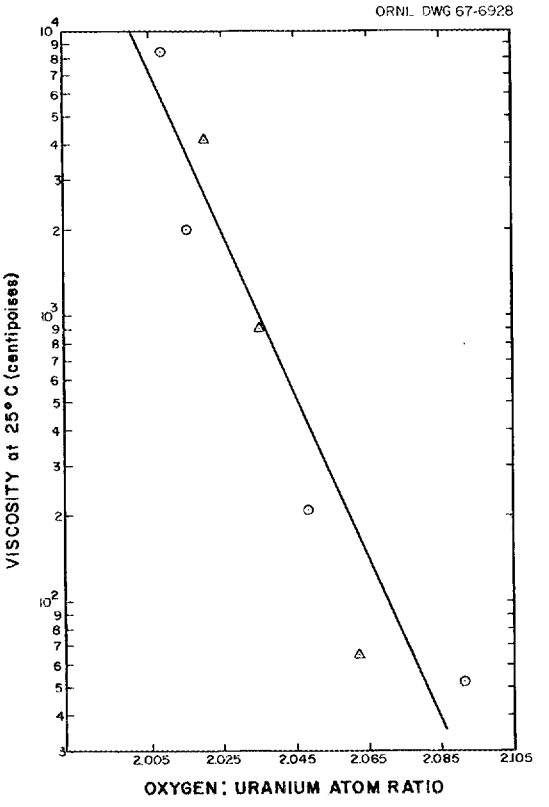

Fig. 17.4. Effect of UO_3 Addition on the Viscosity of Concentrated Chloride-Stabilized UO_2 Sols. Initial conditions: ⊙, 6.4 *M* U, 0.79% U(VI), chloride: uranium atom ratio = 0.45, sp gr of sol = 2.643; △, 6.18 *M* U, 2.1% U(VI), chloride: uranium atom ratio = 0.38, sp gr of sol = 2.5921.

duction of uranyl chloride with hydrogen. The precipitate is then washed until peptization begins to occur and is then converted to a sol either by vigorous stirring for 2 to 3 hr at 60 to 65°C or by aging for several days at ambient temperature. The sols are concentrated in a rotary vacuum evaporator. After reduction, all operations are carried out in an argon atmosphere. The sols prepared in this manner could be concentrated to >8 *M*, which is a much higher concentration than has been achieved with nitrate-stabilized sols.

Viscosity was measured with a Brookfield viscometer at 25°C, and the effect of the addition of UO_3 on the viscosity of the sol was studied. In all instances a very significant decrease in viscosity was obtained (Fig. 17.4). The viscosities of these sols also tended to decrease with time, perhaps because of additional oxidation.

Electron photomicrographs showed loosely held agglomerates of particles in the concentrated sols. A possible explanation for the decrease of viscosity with added U(VI) is that it breaks down the agglomerates. The crystallite size of the same sols, measured by x-ray line broadening, stayed constant at 35 to 37 A, regardless of the addition of the UO_3.

18. Assistance Programs

The Division provided assistance to others on several projects, principally the Eurochemic Assistance Program and a program in which the radiation resistance of a number of selected materials is being determined. The latter effort involves the exposure of protective coatings, lubricants, gasket materials, sealants, electrical insulations, and glasses to a ^{60}Co gamma source (intensity, 8×10^5 r/hr) until failure is observed or until a total dose of 10^{10} rads is received.

18.1 EUROCHEMIC ASSISTANCE PROGRAM

The Laboratory continued to coordinate the Eurochemic Assistance Program for the exchange of information between Eurochemic and the several AEC sites included in the program. In addition, the Laboratory is supplying the services of the U.S. Technical Advisor, E. M. Shank, who will remain at Mol, Belgium, during the construction and startup phases of the Eurochemic plant.

During the past year, 390 USAEC-originated documents and 32 drawings and miscellaneous items of information were sent to Eurochemic. Twenty-four Eurochemic documents written in English were received, reproduced, and distributed. In addition, one Eurochemic report (French) was translated for distribution in English.

Construction and "cold" startup operation of the Eurochemic facility were completed, and the processing of fuels from several European reactors has now been successfully accomplished.

18.2 EVALUATION OF THE RADIATION RESISTANCE OF SELECTED PROTECTIVE COATINGS AND OTHER MATERIALS

In a continuing evaluation program for determining the radiation resistance of protective coatings for radiochemical plant uses,[1–6] a total of 30 coating specimens (from five different manufacturers) and 13 miscellaneous materials are currently being evaluated. The results for coatings that were exposed to a ^{60}Co gamma source at an intensity of 8×10^5 r/hr and a temperature of 40 to 50°C are as follows:

1. Two specimens, one epoxy and one polyurethane, showed excellent radiation resistance (had not failed after exposure to 1×10^{10} rads in air).
2. Eight specimens, seven epoxy and one polyurethane, failed by embrittlement or cracking at exposure to 1×10^{10} rads in air.
3. Seven epoxy specimens failed at exposures to between 3 and 9×10^9 rads in air.
4. Seventeen specimens, 3 epoxy and 14 modified phenolic, submerged in deionized water, failed at exposures to 1×10^8 to 2.6×10^9 rads.
5. Thirteen specimens, 1 phenolic and 12 modified phenolic, exposed to 1.5 to 4.0×10^9 rads in air, showed excellent resistance. Tests will be continued with these coatings until they have failed or until they have received a dose of 1×10^{10} rads.

---

[1] *Chem. Technol. Div. Ann. Progr. Rept. May 31, 1966*, ORNL-3945, pp. 250–55.

[2] C. D. Watson and G. A. West, "Protective Coatings (Paints)," chap. 12 in *Decontamination of Nuclear Reactors and Equipment* (ed. by J. A. Ayres), sponsored by Division of Technical Information, USAEC, Washington, D.C. (in press).

[3] C. D. Watson, "Buildings and Laboratories," sect. 20-3 of chap. 20 in *Decontamination of Nuclear Reactors and Equipment* (ed. by J. A. Ayres), sponsored by Division of Technical Information, USAEC, Washington, D.C. (in press).

[4] C. D. Watson *et al.*, United States Standard, "Protective Coatings (Paints) for the Nuclear Industry," United States Standards Institute, 1967.

[5] C. D. Watson and G. A. West, "A Ten-Year Look at Protective Coatings (Paints) in the Nuclear Industry," presented at the National Association of Corrosion Engineers, 22d Annual NACE Conference and 1966 Corrosion Show, Miami Beach, Fla., Apr. 18–22, 1966.

[6] C. D. Watson and G. A. West, "Radiation Effects on Paints," *Mater. Protect.* 6(2), 44–49 (February 1967).

Table 18.1. Gamma-Radiation Resistance of Several Protective Coatings

Radiation source: ^{60}Co at 8×10^5 r/hr intensity and 40 to 50°C temperature

Coating	Manufacturer[a]	Substrate	Exposure[b] in Demineralized Water (rads)	Effect[c]	Exposure[b] in Air (rads)	Effect[c]
Epoxy, OX-1055[d] (FG-3)	2	Concrete	1.5×10^9 [e]	A	9.7×10^9	C
Epoxy, SX-1655[d] (FG-6)	2	Concrete	1.5×10^9 [e]	A	8.3×10^9	C
Epoxy, SX-1346 (Cat. 48101) (FC-1)	2	Concrete	5.4×10^8 [e]	C	1.0×10^{10}	D
Epoxy, SX-1055 (Cat. 48101) (FC-2)	2	Concrete	1.4×10^9 [e]	A, B	1.0×10^{10}	B, D
Epoxy, OX-1055 (FC-3)	2	Concrete	1.4×10^9 [e]	A, B	1.0×10^{10}	F
Epoxy, SX-1665 (FC-5)	2	Concrete	1.4×10^9 [e]	A, B	1.0×10^{10}	F
Epoxy, SX-1665 (FC-6)	2	Concrete	1.4×10^9 [e]	A, B	1.0×10^{10}	B, C
Epoxy, 46614 (Cat. 46610) (FS-2)	2	Steel	5.4×10^8 [e]	C	1.0×10^{10}	B
Epoxy, SX-1665 (Cat. 46000) (FS-3B)	2	Steel	9.0×10^8 [e]	C	1.0×10^{10}	B
Epoxy, SX-1665 (Cat. 46000) (FS-3C)	2	Steel	1.4×10^9 [e]	A, B, E	1.0×10^{10}	
Epoxy, K-30 (7-W-20)	5	Steel	1.3×10^8	C	5.1×10^9	A
Epoxy, 5-Y-30 (7-W-20)	5	Steel	1.3×10^8	C	3.7×10^9	B
Mod. phenolic, Phenoline 368-A[d]	1	Concrete	1.2×10^9	C	$>4.0 \times 10^9$	
Mod. phenolic, Phenoline 368-B[d]	1	Steel	2.6×10^9	A	$>4.0 \times 10^9$	
Mod. phenolic, Phenoline 368-C[d]	1	Concrete	1.2×10^9	C	$>4.0 \times 10^9$	
Mod. phenolic, Phenoline 368-D[d]	1	Steel	2.6×10^9	A	$>4.0 \times 10^9$	
Mod. phenolic, Phenoline 368-E[d]	1	Concrete	2.6×10^9	A	$>4.0 \times 10^9$	
Mod. phenolic, Phenoline 368-F[d]	1	Steel	2.6×10^9	B	$>4.0 \times 10^9$	
Mod. phenolic, Phenoline 368-G[d]	1	Concrete	2.6×10^9	A	$>4.0 \times 10^9$	
Mod. phenolic, Phenoline 368-H[d]	1	Steel	2.6×10^9	C	$>4.0 \times 10^9$	
Mod. phenolic, Phenoline 368-I	1	Concrete	7.8×10^8	C	$>4.0 \times 10^9$	
Mod. phenolic, Phenoline 368-J	1	Steel	7.8×10^8	C	$>4.0 \times 10^9$	
Mod. phenolic, Phenoline 368-O[d]	1	Concrete	7.9×10^8	C	$>4.0 \times 10^9$	
Mod. phenolic, Phenoline 368-P[d]	1	Steel	7.9×10^8	C	$>4.0 \times 10^9$	
Phenolic, Q-Kote	3	Concrete	1.9×10^8	C	$>3.0 \times 10^9$	
Phenolic, Q-Kote	3	Steel	1.9×10^8	C	$>3.0 \times 10^9$	
Polyurethane, Z552 (A)	4	Concrete	1.0×10^9 [e]	C	1.0×10^{10}	F
Polyurethane, Z552 (A)	4	Steel	1.68×10^8 [e]	C	2.9×10^9	B, C
Polyurethane, Z651 (B)	4	Concrete	1.0×10^9	C	1.0×10^{10}	
Polyurethane, Z651 (B)	4	Steel	1.0×10^9	D	4.6×10^9	B
Polyurethane, Carboline 1341	1	Concrete	1.3×10^8	C	1.6×10^9	C
Polyurethane, Carboline 1341	1	Steel	1.3×10^8	C	1.8×10^9	C
Vinyl, SX-1666 (FS-5)	2	Steel	1.8×10^8	C	7.5×10^9	B, D

[a]Manufacturers: 1, Carboline Co.; 2, Celanese Coating Co.; 3, Chemline Coatings Co., Division of Dixie Paint and Varnish Co.; 4, Hughson Chemical Co.; 5, Rowe Products Inc.

[b]The materials were inspected for radiation damage at various dose intervals: $\sim 1 \times 10^7$, $\sim 5 \times 10^7$, $\sim 1 \times 10^8$, $\sim 2.5 \times 10^8$, $\sim 5 \times 10^8$, and each additional 5×10^8 rads thereafter. The exposure values listed represent the cumulative irradiation dose that had been received at the time the adverse effects were first observed.

[c]Effects: A, chalked; B, embrittled; C, blistered; D, loss of adhesion; E, interfacial area attack; F, alligator cracking.

[d]Coating reinforced with woven glass fabric laminate.

[e]Reported previously in ORNL-3945.

Further data on protective coatings are given in Table 18.1. Materials, other than coatings, that were evaluated for possible use in radiochemical environments include: (1) lubricants, (2) gasket material, (3) sealants, (4) electric cable insulation, (5) plastics, and (6) viewing-window glass. The results for these materials are presented in Table 18.2.

Table 18.2. Radiation Resistance of Selected Lubricants, Gasket Materials, Sealants, Electrical Insulations, and Glasses[a]

Materials and Manufacturer	Use	Results
Bemol moly grease (5% MoS_2 in medium bonded Li grease), Bemol Corp.	Lubricant	Failure by hardening at 2 to 3×10^9 rads
Way-Lube oil, Texaco Co.	Lubricant	Failure by extreme tackiness at 1 to 2×10^9 rads
Hi Temp. silicone rubber, General Electric Co.	Gasket, etc.	Failure by hardening and embrittling at 1 to 5×10^9 rads
Polyurethane seal rings, Dysogrin Industries	Gaskets	Failure by progressive hardening at 1 to 3×10^9 rads
Sealer No. 130 (polyisobutylene with inert pigment and asbestos), Electro-Cote Co.	Caulking	Satisfactory at 1×10^9 rads
Sylguard No. 185, Dow-Corning	Potting and encapsulating	Failure by hardening and embrittling at 4 to 9×10^8 rads
Multiconductor (polyvinyl), Spectra-Strip Wire and Cable Co.	Electric cable insulation	Failure by hardening and embrittling at 5×10^8 to 1×10^9 rads
Multiconductor (Hypalon), Boston Insul. Wire Co.	Electric cable	Failure by hardening and embrittling at 5×10^8 to 1×10^9 rads
Type H Corite resin, Corite-Reynolds Corp.	Rigid plastic equipment	Failure by cracking at 2 to 4×10^9 rads
Epoxy pipe, Tube Turn Plastic Div.	Pipe	Failure by deforming at 1×10^9 rads[b]
Penton plastic, Hercules Powder Co.	Pipe	Failure by embrittling at 1×10^7 to 1×10^8 rads
Plastic screen (vinyl-coated Fiberglas), Owens-Corning Fiberglas Corp.	Screen	Failure by embrittlement of coating at 1 to 5×10^8 rads
Plate glass (laminated, 2-in. thick), Pittsburgh Plate Glass Co.	Viewing windows	Light transmission loss of 11 and 39% at 5×10^8 and 6×10^9 rads respectively

[a] All materials exposed to gamma radiation source in air at 40 to 50°C.

[b] Failure by deterioration at 5×10^8 to 1×10^9 rads when material was exposed to gamma radiation in deionized water at 40 to 50°C.

19. Water Research Program

Work by the Chemical Technology Division on the Water Research Program is reported directly to the Office of Saline Water, and only an abstract appears in this report (see the Summary).

20. Chemistry of Carbides and Nitrides

The basic chemistry of the carbides of uranium, thorium, and other metals is being investigated, with emphasis on reactions in aqueous systems. This work has application to the processing of power reactor fuels, reactor safety, and high-temperature materials development. Previous studies were primarily concerned with the reaction of water with uranium and thorium carbide specimens that had been carefully characterized by advanced analytical and metallographic techniques. The reactions of the uranium carbides with nitric acid and of the thorium carbides with sodium hydroxide have also been examined. During the past year the reactions of the uranium and thorium carbides with aqueous solutions of hydrochloric and sulfuric acids and of uranium monocarbide with sodium hydroxide solutions were studied. The latter experiments were useful in devising processing methods for SAP-clad carbide fuel (see Sect. 1.5). To gain insight into the mechanisms of the reactions (which are quite complex), the hydrolysis of the carbides of uranium, thorium, and aluminum in D_2O and the simpler reactions of the carbides of calcium and barium with 0 to 16 *M* HNO_3 were also studied. Work already reported in the open literature[1-3] has only been briefly summarized here.

The reactions of the uranium and thorium carbides with 3 to 9 *M* HCl and with 6 *M* H_2SO_4 at 80°C were found to be hydrolysis reactions, with no oxidation or formation of C-S, C-O-S, or C-Cl bonds occurring.[1] Ninety percent or more of the carbon in the uranium and thorium monocarbides was hydrolyzed to methane, whereas uranium sesquicarbide, uranium dicarbide, and thorium dicarbide produced complex aliphatic hydrocarbon mixtures similar to those obtained with water. Hydrochloric acid was found to affect the extent of polymerization of the C_2 groups from the dicarbides; it increased wax formation with uranium dicarbide and decreased polymerization (i.e., yielded more gaseous hydrocarbons) with thorium dicarbide. In the experiments with hydrochloric acid more than 99% of the uranium was found as soluble U(IV), and all of the thorium was found as soluble Th(IV). With 6 *M* H_2SO_4 the products were crystalline $U(SO_4)_2 \cdot 4H_2O$ and crystalline $Th(SO_4)_2 \cdot xH_2O$, where *x* was in the range of 2.5 to 3.5. With 12 *M* H_2SO_4 the monocarbides yielded primarily methane. The reactions of uranium sesquicarbide, uranium dicarbide, and thorium dicarbide with 12 *M* H_2SO_4 at 80°C were so slow that they were terminated after 16 days when they were only about half completed. The collected gas contained mostly hydrogen, plus some hydrocarbons and a small amount of SO_2. No compounds containing C-O, C-S, or C-O-S bonds were found in the gas. Surprisingly, with 12 *M* H_2SO_4 30% of the uranium was found as UO_2, and some of the thorium was found as ThO_2 (7% from ThC and 40% from ThC_2); the remaining salt was $U(SO_4)_2$ or $Th(SO_4)_2$ (the extent of hydration could not be determined).

There are pronounced differences between the chemical behavior of the alkaline-earth dicarbides and that of the actinide dicarbides. The reactions of calcium carbide with 0 to 16 *M* HNO_3 and of barium carbide with 0 to 8 *M* HNO_3 at 25°C produced acetylene as the only carbon-containing product.[2] With 10 to 16 *M* HNO_3, part of the carbide carbon in barium carbide was oxidized to free carbon and carbon oxides, although some was hydrolyzed to acetylene. There was no passivation of either carbide in dilute nitric acid. In

[1] M. B. Sears and L. M. Ferris, "Reactions of Uranium and Thorium Carbides with Aqueous Solutions of Hydrochloric Acid and Sulfuric Acid," to be published in the *Journal of Inorganic and Nuclear Chemistry*.

[2] M. B. Sears and L. M. Ferris, *J. Inorg. Nucl. Chem.* 29, 1255 (1967).

[3] M. B. Sears and L. M. Ferris, *J. Inorg. Nucl. Chem.* 28, 2055 (1966).

contrast, the uranium and thorium dicarbides yielded complex aliphatic hydrocarbon mixtures when hydrolyzed[4,5] and complex aromatic compounds when oxidized by nitric acid.[6-8] Furthermore, uranium dicarbide was passive in dilute (0.005 to 0.05 *M*) nitric acid, although it reacted readily with water and with more-concentrated (>1 *M*) nitric acid.[6] The alkaline-earth dicarbides and the actinide dicarbides all contain C_2 groups in the crystal lattice; the only difference is in the carbon-to-carbon bond length, which is about that of a triple bond in calcium carbide[9] vs a double bond in the uranium[9] and thorium dicarbides.[10] Actually, one would expect the acetylide group to polymerize more readily than the ethylide group. Therefore, it seems likely that differences in the cations, rather than in the anions, are responsible for observed differences in the chemical behavior of the alkaline-earth dicarbides and the actinide dicarbides.

The rate-determining step in the hydrolysis of the uranium and thorium carbides probably does not involve cleavage of the H-O bond in the water, since the reactions with D_2O at 80°C were identical to the corresponding reaction with H_2O except that deuterium was substituted for hydrogen in the products.[3] In contrast, hydrolysis of aluminum carbide at 80°C to produce methane was four times more rapid in H_2O than in D_2O and probably involved cleavage of the H-O bond in the rate-determining step.[3] An isotope effect has also been reported for the calcium carbide–water reaction.[11,12] The difference in the reaction mechanisms is not surprising in view of differences between the chemical behavior of calcium dicarbide and that of the actinide dicarbides.

The hydrolysis of uranium monocarbide with 2 to 18 *M* NaOH at 80°C in glass equipment produced the expected methane, some amorphous U(IV) oxide, and traces of higher hydrocarbons; in addition, the amount of hydrogen formed was significantly higher than that found in the reaction with water (Table 20.1). Furthermore, some of the uranium was oxidized to a higher valence state, which was not the case with water. The amount of free hydrogen increased nonlinearly from 1.1 to 3.9 milligram-atoms per gram of carbide as the sodium hydroxide concentration increased from 0 to 18 *M*, reaching a plateau of about 2.4 milligram-atoms in the 2 to 6 *M* region. The amount of methane decreased slightly with increasing sodium hydroxide concentration, while the small quantity of C_2- to C_8-hydrocarbons (probably from the trace of dicarbide impurity in the specimens) showed little variation. After the residue was dissolved in hydrochloric acid, about 1 gram-atom of U(VI) was found for each mole of hydrogen produced in excess of the amount found when the specimen was hydrolyzed in water (Table 20.2) in accordance with

$$U^{4+} + 2H^+ \xrightarrow{[OH^-]} U^{6+} + H_2 ,$$

where U^{x+} refers to the oxidation state of the uranium and does not signify an ion. The U(VI) values are probably slightly high because the corrosion products from the glass plugged the filters, allowing time for some oxidation by air during preparation of the uranium solutions for analysis. The actual uranium-containing products have not been identified. They were greenish, gelatinous precipitates, which oxidized rapidly when exposed to air; x-ray studies showed them to be amorphous. The solids were contaminated with sodium silicates from the glass, so that chemical analysis was of value only in determining the oxidation state of the uranium. The reaction of uranium monocarbide with 6 *M* NaOH gave the same products at 40, 80, and 99°C (Table 20.1). At 80°C, the time required to hydrolyze 95% of a 3- to 4-g specimen increased nonlinearly from 2.3 hr with water, to 5 hr with 2 to 6 *M* NaOH, and to about 40 hr with 18 *M* NaOH. The constant rate in the 2 to 6 *M* range is consistent with the constant gas composition noted earlier. Although varying the temperature had no effect on the products, the rate of reaction with 6 *M* NaOH decreased markedly from 3 hr at 99°C for 95%

---

[4] M. J. Bradley and L. M. Ferris, *Inorg. Chem.* **3**, 189 (1964).

[5] M. J. Bradley and L. M. Ferris, *J. Inorg. Nucl. Chem.* **27**, 1021 (1965).

[6] L. M. Ferris and M. J. Bradley, *J. Am. Chem. Soc.* **87**, 1710 (1965).

[7] P. L. Pausen, J. McLean, and W. J. Clelland, *Nature* **197**, 1200 (1963).

[8] H. Imai and S. Uruno, *Nature* **206**, 691 (1965).

[9] M. Atoji, *J. Chem. Phys.* **35**, 1950 (1961).

[10] E. B. Hunt and R. E. Rundle, *J. Am. Chem. Soc.* **73**, 4777 (1951).

[11] H. L. Johnston and C. O. Davis, *J. Am. Chem. Soc.* **64**, 2613 (1942).

[12] E. D. Hughes, C. K. Ingold, and C. L. Wilson, *J. Chem. Soc.*, 493 (1934).

Table 20.1. Reaction of UC with NaOH Solutions, Using Glass Equipment

Specimen 14A: U = 4.00 milligram-atoms/g; total C = 3.96 milligram-atoms/g; free C = 0.01 milligram-atom/g

Temperature (°C)	NaOH Concentration (*M*)	Volume of Gas Evolved [ml(STP) per gram of carbide]	Gas Composition (vol %)			Carbon (milligram-atoms per gram of carbide)			Hydrogen (milligram-atoms per gram of carbide)		Uranium (milligram-atoms per gram of carbide)	
			Hydrogen	Methane	C_2- to C_8-Hydrocarbons	Methane	Gaseous C_2- to C_8-Hydrocarbons	Insoluble Residue	Free Hydrogen	Gaseous Hydrocarbons	U(IV)[a]	Total U
80	0	96	13	84	3	3.6	0.3		1.1	15.2	4.0	4.0
	2	103	25	72	3	3.3	0.3	<0.1	2.3	14.3	3.3	4.2
	4	105	26	71	4	3.3	0.4	<0.1	2.4	14.5	3.2	4.0
	6	104	25	72	3	3.3	0.3	<0.3	2.4	14.2	3.2	3.9
	9	111	32	65	3	3.2	0.4	<0.3	3.2	13.8	3.1	3.9
	12	115	36	60	4	3.1	0.5	<0.3	3.7	13.6	2.8	3.7
	18	119	36	60	3	3.2	0.4	<0.4	3.9	14.0	2.6	4.1
	19[b]	111	31	65	4	3.2	0.5	?	3.1	14.2	2.8	4.0
40	6	105	27	69	4	3.3	0.3	?	2.5	13.7	2.9	4.0
99	6	107	26	71	3	3.4	0.3		2.5	14.5	3.2	4.0

[a]Values are probably slightly low because some air oxidation occurred during preparation of the solutions for analysis.

[b]Specimen 2D: U = 4.00 milligram-atoms/g; total C = 3.96 milligram-atoms/g; free C = 0.02 milligram-atom/g.

Table 20.2. Correlation of "Excess" Hydrogen with U(VI) Formed in the Reaction of UC with NaOH Solutions (Glass Equipment)

Temperature (°C)	NaOH Concentration (*M*)	"Excess" H_2[a] (millimoles/g)	U(VI)[b] (milligram-atoms/g)
80	2	0.6	0.7
	4	0.6	0.9
	6	0.6	0.7
	9	1.0	0.8
	12	1.3	0.9
	18	1.4	1.5
	19	1.0	1.2
40	6	0.7	1.1
99	6	0.7	0.8

[a]Free hydrogen from NaOH reaction minus free hydrogen from water reaction.

[b]Total uranium minus U(IV); values are probably slightly high because there was some oxidation by air during preparation of the solutions for analysis.

hydrolysis of a 3-g specimen to four days at 40°C for a 1-g specimen.

To date, no practical alternative to glass equipment has been found. This is not necessarily serious, since the corrosion products from glass had no effect on the reactions of the thorium carbides with 2 to 18 *M* NaOH.[13] The hydrated U(IV) product is readily air-oxidized and must be dissolved in situ in a nonoxidizing acid under an inert atmosphere. This acid solution can then be handled briefly in air without appreciable oxidation of the U(IV). Hydrochloric acid is the logical choice, since the acid must also neutralize the sodium hydroxide and all the salts must be dissolved without diluting the uranium unnecessarily. Unfortunately, the common metals (e.g., copper, stainless steel, or aluminum) react with either hydrochloric acid or caustic. Some experiments were conducted using a Nalgene liner inside a glass reactor. Results were qualitatively similar to those reported in Table 20.1; however, less precise data were obtained because of the gap between the liner and the reactor. The Nalgene liner cannot be used in studies with either uranium sesquicarbide or dicarbide because it reacts with some of the waxes that are formed.

The oxidation by the NaOH solutions of some of the uranium in the uranium monocarbide from the tetravalent state to the hexavalent state, with the accompanying evolution of hydrogen, was unexpected. Hydrates of UO_2 are prepared by precipitating U(IV) solutions with alkalies,[14] and thermodynamic calculations show that "UO_2 cannot be expected to reduce water."[15] Experiments confirmed that the addition of NaOH to a uranous chloride solution merely effected precipitation of a UO_2 hydrate; no hydrogen was evolved. However, the in situ addition of NaOH to the amorphous residue from the hydrolysis of uranium monocarbide resulted in the oxidation of 14% of the uranium to the hexavalent state and the evolution of at least 0.26 mole of hydrogen per gram of original carbide. The NaOH concentration was about 8 *M* after dilution by the water used in the hydrolysis; only a portion of the hydrogen was collected. Additional work on the reactions of sodium hydroxide with the uranium carbides is in progress.

---

[13] M. J. Bradley, M. D. Pattengill, and L. M. Ferris, *Inorg. Chem.* 4, 1080 (1965).

[14] J. J. Katz and E. Rabinowitch, *The Chemistry of Uranium the Element, Its Binary and Related Compounds*, p. 281, McGraw-Hill, New York, 1951.

[15] *Ibid.*, p. 309.

21. Industrial Applications of Nuclear Energy

Use of low-cost power produced by a large nuclear reactor in an industrial-desalination complex may have economic advantages both in the industrial processes and in the production of fresh water by desalination. Recent estimates indicate that electricity can be obtained at costs 2.5 to 3.2 mills/kwhr for 50- to 500-Mw (electrical) blocks of incremental power and, ultimately, as low as 1.6 mills/kwhr from 5000-Mw (electrical) dual-purpose desalination reactors. The cost of off-peak power may be as low as 0.5 to 0.8 mill/kwhr. However, there is some question concerning the ability to utilize the large blocks of power [3000 to 5000 Mw (electrical)] that may be produced at such desalting stations. Certainly, if the area is highly industrialized, the power could be put into the existing system. But some regions of the world are not sufficiently industrialized to use large blocks of power. Plants for producing industrial chemicals at the site of a nuclear desalting station would provide a ready market for surplus power.

A general economic survey was made to determine which industries should be located at a nuclear desalination complex for their mutual benefit.[1] The production of hydrogen and fertilizers ranked high in this evaluation, and, therefore, further detailed studies of the production of hydrogen,[2] ammonia,[3] and ammonium nitrate[4] were made. Detailed studies of phosphate or potash fertilizers are still in progress. A chemical system was proposed and an initial evaluation was completed for a process for removing scale-forming elements from seawater, using only chemicals from the sea and low-cost electrical power. Hydrogen and chlorine are obtained as by-products. The hydrogen, along with nitrogen from the air and carbon dioxide from the seawater, can be combined to form ammonia and urea by standard industrial techniques.[5] A preliminary cost study was prepared to show the economic feasibility of using oxygen instead of air for the treatment of sewage sludge by a modified wet-air oxidation (Zimmermann) process.[6] Finally, a literature survey was made to determine promising applications for nuclear energy in the treatment of sewage or industrial waste waters.[7] Only the first two of these studies are discussed here.

21.1 SURVEY OF PROCESS APPLICATIONS IN A DESALINATION COMPLEX

A survey of the chemical and metallurgical industries was made to ascertain which process

---

[1] J. M. Holmes and J. W. Ullmann, *Survey of Process Applications in a Desalination Complex*, ORNL-TM-1561 (October 1966).

[2] R. E. Blanco, J. M. Holmes, R. Salmon, and J. W. Ullmann, "An Economic Study of the Production of Ammonia and Other Chemicals with the Use of Electricity from a Nuclear Desalination Reactor Complex," *Chem. Eng. Progr., Symp. Ser.* 63, No. 71 (1967).

[3] R. E. Blanco, J. M. Holmes, R. Salmon, and J. W. Ullmann, *An Economic Study of the Production of Ammonia Using Electricity from a Nuclear Desalination Reactor Complex*, ORNL-3882 (June 1966).

[4] R. E. Blanco, J. M. Holmes, R. Salmon, and J. W. Ullmann, "The Production of Ammonium Nitrate Fertilizer by Using Low-Cost Energy from a Nuclear Desalination Reactor," submitted for publication in *Chemical Engineering*.

[5] R. E. Blanco, W. C. Yee, W. E. Clark, J. M. Holmes, and R. Salmon, *A Closed-Cycle Descaling Process for Preventing Scale Formation in Evaporators and Producing Industrial Chemicals at a Nuclear Desalination Plant*, ORNL-4057 (in press).

[6] W. F. Shaffer, Jr., *Cost Study of the Treatment of Sewage Sludge by the Wet-Air Oxidation Process, Using Oxygen Produced by Low-Cost Electricity from Large Nuclear Reactors*, ORNL-TM-1629 (August 1966).

[7] I. Spiewak and W. F. Schaffer, Jr., *Survey of the Potential Use of Nuclear Derived Energy Sources in Waste Water Treatment*, ORNL-TM (in preparation).

should be given priority for further detailed study as possible components of a nuclear industrial-desalination complex.[1] Factors studied included market potential, demand for large quantities of power or steam, shipping costs, production costs, and economics expressed as turnover ratios.

A comparison of 20 industrial processes showed that nitrogenous and phosphatic fertilizer production should be given first priority, after which chlorine and caustic production should be considered (Table 21.1). The production of metals such as iron, steel, aluminum, ferroalloys, and magnesium falls next in priority. The production of acetylene via calcium carbide and the electric arc furnace also appeared promising. Processes that extract potassium, bromine, and sodium chloride from the sea appeared less attractive because of low product prices or high capital costs. Oxygen production for external consumption did not appear promising because of high shipping costs but would be attractive for internal use at the desalination site.

The improvement in profits that might be achieved was calculated for one case, aluminum production. Assuming that the sales price of aluminum remained stable, a 64% increase in profits could be achieved by reducing power costs from 5 to 1.6 mills/kwhr. Data reported in the literature concerning production costs for ten processes indicate that reducing power rates to 1.6 mills/kwhr would reduce manufacturing costs 7 to 27%.

21.2 PRODUCTION OF HYDROGEN BY THE ELECTROLYSIS OF WATER

An economic study of the production of ammonia using electrolytic hydrogen by Blanco *et al.*[3] indi-

Table 21.1. Order of Preference of Industries for Nuclear Desalination Complex

1.	Ammonia fertilizer via electrolytic hydrogen	Fertilizer intermediates and products
2.	Nitric acid via electrolytic hydrogen	
3.	Ammonium nitrate fertilizer via electrolytic hydrogen	
4.	Chlorine and caustic via electrolysis	
5.	Nitrophosphate fertilizer via electrolytic hydrogen and electric furnace phosphorus	Fertilizer intermediates and products
6.	Phosphorus via electric furnace	
7.	Iron ore reduction – electric furnace	Metals
8.	Steel via electric furnace	
9.	Iron ore reduction – electrolytic hydrogen	
10.	Aluminum via electrolysis	
11.	Ferromanganese via electric furnace	
12.	Magnesium from seawater	
13.	Triple superphosphate fertilizer from electric furnace phosphorus	
14.	Calcium carbide via electric furnace	Intermediates for organics
15.	Acetylene and ethylene via arc process	
16.	Copper via electrolysis	
17.	Potassium extracted from seawater	Seawater products
18.	Salt from concentrated seawater	
19.	Bromine from seawater	
20.	Oxygen via distillation of air	

cated that, with the use of new, advanced electrolytic cells to synthesize hydrogen, ammonia produced by the use of low-cost electricity available from large nuclear desalination reactors could compete, in selected locations in the United States, with that produced by the large single-train steam-methane reforming plants. The production of fertilizer using such low-cost electricity might be very attractive in underdeveloped countries needing large amounts of fresh water but not having a market for the electric power. Laboratory studies were performed with this new cell to assess the simultaneous effects of high temperatures (up to 194°F) and high current densities (up to 4600 amp/ft^2) on performance.

The electrolysis cell and the electrolyte circulation system were described in a previous report.[8] Modifications of the system, which were necessary to eliminate galvanic corrosion caused by bimetallic connections, included the replacement of all stainless steel tubing and connectors with nickel tubing and Teflon "Varigrip" connectors. Iron, appearing in the electrolyte as a result of the corrosion of stainless steel, was reduced and deposited on the back of the cathode. In a large plant this would result in flaking off and blockage of electrolyte flow channels.

Corrosion Tests

Corrosion tests were performed in the laboratory to determine the reason for the deposition of abnormal amounts of iron on the cathode. Types 316 and 304 stainless steels were tested individually and as a mechanically coupled unit in 34% KOH at 116°C for 146 hr. The two steels, uncoupled, corroded at the rates of 3.1 and 1.8 μg cm^{-2} hr^{-1} respectively. Coupling caused a 75% increase in the corrosion rate for type 316; however, the corrosion rate for type 304 remained essentially constant. Under these conditions, nickel showed no measurable corrosion and thus appears to be a suitable construction material for a system to be operated at temperatures to 120°C.

Monel metal and nickel were also tested in 50% KOH at 144°C for use in an electrolysis system to be operated at temperatures as high as 200°C. When coupled together, nickel corroded at the rate of 0.7 μg cm^{-2} hr^{-1} and Monel metal corroded at the rate of 1.4 μg cm^{-2} hr^{-1}. The color of the electrolyte solution turned amber from exposure to Monel metal alone under these conditions, thereby indicating this material to be unsatisfactory as a construction material. Nickel should be suitable, since any reduction of its corrosion product occurring at the cathode would result in the plateout of nickel on a porous nickel electrode.

Membrane Studies

The easiest means of reducing the voltage of this electrolytic cell is to reduce the voltage drop due to internal resistance. To accomplish this, three different types of asbestos membranes were evaluated; Table 21.2 lists the properties of these materials. Fuel cell asbestos (available in 10-, 20-, and 30-mil thicknesses) and Quinterra (10-mil only) asbestos are obtainable commercially; ACCO-1 (20-mil only) is available only in small amounts. Figure 21.1 shows the effect of different porosities

[8] *Chem. Technol. Div. Ann. Progr. Rept. May 31, 1966*, ORNL-3945 (September 1966).

Table 21.2. Properties of Asbestos Matrices

Material	Mineral Form	Skeletal Density	Bulk Density	Calculated Void Volume		Percent Fe	Bubble Pressure (psi)
				(%)	(cc/g)		
Fuel-cell asbestos[a]	Chrysotile, $Mg_6(OH)_8Si_4O_{10}$	2.5	0.78	69	0.88	0.34	15–20
Quinterra[a]	Chrysotile	2.5	0.54	78	1.4	1.97	15–20
ACCO-I asbestos[b]	Tremolite, $Ca_2Mg_5Si_8O_{22}(OH)_2$	3.0	0.37	88	2.4	Unknown	2–3

[a] Johns-Manville Co.

[b] American Cyanamid Co.

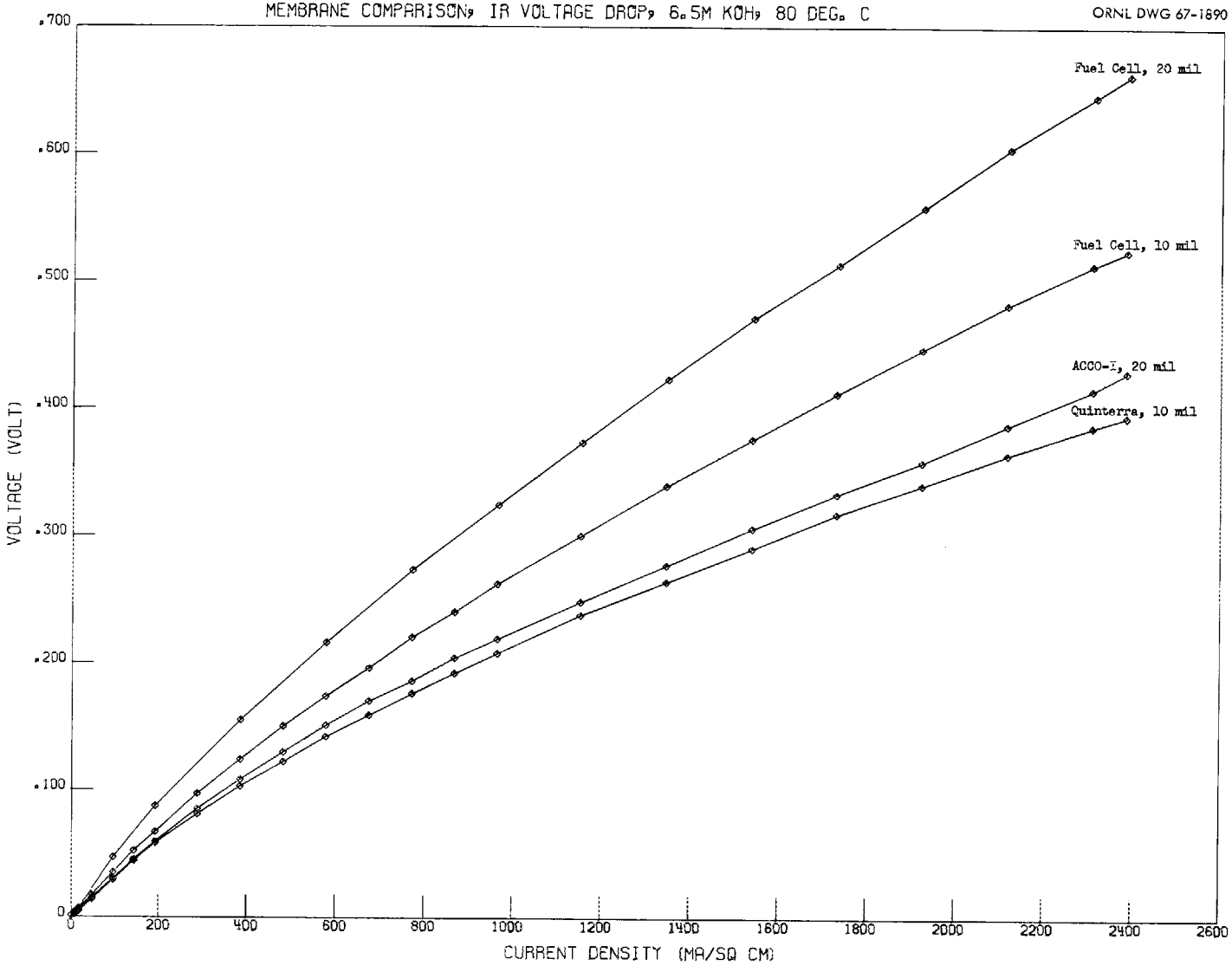

Fig. 21.1. Effect of Different Membranes on the Internal Resistance Losses of an Electrolytic Cell.

and thicknesses on the internal resistance. From the standpoint of resistance per unit thickness, ACCO-1 is superior; but its low bubble pressure of 2 to 3 psi (differential pressure that the membrane can withstand before allowing gas cross-leakage) would preclude its use in a cell operated above atmospheric pressure. Type 10 Quinterra asbestos appears to be the best material, considering both resistance and bubble pressure, if the increased amount of iron can be tolerated without adverse effects.

Laboratory Tests to Determine Expected Life of Cell Components

Tests to determine the expected life of all components of the electrolytic cell under dynamic conditions are necessary in order to make accurate cost estimates for large plants. At the present, no comparable data are available for the electrodes and the membrane of this advanced cell under the conditions projected for operation of a full-size plant, namely, 1600 amp/ft^2 and 250°F.[9]

To obtain information about electrodes and membranes during longer-term exposure to high current densities and high temperatures, a small-scale laboratory life test was performed. The cell, containing electrodes 10 cm^2 in area, was operated continuously for 82 hr at a current density of 1860 amp/ft^2 at 194°F. Since pressurization of the laboratory cell was not feasible, we were not able to use temperatures as high as 250°F. Figure 21.2 shows that the cell voltage remained almost constant over the period of the test, the initial and the final steady-state voltages being 2.320 and 2.323 v respectively. The anode showed no measurable loss in weight over this period, suggesting that anode corrosion should not be a problem. These data indicate that performance of this cell will be stable over extended periods of time; however, long-term performance tests of larger electrodes will be required to demonstrate this conclusively.

[9]*Design Study of Hydrogen Production by Electrolysis*, vol. I, ACSDS 0 106643 (October 1966).

Ultrahigh Current Density Experiments

Electrodes 5 cm^2 in area were operated at current densities up to 4620 amp/ft^2; the system was operated at this maximum current density at 80 and 90°C for about 65 hr on a 7-hr/day basis. Figure 21.3 shows the cell voltage data as a function of current density and graphically illustrates the beneficial effects of gas release from the back of the electrodes. This technique eliminates steep increases in the *IR* losses that accompany the formation of voids in the conducting path between the electrodes.

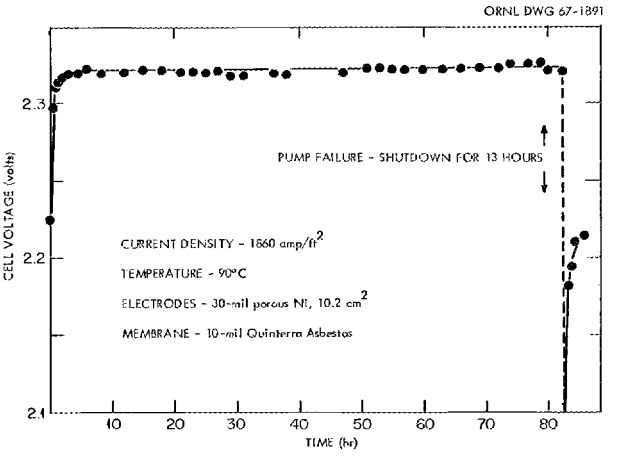

Fig. 21.2. Voltages Measured During Continuous Testing of an Electrolytic Cell.

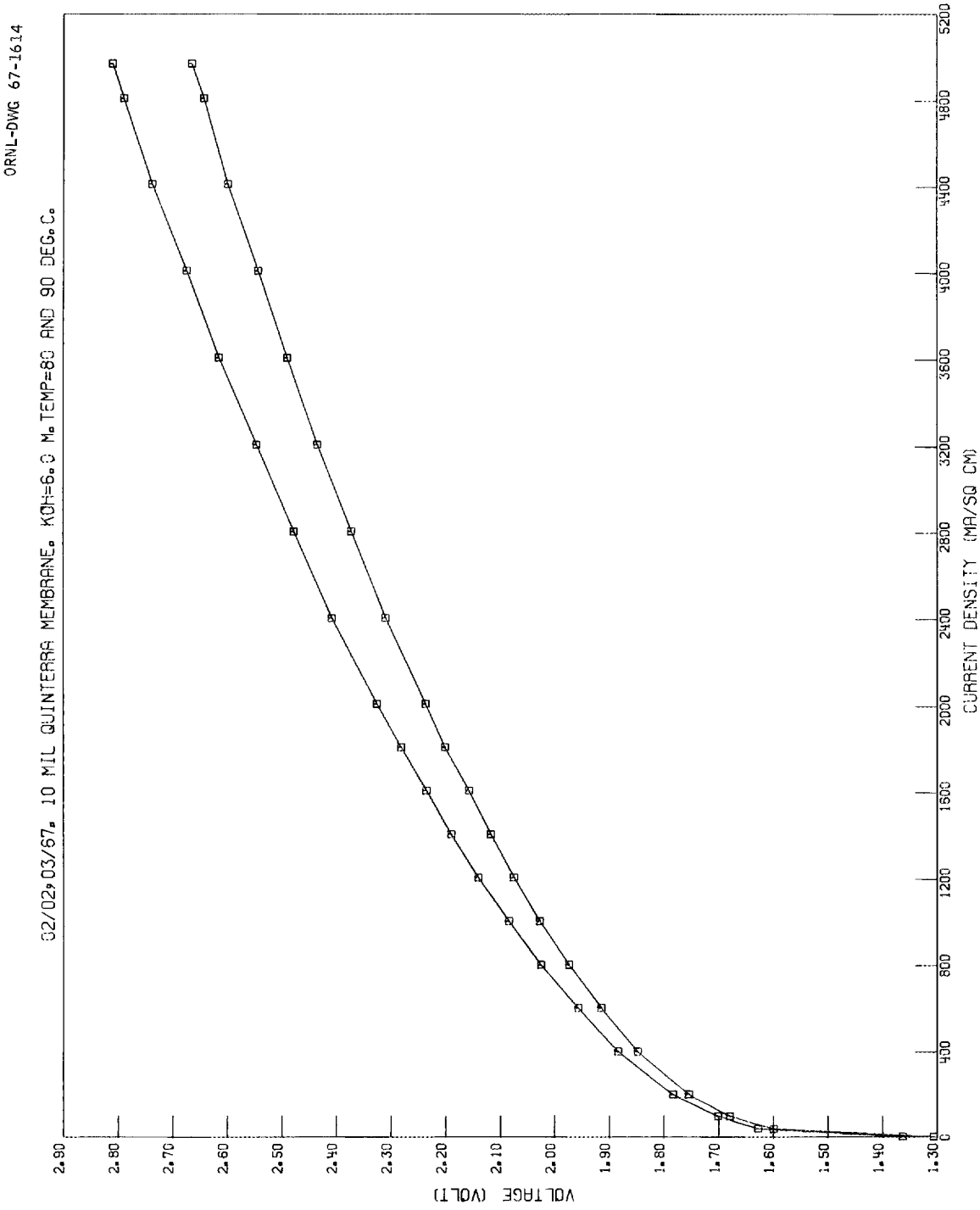

Fig. 21.3. Voltages of Electrolytic Cell Obtained During Ultrahigh Current Density Studies at 80 and 90°C.

22. Safety Studies of Fuel Transport

22.1 CASK TRANSPORT STUDIES

A new program was organized in the early part of 1966 to develop an acceptance *Criteria* for casks designed for use in shipping irradiated fuel. The *Criteria* is intended to provide a uniform engineering basis for cask design and fabrication that will ensure compliance with the performance specifications imposed by AEC regulations.[1] The program will culminate in the issuance of two volumes; the first will contain the design and fabrication *Criteria*, and the second will consist of a technical supplement describing the engineering development on which the *Criteria* is based.

The design and fabrication *Criteria* will set forth engineering standards for the design, fabrication, testing, inspection, and maintenance of shipping casks for irradiated fuel and thus should solve many of the designer's problems which now may include (1) determination of acceptable materials, (2) destructive testing to confirm design assumptions, and (3) uncertainty of thermal and criticality analyses. The *Criteria* is not expected or intended to inhibit the ingenuity or the technical aggresiveness of the designer.

The technical supplement, or second volume, will provide detailed data concerning the basis and the development of the *Criteria* and will indicate the margin of safety and relative degree of conservatism that is assumed.

The following sections describe the work that has been done to date; this material will also be included in the *Criteria*.

Literature Search

Battelle Memorial Institute, working under a subcontract, has assembled a bibliography of approximately 600 abstracts of journals, reports, patents, etc., dealing with all aspects of the transportation and the handling of radioactive materials. Each abstract has been key-worded and listed on the Radiation Safety Information Center's electronic data-processing machine. The report containing these abstracts has been issued as ORNL-NSIC-33.[2]

Cask Structural Design

The analysis and approval of structural integrity normally requires the development and submission of a mass of supporting data.[1] Consequently a large portion of the *Criteria* will be devoted to this problem. The cask designer will have a choice of methods for developing individual components of the cask, but in every instance a simple approach has been set forth that will permit him to design quickly though conservatively.

The following equations are examples of this approach; however, more-detailed analytical procedures will also be provided to enable the designer to reduce to some extent the high factor of conservatism afforded by the simple approach and, perhaps to achieve a more economical design that will comply fully with regulations.[1]

Inner Shell Thickness. – The thickness of the inner cask shell, t_1, must be at least as great as the largest t_1 computed by Eqs. (1) and (2):

$$t_1 \geq \frac{R_1 P_i}{eS}, \tag{1}$$

$$t_1 \geq 10 R_1 (1 - \nu) \left(\frac{P_e}{E}\right)^{1/2}, \tag{2}$$

[1] "Safety Standards for the Packaging of Radioactive and Fissile Materials," chap. 0529 in *AEC Manual*.

[2] L. B. Shappert and R. S. Burns, *Indexed Bibliography on Transportation and Handling of Radioactive Materials*, ORNL-NSIC-33 (June 1967).

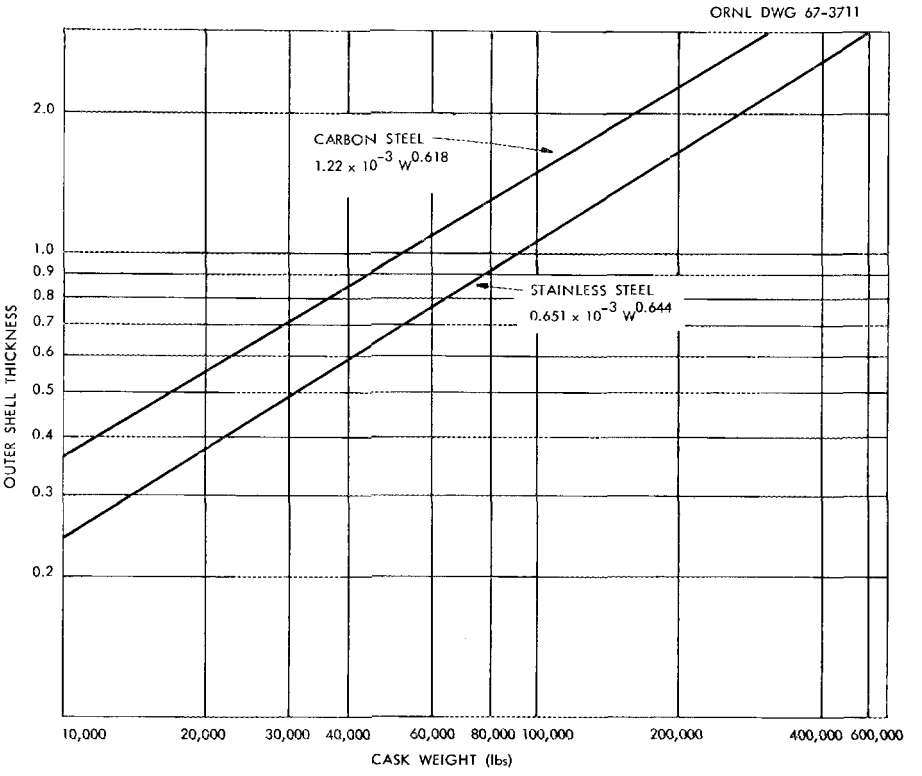

Fig. 22.1. Outer Shell Thickness as a Function of Cask Weight.

where

t_l = inner shell thickness, in.;

P_i = internal pressure, psi;

R_l = shell radius, in.;

e = weld efficiency;

S = stress intensity, psi;

ν = Poisson's ratio of the steel shell;

P_e = maximum external pressure, psi;

E = modulus of elasticity, psi.

Equation (1) is based on the resistance to a maximum internal pressure, whereas Eq. (2) is based on the resistance to a maximum external pressure (such as molten lead).

Outer Shell Thickness. – The thickness for outer carbon-steel shells must be

$$t_s \geq (1.22 \times 10^{-3})\, W^{0.618} ,$$

while that for stainless steel shells must be

$$t_s \geq (0.651 \times 10^{-3})\, W^{0.644} ,$$

where W is the cask weight in pounds and t_s is the outer shell thickness in inches. These equations are plotted in Fig. 22.1.

Dynamic Behavior of Lead. – Several cask designers have considered the effects of lead under impact conditions and have assumed, for lack of better information, that the lead flows easily and behaves like a liquid. However, tests have indicated that this assumption is erroneous under certain conditions and, therefore, theoretical calculations based on it may be incorrect.

Results of cask impact tests performed by Langhaar (Du Pont), Peterson (Knapp Mills), and Clarke (Franklin Institute) were examined in detail.

The relative movement of lead shielding and steel shells for unbonded containers was reported by Clarke,[3] who described three cubic models: one was dropped 35 ft on edge, the second was dropped 42 ft on edge, and the third was dropped 80 ft on a

[3] H. G. Clarke, *International Symposium for Packaging and Transportation of Radioactive Materials*, SC-RR-65-98, p. 261 (Jan. 12–15, 1965).

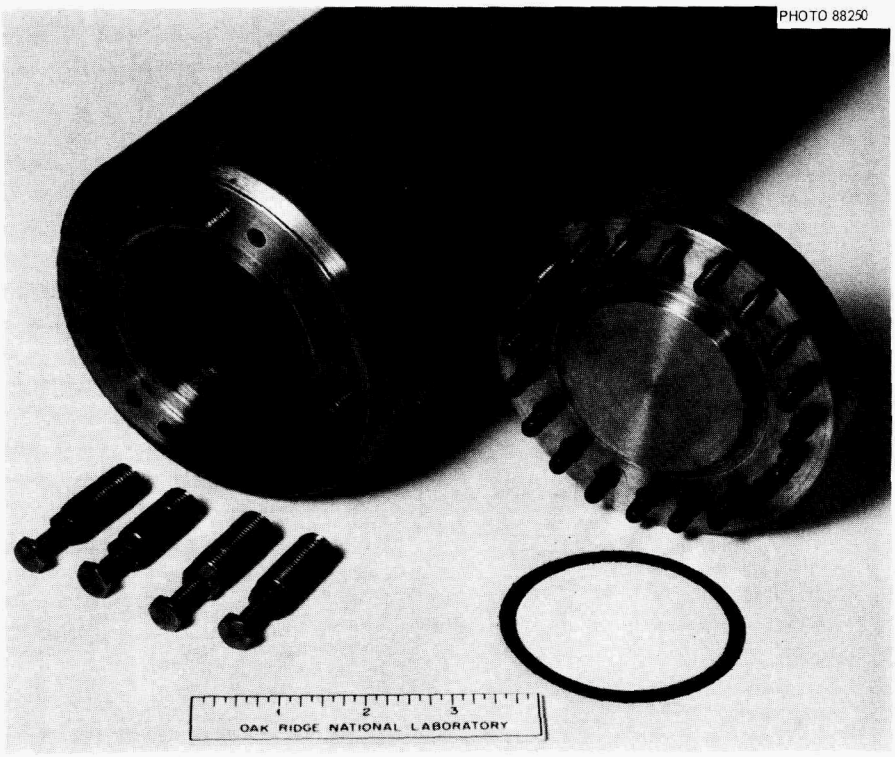

Fig. 22.2. A Model Cask Closure.

corner. The three models were then sectioned. Results indicated that gross localized lead deformation had occurred only at the point of impact and the shielding tended to behave as a unit.

Recent tests at both the University of Tennessee and the Franklin Institute indicated that an appreciable amount of lead settling can occur as the result of a 30-ft impact if the lead is unbonded, thereby leaving a void volume in the shielding annulus at the opposite end from the point of impact. On the other hand, tests with bonded casks indicate that the settling of lead under impact is very small.

Closures, Gasketing, and Bolting. – A report on closures and related equipment[4] is being condensed for inclusion in the *Criteria*. Discussions and examples of typical gasket design, temperature restrictions on various gasket materials, and important bolting designs will be included.

Investigators at the University of Tennessee, under subcontract, will perform detailed studies and model tests that are aimed at establishing design data for a closure that will not fail under impact. Figure 22.2 shows the closure of a model cask that will be tested in this program.

Shock-Absorbing Structures. – The method involving absorption of kinetic energy by deformation of a structure surrounding a shipping cask has been investigated and applied by Hanford.[5] Such a structure may assume many different forms, although materials of construction are limited to those that can absorb considerable energy in small volumes.

Hard rubber was first used by Hanford as the energy-absorbing medium in the HAPO I and II casks. Subsequently, aluminum honeycomb, which is not dependent upon the temperature, has been tested and is considered to be a satisfactory substitute for the rubber.

---

[4]A. E. Spaller, *Structural Analysis of Shipping Casks. Vol. 4. Equations for Designing Top Closures of Casks*, ORNL-TM-1312 (November 1966).

[5]C. W. Smith *et al.*, "Application of External Impact Energy Sorption to Large Radioisotope Shipping Casks," *Summary Report of the AEC Symposium on Packaging and Regulatory Standards for Shipping Radioactive Material, Germantown, Md., Dec. 3–5, 1962*, TID-7651, p. 265.

Materials and Fabrication

Ductility is a prime consideration in the selection of structural materials for the cask because of the necessity of avoiding brittle fracture of the outer or inner shell during normal operating temperatures (−40 to +130°F). The problem centers around the ductility and impact properties of the shell material at low (−40°F) temperatures; many grades of structural carbon steels are subject to brittle fracture at such temperatures.

Since fine-grained carbon steels, such as A-516, have excellent impact properties at low temperatures, they are recommended for use as shell material by the *Criteria*. A-516 steel is essentially a normalized version of A-212; it costs about the same and is widely available.

In almost every impact failure, the cask shell failed at a weld. Weld design, welder and procedure qualification, and weld inspection methods will therefore be described in detail in the *Criteria*.

The chapter on fabrication outlines cask requirements as set forth in the ASME Pressure Vessel Code, Sect. III, VIII, and IX. To assure the cask purchaser, as well as the AEC, that proper fabrication practices are followed and recorded, the functions and the responsibility of an independent fabrication inspector are outlined.

Shielding

Even though detailed shielding analyses are recommended, simplified methods of analysis will be presented in the *Criteria* so that particular shielding thicknesses may be checked with a reasonable degree of accuracy. Graphs have been developed for predicting the amount of shielding required for specified reactor irradiation and cooling conditions. Such a graph is expected to predict the amount of necessary shielding to within 10% of the amount that would be determined from a detailed machine calculation.

Criticality

The shipper of fissile materials must demonstrate to the AEC not only that his container has incorporated sound engineering design and fabrication but also that the shipment will remain subcritical at all times during shipment, including loading and unloading, and under hypothetical accident conditions.

The criticality evaluation problem is not so much concerned with the method of maintaining subcriticality as it is with the proof of adherence to the requirement of subcriticality. The chapter on criticality provides a framework within which to judge the accuracy of the proof.

Heat Transfer

Investigators at Battelle Memorial Institute (BMI), under subcontract, are studying the heat-transfer processes that occur inside and outside the shipping cask. Present regulations do not specify the maximum permissible fuel temperature; however, it is prudent to keep temperatures as low as possible, certainly below the sheath failure temperature. Information to be reported in the *Criteria* will concern heat sources, internal heat transfer, and cask behavior in a fire.

Heat Sources. – BMI has developed a nomogram that shows the heat release of a spent fuel element as a function of operating power in the reactor, operating time, and cooling time.

A second heat source that should be considered is the sun; thus, a nomogram that will predict maximum values to be expected from solar heating has also been developed. It should provide conservative estimates of temperature responses in shipping casks under normal operating conditions.

Internal Heat Transfer. – The interior of the cask is often a complex arrangement of spent fuel elements, nuclear poison plates, coolants, and support structures. With such an arrangement, the determination of the temperature distribution throughout the cavity becomes quite difficult.

Complex computer codes can account for all modes of heat transfer in an air-filled cavity (the situation that will impose the highest potential temperatures on the fuel during transit). Several specific cases that are typical of power reactor fuel shipments have been analyzed; these assume that any liquid coolant present at the start of the shipment is lost.

The code used to analyze these cases accounted for conduction and radiation within the fuel assembly, as well as conduction, convection, and radiation outside it. Figure 22.3 shows the temperature response of a loaded cask under the conditions specified in the figure. Ambient air temperature was assumed to be 130°F.

Additional cases are being analyzed in the expectation of providing conservative, yet simplified, methods for predicting the maximum fuel element temperature under the specified conditions.

Cask Behavior in a Fire. – One of the most difficult problems in cask design is to assess the behavior of the cask in a 1475°F fire for 30 min, as postulated by AEC regulations. The cask must survive such a fire and still be capable of protecting the public from its contents.

Before the structural damage to the cask can be predicted, the temperature distribution and the physical state of the lead shield must be known. To this end, BMI has developed a finite-difference technique to determine the temperature distribution as a function of time in a fire. This technique can account for physical changes, such as melting of the lead shielding, and may be handled by either hand or machine methods.

The technique may also be used to analyze cylinders of finite dimensions by multiplying the solution of the temperature-distribution equation for an infinite cylinder by that for an infinite slab.

Figure 22.4 shows the temperature distribution through the center plane of a specific cask (the solid line) and through the corner of the cask at certain times after the start of a fire. The temperature was assumed to be uniform (180°F) at time zero.

ORNL DWG 67-6904

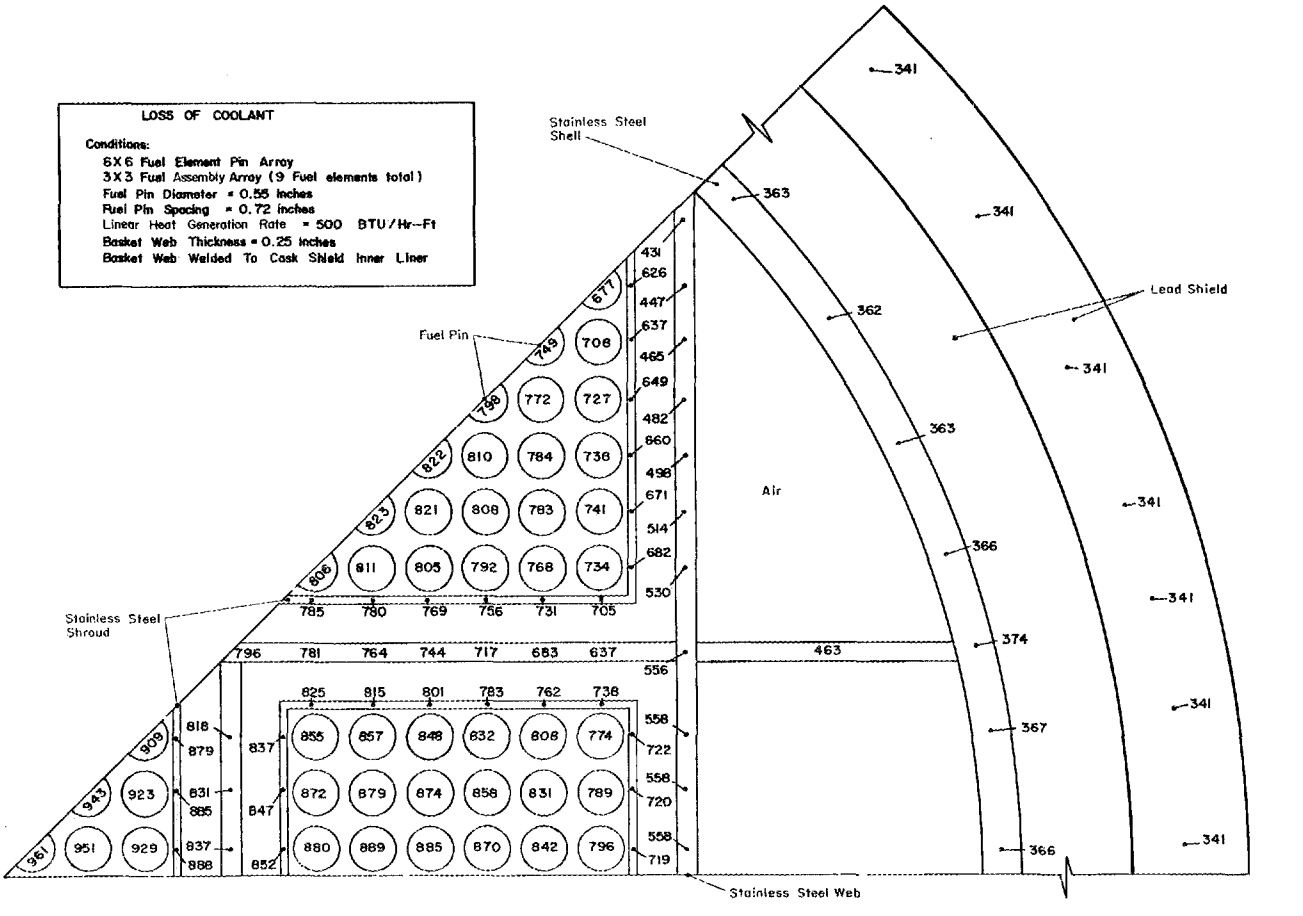

Fig. 22.3. Equilibrium Temperatures in Spent Fuel Shipping Cask and Fuel Following a Loss-of-Coolant Accident. Numbers on drawing are °F.

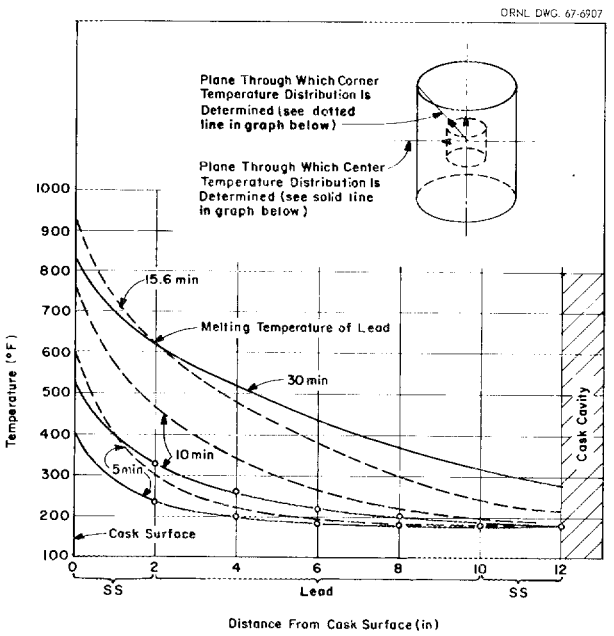

Fig. 22.4. Temperature Profiles for a Cylindrical Cask.

Results indicate that the temperature in the center plane of the cask does not exceed the melting temperature of lead (621°F) after 30 min; however, melting begins in the corners of the cask in slightly less than 16 min.

Information concerning temperatures and the extent of melting may then be utilized to predict not only thermal and mechanical stresses induced during the fire but also the extent of deformation and subsequent rearrangement of shielding after a fire.

Publications, Speeches, and Seminars

ASSISTANCE PROGRAMS

Goeller, H. E., E. M. Shank, and W. M. Sproule, *List of Information Sent to and Received from the Eurochemic Co., January 1, 1966 Through June 30, 1966 (Categorized)*, ORNL-TM-685, suppl. 6 (Aug. 1, 1966).

Goeller, H. E., E. M. Shank, and W. M. Sproule, *List of Information Sent to and Received from the Eurochemic Co., July 1, 1966 Through December 31, 1966 (Categorized)*, ORNL-TM-685, suppl. 7 (Feb. 15, 1967).

BIOCHEMICAL SEPARATIONS

Egan, B. Zane, "Molecular Weights of Transfer Ribonucleic Acids," presented at the ACS Southeastern Regional Meeting, Louisville, Ky., Oct. 27–29, 1966.

Kelmers, A. D., "Preparation of a Highly Purified Phenylalanine Transfer Ribonucleic Acid," *J. Biol. Chem.* **241**, 3540–45 (August 1966).

Kelmers, A. D., "Preparation of a Highly Purified Leucine Transfer Ribonucleic Acid," *Biochem. Biophys. Res. Commun.* **25**(5), 562–66 (1966).

Kelmers, A. D., "Separation of Transfer Ribonucleic Acids," presented at the Gordon Research Conference on Nucleic Acids, New Hampton, N.H., June 19–23, 1967.

Scott, C. D., J. E. Attrill, and N. G. Anderson, "Automatic, High-Resolution Analysis of Urine for Its Ultraviolet-Absorbing Constituents," *Proc. Soc. Exptl. Biol. Med.* **125**, 181 (1967).

Weiss, J. F., A. D. Kelmers, and M. P. Stulberg, "A New Chromatographic System for Increased Resolution of Transfer RNAs," presented at 51st Annual Meeting, Federation of American Societies for Experimental Biology, Chicago, Ill., Apr. 16–21, 1967.

CHEMICAL ENGINEERING RESEARCH

Finsterwalder, L. O., *Geometric Scaling of Stacked-Clone Contactors*, ORNL-4088 (April 1967).

CHEMICAL PROCESSING FOR THE MOLTEN-SALT EXPERIMENT

McNeese, L. E., *Considerations of Low Pressure Distillation and Its Application to Processing of Molten-Salt Breeder Reactor Fuels*, ORNL-TM-1730 (March 1967).

CLASSIFIED

Robinson, R. A. (Isotopes Division), J. P. Nichols, *et al.*, ORNL-TM-1691 (December 1966) (classified).

DEVELOPMENT OF THE THORIUM FUEL CYCLE

Anderson, J. W., A. R. Irvine, J. P. Jarvis, and D. M. Shepherd, *Leak Testing of TUFCDF Cell Supply Ducts by Temperature Compensated Differential Pressure Method*, ORNL-TM-1728 (May 1967).

Bond, W. D., S. D. Clinton, P. A. Haas, A. T. Kleinsteuber, and A. B. Meservey, *Preparation of $^{235}UO_2$-ThO_2 Microspheres by a Sol-Gel Method*, ORNL-TM-1601 (Aug. 8, 1966).

Ferguson, D. E., B. A. Hannaford, and E. L. Nicholson, "Status of Process Development for Thorium-Bearing HTGR Fuels," presented at the ANS Annual Meeting, Denver, Colo., June 20–23, 1966; abstract published in *Trans. Am. Nucl. Soc.* **9**, 315 (1966).

Haas, P. A., and S. D. Clinton, "Preparation of Thoria and Mixed-Oxide Microspheres," *Ind. Eng. Chem., Prod. Res. Develop.* **5**(3), 236–44 (September 1966).

Haws, C. C., and J. W. Snider, "Development and Full-Scale Testing of Process Equipment for the Thorium-Uranium Recycle Facility," presented at the 13th Annual ANS Meeting, San Diego, Calif., June 11–16, 1967.

Meservey, A. B., "UO_2-ThO_2 and UO_3-ThO_2 Sols Prepared by Precipitation-Peptization Processes," presented at the 153d National ACS Meeting, Miami, Fla., Apr. 9–14, 1967; also published as ORNL-TM-1782 (Mar. 20, 1967).

Moore, J. G., "Preparation of Thorium-Uranium Oxide Sols by Amine Denitration," presented at the 13th Annual ANS Meeting, San Diego, Calif., June 11–15, 1967.

Notz, K. J., "Properties of Thoria-Carbon Sols and the Preparation of Thorium Carbides and Porous Thoria," presented at the 153d National ACS Meeting, Miami, Fla., Apr. 9–14, 1967.

Notz, K. J., "Dispersal of Carbon Blacks to Individual Crystallites," *J. Phys. Chem.* **71**, 1965 (1967).

FLUORIDE VOLATILITY PROCESSING

Katz, Sidney, and G. I. Cathers, "A Gas Sorption-Desorption Recovery Method for Plutonium Hexafluoride," presented at the 152d National ACS Meeting, New York City, Sept. 11–16, 1966.

Mailen, J. C., "Recovery of Uranium and Plutonium from Falling Droplets of Molten Fluoride Salt by Fluorination," presented at the 153d National ACS Meeting, Miami, Fla., Apr. 9–14, 1967.

Miles, F. W., *Plutonium-Related Safety Aspects in Designing the Fluidized-Bed Volatility Pilot Plant*, ORNL-TM-1593 (November 1966).

Miller, P. D., W. E. Berry, W. N. Stiegelmeyer, and W. K. Boyd (employed by Battelle Memorial Institute under subcontract No. 988), *Intergranular Modifications in Nickel from the Fluidized-Bed Fluoride Volatility Process*, BMI-X-417 (Nov. 28, 1966).

Miller, P. D., E. F. Stephan, W. E. Berry, and W. K. Boyd (employed by Battelle Memorial Institute under subcontract No. 988), *Corrosion of Construction Materials in Boiling 13 M Nitric–0.1 M Hydrofluoric Acids*, BMI-X-434 (Mar. 30, 1967).

Nicol, R. G., "Engineering and Maintenance Problems in a Fuel Processing Pilot Plant Using the Volatility Method," presented at the 14th ANS Conference on Remote Systems Technology, Pittsburgh, Pa., Oct. 30–Nov. 4, 1966; published in *Trans. Am. Nucl. Soc.* **9**, 622 (1966).

MISCELLANEOUS

Bell, J. T., and R. E. Biggers, "The Absorption Spectrum of the Uranyl Ion in Perchlorate Media. Part II. The Effects of Hydrolysis on the Resolved Spectral Bands," presented at the Southeastern Regional ACS Meeting, Louisville, Ky., Oct. 27–29, 1966.

Bell, J. T., and R. E. Biggers, "The Absorption Spectra of the Uranyl Ion in Perchlorate Media. Part II. The Effects of Hydrolysis on the Resolved Spectral Bands," *J. Mol. Spectry.* **22**, 262–71 (1967).

Biggers, R. E., J. T. Bell, E. C. Long, and O. W. Russ, "MROCOS/MROPLT – a Computer Program for the Mathematical Resolution of Complex Overlapping Spectra and Fine Structure by Nonlinear, Least-Squares Approximation Methods," presented at the Seminar on Automated Spectrometry, National Research Council of Canada, Ottawa, Ontario, July 6–7, 1966.

Blanco, R. E., "Industrial Applications of Nuclear Energy," presented at the Water and Desalination Information Meeting, ORNL, Mar. 28–29, 1967.

Blanco, R. E., "Production of Industrial Chemicals in a Nuclear Desalination Complex," presented at the Technical University, Aachen, Germany, July 10–21, 1967.

Blanco, R. E., *et al., Survey of a Site for a Nuclear Fuel Processing Plant and Waste Disposal Area at Oak Ridge*, ORNL-TM-1748 (Jan. 13, 1967).

Blanco, R. E., J. M. Holmes, R. Salmon, and J. W. Ullmann, *An Economic Study of the Production of Ammonia Using Electricity from a Nuclear Desalination Reactor Complex*, ORNL-3882 (June 1966).

Blanco, R. E., J. M. Holmes, R. Salmon, and J. W. Ullmann, "Ammonia Costs and Electricity," *Chem. Eng. Progr.* **63**(4), 46–50 (1967).

Blanco, R. E., J. M. Holmes, R. Salmon, and J. W. Ullmann, "An Economic Study of the Production of Ammonia and Other Chemicals Using Electricity from a Nuclear Desalination Reactor Complex," *Chem. Eng. Progr., Symp. Ser.* **63**(71), 18–30 (1967).

Ferris, L. M., "Solubility of Niobic Oxide and Niobium Dioxyfluoride in Nitric Acid–Hydrofluoric Acid Solutions at 25°C," *J. Chem. Eng. Data* **11**, 343–46 (1966).

Haas, P. A., and H. F. Johnson, "Model and Experimental Results for Drainage of Solution Between Foam Bubbles," *Ind. Eng. Chem., Fundamentals* **6**, 225 (1967).

Hannon, F. L., "Construction Problems in the Transuranium Facility," presented at General Engineering and Construction Seminar, Feb. 8, 1967.

Hannon, F. L., "Transuranium Procurement," presented at General Engineering and Construction Seminar, Mar. 8, 1967.

Holmes, J. M., and J. W. Ullmann, *Survey of Process Applications in a Desalination Complex*, ORNL-TM-1561 (October 1966).

Johnson, J. S., K. A. Kraus, J. J. Perona, and F. H. Butt, "Hyperfiltration of Paper Mill Wastes," presented at ORNL Desalination Information Meeting, Mar. 28–29, 1967.

Jolley, R. L., B. J. Robinson, and J. S. Wike, "Dissolution and Analysis of Highly Irradiated Plutonia," presented at the 10th Conference on Analytical Chemistry, Gatlinburg, Tenn., Sept. 27–29, 1966.

Jury, S. H., *Foam Decontamination of Air Containing Radioactive Iodine and Particulates Following a Nuclear Incident*, ORNL-TM-1589 (October 1966).

Landry, J. W., "From Weapon to Welfare – Civilian Uses of Nuclear Explosives," presented at the dinner meeting of the Sixth Annual United States Army Nuclear Science Seminar, Oak Ridge, Tenn., July 15, 1966.

Landry, J. W., "Tapping Earth's Steam Kettle with Nuclear Explosives," presented at the dinner meeting of the Second Annual Southeastern Seminar on Thermal Sciences, Oak Ridge, Tenn., July 25, 1966.

Landry, J. W., "The Benevolent Bomb," presented to the Exhibit Managers of the American Museum of Atomic Energy, Oak Ridge, Tenn., Aug. 1, 1966.

Landry, J. W., "Industrial and Scientific Uses of Nuclear Explosives," presented at the dinner meeting of the First North American Symposium on Electromagnetic Separations, Oak Ridge, Tenn., Sept. 8, 1966.

Landry, J. W., "Peaceful Nuclear Explosives – Their Uses and Problems," presented at the Joint Health Physics Society Meeting, Cumberland Falls, Ky., Sept. 10, 1966.

Landry, J. W., "The Reformed Sword: Peaceful Nuclear Explosives," presented at the Armistice Day dinner of the Athens, Tenn., Kiwanis Club, Athens, Tenn., Nov. 11, 1966.

Landry, J. W., "Geographic Engineering with Peaceful Nuclear Explosives," presented at the Quarterly Dinner Meeting of the Atlanta Chapter of the Military Order of the World Wars, Fort McPherson, Atlanta, Ga., Nov. 16, 1966.

Landry, J. W., "The Converted Sword," presented to the Catholic Youth Organization, Oak Ridge, Tenn., Nov. 27, 1966.

Landry, J. W., "Nuclear Digging for Canals and Harbors," presented to the Annual United States Navy Nuclear Science Seminar, Oak Ridge, Tenn., Dec. 2, 1966.

Landry, J. W., "The Engineering Explosion Is Coming!" presented to the Nashville subsection of the American Society of Mechanical Engineers, Nashville, Tenn., Dec. 14, 1966.

Landry, J. W., "Engineers Are Thinking Bigger with Nuclear Explosives," presented under the ORNL Traveling Lecture Program to the College of Engineering Seminar, University of South Carolina, Jan. 5, 1967.

Landry, J. W., "Project Earth Furnace – Industrial Chemicals from Peaceful Nuclear Explosives," presented under the ORNL Traveling Lecture Program to the Student Chapter of American Institute of Chemical Engineers, University of Mississippi, Feb. 6, 1967.

Landry, J. W., "Physicists Provide Potent Packages of Power for Progress – Peaceful Nuclear Explosives," presented under the ORNL Traveling Lecture Program to the Physics Department Seminar, University of Southern Mississippi, Feb. 7, 1967.

Landry, J. W., "Scientific Applications of Nuclear Explosives," presented under the ORNL Traveling Lecture Program to the Physics and Nuclear Engineering classes at the University of Southern Mississippi, Feb. 8, 1967.

Landry, J. W., "Chemical Applications of Nuclear Explosives," presented to the Oak Ridge High School Chemiteers, Oak Ridge, Tenn., Mar. 7, 1967.

Landry, J. W., "Quick and Dirt Cheap: Projects from Peaceful Nuclear Explosives," presented to the dinner meeting of the QAD Seminar-Workshop conducted by the Radiation Shielding Information Center, ORNL and LASL, Oak Ridge, Tenn., Apr. 17, 1967.

Landry, J. W., "Peaceful Uses of Nuclear Explosives, or, How I Learned to Love the H Bomb," presented to the dinner meeting of the Civil Defense Research Project Annual Information Meeting, Oak Ridge, Tenn., Apr. 25, 1967.

Landry, J. W., "Canals and Other Colossal Construction with Nuclear Explosives," presented to the U.S. Navy Research Reserve Nuclear Science Seminar, Oak Ridge, Tenn., May 21, 1967.

Mrochek, J. E., and A. H. Kibbey, *Laboratory Studies of the Electrolysis of Water. The Feasibility of Electrolysis at Temperatures to 400°F*, ORNL-TM-1716 (Dec. 7, 1966).

Nichols, J. P., and D. R. Winkler, *A Program for Calculating Optimum Dimensions of Alpha Radioisotope Capsules Exposed to Varying Stress and Temperature*, ORNL-TM-1735 (April 1967); also NASA CR-72172 (April 1957).

Nichols, J. P., "Containment Potential of the HFIR Pressure Vessel and Primary Coolant System," pp. 227–44 in *The High Flux Isotope Reactor, Accident Analysis*, ORNL-3573 (April 1967).

Rainey, R. H., "Application of the Mixing Equation to the Displacement of Pollution from Lakes," presented at Discussion at International Symposium on Eutrophication, University of Wisconsin, Madison, Wis., June 12–16, 1967.

Rainey, R. H., *Criteria for Noble-Gas Removal Using Permselective Membranes*, ORNL-TM-1822 (Apr. 3, 1967).

Rainey, R. H., "Natural Displacement of Pollution from the Great Lakes," *Science* **155**, 1242 (1967).

Rom, A. M., *Design of a Critically Safe ^{233}U Batch Dissolver for Building 3019*, ORNL-4029 (October 1966).

Rom, A. M., *Design of a Criticality-Proof Batch Dissolver for ^{233}U Located in Building 3019*, ORNL-TM-1568 (Aug. 8, 1966).

Schaffer, W. F., Jr., *Cost Study of the Treatment of Sewage Sludge by the Wet-Air Oxidation Process, Using Oxygen Produced by Low-Cost Electricity from Large Nuclear Reactors*, ORNL-TM-1629 (August 1966).

Schonfeld, Ernest, "Alpha – a Computer Program for the Determination of Radioisotopes by Least-Squares Resolution of the Gamma-Ray Spectra," *Nucl. Instr. Methods* **42**, 213–18 (1966).

Schonfeld, E., *Alpha M – an Improved Computer Program for Determining Radioisotopes by Least-Squares Resolution of the Gamma-Ray Spectra*, ORNL-3975 (September 1966).

Schonfeld, E., "Improved Accuracy in Determination of Radionuclide Concentrations in Solutions Containing Fast-Decaying Isotopes by Least-Squares Resolution of the Gamma-Ray Spectra," pp. 279–83 in *Proceedings of the 2d International Conference on Modern Trends in Activation Analysis, Texas A & M University, 1966*.

Schonfeld, Ernest, "Computer Programs for the Analysis of Samples Containing Several Radioisotopes," presented at the ACS National Meeting, Miami, Fla., Apr. 11–14, 1967.

Schonfeld, E., "Pulse-Height Analysis of Gamma-Ray Spectra of Samples Containing Very Low Levels of Radioactivity," presented at the National ANS Meeting, San Diego, Calif., June 11–15, 1967.

Schonfeld, E., W. Davis, Jr., and A. H. Kibbey, "Rapid, Low-Cost Analyses of Isotope Mixtures," published in *Fundamental Nuclear Energy Research* (USAEC Annual Report to Congress for 1966), pp. 155–56 (December 1966).

Schonfeld, E., J. F. Emery, F. F. Dyer, and T. Alexander, "The Evaluation of Computer Programs for Gamma-Ray Spectrometry in Activation Analysis," pp. 212–15 in *Proceedings of the 2d International Conference on Modern Trends in Activation Analysis, Texas A & M University, 1966*.

Schonfeld, E., A. H. Kibbey, and W. Davis, Jr., "Determination of Nuclide Concentrations in Solutions Containing Low Levels of Radioactivity by Least-Squares Resolution of the Gamma-Ray Spectra," *Nucl. Instr. Methods* **45**, 1–21 (1966).

Schonfeld, E., and D. C. Stewart, "Effect of Temperature on Rare Earth Separations on Cation Resin Columns with Lactate," *Radiochim. Acta* **5**, 176 (1966).

Sears, M. B., and L. M. Ferris, "Hydrolysis of Uranium, Thorium, and Aluminum Carbides in D_2O," *J. Inorg. Nucl. Chem.* **28**, 2055–59 (1966).

Sears, M. B., and L. M. Ferris, "The Reaction of Calcium and Barium Carbides with 0 to 16 *M* Nitric Acid," *J. Inorg. Nucl. Chem.* **29**, 1255 (1967).

Watson, C. D., and G. A. West, "Protective Coatings (Paints)," chap. 12 in *Decontamination of Nuclear Reactors and Equipment* (ed. by J. A. Ayres), USAEC Division of Technical Information.

Watson, C. D., and G. A. West, "Radiation Effects on Paints," *Mater. Protect.* **6**, 44–49 (February 1967).

Watson, C. D., *et al.* (United States Standard), "Protective Coatings (Paints) for the Nuclear Industry," sponsored by the American Institute of Chemical Engineers and approved by the United States Standards Institute.

POWER REACTOR FUEL PROCESSING

Abraham, G. E., and B. C. Finney, *Calculated Maximum Temperatures of Spent Yankee Atomic Type Power Reactor Fuel During Shear-Leach Processing*, ORNL-3948 (November 1966).

Blanco, R. E., "Survey of Aqueous Fuel Processing Methods," presented at the Technical University, Aachen, Germany, July 10–21, 1967.

Blanco, R. E., "Survey of Thorium Nuclear Fuel Processing and Industrial Uses of Nuclear Power," presented at the KFA, Juelich, Germany, July 10–21, 1967.

Blanco, R. E., "Survey of Nuclear Fuel Processing and Industrial Uses of Nuclear Power," presented at the Technical University, Aachen, Germany, July 10–21, 1967.

Blanco, R. E., "Survey of Nonaqueous Fluoride Volatility and Molten Salt Reactor Fuel Processing Methods," presented at the Technical University, Aachen, Germany, July 10–21, 1967.

Ferris, L. M., *Experimental Survey of Close-Coupled Processing Methods for Fuels Containing Uranium and Thorium*, ORNL-3952 (June 1966).

Ferris, L. M., *Possible Head-End Processes for Heavy-Water-Moderated Organic-Cooled Reactor (HWOCR) Fuels*, ORNL-4109 (June 1967).

Ferris, L. M., *Grind-Leach Process for Graphite-Base Reactor Fuels That Contain Coated Particles: Laboratory Development*, ORNL-4110 (June 1967).

Goode, J. H., *Hot Cell Evaluation of the Release of Tritium and ^{85}Krypton During Processing of ThO_2-UO_2 Fuels*, ORNL-3956 (June 1966).

Goode, J. H., "The Release of Tritium and ^{85}Krypton to the Atmosphere During Processing of ThO_2-UO_2 Reactor Fuel," presented at the ANS Annual Meeting, Denver, Colo., June 20–23, 1966.

Goode, J. H., and J. R. Flanary, *Hot Cell Evaluation of the Grind-Leach Process with Irradiated Pyrolytic-Carbon-Coated Sol-Gel Thoria-Urania Particles*, ORNL-TM-1880 (May 26, 1967).

Haas, P. A., and L. M. Ferris, "Dissolution of Graphite-Base Reactor Fuels by Pressurized Aqueous Processes," *Ind. Eng. Chem., Process Design Develop.* **5**, 234–38 (1966).

Nicholson, E. L., *Preliminary Investigation of Processing Fast-Reactor Fuel in an Existing Plant*, ORNL-TM-1784 (April 1967).

Warren, K. S., and L. M. Ferris, *Oxidation and Chlorination of UO_2-PuO_2*, ORNL-3977 (July 1966).

Witte, H. O., *Calculation of Fission Product Radioactivity in Off-Gases from a Burn-Leach Process for Graphite-Base Fuels*, ORNL-TM-1506 (Apr. 27, 1966).

PROGRESS REPORTS

Blake, C. A., Jr., K. B. Brown, and D. J. Crouse, *Chemical Applications of Nuclear Explosions (CANE): Progress Report for October 1 to December 31, 1966*, ORNL-TM-1775 (Feb. 21, 1967).

Blake, C. A., Jr., K. B. Brown, and D. J. Crouse, *Chemical Applications of Nuclear Explosions (CANE): Progress Report for July 1 to September 30, 1966*, ORNL-TM-1688 (Nov. 9, 1966).

Blake, C. A., Jr., K. B. Brown, and D. J. Crouse, *Chemical Applications of Nuclear Explosions (CANE): Progress Report for April 1 to June 30, 1966*, ORNL-TM-1582 (July 29, 1966).

Burch, W. D., *Transuranium Quarterly Progress Report for Period Ending October 31, 1965*, ORNL-3965 (October 1966).

Ferguson, D. E., and staff, *Chemical Technology Division Annual Progress Report for Period Ending May 31, 1966*, ORNL-3945 (September 1966).

Milford, R. P., G. I. Cathers, R. W. Horton, and W. H. Carr, *Fluoride Volatility Processing Semiannual Progress Report for Period Ending November 30, 1966*, ORNL-TM-1849 (July 1967).

Whatley, M. E., *et al., Unit Operations Section Quarterly Progress Report, October–December 1965*, ORNL-3958 (July 1966).

Whatley, M. E., *et al., Unit Operations Section Quarterly Progress Report for January–March 1966*, ORNL-3995 (September 1966).

Whatley, M. E., *et al., Unit Operations Section Quarterly Progress Report, April–June 1966*, ORNL-4074 (April 1967).

Wymer, R. G., and D. A. Douglas, Jr., *Status and Progress Report for Thorium Fuel Cycle Development for Period Ending December 31, 1964*, ORNL-3831 (May 1966).

Wymer, R. G., and A. L. Lotts, *Status and Progress Report for Thorium Fuel Cycle Development for Period Ending December 31, 1965*, ORNL-4001 (October 1966).

REACTOR EVALUATION STUDIES

Arnold, E. D., *Individual Fission Products Produced in High-Exposure, Gas-Cooled Thorium Reactor Fuel*, ORNL-TM-1556 (June 15, 1966).

Arnold, E. D., "Formation of ^{236}Pu and ^{232}U in Slightly Enriched Power Reactors," presented at the National ANS Meeting, Denver, Colo., June 20–23, 1966; published in *Trans. Am. Nucl. Soc.* **9**(1), 294 (1966).

Arnold, E. D., *PHOEBE – a Code for Calculating Beta and Gamma Activity and Spectra for ^{235}U Fission Products*, ORNL-3931 (July 1966).

Arnold, E. D., and B. F. Maskewitz, *SDC, a Shielding-Design Calculation Code for Fuel-Handling Facilities*, ORNL-3041 (March 1966).

Harrington, F. E., "Fuel Preparation Cost," chap. 9 in *An Evaluation of Heavy-Water-Moderated Organic-Cooled Reactors*, ORNL-3921 (January 1967).

Harrington, F. E., and J. T. Roberts, "Fuel Preparation Costs," sect. 9.1 in *An Evaluation of Heavy-Water-Moderated Organic-Cooled Reactors*, ORNL-3921 suppl. (May 1967).

Roberts, J. T., "Spent-Fuel Processing Costs," chap. 11 in *An Evaluation of Heavy-Water-Moderated Organic-Cooled Reactors*, ORNL-3921 (January 1967).

Roberts, J. T., "Fuel Processing Costs," sect. 9.3 in *An Evaluation of Heavy-Water-Moderated Organic-Cooled Reactors*, ORNL-3921 suppl. (May 1967).

Salmon, R., "Fuel Shipping Costs," chap. 12 in *An Evaluation of Heavy-Water-Moderated Organic-Cooled Reactors*, ORNL-3921 (January 1967).

Salmon, R., "Fuel Shipping Costs," sect. 9.4 in *An Evaluation of Heavy-Water-Moderated Organic-Cooled Reactors*, ORNL-3921 suppl. (May 1967).

Salmon, Royes, *A Procedure and a Computer Code (POWERCO) for Calculating the Cost of Electricity Produced by Nuclear Power Stations*, ORNL-3944 (June 1966).

SEPARATIONS CHEMISTRY RESEARCH

Baybarz, R. D., "Anion Exchange Behavior of the Transplutonium Elements with Ethylenediaminetetraacetic Acid," *J. Inorg. Nucl. Chem.* **28**, 1723–31 (1966).

Blake, C. A., "Solvent Extraction Research at the Chemical Technology Division of the Oak Ridge National Laboratory," presented at seminar at Ames Laboratory, Ames, Iowa, Dec. 8, 1966.

Campbell, D. O., and H. D. Harmon, "Amine Extraction of Sulfuric Acid," presented at the Tennessee Academy of Science Meeting, Harrogate, Tenn., Apr. 28–29, 1967.

Coleman, C. F., and J. W. Roddy, "Mass Action and Non-Ideality in Extraction by Amine Sulfate," presented at the International Conference on Solvent Extraction Chemistry, Göteborg, Sweden, Aug. 29–Sept. 1, 1966.

Davis, W., Jr., and J. Mrochek, "Activities of Tributyl Phosphate in Tributyl Phosphate–Uranyl Nitrate–Water Solutions," presented at the International Conference on Solvent Extraction Chemistry, Göteborg, Sweden, Aug. 29–Sept. 1, 1966.

Davis, W., Jr., J. Mrochek, and C. J. Hardy, "The System: Tri-*n*-butyl Phosphate (TBP)–Nitric Acid–Water. 1. Activities of TBP in Equilibrium with Aqueous Nitric Acid and Partial Molar Volumes of the Three Components in the TBP Phase," *J. Inorg. Nucl. Chem.* **28**, 2001–14 (1966).

McDowell, W. J., and C. F. Coleman, "Investigation of Possible Intermolecular Bonding in Some Mixtures of Phosphate Extractants by Use of Dielectric Measurements," *J. Tenn. Acad. Science* **41**(2), 78–80 (April 1966).

McDowell, W. J., and C. F. Coleman, "Interface and Transferring Species in Amine Extraction of Uranium," presented at the International Conference on Solvent Extraction Chemistry, Göteborg, Sweden, Aug. 29–Sept. 1, 1966.

McDowell, W. J., and C. F. Coleman, "Extraction of Alkaline Earths from Sodium Nitrate Solutions by Di(2-ethylhexyl)phosphate in Benzene: Mechanisms and Equilibria," *J. Inorg. Nucl. Chem.* **28**, 1083–89 (1966).

McDowell, W. J., and C. F. Coleman, "Interface Mechanism for Uranium Extraction by Amine Sulfate," *J. Inorg. Nucl. Chem.* **29**, 1325 (1967).

McDowell, W. J., C. F. Coleman, and R. M. Fuoss (Yale University), "Precision Manometer for Differential Vapor Pressures," *Chem. Eng.* **72**(26), 120–22 (1965).

Roddy, J. W., and C. F. Coleman, "Activity Coefficients and Aggregation Numbers in the Tri-*n*-octylamine–Sulfuric Acid–Benzene System," presented at the 152d Annual ACS Meeting, New York, N.Y., Sept. 12–16, 1966.

Seeley, F. G., and D. J. Crouse, "Extraction of Metals from Chloride Solutions with Amines," *J. Chem. Eng. Data* **11**(3), 424–29 (July 1966).

Zingaro, R. A. (Texas A & M University), and C. F. Coleman, "Synergism and Diluent Effects in the Extraction of Cesium by 4-sec-Butyl-2-(α-methylbenzyl)phenol (BAMBP)," *J. Inorg. Nucl. Chem.* **29**, 1287 (1967).

SEPARATIONS PROCESS DEVELOPMENT

Arnold, W. D., and D. J. Crouse, "Radium Removal from Uranium Mill Effluents with Inorganic Ion Exchangers," *Ind. Eng. Chem., Process Design Develop.* **4**, 333 (1965).

Arnold, W. D., D. J. Crouse, and K. B. Brown, "Solvent Extraction of Cesium (and Rubidium) from Ore Liquors with Substituted Phenols," *Ind. Eng. Chem., Process Design Develop.* **4**, 249 (1965).

Egan, B. Z., and W. D. Arnold, "The Purity, Properties and Analytical Determination of 4-sec-Butyl-2-(α-methylbenzyl)phenol (BAMBP)," *Anal. Chem.* **38**, 950 (1966).

Hurst, F. J., D. J. Crouse, K. B. Brown, and A. H. Ross, *Estimated Costs for Processing Granites for Recovery of Thorium and Uranium*, ORNL-3988 (November 1966).

Hurst, F. J., D. J. Crouse, and K. B. Brown, *Recovery of Thorium (and Uranium) from Granitic Rocks*, ORNL-3987 (October 1966).

SOL-GEL STUDIES

Baybarz, R. D., "Preparation of Curium Hydroxide Sol-Gel Spheres as an Intermediate to CmO_2 Microsphere Preparation," *Inorg. Nucl. Chem. Letters* **2**, 129–32 (1966).

Buxton, S. R., C. J. Hardy, and M. H. Lloyd, "Analysis and Significance of Rare-Earth Oxides Produced by a Sol-Gel Method," presented at the 3d International Materials Symposium on Ceramic Microstructure, Berkeley, Calif., June 13–16, 1966; also ORNL-TM-1682 (Sept. 7, 1966).

Gens, T. A., *Preparation of Uranium and Thorium Oxide Microspheres with Controlled Porosity by a Sol-Gel Process*, ORNL-TM-1530 (May 31, 1966).

Gens, T. A., *Formation of Uranium, Zirconium, and Thorium Oxide Microspheres by Hydrolysis of Droplets*, ORNL-TM-1508 (July 10, 1966).

Gens, T. A., *Laboratory Preparation of Several Kinds of Nuclear Fuel Microspheres Using a Sol-Gel Method*, ORNL-TM-1785 (Mar. 10, 1967).

Haas, P. A., F. G. Kitts, and H. Beutler, "Preparation of Reactor Fuels by Sol-Gel Processes," presented at AIChE National Meeting, Salt Lake City, Utah, May 21–24, 1967.

Hardy, C. J., *Examination of Hydrous Uranium Dioxide Precipitates and Sols by Electron Microscopy, Electron Diffraction, and Spectrophotometry*, ORNL-3963 (August 1966).

Hardy, C. J., *Sol-Gel Preparation of Lanthanide Oxide Microspheres and Characterization of Sols and Gels of Lanthanide Hydroxides, Thoria, Urania, and Plutonia*, ORNL-TM-1592 (Aug. 12, 1966).

Hardy, C. J., S. R. Buxton, and T. E. Willmarth, "The Structure of Precipitates, Sols, and Gels of Rare-Earth Hydroxides," presented at 6th Rare-Earth Research Conference, Gatlinburg, Tenn., May 3–7, 1967.

Hardy, C. J., S. R. Buxton, and T. E. Willmarth, "The Structure and Properties of Europium Oxide Spheres Prepared from Sols and Gels of Colloidal Europium Hydroxide," presented at 6th Rare-Earth Research Conference, Gatlinburg, Tenn., May 3–7, 1967.

Lloyd, M. H., and E. J. Kosiancic, *Investigation of Denitration of High-Nitrate Plutonia Sols by Baking*, ORNL-TM-1558 (June 22, 1966).

McCorkle, K. H., "Preparation and Properties of Sol-Gel Oxides," presented at the Gordon Research Conference, Meriden, N.H., Aug. 1–5, 1966.

Wymer, R. G., and J. H. Coobs, "Preparation, Coating, Evaluation, and Irradiation Testing of Sol-Gel Oxide Microspheres," *Proc. Brit. Ceram. Soc.*, No. **7**, 61–79 (February 1967).

THESES

McCorkle, K. H., *Surface Chemistry and Viscometry of Thoria Sols*, ORNL-TM-1536 (July 1966).

Pitt, W. W., Jr., *Vapor-Liquid Equilibria of the Binary System Uranium Hexafluoride–Niobium Pentafluoride*, ORNL-TM-1683 (January 1967).

Scott, C. D., *Oxidation of Hydrogen and Carbon Monoxide in a Helium Stream by Copper Oxide. Analysis of Combined Film and Pore Diffusion with Rapid Irreversible Reaction for Two Components in a Fixed-Bed Process*, ORNL-TM-1540 (August 1966).

TRANSURANIUM ELEMENT PROCESSING

Baybarz, R. D., "An Alpha-Gamma-Neutron Hot Cell for Transplutonium Element Handling," presented at the 10th Conference on Analytical Chemistry in Nuclear Technology, Gatlinburg, Tenn., Sept. 27–29, 1966.

Bigelow, J. E., "Optimizing Schedules at the TRU-HFIR Complex to Maximize ^{249}Cf or ^{252}Cf as Alternative Products," presented at the Annual ANS Meeting, San Diego, Calif., June 11–16, 1967.

Bottenfield, B. F., F. L. Hannon, R. McCarter, C. A. Hahs, and F. L. Peishel, "Remote Maintenance Systems in the Transuranium Processing Plant," presented at the 14th Fall Conference of ANS Remote Systems Technology Division, Pittsburgh, Pa., Oct. 30–Nov. 4, 1966; published in *Trans. Am. Nucl. Soc.* **9**, 623–24 (1966).

Burch, W. D., F. L. Peishel, and O. O. Yarbro, "Philosophy of Chemical Processing Equipment Design and Installation in the Transuranium Processing Plant," presented at the 14th ANS Conference on Remote Systems Technology, Pittsburgh, Pa., Oct. 30–Nov. 4, 1966; also published in *Trans. Am. Nucl. Soc.* **9**, 627 (1966).

King, L. J., and J. L. Matherne, "Containment of Radioactive Material in the Transuranium Processing Plant," presented at the 14th ANS Conference on Remote Systems Technology, Pittsburgh, Pa., Oct. 30–Nov. 4, 1966; published in *Trans. Am. Nucl. Soc.* **9**, 610 (1966).

URANIUM FUEL CYCLE SOL-GEL PROCESSES

Haas, P. A., S. D. Clinton, and A. T. Kleinsteuber, "Preparation of Urania and Urania-Zirconia Microspheres," *Can. J. Chem. Eng.* **44**(6), 348–53 (1966).

Irvine, A. R., J. M. Chandler, P. A. Haas, and K. H. McCorkle, "The Design and Performance of Continuous Process Equipment for Preparation of Urania Sol," presented at the 13th Annual ANS Meeting, San Diego, Calif., June 11–16, 1967; to be published in the Transactions.

WASTE TREATMENT AND DISPOSAL

Blanco, R. E., "Waste By-Product Production," presented at Nuclear Power Briefing for the Coal Industry Conference, Oak Ridge, Tenn., Sept. 29–30, 1966.

Blanco, R. E., "Solving the Waste Disposal Problem," *Nucleonics* **25**(2), 58–61 (1967).

Blanco, R. E., "Survey of Radioactive Waste Treatment Methods," presented at the Technical University, Aachen, Germany, July 10–21, 1967.

Blomeke, J. O., and F. E. Harrington, "Power-Reactor Waste Management," presented at 13th Annual ANS Meeting, San Diego, Calif., June 11–15, 1967.

Clark, W. E., and C. L. Fitzgerald, *Laboratory Development of Processes for Fixation of High-Level Radioactive Wastes in Glassy Solids. (5) Continuous Fixation of Aqueous Wastes: The Con-Potglass Process*, ORNL-4017 (January 1967).

Clark, W. E., *et al.*, *Development of Processes for Solidification of High Level Radioactive Waste: Summary for Pot Calcination and Rising Level Potglass Processes*, ORNL-TM-1584 (Aug. 12, 1966).

Godbee, H. W., R. E. Blanco, E. J. Frederick, W. E. Clark, and N. S. S. Rajan, *Laboratory Development of a Process for Incorporation of Radioactive Waste Solutions and Slurries in Emulsified Asphalt*, ORNL-4003 (April 1967).

Rom, A. M., *Incorporation of Intermediate-Level Waste in Asphalt: Preliminary Design and Cost Estimate of a Full-Scale Plant for ORNL*, ORNL-TM-1697 (December 1966).

Rom, A. M., *Development of the Waste-Asphalt Process on a Semiworks Scale: Design and Installation of Evaporator Equipment in Building 4505*, ORNL-TM-1637 (Sept. 21, 1966).

Schonfeld, E., and A. H. Kibbey, "Improving Strontium Removal from Solution by Controlled Reflux Foam Separation," *Nucl. Appl.* **3**, 353 (1967).

Suddath, J. C., C. W. Hancher, and J. M. Holmes, "Engineering Development of the Pot Processes for Solidification of Radioactive Waste," pp. 301–25 in *Proceedings of the Symposium on the Solidification and Long-Term Storage of Highly Radioactive Wastes, Feb. 14–18, 1966, Richland, Washington*, November 1966.

Yee, W. C., "The Influence of Calcium Ion on the Chemical Removal of Phosphates from Waste Effluents," presented at Gordon Research Conference on Environmental Sciences and Engineering, New Hampton, N.H., June 13–17, 1966.

SEMINARS

1966

Feb. 1	Hot Flowsheet Demonstration (Talspeak, Cerex, Dapex) – Cm Recovery Facility	F. A. Kappelmann J. E. Bigelow
Feb. 8	Project Salt Vault – Design and Demonstration of Equipment	W. F. Schaffer, Jr.
	Estimated Costs of High-Level Waste Management	J. O. Blomeke
Feb. 15	The Potential Uses of Activated Carbons for the Adsorption of Metallic Ions	E. A. Sigworth (West Virginia Pulp and Paper Co., Chemicals Division)
Feb. 22	Project Plowshare: Application to Copper Ores	W. D. Arnold F. J. Hurst
Feb. 25	Densification of Thoria	M. E. Wadsworth
Mar. 1	Extraction of Alkalies and Alkaline Earths by HDEHP	W. J. McDowell
Mar. 8	Activity Measurements in the Water, Sulfuric Acid, Trioctylamine, Diluent System	J. W. Roddy
Mar. 15	Plowshare, Possible Applications: Stimulation of Gas Production from Wells and Recovery of Oil for Shales	C. A. Blake
Mar. 22	Waste Disposal by Hydrofracture	H. O. Weeren
Mar. 29	Thermal Conductivity of Sheared Fuel Elements	H. W. Godbee

Apr. 12	Rare Earth Sol-Gel Development and Application of Spectroscopy to the Study of Sol-Gel Processes	C. J. Hardy
Apr. 19	Plutonia Sol-Gel Development	R. G. Haire
May 24	Comments on Design and Construction of TURF	A. R. Irvine J. W. Anderson
May 31	Laboratory Testing of the Fluid-Bed Volatility Process	J. C. Mailen
June 6	Tracer and Kinetic Studies of the Catalytic Decomposition of Hydrocarbons over Silica-Alumina Catalysts	Paul H. Emmett
June 7	Physical Adsorption of Gases on Solids	Paul H. Emmett
June 8	Multilayer Physical Adsorption and Surface Area Measurements on Porous Solids	Paul H. Emmett
June 9	Measurement of Pore Size Distribution in Solids	Paul H. Emmett
June 10	Chemical Adsorption	Paul H. Emmett
June 13	Reactions of Clean Metal Surfaces	Robert S. Hansen
June 14	Physical Adsorption and the Potential Model	Robert S. Hansen
June 15	The Electrical Double Layer	Robert S. Hansen
June 16	Stability of Lyophobic Colloids	Robert S. Hansen
June 17	Surface Films and Capillary Waves	Robert S. Hansen
June 20	Continuity in Ideal, One Dimensional Flow System	H. A. Deans
June 21	Hyperbolic Continuity	H. A. Deans
June 22	Implicit vs Explicit Chromatographic Systems	H. A. Deans
June 23	The Theory of Distinguishable Pulses in a Perturbed Equilibrium System Effects of Dispersion (Peak-Spreading) on Equilibrium Theory	H. A. Deans
June 24	Chemical Reactions in Chromatographic Systems	H. A. Deans
June 27	Generalization of Gas-Liquid Partition Chromatography to Study High Pressure Vapor-Liquid Equilibria – Part I	R. Kobayashi
June 28	Generalization of Gas-Liquid Partition Chromatography to Study High Pressure Vapor-Liquid Equilibria – Part II	R. Kobayashi
June 29	Generalization of Gas-Solid Chromatography to Study Adsorption in High Pressure Systems – Part I	R. Kobayashi
June 30	Generalization of Gas-Solid Chromatography to Study Adsorption in High Pressure Systems – Part II	R. Kobayashi
July 1	The Study of Diffusion in Dilute and Moderately Dense Gases by a Perturbation Technique	R. Kobayashi
July 12	Ruthenium Chemistry – Coordination Chemists's Delight, Process Chemist's Nightmare	C. J. Hardy

Sept. 27	Status of the ORNL Civil Defense Research Project	J. C. Bresee
Oct. 25	Fuel Reprocessing Studies – Refractory Materials and Plasma Technology at K-25	S. H. Smiley
Nov. 22	An Introduction to Linear Programming and Its Application to the Current Reactor Systems Analysis Project	R. Salmon
Nov. 29	Urania Sol-Gel Process	
	I. Preparation of Urania Sols	J. P. McBride
	II. Drying and Firing of UO_2 Gel Microspheres	W. D. Bond
Dec. 6	Preparation of Sols by Amine Extraction	
	Part 1. Mixed Thorium-Uranium Sols	J. G. Moore
	Part 2. Urania Sols	L. E. Morse
Dec. 13	UO_2-ThO_2 Sols and UO_3-ThO_2 Sols Prepared by Precipitation-Peptization Processes	A. B. Meservey
	Properties of Thoria-Carbon Sols and the Preparation of Thorium Carbides and Porous Thoria	K. J. Notz
1967		
Jan. 10	Advantages and Disadvantages of Factorial Experiments	John T. Holmes (ANL) Lowell E. Koppel (Purdue University)
Jan. 24	Microsphere Forming Column Engineering Studies	C. C. Haws
	Chemistry of the Microsphere Forming Column	W. D. Bond
Feb. 21	Production of Hydrogen by Electrolysis of Water	J. E. Mrochek
Feb. 28	Analysis of Complex Gamma-Ray Spectra of Radionuclides	E. Schonfeld
	Foam Separation with Reflux	A. H. Kibbey
Mar. 6	Solvent Extraction at Ames Laboratory	Morton Smutz (Ames Laboratory)
Apr. 4	Construction Problems in the Transuranium Facility	F. L. Hannon
Apr. 11	Processing of HWOCR Fuels	L. M. Ferris
	Hot-Cell Studies of the Combustion-Leach Process	H. O. Witte
Apr. 17	"AKUFVE," an Automatic System for Measuring Liquid-Liquid Partition Data	Lars G. Erwall (Incentive Research and Development AB, Stockholm)
Apr. 25	MSBR and Blanket Processing	W. L. Carter
	Unit Operations Results in Vacuum Distillation of MSR Salts	L. E. McNeese
	The Hand Trap (safety film)	J. B. Ruch
May 2	Startup of TRU	
	a. Processing to Date	L. J. King
	b. The Recent Maintenance Program in Cell 7	J. L. Matherne
	c. Present Status and Future Plans	W. D. Burch
May 16	HDEHP Extraction Kinetics	J. W. Roddy

CHEMICAL TECHNOLOGY DIVISION

D. E. FERGUSON, DIRECTOR
K. B. BROWN, ASSISTANT DIRECTOR
NANCY BEACH, SECRETARY
ELAINE HICKMAN, SECRETARY
J. B. RUCH, RADIATION AND SAFETY CONTROL OFFICER
A. T. GRESKY, SPECIAL ASSIGNMENT
MARTHA STEWART,* REPORTS EDITOR

H. B. GRAHAM, ADMINISTRATIVE ASSISTANT
JUNE REDMOND, SECRETARY
W. O. GREEVER, PROCUREMENT
LUCILLE KUYKENDALL, SECRETARY

LONG RANGE PLANNING COMMITTEE
J. T. ROBERTS, CHAIRMAN
E. D. ARNOLD
C. F. GUTHRIE
H. SALMON
J. W. ULLMANN
O. L. CULBERSON, CONSULTANT, U.T.
PEGGY MASKEWITZ, SECRETARY
TECHNICIAN: P. P. HAYDON

CHEMICAL DEVELOPMENT SECTION A

R. G. WYMER, SECTION CHIEF
R. E. LEUZE, ASSISTANT SECTION CHIEF
C. F. COLEMAN,[1] ASSISTANT SECTION CHIEF
ALICE McWILLIAMS, SECRETARY
CAROLYN WHEAT, SECRETARY
TECHNICIANS: C. F. KECK
A. S. LYLE[2]
R. G. MANSFIELD, TRANSLATIONS

SOL-GEL STUDIES
J. P. McBRIDE, GROUP LEADER
K. H. McCORKLE
L. E. MORSE
W. L. PATTISON

FUEL CYCLE STUDIES
W. D. BOND, GROUP LEADER
A. B. MESERVEY
K. J. NOTZ
TECHNICIANS: C. W. GREENE
J. E. KERLEY
D. E. SPANGLER

PROTACTINIUM CHEMISTRY
D. O. CAMPBELL, PROBLEM LEADER

SEPARATIONS CHEMISTRY RESEARCH
C. F. COLEMAN,[1] GROUP LEADER
W. J. McDOWELL
J. W. RODDY
TECHNICIANS: G. N. CASE
J. E. THOMPSON

ALPHA MATERIAL PROCESSING
M. H. LLOYD, COORDINATOR[1]
J. R. FLANARY, TRU FLOWSHEETS
B. WEAVER, GROUP LEADER, SEPARATIONS AND CHEMISTRY OF ACTINIDES AND LANTHANIDES
TECHNICIAN: R. R. SHOUN
R. D. BAYBARZ, GROUP LEADER, TRU FINAL SEPARATIONS
A. DELLE SITE[3]
F. A. KAPPELMANN
P. B. ORR
TECHNICIANS: E. C. HENDREN[4]
R. L. HICKEY
J. T. WIGGINS
M. H. LLOYD,[1] GROUP LEADER, TRU PROCESS RESEARCH AND DEVELOPMENT
S. R. BUXTON
J. M. CHILTON
J. J. FARDY[3]
R. G. HAIRE
J. D. HOESCHELE
O. K. TALLENT
TECHNICIAN: S. A. McCOSH

ACTINIDE ELEMENT OXIDES AND RADIATION EFFECTS
N. A. KROHN,[1] GROUP LEADER
TECHNICIANS: D. H. NEWMAN
J. F. TALLEY

ACTINIDE ELEMENT SPECTROPHOTOMETRY
N. A. KROHN,[1] GROUP LEADER
R. E. BIGGERS[4]
J. T. BELL
TECHNICIAN: D. M. HELTON

BIOCHEMICAL SEPARATIONS
A. D. KELMERS, GROUP LEADER
B. Z. EGAN
R. W. RHEAR
R. L. PEARSON
J. F. WEISS
TECHNICIANS: J. P. EUBANKS
D. E. HEATHERLY

BODY FLUID ANALYSES
C. D. SCOTT, GROUP LEADER
K. S. WARREN
R. L. JOLLEY
C. A. BURTIS[4]
TECHNICIAN: M. L. FREEMAN[4]

CHEMICAL DEVELOPMENT SECTION B

R. E. BLANCO, SECTION CHIEF
D. J. CROUSE,[1] ASSISTANT SECTION CHIEF
L. M. FERRIS,[1] ASSISTANT SECTION CHIEF
W. E. CLARK[2]
BRENDA MOSES, SECRETARY
BEA GARBER, SECRETARY
KAY NICHOLS, SECRETARY
J. E. FARMER, DRAFTSMAN

MECHANISMS OF SEPARATIONS PROCESSES
W. DAVIS, JR., GROUP LEADER
A. H. KIBBEY
J. E. MROCHEK
E. SCHONFELD

WASTE STUDIES
H. W. GODBEE, GROUP LEADER
N. M. DAVIS
C. L. FITZGERALD
W. C. YEE
TECHNICIANS: G. D. DAVIS
W. E. SHOCKLEY

POWER REACTOR FUEL PROCESSING
V. C. A. VAUGHEN, GROUP LEADER, *FLOWSHEET DEMONSTRATION ON RADIOACTIVE FUELS*
J. H. GOODE
H. O. WITTE[3]
TECHNICIANS: L. A. BYRD
O. L. KIRKLAND
G. E. WOODALL

L. M. FERRIS,[1] GROUP LEADER, *MOLTEN-SALT REACTOR HEAD END, AND HTGR FUEL PROCESSING*
C. E. SCHILLING
M. D. SEARS[5]
F. J. SMITH
TECHNICIANS: J. F. LAND
C. T. THOMPSON

R. H. RAINEY, GROUP LEADER, *FAST REACTOR PROCESSING AND RARE GAS REMOVAL*
D. E. HORNER
TECHNICIANS: J. R. COLLINS
R. C. LOVELACE

G. I. CATHERS, GROUP LEADER, *VOLATILITY PROCESSING*
M. R. BENNETT
S. KATZ
J. C. MAILEN
E. D. NOGUEIRA[3]
H. F. SOARD
TECHNICIANS: T. E. CRABTREE
C. J. SHIPMAN

SEPARATIONS PROCESSES AND FISSION PRODUCT RECOVERY
D. J. CROUSE,[1] GROUP LEADER
W. D. ARNOLD
F. J. HURST
J. G. MOORE
F. G. SEELEY
TECHNICIAN: W. B. HOWERTON

DESCRIPTIVE CHEMISTRY OF SEPARATIONS SYSTEMS
C. A. BLAKE,[1] GROUP LEADER
J. M. SCHMITT

PLOWSHARE PROGRAM
C. A. BLAKE[1]
D. J. CROUSE[1]
W. D. ARNOLD[1]
F. J. HURST[1]
J. M. SCHMITT[1]

UNIT OPERATIONS SECTION

M. E. WHATLEY, SECTION CHIEF
A. D. RYON, ASSISTANT SECTION CHIEF
JANE POSEY, SECRETARY

FUEL CYCLE STUDIES AND THORIUM UTILIZATION
P. A. HAAS, GROUP LEADER
S. D. CLINTON
C. C. HAWS
J. T. LONG
TECHNICIANS: R. D. ARTHUR
E. W. BROWN
D. A. McWHIRTER
D. E. WILLIS
E. R. JOHNS[3]

FLUORIDE VOLATILITY PROCESS
R. W. HORTON, GROUP LEADER
R. S. LOWRIE
W. W. PITT, JR.[3]
S. H. JURY[3]
TECHNICIANS: V. L. FOWLER
F. G. KILPATRICK

MOLTEN SALT PROCESSING
L. E. McNEESE, PROBLEM LEADER
J. R. HIGHTOWER
B. A. HANNAFORD
J. S. WATSON
TECHNICIANS: J. BEANS
R. O. PAYNE

CHEMICAL ENGINEERING RESEARCH
A. D. RYON, GROUP LEADER
F. L. DALEY
W. S. GROENIER
W. M. WOODS
TECHNICIANS: G. JONES, JR.
K. LADD
C. H. TIPTON

BIOCHEMICAL SEPARATIONS
C. D. WATSON, GROUP LEADER
C. W. HANCHER
H. O. WEEREN
H. F. JOHNSON[4]
TECHNICIANS: G. E. DINSMORE
J. S. TAYLOR

POWER REACTOR FUEL PROCESSING
C. D. WATSON, GROUP LEADER
B. C. FINNEY
G. A. WEST
TECHNICIANS: F. L. ROGERS
J. C. ROSE

DESALINATION STUDIES
J. C. SUDDATH
J. J. PERONA
TECHNICIAN: W. G. SISSON

PROCESS DESIGN SECTION

H. E. GOELLER, SECTION CHIEF
W. E. UNGER, ASSISTANT SECTION CHIEF
E. M. SHANK, *EUROCHEMIC ASSISTANCE*
W. M. SPROULE,[13] TECHNICIAN
J. W. LANDRY, *PLOWSHARE PROGRAM*
W. G. STOCKDALE, *ECONOMIC STUDIES*
P. L. ROBERTSON, *COST ESTIMATES*
J. M. HOLMES,[9] *INDUSTRIAL CHEMICAL STUDIES*
F. E. HARRINGTON, *PU SOL-GEL STUDIES*
A. M. ROM,[1] *PU SOL-GEL STUDIES*
W. F. SCHAFFER, JR.,[1] *WATER CLEANUP STUDIES*
W. L. CARTER,[1] *RARE GAS MEMBRANE SEPARATION STUDIES*
J. P. NICHOLS,[1] *SHIELDING STUDIES*
L. B. SHAPPERT, *FUEL SHIPPING SAFETY STUDIES*
J. B. RUCH, *RADIATION CONTROL OFFICER*
B. F. BOTTENFIELD, *HLW DESIGN*
F. L. PEISHEL, *TRANSURANIUM ASSISTANCE*
F. N. BROWDER, ON LEAVE, *IAEA, VIENNA*
E. L. NICHOLSON,[1] *FAST BREEDER REACTOR PROCESSING*
MAY E. PEPPER, SECRETARY
JO B. DeCARLO, SECRETARY
SUE R. DAMEWOOD, SECRETARY
PATRICIA J. TRENT, SECRETARY
MARY S. BROWN, SECRETARY
K. F. STOOKSBURY, CLERK

DRAFTSMEN
D. E. DUNNING,[11] DRAFTING SUPERVISOR
S. H. BEASLEY[11]
J. W. DAY
B. G. DeWALL
H. W. FALLON[11]
R. G. FARLEY[11]
A. J. FARMER
G. K. FORD[11]
BARBARA A. HISE
L. C. HUBBARD[11]
R. P. OLIVER[11]
J. D. PHILLIPS[11]
J. N. WHEELER[11]

THORIUM FUEL CYCLE
A. R. IRVINE, GROUP LEADER
J. W. ANDERSON,[12] CONSTRUCTION LIAISON
J. P. JARVIS,[12] CONSTRUCTION LIAISON
J. M. CHANDLER,[10] PROCESS EQUIPMENT
J. W. SNIDER, PROCESS EQUIPMENT
F. L. HANNON,[11] PROCESS EQUIPMENT
G. B. BERRY,[11] PROCESS EQUIPMENT
R. V. FOLTZ,[11] PROCESS EQUIPMENT
J. H. FREELS,[11] CRITICAL PATH SCHEDULE

VOLATILITY STUDIES
R. P. MILFORD, GROUP LEADER
S. MANN, *SAMPLING AND ACCOUNTABILITY*
H. W. MILES, *RADIATION AND PLUTONIUM*
E. L. YOUNGBLOOD, *SAFETY ANALYSIS*
B. B. KLIMA, *PROCUREMENT*
G. E. PIERCE,[12] *PROJECT LIAISON*
J. T. HUFFSTETLER, *CRITICAL PATH SCHEDULE*

WASTE STUDIES
J. O. BLOMEKE, GROUP LEADER
E. J. FREDERICK, *FBVPP WASTE STUDIES*
A. M. ROM,[1] *ASPHALT WASTE STUDIES*

MSR STUDIES
E. L. NICHOLSON,[1] GROUP LEADER
W. L. CARTER,[1] *MSBR FUEL PROCESSING*
J. P. NICHOLS,[1] *COMPUTER STUDIES*
W. F. SCHAFFER, JR.,[1] *^{233}U MSRE LOADING*

PILOT PLANT SECTION

R. E. BROOKSBANK, SECTION CHIEF
R. B. LINDAUER, *MSRE PROCESSING PLANT DESIGN*
BOBBIE HOYLE, SECRETARY
JANET MASON, SECRETARY
NANCY WEXLER, SECRETARY
E. C. BRANTLEY, CLERK
R. B. WATERS, DRAFTSMAN

TRANSURANIUM FACILITY
W. D. BURCH, GROUP LEADER
O. O. YARBRO, *OPERATIONS*
L. J. KING, *TECHNICAL GROUP*
J. L. MATHERNE, *ENGINEERING PLANT SAFETY*
F. L. PEISHEL[13]
F. R. CHATTIN
E. D. COLLINS
W. W. EVANS
J. E. VAN CLEVE[14]
J. E. BIGELOW

PROCESS SUPERVISORS
C. E. WADDELL
B. J. STRADER
R. C. SHIPWASH
C. L. SHEPHERD

TECHNICIANS
K. D. BAYNE[14]
C. W. BOATMAN
J. H. BROCK
W. J. BRYAN
H. S. CALDWELL
T. L. DOUGLASS
J. T. EAST[14]
J. H. GROOVER
M. C. HILL
C. H. JONES
R. R. LAXSON
J. B. OVERTON
D. B. OWSLEY
R. E. POTTER
W. M. SPROULE
H. C. THOMPSON
A. V. WILDER

FLUORIDE VOLATILITY
W. H. CARR, GROUP LEADER
W. T. McDUFFEE
R. J. NICOL
R. J. SHANNON

RADIOCHEMICAL OPERATIONS
J. R. PARROTT, GROUP LEADER, *^{233}U DISPENSING PLANT SAFETY*
W. A. SHANNON
TECHNICIANS: C. W. MARTIN
J. H. WALKER
W. A. LINDSEY

SOL-GEL DEMONSTRATION
F. G. KITTS, GROUP LEADER
W. R. WHITSON
TECHNICIANS: S. E. SHELL
R. E. PURKEY

MSRE FUEL PREPARATION
J. M. CHANDLER,[15] GROUP LEADER
TECHNICIAN: W. T. BOSTIC

HOT CELL FACILITY
V. C. A. VAUGHEN,[1] GROUP LEADER
TECHNICIAN: D. R. TAYLOR

*ON LOAN FROM TECHNICAL INFORMATION DIVISION
[1]DUAL CAPACITY
[2]ASSIGNED TO THE WATER PROGRAM
[3]GUEST SCIENTIST FROM ABROAD
[4]ASSIGNED TO THIS PROBLEM BY THE ANALYTICAL CHEMISTRY DIVISION
[5]LEAVE OF ABSENCE
[6]CONSULTANT
[7]ON LOAN FROM SECTION A
[8]EDUCATIONAL LEAVE, U.T.
[9]CONSULTANT, U.T.
[10]PART TIME FROM PILOT PLANT SECTION
[11]ON LOAN FROM GENERAL ENGINEERING AND CONSTRUCTION DIVISION
[12]ON LOAN FROM PLANT AND EQUIPMENT DIVISION
[13]ON LOAN FROM PROCESS DESIGN SECTION
[14]ON LOAN FROM METALS AND CERAMICS DIVISION
[15]ON LOAN TO METALS AND CERAMICS DIVISION
NOTE: CO-OP AND SUMMER EMPLOYEES NOT INCLUDED ON CHART

ORNL-4145
UC-10 – Chemical Separations Processes
for Plutonium and Uranium

INTERNAL DISTRIBUTION

1. Biology Library
2–4. Central Research Library
5. Laboratory Shift Supervisor
6–7. ORNL – Y-12 Technical Library
Document Reference Section
8–28. Laboratory Records Department
29. Laboratory Records, ORNL R.C.
30–31. E. L. Anderson
32. S. E. Beall
33. Arnold Berman
34. D. S. Billington
35. C. A. Blake
36. R. E. Blanco
37. J. O. Blomeke
38. C. J. Borkowski
39. R. E. Brooksbank
40. G. E. Boyd
41. J. C. Bresee
42. R. B. Briggs
43. K. B. Brown
44. F. R. Bruce
45. W. D. Burch
46. W. H. Carr
47. G. I. Cathers
48. J. M. Chandler
49. W. E. Clark
50. C. F. Coleman
51. J. A. Cox
52. D. J. Crouse
53. F. L. Culler
54. W. Davis, Jr.
55. D. A. Douglas
56–185. D. E. Ferguson
186. L. M. Ferris
187. J. R. Flanary
188. J. L. Fowler
189. J. H. Frye, Jr.
190. J. H. Gillette
191. H. E. Goeller
192. A. T. Gresky
193. W. R. Grimes
194. P. A. Haas
195. Richard Hamburger
196. J. P. Hammond
197. C. S. Harrill
198. A. Hollaender
199. R. W. Horton
200. A. R. Irvine
201. M. A. Kastenbaum
202. W. H. Jordan
203. M. T. Kelley
204. R. F. Kimball
205. J. A. Lane
206. C. E. Larson
207. R. E. Leuze
208. M. H. Lloyd
209. R. S. Livingston
210. H. G. MacPherson
211. F. C. Maienschein
212. W. J. McDowell
213. R. A. McNees
214. R. P. Milford
215. D. R. Miller
216. E. C. Miller
217. K. Z. Morgan
218. E. L. Nicholson
219–220. R. B. Parker
221. R. E. Pahler
222. R. H. Rainey
223. J. T. Roberts
224. A. D. Ryon
225. A. F. Rupp
226. H. E. Seagren
227. M. J. Skinner
228. A. H. Snell
229. J. C. Suddath
230. E. H. Taylor
231. V. C. A. Vaughen
232. W. E. Unger
233. B. J. Young
234. C. D. Watson
235. B. S. Weaver
236. A. M. Weinberg
237. M. E. Whatley
238. G. C. Williams
239. R. G. Wymer
240. J. J. Katz (consultant)
241. C. W. J. Wende (consultant)
242. P. H. Emmett (consultant)
243. E. A. Mason (consultant)

EXTERNAL DISTRIBUTION

244. J. A. Swartout, 270 Park Avenue, New York 17, New York
245. Sylvania Electric Products, Inc.
246. Dr. Barendregt, Eurochemic, Mol, Belgium
247. Giacomo Calleri, CNEN, c/o Vitro via Bacdisseras, Milano, Italy
248. D. J. Carswell, Radiochemical Laboratory, The New South Wales University of Technology, P.O. Box 1, Kensington, Sydney, N.S.W., Australia
249. E. Cerrai, Laboratori CISE, Casella Postale N. 3986, Milano, Italy
250. David Dryssen, The Royal Institute of Technology, Department of Inorganic Chemistry, Kemisträgen 37, Stockholm 70, Sweden
251. Syed Fareeduddin, Indian Rare Earths Ltd., Army and Navy Building, 148 Mahatma Gandhi Road, Bombay 1, India
252. J. M. Fletcher, United Kingdom Atomic Energy Authority, Atomic Energy Research Establishment, Harwell, Berks, England
253. W. A. Graf, Manager, Plant Design, Atomic Products Division, General Electric Company, Box 450, Palo Alto, Calif.
254. H. Irving, Department of Inorganic Chemistry, University of Leeds, Leeds, England
255. T. Ishihara, Division of Fuel Research and Development, Tokai Research Establishment, JAERI, Tokai-mura, Ibaraki-ken, Japan
256. A. S. Kertes, Hebrew University, Jerusalem
257. Jorgen Klitgaard, Eurochemic, Mol. Belgium
258. Y. Marcus, Israel Atomic Energy Commission, Tel Aviv, Israel
259. E. Glueckauf, Atomic Energy Research Establishment, Harwell, Berks, England
260. P. Rengnaut, C.E.N. Fontenay-aux-Roses, Boite Postale No. 6, Fontenay-aux-Roses, Seine, France
261. R. Rometsch, Eurochemic, Mol. Belgium
262. A. J. A. Roux, Director of Atomic Energy Research, South African Council for Scientific and Industrial Research, Box 395, Pretoria, South Africa
263. Jan Rydberg, Department of Nuclear Chemistry, Chalmers Tekniska Hogskola, Gibraltargatan 5 H. Goteborg, Sweden
264. M. Shaw, AEC, Washington
265. Erik Svenke, Director, Department of Chemistry, Atomic Energy Company, Stockholm 9, Sweden
266. D. G. Tuck, Associate Professor, Department of Chemistry, Simon Fraser University, Burnaby 2, British Columbia, Canada
267. B. F. Warner, United Kingdom Atomic Energy Authority, Production Group, Windscale and Calder Works, Sellafield, Seascale, Cumberland, England
268. R. A. Wells, Dept. of Scientific and Industrial Research, National Chemical Laboratory, Teddington, Middlesex, England
269. M. Zifferero, Comitato Nazionale per l'Energia, Nucleare, Laboratorio Trattamento Elementi Combustibili, c/o Instituto di Chemica Farmaceutica e Tossicologica dell 'Universita, Piazzale delle Scienze, 5, Rome, Italy
270. M. Claude Jean Jouannaud, Department Head, Plutonium Extraction Plant, Marcoule (Gard), France
271. Prof. Louis Gutierrez-Jadra, Director de Planta Pilotos e Industriales, Junta de Energia Nuclear, Ciudad Universitaris, Madrid (3), Spain
272. W. G. Belter, AEC, Washington
273. J. A. Lieberman, AEC, Washington
274. W. H. Regan, AEC, Washington
275. H. Bernard, AEC, Washington
276. P. Schmid, Federal Institute for Reactor Research, Wurenlingen, AG, Switzerland
277. Atou Shimozato, Nuclear Reactor Design Section, Nuclear Power Plant Department, Hitachi Ltd., Hitachi Works, Hitachi-Shi, Ibaraki-Ken, Japan
278. R. S. Brodsky, Division of Naval Reactors, Atomic Energy Commission, Washington, D.C. 20545

279. Theodore Rockwell III, Chairman, AIF Safety Task Force, MPR Associates, Inc., 815 Connecticut Avenue, N.W., Washington, D.C. 20006
280. Guenther Wirths, NUKEM, Hanau, Germany
281. Riki Kobayashi, Professor, Rice University
282. W. W. Grigorieff, Assistant to the Executive Director, Oak Ridge Associated Universities
283. G. R. Hall, Nuclear Technology Laboratories, Department of Chemical Technology, Imperial College, Prince Consort Road, London, S.W. 7, England
284. Giuseppe Orsenigo, CNEN, Via Belisario 15, Rome, Italy
285. Laboratory and University Division, AEC, ORO

286–468. Given distribution as shown in TID-4500 under Chemical Separations Processes for Plutonium and Uranium (25 copies – CFSTI)